Investigation of Apoptosis and Metabolism as Mechanisms of Trichloroethylene Toxicity During Pregnancy

by

Anthony Su

A dissertation submitted in partial fulfillment
of the requirements for the degree of
Doctor of Philosophy
(Toxicology)
in the University of Michigan
2020

Doctoral Committee:

Professor Rita Loch-Caruso, Chair
Assistant Professor Justin Colacino
Professor Craig Harris
Professor Lawrence Lash, Wayne State University
Professor Stephen W. Ragsdale

Anthony Su

ansu@umich.edu

ORCID iD: 0000-0002-5280-6423

Dedication

To my family and friends

Acknowledgements

I gratefully acknowledge all my sources of support during my time at the University of Michigan. Firstly, my primary mentor and advisor, Dr. Rita Loch-Caruso, deserves special thanks for guiding me with patience, understanding, and a critical yet open mind that I claim has fostered crucial developments to my cognitive skills, including creativity. I am deeply humbled yet proud about many findings contained within this dissertation. I also give huge thanks to my dissertation committee members Dr. Justin Colacino, Dr. Craig Harris, Dr. Lawrence Lash, and Dr. Stephen Ragsdale for unwavering contributions of expertise, time, mentorship, and constructive criticism and assessment to develop my work into what it is today.

Thank you to all past and current members of the Loch-Caruso laboratory who have exerted profound influence on my scientific training, whether it be laboratory techniques, experimental designs, experimental analyses, or experimental interpretations. These individuals with Loch-Caruso laboratory affiliations have all deeply influenced how I think about scientific research, whether broadly or directly applicable to my work: Dr. Elana Elkin, Dr. Sean Harris, Faith Bjork, Kyle Campbell, Dr. Kelly Bakulski, Dr. Kelly Hogan, Dr. Iman Hassan, Catherine Robeson, Monica Smolinski, Thomas Onsi, Maggie Rubens, Gloria Choi, and Eva Antibi-Lerman. Additionally, many of these individuals have made the Loch-Caruso laboratory a pleasant and gratifying place to work.

Thank you to the many collaborators of this work. I thank Dr. Maureen Kachman, Charles Evans, Dr. Angela Wiggins, Kari Bonds from the University of Michigan Metabolomics Core. Sincere thanks also goes to Dr. Alla Karnovsky and Dr. Maureen Sartor of the

Table of Contents

vii

List of Tables

List of Figures

Abstract

Trichloroethylene (TCE), an organic solvent with multiple industrial uses, is associated with adverse pregnancy outcomes in epidemiological studies. In timed-pregnant Wistar rats, TCE exposure reduces fetal weight. Additionally, the TCE metabolite S-(1,2-dichlorovinyl)-L-cysteine (DCVC) stimulates reactive oxygen species (ROS) generation and apoptosis in HTR-8/SVneo placental cells as mechanisms of toxicity. By using aminooxyacetic acid (AOAA) to decrease cysteine conjugate beta-lyase (CCBL) activity and resulting toxicity of DCVC, prior studies in kidney cells demonstrated that the metabolism of DCVC into 1,2-dichlorovinylthiol (DCVT) by CCBL is critical for producing cell death. N-acetyl-L-cysteine (NAC) is a compound with ROS-scavenging properties and a supplier of an acetyl group that contributes to N-acetylation of DCVC. Because metabolism of DCVC is crucial for TCE toxicity, this dissertation hypothesizes that modification of TCE or DCVC metabolism during pregnancy modulates TCE or DCVC-stimulated apoptosis and toxicity. This dissertation uses AOAA and NAC as modulators of TCE or DCVC-stimulated toxicity.

Chapter 2 described TCE-induced decreased fetal weight in timed-pregnant Wistar rats that was prevented by AOAA but not NAC pre/co-treatment. However, AOAA reduced CCBL activity in maternal kidney, but not maternal liver or placenta, suggesting that inhibition of kidney metabolism may have a role in the AOAA effect. Morphometric analysis of the placenta indicated that NAC pre/co-treatment with TCE relative to TCE treatment alone altered placental dimensions consistent with a delayed developmental phenotype. Treatments failed to stimulate any indication of placental apoptosis.

Chapter 3 findings showed that TCE exposure stimulates changes in amniotic fluid of the rats. Changes in amniotic fluid of both sexes include decreased adenosine triphosphate, decreased adenosine diphosphate, decreased guanosine diphosphate, and altered pentose phosphate pathway and folate biosynthesis.

Chapter 4 described mechanisms of DCVC-stimulated toxicity in the *in vitro* human trophoblast BeWo cell model. BeWo cells are known to syncytialize, or multinucleate and fuse, in response to forskolin to create the syncytiotrophoblast cell type that is the maternal-fetal interface *in vivo*. DCVC was found to increase caspase 3/7 activity and nuclear condensation or fragmentation, markers of apoptosis, in unsyncytialized BeWo cells, BeWo cells undergoing syncytialization, and syncytialized BeWo cells. DCVC also stimulated changes consistent with increased ROS production in all three BeWo cell types, including increased hydrogen peroxide abundance and decreased *PRDX2* mRNA expression.

Chapter 5 showed NAC and AOAA pre/co-treatment modulation of DCVC-stimulated toxicity. NAC either exacerbated or did not affect the DCVC-stimulated response. Because NAC exerted a significant effect on increased *CYP3A4* mRNA expression, it is possibile that NAC could have contributed to the CYP3A4-generation of the toxic *N*-acetyl DCVC sulfoxide (NAcDCVCS) metabolite. AOAA did not modify CCBL activity in BeWo cells regardless of differentiation status. However, syncytialized BeWo cells exhibited higher CCBL activity than unsyncytialized BeWo cells, which could explain increased susceptibility of syncytialized BeWo to DCVC apoptosis compared with unsyncytialized BeWo cells.

Chapter 6 revealed that DCVC treatment during syncytialization could either exacerbate or reverse some cellular energy metabolism changes stimulated by syncytialization by itself. Notable reversal effects included ratios within purine metabolism.

This research indicates a critical role for CCBL in DCVC- and TCE-stimulated toxicity during pregnancy and raises the possibility that NAC pre/co-treatment with TCE or DCVC could be detrimental. Apoptosis and disrupted energy metabolism could be major mechanisms of TCE or DCVC-stimulated toxicity. Important future work includes detection of reactive TCE metabolites and identification of enzyme targets of TCE.

Chapter I. Introduction

Adverse pregnancy outcomes as a major public health concern

Adverse pregnancy outcomes are numerous and can be severe in nature. These outcomes can range from maternal mortality, infant mortality, stillbirth, miscarriage, preeclampsia, low birth weight, intrauterine growth restriction, and preterm birth (World Health Organization, 1970). The most serious adverse outcomes are common. The maternal mortality ratio was reported as 216 per 100,000 live births globally in 2015, with an estimate of 12 per 100,000 for high-income countries and 546 per 100,000 in sub-Saharan Africa (Alkema *et al.*, 2016). In the United States in 2013, infant mortality occurred at a rate of 596 per 100,000 live births, which is high compared to that of other developed countries (Murphy *et al.*, 2017).

Along with the occurrence of maternal and infant mortality, adverse pregnancy outcomes of preeclampsia, intrauterine growth restriction, and preterm birth are also common with profound consequences. Preeclampsia, or hypertension with proteinuria during pregnancy, affected 4.6% of all deliveries in a study involving 39 million women from 40 countries worldwide (Abalos *et al.*, 2013). Preeclampsia also increases risk of maternal death from other diseases such as cardiovascular disease (2.7-8.1 hazard ratio compared to control) and stroke (1.6-5.1 hazard ratio compared to control) (Fraser *et al.*, 2012). Intrauterine growth restriction occurs in 10-15% of pregnancies (Longo *et al.*, 2013) and is associated with higher insulin, lower adiponectin, and higher abdominal fat in the offspring (Crume *et al.*, 2014). Finally, preterm birth is estimated to have a rate of 10.02% in the United States in 2018 (Martin *et al.*, 2019), and

is the primary cause of death in infants below five years of age (World Health Organization, 2016).

Exposures and health conditions as associated with adverse pregnancy outcomes

Despite the aforementioned knowledge of adverse pregnancy outcomes, causes of such outcomes remain largely unknown and are an active area of research. It has been reported that low energy intake, short stature, low body mass index (BMI) before pregnancy, and cigarette smoking are associated with intrauterine growth restriction (Kramer, 2003). Additionally, low body mass index (BMI) before pregnancy, genital tract infection, incompetent cervix, and cigarette smoking are associated with preterm birth (Kramer, 2003).

Exposures to specific chemicals are increasingly associated with adverse pregnancy outcomes. Nitrogen dioxide (NO_2) exposure as a form of air pollution has been linked to small for gestational age and decreased term birth weight (Stieb *et al.*, 2016). Additionally, women who delivered preterm were found to have higher concentrations of selected phthalate metabolites in urine compared to women who delivered after 37 gestational weeks (Meeker *et al.*, 2009). Furthermore, a study found that maternal plasma concentrations of polychlorinated biphenyls (PCBs) were inversely associated with both placenta and birth weights (Halldorsson *et al.*, 2008).

Trichloroethylene (TCE) as an environmental toxicant and potential contributor to adverse pregnancy outcomes

Trichloroethylene (TCE) is an organic solvent primarily used as a metal degreaser and in synthesis of other chemicals (Agency for Toxic Substances and Disease Registry, 2019). During manufacture, formulation, and use, TCE is released into air, soil, and surface water (Agency for Toxic Substances and Disease Registry, 2019). Despite the decrease of TCE release into the total

environment from over 57 million pounds in 1988 to 2.4 million pounds in 2010 (Chiu *et al.*, 2013), the legacy of TCE as a Superfund hazardous waste site pollutant and a drinking water contaminant remains particularly severe. Indeed, TCE has been found in 761 out of 1300 hazardous waste sites designated by the United States Environmental Protection Agency as of 2011 (United States Environmental Protection Agency, 2011a; Chiu *et al.*, 2013) and has been estimated to be in one-third of the municipal water supplies of the United States (Jollow *et al.*, 2009).

The toxicity of TCE is well-documented. TCE negatively affects the central nervous system (Bale *et al.*, 2011), kidney (Green *et al.*, 1997a; Lash *et al.*, 2000b), and liver (Bull, 2000). Two case-control epidemiological studies associated TCE exposure with renal cell cancer (Charbotel *et al.*, 2006; Moore *et al.*, 2010). In mice and rats, exposure to TCE increases incidence of liver, kidney, lung, testes, and hematopoietic system tumors (Guha *et al.*, 2012). Studies of TCE as a carcinogen led the International Agency for Research on Cancer to classify TCE as a Group 1 known human carcinogen in 2014 (Guha *et al.*, 2012; International Agency for Research on Cancer, 2014). The United States Environmental Protection Agency (U.S. EPA) also determined that TCE is carcinogenic, in large part for its involvement in kidney and liver tumor formation (United States Environmental Protection Agency, 2011c).

The link between TCE exposure and adverse pregnancy outcomes has been documented, as well. In an epidemiological study, maternal exposure to TCE in drinking water was associated with decreased birth weight of the offspring (Rodenbeck *et al.*, 2000). Similarly, maternal inhalation of TCE was associated with adverse pregnancy outcomes such as low birth weight, small for gestational age, and presence of cardiac and conotruncal defects (Forand *et al.*, 2012). Additional epidemiological studies at Camp Lejeune in North Carolina found that TCE exposure

through contaminated drinking water was associated with small for gestational age, decreased

term birth weight (Ruckart *et al.*, 2014), and increased presence of neural tube defects (Ruckart

et al., 2013). A final epidemiological study has seen TCE ingestion through drinking water to be

associated with small for gestational age, fetal eye malformations, fetal cleft lip, fetal death, and

fetal neural tube defects (Bove *et al.*, 2002). In the pregnant Wistar rat, maternal inhalation of

TCE decreased fetal weight and increased incidence of skeletal ossification (Healy *et al.*, 1982).

TCE metabolism

TCE can be metabolized to a wide range of metabolites with varying degrees of toxicity

(**Figure 1.1**). A first pathway by which TCE is metabolized is through the oxidative cytochrome

P450 (CYP) pathway (Lash *et al.*, 2014a). In this oxidation pathway, TCE is first converted to a

transient CYP-bound intermediate, or TCE-O-CYP complex (Lash *et al.*, 2014a), which

spontaneously reforms into either N-(hydroxyacetyl)-aminoethanol, chloral (CHL), or TCE

epoxide (TCE-O) (Lash *et al.*, 2014a). TCE-O can reform into oxalate or another unstable

compound, dichloroacetyl chloride (DCAC), which rearranges into dichloroacetic acid (DCA)

(Lash *et al.*, 2014a). CHL is in equilibrium with chloral hydrate (CH), which together can be

converted to trichloroethanol (TCOH) by alcohol dehydrogenases or CYPs (Lash *et al.*, 2014a).

TCOH can be metabolized to its glucuronide trichloroethanol glucuronide (TCOG) by UDP-

glucuronosyltransferase (Lash *et al.*, 2014a). The CH/CHL mixture can also be converted to

trichloroacetic acid (TCA) by aldehyde dehydrogenases, and TCA can be converted to DCA.

DCA undergoes multiple fates, including conversion to either monochloroacetic acid (MCA),

glyoxylic acid, or oxalate (Lash *et al.*, 2014a). Of all these compounds formed from CYP-

dependent oxidation of TCE, the metabolites TCOH, TCOG, TCA, DCA, MCA, and oxalate are

hydrophilic and recoverable in urine (Lash *et al.*, 2014a). Additionally, it is known that CH is genotoxic and clastrogenic, and that TCA and DCA are liver carcinogens (Lash *et al.*, 2000a).

The second pathway by which TCE is metabolized is through the glutathione (GSH) conjugation pathway. In this pathway, TCE is first converted to *S*-(1,2-dichlorovinyl)glutathione (DCVG) by glutathione-S-transferases (GSTs) (Lash *et al.*, 2014a). DCVG is then metabolized into *S*-(1,2-dichlorovinyl)-L-cysteine (DCVC) in a two-part process involving γ-glutamyltransferase (GGT) and cysteinyl-glycine dipeptidase (DP) (Lash *et al.*, 2014a). DCVC can either be converted to 1,2-dichlorovinylthiol (DCVT) by cysteine conjugate β-lyase (CCBL) or into *N*-acetyl-*S*-(1,2-dichlorovinyl)-L-cysteine (NAcDCVC) via *N*-acetyltransferases (Lash *et al.*, 2014a). NAcDCVC can be bioactivated into its sulfoxide (NAcDCVCS) by CYP3As (Werner *et al.*, 1996; Lash *et al.*, 2014a). Additionally, DCVC can be converted into its sulfoxide, DCVCS, by flavin-containing monooxygenase 3 (FMO3). Both DCVT and DCVCS spontaneously rearrange into chlorothioketene (CTK) or chlorothionoacetyl chloride (CTAC), which are in equilibrium with each other (Lash *et al.*, 2014a). Of the metabolites from the GSH conjugation pathway, DCVT, DCVCS, CTK, and CTAC are all unstable and reactive (Lash *et al.*, 2014a). Additionally, NAcDCVCS is toxic and reduces viability in cells compared to NAcDCVC (Werner *et al.*, 1996; Lash *et al.*, 2014a). Whereas DCVT is both nephrotoxic and nephrocarcinogenic (Lash *et al.*, 2000a), NAcDCVC is only nephrotoxic after it is deacetylated to DCVC (Wolfgang *et al.*, 1989; Zhang and Stevens, 1989). As a whole, it is widely regarded that the GSH conjugation pathway of TCE metabolism is the more toxic metabolic pathway, leading to generation of more unstable metabolites and fewer metabolites that are recovered in urine compared to the CYP-dependent oxidative pathway of TCE metabolism (Lash *et al.*, 2014a).

The metabolism of TCE is highly dependent on gender, organ, and species (Lash *et al.*, 2000a; Lash *et al.*, 2014a). For instance, the CYP pathway occurs mostly in the liver, and CYP1A1/2, CYP2B1/2, CYP2E1, and CYP2C6/11 have been documented as most active with TCE metabolism (Lash *et al.*, 2000a; Lash *et al.*, 2014a). Additionally, mice have a higher rate of TCE metabolism to TCA compared to rats, as depicted by blood TCA concentrations following oral TCE exposure (Larson and Bull, 1992). Although no direct comparisons in TCA concentrations were made for humans to date, findings that human liver and testes express high levels of CYP2E1 (Forkert *et al.*, 2003), especially compared to human kidney (Sasso *et al.*, 2013), indicate potential for humans to generate CYP-pathway metabolites dependent on organ. Specific to pregnancy, the rate of TCE metabolism to CH has been shown to decrease almost two-fold in pregnancy (Nakajima *et al.*, 1992). Regarding the glutathione conjugation pathway, the liver and kidney are thought to be the organs principally involved (Lash *et al.*, 2000a). Moreover, rats have higher GGT activity compared to mice, and both have higher GGT activity compared to humans (Lash *et al.*, 2000a). Finally, although the rate of GSH conjugation in male rats is greater than the rate of GSH conjugation in female rats (Green *et al.*, 1997a; Lash *et al.*, 1998), literature is sparse on enzymatic activity in pregnant rats.

Role of TCE metabolism in TCE-stimulated toxicity

A first line of evidence that TCE metabolism is critical for its toxicity stems from findings that DCVC as an exposure produces adverse outcomes in several types of cells, thus suggesting that DCVC and/or its downstream metabolites are toxic TCE metabolites. Supporting evidence includes findings that DCVC induces apoptosis and mitochondrial dysfunction in kidney cells (Xu *et al.*, 2008; Lash *et al.*, 2014b). Additionally, in human cytotrophoblastic HTR-8/SVneo cells (Graham *et al.*, 1993), DCVC exposure generates increased reactive oxygen

species (ROS), pro-inflammatory response (Hassan *et al.*, 2016), apoptosis (Elkin *et al.*, 2018), mitochondrial dysfunction (Elkin *et al.*, 2019), and altered energy metabolism (Elkin *et al.*, 2020a). In contrast, CYP metabolism-derived metabolites TCA and DCA do not stimulate toxicity in HTR-8/SVneo cells (unpublished data), suggesting GSH conjugation metabolites to be more important for toxicity in placenta.

Studies have addressed how DCVC metabolism contributes to its toxicity. In kidney cells, the administration of aminooxyacetic acid (AOAA), which decreases CCBL activity, reduces DCVC-induced toxicity (Elfarra and Anders, 1984; Lash *et al.*, 1986; Lash *et al.*, 1994). This suggests that the metabolism of DCVC to DCVT by CCBL is necessary for DCVC toxicity. Similarly, in human placental HTR-8/SVneo cells, it was shown that 1 mM AOAA pretreatment reduced interleukin-6 (IL-6) release stimulated by 20 µM DCVC (Hassan *et al.*, 2016).

Potential for modulation of toxicity based on modulation of TCE metabolism

Based on the aforementioned literature suggesting that inhibition of CCBL activity via AOAA administration is a mechanism to reduce DCVC toxicity (Elfarra and Anders, 1984; Lash *et al.*, 1986; Lash *et al.*, 1994), the choice of utilization of AOAA as an exposure that could modulate DCVC toxicity remains plausible. However, it is only known that AOAA is a CCBL inhibitor in kidney cells (Elfarra and Anders, 1984; Lash *et al.*, 1986), so its effectiveness as a CCBL inhibitor in placental cells is unknown prior to this dissertation. Additionally, it is unknown if modulation of other pathways of DCVC metabolism could result in modulation of DCVC toxicity. Because DCVC can be N-acetylated to form NAcDCVC by N-acetyltransferases (Lash *et al.*, 2014a), it is plausible that administration of chemicals that are a source of acetyl groups could favor DCVC metabolism towards production of NAcDCVC and its sulfoxide, NAcDCVCS. N-acetyl-L-cysteine (NAC) is a provider of an acetyl group (Aldini *et al.*, 2018)

that could potentially modulate DCVC toxicity. Additionally, NAC is a ROS scavenger by itself and through its property as a GSH precursor (Aldini *et al.*, 2018), so it could modulate DCVC toxicity through that means. The two potential modulators of DCVC toxicity used in this dissertation are NAC and AOAA.

<center>**The placenta as a target organ for TCE**</center>

Despite the presence of a significant amount of work on TCE in the kidney and liver, (Lash *et al.*, 2000a), research into effects of TCE in the placenta is more limited. Many reasons exist to suspect that the placenta is a target organ for TCE. Firstly, maternal blood flow to the placenta at term has been estimated to be 600-700 mL/min (Wang and Zhao, 2010), meaning that toxicants in circulating blood encounter the placenta. Secondly, the placenta transports nutrients between mother and fetus, metabolizes xenobiotic agents, and secretes hormones (Prouillac and Lecoeur, 2010), highlighting how placenta disruption could have major consequences. Thirdly, placental cytotrophoblasts fuse to become multinucleated syncytiotrophoblasts that form the maternal-fetal interface during pregnancy (Potgens *et al.*, 2002; Wang *et al.*, 2014). Given this dynamic nature of the placental surface, lipophilic compounds known to cross membranes or utilize placental organic xenobiotic transporters are known to have associations with placenta-related adverse outcomes (Leazer and Klaassen, 2003; Chao *et al.*, 2007). Indeed, TCE is a lipophilic and volatile compound (Yoon *et al.*, 2007) that has been shown to readily cross the placenta (Beppu, 1968; Laham, 1970), and DCVC has been detected in the amniotic fluid of pregnant Wistar rats (Hassan, 2015).

The plausibility of the placenta as a target organ for TCE toxicity also stems from the fact that many of the enzymes needed to produce the toxic TCE metabolites are located in the placenta. Both CYP1A1 and GST are active in the placenta of pregnant Wistar rats (Serafini *et*

<center>8</center>

al., 1991; Wang *et al.*, 2009). Finally, TCE-exposed and control pregnant Wistar rats have detectable GGT activity in the placenta, and TCE exposure significantly increases placental GST activity compared to control rats (Loch-Caruso *et al.*, 2019).

Similarities and differences between human and rat placenta

The human and rat placentae share similarities but also have differences in their anatomy and function. Among similarities between the placentae, proper levels of similar molecules such as nuclear factor erythroid 2-related factor-2 (Nrf2) and peroxiredoxin 6 (Prdx6) play a role in preventing pregnancy disorders such as hypertension and intrauterine growth restriction in both species (Acar *et al.*, 2014). Despite anatomical differences in the number of cell layers between mother and fetus, and implantation types, rat and human placentae are both hemochorial (Furukawa *et al.*, 2011).

A major difference between rat and human placenta concerns the quantity and type of hormone production. The rat placenta synthesizes significantly less estrogen and progesterone compared to the human placenta (Sybulski, 1969; Townsend and Ryan, 1970; Matt and MacDonald, 1984). Additionally, the rat placenta uses cholesterol to synthesize androgen, whereas the human placenta uses cholesterol to synthesize pregnenolone (Furukawa *et al.*, 2011). Because of these differences, it is necessary to use caution when extrapolating endocrine-related endpoints in rat placenta to humans.

The BeWo human placental trophoblast cell model

The BeWo cell line is a human choriocarcinoma villous cytotrophoblastic cell line (Pattillo and Gey, 1968). Through fusion and multinucleation, cytotrophoblasts differentiate into syncytiotrophoblasts as part of normal placentation, a process known as syncytialization (Potgens *et al.*, 2002; Wang *et al.*, 2014). Syncytiotrophoblasts form the outermost layer of the

fetal side of the placenta in contact with maternal blood, providing the maternal-fetal interface for nutrient, gas, and waste exchange (Potgens *et al.*, 2002; Wang *et al.*, 2014). The BeWo cell line can be induced to differentiate, or syncytialize, into syncytiotrophoblasts upon addition of forskolin (Wice *et al.*, 1990; Nampoothiri *et al.*, 2007), an adenylate cyclase activator (Daly, 1984). This process is characterized by the increased expression of syncytin-1 and syncytin-2, often used as biomarkers of syncytialization (Vargas *et al.*, 2009). These characteristics make the BeWo cell line a useful *in vitro* model for studying cytotrophoblasts, syncytiotrophoblasts, and the process of syncytialization.

BeWo cells as cytotrophoblasts, syncytiotrophoblasts, and in the process of syncytialization provide a model for study of signaling pathways leading to apoptosis in the context of syncytialization. Particularly, BeWo cells have been studied in the context of ROS generation, pro-inflammatory response, and apoptosis itself, which are known mechanisms of DCVC toxicity. Firstly, syncytialization decreases the quantity of proteins involved in apoptosis, such as galectin-3 (Hu *et al.*, 2007), and apoptosis promoted by tumor necrosis factor-α (TNF-α) hampers syncytialization (Al-Nasiry *et al.*, 2006). Secondly, proper control of *BCL2*, which is anti-apoptotic, is crucial to prevent excessive cell death during syncytialization (Huppertz *et al.*, 1998; Zheng *et al.*, 2016). Furthermore, p38-MAPK, a protein sensitive to ROS generation, is in the cascade leading to increased syncytin-1 expression and subsequent syncytialization (Gupta *et al.*, 2016). Moreover, proteins that may mediate antioxidant response, such as peroxiredoxin 1 and peroxiredoxin 2, are upregulated when syncytialization occurs (Hu *et al.*, 2007). Likewise, silencing expression of peroxiredoxin 2 prevents BeWo cell syncytialization (Wu *et al.*, 2017). Finally, ROS generation and pro-inflammatory response are established precursors of apoptosis in cytotrophoblasts (Bai *et al.*, 2009; Khera *et al.*, 2017). Therefore, BeWo cells provide a model

to study ROS, pro-inflammatory response, and apoptosis endpoints that are relevant to DCVC toxicity.

Apoptosis as an endpoint of interest in the placenta

Apoptosis is a form of programmed cell death that involves the activation of multiple caspases (Parrish *et al.*, 2013). Apoptosis can proceed via an extrinsic pathway involving a membrane receptor or an intrinsic pathway involving the mitochondria (Parrish *et al.*, 2013). In trophoblastic JEG-3 (Kohler and Bridson, 1971; Kohler *et al.*, 1971), BeWo (Pattillo and Gey, 1968), and Swan-71 cells (Straszewski-Chavez *et al.*, 2009), ROS generation precedes apoptosis (Khera *et al.*, 2017). Similarly, pro-inflammatory response has been linked to apoptosis in cytotrophoblasts (Bai *et al.*, 2009). DCVC stimulates ROS generation, pro-inflammatory response, and apoptosis in human placental HTR-8/SVneo cells (Hassan *et al.*, 2016; Elkin *et al.*, 2018). DCVC also stimulates apoptosis in kidney cells (Xu *et al.*, 2008; Lash *et al.*, 2014b) Thus, it is plausible that apoptosis, ROS generation, and pro-inflammatory response are endpoints affected by DCVC exposure across multiple cell types. However, knowledge of the cellular signaling pathways by which TCE or DCVC exposure lead to apoptosis in placental cells remain unclear or incomplete.

Placental apoptosis is a mechanism of relevance to adverse pregnancy outcomes. For instance, a study found that preeclamptic placentae had altered gene expression relative to control placentae of *RELL2*, whose gene product is involved in apoptosis (Sober *et al.*, 2015). Additionally, apoptosis of syncytiotrophoblasts is associated with intrauterine growth retardation and preeclampsia as determined by bcl-2 expression and terminal deoxynucleotidyl transferase dUTP nick-end labeling (Ishihara *et al.*, 2002). The prior publications provide rationale for further investigation of the role of placental cell apoptosis in adverse pregnancy outcomes.

Study of potential mechanisms of ROS and pro-inflammatory response are supported by known relationships to apoptosis and adverse pregnancy outcomes. Increased ROS in maternal serum is associated with preeclampsia (Matsubara *et al.*, 2010). Similarly, increased systemic IL-6, a pro-inflammatory cytokine, has been associated with infertility, recurrent miscarriage, preterm birth, and preeclampsia (Prins *et al.*, 2012). Additionally, TNF-R1, IL-6, TNF-α, IFN-γ, and IL-1β are all molecules that have pro-inflammatory properties (Chen and Goeddel, 2002; Prins *et al.*, 2012; Turner *et al.*, 2014), participate in regulation of apoptosis (Garcia-Lloret *et al.*, 2000; Chen and Goeddel, 2002; Fortunato and Menon, 2003; Al-Nasiry *et al.*, 2006; Sun *et al.*, 2007; Bai *et al.*, 2009; Saquib *et al.*, 2013; Cao *et al.*, 2015; Jiang *et al.*, 2015; Maurya and Vinayak, 2015), and are relevant to placental health (Maymon *et al.*, 1999; Garcia-Lloret *et al.*, 2000; Fortunato and Menon, 2003; Hebisch *et al.*, 2004; Al-Nasiry *et al.*, 2006; Sun *et al.*, 2007; Bai *et al.*, 2009; Vitoratos *et al.*, 2010; Mulla *et al.*, 2011; Prins *et al.*, 2012; Saquib *et al.*, 2013).

Energy metabolism as an endpoint of interest during pregnancy

Energy metabolism is an important endpoint for DCVC toxicity and pregnancy health. Specifically, in HTR-8/SVneo placental cells, DCVC exposure altered some metrics of energy metabolism, including the increase of several amino acids, including alanine, glutamine, glutamate, and tryptophan, and decreased the adenosine triphosphate (ATP) to adenosine diphosphate (ADP) ratio (Elkin *et al.*, 2020a). These DCVC-induced alterations suggest a role for energy metabolism in a mechanism of DCVC-induced toxicity in placental cells.

Likewise, energy metabolism is critical to pregnancy health. Changes in energy metabolism in amniotic fluid have been associated with adverse pregnancy outcomes. These include decreased amino acids and carbohydrates, including alanine, glycine, proline, glutamine, galactose, mannose, and inositol in the amniotic fluid of preterm birth deliveries versus control

12

(Romero *et al.*, 2010). Similarly, Virgiliou *et al.* found changes in metabolites, including decreased alanine, glutamine, creatine, ornithine, pyruvate, tyrosine, and inositol but increased glutamate, in amniotic fluid of preterm birth deliveries versus control (Virgiliou *et al.*, 2017). Additional literature about amniotic fluid metabolomics and associations with a focus on preterm birth have been reviewed by Gil and Duarte (Gil and Duarte, 2018). Altered amino acids and energy metabolism metabolites, such as decreased aspartate and uridine monophosphate (UMP) and increased creatine, creatinine, and ribose 5-phosphate, were found in placenta of early-onset preeclampsia patients versus control (Kawasaki *et al.*, 2019). Changes in serum metabolites associated with late-onset preeclampsia versus control include increased valine, glucose, citrate, creatine, creatinine, and pyruvate, and decreased acetamide (Bahado-Singh *et al.*, 2013).

In a slime mold model of multinucleation, decreases in glutathione (GSH) concentration and oxygen consumption rate occurred as differentiation proceeded (Allen *et al.*, 1985). Similarly, D-amino oxidase activity induces differentiation in the slime mold (Allen *et al.*, 1988). Furthermore, L-gamma-carboxyglutamic acid has been implicated to be important in the multinucleation of osteoclasts (Kahn *et al.*, 1982). Although these prior reports suggest energy metabolism as critical in other systems of multinucleation, it is currently unknown if a similar mechanism involving energy metabolism is involved in syncytialization in BeWo cells. However, specific to pregnancy, provision or adequate supply of proline is critical to the development of the fetus (Wu *et al.*, 2005; Wu *et al.*, 2008).

Overarching hypothesis and experimental design

Given the importance of adverse pregnancy outcomes and the potential of TCE to affect pregnancy through actions on the placenta, this dissertation aims to advance our understanding of the mechanisms by which TCE or its metabolite DCVC stimulate changes in the placenta or

13

during pregnancy that could lead to adverse pregnancy outcomes. Additionally, this dissertation aims to modulate TCE- or DCVC-stimulated toxicity using treatments that modify TCE metabolism.

The overarching hypothesis of this dissertation is that TCE or its metabolite DCVC stimulates adverse outcomes of pregnancy by increasing ROS generation, increasing pro-inflammatory response, increasing apoptosis, and decreasing supply of energy metabolites, with outcomes modifiable by modulation of TCE or DCVC metabolism. Experimental goals are indicated by thesis chapter and summarized in **Figure 1.2**. This dissertation uses a timed-pregnant Wistar rat model of fetal growth restriction to investigate how TCE-stimulated outcomes may be modified by NAC or AOAA pre/co-treatment to TCE (Chapter 2). Using the same rat model, this dissertation investigates energy metabolism in male and female amniotic fluid samples as it is modified by maternal exposure to TCE (Chapter 3). The remaining dissertation data chapters use the *in vitro* model consisting of the BeWo cell line, a cytotrophoblast cell line capable of fusing to form syncytiotrophoblasts (Pattillo and Gey, 1968; Nampoothiri *et al.*, 2007). This dissertation investigates how DCVC exposure could activate apoptosis in unsyncytialized BeWo cells, BeWo cells undergoing syncytialization, and syncytialized BeWo cells (Chapter 4). Subsequently, this dissertation examines how NAC or AOAA pre/co-treatment with DCVC exposure could modulate DCVC-stimulated toxicity in BeWo cells (Chapter 5). Finally, the dissertation investigatates how energy metabolism in BeWo cells is altered by syncytialization and DCVC treatment during syncytialization (Chapter 6).
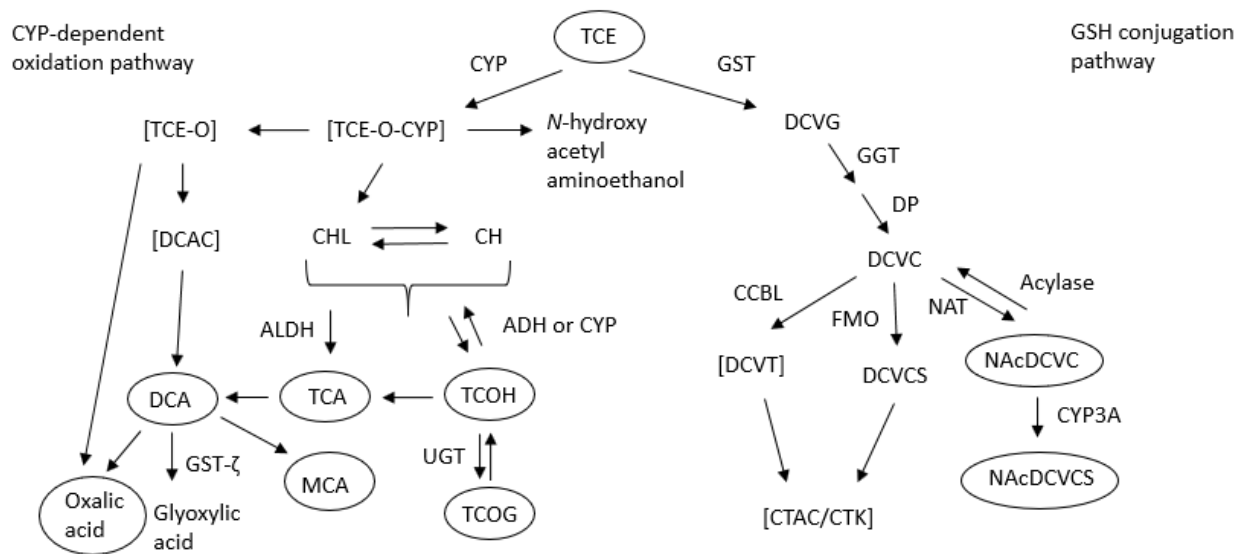
Figure 1.1. Trichloroethylene (TCE) is biotransformed by two different metabolic pathways. The two metabolic pathways by which TCE can be biotransformed are the cytochrome P450 (CYP)-dependent oxidation pathway or the glutathione (GSH) conjugation pathway. Unstable metabolites and metabolites recoverable in urine are depicted in brackets and ovals, respectively. All TCE metabolites, except for the unstable metabolites and DCVCS, are systemically available (Lash et al. 2014). Additional abbreviations: TCE-O, TCE-epoxide; TCE-O-CYP, CYP-bound TCE-epoxide; DCAC, dichloroacetyl chloride; CHL, chloral; CH, chloral hydrate; DCA, dichloroacetic acid; TCA, trichloroacetic acid; TCOH, trichloroethanol; TCOG, trichloroethanol glucuronide; MCA, monochloroacetic acid; ALDH, aldehyde dehydrogenase; ADH, alcohol dehydrogenase; GST, glutathione *S*-transferase; UGT, UDP-glucuronosyltransferase; DCVG, *S*-(1,2-dichlorovinyl)glutathione; DCVC, *S*-(1,2-dichlorovinyl)-L-cysteine; DCVT, 1,2-dichlorovinylthiol; DCVCS, DCVC sulfoxide; NAcDCVC, N-acetyl-S-(1,2-dichlorovinyl)-L-cysteine; NAcDCVCS, NAcDCVC sulfoxide; CTAC, chlorothionoacetyl chloride; CTK, chlorothioketene; GGT, γ-glutamyltransferase; DP, cysteinyl-glycine dipeptidase; CCBL, cysteine conjugate β-lyase; FMO, flavin-containing monooxygenase; NAT, N-acetyltransferase. This figure was modified from Lash et al. 2014 and Elkin et al. 2020 (Lash *et al.*, 2014a; Elkin *et al.*, 2020b).

TCE ----------------------------------> DCVC

Chapter 2
Toxic responses
stimulated by TCE
during pregnancy
and modulation by
NAC or AOAA

Chapter 3
Energy
metabolism
responses in
amniotic fluid
stimulated by
TCE

Chapter 4
ROS-relevant, pro-
inflammatory, and
apoptotic
responses
stimulated by
DCVC

Chapter 5
Modulation of
DCVC-stimulated
responses by NAC
or AOAA

Chapter 6
Cellular energy
metabolism
responses from
syncytialization
and from DCVC
treatment during
syncytialization

Timed-pregnant Wistar rats   Human villous trophoblast BeWo cells

Figure 1.2. Summary of Chapter 2 through Chapter 6 of this dissertation. This dissertation investigates responses stimulated by TCE in timed-pregnant Wistar rats and how NAC or AOAA pre/co-treatment to TCE could modulate responses induced by TCE (Chapter 2). For the timed-pregnant Wistar rats, the dissertation uses a metabolomics approach to investigate how TCE alters the abundance of metabolites in amniotic fluid of associated male and female fetuses (Chapter 3). Sunsequently, the dissertation uses an *in vitro* BeWo human placental trophoblast model to examine how DCVC may stimulate toxic responses in unsyncytialized BeWo cells, BeWo cells undergoing syncytialization, and syncytialized BeWo cells (Chapter 4). The dissertation investigates how DCVC-stimulated responses in BeWo cells could be modified by NAC or AOAA pre/co-treatment (Chapter 5). Finally, this dissertation examines how metabolites in energy metabolism are altered by syncytialization and DCVC treatment during syncytialization (Chapter 6). Abbreviations: TCE, trichloroethylene; DCVC, *S*-(1,2-dichlorovinyl)-L-cysteine; NAC, N-acetyl-L-cysteine; AOAA, aminooxyacetic acid; ROS, reactive oxygen species.

References

Abalos, E., Cuesta, C., Grosso, A.L., Chou, D., Say, L., 2013. Global and regional estimates of preeclampsia and eclampsia: a systematic review. Eur J Obstet Gynecol Reprod Biol **170**, 1-7.

Acar, N., Soylu, H., Edizer, I., Ozbey, O., Er, H., Akkoyunlu, G., Gemici, B., Ustunel, I., 2014. Expression of nuclear factor erythroid 2-related factor 2 (Nrf2) and peroxiredoxin 6 (Prdx6) proteins in healthy and pathologic placentas of human and rat. Acta Histochem **116**, 1289-1300.

Agency for Toxic Substances and Disease Registry, 2019. Toxicological Profile for Trichloroethylene. In U.S. Department of Health and Human Services, A.f.T.S.a.D.R.A., (Ed.), Atlanta, GA, pp.

Al-Nasiry, S., Spitz, B., Hanssens, M., Luyten, C., Pijnenborg, R., 2006. Differential effects of inducers of syncytialization and apoptosis on BeWo and JEG-3 choriocarcinoma cells. Hum Reprod **21**, 193-201.

Aldini, G., Altomare, A., Baron, G., Vistoli, G., Carini, M., Borsani, L., Sergio, F., 2018. N-Acetylcysteine as an antioxidant and disulphide breaking agent: the reasons why. Free Radic Res **52**, 751-762.

Alkema, L., Chou, D., Hogan, D., Zhang, S., Moller, A.B., Gemmill, A., Fat, D.M., Boerma, T., Temmerman, M., Mathers, C., Say, L., United Nations Maternal Mortality Estimation Inter-Agency Group, c., technical advisory, g., 2016. Global, regional, and national levels and trends in maternal mortality between 1990 and 2015, with scenario-based projections to 2030: a systematic analysis by the UN Maternal Mortality Estimation Inter-Agency Group. Lancet **387**, 462-474.

Allen, R.G., Balin, A.K., Reimer, R.J., Sohal, R.S., Nations, C., 1988. Superoxide dismutase induces differentiation in microplasmodia of the slime mold Physarum polycephalum. Arch Biochem Biophys **261**, 205-211.

Allen, R.G., Newton, R.K., Sohal, R.S., Shipley, G.L., Nations, C., 1985. Alterations in superoxide dismutase, glutathione, and peroxides in the plasmodial slime mold Physarum polycephalum during differentiation. J Cell Physiol **125**, 413-419.

Bahado-Singh, R.O., Akolekar, R., Mandal, R., Dong, E., Xia, J., Kruger, M., Wishart, D.S., Nicolaides, K., 2013. First-trimester metabolomic detection of late-onset preeclampsia. Am J Obstet Gynecol **208**, 58 e51-57.

Bai, X., Williams, J.L., Greenwood, S.L., Baker, P.N., Aplin, J.D., Crocker, I.P., 2009. A placental protective role for trophoblast-derived TNF-related apoptosis-inducing ligand (TRAIL). Placenta **30**, 855-860.

Bale, A.S., Barone, S., Jr., Scott, C.S., Cooper, G.S., 2011. A review of potential neurotoxic mechanisms among three chlorinated organic solvents. Toxicol Appl Pharmacol **255**, 113-126.

Beppu, K., 1968. Transmission of the anesthetic agents through the placenta in painless delivery and their effects on newborn infants. Keio J Med **17**, 81-107.

Bove, F., Shim, Y., Zeitz, P., 2002. Drinking water contaminants and adverse pregnancy outcomes: a review. Environ Health Perspect **110 Suppl 1**, 61-74.

Bull, R.J., 2000. Mode of action of liver tumor induction by trichloroethylene and its metabolites, trichloroacetate and dichloroacetate. Environ Health Perspect **108 Suppl 2**, 241-259.

Cao, Z.H., Zheng, Q.Y., Li, G.Q., Hu, X.B., Feng, S.L., Xu, G.L., Zhang, K.Q., 2015. STAT1-mediated down-regulation of Bcl-2 expression is involved in IFN-gamma/TNF-alpha-induced apoptosis in NIT-1 cells. PLoS One **10**, e0120921.

Chao, H.R., Wang, S.L., Lin, L.Y., Lee, W.J., Papke, O., 2007. Placental transfer of polychlorinated dibenzo-p-dioxins, dibenzofurans, and biphenyls in Taiwanese mothers in relation to menstrual cycle characteristics. Food Chem Toxicol **45**, 259-265.

Charbotel, B., Fevotte, J., Hours, M., Martin, J.L., Bergeret, A., 2006. Case-control study on renal cell cancer and occupational exposure to trichloroethylene. Part II: Epidemiological aspects. Ann Occup Hyg **50**, 777-787.

Chen, G., Goeddel, D.V., 2002. TNF-R1 signaling: a beautiful pathway. Science **296**, 1634-1635.

Chiu, W.A., Jinot, J., Scott, C.S., Makris, S.L., Cooper, G.S., Dzubow, R.C., Bale, A.S., Evans, M.V., Guyton, K.Z., Keshava, N., Lipscomb, J.C., Barone, S., Jr., Fox, J.F., Gwinn, M.R., Schaum, J., Caldwell, J.C., 2013. Human health effects of trichloroethylene: key findings and scientific issues. Environ Health Perspect **121**, 303-311.

Crume, T.L., Scherzinger, A., Stamm, E., McDuffie, R., Bischoff, K.J., Hamman, R.F., Dabelea, D., 2014. The long-term impact of intrauterine growth restriction in a diverse U.S. cohort of children: the EPOCH study. Obesity (Silver Spring) **22**, 608-615.

Daly, J.W., 1984. Forskolin, adenylate cyclase, and cell physiology: an overview. Adv Cyclic Nucleotide Protein Phosphorylation Res **17**, 81-89.

Elfarra, A.A., Anders, M.W., 1984. Renal processing of glutathione conjugates. Role in nephrotoxicity. Biochem Pharmacol **33**, 3729-3732.

Elkin, E.R., Bridges, D., Harris, S.M., Loch-Caruso, R.K., 2020. Exposure to Trichloroethylene Metabolite S-(1,2-Dichlorovinyl)-L-cysteine Causes Compensatory Changes to Macronutrient Utilization and Energy Metabolism in Placental HTR-8/SVneo Cells. Chem Res Toxicol.

Elkin, E.R., Bridges, D., Loch-Caruso, R., 2019. The trichloroethylene metabolite S-(1,2-dichlorovinyl)-L-cysteine induces progressive mitochondrial dysfunction in HTR-8/SVneo trophoblasts. Toxicology **427**, 152283.

Elkin, E.R., Harris, S.M., Loch-Caruso, R., 2018. Trichloroethylene metabolite S-(1,2-dichlorovinyl)-l-cysteine induces lipid peroxidation-associated apoptosis via the intrinsic and extrinsic apoptosis pathways in a first-trimester placental cell line. Toxicol Appl Pharmacol **338**, 30-42.

Forand, S.P., Lewis-Michl, E.L., Gomez, M.I., 2012. Adverse birth outcomes and maternal exposure to trichloroethylene and tetrachloroethylene through soil vapor intrusion in New York State. Environ Health Perspect **120**, 616-621.

Forkert, P.G., Lash, L., Tardif, R., Tanphaichitr, N., Vandevoort, C., Moussa, M., 2003. Identification of trichloroethylene and its metabolites in human seminal fluid of workers exposed to trichloroethylene. Drug Metab Dispos **31**, 306-311.

Fortunato, S.J., Menon, R., 2003. IL-1 beta is a better inducer of apoptosis in human fetal membranes than IL-6. Placenta **24**, 922-928.

Fraser, A., Nelson, S.M., Macdonald-Wallis, C., Cherry, L., Butler, E., Sattar, N., Lawlor, D.A., 2012. Associations of pregnancy complications with calculated cardiovascular disease risk and cardiovascular risk factors in middle age: the Avon Longitudinal Study of Parents and Children. Circulation **125**, 1367-1380.

Furukawa, S., Hayashi, S., Usuda, K., Abe, M., Hagio, S., Ogawa, I., 2011. Toxicological pathology in the rat placenta. J Toxicol Pathol **24**, 95-111.

Garcia-Lloret, M.I., Winkler-Lowen, B., Guilbert, L.J., 2000. Monocytes adhering by LFA-1 to placental syncytiotrophoblasts induce local apoptosis via release of TNF-alpha. A model for hematogenous initiation of placental inflammations. J Leukoc Biol **68**, 903-908.

Gil, A.M., Duarte, D., 2018. Biofluid Metabolomics in Preterm Birth Research. Reprod Sci **25**, 967-977.

Graham, C.H., Hawley, T.S., Hawley, R.G., MacDougall, J.R., Kerbel, R.S., Khoo, N., Lala, P.K., 1993. Establishment and characterization of first trimester human trophoblast cells with extended lifespan. Exp Cell Res **206**, 204-211.

Green, T., Dow, J., Ellis, M.K., Foster, J.R., Odum, J., 1997. The role of glutathione conjugation in the development of kidney tumours in rats exposed to trichloroethylene. Chem Biol Interact **105**, 99-117.

Guha, N., Loomis, D., Grosse, Y., Lauby-Secretan, B., El Ghissassi, F., Bouvard, V., Benbrahim-Tallaa, L., Baan, R., Mattock, H., Straif, K., International Agency for Research on Cancer Monograph Working, G., 2012. Carcinogenicity of trichloroethylene, tetrachloroethylene, some other chlorinated solvents, and their metabolites. Lancet Oncol **13**, 1192-1193.

Gupta, S.K., Malhotra, S.S., Malik, A., Verma, S., Chaudhary, P., 2016. Cell Signaling Pathways Involved During Invasion and Syncytialization of Trophoblast Cells. Am J Reprod Immunol **75**, 361-371.

Halldorsson, T.I., Thorsdottir, I., Meltzer, H.M., Nielsen, F., Olsen, S.F., 2008. Linking exposure to polychlorinated biphenyls with fatty fish consumption and reduced fetal growth among Danish pregnant women: a cause for concern? Am J Epidemiol **168**, 958-965.

Hassan, I., 2015. The effect of trichloroethylene on adverse birth outcomes., Toxicology. University of Michigan, Ann Arbor, MI, pp.

Hassan, I., Kumar, A.M., Park, H.R., Lash, L.H., Loch-Caruso, R., 2016. Reactive Oxygen Stimulation of Interleukin-6 Release in the Human Trophoblast Cell Line HTR-8/SVneo by the Trichlorethylene Metabolite S-(1,2-Dichloro)-l-Cysteine. Biol Reprod **95**, 66.

Healy, T.E., Poole, T.R., Hopper, A., 1982. Rat fetal development and maternal exposure to trichloroethylene 100 p.p.m. Br J Anaesth **54**, 337-341.

Hebisch, G., Neumaier-Wagner, P.M., Huch, R., von Mandach, U., 2004. Maternal serum interleukin-1 beta, -6 and -8 levels and potential determinants in pregnancy and peripartum. J Perinat Med **32**, 475-480.

Hu, R., Jin, H., Zhou, S., Yang, P., Li, X., 2007. Proteomic analysis of hypoxia-induced responses in the syncytialization of human placental cell line BeWo. Placenta **28**, 399-407.

Huppertz, B., Frank, H.G., Kingdom, J.C., Reister, F., Kaufmann, P., 1998. Villous cytotrophoblast regulation of the syncytial apoptotic cascade in the human placenta. Histochem Cell Biol **110**, 495-508.

International Agency for Research on Cancer, 2014. Trichloroethylene, Tetrachloroethylene, and Some Other Chlorinated Agents. (IARC Monographs on the Evaluation of Carcinogenic Risks to Humans). IARC Working Group on the Evaluation of Carcinogenic Risk to Humans, Lyon, France, pp.

Ishihara, N., Matsuo, H., Murakoshi, H., Laoag-Fernandez, J.B., Samoto, T., Maruo, T., 2002. Increased apoptosis in the syncytiotrophoblast in human term placentas complicated by

either preeclampsia or intrauterine growth retardation. Am J Obstet Gynecol **186**, 158-166.

Jiang, Q., Li, Q., Chen, H., Shen, A., Cai, Q., Lin, J., Peng, J., 2015. Scutellaria barbata D. Don inhibits growth and induces apoptosis by suppressing IL-6-inducible STAT3 pathway activation in human colorectal cancer cells. Exp Ther Med **10**, 1602-1608.

Jollow, D.J., Bruckner, J.V., McMillan, D.C., Fisher, J.W., Hoel, D.G., Mohr, L.C., 2009. Trichloroethylene risk assessment: a review and commentary. Crit Rev Toxicol **39**, 782-797.

Kahn, A.J., Teitelbaum, S.L., Malone, J.D., Krukowski, M., 1982. The relationship of monocytic cells to the differentiation and resorption of bone. Prog Clin Biol Res **110 Pt B**, 239-248.

Kawasaki, K., Kondoh, E., Chigusa, Y., Kawamura, Y., Mogami, H., Takeda, S., Horie, A., Baba, T., Matsumura, N., Mandai, M., Konishi, I., 2019. Metabolomic Profiles of Placenta in Preeclampsia. Hypertension **73**, 671-679.

Khera, A., Vanderlelie, J.J., Holland, O., Perkins, A.V., 2017. Overexpression of Endogenous Anti-Oxidants with Selenium Supplementation Protects Trophoblast Cells from Reactive Oxygen Species-Induced Apoptosis in a Bcl-2-Dependent Manner. Biol Trace Elem Res **177**, 394-403.

Kohler, P.O., Bridson, W.E., 1971. Isolation of hormone-producing clonal lines of human choriocarcinoma. J Clin Endocrinol Metab **32**, 683-687.

Kohler, P.O., Bridson, W.E., Hammond, J.M., Weintraub, B., Kirschner, M.A., Van Thiel, D.H., 1971. Clonal lines of human choriocarcinoma cells in culture. Acta Endocrinol Suppl (Copenh) **153**, 137-153.

Kramer, M.S., 2003. The epidemiology of adverse pregnancy outcomes: an overview. J Nutr **133**, 1592S-1596S.

Laham, S., 1970. Studies on placental transfer. Trichlorethylene. IMS Ind Med Surg **39**, 46-49.

Larson, J.L., Bull, R.J., 1992. Species differences in the metabolism of trichloroethylene to the carcinogenic metabolites trichloroacetate and dichloroacetate. Toxicol Appl Pharmacol **115**, 278-285.

Lash, L.H., Chiu, W.A., Guyton, K.Z., Rusyn, I., 2014a. Trichloroethylene biotransformation and its role in mutagenicity, carcinogenicity and target organ toxicity. Mutat Res Rev Mutat Res **762**, 22-36.

Lash, L.H., Elfarra, A.A., Anders, M.W., 1986. Renal cysteine conjugate beta-lyase. Bioactivation of nephrotoxic cysteine S-conjugates in mitochondrial outer membrane. J Biol Chem **261**, 5930-5935.

Lash, L.H., Fisher, J.W., Lipscomb, J.C., Parker, J.C., 2000a. Metabolism of trichloroethylene. Environ Health Perspect **108 Suppl 2**, 177-200.

Lash, L.H., Parker, J.C., Scott, C.S., 2000b. Modes of action of trichloroethylene for kidney tumorigenesis. Environ Health Perspect **108 Suppl 2**, 225-240.

Lash, L.H., Putt, D.A., Benipal, B., 2014b. Multigenerational study of chemically induced cytotoxicity and proliferation in cultures of human proximal tubular cells. Int J Mol Sci **15**, 21348-21365.

Lash, L.H., Qian, W., Putt, D.A., Jacobs, K., Elfarra, A.A., Krause, R.J., Parker, J.C., 1998. Glutathione conjugation of trichloroethylene in rats and mice: sex-, species-, and tissue-dependent differences. Drug Metab Dispos **26**, 12-19.

Lash, L.H., Sausen, P.J., Duescher, R.J., Cooley, A.J., Elfarra, A.A., 1994. Roles of cysteine conjugate beta-lyase and S-oxidase in nephrotoxicity: studies with S-(1,2-dichlorovinyl)-

L-cysteine and S-(1,2-dichlorovinyl)-L-cysteine sulfoxide. J Pharmacol Exp Ther **269**, 374-383.

Leazer, T.M., Klaassen, C.D., 2003. The presence of xenobiotic transporters in rat placenta. Drug Metab Dispos **31**, 153-167.

Loch-Caruso, R., Hassan, I., Harris, S.M., Kumar, A., Bjork, F., Lash, L.H., 2019. Trichloroethylene exposure in mid-pregnancy decreased fetal weight and increased placental markers of oxidative stress in rats. Reprod Toxicol **83**, 38-45.

Longo, S., Bollani, L., Decembrino, L., Di Comite, A., Angelini, M., Stronati, M., 2013. Short-term and long-term sequelae in intrauterine growth retardation (IUGR). J Matern Fetal Neonatal Med **26**, 222-225.

Martin, J.A., Hamilton, B.E., Osterman, M.J.K., Driscoll, A.K., 2019. Births: Final data for 2018. In Statistics, N.C.f.H., (Ed.). National Vital Statistics Reports, Hyattsville, MD, pp. 1-47.

Matsubara, K., Matsubara, Y., Hyodo, S., Katayama, T., Ito, M., 2010. Role of nitric oxide and reactive oxygen species in the pathogenesis of preeclampsia. J Obstet Gynaecol Res **36**, 239-247.

Matt, D.W., MacDonald, G.J., 1984. In vitro progesterone and testosterone production by the rat placenta during pregnancy. Endocrinology **115**, 741-747.

Maurya, A.K., Vinayak, M., 2015. Modulation of PKC signaling and induction of apoptosis through suppression of reactive oxygen species and tumor necrosis factor receptor 1 (TNFR1): key role of quercetin in cancer prevention. Tumour Biol **36**, 8913-8924.

Maymon, E., Ghezzi, F., Edwin, S.S., Mazor, M., Yoon, B.H., Gomez, R., Romero, R., 1999. The tumor necrosis factor alpha and its soluble receptor profile in term and preterm parturition. Am J Obstet Gynecol **181**, 1142-1148.

Meeker, J.D., Hu, H., Cantonwine, D.E., Lamadrid-Figueroa, H., Calafat, A.M., Ettinger, A.S., Hernandez-Avila, M., Loch-Caruso, R., Tellez-Rojo, M.M., 2009. Urinary phthalate metabolites in relation to preterm birth in Mexico city. Environ Health Perspect **117**, 1587-1592.

Moore, L.E., Boffetta, P., Karami, S., Brennan, P., Stewart, P.S., Hung, R., Zaridze, D., Matveev, V., Janout, V., Kollarova, H., Bencko, V., Navratilova, M., Szeszenia-Dabrowska, N., Mates, D., Gromiec, J., Holcatova, I., Merino, M., Chanock, S., Chow, W.H., Rothman, N., 2010. Occupational trichloroethylene exposure and renal carcinoma risk: evidence of genetic susceptibility by reductive metabolism gene variants. Cancer Res **70**, 6527-6536.

Mulla, M.J., Myrtolli, K., Potter, J., Boeras, C., Kavathas, P.B., Sfakianaki, A.K., Tadesse, S., Norwitz, E.R., Guller, S., Abrahams, V.M., 2011. Uric acid induces trophoblast IL-1beta production via the inflammasome: implications for the pathogenesis of preeclampsia. Am J Reprod Immunol **65**, 542-548.

Murphy, S.L., Mathews, T.J., Martin, J.A., Minkovitz, C.S., Strobino, D.M., 2017. Annual Summary of Vital Statistics: 2013-2014. Pediatrics **139**.

Nakajima, T., Wang, R.S., Katakura, Y., Kishi, R., Elovaara, E., Park, S.S., Gelboin, H.V., Vainio, H., 1992. Sex-, age- and pregnancy-induced changes in the metabolism of toluene and trichloroethylene in rat liver in relation to the regulation of cytochrome P450IIE1 and P450IIC11 content. J Pharmacol Exp Ther **261**, 869-874.

Nampoothiri, L.P., Neelima, P.S., Rao, A.J., 2007. Proteomic profiling of forskolin-induced differentiated BeWo cells: an in-vitro model of cytotrophoblast differentiation. Reprod Biomed Online **14**, 477-487.

Parrish, A.B., Freel, C.D., Kornbluth, S., 2013. Cellular mechanisms controlling caspase activation and function. Cold Spring Harb Perspect Biol **5**.

Pattillo, R.A., Gey, G.O., 1968. The establishment of a cell line of human hormone-synthesizing trophoblastic cells in vitro. Cancer Res **28**, 1231-1236.

Potgens, A.J., Schmitz, U., Bose, P., Versmold, A., Kaufmann, P., Frank, H.G., 2002. Mechanisms of syncytial fusion: a review. Placenta **23 Suppl A**, S107-113.

Prins, J.R., Gomez-Lopez, N., Robertson, S.A., 2012. Interleukin-6 in pregnancy and gestational disorders. J Reprod Immunol **95**, 1-14.

Prouillac, C., Lecoeur, S., 2010. The role of the placenta in fetal exposure to xenobiotics: importance of membrane transporters and human models for transfer studies. Drug Metab Dispos **38**, 1623-1635.

Rodenbeck, S.E., Sanderson, L.M., Rene, A., 2000. Maternal exposure to trichloroethylene in drinking water and birth-weight outcomes. Arch Environ Health **55**, 188-194.

Romero, R., Mazaki-Tovi, S., Vaisbuch, E., Kusanovic, J.P., Chaiworapongsa, T., Gomez, R., Nien, J.K., Yoon, B.H., Mazor, M., Luo, J., Banks, D., Ryals, J., Beecher, C., 2010. Metabolomics in premature labor: a novel approach to identify patients at risk for preterm delivery. J Matern Fetal Neonatal Med **23**, 1344-1359.

Ruckart, P.Z., Bove, F.J., Maslia, M., 2013. Evaluation of exposure to contaminated drinking water and specific birth defects and childhood cancers at Marine Corps Base Camp Lejeune, North Carolina: a case-control study. Environ Health **12**, 104.

Ruckart, P.Z., Bove, F.J., Maslia, M., 2014. Evaluation of contaminated drinking water and preterm birth, small for gestational age, and birth weight at Marine Corps Base Camp Lejeune, North Carolina: a cross-sectional study. Environ Health **13**, 99.

Saquib, Q., Al-Khedhairy, A.A., Ahmad, J., Siddiqui, M.A., Dwivedi, S., Khan, S.T., Musarrat, J., 2013. Zinc ferrite nanoparticles activate IL-1b, NFKB1, CCL21 and NOS2 signaling to induce mitochondrial dependent intrinsic apoptotic pathway in WISH cells. Toxicol Appl Pharmacol **273**, 289-297.

Sasso, A.F., Schlosser, P.M., Kedderis, G.L., Genter, M.B., Snawder, J.E., Li, Z., Rieth, S., Lipscomb, J.C., 2013. Application of an updated physiologically based pharmacokinetic model for chloroform to evaluate CYP2E1-mediated renal toxicity in rats and mice. Toxicol Sci **131**, 360-374.

Serafini, M.T., Arola, L., Romeu, A., 1991. Glutathione and related enzyme activity in the 11-day rat embryo, placenta and perinatal rat liver. Biol Neonate **60**, 236-242.

Sober, S., Reiman, M., Kikas, T., Rull, K., Inno, R., Vaas, P., Teesalu, P., Marti, J.M.L., Mattila, P., Laan, M., 2015. Extensive shift in placental transcriptome profile in preeclampsia and placental origin of adverse pregnancy outcomes. Sci Rep **5**, 13336.

Stieb, D.M., Chen, L., Hystad, P., Beckerman, B.S., Jerrett, M., Tjepkema, M., Crouse, D.L., Omariba, D.W., Peters, P.A., van Donkelaar, A., Martin, R.V., Burnett, R.T., Liu, S., Smith-Doiron, M., Dugandzic, R.M., 2016. A national study of the association between traffic-related air pollution and adverse pregnancy outcomes in Canada, 1999-2008. Environ Res **148**, 513-526.

Straszewski-Chavez, S.L., Abrahams, V.M., Alvero, A.B., Aldo, P.B., Ma, Y., Guller, S., Romero, R., Mor, G., 2009. The isolation and characterization of a novel telomerase immortalized first trimester trophoblast cell line, Swan 71. Placenta **30**, 939-948.

Sun, Q.H., Peng, J.P., Xia, H.F., Yang, Y., 2007. IFN-gamma promotes apoptosis of the uterus and placenta in pregnant rat and human cytotrophoblast cells. J Interferon Cytokine Res **27**, 567-578.

Sybulski, S., 1969. Testosterone metabolism by rat placenta. Steroids **14**, 427-440.

Townsend, L., Ryan, K.J., 1970. In vitro metabolism of pregnenolone-7-alpha-3H, progesterone-4-14C and androstenedione-4-14C by rat placental tissue. Endocrinology **87**, 151-155.

Turner, M.D., Nedjai, B., Hurst, T., Pennington, D.J., 2014. Cytokines and chemokines: At the crossroads of cell signalling and inflammatory disease. Biochim Biophys Acta **1843**, 2563-2582.

United States Environmental Protection Agency, 2011a. EPA Releases Final Health Assessment for TCE. In Newsroom, U.S.E.P.A., (Ed.), Washington, D.C., pp.

United States Environmental Protection Agency, 2011b. Trichloroethylene: CASRN 79-01-6 (IRIS Assessment). In Integrated Risk Information System (IRIS), U.S.E.P.A.U.S.E., (Ed.), Washington, D.C., pp.

Vargas, A., Moreau, J., Landry, S., LeBellego, F., Toufaily, C., Rassart, E., Lafond, J., Barbeau, B., 2009. Syncytin-2 plays an important role in the fusion of human trophoblast cells. J Mol Biol **392**, 301-318.

Virgiliou, C., Gika, H.G., Witting, M., Bletsou, A.A., Athanasiadis, A., Zafrakas, M., Thomaidis, N.S., Raikos, N., Makrydimas, G., Theodoridis, G.A., 2017. Amniotic Fluid and Maternal Serum Metabolic Signatures in the Second Trimester Associated with Preterm Delivery. J Proteome Res **16**, 898-910.

Vitoratos, N., Economou, E., Iavazzo, C., Panoulis, K., Creatsas, G., 2010. Maternal serum levels of TNF-alpha and IL-6 long after delivery in preeclamptic and normotensive pregnant women. Mediators Inflamm **2010**, 908649.

Wang, R., Dang, Y.L., Zheng, R., Li, Y., Li, W., Lu, X., Wang, L.J., Zhu, C., Lin, H.Y., Wang, H., 2014. Live cell imaging of in vitro human trophoblast syncytialization. Biol Reprod **90**, 117.

Wang, T., Chen, M., Yan, Y.E., Xiao, F.Q., Pan, X.L., Wang, H., 2009. Growth retardation of fetal rats exposed to nicotine in utero: possible involvement of CYP1A1, CYP2E1, and P-glycoprotein. Environ Toxicol **24**, 33-42.

Wang, Y., Zhao, S., 2010. Vascular Biology of the Placenta. Morgan & Claypool Life Sciences, San Rafael, CA.

Werner, M., Birner, G., Dekant, W., 1996. Sulfoxidation of mercapturic acids derived from tri- and tetrachloroethene by cytochromes P450 3A: a bioactivation reaction in addition to deacetylation and cysteine conjugate beta-lyase mediated cleavage. Chem Res Toxicol **9**, 41-49.

Wice, B., Menton, D., Geuze, H., Schwartz, A.L., 1990. Modulators of cyclic AMP metabolism induce syncytiotrophoblast formation in vitro. Exp Cell Res **186**, 306-316.

Wolfgang, G.H., Gandolfi, A.J., Stevens, J.L., Brendel, K., 1989. N-acetyl S-(1,2-dichlorovinyl)-L-cysteine produces a similar toxicity to S-(1,2-dichlorovinyl)-L-cysteine in rabbit renal slices: differential transport and metabolism. Toxicol Appl Pharmacol **101**, 205-219.

World Health Organization, 1970. The prevention of perinatal mortality and morbidity. In Series, W.H.O.T.R., (Ed.), Geneva, Switzerland, pp.

World Health Organization, 2016. Preterm birth: Fact Sheet. In Centre, W.H.O.M., (Ed.),
    Geneva, Switzerland, pp.

Wu, F., Tian, F., Zeng, W., Liu, X., Fan, J., Lin, Y., Zhang, Y., 2017. Role of peroxiredoxin2
    downregulation in recurrent miscarriage through regulation of trophoblast proliferation
    and apoptosis. Cell Death Dis **8**, e2908.

Wu, G., Bazer, F.W., Datta, S., Johnson, G.A., Li, P., Satterfield, M.C., Spencer, T.E., 2008.
    Proline metabolism in the conceptus: implications for fetal growth and development.
    Amino Acids **35**, 691-702.

Wu, G., Bazer, F.W., Hu, J., Johnson, G.A., Spencer, T.E., 2005. Polyamine synthesis from
    proline in the developing porcine placenta. Biol Reprod **72**, 842-850.

Xu, F., Papanayotou, I., Putt, D.A., Wang, J., Lash, L.H., 2008. Role of mitochondrial
    dysfunction in cellular responses to S-(1,2-dichlorovinyl)-L-cysteine in primary cultures
    of human proximal tubular cells. Biochem Pharmacol **76**, 552-567.

Yoon, M., Madden, M.C., Barton, H.A., 2007. Extrahepatic metabolism by CYP2E1 in PBPK
    modeling of lipophilic volatile organic chemicals: impacts on metabolic parameter
    estimation and prediction of dose metrics. J Toxicol Environ Health A **70**, 1527-1541.

Zhang, G.H., Stevens, J.L., 1989. Transport and activation of S-(1,2-dichlorovinyl)-L-cysteine
    and N-acetyl-S-(1,2-dichlorovinyl)-L-cysteine in rat kidney proximal tubules. Toxicol
    Appl Pharmacol **100**, 51-61.

Zheng, R., Li, Y., Sun, H., Lu, X., Sun, B.F., Wang, R., Cui, L., Zhu, C., Lin, H.Y., Wang, H.,
    2016. Deep RNA sequencing analysis of syncytialization-related genes during BeWo cell
    fusion. Reproduction.

Chapter II. Differential Modulation by N-acetyl-L-cysteine and Aminooxyacetic Acid of Trichloroethylene Toxicity in Wistar Rats

Abstract

Exposure to trichloroethylene (TCE), a colorless chlorinated organic solvent with many industrial purposes, has been associated with adverse pregnancy outcomes in epidemiological studies, decreased fetal weight in timed-pregnant rats, and increased expression of markers of oxidative stress in rat placenta. The toxicity of TCE can be manifest through formation of reactive metabolites via its glutathione (GSH) conjugation metabolic pathway. However, exact mechanisms of TCE toxicity during pregnancy remain incomplete or unclear. To understand the contribution of the GSH conjugation metabolic pathway and oxidative stress to TCE toxicity during pregnancy, we exposed rats orally to 480 mg TCE/kg/day from gestational day (GD) 6 to GD 16 with and without N-acetyl-L-cysteine (NAC) at 200 mg/kg/day or aminooxyacetic acid (AOAA) at 20 mg/kg/day as pre/co-treatments from GD 5 to GD 16. NAC was included as a scavenger of reactive oxygen species that can also modify the GSH conjugation pathway. AOAA was included as an inhibitor of cysteine conjugate β-lyase (CCBL), an enzyme responsible for metabolic activation of DCVC. TCE decreased fetal weight, and this was prevented by AOAA but not NAC pre/co-treatment to TCE. Although AOAA inhibited CCBL activity in maternal kidney, it was not an effective inhibitor of CCBL activity in maternal liver and placenta, suggesting that AOAA prevention of TCE-stimulated decreased fetal weight was due to CCBL activity inhibition in the kidneys, not in the liver or placenta. Exposure to NAC pre/co-treatment with TCE, relative to TCE treatment alone, altered placental morphology consistent with a

delayed developmental phenotype. Immunohistochemical staining revealed that the decidua basale, relative to basal zone and labyrinth zone, expressed the highest abundance of CCBL1, flavin-containing monooxygenase 3, and cleaved caspase-3. As a whole, TCE by itself produced modest changes to placenta. Together, the findings of the current study show that NAC and AOAA differentially modulated TCE-induced pregnancy outcomes and suggests additional approaches and future directions to protect against TCE toxicity during pregnancy.

Introduction

Trichloroethylene (TCE) is a chlorinated environmental contaminant commonly used as a metal degreaser and in synthesis of chemicals such as refrigerants (Agency for Toxic Substances and Disease Registry, 2019). Exposure to TCE can occur by inhalation of contaminated air, ingestion of contaminated drinking water, and, to a lesser extent, ingestion of contaminated foods and dermal contact with contaminated consumer products (Agency for Toxic Substances and Disease Registry, 2019). Release of TCE into air has been widespread throughout the United States (United States Environmental Protection Agency, 2011b), although total environmental emission in any media of TCE decreased from 57.4 million pounds in 1988 to 2.18 million pounds in 2018 (United States Environmental Protection Agency, 2020). Relatively recent publications indicate continued water and other environmental media contamination by TCE (Jollow *et al.*, 2009; Agency for Toxic Substances and Disease Registry, 2019). TCE is found in over half of current or former National Priorities List hazardous waste sites designated by the United States Environmental Protection Agency (Agency for Toxic Substances and Disease Registry, 2019), and TCE was detected in about a third of municipal water supplies in the United States (Jollow *et al.*, 2009). Significantly, TCE is classified as a Group 1 known human carcinogen by the International Agency for Research on Cancer (Guha *et al.*, 2012; International

Agency for Research on Cancer, 2014) and classified as a known human carcinogen via all routes of exposure by the United States Environmental Protection Agency (United States Environmental Protection Agency, 2011c). TCE is a suggested toxicant to multiple organs, including liver (Bull, 2000), kidney (Green *et al.*, 1997a), lungs (Forkert *et al.*, 1985; Green *et al.*, 1997b), and the immune (Cooper *et al.*, 2009), nervous (Bale *et al.*, 2011), reproductive (Healy *et al.*, 1982; Manson *et al.*, 1984; Lamb and Hentz, 2006; Loch-Caruso *et al.*, 2019), and developmental systems (Saillenfait *et al.*, 1995).

Of specific relevance to the present study, epidemiological studies have identified adverse effects of TCE on pregnancy outcomes. Rodenbeck *et al.* associated maternal exposure to TCE via contaminated water to very low birth weight offspring (Rodenbeck *et al.*, 2000). Similarly, Forand *et al.* found an association between TCE exposure through vapor intrusion to low birth weight, small for gestational age, and term low birth weight (Forand *et al.*, 2012). Finally, Ruckart *et al.* found maternal TCE exposure through drinking water to be associated with small for gestational age (Ruckart *et al.*, 2014).

The metabolism of TCE has been extensively studied and is thought to be responsible for the toxicity of TCE. TCE is metabolized through two metabolic pathways: a cytochrome P450 (CYP)-dependent oxidative pathway and a glutathione (GSH) conjugation metabolic pathway (Lash *et al.*, 2014a). The CYP-dependent oxidative pathway includes formation of reactive and unstable epoxide intermediates that precedes formation of stable metabolites such as dichloroacetic acid (DCA), trichloroacetic acid (TCA), and monoacetic acid (MCA) that can be recovered in urine (Lash *et al.*, 2014a). In contrast, the GSH conjugation pathway is initiated by TCE conjugation with GSH to form *S*-(1,2-dichlorovinyl)glutathione (DCVG). DCVG is metabolized by γ-glutamyltransferase (GGT) and cysteinyl-glycine dipeptidase (DP) to form *S*-

(1,2-dichlorovinyl)-L-cysteine (DCVC) (Lash *et al.*, 2014a). DCVC can then be metabolized

through three different pathways, each generating at least one reactive metabolite. Firstly, DCVC

can be metabolized by cysteine conjugate β-lyase (CCBL) to yield 1,2-dichlorovinylthiol

(DCVT), which spontaneously rearranges to form chlorothionoacetyl chloride (CTAC) and

chlorothioketene (CTK) (Lash *et al.*, 2014a). Secondly, flavin-containing monooxygenase 3

(FMO3) can metabolize DCVC into DCVC sulfoxide (DCVCS), which also spontaneously

forms CTAC and CTK (Lash *et al.*, 2014a). Lastly, DCVC can be metabolized by N-acetyl-

transferases (NATs) into N-acetyl-*S*-(1,2-dichlorovinyl)-L-cysteine (NAcDCVC), a reaction that

can be reversed by aminoacylase III (Uttamsingh and Anders, 1999; Uttamsingh *et al.*, 2000;

Lash *et al.*, 2014a). NAcDCVC can be bioactivated by CYP3As into NAcDCVCS (Werner *et

al.*, 1996; Lash *et al.*, 2014a). DCVT, DCVCS, CTAC, and CTK are all chemically unstable and

reactive (Lash *et al.*, 2014a). NAcDCVCS is an additional toxic metabolite (Werner *et al.*, 1996;

Lash *et al.*, 2014a). Through studies of using the CCBL inhibitor aminooxyacetic acid (AOAA)

to reduce toxicity of DCVC in kidney cells (Elfarra and Anders, 1984; Lash *et al.*, 1986; Lash *et

al.*, 1994), it has been established that TCE toxicity likely results from DCVC metabolism via

CCBL into reactive metabolites.

Toxicological studies have contributed to the understanding of how TCE metabolism

contributes to its toxicity. The TCE metabolite DCVC stimulates reactive oxygen species

generation, pro-inflammatory response, and cell death in the HTR-8/SVneo human placental

cytotrophoblast cell line (Hassan *et al.*, 2016; Elkin *et al.*, 2018), suggesting that the GSH

conjugation metabolic pathway has a role in placental toxicity. Additionally, inhibiting CCBL

activity in kidney cells via aminooxyacetic acid (AOAA) treatment reduces DCVC-stimulated

toxicity (Elfarra and Anders, 1984; Lash *et al.*, 1986; Lash *et al.*, 1994). Together, these studies

suggest that TCE metabolism, particularly downstream of DCVC, contributes to the toxicity of TCE.

Because of the requirement of metabolism in TCE toxicity, modulation of TCE metabolism by pharmacological agents has the potential to modify TCE toxicity. One approach can be through use of N-acetyl-L-cysteine (NAC), which is commonly thought of as a scavenger of reactive oxygen species generation, either in part by itself or because of its function as a GSH precursor (Aldini *et al.*, 2018). Importantly, NAC is cleaved into an acetyl group and cysteine by aminoacylase I (Uttamsingh and Anders, 1999; Uttamsingh *et al.*, 2000). Because DCVC can be *N*-acetylated to form NAcDCVC, NAC could contribute to its formation. This could have toxicity manifestations because NAcDCVC is metabolized by CYP3As into NAcDCVCS, a toxic metabolite (Werner *et al.*, 1996; Lash *et al.*, 2014a). Secondly, NAC, by metabolism into GSH (Aldini *et al.*, 2018), could provide substrate for glutathione S-transferases (GSTs), the enzyme responsible for forming DCVG as the first step of TCE GSH conjugation (Lash *et al.*, 2014a).

Another approach to modify TCE metabolism is through the use of AOAA, a CCBL inhibitor in kidney (Elfarra and Anders, 1984; Lash *et al.*, 1986; Lash *et al.*, 1994). However, the contribution of AOAA as a CCBL inhibitor in other organs, such as liver and placenta, is currently unknown. The different composition of CCBLs as a function of organ (Lash, 2010) gives rise to the possibility that AOAA may be more effective as a CCBL inhibitor in some organs compared to others. Although the exact composition of CCBLs in placenta is currently unknown, the finding that AOAA decreased DCVC-stimulated increase in interleukin-6 in media of HTR-8/SVneo human placental cells (Hassan *et al.*, 2016) indicates that AOAA may have a mechanism of action relevant to DCVC in placental cells. However, because CCBL activity was

not measured in the prior study, it remains unclear if this response could be attributable to CCBL activity.

Investigation of mechanisms to explain TCE-stimulated decreased fetal weight (Loch-Caruso *et al.*, 2019) is a goal of the present study. A mechanism by which decreased fetal weight could occur is through apoptosis in placenta or activation of pro-inflammatory response in maternal serum. As an example, it has been demonstrated that administration of L-arginine to the mother increased fetal weight while decreasing anti-apoptotic Bcl-2 placenta staining and increasing apoptotic Bax placenta staining (Shen and Hua, 2011). Additionally, intrauterine growth retardation is associated with the apoptosis, as verified by Bcl-2 and TUNEL staining, of placental syncytiotrophoblasts (Ishihara *et al.*, 2002), a crucial cell type at the maternal-fetal interface (Potgens *et al.*, 2002; Wang *et al.*, 2014). Furthermore, decreased fetal weight is associated with increased maternal serum levels of high sensitive-C-reactive protein, interleukin-6 (IL-6), and tumor necrosis factor-α (TNF-α) (Guven *et al.*, 2009).

Because the toxicity of TCE could be manifest via the GSH conjugation metabolic pathway and involves ROS generation, pro-inflammatory response, and cell death, we hypothesize that modifiers of metabolism could impact these TCE-stimulated responses in an *in vivo* timed-pregnant Wistar rat model. The potential modifiers of TCE toxicity we chose to use for this study are NAC and AOAA. In summary, the current study tests thr hypothesis that TCE-induced fetal weight decrease is due to apoptosis, oxidative stress, and pro-inflamatory responses that require metabolic activation through the TCE GSH conjugation metabolic pathway, and thus are modifiable by NAC and AOAA.

Materials and Methods

Chemicals and reagents

Trichloroethylene (TCE), N-acetyl-L-cysteine (NAC), aminooxyacetic acid (as *O*-(carboxymethyl)hydroxylamine hemihydrochloride) (AOAA), potassium phosphate dibasic (K_2HPO_4), potassium phosphate monobasic (KH_2PO_4, anhydrous), sucrose, potassium hydroxide (KOH), boric acid, and trichloroacetic acid were purchased from Sigma-Aldrich (St. Louis, MO). Vanilla wafers (Nabisco) were purchased locally. *S*-(2-Benzothiazolyl)-L-cysteine (BTC) was purchased from Toronto Research Chemicals (Toronto, ON).

Handling and treatment of rats

Timed-pregnant Wistar rats between 60 and 90 days of age were purchased from Charles River Laboratories (Portage, MI) and arrived at the University of Michigan School of Public Health Animal Facility on gestational day (GD) 2, with GD 0 designated as day of copulation. Rats were individually housed in a controlled environment with a 12-hour light/dark cycle and provided with standard rat chow (Purina 5001) and water *ad libitum*. On GD 3, the rat weights ranged from 121 to 224 g. All procedures with the rats were approved by the University of Michigan Institutional Animal Care & Use Committee (IACUC) (Approval #PRO00006981).

Rats were exposed to chemical treatments using a vanilla wafer treat developed by Seegal *et al.* (Seegal *et al.*, 1997). Rats were placed individually in exposure cages without food for one hour prior to presentation with a wafer. Rats were presented with a wafer on GD 3 and GD 4 to train for recognition of the wafers as food. Rats were weighed daily and treatment doses were adjusted to rat weight. Chemicals were added directly to the vanilla wafers and immediately offered to the rats for consumption. NAC and AOAA were dissolved in double-distilled and filtered water prior to pipetting onto the wafer. TCE was pipetted undiluted onto a vanilla wafer. The rats typically finished eating the vanilla wafer within ten minutes of wafer presentation.

The treatment regimen is depicted in **Figure 2.1**. Pregnant rats were exposed from GD 6-16 to 480 mg TCE/kg/day, a dose that is within one order of magnitude of the U.S. Occupational Safety and Health Administration Permissible Exposure Level (Agency for Toxic Substances and Disease Registry, 2007) and similar to TCE dosages used in other studies with rats (Toraason *et al.*, 1999; Liu *et al.*, 2010; Loch-Caruso *et al.*, 2019). Some rats also received NAC or AOAA on GD 5-16 as pre/co-exposures with TCE. The NAC dosage of 200 mg/kg/day (Fukami *et al.*, 2004; Chang *et al.*, 2005; Naik *et al.*, 2006) and AOAA dosage of 20 mg/kg/day (Perry and Hansen, 1978; Donoso and Banzan, 1984) are within the range of dosages used *in vivo* in past reports. The time points of treatment encompass the gestational period when fetuses and placentae start to exhibit rapid growth (Furukawa *et al.*, 2011) and are similar to TCE exposures used in prior studies with rats (Healy *et al.*, 1982; Fisher *et al.*, 1989; Loch-Caruso *et al.*, 2019). In total, 49 timed-pregnant Wistar rats were acquired in eight batch deliveries. Within each batch, at least one rat was assigned randomly to each treatment group. Details of the assignments of rats to treatment group and batch are included in **Table S2.1**. Three of the 49 rats were not pregnant.

Rat tissue collection

Rats were euthanized on GD 16 by carbon dioxide asphyxiation. Euthanasia started directly after completion of vanilla wafer treatment on GD 16, and dams were euthanized in random order. Blood was collected from the rats directly after euthanasia by cardiac puncture. Typically, 6-8 mL of blood was collected from each rat. Blood was allowed to coagulate by incubating at 37°C in 50 mL conical tubes. Subsequently, the blood was centrifuged at 2000 x g for 30 minutes at 4°C to separate clotted blood from serum, yielding 3-4 mL serum per dam. Serum samples were aliquoted into 1.5-mL microcentrifuge tubes and stored at -80°C. Placenta,

maternal kidney, and maternal liver were snap frozen in liquid nitrogen and stored at -80°C, with

the exception of tissue for RNA, which was stored overnight in RNAlater (Qiagen, Germantown,

MD) prior to RNAlater removal and sample transfer to -80°C. Maternal kidney, maternal liver,

placenta, and fetal weights were removed by dissection and weighed individually.

Measurement of cysteine conjugate β-lyase (CCBL) activity

CCBL activity was measured according to a method developed by Dohn and Anders

using S-(2-benzothiazolyl)-L-cysteine (BTC) as the substrate and 2-mercaptobenzothiazole as

the product produced (Dohn and Anders, 1982). Briefly, placenta, maternal kidney, or maternal

liver were thawed on ice, and then added to a solution of 0.1 M potassium phosphate (pH 7.4)

containing 0.25 M sucrose at a 25% (w/v) concentration. Tissues were sonicated twice at 3.5 Hz

for five seconds (MiSonix Sonicator 3000, Misonix Inc., Farmingdale, NY) to dissociate the

tissue for enzyme analysis. The potassium phosphate buffer (0.1 M, pH 7.4) was made from a

mixture of potassium phosphate dibasic (K_2HPO_4) at 69.6 mM and potassium phosphate

monobasic (KH_2PO_4, anhydrous) at 30.4 mM prior to sucrose addition.

The substrate solution was made by suspending 10.15 mg of BTC in 4 mL ddH_2O

representing 40% of total final desired volume. The mass of BTC added corresponds to a final

BTC concentration in substrate solution of 4 mM. Potassium hydroxide (KOH) (1 M in ddH_2O)

was added at 0.25 mL to dissolve BTC. After the BTC dissolved, 5 mL of boric acid (0.2 M in

ddH_2O) was added. The solution pH was adjusted to 8.6 using 1 M KOH, and ddH_2O was then

added to achieve 10 mL desired total volume. In aliquots, this substrate solution was added to 0.1

M potassium borate buffer (made from KOH and boric acid) in a 1.5:1.3 (v/v) ratio and

incubated for 4 minutes at 37°C. Subsequently, enzyme sample was added to this reaction

mixture in a 1:14 (v/v) ratio. Incubation time with the enzyme sample was 30 minutes at 37°C.

After the incubation, trichloroacetic acid at a 10% (w/v) concentration in ddH$_2$O was added to the reaction mixture in a 1:5 (v/v) ratio to terminate the reaction and precipitate protein. A negative control for each sample was made by adding 10% (w/v) trichloroacetic acid into the reaction mix before addition of the enzyme source. All reactions were centrifuged at 11,000 x g for 1.25 minutes to remove precipitated protein. Absorbance of each supernatant was measured at 321 nm wavelength, with a molar extinction coefficient (ε) of 21,600 M^{-1} cm^{-1} for 321 nm, using a SpectraMax M2e microplate reader (Molecular Devices, San Jose, CA). The absorbance corresponding to the negative control was subtracted from the absorbance corresponding to the appropriate reaction to generate a net absorbance used to convert absorbance into nmol of product produced/min/mL, which were converted into nmol/min/mg tissue or nmol/min/mg protein or nmol/min/total tissue. The protein assay used to determine protein concentration was the bicinchoninic acid (BCA) assay using a kit from ThermoFisher Scientific (ThermoFisher Scientific, Waltham, MA).

Hematoxylin and eosin (H&E) staining

Placentae stored in 10% formaldehyde (Fisherbrand, Waltham, MA) were cut in half transversely to expose the maternal and fetal layers. Each half was placed in a biopsy cassette (Fisherbrand, Waltham, MA) submerged in 10% formaldehyde and transferred to the University of Michigan In Vivo Animal Core (IVAC). Placentae were embedded in paraffin using an automated tissue processor (TissueTek, Sakura) and typical histological methods at the core. Sections were cut to 4 µM thickness using a rotary microtome and mounted on glass slides. All placental sections mounted on slides were female in sex because not enough male placentae were collected in 10% formaldehyde at the time of dissection. Tissues were stained with hematoxylin and eosin using a standard hematoxylin and eosin staining protocol assisted by an automated

histostainer (Leica Autostainer XL, Leica Biosystems Inc., Buffalo Grove, IL). The slides were digitally scanned using an Aperio AT2® scanner (Leica Biosystems Inc.), allowing imaging of two vertical transverse sections of the whole placenta. Quantitative morphometric measurements with drawn annotations of placental zones were taken from these images using Aperio ImageScope software (Leica Biosystems Inc.). The placental zones quantified included the labyrinth zone area, basal layer area, total placenta area, labyrinth zone width, basal zone width, and decidua basale width. Decidua basale area was calculated as total placenta area minus labyrinth zone area minus basal layer area. Total placenta width was calculated as labyrinth zone width + basal area width + decidua basale width. Three different measures of width for each of the zones of interest were made at the center region of each zone. Because two sections were taken from each placenta (one from each half) for a slide, a slide for one given placenta had two different area measurements for each of the area metrics and six different width measurements for each of the width metrics. The morphometric measurements were averaged for each placenta prior to further analysis. In the case of the labyrinth zone, basal zone, and decidua basale, absolute dimensions (length and area) and relative dimensions (normalized to the total placenta and reported as percentages) were reported.

Immunohistochemistry (IHC) staining of cleaved caspase-3, CCBL1, FMO3, 3-nitrotyrosine, and CYP3A1

Placental tissue sections were subjected to immunohistochemistry (IHC) staining to detect expression of proteins important in TCE toxicity. These proteins included cysteine conjugate β-lyase (CCBL1) and flavin-containing monooxygenase 3 (FMO3) because of the importance of these enzymes for TCE metabolic activation (Lash *et al.*, 2014a). In addition, 3-

nitrotyosine and cleaved caspase-3 were chosen as markers of protein oxidative stress and apoptosis, respectively (Ahsan, 2013; Crowley and Waterhouse, 2016).

Unstained sections were deparaffinized and rehydrated, then subject to heat-induced antigen retrieval with a commercial antigen retrieval solution (DIVA, Biocare Medical, Pacheco, CA) performed within a pressurized retrieval chamber (Decloaker, Biocare Medical). Staining was performed using an automated immunohistochemical stainer (Biocare Intellipath, Biocare Medical) with inclusion of endogenous peroxidase and non-specific blocking steps. Negative control slides were run concurrently using naïve mouse/rabbit serum (Polymer Universal negative control serum, Biocare Medical) in place of the primary antibody. Positive detection was performed with commercial dextran polymer-based, biotin-free reagents for mouse (MACH4 HRP, Biocare Medical) or rabbit (Biocare Rabbit on Rodent Poly HRP, Biocare Medical) with the chromogen diaminobenzidine. Hematoxylin was utilized as the nuclear counterstain. Slides were dehydrated and mounted with glass cover slips. Details of the primary antibodies, dilutions, and positive controls used are in **Table S2.2**.

After IHC staining, tissue sections were digitally scanned using an Aperio AT2® scanner (Leica Biosystems Inc.), allowing imaging of two vertical whole sections of the placenta. For all IHC stains, stain quantification was performed using QuPath. Each zone of the placenta was traced to allow for quantification specific to each region. From QuPath, we identified a setting to detect all staining, regardless of localization to cytoplasm or nucleus, and a setting to detect only nuclear staining. All detections were based on achieving a specific color threshold. The nuclear only stain detection values were subtracted from the total stain detection values to derive quantification of cytoplasmic stain. For a given placenta, total positive count was normalized to total area for each placental zone. These normalized values were used in statistical analysis.

Detection of fragmented DNA via labeling with terminal deoxynucleotidyl transferase (Tdt)

Unstained placental tissues were embedded in paraffin and mounted on glass slides as described for the H&E staining. Sections were stained for expression of the Tdt enzyme to detect fragmented DNA. Slides were subject to labeling with the Tdt enzyme using the FragEL™ DNA Fragmentation Detection Kit, Fluorescent - TdT Enzyme (Millipore Sigma, Burlington, MA). Paraffin-embedded tissues underwent the protocol as described by the kit manufacturer. Positive and negative control slides with HL-60 cells (provided by manufacturer) were stained according the manufacturer's protocol. The staining protocol consisted of Tdt as stained green whereas nuclei as stained by 4′,6-diamidino-2-phenylindole (DAPI) in the color of blue (used to normalize green staining to total nuclear stain).

An EVOS M7000 Microscope (ThermoFisher Scientific, Waltham, MA) with fluorescence and image stitching capabilities was used to capture images of the placenta stained with Tdt. Images of whole placenta were captured under the DAPI, GFP, and DAPI + GFP overlay channels. The magnification used to capture the images to be stitched were 100X (10 x 10X). QuPath2.0 was used to quantify the staining on the DAPI + GFP overlay images, with quantification performed specific to the labyrinth zone, basal zone, and decidua basale of the placenta as manually annotated using QuPath2.0. A ratio of green to blue stain was obtained for each of the two sections for the placenta for each zone, and the average of these was used for statistical analysis purposes for each zone of a given placenta.

Alizarin Red staining to detect placental calcification

Paraffin-embedded unstained slides of placental tissue were prepared as described for H&E staining. Sections were subject to Alizarin Red staining for mineral detection, using a commercial reagent kit according to the manufacturer recommendations (Alizarin Red C-206,

37

Rowley Biochemical, Inc, Danvers, MA). As with H&E and IHC, slides were digitally scanned

using an Aperio AT2® scanner (Leica Biosystems Inc.), allowing imaging of two vertical whole

sections of the placenta. The labyrinth zone, basal zone, and decidua basale were annotated using

Aperio ImageScope software (Leica Biosystems Inc.). Digital quantitation of staining for each

zone was performed using a commercial algorithm (Leica Aperio Color Deconvolution, v.9.1,

Leica Biosystems Inc.). Settings were calibrated for detection of Alizarin Red slide using a test

area on the slide per manufacturer instructions. Calibrated parameters were set as R=0.223,

G=0.579, B=0.785 and default parameters for intensity were used (range 0-255; weak: 220,

moderate: 175, strong: 100). For each zone of the placenta, the average from the two placental

sections for a given placenta was used for statistical analysis purposes. The percentage of strong

positive and total positive stains were used for statistical analysis.

RNA extraction

Placental samples were thawed and homogenized using a FastPrep-24 tissue and cell

lyser (MP Biomedicals, Solon, OH) with the placenta submerged in RLT Buffer PLUS (Qiagen,

Germantown, MD) containing 1% (v/v) 2-mercaptoethanol (Sigma-Aldrich, St. Louis, MO).

Following homogenization, RNA was extracted using an RNeasy Plus Mini kit (Qiagen,

Germantown, MD) according to the manufacturer's instructions. RNA concentration and purity

were verified using a NanoDrop 2000 UV-Vis Spectrophotometer (Thermo Fisher Scientific,

Waltham, MA). RNA was stored at -80°C until further analysis.

Placental sex determination

The sex of the rat placenta and associated fetus was determined by the presence or

absence of the *Sry* genomic DNA (gDNA). The gDNA was isolated from rat placenta using a

NucleoSpin™ Tissue kit (Machery-Nagel, Bethlehem, PA) according to the manufacturer's

instructions. The concentration and purity of the gDNA were verified using a Nanodrop 2000

UV-Vis Spectrophotometer (Thermo Fisher Scientific, Waltham, MA) and stored -20°C until

further analysis using qRT-PCR. A subset of these placentae also were evaluated for *Sry* mRNA

expression. In the case of one discrepancy between the mRNA and gDNA *Sry* reading (male

classification from gDNA but female classification from mRNA), sex was assigned based on the

gDNA result.

Quantitative real-time polymerase chain reaction (qRT-PCR)

Detection of *Sry* gDNA and mRNA expression of *Nfkb1*, *Bcl2*, *Bax*, *Prdx1*, *Lgals3*,

Kyat1, and *Fmo3* was performed with qRT-PCR. Briefly, cDNA was synthesized using a Bio-

Rad iScript™ cDNA synthesis kit (Bio-Rad Laboratories, Hercules, CA) according to the

manufacturer's instructions. A Bio-Rad CFX Connect™ Real-Time System (Bio-Rad

Laboratories, Hercules, CA) synthesized cDNA under the following protocol: (1) 25°C for 5

minutes, (2) 42°C for 30 minutes, (3) 85°C for 5 minutes, and then (4) cool down to 4°C. The

cDNA samples were stored at -20°C until further use.

Reaction mixtures of 25 µL total were prepared in SsoAdvanced™ Universal SYBR®

Green Supermix (60% v/v; Bio-Rad Laboratories, Hercules, CA) containing 0.32 µM of each

(forward and reverse) primer, and 40 ng of either cDNA template or 50 ng of gDNA. Primer

sequences and sources are listed in **Table S2.3**.

Samples were run and analyzed in Hard-Shell® 96-well plates (Bio-Rad Laboratories,

Hercules, CA) using a Bio-Rad CFX Connect™ Real-Time System using the following protocol:

(1) 95°C for 10 minutes, (2) 95°C for 15 seconds, (3) 60°C for 1 minute, (4) repeat 39 times

steps 2 and 3, (5) 95°C for 1 minute, (6) 65°C for 2 minutes, (7) 65°C to gradual increase to

95°C, stopping at every 0.5°C interval for 5 seconds each. Analysis was performed using the

ΔΔCt method (Yuan *et al.*, 2006). All samples were run and analyzed in duplicate. *B2m* served

as the reference gene.

Detection of IL-1β, TNF-α, and IL-6 in maternal serum

Maternal serum samples stored at -80°C were thawed and pipetted into round-bottom 96-

well plates. Samples were then delivered to the University of Michigan Immunologic Monitoring

Core for IL-1β, TNF-α, and IL-6 for enzyme-linked immunosorbent assay (ELISA) using Duoset

ELISA kits (R&D Systems, Minneapolis, MN) according to the manufacturer's recommended

protocol.

Statistical analysis

Statistical analysis included mixed models analysis of variance (ANOVA), one-way

ANOVA, or two-way ANOVA each followed by Tukey's post-hoc comparison of means. In the

case where two groups were compared, an unpaired two-tailed t-test was used. Mixed models

ANOVA was performed using SPSS software (Chicago, IL) whereas one-way ANOVA, two-

way ANOVA, and t-tests were performed using GraphPad Prism (San Diego, CA). Graphs were

generated using GraphPad Prism (San Diego, CA). A $p<0.05$ was considered statistically

significant. Percentage data were converted to proportion values and arcsine transformed prior to

statistical analysis. The ratio data from the Tdt staining analysis was also arcsine transformed

prior to statistical analysis.

<div align="center">

Results

</div>

Treatment effects on fetal weight

Fetal weight was analyzed for all fetuses and in a subset of males and females in which

placental sex was determined by gDNA. In analysis of all fetuses, exposure to TCE during

pregnancy decreased average fetal weight per dam on GD 16 by 12.8% ($p<0.0001$) (**Figure**

2.2A). TCE suppressed average fetal weight in males by 21.7% relative to control (p<0.0001) but no significant effect was observed in female fetuses (**Figures 2.2B and 2.2C**, respectively). Whereas NAC alone had no significant effect on average fetal weight relative to control, AOAA alone decreased average fetal weight relative to control by 15.1% (p<0.0001) in all fetuses (**Figure 2.2A**), and the same pattern was observed in separate analyses of male and female fetuses (p=0.018 and 0.001, respectively) (**Figures 2.2B and C**, respectively). The combined treatment of AOAA with TCE prevented the depressed average fetal weight elicited by treatment with TCE alone and AOAA alone in all fetuses and the subset of males (**Figures 2.2A and 2.2B**, respectively). In females, the combined AOAA and TCE treatment prevented depressed average fetal weight elicited by treatment with AOAA alone (**Figure 2.2C**). The combined treatment of NAC with TCE decreased average fetal weight relative to control in all fetuses, male fetuses, and female fetuses by 13.3%, 16.7%, and 15.6%, respectively (p<0.0001, p=0.003, and p=0.002, respectively) (**Figures 2.2A, 2.2B, and 2.2C**, respectively).

Treatment effects on placental weight and efficiency

Investigation of placenta weight and placental efficiency revealed treatment-related effects. Placental efficiency is the ratio of fetal weight to placenta weight, an index used to assess placental function (Wilson and Ford, 2001). Although TCE alone had no significant effect on average placental weight (**Figures 2.3A1, B1 and C1**), the combination treatment of TCE with AOAA increased average placental weight relative to control by 8.1% (p=0.008), NAC-only treated by 7.5% (p=0.016), TCE-only treated by 15.2% (p=0.001), and NAC pre/co-treated with TCE by 12.5% (p=0.005) for analysis of all placenta (**Figure 2.3A1**). Moreover, the combination treatment of TCE + AOAA increased average placenta weight relative to TCE-only treatment by 20.7% in males (p=0.003) (**Figure 2.3B1**) whereas there was no statisitically significant effect on

41

female placentae (**Figure 2.3C1**). There were no remarkable treatment-related effects on average placental efficiency (**Figures 2.3A2, B2 and C2**), with the sole statistically significant difference between AOAA treatment alone and NAC alone in all placenta (**Figure 2.3A2**).

Treatment effects on maternal body weight, tissue weights, and litter size

Treatments with TCE, NAC, or AOAA - alone or in combination - had no significant effects on maternal kidney weight, maternal liver weight, litter size, or maternal weight gain (GD3 to GD16) (**Figure 2.4**), indicating lack of overt treatment-related maternal toxicity.

Treatment effects on CCBL activity in maternal tissue and placenta

Consistent with previous literature showing AOAA as an effective CCBL inhibitor in kidney (Elfarra and Anders, 1984; Lash *et al.*, 1986; Lash *et al.*, 1994), exposure to AOAA alone, or AOAA as pre/co-treatment with TCE, markedly reduced CCBL activity in maternal kidney (specific activity on tissue weight basis was reduced by 73.0% and 82.0%, respectively; p=0.0239 and 0.0006, respectively) relative to the control and TCE-only exposed groups, respectively (**Figure 2.5A1**). Similar reductions were observed for CCBL total activity (nmol/min) (p=0.0297 and 0.0001, respectively) (**Figure 2.5A2**). When CCBL specific activity was expressed relative to protein, the AOAA-only treated and AOAA pre/co-treatment with TCE group had reduced CCBL activity compared to NAC only-treated group by 77.2% and 82.5%, respectively (p=0.0280 and 0.0172, respectively) and the TCE only-treated group by 79.3% and 84.1%, respectively (p=0.0110 and 0.0067, respectively) (**Figure 2.5A3**). In contrast to maternal kidney, AOAA failed to inhibit CCBL activity in maternal liver and in placenta, regardless of sex, irrespective of the presence or absence of TCE (**Figures 2.5B1-3, 2.5C1-3, and 2.5D1-3**, respectively). Neither NAC nor TCE, alone or in combination with each other, had an effect on

CCBL specific or total activity in maternal kidney, maternal liver, or placenta (**Figures 2.5A1-3, 2.5B1-3, 2.5C1-3, 2.5D1-3**, respectively).

Treatment effects on placental zone areas and widths

Because pregnancy progression is associated with changes in size to each zone of the rat placenta (Furukawa *et al.*, 2011), we assessed treatment effects on placental morphology. A representative image for a placental section illustrates our method for quantification of area and width in hematoxylin and eosin-stained placental sections (**Figure 2.6**). TCE treatment alone did not alter absolute or relative width and area dimensions in any of the zones nor in the absolute width or area for total placenta (**Figure 2.7**). Unexpectedly, NAC pre/co-treatment with TCE decreased relative area and width of the labyrinth zone by 16.9% and 17.1%, respectively (p=0.0483 and 0.0250, respectively) (**Figures 2.7A1 and 2.7E1**, respectively) and increased relative area and width of the basal zone by 38.1% and 47.2%, respectively (p=0.0167 and 0.0395, respectively) (**Figures 2.7B1 and 2.7F1**) relative to TCE treatment alone. No other changes in absolute or relative dimension were observed with treatments (**Figure 2.7**).

Treatment effects on Alizarin Red staining

Intensity of Alizarin Red staining for calcium disposition did not differ by treatment group (data not shown). A representative image with and without quantification marking is displayed in **Figure 2.8**. To understand if different placental zones vary in calcification, which can inform a role in toxicity (Wallingford *et al.*, 2018), we compared Alizarin Red staining intensity across different zones. Alizarin Red staining intensity differed by placental zone for control rats (analysis only performed for this group). Specifically, in the metric of percentage of strong positive stain, the decidua basale of control rats was increased relative to the labyrinth

zone by 52.9% (p=0.0274) (**Figure 2.9A**). However, in the metric of total positive stain, no placental zones were different compared to each other (**Figure 2.9B**).

Treatment effects on markers of oxidative stress, apoptosis, and pro-inflammatory response

No treatment-related changes were detected with immunohistochemical (IHC) staining for markers of oxidative stress and apoptosis in placenta, including 3-nitrotyrosine and cleaved caspase-3 (**Table S2.4**; method for IHC quantification in **Figure 2.10**). Likewise, no treatment-related changes were observed for mRNA expression of *Prdx1*, *Nfkb1*, *Bcl2*, *Bax*, and *Lgals3* (**Table S2.5**). No treatment-related changes were also observed for Tdt enzyme staining in placenta (quantification method shown in **Figure S2.1**). Moreover, we failed to detect a treatment-related change for 1L-1β in maternal serum (**Figure S.2.2**). We also attempted to detect TNF-α and IL-6 in maternal serum, but stopped at N=2 because one-third (4/12) of the samples for each endpoint had zero values (data not shown).

Detection of proteins via IHC by placental zone in control placenta

Treatment-related changes were not observed for IHC detection of 3-nitrotyrosine, cleaved caspase-3, CCBL1, and FMO3. However, staining for these proteins varied by placental zone in the untreated control placenta (**Figure 2.11**). A pronounced difference occurred for CCBL1, with increased staining in the decidua basale relative to the labyrinth zone for the total metric, nuclear metric, and cytoplasmic metric by 87.0%, 302.8%, and 56.1%, respectively (p=0.0072, 0.0005, and 0.0422, respectively) (**Figures 2.11A1, 2.11A2, 2.11A3**, respectively). Some differences in staining between the different zones is specific to a particular metric (e.g., nuclear). For example, whereas 3-nitrotyrosine was decreased in the basal zone detection relative to the labyrinth zone and dedicua basale for the nuclear metric by 42.8% and 43.9%, respectively (p=0.0123 and 0.0093, respectively), similar reductions were not observed for the total or

cytoplasmic metrics (**Figure 2.11B**). FMO3 was also detected in lower levels for the labyrinth zone compared to the basal zone and decidua basale for the total and cytoplasmic metrics (for total metric, by 99.88% and 99.89%, respectively; p=0.0028 and 0.0027, respectively) (for cytoplasmic metric, by 99.93% and 99.91%, respectively; p= 0.0016 and 0.0016, respectively) (**Figure 2.11C**). Although the yolk sac expression of FMO3 was not quantified because the yolk sac was not present in all placenta sections, qualitative assessment of appearance suggests that the yolk sac expresses FMO3 at a very high level (**Figure 2.10**).

Discussion

This study confirms our prior finding that trichloroethylene exposure during mid-pregnancy decreases fetal weight, using the same exposure regimen (Loch-Caruso *et al.*, 2019). New to the present study, we report that AOAA pre/co-treatment prevented the TCE-induced fetal weight decrease. AOAA is an inhibitor of CCBL (Elfarra and Anders, 1984; Lash *et al.*, 1986; Lash *et al.*, 1994), which metabolizes the TCE glutathione pathway metabolite DCVC into DCVT, a toxic and reactive metabolite (Lash *et al.*, 2014a). We suggest that this effect may be due to AOAA inhibition of CCBL in maternal kidney because we found that AOAA strongly inhibited CCBL activity in maternal kidney but not in placenta or maternal liver. Moreover, although NAC pre/co-treatment did not affect fetal weight relative to TCE alone, the study suggested that NAC pre/co-treatment with TCE could be detrimental to pregnancy because of alterations in placental zone dimensions relative to TCE treatment alone.

Unexpectedly, AOAA treatment alone decreased fetal weight. We suggest that AOAA inhibition of CCBL may have disrupted essential physiological processes. Examples of potentially vulnerable CCBLs include alanine aminotransferases and mitochondrial aspartate aminotransferases (Cooper and Pinto, 2006). Alanine aminotransferase above 50 U/L are used in

clinical diagnosis of hemolysis, elevated liver enzymes, and low platelets (HELLP) syndrome

(Vigil-De Gracia *et al.*, 2003). Importantly, HELPP syndrome also includes the diagnosis of

preeclampsia (Vigil-De Gracia *et al.*, 2003). These prior studies suggest that normal alanine

aminotransferase activity is important for a successful pregnancy. Similarly, mitochondrial

aspartate aminotransferase is part of the malate-aspartate shuttle that is crucial to the metabolism

of lactate in the embryo (Lane and Gardner, 2005), supporting the notion that mitochondrial

aspartate aminotransferase is crucial to embryonic development. Together, these findings suggest

that inhibition of aminotransferase-derived CCBL activity critical for fetal development could at

least partially explain a detrimental effect of treatment with AOAA alone on fetal weight.

Although AOAA treatment alone depressed fetal weight, the mean fetal weight of the

TCE + AOAA group increased relative to the AOAA alone group to a level similar to that

observed in untreated control. As a possible explanation, the TCE + AOAA treatment group

would have more systemic DCVC than the AOAA alone treatment group because of the low

ability of maternal kidney to convert DCVC to DCVT in the TCE + AOAA group and lack of

TCE exposure in the AOAA alone group. The increased circulating DCVC in the TCE + AOAA

group would be accompanied by inhibited generation of reactive downstream TCE metabolites

such as DCVT, CTK, and CTAC. Although currently unstudied, the inhibited CCBL metabolism

of DCVC could lead to build-up of DCVC that subsequently depressed activity of upstream

enzymes such as γ-glutamyltransferase (GGT) and cysteinyl-glycine dipeptidase (DP). Inhibition

of GGT reduces the supply of cysteine, prevents the utilization of extracellular GSH as a source

of cysteine, and has received attention clinically (Hanigan, 2014). Indeed, the potential benefits

of reducing systemic cysteine extends to pregnancy because total plasma cysteine is positively

associated with preeclampsia, very low birth weight, and premature delivery (El-Khairy *et al.*,

2003). Therefore, a mechanism could be that the TCE + AOAA treatment group has lower GGT activity and lower systemic cysteine, which is beneficial for pregnancy (El-Khairy *et al.*, 2003), compared to the AOAA treatment alone group. Similarly, because the reaction catalyzed by DP forms cysteine and cysteine conjugates as products (Knapen *et al.*, 1999; Hanigan, 2014), inhibition of DP metabolism could be beneficial for pregnancy by reducing systemic cysteine. Discovering the likelihood and existence of such mechanisms to explain the finding that TCE + AOAA treatment increased fetal weight relative to AOAA alone remain an important future direction with implications for pregnancy health.

Our finding that AOAA strongly inhibits CCBL activity in maternal kidney but not in placenta or maternal liver is partially supported by previous studies in kidney (Elfarra and Anders, 1984; Lash *et al.*, 1986; Lash *et al.*, 1994) and is very likely attributable to the differences in CCBL composition as a function of organ (Lash, 2010). Whereas AOAA is a known CCBL inhibitor in the kidney (Elfarra and Anders, 1984; Lash *et al.*, 1986; Lash *et al.*, 1994), as supported by our data here, the effectiveness of AOAA as a CCBL inhibitor in liver or placenta had been previously unreported. It is known that kidney and liver express different forms of CCBL (Lash, 2010), which explains why AOAA would inhibit CCBL activity in one but not the other. Specific CCBLs, such as glutamine transaminase K/ kynurenine aminotransferase, are found in kidney but not liver, and kynureninase and mitochondrial aspartate aminotransferase are found in liver but not kidney (Lash, 2010). The exact forms of CCBL in placenta are presently unknown: however, our data suggest that the form(s) of CCBL in the placenta are more similar to that (those) of liver as opposed to kidney. Identification of exact CCBLs in placenta require further research. Finally, we observed that alteration of CCBL activity was specific to AOAA and not TCE or NAC. The lack of effect of TCE or NAC on

47

CCBL activity is not unexpected; in fact, TCE does not stimulate increased activity of γ-glutamyltransferase (Loch-Caruso *et al.*, 2019), which is upstream of CCBL in TCE metabolism.

Mechanistic and physiological explanations exist for how AOAA could inhibit CCBL activity in kidney to prevent TCE-induced decreased fetal weight. DCVG and DCVC are TCE metabolites generated through the glutathione conjugation metabolic pathway that circulate systemically (Lash *et al.*, 2014a). Thus, it is plausible that AOAA pre/co-treatment with TCE could thwart the ability of the kidneys to convert DCVC into reactive and toxic downstream metabolites (Lash *et al.*, 2014a). This mechanism to reduce toxicity may also be manifest in the fetus. Although fetal kidney CCBL composition is currently unknown, the possibility exists that AOAA could inhibit fetal kidney CCBL to limit production of downstream metabolites (DCVT, CTK, and CTAC). Indeed, the existence of peptide transporters in placenta (Leazer and Klaassen, 2003) that could transport DCVC from mother to fetus increases the relevance and plausibility that AOAA pre/co-treatment could exert an effect on fetal weight via fetal kidney.

The morphometric zonal analysis of the placenta indicated that NAC pre/co-treatment with TCE caused multiple effects on placenta morphology relative to TCE treatment alone in a manner consistent with increased toxicity. Specifically, the effects that NAC pre/co-treatment with TCE decreased relative labyrinth zone width and area, and increased relative basal zone area and width, compared to TCE treatment alone are relevant to pregnancy health. Because the labyrinth zone increases as pregnancy progresses in rat and nearly the opposite is true of the basal zone, especially around GD 16 (Furukawa *et al.*, 2011), the changes observed in the NAC + TCE treatment group are consistent with a delayed developmental phenotype compared to the TCE treatment alone group. Although less data variance or inclusion of additional rats might allow detection of statistically significant differences between the NAC + TCE group and the

control group for labyrinth and basal zone measurements, the present findings are important because they affected relative widths and areas of multiple placental zones. A worthy future direction could be to explore how these manifestations could impact fetal or placental weight after GD 16 or if the rats exposed to NAC pre/co-treatment group would give birth later than the other treatment groups.

The suggestion that NAC pre/co-treatment with TCE could be toxic is consistent the delayed placental phenotype observation and is also consistent with our observations in our *in vitro* BeWo human placental trophoblast model in which NAC exacerbated some responses stimulated by DCVC (Chapter 5). The lack of treatment effects on Alizarin Red staining of the rat placentae indicate that enlargement of the basal zone for the NAC pre/co-treatment group was not attributable to placental calcification. Rather, the mechanism of altered placenta zone areas may be related to growth factors and cytokines that are critical for placental growth (Furukawa *et al.*, 2011), although this possibility was untested in the current study. Verification of these mechanisms requires further investigation beyond the scope of the present study.

Investigation into the interaction between NAC and TCE metabolism may prove critical for understanding how NAC exacerbated or failed to prevent TCE toxicity. In the *in vitro* BeWo cell studies, NAC enhancement of DCVC toxicity was associated with an NAC effect of increased *CYP3A4* mRNA expression (Chapter 5), which supports the idea that NAC exacerbation of TCE toxicity occurs downstream of DCVC. A possible mechanism could be that NAC provides an acetyl group via its breakdown by aminoacylase I (Uttamsingh and Anders, 1999; Uttamsingh *et al.*, 2000) to generate NAcDCVC from DCVC (Lash *et al.*, 2014a). NAcDCVC can be metabolized by CYP3As into NAcDCVCS, a known toxic TCE metabolite (Werner *et al.*, 1996; Lash *et al.*, 2014a). Future work could study how NAC and TCE combined

treatment impacts protein expression of CYP3A1, a CYP3A expressed in rat placenta and suggested to be a major CYP in rat placenta (Ejiri *et al.*, 2001; Ejiri *et al.*, 2003). Moreover, NAC could be metabolized to GSH (Aldini *et al.*, 2018) to provide substrate for GSTs that conjugate GSH to TCE (Lash *et al.*, 2014a). However, GSH conjugation of TCE occurs several steps before the formation of any reactive metabolites, so the link to toxicity via increased GSTs or DCVG formation is more difficult to make. The argument for an NAC effect non-specific to TCE is also difficult to make because we failed to observe NAC exert an effect by itself. Regardless, future investigation of the formation of reactive metabolites such as NAcDCVCS could provide insight into the effects observed with NAC and TCE combined treatment.

Although DCVC stimulates ROS generation, pro-inflammatory cytokine release, and apoptosis to HTR-8/SVneo human placental cells *in vitro* (Hassan *et al.*, 2016; Elkin *et al.*, 2018), exposure of pregnant rats to TCE failed to stimulate changes in markers of oxidative stress (3-nitrotyrosine) and apoptosis (cleaved caspase-3 and Tdt enzyme staining) in placental tissue. Additionally, there were no significant changes in placental mRNA expression of genes relevant to oxidative stress and apoptosis pathways (*Prdx1*, *Bcl2*, *Bax*, *Nfkb1* or *Lgals3*). These findings suggest that TCE, NAC, and AOAA may act by mechanisms involving tissues other than placenta *in vivo*, or else their actions on the placenta may involve mechanisms other than oxidative stress and apoptosis. Alternative explanations include the differences in species and concentrations used in the studies. For example, DCVC concentrations in cell culture may not correspond to DCVC concentrations in tissue generated *in vivo* from a given TCE dose, and this may differ as a function of species. Furthermore, rats exhibit higher GGT and renal CCBL activity compared to humans (Hinchman and Ballatori, 1990; Lash *et al.*, 1990) as examples of species differences that can affect detected concentrations of TCE metabolites. Another possible

explanation is that the *in vitro* work was performed on a specific cell type but the *in vivo* work was performed on placental tissue exposed *in vivo*. Additionally, the possibility exists that extravillous cytotrophoblastic cells may be especially vulnerable to TCE or DCVC toxicity compared to placental tissue. However, confirming these explanations would require placental cell isolation methodologies not used in the present study.

Immunohistochemical staining indicated that differences in protein expression were more notable across different zones in placenta, rather than between treatment groups. The differences in zone were highlighted using placenta from the control group of rats, in which we detected more CCBL1 expression in the decidua basale compared to the labyrinth zone. Because CCBL1 can potentially bioactivate DCVC to DCVT (Lash *et al.*, 2014a), this finding suggests that the decidua basale may be more sensitive to DCVC toxicity. We also detected significant differences in FMO3 as a function of zone in the placenta. Of novelty but not quantified because of the lack of yolk sac in some placenta sections, FMO3 was found to be highly expressed in yolk sac. These examples highlight how the current work can provide information about possible zonal sensitivity of the placenta for certain toxicant exposures and interventions.

Although treatments used in this study had only nominal effects on the placenta, some placental changes were observed with the TCE + NAC treatment and TCE + AOAA treatment. The NAC pre/co-treatment with TCE could be acting by a mechanism of DCVC bioactivation to produce toxicity of altered placenta dimensions. TCE + AOAA could be acting in a protective mechanism towards pregnancy by increasing placenta weight. Because AOAA is effective as a CCBL inhibitor in kidney (Elfarra and Anders, 1984; Lash *et al.*, 1986; Lash *et al.*, 1994), which would increase the DCVC/DCVT ratio in kidney and influence the corresponding metabolites in systemic circulation, an untested mechanism to date is that the TCE + AOAA group could have

51

increased DCVC in placenta relative to all treatment groups. The increased DCVC may inhibit activity of upstream enzymes, GGT and DP (Lash *et al.*, 2014a), with the decreased GGT and DP activity as beneficial for pregnancy as described previously (Knapen *et al.*, 1999; El-Khairy *et al.*, 2003; Hanigan, 2014). Measurement of enzyme activity upstream of DCVC remains important future work. Additionally, the finding that NAC treatment alone produced higher placental efficiency compared to AOAA treatment alone raises the question if the difference is attributable to amino acid transport. This possibility is valid because NAC is a precursor of cysteine (Aldini *et al.*, 2018) and AOAA inhibits renal CCBL (Elfarra and Anders, 1984; Lash *et al.*, 1986; Lash *et al.*, 1994), which includes aspartate aminotransferase (Lash, 2010). Knowledge on the specific transport mechanisms and the exact enzymes with CCBL activity susceptible to AOAA inhibition is not definitive at this point.

Wistar rats were selected for the present study for several reasons. They are more responsive to estradiol-stimulated increase in uterine weight compared to Sprague-Dawley rats (Diel *et al.*, 2004), more responsive to bisphenol A-stimulated delayed vaginal opening compared to Sprague-Dawley rats (Tinwell *et al.*, 2002), and are higher in hepatic CYP2D2 content correlated with 4-hydroxylase activity compared to Dark Agouti rats (Schulz-Utermoehl *et al.*, 1999). Significantly, timed-pregnant Wistar rats have been previously reported to have decreased fetal weight in response to TCE exposure (Loch-Caruso *et al.*, 2019). Thus, we chose a rat strain more likely to be sensitive to reproductive effects. We intentionally chose a time point of exposure that encompassed the time point when rat fetuses and placenta exhibit rapid growth and included a time point before the placenta forms (Furukawa *et al.*, 2011).

Likewise, dosages chosen for our study reflect the previous literature. The TCE exposure of 480 mg/kg/day is within an order of magnitude of the Occupational Safety and Health

Administration Permissible Exposure Level of 100 ppm for an 8-hour workday (Agency for Toxic Substances and Disease Registry, 2007). Differences between inhalation and ingestion exposure routes, and subsequent distribution and metabolism, could influence TCE toxicity, however. Moreover, prior studies report effects of TCE at similar exposure levels, including oxidative stress and/or neurodegeneration in rats (Toraason *et al.*, 1999; Liu *et al.*, 2010; Loch-Caruso *et al.*, 2019). The NAC dosage of 200 mg/kg/day was in the effective range of studies using NAC *in vivo* (Fukami *et al.*, 2004; Chang *et al.*, 2005; Naik *et al.*, 2006). In particular, Chang *et al.* found that 100 mg NAC/kg treatment twice a day rescued high blood pressure in timed-pregnant Sprague-Dawley rats (Chang *et al.*, 2005). The AOAA dosage of 20 mg/kg/day is also within the effective *in vivo* range used in prior studies (Perry and Hansen, 1978; Donoso and Banzan, 1984).

In summary, this is the first report that AOAA is capable of preventing TCE-stimulated decreased fetal weight, using a timed-pregnant Wistar rat model. Our data suggest that the mechanism is related to CCBL activity because AOAA was effective in maternal kidney but neither in placenta nor maternal liver. We are also the first to report that NAC pre/co-treatment could be more detrimental to pregnancy than TCE treatment by itself. **Figure 2.12** depicts our proposed mechanism of action of TCE on timed-pregnant Wistar rats, with modulation of TCE toxicity by NAC and AOAA, to explain the impact of the treatments on fetal weight. Importantly, this study failed to find oxidative stress in placenta as a mechanism of toxicity. Future studies could further investigate modulation of the GSH conjugation pathway in TCE metabolism to modify toxicity, including quantification of metabolite concentrations. Finally, because enzymes capable of metabolizing DCVC differed by placental zone, future studies could investigate the toxic effects of TCE or DCVC targeted to different placental cell types.
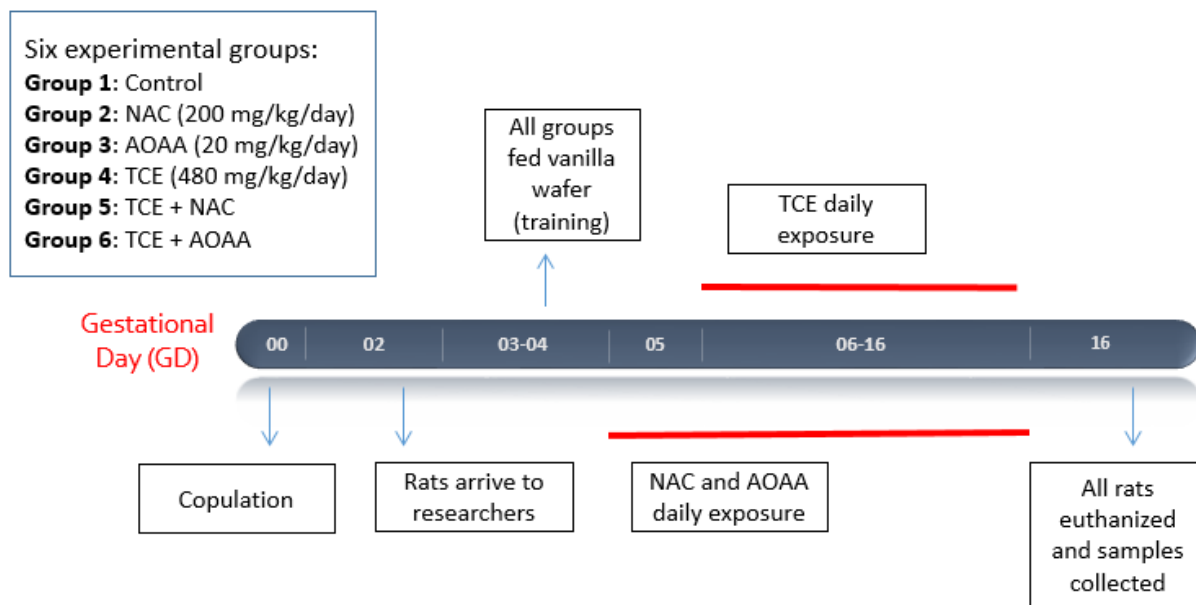
Figure 2.1. Treatment schedule of the timed-pregnant Wistar rats. With gestational day (GD) 0 designated as day of copulation, rats arrive on GD 2, are first trained to eat the vanilla wafer on GD 3, and are euthanized on GD 16. The following dosages of each chemical was used: 200 mg NAC/kg/day, 20 mg AOAA/kg/day, and 480 mg TCE/kg/day.

Fetal weight

(A)

(B)

(C)
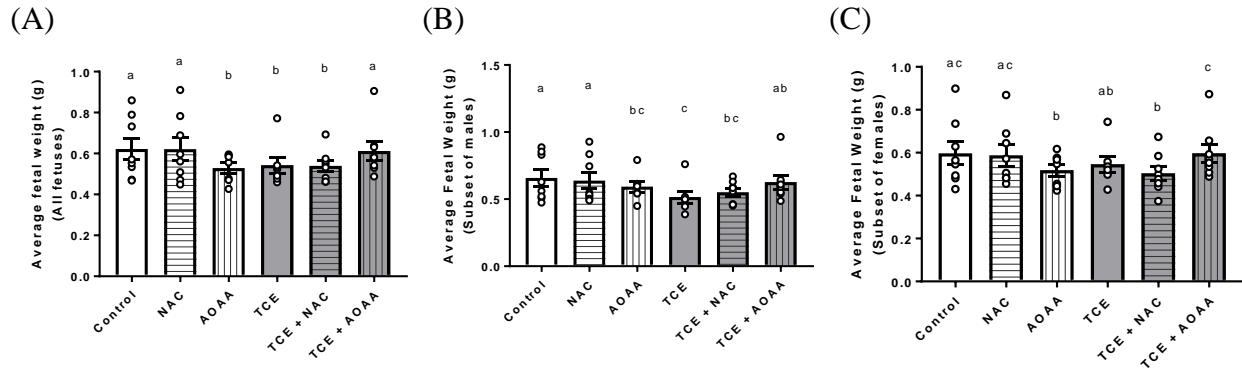
Figure 2.2. Effects of trichloroethylene (TCE), in the presence and absence of N-acetyl-L-cysteine (NAC) and aminooxyacetic acid (AOAA), on fetal weight. The effects for (A) all fetuses, (B) a subset of males, and (C) a subset of females are presented. The subset of males and females are indicated because we were only able to determine the sex for a subset of placenta. Individual data points correspond to average fetal weight for a given dam. Data were analyzed by mixed model ANOVA with treatment as the fixed variable and litter as the random variable. Statistically significant differences are indicated by non-overlapping letters. Error bars represent mean ± SEM. For (A) and (C), N=8 for each treatment group with the exception of the AOAA-only and TCE-only treatment groups, which had N=7 each. For (B), N=8 for each treatment group, with the exception of the AOAA-only and TCE-only treatment groups, which had N=7 and N=6, respectively.

Placental weight

(A1)
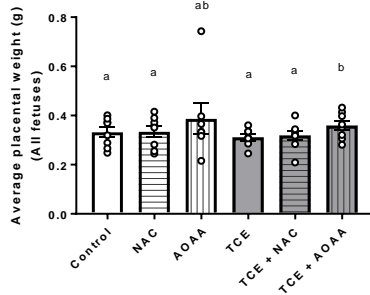
(B1)
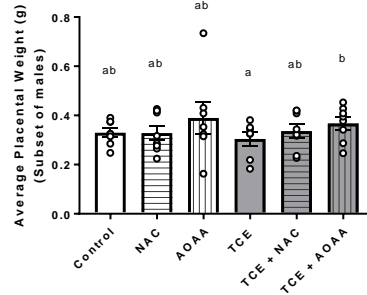
(C1)
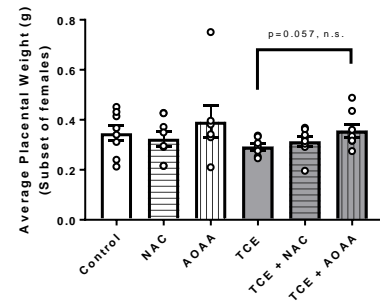
Placental efficiency

(A2)
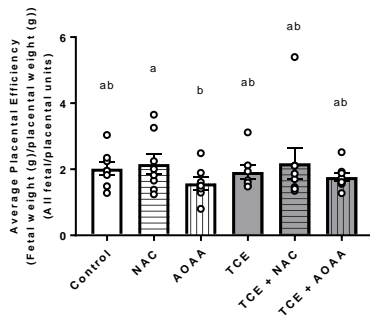
(B2)
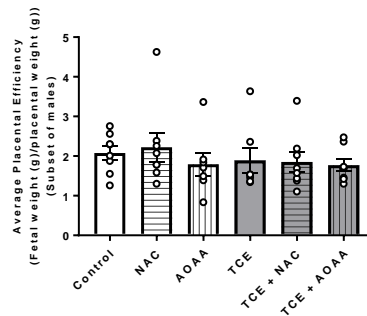
(C2)
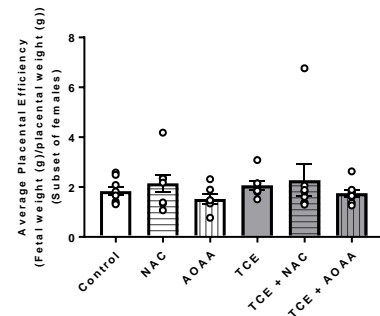
Figure 2.3. Effects of trichloroethylene (TCE), in the presence and absence of N-acetyl-L-cysteine (NAC) and aminooxyacetic acid (AOAA), on placental weight and placental efficiency. The effects for (A) all placentae, (B) a subset of male placentae, and (C) a subset of female placentae are presented. Placental efficiency is defined as placental weight/fetal weight. Individual data points correspond to average placental weight or average placental efficiency for a given dam. Data were analyzed by mixed model ANOVA with treatment as the fixed variable and litter as the random variable. Statistically significant differences are indicated by non-overlapping letters. Error bars represent mean ± SEM. For (A) and (C), N=8 for each treatment group with the exception of the AOAA-only and TCE-only treatment groups, which had N=7 each. For (B), N=8 for each treatment group, with the exception of the AOAA-only and TCE-only treatment groups, which had N=7 and N=6, respectively.

56
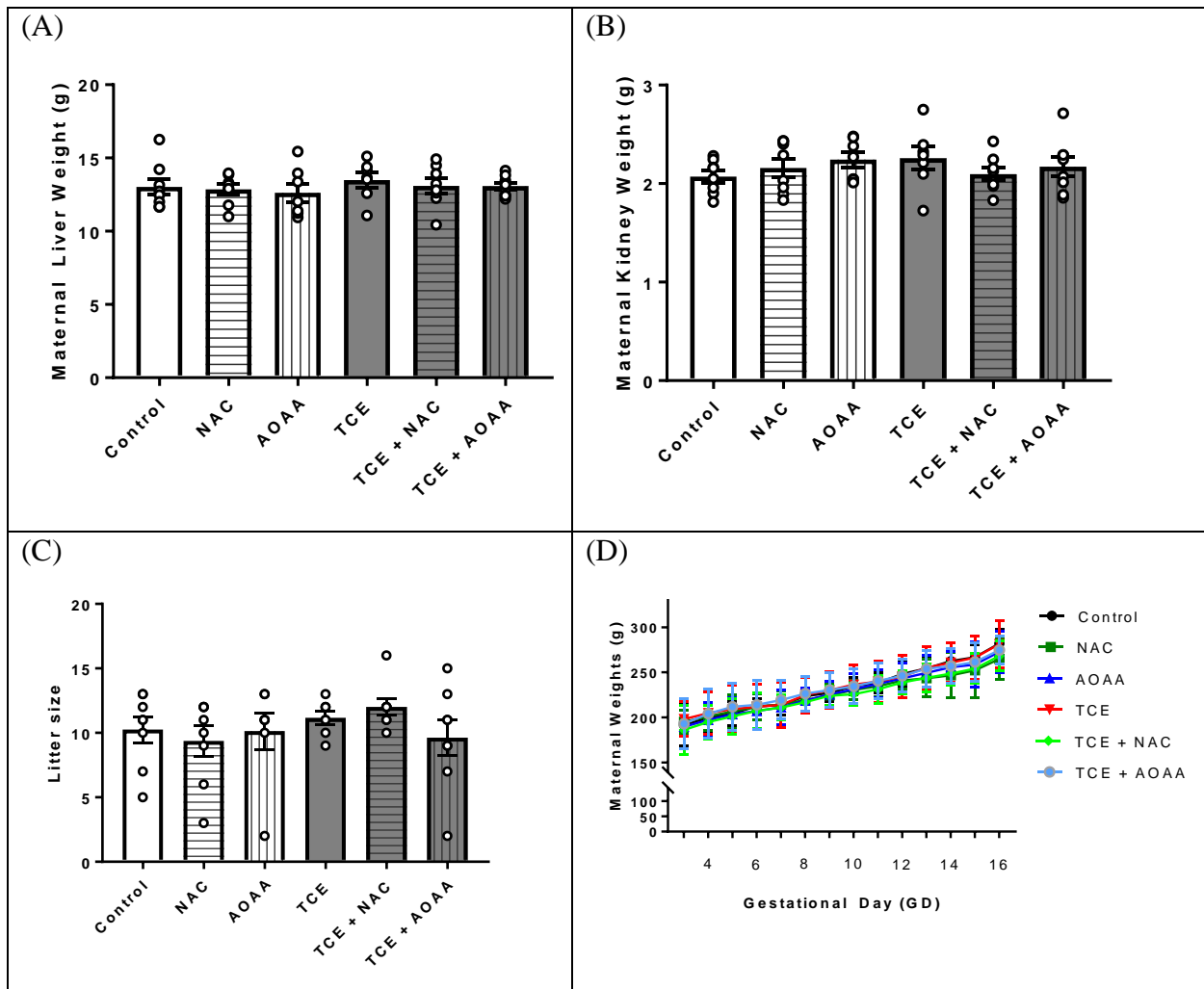
Figure 2.4. Effects of TCE, in the presence and absence of NAC and AOAA, on (A) maternal liver weight, (B) maternal kidney weight, (C) litter size, and (D) maternal weight gain. Data were analyzed by one-way or two-way ANOVA followed by Tukey's post-hoc comparison of means. Error bars represent mean ± SEM. N=8 for the control group, N=8 for the NAC group, N=7 for the AOAA group, N=7 for the TCE group, N=8 for the TCE + NAC group, N8 for the TCE + AOAA group.

CCBL specific activity (nmol/min/mg tissue)
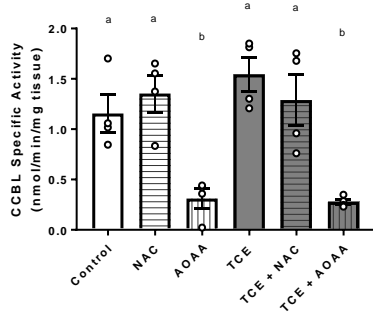
CCBL total activity (nmol/min)
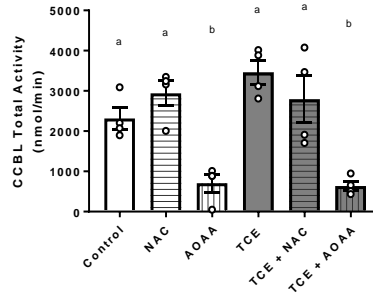
CCBL specific activity (nmol/min/mg protein)

Maternal Kidney
(A1)

(A2)

(A3)
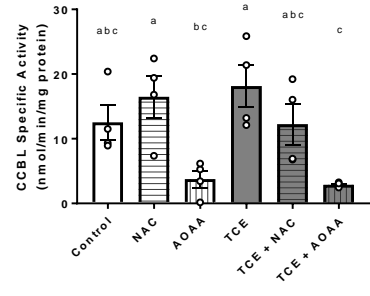
Maternal Liver
(B1)
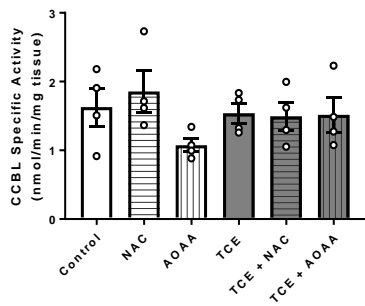
(B2)
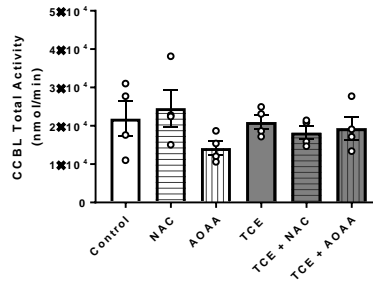
(B3)
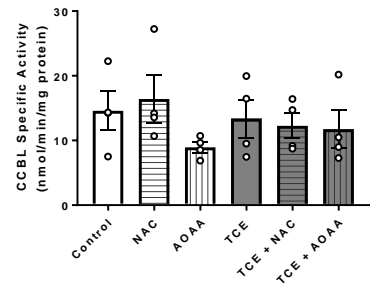
Male Placenta
(C1)
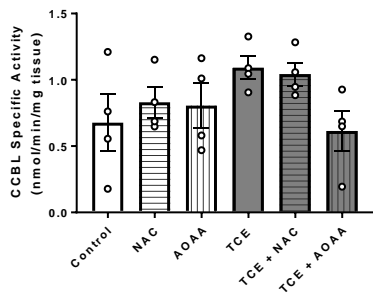
(C2)
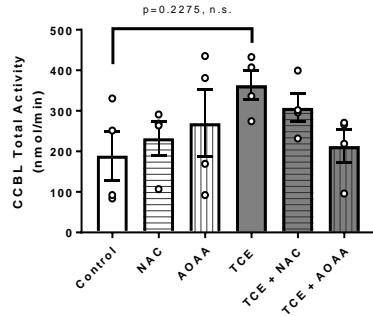
(C3)
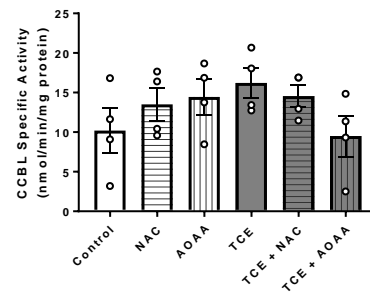
Female Placenta
(D1)

(D2)

(D3)
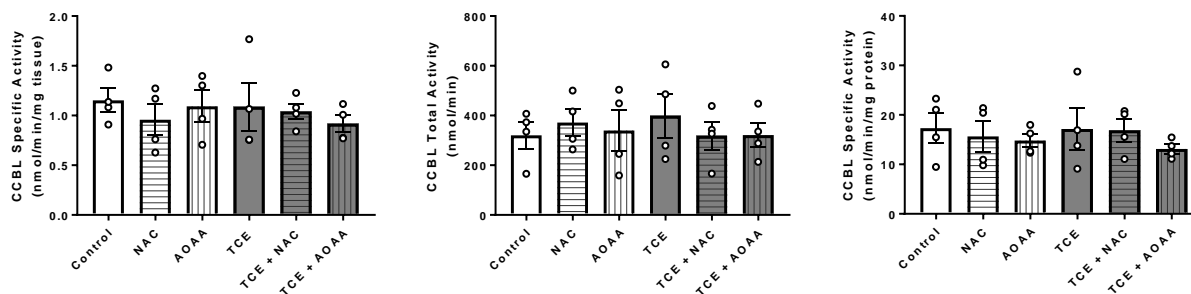
Figure 2.5. Effects of AOAA, TCE and NAC on CCBL activity in (A) maternal kidney, (B) maternal liver, (C) male placenta, and (D) female placenta. Data were analyzed using one-way ANOVA followed by Tukey's post-hoc comparison of means. Statistically significant differences are indicated by non-overlapping letters. Error bars represent mean ± SEM. N=4 dams per experimental group.
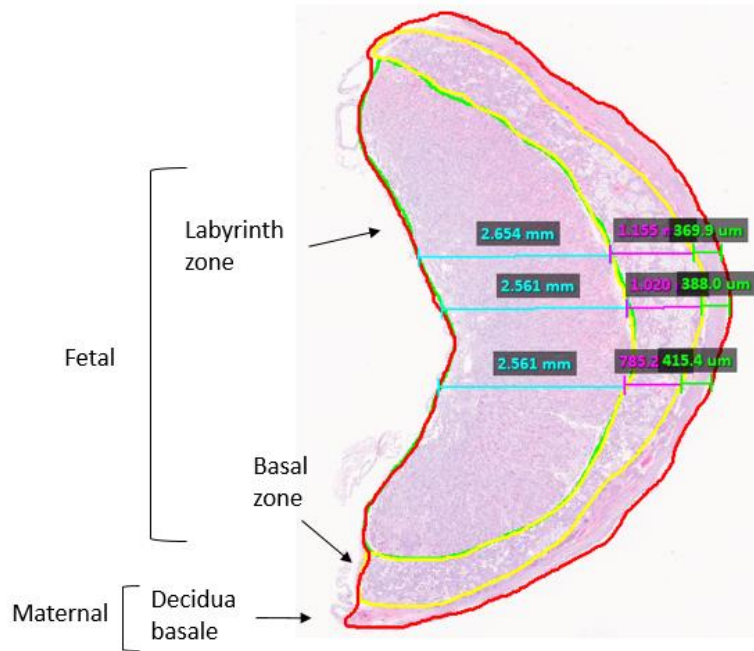
Figure 2.6. Representative image of hematoxylin and eosin (H&E) stained placental section indicating quantification method for placenta morphometric analysis of different placental zones.

	Relative dimensions (normalized to total placenta)	Absolute dimensions (in units of length or area)
Labyrinth zone area	(A1) 	(A2)
Basal zone area	(B1) 	(B2)
Decidua basale area	(C1) 	(C2)
Total placenta area	(D) 	
	Relative dimensions (normalized to total placenta)	Absolute dimensions (in units of length or area)

61

Labyrinth zone width	(E1)	(E2)
Basal zone width	(F1)	(F2)
Decidua basale width	(G1)	(G2)
Total placenta width	(H)	
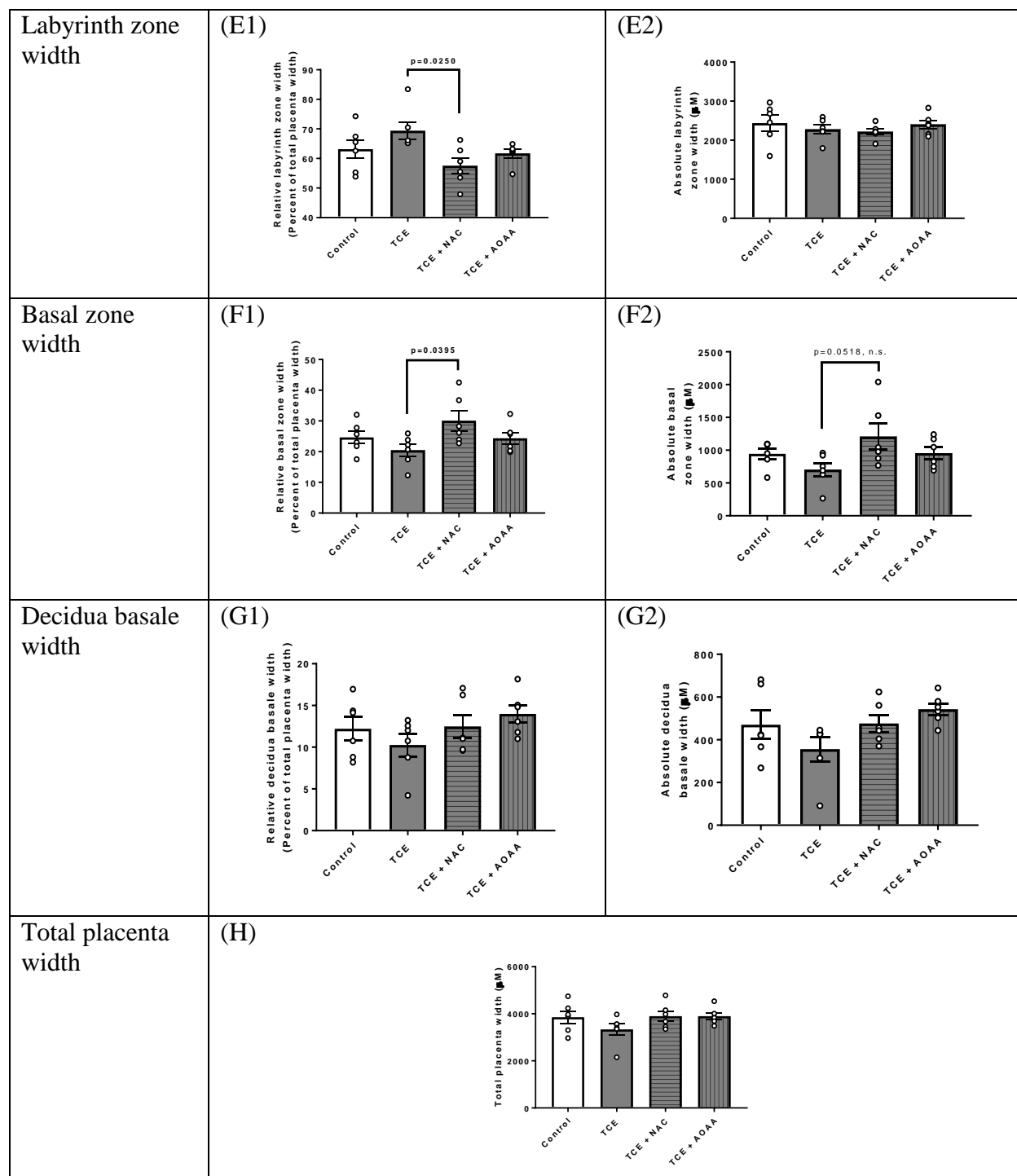
Figure 2.7. Effects of TCE, in the presence and absence of NAC and AOAA, on placental zone morphology. Effects on (A) labyrinth zone area, (B) basal zone area, (C) decidua basale area, (D) total placenta area, (E) labyrinth zone width, (F) basal zone width, (G) decidua basale width, and (H) total placenta width are presented. Data were analyzed by one-way ANOVA followed by Tukey's post-hoc comparison of means. Data of relative dimensions were converted from percent to fraction, then arcsine transformed prior to statistical analysis. N=6 for each

experimental group, with each placenta from a different litter. All placenta used for this figure are female.

(A) Representative Image of Alizarin Red Stain
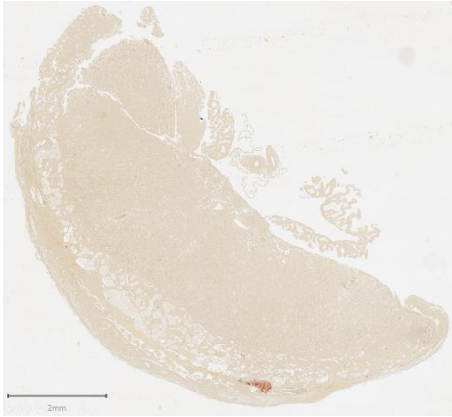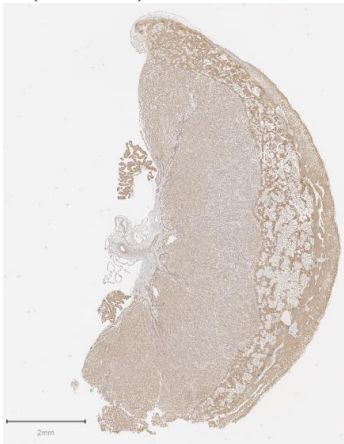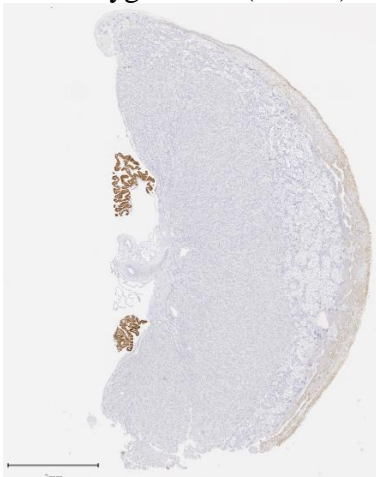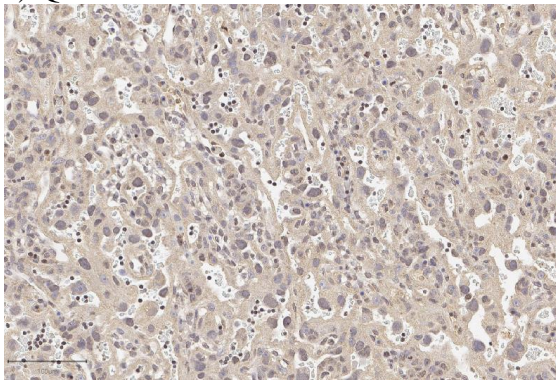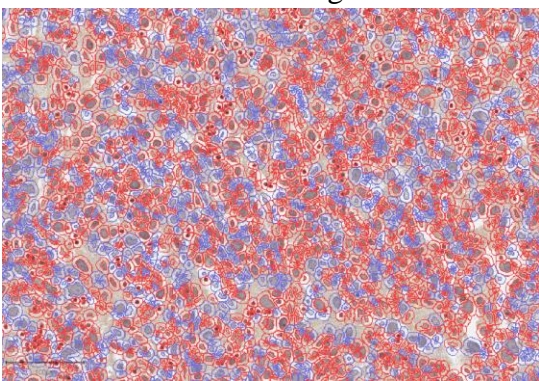
(B) Quantification method
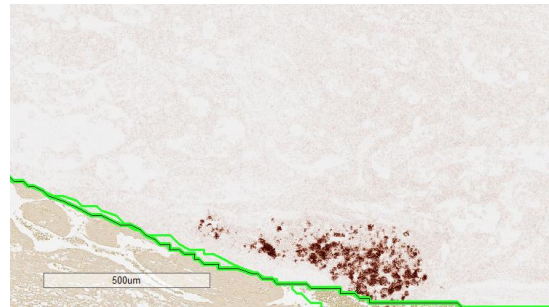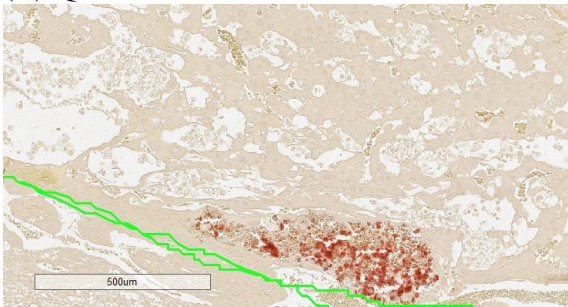
Figure 2.8. Representative image and quantification method for analysis of Alizarin Red staining. (A) Representative image of placenta stained with Alizarin Red. (B) Display of Alizarin Red stain in the basal zone without (left) and with (right) marking from the total positive stain algorithm. The green lines are derived from tracing the basal zone and decidua basale to mark their borders. The images from (B) come from the same placenta as (A) and are from placenta from the control group.
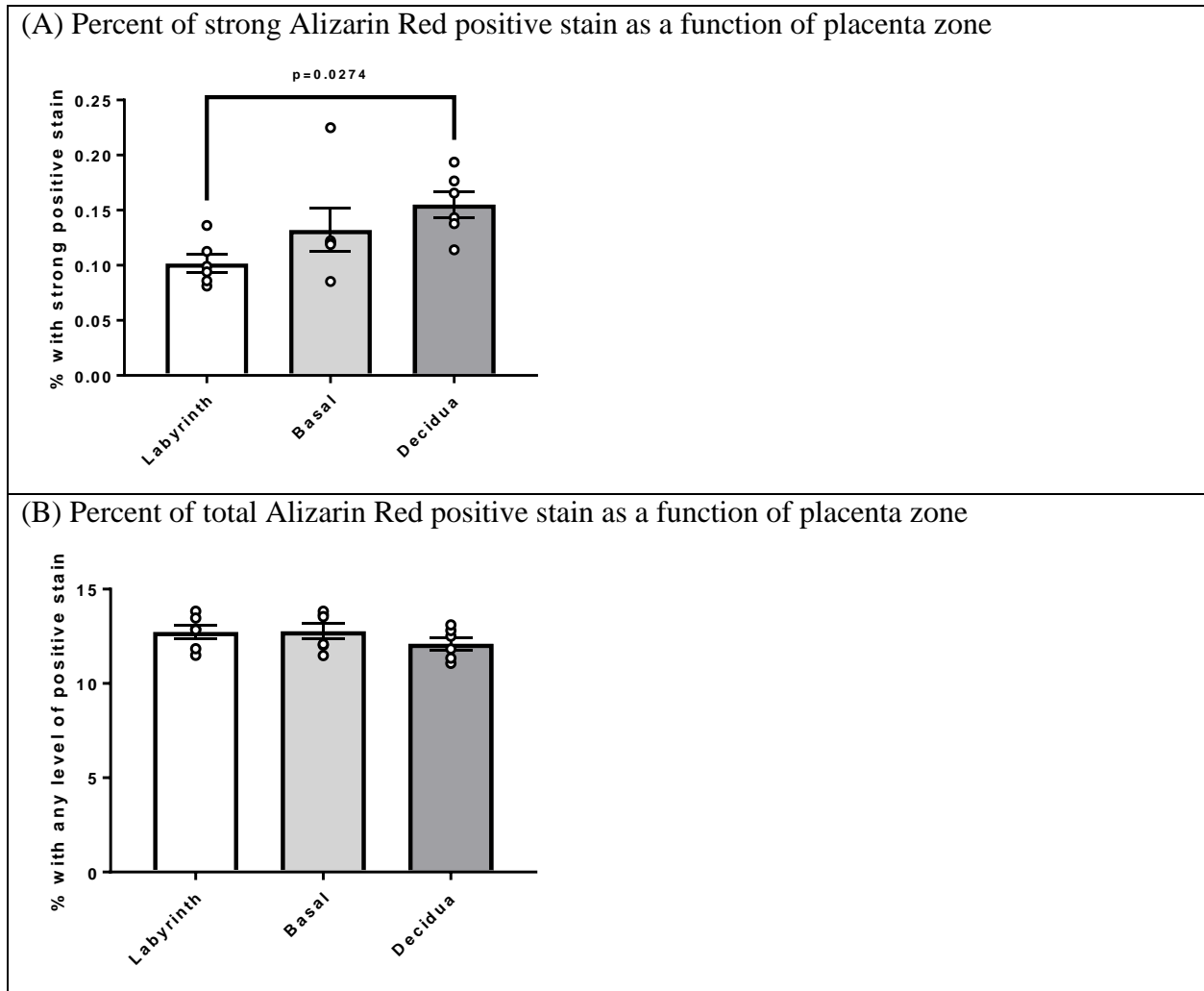
Figure 2.9. Effects of Alizarin Red stain intensity as a function of placental zone in control placenta for (A) strong positive stain and (B) total positive stain. Percent strong positive stain or total positive stain were not altered by treatment group for any zone of the placenta (not shown). Percentage data were converted to fraction values and arcsine transformed prior to statistical analysis by one-way ANOVA followed by Tukey's post-hoc comparison of means. N=6 for each zone and all placenta used to arrive at this figure are female and come from distinct litters.

(A) Cleaved caspase-3	(B) Cysteine conjugate β-lyase 1 (CCBL1)	(C) Flavin-containing monooxygenase 3 (FMO3)

(E) Quantification method used for all IHC stains – total detection reading

(F) Quantification method used for all IHC stains – nuclear detection reading
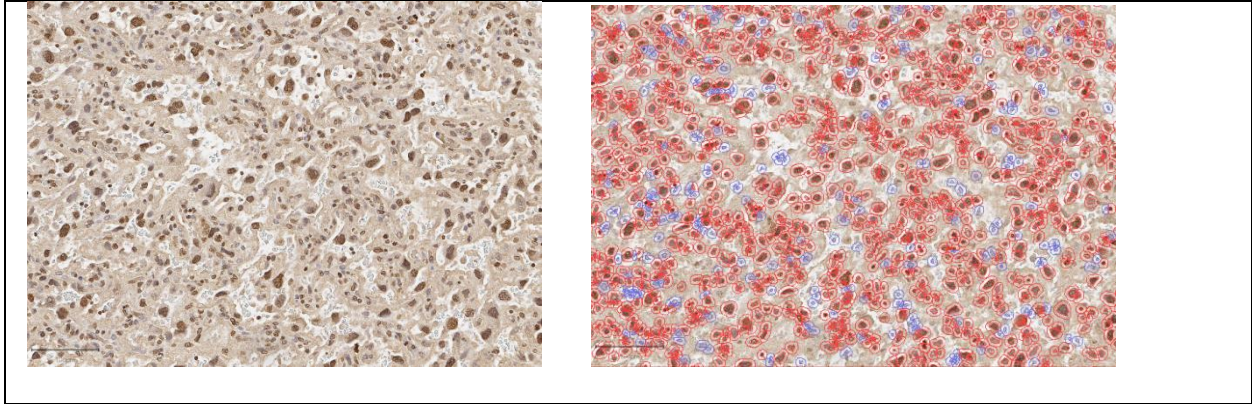
(D) 3-nitrotyrosine

Figure 2.10. Representative images for immunohistochemistry (IHC) staining for (A) cleaved caspase-3, (B) cysteine conjugate β-lyase 1, (C) flavin-containing monooxygenase 3, and (D) 3-nitrotyrosine stains. Quantification method for the (E) total detection reading, and the (F) nuclear detection reading. In (E) and (F), the image on the left an unannotated image whereas the image on the right is the equivalent image containing annotations from the detections. Red markings symbolize a positive detection whereas blue markings symbolize a negative detection. The images from (E) and (F) are all from the labyrinth zone of placenta stained with 3-nitrotyrosine.

Total Positive Detections	Nuclear Positive Detections	Cytoplasmic Positive Detections
Cysteine conjugate β-lyase 1 (CCBL1)		
(A1)	(A2)	(A3)
3-nitrotyrosine		
(B1)	(B2)	(B3)
Flavin-containing monooxygenase 3 (FMO3)		
(C1)	(C2)	(C3)
Cleaved caspase-3		
(D1)	(D2)	(D3)
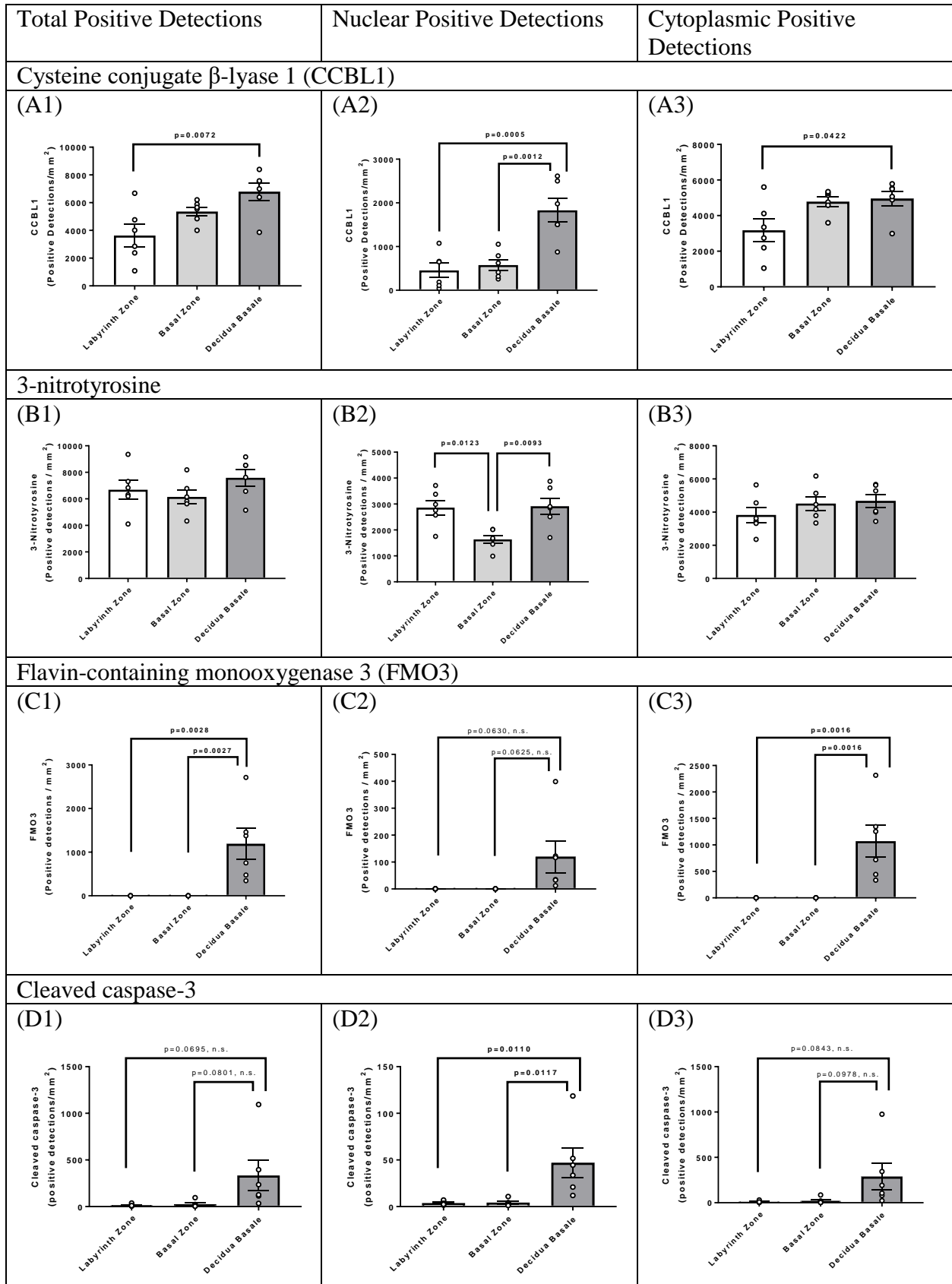
Figure 2.11. Effects of IHC staining of (A) cysteine conjugate β-lyase 1, (B) 3-nitrotyrosine, (C) flavin-containing monooxygenase 3, and (D) cleaved caspase-3 as a function of placental zone in control placenta. Data were analyzed by one-way ANOVA followed by Tukey's post-hoc comparison of means. N=6 for each zone and all placenta used to arrive at this figure are female and come from distinct litters.
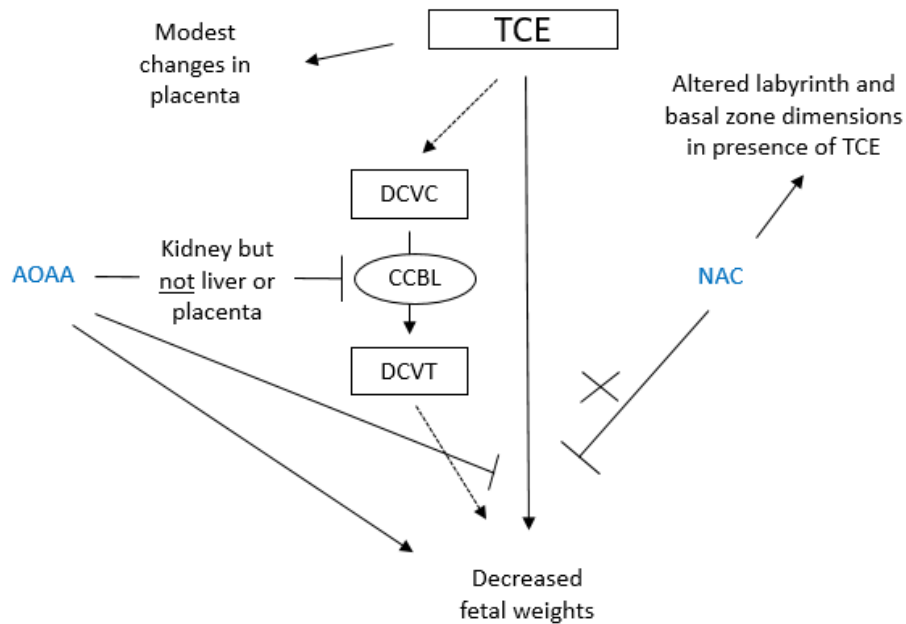
Figure 2.12. Proposed mechanism of action of trichloroethylene (TCE) in the timed-pregnant Wistar rat with modulation by N-acetyl-L-cysteine (NAC) and aminooxyacetic acid (AOAA). Interventions to modulate TCE toxicity are listed in blue. TCE and its metabolites are in rectangular boxes, and an enzyme, cysteine conjugate β-lyase (CCBL), involved in TCE metabolism is in a circular box. Other abbreviations: DCVC, *S*-(1,2-dichlorovinyl)-L-cysteine; DCVT, 1,2-dichlorovinylthiol.

Table S2.1. Assignment of rats across treatment groups and batches.

Treatment	Number of rats	Pregnancy status
Control	8 across 8 batches	All pregnant
NAC	8 across 8 batches	All pregnant
AOAA	9 across 8 batches	Two rats non-pregnant – one from batch 3 and one from batch 7
TCE	8 across 8 batches	One rat from batch 8 non-pregnant
TCE + NAC	8 across 8 batches	All pregnant
TCE + AOAA	8 across 8 batches	All pregnant

Eight total batches of rats arrived at eight separate time points to the researchers. Within each batch, each treatment group was assigned at least once with assignments made in a random fashion.

Table S2.2. Details of primary antibodies used for Immunohistochemistry (IHC) staining and reaction conditions.

Peptide/Protein Target	Antigen Sequence	Manufacturer and Catalog Number	Species Reactivity	Antibody Type	Dilution Used	Positive Control
Cleaved caspase-3	Synthetic peptide of amino-terminal residues adjacent to Asp175 of human caspase-3	Cell Signaling Technology, 9664	Human, Mouse, Rat, Monkey	Rabbit monoclonal	1:500, 30 minutes, room temp	Rat thymus
Cysteine conjugate β-lyase 1 (CCBL1)	Full length fusion protein [human]	ThermoFisher Scientific, PA5-51313	Human, Rat	Rabbit polyclonal	1:500, 1 hour, room temp	Rat Liver/Kidney
Flavin-containing monooxygenase 3 (FMO3)	Synthetic peptide within human FMO3 on amino acids 300-400	Abcam, ab126711	Human, Rat, Mouse	Rabbit monoclonal	1:500, 1 hour, room temp	Rat Kidney
3-nitrotyrosine	3-(4-Hydroxy-3-nitrophenyl acetamido) propionic acid-BSA conjugate	Abcam, ab61392	Any	Mouse monoclonal	1:500 30 minutes, room temp	Rat brain

Table S2.3. Primer sequences used for the current study.

B2m (Beta-2-microglobulin)	
Forward	5'-TCGTGCTTGCCATTCAGAAAAC-3'
Reverse	5'-GCAGTTGAGGAAGTTGGGCT-3'
Source: NCBI nucleotide database	
Nfkb1 (Nuclear factor kappa B subunit 1)	
Forward	5'-ACTGTCAACAGATGGCCCATACC-3'
Reverse	5'-TTCGCACACGTAGCGGAAT-3'
Source: NCBI nucleotide database	
Bcl2 (BCL2 apoptosis regulator)	
Forward	5'-GACTGAGTACCTGAACCGGC-3'
Reverse	5'-AGTTCCACAAAGGCATCCCAG-3'
Source: NCBI nucleotide database	
Bax (BCL2 associated X, apoptosis regulator)	
Forward	5'-TTGCTACAGGGTTTCATCCAGG-3'
Reverse	5'-CACTCGCTCAGCTTCTTGGT-3'
Source: NCBI nucleotide database	
Prdx1 (Peroxiredoxin 1)	
Forward	5'-CTGGCATGGATTAACACACCC-3'
Reverse	5'-AATGGTGCGCTTGGGATCTG-3'
Source: NCBI nucleotide database	
Lgals3 (Galectin-3)	
Forward	5'-CAGTGCCCTACGATATGCCC-3'
Reverse	5'-GAGTGATACTGTTTGCGTTGGG-3'
Source: NCBI nucleotide database	
Fmo3 (Flavin-containing monooxygenase 3)	
Forward	5'-CCTGGGGAACTCAGGTTGTG-3'
Reverse	5'-GGAGCTTATGATGACCTGCTGA-3'
Source: NCBI nucleotide database	
Kyat1 (Kyurenine aminotransferase 1, also codes for cysteine conjugate beta-lyase)	
Forward	5'-TGACAAACGTCCTGGCAAGT-3'
Reverse	5'-CATAGGCACCCACTGTCACC-3'
Source: NCBI nucleotide database	
For sex determination (listed below)	
Sry (Sex determining region Y) (works for both genomic DNA and cDNA input)	

Forward	5'-AAGCGCCCCATGAATGCAT-3'
Reverse	5'-CGATGAGGCTGATATTTATA-3'
Source: (Schulte et al. 2012)	
B2m (Beta-2-microglobulin) (for cDNA input) – spans exon-exon junction	
Forward	5'-TCGTGCTTGCCATTCAGAAAAC-3'
Reverse	5'-GCAGTTGAGGAAGTTGGGCT-3'
Source: NCBI nucleotide database	
B2m (Beta-2-microglobulin) (for genomic DNA input) – does not span exon-exon junction	
Forward	5'-CCCACCCTCATGGCTACTTC-3'
Reverse	5'-TGGGTGATGAAAACCGCACA-3'
Source: NCBI nucleotide database	

Primers for sex determination are at the bottom of the Table. Several criteria were used for primer selection in the case of using the NCBI nucleotide database. Desirable characteristics of the primer pair included a melting point as close to 60 degrees Celsius as possible, an amplicon length preferably between 75 and 150 base pairs, and base pairs as close as possible to 50% GC in composition. Finally, the criterion of the primer spanning an exon-exon junction was selected as a must (except in the case of *Kyat1*, in which no primers could be found with the specification).

Table S2.4. Summary of mainly null immunohistochemistry (IHC) and Tdt stain findings from the treatment group comparisons for each individual zone of the placenta (Cleaved caspase-3, cysteine conjugate β-lyase 1, flavin-containing monooxygenase 3, 3-nitrotyrosine, Tdt).

	p-value ranges when comparing the four different treatment groups via ANOVA followed by Tukey's posthoc comparison of means		
	Labyrinth Zone	**Basal Zone**	**Decidua Basale**
Cleaved caspase-3: Total	0.5960 to 0.9807	0.7445 to >0.9999	0.6168 to 0.9996
Cleaved caspase-3: Nuclear	0.6483 to 0.9994	0.6666 to 0.9984	0.5028 to >0.9999
Cleaved caspase-3: Cytoplasmic	0.5913 to 0.9878	0.7186 to 0.9993	0.6561 to 0.9994
CCBL1: Total	0.9711 to >0.9999	0.9340 to 0.9996	0.4336 to 0.9982
CCBL1: Nuclear	0.7068 to 0.9991	0.7499 to 0.9984	0.4912 to 0.9955
CCBL1: Cytoplasmic	0.9591 to >0.9999	0.9662 to 0.9996	0.5027 to 0.9995
FMO3: Total	0.3556 to 0.9931	0.6706 to >0.9999	0.9334 to 0.9996
FMO3: Nuclear	0.6536 to 0.9997	**0.0384** to 0.7770	0.8619 to 0.9959
FMO3: Cytoplasmic	0.3351 to 0.9982	0.6920 to 0.9997	0.9212 to 0.9985
3-nitrotyrosine: Total	0.5512 to 0.9645	0.2922 to 0.9785	0.5663 to 0.9987
3-nitrotyrosine: Nuclear	0.5979 to 0.9878	0.4095 to 0.9919	0.2486 to 0.9993
3-nitrotyrosine: Cytoplasmic	0.4667 to 0.9859	0.2799 to 0.9896	0.5495 to 0.9923
Tdt (ratio of green to blue)	0.2748 to 0.9997	0.9937 to >0.9999	0.6311 to 0.9961

For the IHC stains, detections were made on QuPath using an algorithm that specifically detected all staining regardless of cytoplasmic or nuclear and an algorithm that specifically detected only nuclear staining (also described in **Figure 2.10**). For Tdt, abundance was quantified as a ratio of green (Tdt enzyme) to blue (DAPI) stain (also described in **Figure S2.1**). Despite almost no differences among treatment groups, many comparisons for IHC staining among zones for control placenta were statistically significant (**Figure 2.11**). The one statistically significant p-value of 0.0384 here corresponds to the Control versus TCE + AOAA comparison, with the TCE + AOAA group having more nuclear FMO3 stain compared to the control group. N=6 for each zone, with all placenta as female and coming from a different litter. Abbreviations: CCBL, cysteine conjugate β-lyase; FMO, flavin-containing monooxygenase; Tdt, terminal deoxynucleotidyl transferase.

Table S2.5. Summary of null findings from qRT-PCR experiments (*Nfkb1*, *Bcl2*, *Bax*, *Prdx1*, *Lgals3*, *Kyat1*, and *Fmo3* mRNA expression).

Comparison of treatment groups within each sex		
	Lowest p-value in ANOVA followed by Tukey's multiple comparison of means (comparison leading to the reported p-value)	
Gene	**Male**	**Female**
Nfkb1	0.5017 (NAC vs. TCE + AOAA)	0.9037 (AOAA vs. TCE)
Bcl2	0.1360 (NAC vs. TCE + AOAA)	0.7482 (AOAA vs. TCE)
Bax	0.5979 (Control vs. TCE)	0.9975 (Control vs. TCE)
Prdx1	0.1517 (Control vs. TCE + AOAA)	0.8321 (Control vs. AOAA)
Lgals3	0.8337 (Control vs. TCE + NAC)	0.6297 (AOAA vs. TCE + AOAA)
Kyat1	0.4311 (Control vs. TCE + AOAA)	0.9181 (Control vs. AOAA)
Fmo3	0.0799 (Control vs. TCE)	0.2744 (TCE + NAC vs. TCE + AOAA)

Comparison of sex within each treatment group (p-values from unpaired, two-tailed t-test)					
Male vs. female (Control)		**Male vs. female (NAC)**		**Male vs. female (AOAA)**	
Gene	p-value	Gene	p-value	Gene	p-value
Nfkb1	0.2183	*Nfkb1*	0.3982	*Nfkb1*	0.3856
Bcl2	0.1089	*Bcl2*	0.2046	*Bcl2*	0.1352
Bax	0.1941	*Bax*	0.6278	*Bax*	0.6414
Prdx1	0.2194	*Prdx1*	0.2473	*Prdx1*	0.623
Lgals3	0.2348	*Lgals3*	0.6009	*Lgals3*	0.7237
Kyat1	0.3651	*Kyat1*	0.3601	*Kyat1*	**0.0386**
Fmo3	0.5854	*Fmo3*	0.3471	*Fmo3*	0.8479
Male vs. female (TCE)		**Male vs. female (TCE + NAC)**		**Male vs. female (TCE + AOAA)**	
Gene	p-value	Gene	p-value	Gene	p-value
Nfkb1	0.8462	*Nfkb1*	0.7751	*Nfkb1*	0.4469
Bcl2	0.1853	*Bcl2*	0.209	*Bcl2*	0.4233
Bax	0.559	*Bax*	0.6149	*Bax*	0.6164
Prdx1	0.8793	*Prdx1*	0.9976	*Prdx1*	0.1535
Lgals3	0.541	*Lgals3*	0.9594	*Lgals3*	0.6371
Kyat1	0.5879	*Kyat1*	0.9229	*Kyat1*	0.4711
Fmo3	0.2447	*Fmo3*	0.1068	*Fmo3*	0.8953

Only one significant p-value was found in the case of a male to female comparison in *Kyat1* expression within the AOAA experimental group, which has limited interpretability because it was not the control group. N=8, 8, 7, 6, 8, 8, respectively for the control, NAC, AOAA, TCE, TCE + NAC, and TCE + AOAA male experimental groups. N=8, 8, 7, 7, 8, 8, respectively, for the control, NAC, AOAA, TCE, TCE + NAC, and TCE + AOAA female experimental groups.

Representative Image of Tdt stain (green) with DAPI counterstain (blue)
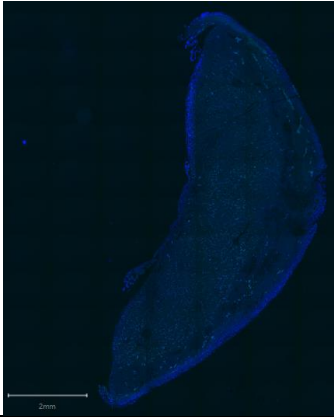
Quantification method to detect Tdt stain (green) (left) and DAPI (blue) (right)
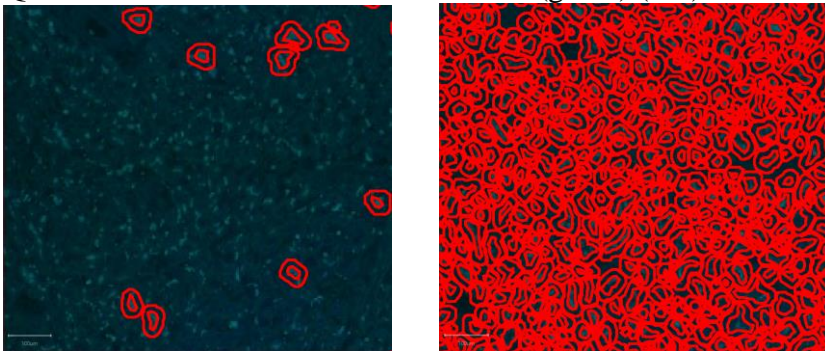
Verification of quantification method (quantification of green to blue ratio for positive and negative control)
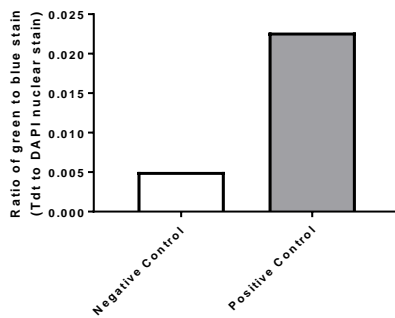
Figure S2.1. Representative image and quantification method for analysis of Tdt enzyme staining. Quantification was performed using QuPath. Negative and positive control staining were performed on manufacturer-supplied slides of HL-60 cells. Generation of negative control was accomplished by substituting the Tdt enzyme with ddH_2O in the reaction mixture as described in the manufacturer-supplied instructions. Generation of positive control was accomplished by incubating the specimen in a Tris-buffered saline (TBS) /1 mM $MgSO_4$ mixture, as described in the instructions provided by the manufacturer.
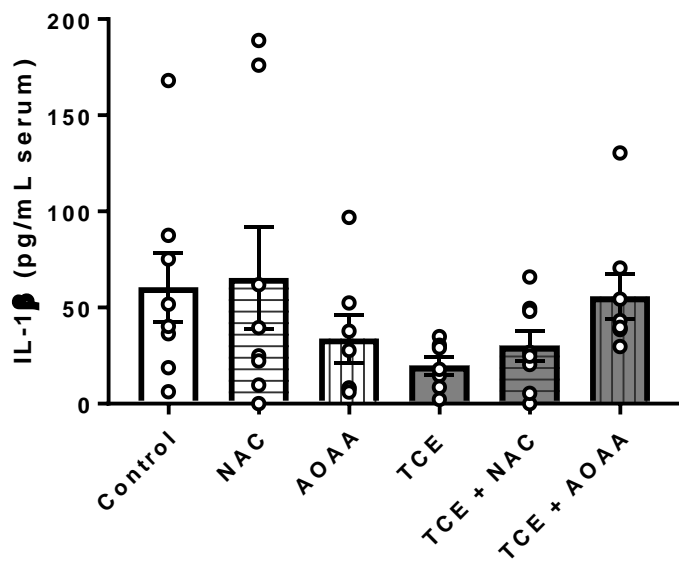
Figure S2.2. Effects of TCE, in the presence and absence of NAC and AOAA, on maternal serum concentrations of IL-1β. Data were analyzed by one way-ANOVA followed by Tukey's post-hoc comparison of means. N=8, 8, 7, 7, 8, 8, for the control, NAC, AOAA, TCE, TCE + NAC, TCE + AOAA groups, respectively. Attempt was also made to detect TNF-α and IL-6 in maternal serum; however, 4 out 12 samples submitted for each of these analyses returned a null value (data not shown) and a decision was made to not proceed with TNF-α and IL-6 detection.

References

Agency for Toxic Substances and Disease Registry, 2007. Trichloroethylene Toxicity: What are the U.S. Standards for Trichloroethylene Exposure? In Agency for Toxic Substances and Disease Registry (ATSDR), E.H.a.M.E., (Ed.), Atlanta, GA, pp.

Agency for Toxic Substances and Disease Registry, 2019. Toxicological Profile for Trichloroethylene. In U.S. Department of Health and Human Services, A.f.T.S.a.D.R.A., (Ed.), Atlanta, GA, pp.

Ahsan, H., 2013. 3-Nitrotyrosine: A biomarker of nitrogen free radical species modified proteins in systemic autoimmunogenic conditions. Hum Immunol **74**, 1392-1399.

Aldini, G., Altomare, A., Baron, G., Vistoli, G., Carini, M., Borsani, L., Sergio, F., 2018. N-Acetylcysteine as an antioxidant and disulphide breaking agent: the reasons why. Free Radic Res **52**, 751-762.

Bale, A.S., Barone, S., Jr., Scott, C.S., Cooper, G.S., 2011. A review of potential neurotoxic mechanisms among three chlorinated organic solvents. Toxicol Appl Pharmacol **255**, 113-126.

Bull, R.J., 2000. Mode of action of liver tumor induction by trichloroethylene and its metabolites, trichloroacetate and dichloroacetate. Environ Health Perspect **108 Suppl 2**, 241-259.

Chang, E.Y., Barbosa, E., Paintlia, M.K., Singh, A., Singh, I., 2005. The use of N-acetylcysteine for the prevention of hypertension in the reduced uterine perfusion pressure model for preeclampsia in Sprague-Dawley rats. Am J Obstet Gynecol **193**, 952-956.

Cooper, A.J., Pinto, J.T., 2006. Cysteine S-conjugate beta-lyases. Amino Acids **30**, 1-15.

Cooper, G.S., Makris, S.L., Nietert, P.J., Jinot, J., 2009. Evidence of autoimmune-related effects of trichloroethylene exposure from studies in mice and humans. Environ Health Perspect **117**, 696-702.

Crowley, L.C., Waterhouse, N.J., 2016. Detecting Cleaved Caspase-3 in Apoptotic Cells by Flow Cytometry. Cold Spring Harb Protoc **2016**.

Diel, P., Schmidt, S., Vollmer, G., Janning, P., Upmeier, A., Michna, H., Bolt, H.M., Degen, G.H., 2004. Comparative responses of three rat strains (DA/Han, Sprague-Dawley and Wistar) to treatment with environmental estrogens. Arch Toxicol **78**, 183-193.

Dohn, D.R., Anders, M.W., 1982. Assay of cysteine conjugate beta-lyase activity with S-(2-benzothiazolyl)cysteine as the substrate. Anal Biochem **120**, 379-386.

Donoso, A.O., Banzan, A.M., 1984. Effects of increase of brain GABA levels on the hypothalamic-pituitary-luteinizing hormone axis in rats. Acta Endocrinol (Copenh) **106**, 298-304.

Ejiri, N., Katayama, K., Doi, K., 2003. Induction of CYP3A1 by dexamethasone and pregnenolone-16alpha-carbonitrile in pregnant rat and fetal livers and placenta. Exp Toxicol Pathol **54**, 273-279.

Ejiri, N., Katayama, K.I., Nakayama, H., Doi, K., 2001. Expression of cytochrome P450 (CYP) isozymes in rat placenta through pregnancy. Exp Toxicol Pathol **53**, 387-391.

El-Khairy, L., Vollset, S.E., Refsum, H., Ueland, P.M., 2003. Plasma total cysteine, pregnancy complications, and adverse pregnancy outcomes: the Hordaland Homocysteine Study. Am J Clin Nutr **77**, 467-472.

Elfarra, A.A., Anders, M.W., 1984. Renal processing of glutathione conjugates. Role in nephrotoxicity. Biochem Pharmacol **33**, 3729-3732.

Elkin, E.R., Harris, S.M., Loch-Caruso, R., 2018. Trichloroethylene metabolite S-(1,2-dichlorovinyl)-l-cysteine induces lipid peroxidation-associated apoptosis via the intrinsic and extrinsic apoptosis pathways in a first-trimester placental cell line. Toxicol Appl Pharmacol **338**, 30-42.

Fisher, J.W., Whittaker, T.A., Taylor, D.H., Clewell, H.J., 3rd, Andersen, M.E., 1989. Physiologically based pharmacokinetic modeling of the pregnant rat: a multiroute exposure model for trichloroethylene and its metabolite, trichloroacetic acid. Toxicol Appl Pharmacol **99**, 395-414.

Forand, S.P., Lewis-Michl, E.L., Gomez, M.I., 2012. Adverse birth outcomes and maternal exposure to trichloroethylene and tetrachloroethylene through soil vapor intrusion in New York State. Environ Health Perspect **120**, 616-621.

Forkert, P.G., Sylvestre, P.L., Poland, J.S., 1985. Lung injury induced by trichloroethylene. Toxicology **35**, 143-160.

Fukami, G., Hashimoto, K., Koike, K., Okamura, N., Shimizu, E., Iyo, M., 2004. Effect of antioxidant N-acetyl-L-cysteine on behavioral changes and neurotoxicity in rats after administration of methamphetamine. Brain Res **1016**, 90-95.

Furukawa, S., Hayashi, S., Usuda, K., Abe, M., Hagio, S., Ogawa, I., 2011. Toxicological pathology in the rat placenta. J Toxicol Pathol **24**, 95-111.

Green, T., Dow, J., Ellis, M.K., Foster, J.R., Odum, J., 1997a. The role of glutathione conjugation in the development of kidney tumours in rats exposed to trichloroethylene. Chem Biol Interact **105**, 99-117.

Green, T., Mainwaring, G.W., Foster, J.R., 1997b. Trichloroethylene-induced mouse lung tumors: studies of the mode of action and comparisons between species. Fundam Appl Toxicol **37**, 125-130.

Guha, N., Loomis, D., Grosse, Y., Lauby-Secretan, B., El Ghissassi, F., Bouvard, V., Benbrahim-Tallaa, L., Baan, R., Mattock, H., Straif, K., International Agency for Research on Cancer Monograph Working, G., 2012. Carcinogenicity of trichloroethylene, tetrachloroethylene, some other chlorinated solvents, and their metabolites. Lancet Oncol **13**, 1192-1193.

Guven, M.A., Coskun, A., Ertas, I.E., Aral, M., Zencirci, B., Oksuz, H., 2009. Association of maternal serum CRP, IL-6, TNF-alpha, homocysteine, folic acid and vitamin B12 levels with the severity of preeclampsia and fetal birth weight. Hypertens Pregnancy **28**, 190-200.

Hanigan, M.H., 2014. Gamma-glutamyl transpeptidase: redox regulation and drug resistance. Adv Cancer Res **122**, 103-141.

Hassan, I., Kumar, A.M., Park, H.R., Lash, L.H., Loch-Caruso, R., 2016. Reactive Oxygen Stimulation of Interleukin-6 Release in the Human Trophoblast Cell Line HTR-8/SVneo by the Trichlorethylene Metabolite S-(1,2-Dichloro)-l-Cysteine. Biol Reprod **95**, 66.

Healy, T.E., Poole, T.R., Hopper, A., 1982. Rat fetal development and maternal exposure to trichloroethylene 100 p.p.m. Br J Anaesth **54**, 337-341.

Hinchman, C.A., Ballatori, N., 1990. Glutathione-degrading capacities of liver and kidney in different species. Biochem Pharmacol **40**, 1131-1135.

International Agency for Research on Cancer, 2014. Trichloroethylene, Tetrachloroethylene, and Some Other Chlorinated Agents. (IARC Monographs on the Evaluation of Carcinogenic Risks to Humans). IARC Working Group on the Evaluation of Carcinogenic Risk to Humans, Lyon, France, pp.

Ishihara, N., Matsuo, H., Murakoshi, H., Laoag-Fernandez, J.B., Samoto, T., Maruo, T., 2002. Increased apoptosis in the syncytiotrophoblast in human term placentas complicated by either preeclampsia or intrauterine growth retardation. Am J Obstet Gynecol **186**, 158-166.

Jollow, D.J., Bruckner, J.V., McMillan, D.C., Fisher, J.W., Hoel, D.G., Mohr, L.C., 2009. Trichloroethylene risk assessment: a review and commentary. Crit Rev Toxicol **39**, 782-797.

Knapen, M.F., Zusterzeel, P.L., Peters, W.H., Steegers, E.A., 1999. Glutathione and glutathione-related enzymes in reproduction. A review. Eur J Obstet Gynecol Reprod Biol **82**, 171-184.

Lamb, J.C., Hentz, K.L., 2006. Toxicological review of male reproductive effects and trichloroethylene exposure: assessing the relevance to human male reproductive health. Reprod Toxicol **22**, 557-563.

Lane, M., Gardner, D.K., 2005. Mitochondrial malate-aspartate shuttle regulates mouse embryo nutrient consumption. J Biol Chem **280**, 18361-18367.

Lash, L.H., 2010. Role of Bioactivation Reactions in Chemically Induced Nephrotoxicity. In Gad, S.C., (Ed.), Pharmaceutical Sciences Encyclopedia: Drug Discovery, Development, and Manufacturing. John Wiley & Sons, Inc., Hoboken, NJ, pp. 1-21.

Lash, L.H., Chiu, W.A., Guyton, K.Z., Rusyn, I., 2014. Trichloroethylene biotransformation and its role in mutagenicity, carcinogenicity and target organ toxicity. Mutat Res Rev Mutat Res **762**, 22-36.

Lash, L.H., Elfarra, A.A., Anders, M.W., 1986. Renal cysteine conjugate beta-lyase. Bioactivation of nephrotoxic cysteine S-conjugates in mitochondrial outer membrane. J Biol Chem **261**, 5930-5935.

Lash, L.H., Sausen, P.J., Duescher, R.J., Cooley, A.J., Elfarra, A.A., 1994. Roles of cysteine conjugate beta-lyase and S-oxidase in nephrotoxicity: studies with S-(1,2-dichlorovinyl)-L-cysteine and S-(1,2-dichlorovinyl)-L-cysteine sulfoxide. J Pharmacol Exp Ther **269**, 374-383.

Leazer, T.M., Klaassen, C.D., 2003. The presence of xenobiotic transporters in rat placenta. Drug Metab Dispos **31**, 153-167.

Liu, M., Choi, D.Y., Hunter, R.L., Pandya, J.D., Cass, W.A., Sullivan, P.G., Kim, H.C., Gash, D.M., Bing, G., 2010. Trichloroethylene induces dopaminergic neurodegeneration in Fisher 344 rats. J Neurochem **112**, 773-783.

Loch-Caruso, R., Hassan, I., Harris, S.M., Kumar, A., Bjork, F., Lash, L.H., 2019. Trichloroethylene exposure in mid-pregnancy decreased fetal weight and increased placental markers of oxidative stress in rats. Reprod Toxicol **83**, 38-45.

Manson, J.M., Murphy, M., Richdale, N., Smith, M.K., 1984. Effects of oral exposure to trichloroethylene on female reproductive function. Toxicology **32**, 229-242.

Naik, A.K., Tandan, S.K., Dudhgaonkar, S.P., Jadhav, S.H., Kataria, M., Prakash, V.R., Kumar, D., 2006. Role of oxidative stress in pathophysiology of peripheral neuropathy and modulation by N-acetyl-L-cysteine in rats. Eur J Pain **10**, 573-579.

Perry, T.L., Hansen, S., 1978. Biochemical effects in man and rat of three drugs which can increase brain GABA content. J Neurochem **30**, 679-684.

Potgens, A.J., Schmitz, U., Bose, P., Versmold, A., Kaufmann, P., Frank, H.G., 2002. Mechanisms of syncytial fusion: a review. Placenta **23 Suppl A**, S107-113.

Rodenbeck, S.E., Sanderson, L.M., Rene, A., 2000. Maternal exposure to trichloroethylene in drinking water and birth-weight outcomes. Arch Environ Health **55**, 188-194.

Ruckart, P.Z., Bove, F.J., Maslia, M., 2014. Evaluation of contaminated drinking water and preterm birth, small for gestational age, and birth weight at Marine Corps Base Camp Lejeune, North Carolina: a cross-sectional study. Environ Health **13**, 99.

Saillenfait, A.M., Langonne, I., Sabate, J.P., 1995. Developmental toxicity of trichloroethylene, tetrachloroethylene and four of their metabolites in rat whole embryo culture. Arch Toxicol **70**, 71-82.

Schulz-Utermoehl, T., Bennett, A.J., Ellis, S.W., Tucker, G.T., Boobis, A.R., Edwards, R.J., 1999. Polymorphic debrisoquine 4-hydroxylase activity in the rat is due to differences in CYP2D2 expression. Pharmacogenetics **9**, 357-366.

Seegal, R.F., Brosch, K.O., Okoniewski, R.J., 1997. Effects of in utero and lactational exposure of the laboratory rat to 2,4,2',4'- and 3,4,3',4'-tetrachlorobiphenyl on dopamine function. Toxicol Appl Pharmacol **146**, 95-103.

Shen, S.F., Hua, C.H., 2011. Effect of L-arginine on the expression of Bcl-2 and Bax in the placenta of fetal growth restriction. J Matern Fetal Neonatal Med **24**, 822-826.

Tinwell, H., Haseman, J., Lefevre, P.A., Wallis, N., Ashby, J., 2002. Normal sexual development of two strains of rat exposed in utero to low doses of bisphenol A. Toxicol Sci **68**, 339-348.

Toraason, M., Clark, J., Dankovic, D., Mathias, P., Skaggs, S., Walker, C., Werren, D., 1999. Oxidative stress and DNA damage in Fischer rats following acute exposure to trichloroethylene or perchloroethylene. Toxicology **138**, 43-53.

United States Environmental Protection Agency, 2011a. Toxicological Review of Trichloroethylene (CAS No. 79-01-6). In EPA), U.S.E.P.A.U.S., (Ed.), Washington, D.C., pp.

United States Environmental Protection Agency, 2011b. Trichloroethylene: CASRN 79-01-6 (IRIS Assessment). In Integrated Risk Information System (IRIS), U.S.E.P.A.U.S.E., (Ed.), Washington, D.C., pp.

United States Environmental Protection Agency, 2020. TRI Explorer: Release Trends Report. In Toxic Release Inventory (TRI) Program, U.S.E.P.A.U.S.E., (Ed.), Washington, D.C., pp.

Uttamsingh, V., Anders, M.W., 1999. Acylase-catalyzed deacetylation of haloalkene-derived mercapturates. Chem Res Toxicol **12**, 937-942.

Uttamsingh, V., Baggs, R.B., Krenitsky, D.M., Anders, M.W., 2000. Immunohistochemical localization of the acylases that catalyze the deacetylation of N-acetyl-L-cysteine and haloalkene-derived mercapturates. Drug Metab Dispos **28**, 625-632.

Vigil-De Gracia, P., Montufar-Rueda, C., Ruiz, J., 2003. Expectant management of severe preeclampsia and preeclampsia superimposed on chronic hypertension between 24 and 34 weeks' gestation. Eur J Obstet Gynecol Reprod Biol **107**, 24-27.

Wallingford, M.C., Benson, C., Chavkin, N.W., Chin, M.T., Frasch, M.G., 2018. Placental Vascular Calcification and Cardiovascular Health: It Is Time to Determine How Much of Maternal and Offspring Health Is Written in Stone. Front Physiol **9**, 1044.

Wang, R., Dang, Y.L., Zheng, R., Li, Y., Li, W., Lu, X., Wang, L.J., Zhu, C., Lin, H.Y., Wang, H., 2014. Live cell imaging of in vitro human trophoblast syncytialization. Biol Reprod **90**, 117.

Werner, M., Birner, G., Dekant, W., 1996. Sulfoxidation of mercapturic acids derived from tri- and tetrachloroethene by cytochromes P450 3A: a bioactivation reaction in addition to

deacetylation and cysteine conjugate beta-lyase mediated cleavage. Chem Res Toxicol **9**, 41-49.

Wilson, M.E., Ford, S.P., 2001. Comparative aspects of placental efficiency. Reprod Suppl **58**, 223-232.

Yuan, J.S., Reed, A., Chen, F., Stewart, C.N., Jr., 2006. Statistical analysis of real-time PCR data. BMC Bioinformatics **7**, 85.

Chapter III. Trichloroethylene Modifies Energy Metabolites in the Amniotic Fluid of Wistar Rats

Abstract

Exposure to trichloroethylene (TCE), an organic solvent with multiple industrial purposes, decreases fetal weight in Wistar rats and is associated with several adverse pregnancy outcomes in epidemiological studies. Altered metabolite abundance in amniotic fluid is also associated with adverse pregnancy outcomes. However, effects of TCE exposure on metabolite abundance in amniotic fluid has not been studied previously to our knowledge. In the current study, timed-pregnant Wistar rats were exposed to TCE via vanilla wafer administration or to vehicle (wafer) alone from gestational day (GD) 6 to 16. Amniotic fluid was collected on GD 16 and analyzed for metabolites important in energy metabolism using a targeted metabolomics platform. Concentrations of the following metabolites decreased in amniotic fluid of dams exposed to TCE regardless of fetal sex: 6-phosphogluconate, guanosine diphosphate, adenosine diphosphate, adenosine triphosphate, and flavin adenine dinucleotide. TCE decreased fructose 1,6-bisphosphate and guanosine triphosphate concentrations in amniotic fluid of male but not female fetuses. Moreover, TCE treatment decreased uridine diphosphate-D-glucuronate concentrations, and increased arginine and phosphocreatine concentrations, in amniotic fluid of female fetuses only. No metabolites were increased in the amniotic fluid of male fetuses. A high concentration of acetate compared to other short-chain fatty acids (SCFAs) was found in the amniotic fluid samples. Pathway analysis revealed that folate biosynthesis and the pentose phosphate pathway were altered by TCE treatment in both sexes. Using metabolite ratios to investigate changes within specific pathways, it was found that some ratio alterations, including

84

those in arginine metabolism and phenylalanine metabolism, occurred in amniotic fluid of female fetuses but not male fetuses. Ratio analysis also identified enzymes, such as gluconokinase, that may be TCE targets. Together, our data suggest that TCE caused some different effects in amniotic fluid based on sex that may inform mechanisms of differential susceptibility to TCE dependent on fetal sex. Future considerations include the detection of additional critical metabolites in pathways, such as folate biosynthesis, to bolster conclusions about specific portions of pathways and use of knowledge from the current study, such as changed metabolites, to inform approaches at modulating TCE toxicity.

Introduction

Trichloroethylene (TCE) is an environmental contaminant commonly used as a metal degreaser and in the synthesis of various chemicals (Agency for Toxic Substances and Disease Registry, 2019). Exposure to TCE is associated with several adverse pregnancy outcomes in women (Rodenbeck *et al.*, 2000; Forand *et al.*, 2012; Ruckart *et al.*, 2014). These adverse pregnancy outcomes include low birth weight (LBW) (Forand *et al.*, 2012), term low birth weight (TLBW) (Forand *et al.*, 2012), small for gestational age (SGA) (Forand *et al.*, 2012; Ruckart *et al.*, 2014), decreased mean birth weight (Ruckart *et al.*, 2014), and very low birth weight (VLBW) (defined as less than 1501 grams) (Rodenbeck *et al.*, 2000). Furthermore, different routes of TCE exposure are associated with distinct adverse pregnancy outcomes: whereas TCE inhalation has been significantly associated with LBW, TLBW, and SGA (Forand *et al.*, 2012), TCE ingestion via drinking contaminated water has been significantly associated with SGA, decreased mean birth weight, and VLBW (Rodenbeck *et al.*, 2000; Ruckart *et al.*, 2014).

Toxicology studies are advancing our understanding of mechanisms that may underlie the TCE associations with adverse pregnancy outcomes. A metabolite of TCE, *S*-(1,2-dichlorovinyl)-L-cysteine (DCVC), stimulates increased reactive oxygen species (ROS) generation (Hassan *et al.*, 2016), pro-inflammatory response (Hassan *et al.*, 2016), and apoptosis in the human placental extravillous trophoblast HTR-8/SVneo cell line (Elkin *et al.*, 2018). Exposure of pregnant rats to TCE (480 mg/kg/day) decreased fetal weight at gestational day (GD) 16 (Loch-Caruso *et al.*, 2019). Additionally, TCE exposure increased expression of oxidative stress markers in placenta of rats in the latter study (Loch-Caruso *et al.*, 2019).

Despite epidemiological studies associating TCE exposure with adverse pregnancy outcomes and toxicological findings suggesting mechanisms by which TCE may contribute to adverse pregnancy outcomes, understanding of the molecular mechanisms by which TCE exposure could lead to adverse pregnancy outcomes remains incomplete. A consideration of a mechanism by which TCE exposure may be toxic is through alteration of metabolites in amniotic fluid, the fluid that bathes the fetus during development. Metabolites in amniotic fluid have not been studied before in the context of TCE or other environmental exposures. However, alteration of amniotic fluid metabolites by environmental exposures could be relevant for pregnancy health.

Ample evidence indicates that the content of amniotic fluid is critical to pregnancy health. Decreased abundance of multiple amino acids, including leucine, valine, methionine, tyrosine, and phenylalanine, were found in amniotic fluid of third trimester versus second trimester patients (Orczyk-Pawilowicz *et al.*, 2016), which highlights the dynamic nature of amino acids in amniotic fluid as pregnancy progresses. Recent studies reported that changes in the concentration of energy metabolism metabolites in amniotic fluid were associated with

preterm birth and other adverse pregnancy outcomes. These associations include decreased amino acids (though increased glutamate), inositol, and pyruvate in second-trimester amniotic fluid in the cases of preterm delivery (Virgiliou *et al.*, 2017). Similarly, Romero *et al.* found a decrease in several amino acids (alanine, proline, glycine, glutamine), several altered carbohydrates, and altered fatty acids (increased oleic acid, decreased palmitic acid, stearic acid, and succinic acid) in amniotic fluid from mid- to late-gestation of preterm delivery cases without infection (Romero *et al.*, 2010). Likewise, Graca *et al.* found decreases in many amino acids, glucose, citrate, and α-oxoisovalerate in amniotic fluid from gestational weeks 16-22 of preterm birth cases (Graca *et al.*, 2013). Additional studies using amniotic fluid from additional gestational time points and using biofluids not limited to amniotic fluid to explore the associations between biofluid metabolites and preterm birth are described in a recent review (Gil and Duarte, 2018).

Changes in aforementioned energy metabolism metabolites are highly relevant to markers of pregnancy health, including ROS generation, pro-inflammatory response, and apoptosis, in placental cells. For example, oleic acid pre-exposure of placental explants decreases IL-6 production (Melody *et al.*, 2015). Additionally, palmitic acid stimulates IL-6 and IL-8 production in Swan 71 placental cells in a caspase-3 and ROS-dependent manner (Shirasuna *et al.*, 2016). Furthermore, oxidative stress decreases neutral amino acid uptake in BeWo placental cells (Araujo *et al.*, 2013). Importantly, in addition to DCVC as a stimulator of ROS, pro-inflammatory (Hassan *et al.*, 2016), and apoptotic responses in placental cells (Elkin *et al.*, 2018), DCVC also stimulates alterations in energy metabolism metabolites in placental cells (Elkin *et al.*, 2020a). Moreover, because ROS, pro-inflammatory response, and apoptosis have relevance to adverse pregnancy outcomes (Al-Gubory *et al.*, 2010; Sharp *et al.*, 2010;

McCullough *et al.*, 2017; Garcia-Flores *et al.*, 2018) and are modifiable by DCVC (Hassan *et al.*, 2016; Elkin *et al.*, 2018), increased possibility exists that changes in metabolites caused by TCE may be relevant to pregnancy.

In the present study, we hypothesize that TCE exposure changes amniotic fluid concentrations of at least several metabolites that have relevance to pregnancy outcomes, focusing on specific portions of energy metabolism pathways altered by TCE. By analyzing metabolite concentrations in amniotic fluid in a pregnant Wistar rat model of fetal weight restriction, we assessed how TCE exposure alters outcomes with relevance to metabolites in energy metabolism and their relevance to pregnancy outcomes.

Materials and Methods

Timed-pregnant Wistar rats

Timed-pregnant Wistar rats were purchased from Charles River Laboratories (Portage, MI) and are a subset of the rats used in Chapter 2. The rats were transported to the University of Michigan School of Public Health animal facility on GD 2, with GD 0 designated as day of copulation. Rats used in this study weighed between 140 and 222 grams on GD 3, the first day the rats were weighed. Rats were individually housed in a 12-hour light/dark cycle controlled environment and fed standard rat chow (Purina 5001) and water *ad libitum*.

Exposures of timed-pregnant Wistar rats

Rats were exposed to trichloroethylene (TCE) (480 mg/kg/day) pipetted onto a vanilla wafer, an exposure method developed by Seegal *et al.* (Seegal *et al.*, 1997). Control rats received vanilla wafer alone. The TCE dosage of 480 mg/kg/day was chosen because similar dosages induce oxidative stress in rats, and 480 mg/kg/day is within an order of magnitude of the United States Occupational Safety and Health Administration Permissible Exposure Level (PEL) for

TCE (Agency for Toxic Substances and Disease Registry, 2007). The dosing regimen is shown in **Figure 3.1**, with GD 16 as the day of euthanasia and tissue collection. These animals were a subset of a larger study (Chapter 2).

Amniotic fluid collection

After euthanasia, the uterine horn of a pregnant rat was excised, and the amniotic fluid was withdrawn using a needle and syringe. Amniotic fluid samples were snap frozen in liquid nitrogen immediately and stored at -80°C until delivery on dry ice to the University of Michigan Metabolomics Core. Amniotic fluid samples were analyzed from one male and one female fetus from each of four dams per treatment for a total of 16 amniotic fluid samples.

Fetal sex determination

Fetal sex was determined through qRT-PCR of placental tissue for the *Sry* gene. Both genomic DNA (gDNA) and RNA were extracted from the placentae. For all samples in this study, fetal sex for our samples was confirmed through both messenger RNA and gDNA. For RNA extraction, placental tissue was stored in RNA later (Qiagen, Germantown, MD) at 4°C overnight, then archived at -80°C without RNA later. To extract RNA, we used the RNeasy Plus Mini kit (Qiagen, Germantown, MD) according to the manufacturer's instructions coupled with use of a FastPrep-24 tissue and cell lyser (MP Biomedicals, Solon, OH) prior to the gDNA elimination step. For DNA extraction, placental tissue was snap frozen in liquid nitrogen then stored at -80°C. DNA was extracted using the NucleoSpin™ Tissue kit (Machery-Nagel, Bethlehem, PA) according to the manufacturer's instructions. Concentration and purity of all nucleic acids were verified using a NanoDrop 2000 UV-Vis Spectrophotometer (Thermo Fisher Scientific, Waltham, MA). Primer sequences for sex-determining region Y (*Sry*) and beta-2

microglobulin (*B2m*) (used as a reference gene) are listed in **Table S3.1**. Reactions and conditions for running and analyzing qRT-PCR are previously described (Chapter 2).

Metabolomics analysis using the tricarboxylic acid plus targeted platform: Sample preparation, LC-MS analysis, and data processing

A 100-µL aliquot of amniotic fluid was transferred to a microtube, and 0.5 mL of a mixture of methanol, chloroform and water (8:1:1) containing isotope-labeled internal standards was added. The mixture was vortexed briefly. Samples were allowed to rest at 4°C for 10 minutes, vortexed a second time, and then centrifuged at 4° C, 14,000 rpm for 10 minutes. The extract was transferred to autosampler vials for mass spectrometry analysis. Aliquots of 10 µL were pooled for each sample and treated identically to individual samples, and the pooled extract was analyzed along with the individual samples for quality control purposes. Calibration standards were prepared and analyzed along with samples to quantify metabolites.

LC-MS analysis was performed on an Agilent system consisting of a 1260 UPLC module coupled with an 6520 Quadrupole-Time-of-flight (QTOF) mass spectrometer (Agilent Technologies, Santa Clara, CA). Metabolites were separated on a 150 x 1 mm Luna NH_2 hydrophilic interaction chromatography column (Phenomenex, Torrance, CA) using 10 mM ammonium acetate in water, adjusted to pH 9.9 with ammonium hydroxide, as mobile phase A, and acetonitrile as mobile phase B. The flow rate was 0.075 mL/min and the gradient was linear 20% to 100% mobile phase A over 15 minutes, followed by isocratic elution at 100% mobile phase A for 5 minutes. The system was returned to starting conditions (20% mobile phase A) in 0.1 minute and held there for 10 minutes to allow for column re-equilibration before injecting another sample. The mass spectrometer was operated in ESI negative mode according to previously published conditions (Lorenz *et al.*, 2011).

Data were processed using MassHunter Quantitative analysis version B.07.00. Metabolites in the glycolysis, tricarboxylic acid (TCA), and pentose phosphate pathways were normalized to the nearest isotope-labeled internal standard and quantitated using two replicated injections of 5 standards to create a linear calibration curve with high accuracy. These compounds were reported in absolute micromolar concentrations. Other compounds in the analysis were normalized to the nearest internal standard, and the peak areas were used for differential analysis between groups. These latter compounds were reported in units of relative response.

Metabolomics analysis using the short chain fatty acid targeted platform: Sample preparation, GC-MS analysis, and data processing

An aliquot of 50 µL of amniotic fluid was transferred to a 15x75 mm glass tube and diluted to 100 µL with 50 µL HPLC grade H_2O. An aliquot of 200 µL of a solution of 30 mM hydrochloric acid plus isotopically-labeled acetate (150 µM), butyrate (10 µM), and hexanoate (2 µM) in water was added to each sample, and then mixed on a vortex mixer for 10 seconds. An aliquot of 300 µL of methyl tert-butyl ether (MTBE) was added to each sample, mixed for 10 seconds to emulsify, held at 4°C for 5 minutes, and then mixed again for 10 seconds. Samples were centrifuged for 1 minute to separate the solvent layers and the MTBE layer was then removed to an autosampler vial for gas chromatography-mass spectrometry (GC-MS) analysis. An aliquot of 10 µL of MTBE was removed from each sample and pooled in a separate autosampler vial for quality control purposes. A series of calibration standards were prepared and analyzed along with samples to quantify metabolites.

GC-MS analysis was performed on an Agilent 69890N GC -5973 MS detector with the following parameters: a 1-µL sample was injected with a 1:10 split ratio on a ZB-WAXplus, 30

m x 0.25 mm x 0.25 µm (Phenomenex Cat#7HG-G013-11) GC column, with He as the carrier gas at a flow rate of 1.1 mL/minute. The injector temperature was 240°C, and the column temperature was isocratic at 310°C.

Data were processed using MassHunter Quantitative analysis version B.07.00. SCFAs were normalized to the nearest isotope labeled internal standard and quantitated using two replicated injections of 5 standards to create a linear calibration curve with high accuracy.

Pathway analysis

Pathway analysis was performed using Metaboanalyst 4.0 (Chong *et al.*, 2018; Chong *et al.*, 2019) and the Rattus Norvegicus (81) selected for the pathway library. All pathways analyzed are stated to be directly in the KEGG database. Additional choices made within the program were as follows: Pathway enrichment analysis (global test as opposed to global ANCOVA); and pathway topology analysis (relative between-ness centrality as opposed to out-degree centrality). Data were generalized log-transformed prior to analysis.

Enrichment analyses

Enrichment analyses for location and drug pathway were performed using Metaboanalyst 4.0 (Chong *et al.*, 2018; Chong *et al.*, 2019). These analyses were not specific to a species. The library for the location enrichment analysis contained 73 metabolite sets pertaining to organ, tissue, or subcellular localization. The library for the drug pathway enrichment analysis contained 461 metabolite sets pertain to drug pathways. Data were generalized log-transformed prior to analysis.

Statistical analysis

An unpaired student's two-tailed t-test was used to assess changes in metabolite concentrations in response to TCE exposure for males and females. Results from this analysis

were most consistent with the results obtained via pathway analysis in which data were split into female and male prior to analysis (i.e., correlation of p-value representing degree of change of a particular metabolite corresponding to p-value magnitude of a particular pathway in which the metabolite is important). With the exception of data involving ratios (fold-change data and data of ratios between two metabolites), which were computed based on the processed data for accuracy, all processed data were generalized log-transformed prior to any analysis given the non-Gaussian distribution of the concentrations and relative responses from the processed data. Pathway and enrichment analyses were conducted using Metaboanalyst 4.0 (Chong *et al.*, 2018; Chong *et al.*, 2019) as described in previous sections. With the exception of the analysis performed by Metaboanalyst 4.0, which automatically computed p-values, statistical analyses were performed using GraphPad Prism 7.0 (GraphPad Software, Inc.; San Diego, CA, USA). For all analyses, a $p<0.05$ was considered statistically significant. P-values computed by Metaboanalyst 4.0 were adjusted for multiple comparisons (Chong *et al.*, 2019) and were similar in magnitude to those computed by GraphPad Prism 7.0.

Results

Quantity of metabolites detected

A total of eight metabolites were detected with the short chain fatty acid (SCFA) platform, and 71 metabolites were detected with the tricarboxylic acid (TCA) plus platform. Each of the following sets of metabolites was detected as an aggregate (i.e., within the set, it was not possible to distinguish one from the other): (1) 2-phosphoglycerate and 3-phosphoglycerate, (2) citrate and isocitrate, (3) fructose 6-phosphate and glucose 6-phosphate, (4) glucose (hexose, etc.), (5) ribose 5-phosphate and xylulose 5-phosphate. Each of these sets was considered as one metabolite in the calculation of total detected metabolites. Additionally, because pathway and

enrichment analyses could not assign such aggregated metabolites to a specific compound, the aforementioned sets were excluded from those analyses. Detected metabolite concentrations or relative responses are listed in **Table S3.2**.

Metabolites in the amniotic fluid altered by TCE exposure

Consistent with the pathway analysis restriction to two-group comparisons, we compared the control and TCE-exposed amniotic fluid results separately for each fetal sex (**Figures 3.2 and 3.3**). TCE exposure significantly altered the abundance of some metabolites, and statistically significant changes were generally associated with a high degree of fold-change (**Figure 3.2**). Most statistically significant alterations were decreases. There was some overlap in the metabolites decreased by TCE in amniotic fluid of male fetuses versus female fetuses, but there were also metabolites decreased in only one sex (**Figure 3.3**). Of the 79 total metabolites, seven were changed in males in response to TCE exposure, and all of these changes were decreases. For females, we detected changes in response to TCE exposure for eight of the 79 total metabolites, and six of the changes were decreases. There were five metabolites that were decreased for both males and females (**Figure 3.3**). The metabolite p-values and fold-change in response to TCE treatment are listed in **Table S3.3**, with metabolites altered by TCE in one or both sexes listed first.

Associations between TCE-stimulated effects on male versus female amniotic fluid

Because some changes stimulated by TCE were detected in amniotic fluid from male fetuses but not amniotic fluid from female fetuses, and vice versa, we analyzed for association of TCE-induced changes in metabolite concentrations between male and female amniotic fluid samples (**Figure 3.4**). In comparison of fold-change of individual metabolite abundances stimulated by TCE in male amniotic fluid samples versus female amniotic fluid samples, a

significant association was observed (p=0.0427 for Spearman correlation), indicating that there was modest association between changes observed in males and females. As depicted in **Figure 3.4**, some metabolites decreased by TCE in males and females (e.g., adenosine diphosphate (ADP) and adenosine triphosphate (ATP)), which appear in the lower left quadrant of the graph and contributed to the positive slope of the best-fit line for the data points, likely drove the associations.

Analysis of pathways altered in male amniotic fluid samples

A total of 54 pathways were able to be analyzed by Metaboanalyst 4.0 from our input data, as shown in **Figure 3.5**. Three pathways were statistically altered by TCE treatment for male amniotic fluid samples (p<0.05). The three pathways were folate biosynthesis, pentose phosphate pathway, and riboflavin metabolism (p=0.015162, 0.019209, 0.022343, respectively). However, the importance of the metabolites detected in these pathways was small (pathway impacts of 0.08974, 0.18522, and 0, respectively), meaning that the changes were not at crucial portions of the pathway despite detection of statistical significance for the pathways. The lowest p-value seen with a pathway impact greater than 0.02 was 0.0835 in the case of the fatty acid elongation pathway. At the other end of the spectrum, the pathway impact associated with the phenylalanine, tyrosine, and tryptophan biosynthesis pathway was 1.0 with an associated p-value of 0.6071.

Analysis of pathways altered in female amniotic fluid samples

For the female amniotic fluid samples, 54 total pathways were able to be analyzed from our input data as shown in **Figure 3.5**, similar to male amniotic fluid samples. Four out of 54 of the pathways were statistically altered by TCE treatment (p<0.05). Riboflavin metabolism (p=0.0269), pentose phosphate pathway (p=0.0310), folate biosynthesis (p=0.0410), and

95

nicotinamide metabolism (p=0.0436) were those four pathways. The pathway impacts for each of

these four pathways were low (impacts of 0, 0.1852, 0.0897, and 0, respectively), and, in general,

few metabolites within each of those pathways were measured. The fifth lowest p-value for a

pathway was 0.1866, the pathway for purine metabolism, and the corresponding pathway impact

was 0.3604. Similar to males, the phenylalanine, tyrosine, and tryptophan biosynthesis pathway

had an associated pathway impact of 1.0 for the female amniotic fluid data, but the

corresponding p-value was 0.38317.

Analysis of ratios between two metabolites to infer at specific portions of pathways impacted

Ratios between metabolites were calculated to infer specific portions of a pathway or

additional measures of biological importance that could be affected by TCE treatment. Ratios of

a metabolite near the beginning of a pathway to a metabolite near the end of the pathway were

also calculated to assess overall change (i.e., could subtleties in specific portions of a pathway

lead to a cumulative change). Lists of the ratios measured and whether or not they were

significantly changed by TCE treatment are shown in **Tables S3.4 through S3.8**, and **Figures**

3.6 through 3.14 display pathways with corresponding metabolite ratios that had statistical

significance for at least one sex. For the males, 11 out of 81 total ratios calculated were altered

by TCE treatment (p<0.05).

A similar analysis of metabolite ratios that had been performed for males was also

performed for females (also included in **Tables S3.4 through S3.8**). Similar to the males, 10 out

of 81 ratios were altered by TCE treatment for females (p<0.05). Five of the ratios were common

between the males and females: (1) arginine to creatine (**Figure 3.6B**), (2) phosphocreatine to

adenosine triphosphate (ATP) (**Figure 3.8B**), (3) creatine to ATP (**Figure 3.8C**), (4) creatine to

adenosine diphosphate (ADP) (**Figure 3.8E**), and (5) gluconate to 6-phosphogluconate (6PG)

(**Figure 3.12B**). Each of the TCE-altered metabolite ratios were in the same direction for both sexes.

Amino acid metabolism as impacted by TCE exposure (ratio analysis)

Within amino acid metabolism pathways, several metabolite ratios in the arginine and proline metabolism pathway were altered in response to TCE treatment (**Figure 3.6, Table S3.4**). These included an increase in the arginine to creatine ratio for males and females (28.8% and 26.3% increase, respectively; p=0.0491 and 0.0147, respectively) (**Figure 3.6B**) and an increase in the arginine to citrulline ratio for females only (67.1% increase, p=0.0345) (**Figure 3.6C**). Relevant to two amino acid pathways (**Figures 3.7A and 3.7B**), the phenylpyruvate to phenylalanine ratio was decreased in females only (10.9% decrease, p=0.0335) (**Figure 3.7C, Table S3.4**).

Further downstream within the arginine and proline metabolism pathway, ratio analysis for the phosphocreatine, ATP shuttling system (**Figure 3.8, Table S3.4**) indicated many more changes in response to TCE exposure. Ratios analyzed in regard to the phosphocreatine, ATP shuttling system included (1) phosphocreatine to ATP (**Figure 3.8B**), (2) creatine to ATP (**Figure 3.8C**), (3) phosphocreatine to ADP (**Figure 3.8D**), (4) creatine to ADP (**Figure 3.8E**) and (5) phosphocreatine to creatine (**Figure 3.8F**). For females, all five of these ratios were altered in response to TCE exposure, and three out of five of these ratios were altered in response to TCE exposure for males. The direction of alteration indicates the increase of phosphocreatine and creatine in comparison to ATP and ADP. The largest fold-change and smallest p-value observed for males came with the creatine to ADP ratio (135.2% increase and p=0.0058 in response to TCE) (**Figure 3.8E**). For the females, the smallest p-value was associated with the creatine to ATP ratio (121.2% increase, and p=0.0023) (**Figure 3.8C**) and the largest fold-

change was associated with the phosphocreatine to ADP ratio (380.4% increase, and p=0.0234) (**Figure 3.8D**).

Purine and pyrimidine metabolism as impacted by TCE exposure (ratio analysis)

Despite the TCE-induced changes observed with adenosine triphosphate (ATP), adenosine diphosphate (ADP), guanosine triphosphate (GTP), and guanosine diphosphate (GDP), only one ratio calculated with relevance to purine or pyrimidine metabolism was altered by TCE exposure (**Figure 3.9, Table S3.5**). The only ratio significantly altered by TCE was GTP to GDP, which was decreased 15.4% in the males (p=0.0208) (**Figure 3.9B**). No ratios detected within the purine or pyrimidine metabolic pathways were altered for the females.

Glycolysis, tricarboxylic acid (TCA) cycle, pentose phosphate pathway, and pyruvate metabolism as impacted by TCE exposure (ratio analysis)

To understand impacts of TCE exposure on specific portions of pathways within glycolysis, TCA cycle, pentose phosphate pathway, and pyruvate metabolism, we calculated ratio of metabolites within each of those pathways (**Figures 3.10, 3.11, 3.12, 3.13, and Table S3.6**). Within the glycolysis pathway (**Figure 3.10 and Table S3.6**), the only significant alteration was a 167.0% increase in males only of the ratio of glucose 6-phosphate and fructose 6-phosphate (early in glycolysis) to acetyl coenzyme A (late in glycolysis) (p=0.0322) (**Figure 3.10B**). This ratio was used to understand if glycolysis as a whole was being affected by TCE treatment.

Relevant to the TCA cycle (**Figure 3.11 and Table 3.6**), TCE treatment decreased the acetyl coenzyme A to citrate and isocitrate ratio in males by 67.2% (p=0.0411) (**Figure 3.11B**). TCE treatment also increased the citrate and isocitrate to malate ratio, a ratio used to assess overall change, in females by 28.1% (p=0.0206) (**Figure 3.11C**). Moreover, TCE treatment

decreased the acetyl coenzyme A to malate ratio in males by 65.3% (p=0.0387) (**Figure 3.11D**), which also has relevance to the pyruvate metabolism pathway.

For the pentose phosphate pathway (**Figure 3.12 and Table 3.6**), TCE treatment increased the gluconate to 6-phosphogluconate ratio in males and females by 58.4% and 73.5%, respectively (p=0.0047 and 0.0166, respectively) (**Figure 3.12B**). In addition, TCA treatment increased the glucose 6-phosphate and fructose 6-phosphate to 6-phosphogluconate ratio and the glyceraldehyde 3-phosphate to erythrose-4-phosphate ratio in males only by 81.1% and 53.7%, respectively (p=0.0310 and 0.0017, respectively) (**Figures 3.12C and 3.12D**, respectively). The acetyl coenzyme A to malate ratio previously discussed is also relevant to the pyruvate metabolism pathway (**Figure 3.13 and Table 3.6**). No other ratios calculated within pyruvate metabolism were significantly changed by TCE treatment for either sex.

Additional metabolite ratios and pathways as impacted by TCE exposure

Table S3.7 contains the ratios calculated with relevance to glutathione metabolism. As shown in **Table S3.8**, some additional ratios between metabolites were calculated. However, none of these metabolite ratios were altered by TCE exposure for males and females. In the case of the folate biosynthesis pathway (**Figure 3.14**) that had significant p-values from Metaboanalyst 4.0 pathway analysis (p=0.0152 and 0.0410 for males and females, respectively), guanosine triphosphate (GTP) was the only metabolite detected in the pathway. GTP was decreased in males but not females in response to TCE treatment (by 31.6%, p=0.0344) (**Figure 3.14B**). Because GTP was the only metabolite detected in the folate biosynthesis pathway, it was not possible to perform analysis of metabolite ratios within that pathway.

Short chain fatty acid (SCFA)-specific analysis

Given the importance of individual and total SCFAs in pregnancy (Priyadarshini *et al.*, 2014; Gray *et al.*, 2017), we performed analyses specific to SCFAs. Consistent with analyses performed specifically for SFCAs (Demehri *et al.*, 2016), we investigated TCE effects on total SCFA concentration and the contribution of each SCFA to total SCFA by experimental group (**Figure S3.1**). In our amniotic fluid samples, total SCFA concentration (consisting of the total of acetate, propionate, butyrate, isovalerate, valerate, hexanoate, heptanoate, and octanoate concentrations) was not altered by TCE treatment for either males or females. However, an unexpected finding was the substantial contribution of acetate to total SCFA concentration for all our experimental groups. Specifically, acetate contributed an average of 89.7%, 87.2%, 87.1% and 89.5% of SCFAs for the control male, control female, TCE male, and TCE female experimental groups, respectively. These values are high compared to other studies looking at composition of acetate relative to other SCFAs (Weaver *et al.*, 1988; den Besten *et al.*, 2013; den Besten *et al.*, 2014; Demehri *et al.*, 2016; Hashemi *et al.*, 2017).

Enrichment analysis to analyze organs, tissues, or subcellular structures affected by TCE exposure

For both male and female samples, our input data allowed for the analysis of 30 organs, tissues, or subcellular structures as impacted by TCE based on the TCE effects on metabolites (**Tables S3.9 and S3.10**). For males (**Table S3.9**), only the thyroid gland was statistically significant (p=0.0361); the second lowest p-value was 0.0598 in the case of endoplasmic reticulum. Interestingly, placenta had a p-value of 0.3220. For females (**Table S3.10**), only the gonad achieved statistical significance (p=0.0454), and the second lowest p-value was 0.0870 for skin. Placenta had the highest p-value (ranked 30/30) in this set at p=0.7912.

Enrichment analysis to analyze drug pathways altered by TCE exposure

Our input data of metabolites led to 352 drug pathways analyzed for statistical significance for both male and female samples based on the TCE effects on metabolites (**Tables S3.11 and S3.12**). For males (**Table S3.11**), 243 drug pathways had a $p<0.05$. The lowest p-value associated with a drug pathway was 0.00014, which was for the acetaminophen metabolism pathway. The following eight pathways tied for the second lowest p-value (0.00019): codeine action pathway, etoposide action pathway, etoposide metabolism pathway, irinotecan action pathway, irinotecan metabolism pathway, morphine action pathway, mycophenolic acid metabolism pathway, and tramadol metabolism pathway. For females (**Table S3.12**), 244 drug pathways had a $p<0.05$. Four pathways were tied for the lowest p-value in this data set (0.0014); these pathways were the glibenclamide action pathway, the gliclazide action pathway, the nateglinide action pathway, and the repaglinide action pathway.

Discussion

The current study, using a pregnant rat model, is the first to our knowledge to investigate amniotic fluid metabolomics with a known environmental exposure, trichloroethylene (TCE). Changes in the abundance of metabolites, including amino acids and sugars, in amniotic fluid have been associated with preterm birth in humans (Romero *et al.*, 2010; Menon *et al.*, 2014; Huang *et al.*, 2017; Virgiliou *et al.*, 2017; Gil and Duarte, 2018). Although these human studies provide supportive evidence that amniotic fluid metabolite composition is important to pregnancy, such studies are often challenged by the lack of environmental exposure data, requiring inferences as to potential environmental causes of the altered metabolites in amniotic fluid. Thus, the current study addresses a knowledge gap by investigating TCE-stimulated outcomes that may be relevant to pregnancy health.

Metabolites altered in amniotic fluid by maternal exposure to TCE

We have shown that TCE exposure in pregnancy modified metabolite concentrations in the amniotic fluid of Wistar rats. The changes in amniotic fluid metabolite concentrations were different depending upon the sex of the placenta and fetus. Some metabolites were altered for female only, some were altered for male only, and some were altered in both sexes. Interestingly, the majority of alterations were decreases in response to TCE exposure, with only two increases observed in females only. Purine multi-phosphates, e.g., guanosine triphosphate (GTP), guanosine diphosphate (GDP), adenosine triphosphate (ATP), and adenosine diphosphate (ADP), were altered by TCE exposure, highlighting TCE alteration of the amniotic fluid energy supply.

The finding that TCE decreased GDP, ATP, and ADP in both sexes and GTP in males only is generally consistent with other studies that investigated TCE effects on the purine multi-phosphate metabolites. In kidney cells, a metabolite of TCE, *S*-(1,2-dichlorovinyl)-L-cysteine (DCVC), decreases ATP levels, albeit at relatively high concentrations (Lash and Anders, 1986; Lash and Anders, 1987). It is noteworthy that the DCVC effect in the latter study occurred intracellularly whereas the TCE-induced change in the present study occurred extracellularly in the amniotic fluid. Mapping the relevance of this extracellular change to an intracellular change is a worthy future direction that may be accomplished by fluxomics not limited to amniotic fluid. A study showed that TCE increases Rho GDP-dissociation inhibitor 1 in human L-02 liver cells (Liu *et al.*, 2007), suggesting a potential upstream mechanism by which TCE exposure may impact purine multi-phosphates. Additional experiments beyond the scope of the present study will be required to advance understanding of the mechanism and relevance to pregnancy. Furthermore, deciphering mechanisms by which altered multi-phosphates do not impact amino acid abundance, which is generally observed in the current study, remain currently unknown.

Arginine and proline metabolism as modified by TCE exposure

An interesting finding from the analysis of metabolite ratios was the impact of TCE on arginine and proline metabolism. Multiple ratios with relevance to arginine and proline metabolism were altered by TCE, with more alterations in the females than the males. According to the KEGG pathway for rats, three metabolites of arginine include citrulline, ornithine, and creatine (via upstream conversion to guanidinoacetic acid). Our data indicate that TCE exposure reduced the conversion of arginine to citrulline in the females and that the conversion of arginine to creatine was reduced in both sexes. Future experiments could focus on the impact of TCE on the enzymology in these steps or investigation of TCE exposure on guanidinoacetic acid itself. Another metabolite of arginine is N-(omega)-hydroxyarginine, which can be converted to nitric oxide. Nitric oxide is a vasodilator, and the role of L-arginine in vasodilation is the basis for its use as a treatment for preeclampsia (Aouache *et al.*, 2018). By suppressing the metabolism of arginine into citrulline (females only) and creatine (both sexes), TCE may favor the metabolism of arginine into N-(omega)-hydroxyarginine. The impact of TCE on N-(omega)-hydroxyarginine and nitric oxide in amniotic fluid remain worthy future directions.

Phosphocreatine shuttling as a phenomenon modified by TCE exposure

Metabolite ratios within phosphocreatine shuttling (Meyer *et al.*, 1984) were also discovered to be changed by TCE exposure. In both sexes, TCE stimulated an abundance of phosphocreatine and creatine relative to the adenosine multi-phosphates (ATP, ADP). The abundance of phosphocreatine is most pronounced in females. In regards to pregnancy, extracellular ATP decreases spiral artery remodeling and is known as a vasoconstrictor (Spaans *et al.*, 2014a; Spaans *et al.*, 2014b). A decreased phosphocreatine:ATP ratio, opposite to what occurred in both sexes seen in this study, has been investigated extensively in heart and is linked

to worsening energetics and lipotoxicity (Scheuermann-Freestone *et al.*, 2003; Shivu *et al.*, 2010). Study of phosphocreatine shuttling also extends to many organs with high energy demand (e.g., brain and skeletal muscle) (Wallimann *et al.*, 1992), similar to the demand experienced by a developing fetus. Prior studies on the implications to pregnancy of phosphocreatine shuttling mainly focus on creatine, which the placenta is capable of synthesizing (Ellery *et al.*, 2017). For example, increased birthweight and birth length are associated with higher maternal urinary creatine (Dickinson *et al.*, 2016). Additionally, creatine has been proposed to benefit the fetus, acting on multiple potential mechanisms that include acid-base balance, antioxidant defense, and protein synthesis (Dickinson *et al.*, 2014). In totality, it would seem that the impact of TCE on the phosphocreatine shuttling system signals an adaptive response that would be beneficial for pregnancy.

Glycolysis, tricarboxylic acid (TCA) cycle, pentose phosphate pathway, and pyruvate metabolism as altered by TCE exposure

We detected sex-specific TCE-induced changes in the glycolysis, TCA cycle, pentose phosphate, and pyruvate metabolism pathways. Although few in number, several of the changes are notable. The overall conversion from acetyl coenzyme A to citrate and isocitrate (both upstream metabolites in TCA cycle) was increased in the case of males, whereas the conversion of citrate and isocitrate (early in TCA cycle) to malate (late in TCA cycle) was decreased in the case of females. Pregnancy progression is accompanied by increased production of energy via the TCA cycle (Lindsay *et al.*, 2015), and our data within females suggest that hampered progression of the TCA cycle could partially explain the purine multi-nucleotide findings of decreased abundance. Whether that is manifest in abnormalities as pregnancy progresses further has yet to be seen. Because acetyl coenzyme A and malate are both involved in pyruvate

metabolism, it is plausible that other metabolites within pyruvate metabolism could be changed by TCE but were not detected in the current study. Examples of such metabolites include S-acetyldihydrolipoamide-E, pyruvate, and oxaloacetate (**Figure 3.13**).

The ratio of gluconate to 6-phosphogluconate was increased by TCE in both sexes, which is interesting because of the importance of both metabolites in the pentose phosphate pathway. Gluconate is converted to 6-phosphogluconate via gluconokinase (Cohen, 1951). In light of our finding, the effect of TCE on gluconokinase in tissues surrounding amniotic fluid (e.g., placenta or fetus) is a topic of worthy consideration and could be relevant to pregnancy given that gluconokinase activity is detected in fetal rat and sheep (Ballard and Oliver, 1964). The concentration of 6-phosphogluconate was decreased in amniotic fluid of both sexes, as well. The impact of 6-phosphogluconate has scarcely been studied in the context of pregnancy. Future studies beyond the scope of the present study could explore whether the TCE-induced decrease in 6-phosphogluconate concentrations are detrimental for pregnancy outcomes.

Folate biosynthesis as impacted by TCE exposure

Within the folate biosynthesis pathway, guanosine triphosphate (GTP) was the only metabolite detected. Because the TCE-stimulated change in GTP was a decreased concentration for males ($p=0.0344$) and approached statistical significance for females ($p=0.0539$), and because GTP is upstream in the folate biosynthesis pathway, a worthy future direction could be to detect metabolites downstream of GTP to see if this decrease persists for downstream metabolites such as folic acid, and to determine if both sexes are affected. Such future work is critical because folic acid is important to pregnancy and fetal development (Higgins and Mc Auliffe, 2010; Laanpere *et al.*, 2010; Ly *et al.*, 2016; Wen *et al.*, 2016). If folic acid were to decrease in amniotic fluid to a larger extent for male fetuses compared to female fetuses with

105

maternal exposure to TCE, it could be possible that folic acid could serve as a mechanism by which TCE could be more deleterious to males than females, such as seen in Chapter 2 with fetal weights.

Effects of TCE exposure on other amino acid metabolism pathways and other metabolite ratios

An additional metabolite ratio changed within amino acid metabolism pathways is the phenylpyruvate to phenylalanine ratio. This ratio represents consecutive metabolites in phenylalanine metabolism and phenylalanine, tyrosine, and tryptophan biosynthesis (**Figure 3.7**). In females, TCE decreased phenylpyruvate relative to phenylalanine, an effect not seen in the males and relevant to pregnancy outcomes. Because decreased phenylalanine has been associated with preeclampsia (Bahado-Singh *et al.*, 2012; Bahado-Singh *et al.*, 2015), the direction of change produced by TCE in the present study could indicate a protective response against a pregnancy adverse outcome. It remains worthy to investigate if this response could explain the decreased susceptibility of female fetuses to TCE-induced decreased fetal weight compared to male fetuses, as reported in Chapter 2 in this dissertation. Additionally, because phenylalanine and phenylpyruvate are consecutive metabolites in the aforementioned amino acid pathways, it is plausible that TCE could target D-amino acid dehydrogenase (Olsiewski *et al.*, 1980) or L-amino-acid oxidase (Wellner and Meister, 1960a; Wellner and Meister, 1960b), both of which can convert phenylalanine to phenylpyruvate.

Our finding that purine multi-phosphates (e.g., ATP, GTP) were changed by TCE exposure but that ratios involving these metabolites were largely unchanged could have several explanations. Firstly, this could suggest that TCE exposure does not impact the enzymes involved in the conversion between the different purine phosphate species (e.g., CD39, CD73,

106

and alkaline phosphatase) (Spaans *et al.*, 2014a), but rather that the changes in purine

multiphosphate abundance more likely result from pathways that supply ATP or GTP such as the

TCA cycle. Consistent with the latter explanation, we observed TCE-altered metabolite ratios

within the TCA cycle of decreased acetyl coenzyme A to malate in males and increased citrate

and isocitrate to malate in females. As a whole, it may be that TCE exposure diminishes the

quantity of select metabolites within purine metabolism without impacting the pathway in

totality. Additionally, the lack of TCE-stimulated changes we observed in metabolite ratios

within pyrimidine metabolism in conjunction with the lack of significant changes in the

metabolites themselves (e.g., uridine diphosphate and cytidine monophosphate) may indicate that

TCE exposure is unlikely to use pyrimidine metabolism as a mechanism of toxicity.

Analysis of effects of TCE exposure on short chain fatty acids (SCFAs) and composition

In our SCFA-specific analysis, our findings make sense in light of the functions of

SCFAs. No SCFAs individually or in totality were changed in response to TCE exposure,

suggesting that TCE does not alter SCFAs as a mechanism of toxicity relevant to adverse

pregnancy outcomes. A prior epidemiological study associated the abundance of SCFAs in

maternal serum with pregnancy outcomes, including newborn weight and length (Priyadarshini

et al., 2014), supporting the relevance of SCFAs to pregnancy. Regardless, the composition of

SCFAs in the amniotic fluid at the time of rat euthanasia in each of our treatment groups was

striking. Acetate contributed to nearly 90% of total SCFA composition for all experimental

groups. Although these values are higher than previously published reports of acetate

composition of SCFAs (Weaver *et al.*, 1988; den Besten *et al.*, 2013; den Besten *et al.*, 2014;

Demehri *et al.*, 2016; Hashemi *et al.*, 2017), the high percentage of acetate makes sense in the

light of the purpose of amniotic fluid during pregnancy. Specifically, acetate is known to be

produced during fasting, regulates energy homeostasis, contributes to heat production, and its metabolism is predictive of lifespan (Shimazu *et al.*, 2010; Schonfeld and Wojtczak, 2016). With respect to pregnancy, acetate provision to mother during pregnancy protects mouse offspring from airway disease later in life (Thorburn *et al.*, 2015). Thus, our finding that acetate is highly abundant compared to other SCFAs in amniotic fluid suggests that acetate may serve an important function.

Limitations and benefits of use of pathway analysis and enrichment analyses as use for studying TCE-stimulated changes in amniotic fluid

A limitation to the current study is that a few inputs into the analyses done on Metaboanalyst 4.0 were not able to be mapped into the pathway and enrichment analysis. This applied for glyceraldehyde 3-phosphate and D-sedoheptulose 7-phosphate, in which the program matched its KEGG ID to one of its KEGG IDs but one that was not in the pathway itself. We tried other alternatives, including entry by KEGG ID as opposed to metabolite name, to attempt to successfully get all of the metabolites to match. Using the metabolite names as entry brought us closest to a match for each metabolite, with glyceraldehyde 3-phosphate and D-sedoheptulose 7-phosphate, as mentioned previously, as the only metabolites that were not matched successfully. Therefore, the results presented with Metabolanalyst 4.0 (Pathway Analysis and Enrichment Analyses) have to be interpreted as if glyceraldehyde 3-phosphate or D-sedoheptulose 7-phosphate were not measured at all. Additionally, because aggregates of metabolites (e.g., citrate versus isocitrate) could not be entered into pathway or enrichment analyses on Metaboanalyst 4.0, the results from these analyses have to be interpreted as if we have no knowledge about the aggregates, as well. Hence, to partially address these issues and also learn if specific regions of pathways were impacted, we manually selected and calculated

ratios of metabolites in specific pathways. However, the ability to decipher between different metabolites in an aggregate (e.g., citrate versus isocitrate) would aid interpretation and may contribute additional insights. Increasing the quantities of metabolites detected and standardizing to absolute concentrations remain outstanding important work. It is also possible that an increase in sample size could allow detection of additional significant metabolites. Finally, we cannot rule out possibility of contamination of other fluids with the amniotic fluid.

Nevertheless, Metaboanalyst 4.0 results provided insights in line with consequences important in pregnancy and literature on TCE exposure. Regarding enrichment analysis, TCE-stimulated changes in male amniotic fluid could have implications to thyroid as an organ based on statistical significance. Possible explanations for this latter finding include pregnancy susceptibility to changes in thyroid-related metabolism (Lieutaud et al., 1999) and association of TCE exposure with benign thyroid disease (but not thyroid cancer) (Axelson *et al.*, 1994; Lynge *et al.*, 1997; Wingren and Axelson, 1997; Wartenberg *et al.*, 2000; Lope *et al.*, 2009). Similarly, TCE has been found to be toxic to ovaries (Henschler *et al.*, 1980; Wu and Berger, 2007; Wu and Berger, 2008) and testes (Kumar *et al.*, 2001; Forkert *et al.*, 2002), consistent with our enrichment analysis finding that TCE-stimulated female amniotic fluid changes could have implications to gonads as a structure based on statistical significance. The enrichment analysis featuring drug metabolism pathways allowed for initial identification and hypotheses generation about how drug metabolism, such as acetaminophen metabolism, could be altered by TCE during pregnancy. Finally, as expected, Metaboanalyst 4.0 pathway analysis resulted in the identification of statistically significant KEGG pathways that involve metabolites changed by TCE exposure, such as GTP in the case of male amniotic fluid samples.

Conclusion

In summary, although TCE exposure did not elicit many changes with known relevance to adverse pregnancy outcomes, our data provide insight about potential mechanisms that could explain TCE toxicity in pregnancy. In general, we found that TCE exposure decreased purine multiphosphates (e.g., ATP, GTP, GDP), highlighting the impact of TCE on direct cellular energy supply that is critical for pregnancy health. Several molecules or metabolite ratios that were altered in amniotic fluid of one fetal sex but not the other also give indication about potential mechanisms by which female fetuses could be more resistant to TCE toxicity compared to males. **Figure 3.15** depicts an overall level of change TCE could have through multiple energy metabolism pathways and shows the region around folate biosynthesis as worthy of further investigation. Importantly, the current study indicates that some changes stimulated by TCE have relevance to adverse pregnancy outcomes such as preeclampsia. Worthy future directions include understanding how some changes to specific portions of the pathways are related to other portions of the pathways, use of the discoveries in the current study to inform methods of modulating TCE toxicity possibly through enzyme modulation, and application of such techniques to other environmental contaminants of interest to evaluate how amniotic fluid could be receptive to change by toxicants beyond TCE. Finally, because some of the metabolite changes included amino acids that could be found in diet, such as arginine, the current study could also be suggestive of potential specific nutritional recommendations to modulate TCE-stimulated toxicity.
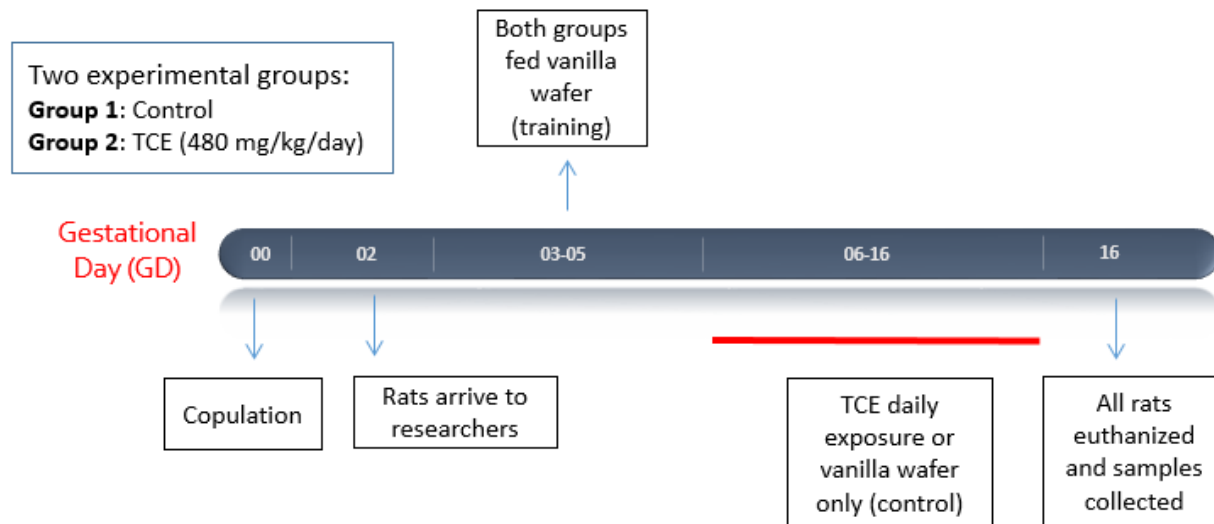
Figure 3.1. Treatment schedule of the timed-pregnant Wistar rats used in the current study. With gestational day (GD) 0 designated as day of copulation, rats arrive on GD 2, are first trained to eat the vanilla wafer on GD 3, and are euthanized on GD 16. The following dosage of TCE was used: 480 mg/kg/day. These rats are a subset of the rats used in Chapter 2 of this dissertation.
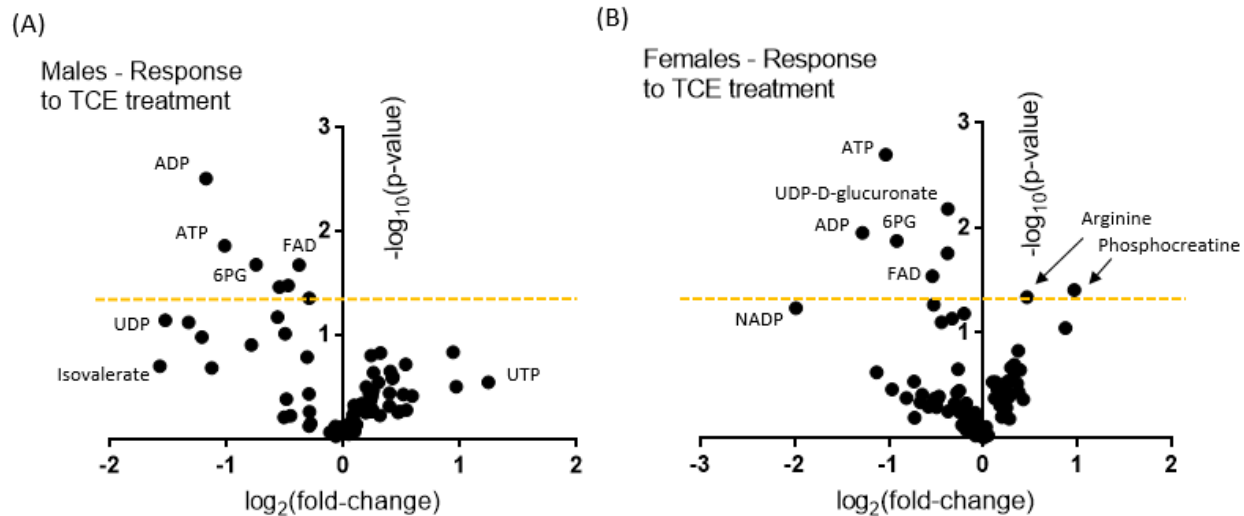
Figure 3.2. Volcano plots displaying the negative[log₁₀(p-value)] as a function of the log₂(fold-change) for each individual metabolite displayed as dots in the control to TCE-treated comparison for each sex. Individual graphs correspond to the display for the effect of TCE on (A) males and (B) females. Individual points correspond to individual metabolites detected, and the gold-dashed lines correspond to the threshold of p=0.05 (approximately where y=1.3 on each graph).
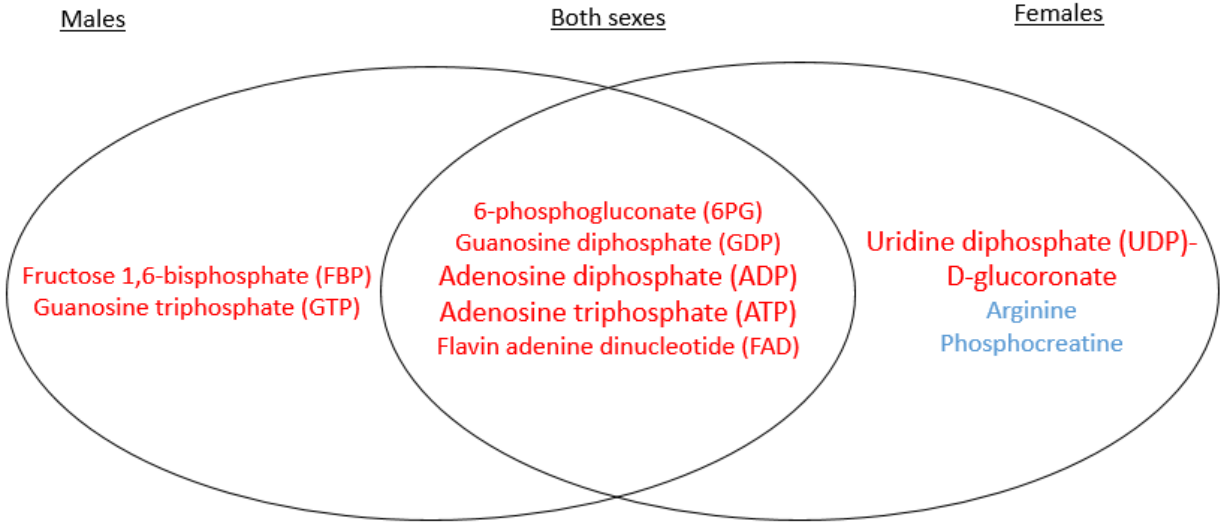
Figure 3.3. Summary of specific metabolites significantly altered by trichloroethylene in amniotic fluid for each sex. Metabolites highlighted in blue or red indicate metabolites increased or decreased, respectively, in response to TCE treatment. All metabolites in smallest font are $p<0.05$ for all associated control to TCE comparisons and metabolites in larger font are $p<0.01$ for one control to TCE comparison (in the case of ADP, $p<0.01$ for males while $p<0.05$ for females; in the case of ATP, $p<0.01$ for females while $p<0.05$ for males).
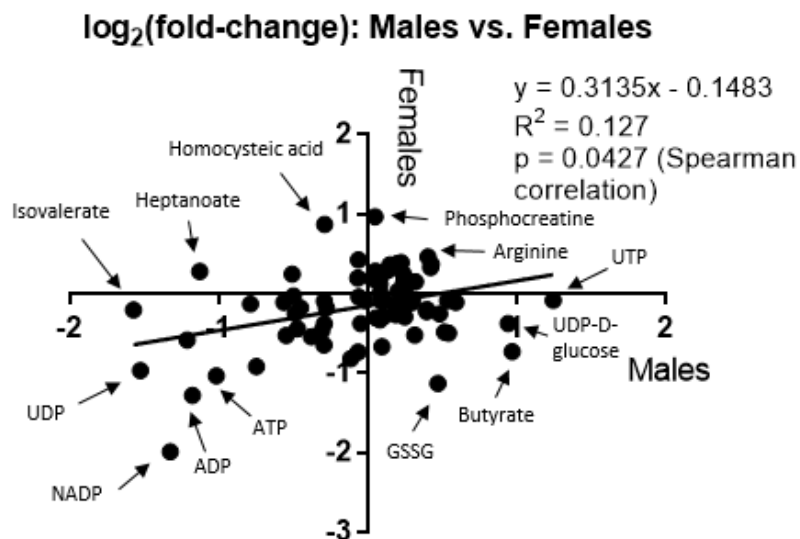
Figure 3.4. Scatterplot showing association between males and females of metabolite fold-changes in response to TCE. X and Y-axes are in units of $\log_2$(fold-change), and individual data points represent individual metabolites detected in amniotic fluid of male and female fetuses. Based on the visualization and Spearman correlation p-value, there is a modest association between the effects seen in males and effects seen in females.
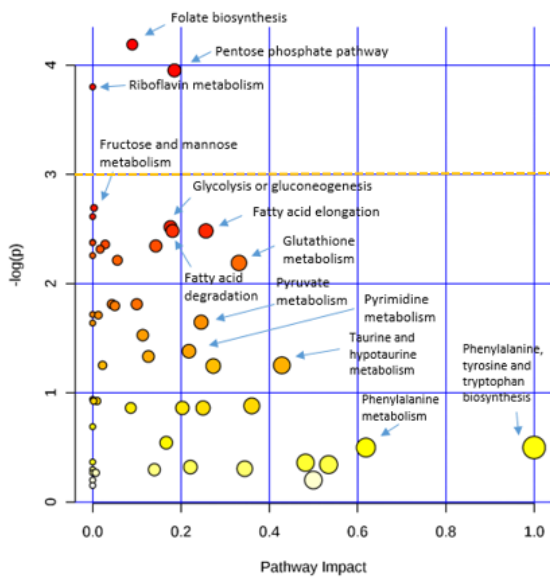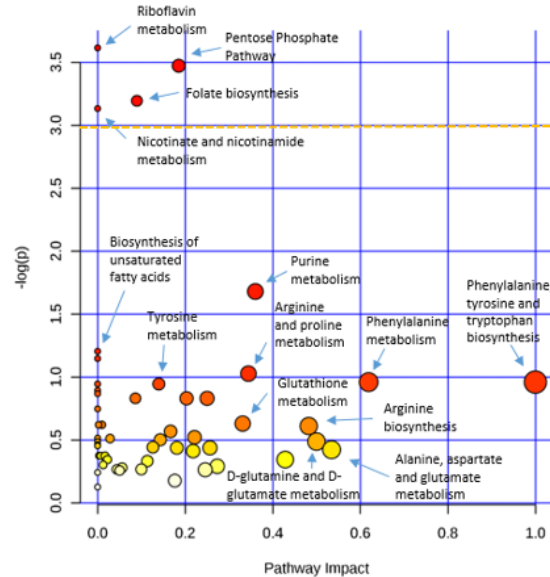
Figure 3.5. Pathway analysis performed by Metaboanalyst 4.0 to reveal changes in KEGG pathways altered by trichloroethylene treatment in (A) males and (B) females. Pathway analysis (specific for *Rattus norvegicus*) was performed by Metaboanalyst 4.0 on the processed data as input into analysis. Generalized log-transformation was performed on the data prior to analysis to achieve normal distribution. Individual circles represent different KEGG pathways. The circle color corresponds to significance of the pathway (white to red in order of increasing significance) whereas circle size corresponds to pathway impact, which is calculated as the matched metabolites as a cumulative percentage contributing to total pathway importance. A horizontal yellow dashed line is put where negative(log(p))=3, which corresponds to a p=0.05 under the $\log_e$ (or ln) scale used in this analysis.

115

(A)
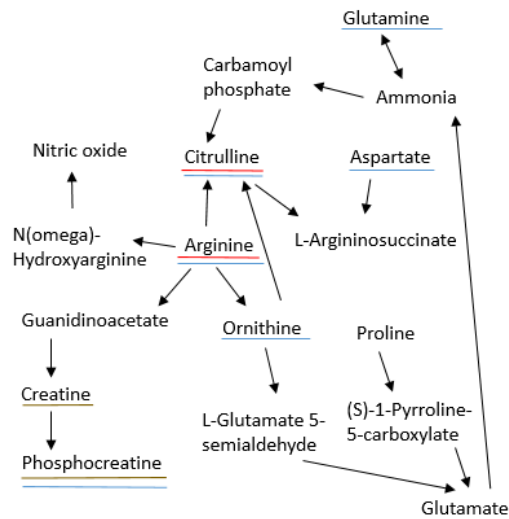
(B)
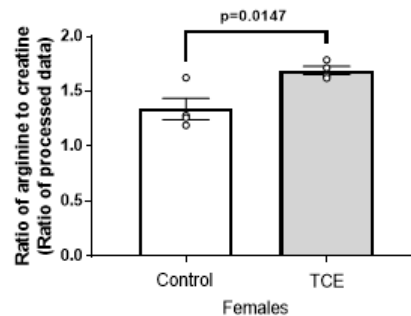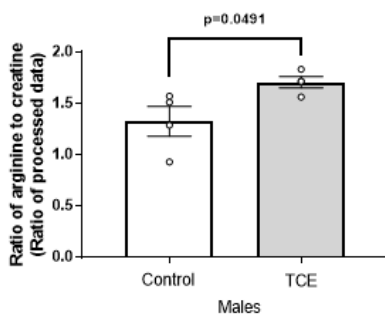
(C)
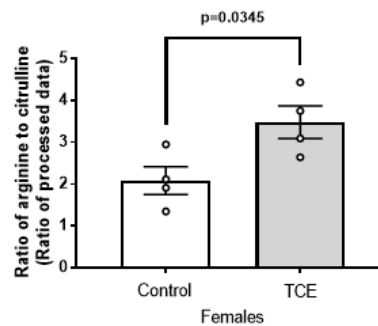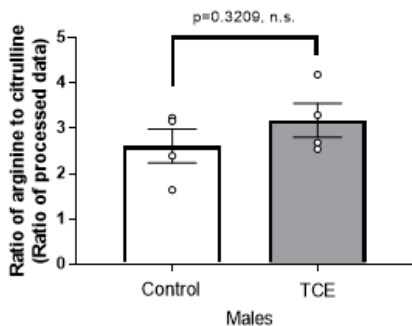
Figure 3.6. Arginine and proline metabolism as modified by trichloroethylene (TCE) treatment in male and female amniotic fluid. (A) Simplified depiction of the purine metabolism KEGG pathway in *Rattus norvegicus*. Metabolites underlined in red correspond to metabolites that are part of ratio altered by TCE treatment in both males and females. Metabolites underlined in dark gold correspond to metabolites that are part of a ratio altered by TCE in females only. Metabolites underlined in blue correspond to metabolites that were analyzed in ratio analysis but not altered by TCE treatment in any sex. Depiction of effects TCE treatment in males and females on (B) the arginine to creatine ratio and (C) the arginine to citrulline ratio. Graphs for the phosphocreatine to creatine ratio are in **Figure 3.8F**. Error bars

116

represent mean ± SEM. Statistical analysis for each sex consisted of a two-tailed unpaired t-test. N= 4 independent experiments.
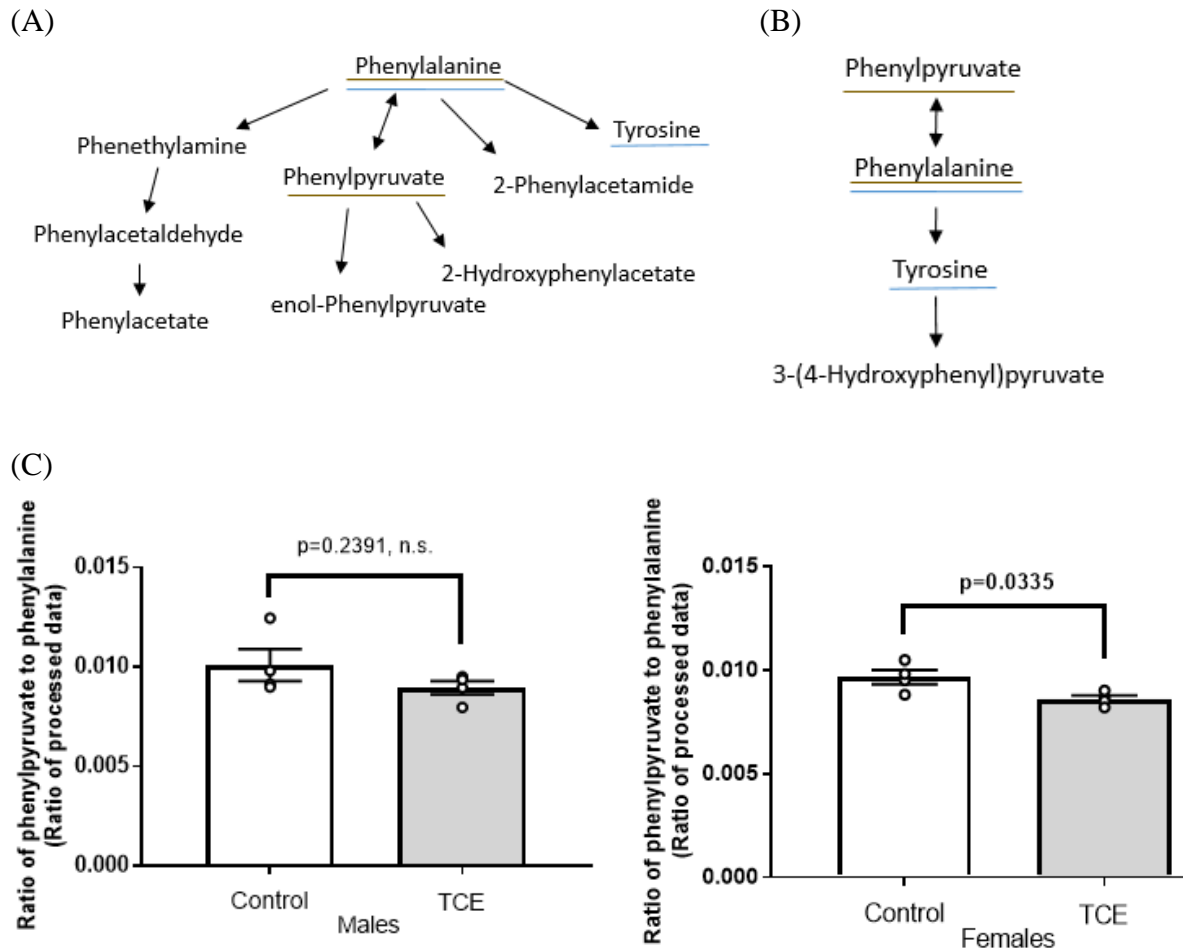
Figure 3.7. Phenylalanine metabolism and phenylalanine, tyrosine, and tryptophan biosynthesis as modified by trichloroethylene (TCE) treatment in male and female amniotic fluid. Simplified depiction of the (A) phenylalanine metabolism KEGG pathway and (B) phenylalanine, tyrosine, and tryptophan biosynthesis pathway in *Rattus norvegicus*. Metabolites underlined in dark gold correspond to metabolites that are part of a ratio altered by TCE in females only. Metabolites underlined in blue correspond to metabolites that were analyzed in ratio analysis but not altered by TCE treatment in any sex. Depiction of effects TCE treatment in males and females on (C) phenylpyruvate to phenylalanine ratio. In the graphs, error bars represent mean ± SEM. Statistical analysis for each sex consisted of a two-tailed unpaired t-test. N= 4 independent experiments.

(A)

(B)

(C)

(D)

(E)

119
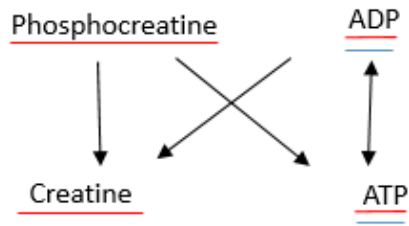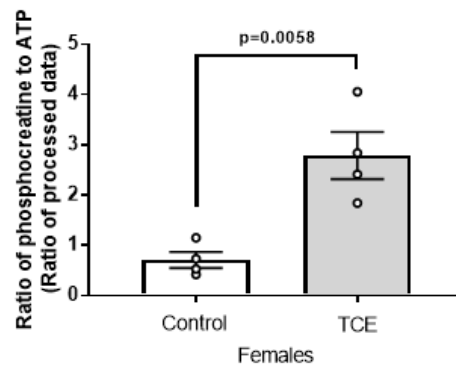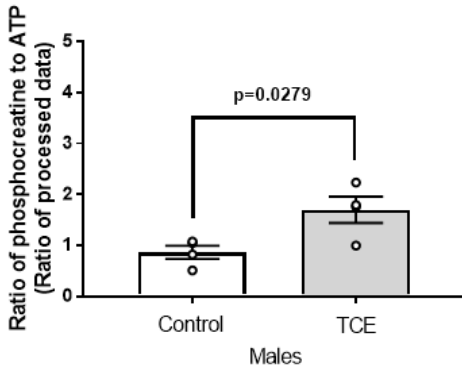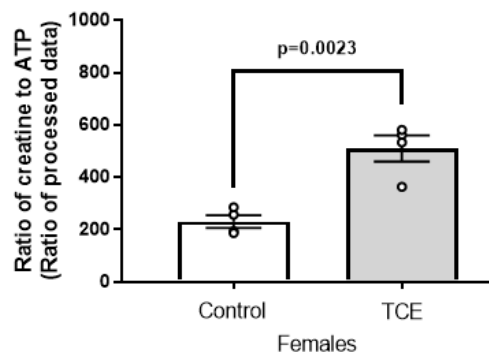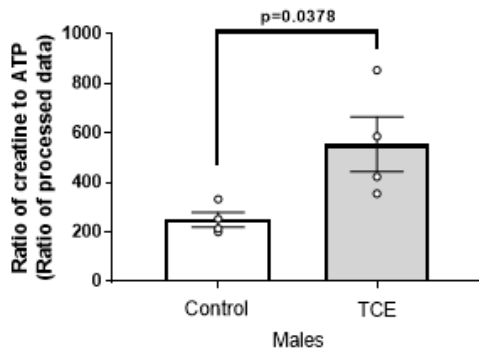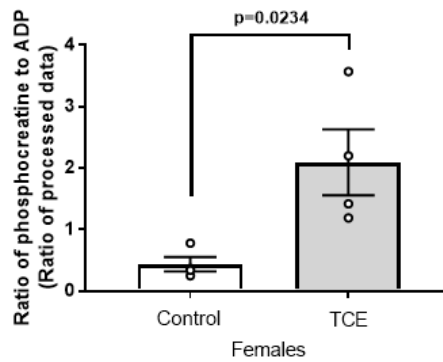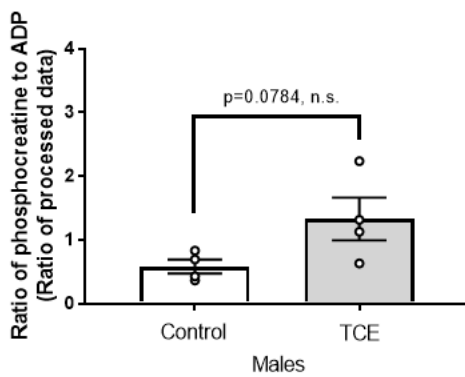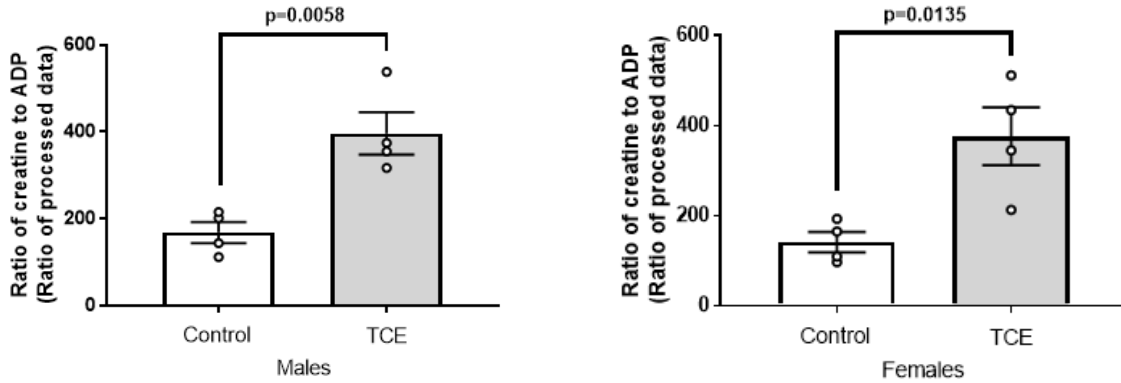
(F)
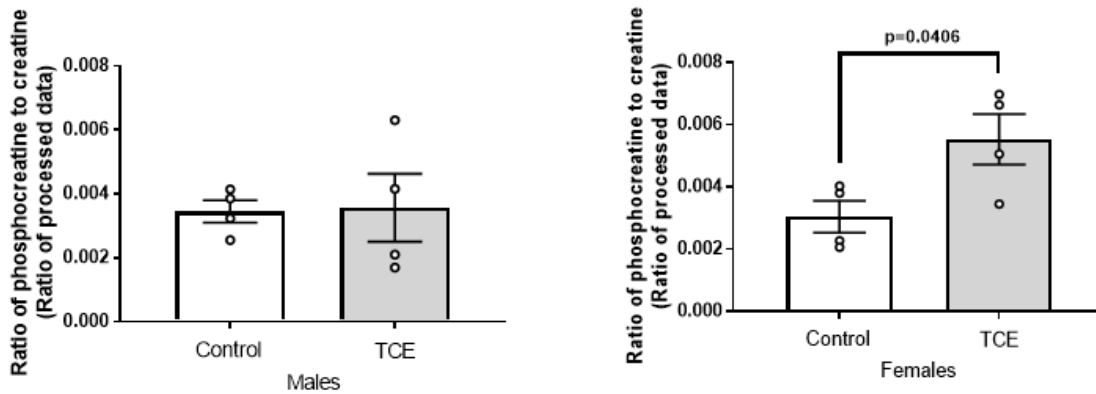
Figure 3.8. Phosphocreatine shuttling as modified by trichloroethylene (TCE) treatment in male and female amniotic fluid. (A) Simplified depiction of extracellular phosphocreatine shuttling. Metabolites underlined in red correspond to metabolites that are part of ratio altered by TCE treatment in both males and females. Metabolites underlined in blue correspond to metabolites that were analyzed in ratio analysis but not altered by TCE treatment in any sex. Depiction of effects TCE treatment in males and females on (B) the phosphocreatine to ATP ratio, (C) the creatine to ATP ratio, (D) the phosphocreatine to ADP ratio, (E) the creatine to ADP ratio, and (F) the phosphocreatine to creatine ratio. (F) is also relevant to **Figure 3.6**. In the graphs, error bars represent mean ± SEM. Statistical analysis for each sex consisted of a two-tailed unpaired t-test. N= 4 independent experiments. Abbreviations: ATP, adenosine triphosphate; ADP, adenosine diphosphate.

(A)

(B)
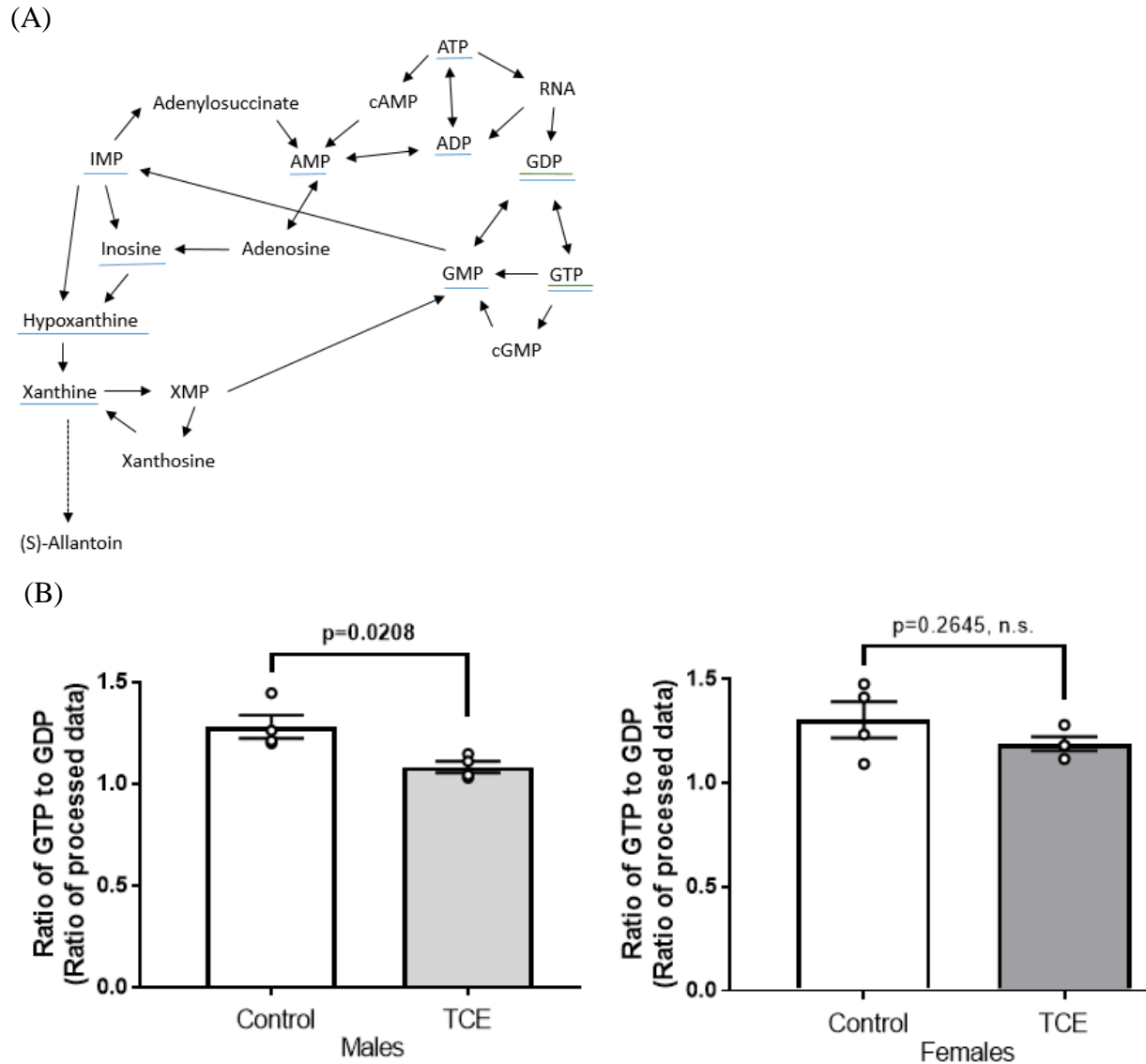
Figure 3.9. Purine metabolism as modified by trichloroethylene (TCE) treatment in male and female amniotic fluid. (A) Simplified depiction of the purine metabolism KEGG pathway in *Rattus norvegicus*. Metabolites underlined in green correspond to metabolites that are part of ratio altered by TCE treatment in males only. Metabolites underlined in blue correspond to metabolites that were analyzed in ratio analysis but not altered by TCE treatment in any sex. Depiction of effects TCE treatment in males and females on (B) the GTP to GDP ratio. In the graphs, error bars represent mean ± SEM. Statistical analysis for each sex consisted of a two-tailed unpaired t-test. N= 4 independent experiments. Abbreviations: IMP, inosine monophosphate; XMP, xanthine monophosphate; AMP, adenosine monophosphate; cAMP, cyclic AMP; ADP, adenosine diphosphate; ATP, adenosine triphosphate; RNA, ribonucleic acid; GDP, guanosine diphosphate; GTP, guanosine triphosphate; GMP, guanosine monophosphate; cGMP, cyclic GMP.

(A)
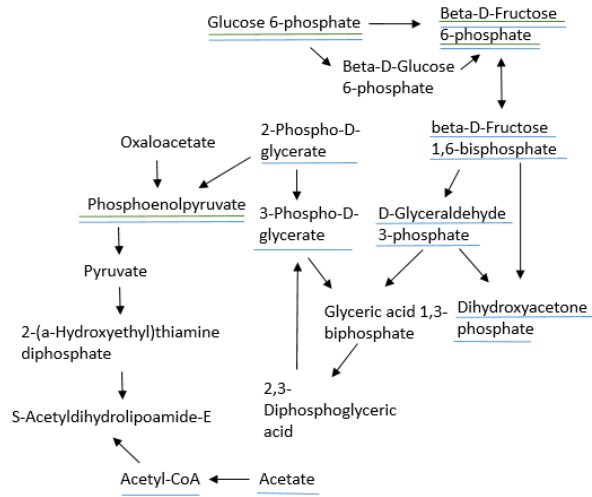
(B)
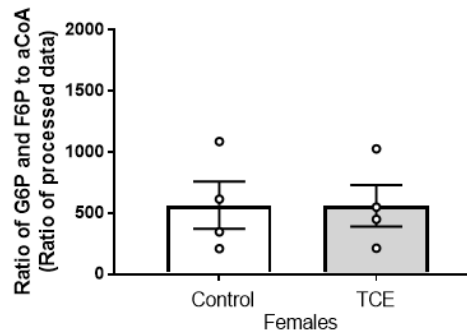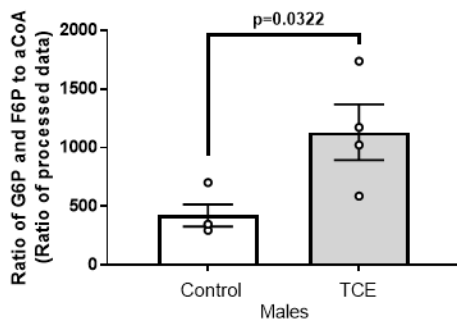
(C)
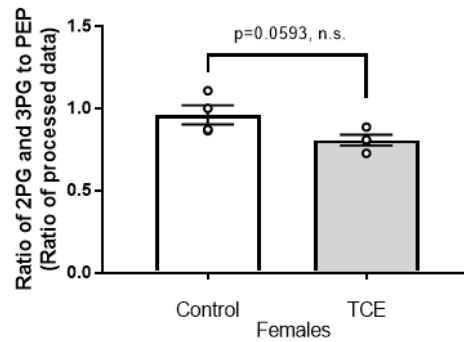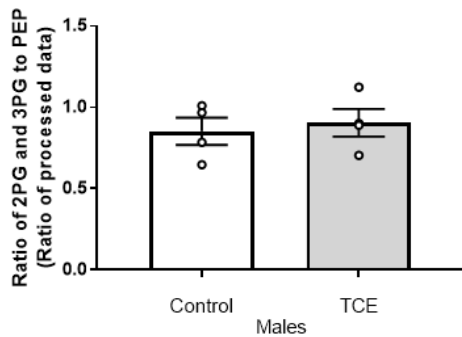
(D)
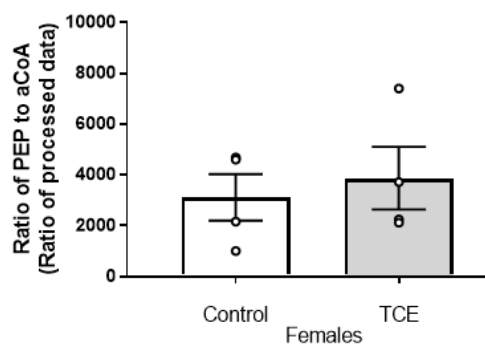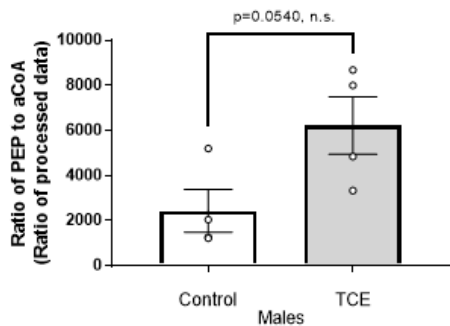
Figure 3.10. Glycolysis or gluconeogenesis as modified by trichloroethylene (TCE) treatment in male and female amniotic fluid. (A) Simplified depiction of the glycolysis or gluconeogenesis metabolism KEGG pathway in *Rattus norvegicus*. Metabolites underlined in green correspond to metabolites that are part of ratio altered by TCE treatment in males only. Metabolites underlined in blue correspond to metabolites that were analyzed in ratio analysis but not altered by TCE treatment in any sex. Depiction of effects TCE treatment in males and females on (B) G6P and F6P to aCoA ratio, (C) the 2PG and 3PG to PEP ratio, and (D) the PEP to aCoA ratio. In the graphs, error bars represent mean ± SEM. Statistical analysis for each sex consisted of a two-tailed unpaired t-test. N= 4 independent experiments. Abbreviations: G6P, glucose 6-phosphate; F6P, fructose 6-phosphate; aCoA or acetyl-CoA, acetyl coenzyme A; 2PG, 2-phosphoglycerate; 3PG, 3-phosphoglycerate; PEP, phosphoenolpyruvate.

(A)
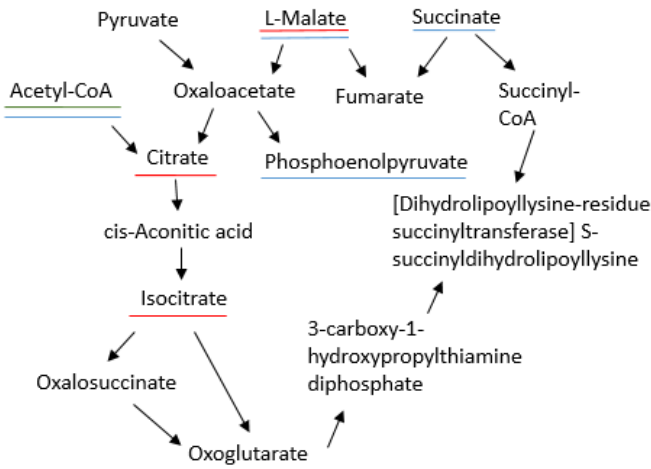
(B)
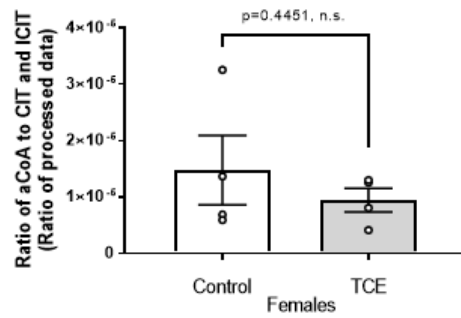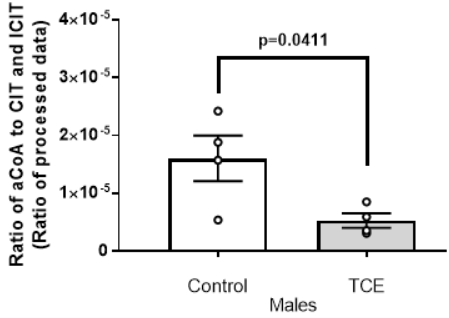
(C)
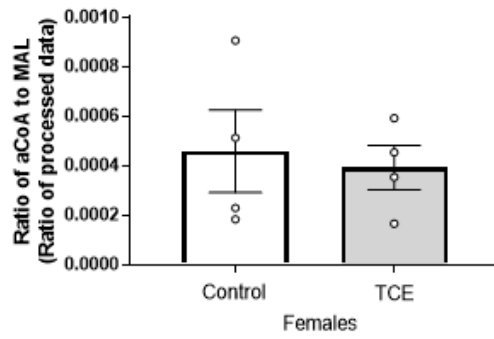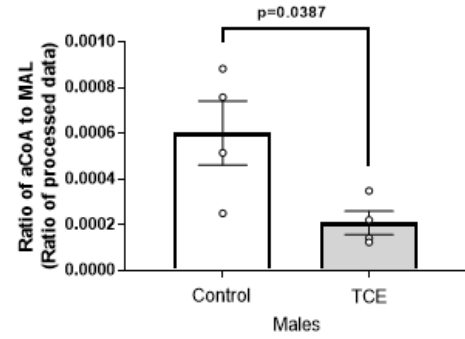
(D)
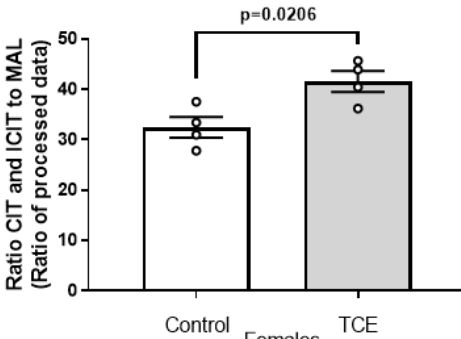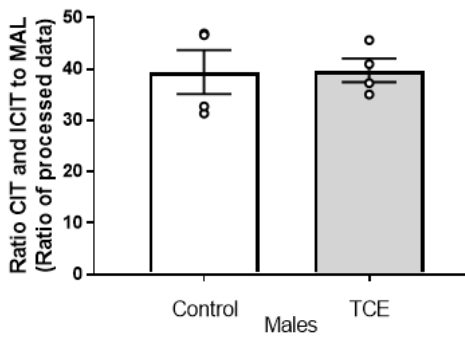
Figure 3.11. Tricarboxylic acid (TCA) cycle as modified by trichloroethylene (TCE) treatment in male and female amniotic fluid. (A) Simplified depiction of the TCA cycle KEGG pathway in *Rattus norvegicus*. Metabolites underlined in red correspond to metabolites that are part of ratio altered by TCE treatment in both males and females. Metabolites underlined in green correspond to metabolites that are part of ratio altered by TCE treatment in males only. Metabolites underlined in blue correspond to metabolites that were analyzed in ratio analysis but not altered by TCE treatment in any sex. Depiction of effects TCE treatment in males and females on (B) the aCoA to CIT and ICIT ratio, (C) the aCoA to MAL ratio, and (D) the CIT and ICIT to MAL ratio. The aCoA to MAL ratio is also relevant to **Figure 3.13**. In the graphs, error bars represent mean ± SEM. Statistical analysis for each sex consisted of a two-tailed unpaired t-test. N= 4 independent experiments. Abbreviations: aCoA or acetyl-CoA, acetyl coenzyme A; CIT, citrate; ICIT, isocitrate; MAL, malate.

(A)
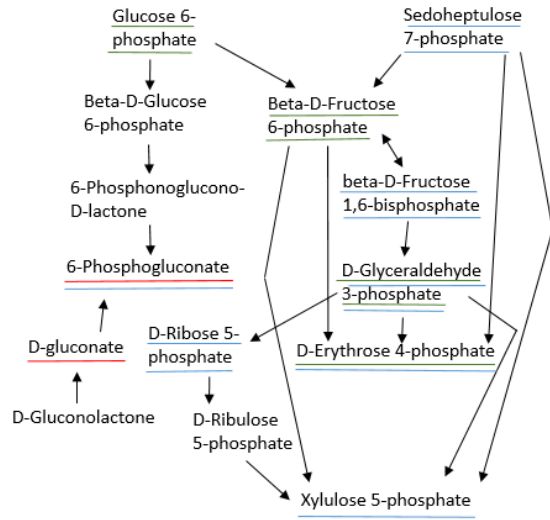
(B)
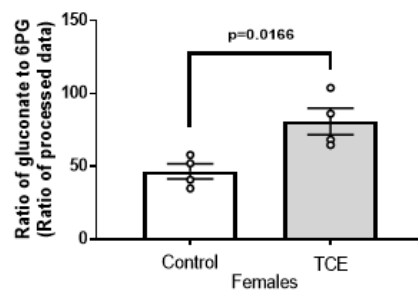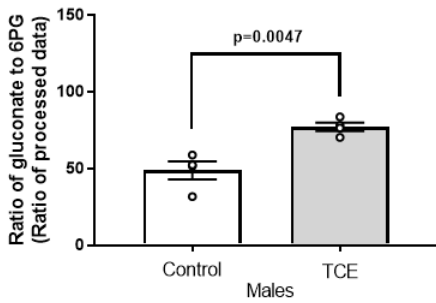
(C)
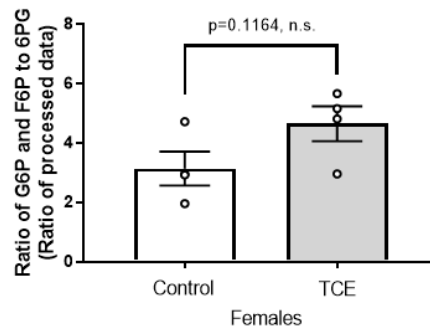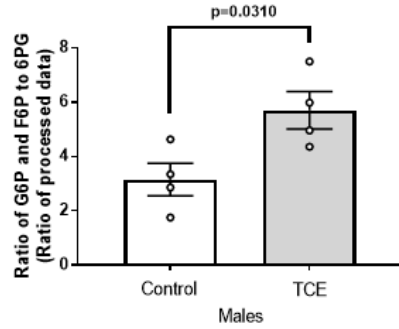
(D)
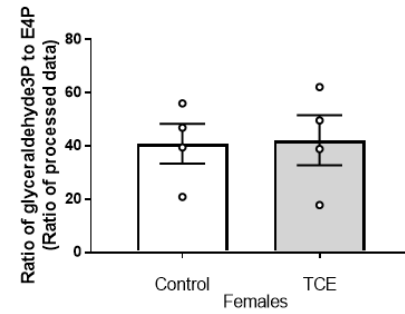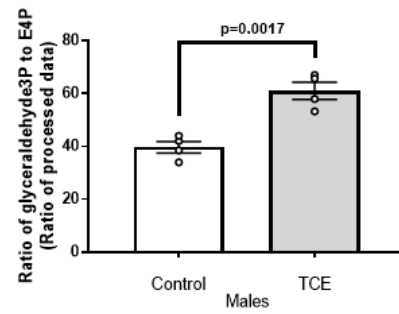
Figure 3.12. Pentose phosphate pathway as modified by trichloroethylene (TCE) treatment in male and female amniotic fluid. (A) Simplified depiction of the pentose phosphate KEGG pathway in *Rattus norvegicus*. Metabolites underlined in red correspond to metabolites that are part of ratio altered by TCE treatment in both males and females. Metabolites underlined in green correspond to metabolites that are part of ratio altered by TCE treatment in males only. Metabolites underlined in blue correspond to metabolites that were analyzed in ratio analysis but not altered by TCE treatment in any sex. Depiction of effects TCE treatment in males and females on (B) the gluconate to 6PG ratio, (C) the G6P and F6P to 6PG ratio, and (D) the glyceraldehyde3P to E4P ratio. In the graphs, error bars represent mean ± SEM. Statistical analysis for each sex consisted of a two-tailed unpaired t-test. N= 4 independent experiments. Abbreviations: 6PG, 6-phosphogluconate; G6P, glucose 6-phosphate; F6P, fructose 6-phosphate; glyceraldehyde3P, glyceraldehyde 3-phosphate; E4P, erythrose 4-phosphate.

(A)
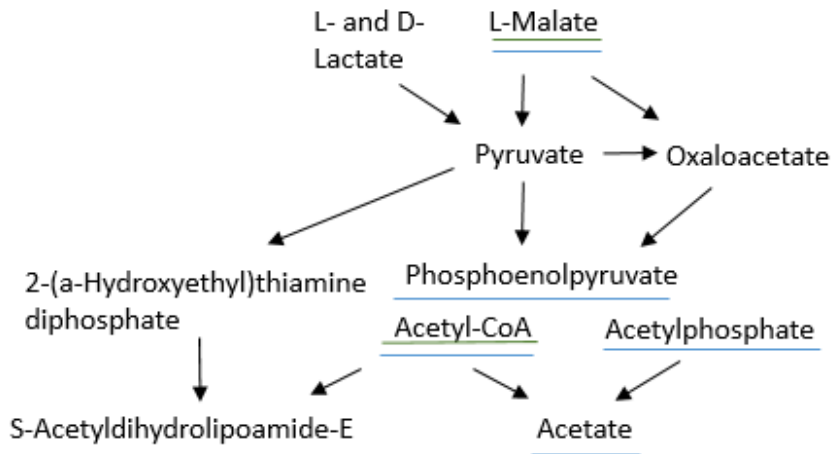
Figure 3.13. Pyruvate metabolism as modified by trichloroethylene (TCE) treatment in male and female amniotic fluid. (A) Simplified depiction of the pyruvate metabolism KEGG pathway in *Rattus norvegicus*. Metabolites underlined in green correspond to metabolites that are part of ratio altered by TCE treatment in males only. Metabolites underlined in blue correspond to metabolites that were analyzed in ratio analysis but not altered by TCE treatment in any sex. Graphs corresponding to the aCoA to MAL ratio are already depicted in **Figure 3.11C**. In the graphs, error bars represent mean ± SEM. Statistical analysis for each sex consisted of a two-tailed unpaired t-test. N= 4 independent experiments. Abbreviations: aCoA or acetyl-CoA, acetyl coenzyme A; MAL, malate.

(A)

GTP

Formamidopyrimidine
nucleoside triphosphate

2,5-Diaminopyrimidine
nucleoside triphosphate

2,5-Diamino-6-(5'-
triphosphoryl-3',4'-
trihydroxy-2'-oxopentyl)-
amino-4-oxopyrimidine

7,8-Dihydroneopterin 3'-
triphosphate

6-Pyruvoyltetrahydropterin

Folate

7,8-Dihydrofolate

7,8-Dihydropteroate

7,8-Dihydroneopterin

6-Lactoyl-5,6,7,8-tetrahydropterin

Tetrahydropteroyldiglutamate

5,6,7,8-Tetrahydrofolate

Tetrahydropteroyl
-[gamma-Glu]n

6,7-Dihydrobiopterin

5,6,7,8-Tetrahydrobiopterin

(B)

Figure 3.14. Folate biosynthesis as modified by trichloroethylene (TCE) treatment in male and female amniotic fluid. (A) Simplified depiction of the folate biosynthesis KEGG pathway in *Rattus norvegicus*. The metabolite underlined in green (GTP) corresponds to a metabolite that is decreased by TCE treatment in males but not females. No other metabolites in the pathway were detected. Depiction of effects TCE treatment in males and females on (B) GTP concentration. In the graphs, error bars represent mean ± SEM. Statistical analysis for each sex consisted of a two-tailed unpaired t-test. N= 4 independent experiments. Abbreviations: GTP, guanosine triphosphate.
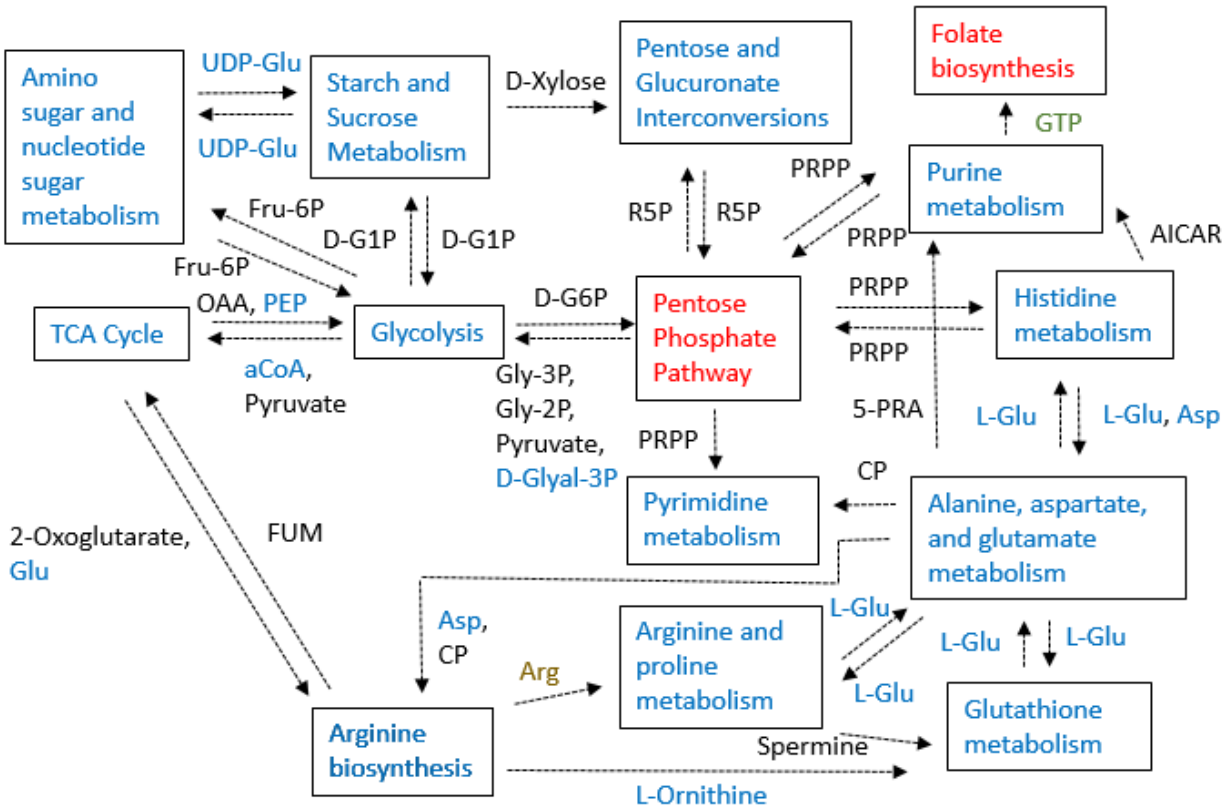
Figure 3.15. The effect of trichloroethylene treatment on a simplified depiction of relationships among multiple KEGG metabolism pathways. Boxes indicate individual KEGG pathways, and unboxed text indicates critical metabolites that connect pathways. Red indicates metabolites or pathways altered in both sexes. Green indicates metabolites or pathways altered in males only. Dark gold indicates metabolites or pathways altered in females only. Blue indicates metabolites or pathways unaltered in either sex. Black indicates metabolites or pathways not detected in the current study. Metabolite concentrations or relative responses and Metabolanalyst 4.0 pathway analysis results were used to determine metabolite and pathway significance, respectively. Dashed arrows indicate multi-step processes. Abbreviations: aCoA, acetyl coenzyme A; OAA, oxaloacetate; D-G1P, alpha-D-glucose 1-phosphate; UDP-Glu, uridine diphosphate-glucose; R5P, D-ribulose 5-phosphate; PRPP, phosphoribosyl pyrophosphate; FUM, fumarate; CP, carbamoyl phosphate, Gly-3P, glycerate 3-phosphate; Gly-2P, glycerate 2-phosphate; D-Glyal-3P, D-glyceraldehyde 3-phosphate; D-G6P, alpha-D-glucose 6-phosphate; 5-PRA, 5-phosphoribosylamine; Fru-6P, fructose 6-phosphate; GTP, guanosine triphosphate.

Table S3.1. Primer sequences used in the current study to identify the sex of the placental and fetal unit associated with the amniotic fluid.

SRY (for both genomic DNA and cDNA input)	
Forward	5'-AAGCGCCCCATGAATGCAT-3'
Reverse	5'-CGATGAGGCTGATATTTATA-3'
Source: (Schulte et al. 2012)	
B2M (for cDNA input) – spans exon-exon junction	
Forward	5'-TCGTGCTTGCCATTCAGAAAAC-3'
Reverse	5'-GCAGTTGAGGAAGTTGGGCT-3'
Source: NCBI nucleotide database	
B2M (for genomic DNA input) – does not span exon-exon junction	
Forward	5'-CCCACCCTCATGGCTACTTC-3'
Reverse	5'-TGGGTGATGAAAACCGCACA-3'
Source: NCBI nucleotide database	

Table S3.2. Concentrations or relative responses of detected metabolites.

I. Short chain fatty acids (data expressed as µM)				

Acetate (µM)

	Control (male)	TCE (male)	Control (female)	TCE (female)
	276.271982866701	257.708408521392	295.30353838664	250.80070608729
	203.444027693933	287.245669109964	207.621963786731	275.111842611805
	385.548239403696	342.078676637373	323.470485854764	364.93071275932
	289.567058405092	220.008514460553	282.985171228317	188.369480922414
Average	288.707827092356	276.760317182321	277.345289814113	269.803185595207

Propionate (µM)

	Control (male)	TCE (male)	Control (female)	TCE (female)
	8.1004852976173	8.79096700437706	11.6756783546484	9.31552978442684
	8.4610411811446	35.9604762615793	16.9697241536998	7.65057962966343
	14.4586725310812	11.5227002760205	11.6581133238875	20.2642263140754
	18.7962475475666	13.2132073983261	15.7003410830218	9.79111421357177
Average	12.4541116393524	17.3718377350757	14.0009642288144	11.7553624854344

Butyrate (µM)

	Control (male)	TCE (male)	Control (female)	TCE (female)
	4.984101743845	6.27015242652338	5.3923125219042	6.496987708135
	6.18056160773178	31.7769388418729	37.0619295902022	4.71449347280659
	8.14532934481046	6.1291109682479	7.41286375984605	8.92454746730236
	8.94359699662898	11.0655026709102	6.87621605762163	14.1797098928921
Average	7.06339742325406	13.8104262268886	14.1858304823935	8.57893463528401

Isovalerate (µM)

	Control (male)	TCE (male)	Control (female)	TCE (female)
	0.470597352293445	0	0.242103915396413	0.0390399273591738
	0.248939377279107	0.324438228002215	0.659009712247637	0.408822382538212
	1.4604822448603	0.249340193304065	0.387029723591049	0.722459609016718
	2.28612157502548	0.927468226507037	0.733685741785168	0.58634098092427
Average	1.11653513736458	0.375311661953329	0.505457273255067	0.439165724959593

Valerate (µM)

	Control (male)	TCE (male)	Control (female)	TCE (female)
	1.66344873422734	2.87973314078432	2.33905429772274	3.07302260533966
	1.62713126923251	3.36738841216542	2.97378059591539	2.00591491173539
	5.39706024045058	1.66067042987601	1.86017249727766	4.3946278839859
	6.38027874345318	2.68419244206085	2.67293026410768	2.21685028085844
Average	3.76697974684090	2.64799610622165	2.46148441375587	2.92260392047985

Hexanoate (µM)

	Control (male)	TCE (male)	Control (female)	TCE (female)
	3.7952513571157	7.58889886327068	5.60791582956784	4.2839793678578
	4.74238481184048	4.98253446716657	7.41046374647852	4.96909298086826
	14.5091027768945	4.68510140633916	7.27523957128617	8.34806877336278
	10.6455501576887	7.38284473326639	9.00802969034518	8.27939771916957
Average	8.42307227588485	6.15984486751070	7.32541220941943	6.47013471031460

Heptanoate (µM)

	Control (male)	TCE (male)	Control (female)	TCE (female)
	0.34381343427593	0.592521837018908	0.321873212646279	0.48777538315166
	0.347893379421463	0.292509609799655	0.474404687838417	0.30526719946079
	1.17722263307827	0.287864845016662	0.344799028123874	0.985571277421056
	1.6589208776074	0.44117992052106	0.544194981587277	0.268398449673147
Average	0.881962581095766	0.403519053089071	0.421317977548962	0.511753077426663

Octanoate (µM)

	Control (male)	TCE (male)	Control (female)	TCE (female)
	0.15973261039682	0.410879239409786	0.149367018948578	0.20468334438462
	0.19890388139438	0.132287002446584	0.167118250150016	0.109903697680086
	0.467972690814254	0.19404017135944	0.249064345280658	0.296850614220606
	0.384676848570042	0.1261259902094	0.279316474005833	0.100615278136368
Average	0.302821507793874	0.215833100856302	0.211216522096271	0.178013233605420

II. Metabolites measured as absolute concentration (TCA Plus targeted platform) (Units: μM)

2-phosphoglycerate and 3-phosphoglycerate (2PG & 3PG) (μM)

	Control (male)	TCE (male)	Control (female)	TCE (female)
	2.29330843295702	3.11684671336996	3.17626750836432	2.36112099248988
	0.736808601954684	1.68955057310398	3.01206769741076	2.55982824741445
	3.73682090294676	2.90525601223677	3.23639578003899	3.12465932845495
	3.16454826826009	3.99559643464801	2.89240749208831	2.66119221122097
Average	2.48287155152964	2.92681243333968	3.07928461947560	2.67670019489506

6-phosphogluconate (6PG) (μM)

	Control (male)	TCE (male)	Control (female)	TCE (female)
	0.2368	0.102	0.2581	0.1254
	0.158	0.1098	0.2211	0.0974
	0.13636	0.0964	0.1659	0.0941
	0.1546	0.1	0.1443	0.1017
Average	0.17144	0.1021	0.1974	0.1047

Citrate and isocitrate (CIT & ICIT) (μM)

	Control (male)	TCE (male)	Control (female)	TCE (female)
	95.1770872998993	121.662546541458	112.122786673005	114.712786034444
	49.5525379497319	89.2440277471424	91.6632300955912	105.717770358297
	115.098501548023	115.145669633639	114.561448766834	125.72759454729
	117.017983468604	123.556499788966	105.527043055531	108.842830286182
Average	94.2115275665645	112.402185927801	105.968627147740	113.750245306553

Erythrose-4-phosphate (E4P) (μM)

	Control (male)	TCE (male)	Control (female)	TCE (female)
	0.468872713830582	0.224265359847	0.342235745983	0.23949779541349
	0.450743935271831	0.424203939567595	0.617668196698293	0.38946281521071
	0.351953089351532	0.18522652588921	0.470626485971941	0.351827766785625
	0.37058759474029	0.328464964129802	0.302941641098863	0.722102340395411
Average	0.410539333298559	0.290540197358402	0.433368017438024	0.425722679451309

Fructose 6-phosphate & glucose 6-phosphate (F6P & G6P) (μM)

	Control (male)	TCE (male)	Control (female)	TCE (female)
	0.793235839817717	0.610682811534276	0.763572008474694	0.647790012255409
	0.277226454587975	0.478828205465435	0.434698935388669	0.469000451413139
	0.631952455874901	0.478518159176854	0.486009139660447	0.533555743859416
	0.442786260887891	0.750601781660329	0.681348887940588	0.301401444584332
Average	0.536300252792121	0.579657739459223	0.591407242866099	0.487936913028074

Fructose 1,6-bisphosphate (FBP) (μM)

	Control (male)	TCE (male)	Control (female)	TCE (female)
	0.276975086490366	0.165726591116647	0.293620904270615	0.159966634833449
	0.221152480519416	0.154723379337304	0.218813012820476	0.152981504336152
	0.190638969746489	0.155596038686046	0.180029604196881	0.159126113844131
	0.179146744479959	0.15003857412507	0.177499158096114	0.168805490707838
Average	0.216978320309058	0.156521145816267	0.217490669846022	0.160219935930393

Guanosine diphosphate (GDP) (μM)

	Control (male)	TCE (male)	Control (female)	TCE (female)
	0.161935044609202	0.117021564793478	0.175888930791753	0.117678938986407
	0.134279107767508	0.108276020650395	0.149163632182011	0.116883603802237
	0.123801285190235	0.106976586430058	0.135491844226981	0.11043308785515

133

| | 0.119767162396773 | 0.10834458528047 | 0.129883848114199 | 0.109467128430997 |
| Average | 0.134945649990930 | 0.110154689288600 | 0.147607063828736 | 0.113615689768698 |

Glycerol 3-phosphate (Gl-OH3P) (µM)

	Control (male)	TCE (male)	Control (female)	TCE (female)
	4.39119529281074	4.20634381522531	4.52165793334052	4.5709112390578
	1.65415368099845	2.97033091688291	3.16393000610236	3.98213983151541
	4.08797187194436	4.3828968145797	5.87657527403507	4.93842733957219
	3.40931819024611	3.92320982702911	4.0830129993303	2.23327680389119
Average	3.38565975899991	3.87069534342926	4.41129405320206	3.93118880350915

Glyceraldehyde 3-phosphate (Glyceraldehyde3P) (µM)

	Control (male)	TCE (male)	Control (female)	TCE (female)
	15.9515472989605	15.0502631574563	16.0298731470094	14.8780449349018
	18.9786392439884	24.6118643553081	12.8718683195233	19.3077260479532
	15.5253638979529	12.1773902399192	18.5532444760988	13.6741209287385
	14.3041497538849	17.4967781491959	16.9510666695505	12.8338033886849
Average	16.1899250486967	17.3340739754699	16.1015131530455	15.1734238250696

Guanosine triphosphate (GTP) (µM)

	Control (male)	TCE (male)	Control (female)	TCE (female)
	0.234347288577464	0.120560983548974	0.248415731451544	0.150596672595084
	0.161154817262453	0.124301107128232	0.220052315629347	0.137728382605887
	0.150255704833941	0.118921464215364	0.147981036725891	0.130330523608576
	0.151304816211229	0.113163737377275	0.160225864002402	0.122070468535473
Average	0.174265656721272	0.119236823067461	0.194168736952296	0.135181511836255

Malate (MAL) (µM)

	Control (male)	TCE (male)	Control (female)	TCE (female)
	3.035138659769	2.96838238271834	4.02235282425872	3.16714807621585
	1.05570518636575	1.95567084470598	2.44102289380379	2.40530440172018
	3.51563989482841	3.28557814942716	3.42606777788102	3.1059370882642
	2.50877907212521	3.31363014460084	3.40404022677933	2.38323289049305
Average	2.52881570327209	2.88081538036308	3.32337093068071	2.76540561417332

Phosphoenolpyruvate (PEP) (µM)

	Control (male)	TCE (male)	Control (female)	TCE (female)
	2.91922424166332	3.45591325756795	3.66987192412319	3.24416329584767
	1.13721251302886	2.39392778754701	2.71651549514247	3.18200448005706
	3.69757513194478	3.26191386266909	3.70525646120795	3.85200265636012
	3.26840639861618	3.55447359178573	2.88721130252671	2.99649429550287
Average	2.75560457131329	3.16655712489244	3.24471379575008	3.31866618194193

Succinate (SUC) (µM)

	Control (male)	TCE (male)	Control (female)	TCE (female)
	4.56400949655562	4.15545165034285	6.5323931810397	4.3387287410853
	1.09112299082636	2.46660586877778	3.25465871210832	2.960926877429
	4.39231788212427	4.71276965881976	7.85057932981988	7.87998182232565
	3.99031951666285	5.3233454343676	3.76296429338289	2.34347506540461
Average	3.50944247154228	4.16454315307700	5.35014887908770	4.38077812656114

III. Metabolites measured as relative concentrations (TCA Plus targeted platform) (Units: Relative response)

3-Phosphoserine (Relative response)

	Control (male)	TCE (male)	Control (female)	TCE (female)
	0.00502927153591151	0.00285506809483588	0.00462739050089528	0.00137192385104196
	0.00146684709815593	0.00156814603320146	0.00301277132021785	0.00525966025163523
	0.00476299497715687	0.00171561007307246	0.00302728418091881	0.00568673788283254
	0.00487517780549056	0.0032082769225232	0.00588059879316144	0.00283377154890839
Average	0.00403357285417872	0.00233677528090825	0.00413701119879835	0.00378802338360453

Acetylphosphate (Relative response)

	Control (male)	TCE (male)	Control (female)	TCE (female)
	0.102272689109334	0.0910005750539508	0.113942443329736	0.0986783814118296
	0.0370208196005331	0.0698097427526974	0.0790482378321081	0.0854337252424941
	0.103642069179313	0.10707228988991	0.144288209051687	0.148701130187443
	0.0983823996997104	0.122274395951951	0.0917819925350769	0.0599437912017978
Average	0.0853294943972226	0.0975392509121273	0.1072652206871520	0.0981892570108911

Arginine (Relative response)

	Control (male)	TCE (male)	Control (female)	TCE (female)
	5.6837037185127	4.45289391631858	5.30885217232204	5.0551217365079
	2.11363610405434	6.64670861316916	3.87158980882508	7.5557548038064
	4.15349247567646	5.11345805563055	3.75071676166752	6.30280062559677
	5.25928842682884	6.53771226666437	4.40845392721576	5.01864600070357
Average	4.30253018126808	5.68769321311440	4.33490316750760	5.98308079165366

Asparagine (Relative response)

	Control (male)	TCE (male)	Control (female)	TCE (female)
	2.97918642132418	3.4204848193291	2.22269151334002	3.4832111662888
	4.91084773905832	3.05515444321032	5.07050995818347	3.39018175101142
	4.5101995667538	3.00145953492596	6.85380015830096	3.72564329824483
	3.34305146059008	3.22394623155469	3.01435315333176	1.79727637619753
Average	3.93582129693159	3.17526125725502	4.29033869578905	3.09907814793565

Aspartate (Relative response)

	Control (male)	TCE (male)	Control (female)	TCE (female)
	0.0582964299540356	0.0647763365252277	0.0902107007574525	0.0922724780581186
	0.0404454017726727	0.0537388310965087	0.0375429766765787	0.0520336382887273
	0.0279835981894312	0.0220495636896825	0.03539358850456	0.0522868065574622
	0.0374650555623649	0.0756903481502986	0.0713224636934267	0.00789013727192886
Average	0.0410476213696261	0.0540637698654294	0.0586174324080045	0.0511207650440592

Citrulline (Relative response)

	Control (male)	TCE (male)	Control (female)	TCE (female)
	1.75943242890966	1.75049823148628	1.79842691879792	1.63359562294114
	0.883573888009974	1.58812438879269	2.02639120697304	1.70315304689964
	2.52674982763964	1.90289126406474	2.77879707798213	1.67985391717891
	1.66418242785741	1.98533846559812	2.08067238311648	1.89955749644303
Average	1.70848464310417	1.80671308748546	2.17107189671739	1.72904002086568

Cytidine monophosphate (CMP) (Relative response)

	Control (male)	TCE (male)	Control (female)	TCE (female)
	0.0238107139016127	0.0258960376777033	0.0300138133426855	0.0359058179661057
	0.0120366872563003	0.0200315975017078	0.00954664027239051	0.0220955582508235
	0.0227721931419426	0.00862138951657184	0.0142513979516159	0.0184930168639229
	0.0109422007240324	0.0501890161007984	0.0316612505126822	0.00287338771061321
Average	0.0173904487559720	0.0261845101991953	0.0213682755198435	0.0198419451978663

Creatine (Relative response)

	Control (male)	TCE (male)	Control (female)	TCE (female)
	3.61527400683645	2.84625965152958	3.27016978778538	3.07998639057688
	2.26902135422181	3.87008332332548	3.02295904936944	4.40572468140206
	3.22028591529816	2.78908618480442	3.147468895781	3.529560220109
	3.47763788735447	3.80841981836494	3.50133192283815	3.0967231019289
Average	3.14555479092772	3.32846224450611	3.23548241394349	3.52799859850421

Creatinine (Relative response)

	Control (male)	TCE (male)	Control (female)	TCE (female)
	1.00134721958411	0.951735523056672	1.17055821642664	0.826651300987152
	0.356371789794643	0.984156677374242	0.687145994632588	1.03039113258861
	0.926040282576031	0.915443917809827	0.839095301676743	0.935085442899104
	0.972101528378523	1.00497125814925	1.1232159565528	0.966194047141943
Average	0.813965205083327	0.964076844097498	0.955003867322193	0.939580480904202

135

Deoxyuridine (Relative response)

	Control (male)	TCE (male)	Control (female)	TCE (female)
	0.437545991573401	0.483692119766459	0.414992350498703	0.629065514407773
	0.0999213830356527	0.618617884321005	0.404110368446751	0.649381055091212
	0.499757949335196	0.544106658951022	0.464204266443553	0.687984079547692
	0.590482028955387	0.533576777934412	0.577958946772988	0.374296273479921
Average	0.406926838224909	0.544998360243224	0.465316483040499	0.585181730631650

Dihydroxy-acetone phosphate (DAP) (Relative response)

	Control (male)	TCE (male)	Control (female)	TCE (female)
	0.06816515783158	0.0364917237462659	0.0623390439508838	0.0591169577150902
	0.0641536494530438	0.0389615503625285	0.0926463768252128	0.0463655807683666
	0.0782415590913062	0.0570043277683071	0.0665033325010187	0.0296629602657331
	0.0415238381790572	0.0381007031942375	0.0388573725634919	0.106666191724361
Average	0.0630210511387468	0.0426395762678348	0.0650865314601518	0.0604529226183877

Gluconate (Relative response)

	Control (male)	TCE (male)	Control (female)	TCE (female)
	7.52267676034018	7.9845985228919	10.5820408409387	8.5779493946241
	8.19552189253673	8.40409686820758	7.764367083852	8.4032126497332
	8.0421362380594	8.08166197129308	8.66749064109869	9.78475006160488
	8.1157426916426	7.04172603607755	8.37771017289613	6.59619229202214
Average	7.96901939564473	7.87802084961753	8.84790218469638	8.34052609949608

Glutamate (Relative response)

	Control (male)	TCE (male)	Control (female)	TCE (female)
	0.307961913155044	0.402649714837443	0.417987776399223	0.522465477411086
	0.371635593219584	0.364665666809564	0.204378305367296	0.346804271840605
	0.276576716242478	0.135636911247062	0.241159174098423	0.332783553075544
	0.199021326753188	0.466495432055383	0.313116237745024	0.018702404226687
Average	0.288798887342573	0.342361931237363	0.294160373402492	0.305188926638481

Glutamine (Relative response)

	Control (male)	TCE (male)	Control (female)	TCE (female)
	148.45156615073	180.05260885779	132.785099913393	174.094302488731
	130.751805673928	177.571367040976	195.752262645839	185.33524694511
	211.171626281737	183.81153381775	226.829995093613	199.301907855555
	174.789006234658	168.141047322105	170.642807020059	121.110374069343
Average	166.291001085263	177.394139259655	181.502541168226	169.960457839685

Glutathione disulfide (GSSG) (Relative response)

	Control (male)	TCE (male)	Control (female)	TCE (female)
	0.00930794619774362	0.0154332913073681	0.0286315869517131	0.0138583805088712
	0.00340130488916917	0.00438147649249482		0.00534678219369634
	0.0103265247281325	0.00143237120348074	0.00470744678487935	0.00832539966523493
	0.00454054060280377	0.0169715869806743	0.0149500296549962	0.00191474409604791
Average	0.00689407910446226	0.00955468149600449	0.01609635446386290	0.00736132661596259

Glutathione (GSH) (Relative response)

	Control (male)	TCE (male)	Control (female)	TCE (female)
	0.00715762187768489	0.0083225337638274	0.0127099634995166	0.0137779396850745
	0.00493605303315922	0.00530309934558272	0.00836530168936515	0.0086278993719756
	0.00607868763057336	0.00589586624314627	0.00629048733871203	0.00925638352323385
	0.00315840295313328	0.0113734184594304	0.0114036773620578	0.00490543765811772
Average	0.00533269137363769	0.00772372945299670	0.00969235747241290	0.00914191505960042

Hexose (glucose etc.) (Relative response)

	Control (male)	TCE (male)	Control (female)	TCE (female)
	116.270990373226	104.082771202489	124.936339420717	135.182357932123
	51.7533190453476	160.569901166951	72.6580141395736	138.622912952932
	114.323956473361	103.040960254044	101.813368479715	148.9844114225

	118.037403458686	103.432732415122	135.831997098081	97.790394968478
Average	100.096417337655	117.781591259651	108.809929784522	130.145019319008

Histidine (Relative response)

	Control (male)	TCE (male)	Control (female)	TCE (female)
	5.18199859497625	6.56322432954156	5.63777177740812	8.06730351274919
	7.59706309645618	6.93416710655496	4.88627626710831	7.72510187587655
	5.8995445198083	5.80632732086946	5.89315569947654	7.49264677532566
	7.81522751089826	5.98326291644746	7.04011464648112	3.65471138487619
Average	6.62345843053475	6.32174541835336	5.86432959761852	6.73494088720690

Homocysteic acid (Relative response)

	Control (male)	TCE (male)	Control (female)	TCE (female)
	0.0165534420175248	0.00885784912943457	0.00325665117859514	0.00558134969322661
	0.00470245126480873	0.00786736624885914	0.00617036715778341	0.0116285165397493
	0.0100403484450849	0.0141480729006386	0.00440186795399468	0.0144740210981528
	0.012652328644841	0.00508744130147274	0.00769155873525647	0.00772898389754247
Average	0.0109871425930649	0.00899018239510126	0.00538011125640742	0.00985321780716780

Hypoxanthine (Relative response)

	Control (male)	TCE (male)	Control (female)	TCE (female)
	1.28910438750246	1.62038610294412	1.35233837227273	1.5148519684768
	1.02599655507051	1.45445174143139	1.15286478699761	1.50376110388397
	1.68472777788512	1.52010820578561	1.5019163014639	1.66129257701654
	1.38606573540508	1.76059273769494	1.40859636306096	1.25882174287346
Average	1.34647361396579	1.58888469696401	1.35392895594880	1.48468184806269

Inosine monophosphate (IMP) (Relative response)

	Control (male)	TCE (male)	Control (female)	TCE (female)
	0.00263783013620089	0.00663475072936561	0.00223287876825929	0.00393434285553368
	0	0.000931712975730085	0.00153295252320881	0.00567437930764282
	0.00492560106710619	0.0054639211559046	0.0031377235260751	0.00593872171754603
	0.0100382118978335	0.00382216464761877	0.0065451776879585	0.00251922197890681
Average	0.00440041077528515	0.00421313737715477	0.003362183126375430	0.00451666646490734

Inosine (Relative response)

	Control (male)	TCE (male)	Control (female)	TCE (female)
	1.65623602504098	1.25094810845345	2.15150834694522	1.32830104004165
	0.416283694182781	1.0951053308403	0.438842384243419	1.36481809126711
	1.42501020065998	0.510773945890011	1.04622698051948	1.09647976538458
	0.545348345542713	3.02661469865942	1.82896873090907	0.0917967754556645
Average	1.01071956635661	1.47086052096080	1.36638661065430	0.970348918037251

Leucine & isoleucine (Relative response)

	Control (male)	TCE (male)	Control (female)	TCE (female)
	120.392156175101	126.03929692653	123.996858296221	156.554550943523
	84.0936520190014	158.063386572106	86.2049263738705	187.474515796931
	126.878656448281	134.99430365122	127.726994617859	205.074970942545
	164.146315334345	148.894073518943	147.97748315866	83.2749721179156
Average	123.877694994182	141.997765167200	121.476565611653	158.094752450229

Lysine (Relative response)

	Control (male)	TCE (male)	Control (female)	TCE (female)
	28.7946956488402	30.9915390624879	22.5234231633974	30.6365322390061
	10.6828316032565	35.8257793363831	25.8709827225469	42.3645472536058
	33.3411742330367	28.2174944873146	32.2686079560879	32.7709736423354
	33.9788398730765	31.411086685645	33.1533640364618	24.3477123243223
Average	26.6993853395525	31.6114748929576	28.4540944696235	32.5299413648174

Methionine (Relative response)

	Control (male)	TCE (male)	Control (female)	TCE (female)
	15.373062522475	14.9485492900276	14.7998422087813	17.2284709251448

	7.16411737615423	18.5844114330434	9.49809241757088	21.3936387492344
	16.9830570309393	16.3215238439866	14.7921889878151	23.282780712636
	17.6236581973945	16.877307463463	17.2092998101684	12.0092179839734
Average	14.2859737817408	16.6829480076301	14.0748558560839	18.4785270927472

N-Acetyl-glucosamine (Relative response)

	Control (male)	TCE (male)	Control (female)	TCE (female)
	0.0660358760241889	0.0546584272955955	0.0759277420956322	0.0675602385690794
	0.0252663312388139	0.0460608624063941	0.0373681866665481	0.048534113578411
	0.058962731215075	0.0411907496034425	0.0497543236708654	0.0599356174273915
	0.0433492623226577	0.0666362888446834	0.0555750751203564	0.0307651891300912
Average	0.0484035502001839	0.0521365820375289	0.0546563318883505	0.0516987896762433

Oleic acid (Relative response)

	Control (male)	TCE (male)	Control (female)	TCE (female)
	3.30228190015226	3.87337011608256	4.61712954746185	4.42898260413718
	2.29184247356761	3.30680615968643	2.73704832156423	3.81827706166149
	3.25309137578706	2.62244359686498	2.38975217228124	3.50199696284627
	2.78960846979286	4.12073358802994	2.81037008648587	2.48993648755509
Average	2.90920605482495	3.48083836516598	3.13857503194830	3.55979827905001

Ornithine (Relative response)

	Control (male)	TCE (male)	Control (female)	TCE (female)
	1.70628755685181	1.47808031697535	1.49851739444816	1.54020746062397
	0.676596081328696	1.84096100813614	1.07764018588357	2.19586621138424
	1.60398971945093	1.23143035077469	1.42948495338061	1.89325694005179
	1.46209103428039	1.17547551086638	1.49711277418818	0.994799813265531
Average	1.36224109797796	1.43148679668814	1.37568882697513	1.65603260633138

Palmitic Acid (Relative response)

	Control (male)	TCE (male)	Control (female)	TCE (female)
	8.32433531441293	9.27164784954155	11.2432200569048	10.0089215619642
	6.14020317719046	7.53719424100165	10.4772853856549	9.98230259312304
	9.12563893216807	11.0271271487329	7.03901122295498	12.2157037744871
	8.12619071689764	11.7266311471852	10.0128062821848	10.8978815672703
Average	7.92909203516728	9.89065009661533	9.69308073692487	10.7762023742112

Pantothenate (Relative response)

	Control (male)	TCE (male)	Control (female)	TCE (female)
	15.9400252022871	19.9375558916484	13.6212037934301	16.6314270515212
	49.1708150068296	26.4508573402717	28.1475500132176	24.235264558982
	24.0587745779932	24.438947756883	26.4972301795193	27.5511324256898
	14.1731980718376	13.5972968990489	13.5922732579102	8.52474716114498
Average	25.8357032147369	21.1061644719630	20.4645643110193	19.2356427993345

Phenylalanine (Relative response)

	Control (male)	TCE (male)	Control (female)	TCE (female)
	65.4710579488895	69.6254440705336	69.9374718187747	81.4747309893265
	39.3658390623823	86.5593410866756	45.5329515425566	93.9719115807344
	71.8751253836729	66.4335914809522	63.9838095771308	103.271636881263
	88.6611813830943	71.6059529982972	74.5797356022803	47.9495460525198
Average	66.3433009445097	73.5560824091147	63.5084921351856	81.6669563759609

Phenylpyruvate (Relative response)

	Control (male)	TCE (male)	Control (female)	TCE (female)
	0.641794475852842	0.554991097580126	0.617107662808514	0.70743195498099
	0.490133214872309	0.774988941208173	0.477615489058907	0.800586140937473
	0.656069180828189	0.631167177155369	0.609317984396435	0.848021537726063
	0.797433217672889	0.670864100378659	0.732364212183068	0.432592070516086
Average	0.646357522306557	0.658002829080582	0.609101337111731	0.697157926040153

Phosphocreatine (Relative response)

	Control (male)	TCE (male)	Control (female)	TCE (female)
	0.00923126422288645	0.0118323738435359	0.0124272942900106	0.0204443067257476
	0.00874636132840988	0.00656835272626641	0.006870499856445	0.0222706593852555
	0.0133444324097765	0.0175739820608964	0.00648527984199975	0.0246034141864023
	0.0112491156550662	0.00799977077461321	0.0141208581080308	0.0106806739471165
Average	0.0106427934040348	0.0109936198513280	0.00997598302412154	0.0194997635611305

Proline (Relative response)

	Control (male)	TCE (male)	Control (female)	TCE (female)
	24.4319495088047	22.0931191735174	20.9604100159154	27.2426168212099
	15.4975861290219	27.1444717512963	19.9563425191946	31.0739226020547
	23.2088157215199	21.9664121745276	23.4678821712094	30.2650194575506
	27.5022914038966	25.4924771364715	25.6124770121144	17.7761605358969
Average	22.6601606908108	24.1741200589532	22.4992779296084	26.5894298541780

Serine (Relative response)

	Control (male)	TCE (male)	Control (female)	TCE (female)
	2.84411094158385	3.6119121509406	2.22397294076109	3.73634912502962
	1.87920004182018	3.07053475302572	4.05855423849056	3.14508491164355
	3.94365982281308	2.82218040310008	5.47187110239556	3.44663141113368
	3.42454953972271	3.05103426413128	3.20144798539712	1.81530869120788
Average	3.02288008648495	3.13891539279942	3.73896156676108	3.03584353475368

Stearic acid (Relative response)

	Control (male)	TCE (male)	Control (female)	TCE (female)
	6.91309120801016	7.53332825147143	7.93436466515582	7.78232163866481
	4.87134316455594	4.8659058076917	7.98100307448258	7.81067494919926
	6.63053315682201	10.8566227425942	4.99227232317821	11.6336049211439
	6.70754701723224	10.4698212685035	8.25559960790603	10.5342609772304
Average	6.28062863665509	8.43141951756521	7.29080991768066	9.44021562155959

Taurine (Relative response)

	Control (male)	TCE (male)	Control (female)	TCE (female)
	43.043378826464	46.4038091148418	55.2665878698384	38.4541217807254
	20.0822852645387	50.3794736843447	31.3669539554034	58.9464876935046
	59.1087334469787	57.9914822926646	51.2413176713261	41.8856552429641
	40.7547469586846	45.966197447735	54.2264936502988	39.0150415220936
Average	40.7472861241665	50.1852406348965	48.0253382867167	44.5753265598219

Threonine (Relative response)

	Control (male)	TCE (male)	Control (female)	TCE (female)
	26.5420764860022	25.3621321158205	21.6101427765488	26.1920945647155
	15.5664068054416	28.1049357860643	25.3375902592003	30.7539180473155
	28.5651419261022	24.4903955482921	29.80681448867	27.1990178468201
	28.0991613174298	26.6559267395848	27.1671781975568	20.256887999177
Average	24.6931966337440	26.1533475474404	25.9804314304940	26.1004796145070

Tryptophan (Relative response)

	Control (male)	TCE (male)	Control (female)	TCE (female)
	22.929500024936	24.5483681428409	25.3767889645271	27.469370591777
	12.7706124682438	28.3404384770958	18.4547752044255	32.4320060766087
	25.8799870674171	23.1094969203151	21.8962128270221	31.9109356926997
	28.4239605261903	22.7238760587342	24.910122391868	19.4735655817221
Average	22.5010150216968	24.6805448997465	22.6594748469607	27.8214694857019

Tyrosine (Relative response)

	Control (male)	TCE (male)	Control (female)	TCE (female)
	24.6509762455246	23.2712737632419	26.0342016608107	29.630537202672
	20.0021828323961	32.4001226913387	17.1165270912691	33.5005878690139
	27.6201399435239	25.9674033312299	22.5713434235082	36.1443975997278
	34.3982877739876	28.7289204311099	30.3339914982273	17.8693649893354
Average	26.6678966988581	27.5919300542301	24.0140159184538	29.2862219151873

139

Uridine diphosphate (UDP) (Relative response)

	Control (male)	TCE (male)	Control (female)	TCE (female)
	0.0033518685337579	0.0031522836087468	0.0153012826081498	0.00161097878565159
	0.00590550981546839	0.00219599257060329	0.00415648803688101	0.00365097711451088
	0.0145589703046561	0.00194907818723399	0.00473420871564339	0.00328549053214651
	0.00919455711140681	0.00416900942747892	0.00167351677546891	0.00470039945334479
Average	0.00825272644132230	0.00286659094851575	0.00646637403403578	0.00331196147141344

UDP-D-glucose (Relative response)

	Control (male)	TCE (male)	Control (female)	TCE (female)
	0.00670994037692693	0.0132905864697261	0.00814772892556413	0.0104882047204441
	0.00516975023734205	0.0168958426173064	0.00360393773695179	0.0047731829158808
	0.00627196530502524	0.00256552746324231	0.00591909017062665	0.00758903057646178
	0.00867898380394269	0.0187527903745959	0.0143916361244371	0.00194074933525791
Average	0.00670765993080923	0.0128761867312177	0.00801559823939492	0.00619779188701115

UDP-D-glucuronate (Relative response)

	Control (male)	TCE (male)	Control (female)	TCE (female)
	0.00471392646828303	0.00346694463448202	0.00408505129594013	0.00349561226252208
	0.00274720140636131	0.0043578868241915	0.00438882473959075	0.00351604767528023
	0.00456518116533876	0.00379733205942947	0.0046260766560671	0.00286452983453633
	0.00459118235876267	0.00445365316820503	0.0037990716865722	0.00316218479602178
Average	0.00415437284968644	0.00401895417157701	0.00422475609454255	0.00325959364209010

UDP-N-acetyl-D-glucosamine (Relative response)

	Control (male)	TCE (male)	Control (female)	TCE (female)
	0.017063582781425	0.0192122136908619	0.0297903679484937	0.0207281902856347
	0.0126368466921788	0.0279656617825415	0.0102726999330243	0.0167880594052918
	0.0163431153984168	0.00352922697109525	0.01173492173956	0.0146910827782388
	0.0115739731504456	0.0315453985196349	0.0235893422897365	0.00181393931681517
Average	0.0144043795056166	0.0205631252410334	0.0188468329777036	0.0135053179464951

Uridine monophosphate (UMP) (Relative response)

	Control (male)	TCE (male)	Control (female)	TCE (female)
	0.0368610588212438	0.0384572551611765	0.0384316837275267	0.0517829664163903
	0.0237788500214308	0.0363185812155498	0.0147581466924772	0.0234802041629992
	0.0260841424669152	0.0070419748487491	0.0168520318275162	0.0254934927569337
	0.0206169961202269	0.0592558427341418	0.0501673432868343	0.0021574110721452
Average	0.0268352618574542	0.0352684134899043	0.0300523013835886	0.0257285186021171

Uridine triphosphate (UTP) (Relative response)

	Control (male)	TCE (male)	Control (female)	TCE (female)
	0.0126490875078588	0.00319790805661974	0.00622141873974524	0.0200919200499327
	0.00211590704998849	0.00262880403884767	0.00272314163280093	0.00171444653806044
	0.00221911755798365	0.0201211011856383	0.00250441501041233	0.000999128367882522
	0.00444034400717764	0.0247789984384867	0.0140831063636847	0.00135699107472546
Average	0.00535611403075214	0.0126817029298981	0.00638302043666080	0.00604062150765028

Valine (Relative response)

	Control (male)	TCE (male)	Control (female)	TCE (female)
	49.370396422706	50.3161715704592	46.835277928922	56.1940808338651
	25.2264030689883	56.6150828869612	33.2183617117957	65.3861835732668
	51.0743702134923	46.3957859493568	45.400079357805	65.9606445149623
	59.5782956247264	53.2051145759724	52.9947785349814	37.0353220080988
Average	46.3123663324782	51.6330387456874	44.6121243833760	56.1440577325483

Xanthine (Relative response)

	Control (male)	TCE (male)	Control (female)	TCE (female)
	0.850855968452767	0.560425862505936	1.93173951991926	1.11430761853677
	0.356227281452005	0.458143734892495	0.407456897551187	0.404838264675126
	0.736787256278116	0.434408759792168	0.873838590834073	0.92848925845376

	0.63592566631639	0.649674377706509	0.888156649337771	0.174616410967954
Average	0.644949043124819	0.525663183724277	1.02529791441057	0.655562888158403

Acetyl Coenzyme A (aCoA) (Relative response)

	Control (male)	TCE (male)	Control (female)	TCE (female)
	0.00230367205791236	0.00103514271900399	0.00365335863830654	0.00144201215826825
	0.000933218924623687	0.000275611158176368	0.00125560575037268	0.000855204749019865
	0.00181074300118018	0.000407446594157108	0.000790456346177375	0.000520154001048692
	0.0006281626074971	0.000733071454520461	0.000627070436249632	0.00141546264663345
Average	0.00141894914780333	0.000612817981464482	0.00158162279277656	0.00105820838874256

Adenosine diphosphate (ADP) (Relative response)

	Control (male)	TCE (male)	Control (female)	TCE (female)
	0.0250695558872703	0.00897293633193122	0.0334025112834971	0.0143969696005388
	0.0201962162705393	0.0103228955992135	0.0274427353374992	0.0101199284641065
	0.0159519736371863	0.00785313065056357	0.0189611991123682	0.00689112311275041
	0.0161315081927367	0.0070754086986106	0.018082484181631	0.00895210651836235
Average	0.0193373134969331	0.0085560928200797	0.0244722324787489	0.0100900319239395

Adenosine monophosphate (AMP) (Relative response)

	Control (male)	TCE (male)	Control (female)	TCE (female)
	0.022937661063937	0.0263331660219209	0.0300127481701151	0.0358153928082896
	0.0217343026523885	0.0528775504621689	0.0172054115640828	0.00970554978274255
	0.0195139978985843	0.00683140336579784	0.0162002507945092	0.023664278998876
	0.0244899309625638	0.0241821114459859	0.0485116198554833	0.00904909525021646
Average	0.0221689731443684	0.0275560578239684	0.0279825075960476	0.0195585792100312

Adenosine triphosphate (ATP) (Relative response)

	Control (male)	TCE (male)	Control (female)	TCE (female)
	0.0180522516459992	0.00671926183990436	0.016896126867039	0.00846967787427657
	0.0106284612540424	0.00659045698023559	0.0161845753593636	0.00784222391166403
	0.0127466447429012	0.00785534859155683	0.0122498679213039	0.00606807910118435
	0.0104428010047217	0.0044559081504387	0.0122722372137768	0.00579842376741688
Average	0.0129675396619161	0.00640524389053387	0.0144007018403708	0.00704460116363546

Flavin adenine dinucleotide (FAD) (Relative response)

	Control (male)	TCE (male)	Control (female)	TCE (female)
	0.00390674695111207	0.00297182014845727	0.00506321239705208	0.00217606570718083
	0.00293330144689455	0.00291967732047542	0.00351504698944016	0.00311747835491235
	0.00385131662110685	0.00234733047735774	0.00350515767335303	0.00278075857592129
	0.00356789179657924	0.00273464752741646	0.00439723555479168	0.0032719789148241
Average	0.00356481420392318	0.00274336886842672	0.00412016315365924	0.00283657038820964

Guanosine monophosphate (GMP) (Relative response)

	Control (male)	TCE (male)	Control (female)	TCE (female)
	0.0220549778155518	0.0161137153404319	0.0267908371683052	0.0219804221338922
	0.0131379142522881	0.0126432041795463	0.0108501649996937	0.00890725905059403
	0.0114833023072668	0.00494910791393415	0.0112376289511407	0.00875986190723127
	0.00835507758761448	0.0188458868922096	0.0183623743515446	0.000863378438572987
Average	0.0137578179906803	0.0131379785815305	0.0168102513676711	0.0101277303825726

Nicotinamide adenine dinucleotide phosphate (NADP) (Relative response)

	Control (male)	TCE (male)	Control (female)	TCE (female)
	0.0131634487544033	0.00244234325500697	0.0178761349227166	0.00236423732715881
	0.0068291556632232	0.0036180119716935	0.0105690567941261	0.00280379042256425
	0.00637540546516435	0.00341562081729896	0.00543222423897134	0.00233739752658422
	0.0052977290900525		0.00450773195038907	0.00219170282335837
Average	0.00791643474321084	0.00315865868133314	0.00959628697655078	0.00242428202491641

Nicotinamide adenine dinucleotide phosphate hydrogen (NADPH) (Relative response)

	Control (male)	TCE (male)	Control (female)	TCE (female)

	0.000522216003857349		0.00215842175567091	
	0.000194430213628183	0.000526973129512696	0.00108203922503506	0.000751800335102332
	0.000721631144197339	0.000551997455421326	0.000607063162576973	0.000286584834522448
	0.00089610310662185		0.00025412183176231	0.000712903190261333
Average	0.000583595117076180	0.000539485292467011	0.001025411493761310	0.000583762786628704

Ribose 5-phosphate & xylulose 5-phosphate (R5P & X5P) (Relative response)

	Control (male)	TCE (male)	Control (female)	TCE (female)
	0.0148367020750656	0.0129333820807472	0.0470602976325785	0.0280443019937553
	0.0142973189301044	0.00595517768858172		0.0145260309080153
	0.0135073752465351	0.00957128784437392	0.00791059906467256	0.0207267889250782
	0.00812166299756489	0.0257399176624197	0.0217021626795717	0.00114466919829366
Average	0.0126907648123175	0.0135499413190306	0.0255576864589409	0.0161104477562856

Sedoheptulose 7-phosphate (S7P) (Relative response)

	Control (male)	TCE (male)	Control (female)	TCE (female)
	0.0215699092275346	0.0132299558340737	0.0267488929311904	0.0142098280524287
	0.00300880737726382	0.00495177856461123	0.00143397974475791	0.00454492632835358
	0.0112446588007931	0.00394995710112161	0.0100689652747451	0.0145157730902237
	0.0064667969662319	0.0127381394729425	0.0119427057840659	
Average	0.0105725430929559	0.00871745774318726	0.0125486359336898	0.0110901758236687

Table S3.3. Metabolites increased or decreased in response to trichloroethylene treatment for male and female amniotic fluid samples. Metabolites altered in any sex are listed first and followed by metabolites that are not altered in any sex. The values placed in **boldface** correspond to values associated with a p<0.05.

Metabolite	Change in response to TCE exposure (Male)		Change in response to TCE exposure (Female)	
	p-value	**Fold-change**	**p-value**	**Fold-change**
Adenosine diphosphate (ADP)	**0.0031**	**0.44247**	**0.0111**	**0.41231**
Adenosine triphosphate (ATP)	**0.0138**	**0.49394**	**0.0020**	**0.48918**
6-Phosphogluconate (6PG)	**0.0209**	**0.59525**	**0.0133**	**0.53028**
Flavin adenine dinucleotide (FAD)	**0.0211**	**0.76957**	**0.0287**	**0.68846**
Fructose 1,6-bisphosphate (FBP)	**0.0333**	**0.72137**	0.0792	0.73667
Guanosine triphosphate (GTP)	**0.0344**	**0.68422**	0.0539	0.69621
Guanine diphosphate (GDP)	**0.0441**	**0.81629**	**0.0174**	**0.76972**
Arginine	0.2228	1.3219	**0.0457**	**1.3802**
Uridine diphosphate (UDP)-D-glucoronate	0.8083	0.96740	**0.0066**	**0.77155**
Phosphocreatine	0.9001	1.0330	**0.0391**	**1.9547**
2-phosphoglyercerate / 3-phosphoglycerate (2PG/3PG)	0.5445	1.1788	0.0655	0.86926
Erythrose 4-phosphate (E4P)	0.0970	0.70770	0.9323	0.98236
Citrulline	0.6594	1.0575	0.0732	0.79640
Dihydroxyacetone phosphate	0.0670	0.67659	0.8228	0.92881
Homocysteic acid	0.5470	0.81825	0.0897	1.8314
Uridine diphosphate (UDP)	0.0720	0.34735	0.3462	0.51218
Nicotinamide adenine dinucleotide phosphate (NADP)	0.0754	0.39900	0.0580	0.25263
Acetate	0.8591	0.95862	0.8094	0.97281
Propionate	0.5452	1.3949	0.3556	0.83961
Butyrate	0.3131	1.9552	0.6450	0.60475
Isovalerate	0.1984	0.33614	0.7273	0.86885
Valerate	0.6197	0.70295	0.5180	1.18733
Hexanoate	0.5989	0.73131	0.4685	0.88325
Heptanoate	0.2075	0.45752	0.6580	1.21465
Octanoate	0.4141	0.71274	0.5692	0.84280

Citrate/ isocitrate (CIT/ICIT)	0.3423	1.19308	0.2945	1.07343
Fructose 6-phosphate / glucose 6-phosphate (F6P/G6P)	0.7217	1.08085	0.3723	0.82504
Glycerol 3-phosphate (Gl-OH3P)	0.4683	1.14326	0.5686	0.89116
Glyceraldehyde 3-phosphate (Glyceraldehyde3P)	0.8096	1.0707	0.6142	0.94236
Malate (MAL)	0.5381	1.1392	0.2223	0.83211
Phosphoenolpyruvate (PEP)	0.4830	1.1491	0.7881	1.0228
Succinate (SUC)	0.5198	1.1867	0.5050	0.81881
3-Phosphoserine	0.1241	0.57933	0.7862	0.91564
Acetylphosphate	0.5575	1.1431	0.7119	0.91539
Asparagine	0.1623	0.80676	0.4050	0.72234
Aspartate	0.3622	1.3171	0.7425	0.87211
Cytidine monophosphate (CMP)	0.3861	1.5057	0.8677	0.92857
Creatine	0.6804	1.0581	0.4204	1.0904
Creatinine	0.3666	1.1844	0.9579	0.98385
Deoxyuridine	0.2609	1.3393	0.2013	1.2576
Gluconate	0.7712	0.98858	0.5771	0.94266
Glutamate	0.5448	1.1855	0.9475	1.0375
Glutamine	0.4750	1.0668	0.7008	0.93641
Glutathione – oxidized (GSSG)	0.5554	1.3859	0.2383	0.45733
Glutathione – reduced (GSH)	0.1913	1.4484	0.8208	0.94321
Hexose (glucose, etc.)	0.4263	1.1767	0.2908	1.1961
Histidine	0.7575	0.95445	0.6331	1.1485
Hypoxanthine	0.1574	1.1800	0.2943	1.0966
Inosine monophosphate (IMP)	0.9409	0.95744	0.4311	1.3434
Inosine	0.5250	1.4553	0.5125	0.71016
Leucine / Isoleucine	0.3162	1.1462	0.3680	1.3014
Lysine	0.3909	1.1840	0.4201	1.1432
Methionine	0.3699	1.1678	0.2252	1.3129
N-Acetyl-glucosamine	0.7373	1.0771	0.8029	0.94589
Oleic acid	0.2303	1.1965	0.4952	1.1342
Ornithine	0.7584	1.0508	0.4140	1.2038
Palmitic acid	0.1480	1.2474	0.3437	1.1117
Pantothenate	0.7510	0.81694	0.7860	0.93995
Phenylalanine	0.4728	1.1087	0.3042	1.2859
Phenylpyruvate	0.8738	1.0180	0.4657	1.1446

Proline	0.5657	1.0668	0.3334	1.1818
Serine	0.7065	1.0384	0.4707	0.81195
Stearic acid	0.2540	1.3424	0.1483	1.2948
Taurine	0.2859	1.2316	0.7092	0.92816
Threonine	0.5886	1.0591	0.9983	1.0046
Tryptophan	0.5059	1.0969	0.2145	1.2278
Tyrosine	0.7434	1.0346	0.3888	1.2195
UDP-D-glucose	0.1459	1.9196	0.5618	0.77322
UDP-N-acetyl-D-glucosamine	0.3723	1.4276	0.4249	0.71658
Uridine monophosphate (UMP)	0.4839	1.3143	0.7560	0.85612
Uridine triphosphate (UTP)	0.2849	2.3677	0.9512	0.94636
Valine	0.4592	1.1149	0.2405	1.2585
Xanthine	0.3687	0.81505	0.3869	0.63939
Acetyl coenzyme A (aCoA)	0.1044	0.43188	0.5052	0.66906
Adenosine monophosphate (AMP)	0.5936	1.2430	0.4262	0.69896
Guanine monophosphate (GMP)	0.8879	0.95495	0.2903	0.60247
Nicotinamide adenine dinucleotide phosphate hydrogen (NADPH)	0.8627	0.92442	0.4192	0.56930
Ribose 5-phosphate / xylulose 5-phosphate (R5P/X5P)	0.8574	1.0677	0.4571	0.63036
D-sedoheptulose 7-phosphate (S7P)	0.7089	0.82454	0.8385	0.88378

Table S3.4. Effect of trichloroethylene treatment on amino acid metabolism-relevant metabolite ratios in male and female amniotic fluid samples. Abbreviations: ATP, adenosine triphosphate; ADP, adenosine diphosphate. The values placed in **boldface** correspond to values associated with a $p<0.05$.

Ratio	Male: response to TCE treatment		Female: response to TCE treatment	
	p-value	**Fold-change**	**p-value**	**Fold-change**
Arginine to creatine	**0.0491**	**1.2876**	**0.0147**	**1.2629**
Arginine to citrulline	0.3209	1.2189	**0.0345**	**1.6714**
Arginine to ornithine	0.1654	1.2923	0.2642	1.1884
Ornithine to citrulline	0.9921	0.99812	0.1282	1.4940
Aspartate to citrulline	0.8422	1.0716	0.9072	1.0571
Glutamine to citrulline	0.7117	0.94061	0.2689	1.1907
Aspartate to glutamine	0.6272	1.1751	0.6358	0.78764
Arginine to phosphocreatine	0.3062	1.5258	0.1306	0.69773
Glutamine to glutamate	0.8737	1.0703	0.4228	2.8765
Asparagine to aspartate	0.3311	0.68185	0.9793	1.0160
Glutamate to succinate	0.6104	0.69329	0.7084	1.1954
Phenylpyruvate to phenylalanine	0.2391	0.88653	**0.0335**	**0.89082**
Phenylalanine to tyrosine	0.2898	1.0929	0.2331	1.0428
Serine to 3-Phosphoserine	0.0637	1.7231	0.8802	1.0929
Homocysteic acid to methionine	0.2378	0.71793	0.3195	1.3212
Phosphocreatine to ATP	**0.0279**	**1.9634**	**0.0058**	**3.9260**
Phosphocreatine to creatine	0.9198	1.0340	**0.0406**	**1.8175**
Phosphocreatine to ADP	0.0784	2.2797	**0.0234**	**4.8037**
Creatine to ATP	**0.0378**	**2.2219**	**0.0023**	**2.2125**
Creatine to ADP	**0.0058**	**2.3524**	**0.0135**	**2.6553**
Creatinine to creatine	0.3142	0.80783	0.6015	1.0654

Table S3.5. Effect of trichloroethylene treatment on purine and pyrimidine metabolism-relevant metabolite ratios in male and female amniotic fluid samples. Abbreviations: ATP, adenosine triphosphate; ADP, adenosine diphosphate; AMP, adenosine monophosphate; GTP, guanosine triphosphate; GDP, guanosine diphosphate; GMP, guanosine monophosphate; IMP, inosine monophosphate. The values placed in **boldface** correspond to values associated with a $p<0.05$.

Ratio	Male: response to TCE treatment		Female: response to TCE treatment	
	p-value	Fold-change	p-value	Fold-change
ATP to ADP*	0.4649	1.1205	0.1700	1.1947
ADP to AMP	0.1624	0.56545	0.2783	0.64104
ATP to AMP	0.5529	0.72759	0.5112	0.77273
GTP to GDP	**0.0208**	**0.84585**	0.2645	0.91177
GDP to GMP	0.9750	1.0120	0.3500	4.0025
GTP to GMP	0.7176	0.87540	0.3647	3.4711
IMP to GMP	0.9772	1.0242	0.2012	5.1283
IMP to inosine	0.7910	0.77228	0.2647	3.5989
IMP to AMP	0.5805	1.5791	0.1276	2.4870
Inosine to hypoxanthine	0.6686	1.2219	0.3237	0.63464
Xanthine to hypoxanthine	0.0754	0.69121	0.2782	0.56857
UTP to UDP	0.1998	3.8760	0.8154	1.3526
UDP to UMP	0.1151	0.36442	0.5016	2.5091
UTP to UMP	0.3556	4.6834	0.5590	1.4557
IMP to xanthine	0.7039	1.2645	0.1121	2.4165
GMP to xanthine	0.8563	1.0571	0.4214	0.75786

*denotes relevance to both purine metabolism and phosphocreatine shuttling

Table S3.6. Effect of trichloroethylene treatment on glycolysis, tricarboxylic acid cycle, pentose phosphate pathway, and pyruvate metabolism-relevant metabolite ratios in male and female amniotic fluid samples. The values placed in **boldface** correspond to values associated with a $p<0.05$. Abbreviations: G6P, glucose 6-phosphate; F6P, fructose 6-phosphate; FBP, fructose 1,6-bisphosphate; Glyceraldehyde3P, glyceraldehyde 3-phosphate; DAP, dihydroxyacetone phosphate; 2PG, 2-phosphoglycerate; 3PG, 3-phosphoglycerate; PEP, phosphoenolpyruvate; aCoA, acetyl coenzyme A; CIT, citrate; ICIT, isocitrate; 6PG, 6-phosphogluconate; R5P, ribose 5-phosphate; X5P, xylulose 5-phosphate; E4P, erythrose 4-phosphate; S7P, sedoheptulose 7-phosphate.

Glycolysis (aka glycolysis or gluconeogenesis)				
Ratio	**Male: response to TCE treatment**		**Female: response to TCE treatment**	
	p-value	**Fold-change**	**p-value**	**Fold-change**
G6P/F6P to FBP	0.0980	1.5002	0.6605	1.1014
FBP to Glyceraldehyde3P*	0.0976	0.71815	0.2686	0.78329
FBP to DAP	0.6988	1.0644	0.7398	0.90280
Glyceraldehyde3P to DAP	0.1301	1.6005	0.7399	1.1243
Glyceraldehyde3P to 2PG/3PG	0.5814	0.67570	0.5352	1.1018
2PG/3PG to PEP	0.6768	1.0616	0.0593	0.83946
PEP to aCoA**	0.0540	2.5567	0.6388	1.2434
Acetate to aCoA***	0.1423	2.4024	0.7358	1.2020
G6P/F6P to PEP	0.5518	0.89379	0.2768	0.79725
G6P/F6P to aCoA	**0.0322**	**2.6695**	0.9850	0.99101
TCA cycle				
Ratio	**Male: response to TCE treatment**		**Female: response to TCE treatment**	
	p-value	**Fold-change**	**p-value**	**Fold-change**
aCoA to CIT/ICIT	**0.0411**	**0.32849**	0.4451	0.63937
CIT/ICIT to Succinate	0.7316	0.92860	0.2638	1.4158
Succinate to Malate	0.5955	1.0604	0.8968	0.96335
CIT/ICIT to Malate	0.9498	1.0081	**0.0206**	**1.2807**
aCoA to Malate****	**0.0387**	**0.34666**	0.7377	0.85561
Pentose phosphate pathway				
Ratio	**Male: response to TCE treatment**		**Female: response to TCE treatment**	
	p-value	**Fold-change**	**p-value**	**Fold-change**
R5P/X5P to S7P	0.7599	0.83883	0.2962	1.5125
Glyceraldehyde3P to E4P	**0.0017**	**1.5370**	0.9159	1.0324
FBP to E4P	0.5482	1.1396	0.4883	0.80103
S7P to E4P	0.6138	1.2811	0.9290	1.0593
G6P/F6P to 6PG	**0.0310**	**1.8105**	0.1164	1.4802

Gluconate to 6PG	**0.0047**	**1.5841**	**0.0166**	**1.7354**
S7P to 6PG	0.3997	1.4638	0.3033	1.6523
E4P to 6PG	0.4867	1.1485	0.1408	1.8494
R5P/X5P to 6PG	0.2433	1.7646	0.7353	1.1914
R5P/X5P to Glyceraldehyde3P	0.8298	1.0760	0.5588	0.68535
R5P/X5P to gluconate	0.7868	1.1205	0.5008	0.68769
E4P to gluconate	0.1181	0.71645	0.8466	1.0857
S7P to gluconate	0.7437	0.83688	0.8843	0.92607
S7P to FBP	0.6856	1.1906	0.6089	1.2663
R5P/X5P to FBP	0.3704	1.4914	0.8962	0.93566
S7P to Glyceraldehyde3P	0.6616	0.79365	0.9895	0.99186
Pyruvate metabolism pathway				
Ratio	**Male: response to TCE treatment**		**Female: response to TCE treatment**	
	p-value	**Fold-change**	**p-value**	**Fold-change**
Acetylphosphate to acetate	0.3736	1.2621	0.4763	0.93020
Malate to PEP	0.8095	0.98072	0.0617	0.81347
Malate to acetate	0.3262	1.2661	0.3394	0.88615

*denotes relevance to both glycolysis and pentose phosphate pathway

**denotes relevance to glycolysis, tricarboxylic acid cycle, and pyruvate metabolism

***denotes relevance to both glycolysis and pyruvate metabolism

****denotes relevance to tricarboxylic acid cycle and pyruvate metabolism

Table S3.7. Effect of trichloroethylene treatment on glutathione metabolism-relevant metabolite ratios in male and female amniotic fluid samples. Abbreviations: GSH, glutathione; GSSG, glutathione disulfide; NADP, nicotinamide adenine dinucleotide phosphate; NADPH, nicotinamide adenine dinucleotide phosphate hydrogen.

Ratio	Male: response to TCE treatment		Female: response to TCE treatment	
	p-value	**Fold-change**	**p-value**	**Fold-change**
GSH to GSSG	0.4133	1.8650	0.1888	1.8526
GSSG to NADP	0.3219	2.8786	0.4660	1.5823
NADP to NADPH	0.3030	0.34773	0.0882	0.44586
GSH to NADPH	0.7516	0.81284	0.9805	0.98090
GSH to glutamate	0.3244	1.3857	0.4136	2.5504

Table S3.8. Effect of trichloroethylene treatment on other important metabolite ratios in male and female amniotic fluid samples. Abbreviations: DAP, dihydroxyacetone phosphate; UDP, uridine diphosphate.

Ratio	Male: response to TCE treatment		Female: response to TCE treatment		Significance
	p-value	Fold-change	p-value	Fold-change	
DAP to glycerol 3-phosphate	0.1414	0.51982	0.7434	1.2260	Glycerophospholipid metabolism
Stearic acid to oleic acid	0.5634	1.1657	0.5393	1.1754	Fatty acid biosynthesis
Stearic acid to palmitic acid	0.6174	1.0503	0.0890	1.1592	Fatty acid biosynthesis
Oleic acid to palmitic acid	0.9019	0.98367	0.8439	1.0372	Fatty acid biosynthesis
UDP-D-glucose to UDP-D-glucuronate	0.1233	1.9175	0.9415	0.96671	Various pathways

(A)
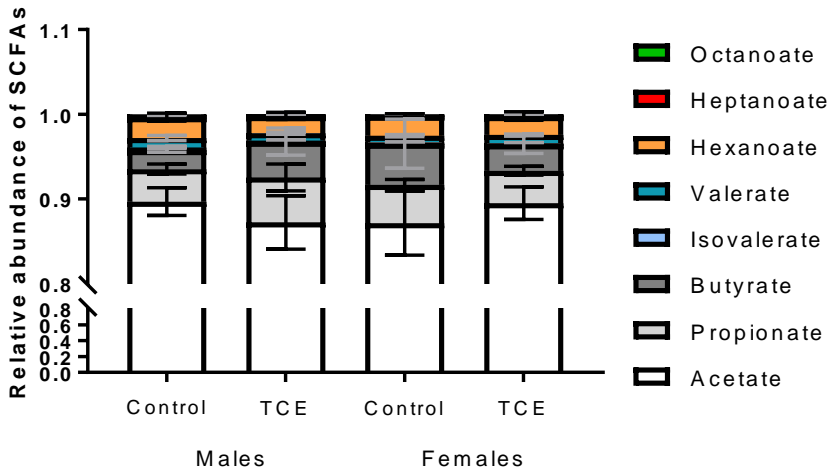
(B)
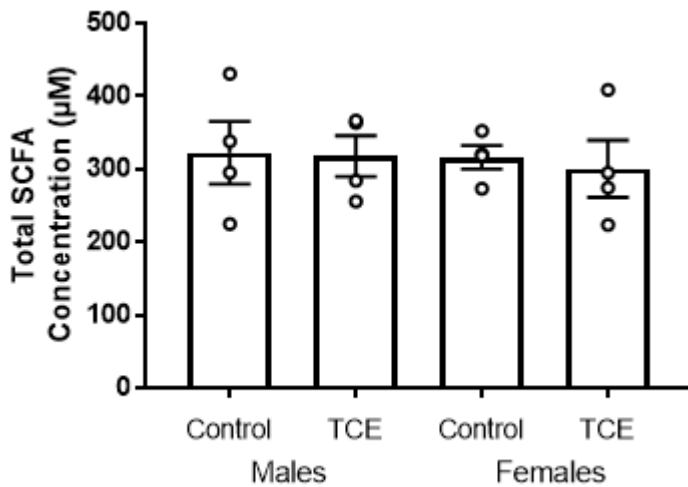
Figure S3.1. Short chain fatty acid (SCFA)-specific analysis. (A) Regardless of treatment group or sex, acetate contributed to the vast majority of SCFAs in the amniotic fluid. (B) Total SCFA concentration was unchanged by TCE treatment for both sex groups, as assessed by a student's unpaired two-tailed t-test on the data (generalized log-transformed). Each individual SCFA was unchanged by TCE treatment for both sexes, as well. Error bars represent mean ± SEM for both (A) and (B). N=4 independent experiments.

Table S3.9. Enrichment analysis results of organ, tissue, and subcellular structures predicted to be altered by trichloroethylene treatment based on male amniotic fluid alterations.

	Total Compounds	Hits	Statistic Q^a	Expected Q^a	Raw p	Holm p	FDR[b]
Thyroid Gland	12	1	54.638	14.286	0.036134	1	0.57884
Endoplasmic Reticulum	53	7	26.473	14.286	0.059796	1	0.57884
Nucleus	23	2	30.904	14.286	0.094831	1	0.57884
Skeletal Muscle	123	15	23.062	14.286	0.11952	1	0.57884
Peroxisome	37	5	26.829	14.286	0.13197	1	0.57884
Golgi Apparatus	14	4	24.865	14.286	0.16007	1	0.57884
Muscle	160	19	21.944	14.286	0.16304	1	0.57884
Brain	122	2	24.265	14.286	0.18448	1	0.57884
Platelet	108	5	22.281	14.286	0.19659	1	0.57884
Prostate	267	37	18.691	14.286	0.22415	1	0.57884
Gonad	42	1	23.403	14.286	0.22452	1	0.57884
Bladder	87	10	18.69	14.286	0.23154	1	0.57884
Mitochondria	98	12	19.028	14.286	0.25304	1	0.58248
Bone Marrow	21	1	18.175	14.286	0.29221	1	0.58248
Spleen	170	10	17.975	14.286	0.29922	1	0.58248
Placenta	183	16	16.854	14.286	0.32203	1	0.58248
Testes	72	4	16.551	14.286	0.33007	1	0.58248
Intestine	251	16	15.997	14.286	0.3682	1	0.61367
Liver	234	5	13.052	14.286	0.4101	1	0.62327
Kidney	164	6	15.019	14.286	0.43653	1	0.62327
Erythrocyte	34	2	10.69	14.286	0.43695	1	0.62327
Pancreas	118	12	13.21	14.286	0.45707	1	0.62327
Fibroblasts	183	10	11.856	14.286	0.52	1	0.67826
Neuron	69	4	11.892	14.286	0.55754	1	0.69692
Nervous Tissue	12	2	8.0256	14.286	0.60247	1	0.72297
Epidermis	216	19	10.911	14.286	0.67558	1	0.77951
Nerve Cells	35	3	5.4681	14.286	0.70714	1	0.78571
Heart	8	1	1.1425	14.286	0.80111	1	0.82729
Smooth Muscle	9	1	1.1425	14.286	0.80111	1	0.82729
Skin	125	5	6.6796	14.286	0.82729	1	0.82729

[a]The equation for the Q statistics can be found in Goeman *et al.* 2004 (Goeman *et al.*, 2004). Q can be considered as a squared covariance aggregate between metabolite concentrations and treatment.
[b]FDR refers to false discovery rate.

Table S3.10. Enrichment analysis results of organ, tissue, and subcellular structures predicted to be altered by trichloroethylene treatment based on female amniotic fluid alterations.

	Total Compounds	Hits	Statistic Q^a	Expected Q^a	Raw p	Holm p	FDR[b]
Gonad	42	1	51.374	14.286	0.045424	1	0.70489
Skin	125	5	31.686	14.286	0.08703	1	0.70489
Bladder	87	10	24.719	14.286	0.17509	1	0.70489
Bone Marrow	21	1	22.059	14.286	0.24031	1	0.70489
Heart	8	1	21.381	14.286	0.24866	1	0.70489
Smooth Muscle	9	1	21.381	14.286	0.24866	1	0.70489
Neuron	69	4	17.371	14.286	0.30335	1	0.70489
Muscle	160	19	16.308	14.286	0.31482	1	0.70489
Mitochondria	98	12	16.643	14.286	0.3263	1	0.70489
Nerve Cells	35	3	15.584	14.286	0.33211	1	0.70489
Liver	234	5	15.507	14.286	0.33285	1	0.70489
Endoplasmic Reticulum	53	7	16.795	14.286	0.33515	1	0.70489
Skeletal Muscle	123	15	15.213	14.286	0.34157	1	0.70489
Intestine	251	16	14.808	14.286	0.34661	1	0.70489
Platelet	108	5	14.675	14.286	0.35691	1	0.70489
Erythrocyte	34	2	11.924	14.286	0.40689	1	0.70489
Thyroid Gland	12	1	10.565	14.286	0.43212	1	0.70489
Testes	72	4	11.336	14.286	0.4462	1	0.70489
Fibroblasts	183	10	10.683	14.286	0.44643	1	0.70489
Peroxisome	37	5	12.05	14.286	0.50178	1	0.72568
Kidney	164	6	8.6464	14.286	0.56822	1	0.72568
Nucleus	23	2	6.4037	14.286	0.58206	1	0.72568
Epidermis	216	19	9.7735	14.286	0.59021	1	0.72568
Prostate	267	37	9.6945	14.286	0.59838	1	0.72568
Spleen	170	10	7.8139	14.286	0.62296	1	0.72568
Brain	122	2	7.615	14.286	0.62892	1	0.72568
Pancreas	118	12	7.3092	14.286	0.67052	1	0.74502
Golgi Apparatus	14	4	7.2038	14.286	0.6977	1	0.74521
Nervous Tissue	12	2	5.2748	14.286	0.72037	1	0.74521
Placenta	183	16	6.1075	14.286	0.79124	1	0.79124

[a]The equation for the Q statistics can be found in Goeman *et al.* 2004 (Goeman *et al.*, 2004). Q can be considered as a squared covariance aggregate between metabolite concentrations and treatment.
[b]FDR refers to false discovery rate.

Table S3.11. Enrichment analysis results of top ten drug pathways altered by trichloroethylene treatment in the male amniotic fluid samples. The 10th pathway on the list, citalopram action pathway, was the only pathway with a raw p-value of 0.001435.

	Total Compounds	Hits	Statistic Q^a	Expected Q^a	Raw p	Holm p	FDR[b]
Acetaminophen Metabolism Pathway	17	5	58.661	14.286	0.000135	0.04769	0.004415
Codeine Action Pathway	21	4	63.58	14.286	0.000191	0.067134	0.004415
Etoposide Action Pathway	15	4	63.58	14.286	0.000191	0.067134	0.004415
Etoposide Metabolism Pathway	15	4	63.58	14.286	0.000191	0.067134	0.004415
Irinotecan Action Pathway	12	4	63.58	14.286	0.000191	0.067134	0.004415
Irinotecan Metabolism Pathway	12	4	63.58	14.286	0.000191	0.067134	0.004415
Morphine Action Pathway	16	4	63.58	14.286	0.000191	0.067134	0.004415
Mycophenolic Acid Metabolism Pathway	20	4	63.58	14.286	0.000191	0.067134	0.004415
Tramadol Metabolism Pathway	18	4	63.58	14.286	0.000191	0.067134	0.004415
Citalopram Action Pathway	28	3	78.238	14.286	0.001435	0.49219	0.004415

[a]The equation for the Q statistics can be found in Goeman *et al.* 2004 (Goeman *et al.*, 2004). Q can be considered as a squared covariance aggregate between metabolite concentrations and treatment.
[b]FDR refers to false discovery rate.

Table S3.12. Enrichment analysis results of top 5 drug pathways altered by trichloroethylene treatment in the female amniotic fluid samples. The 5th pathway on the list, citalopram action pathway, was the only pathway with a raw p-value of 0.002027, and the next 120 pathways on the list had a raw p-value of 0.003382.

	Total Compounds	Hits	Statistic Q^a	Expected Q^a	Raw p	Holm p	FDR[b]
Glibenclamide Action Pathway	5	1	84.029	14.286	0.001358	0.47789	0.009186
Gliclazide Action Pathway	6	1	84.029	14.286	0.001358	0.47789	0.009186
Nateglinide Action Pathway	5	1	84.029	14.286	0.001358	0.47789	0.009186
Repaglinide Action Pathway	5	1	84.029	14.286	0.001358	0.47789	0.009186
Citalopram Action Pathway	28	3	75.516	14.286	0.002027	0.70555	0.009186

[a]The equation for the Q statistics can be found in Goeman *et al.* 2004 (Goeman *et al.*, 2004). Q can be considered as a squared covariance aggregate between metabolite concentrations and treatment.
[b]FDR refers to false discovery rate.

References

Agency for Toxic Substances and Disease Registry, 2007. Trichloroethylene Toxicity: What are the U.S. Standards for Trichloroethylene Exposure? In Agency for Toxic Substances and Disease Registry (ATSDR), E.H.a.M.E., (Ed.), Atlanta, GA, pp.

Agency for Toxic Substances and Disease Registry, 2019. Toxicological Profile for Trichloroethylene. In U.S. Department of Health and Human Services, A.f.T.S.a.D.R.A., (Ed.), Atlanta, GA, pp.

Al-Gubory, K.H., Fowler, P.A., Garrel, C., 2010. The roles of cellular reactive oxygen species, oxidative stress and antioxidants in pregnancy outcomes. Int J Biochem Cell Biol **42**, 1634-1650.

Aouache, R., Biquard, L., Vaiman, D., Miralles, F., 2018. Oxidative Stress in Preeclampsia and Placental Diseases. Int J Mol Sci **19**.

Araujo, J.R., Correia-Branco, A., Pereira, A.C., Pinho, M.J., Keating, E., Martel, F., 2013. Oxidative stress decreases uptake of neutral amino acids in a human placental cell line (BeWo cells). Reprod Toxicol **40**, 76-81.

Axelson, O., Selden, A., Andersson, K., Hogstedt, C., 1994. Updated and expanded Swedish cohort study on trichloroethylene and cancer risk. J Occup Med **36**, 556-562.

Bahado-Singh, R.O., Akolekar, R., Mandal, R., Dong, E., Xia, J., Kruger, M., Wishart, D.S., Nicolaides, K., 2012. Metabolomics and first-trimester prediction of early-onset preeclampsia. J Matern Fetal Neonatal Med **25**, 1840-1847.

Bahado-Singh, R.O., Syngelaki, A., Akolekar, R., Mandal, R., Bjondahl, T.C., Han, B., Dong, E., Bauer, S., Alpay-Savasan, Z., Graham, S., Turkoglu, O., Wishart, D.S., Nicolaides, K.H., 2015. Validation of metabolomic models for prediction of early-onset preeclampsia. Am J Obstet Gynecol **213**, 530 e531-530 e510.

Ballard, F.J., Oliver, I.T., 1964. Ketohexokinase, isoenzymes of glucokinase and glycogen synthesis from hexoses in neonatal rat liver. Biochem J **90**, 261-268.

Chong, J., Soufan, O., Li, C., Caraus, I., Li, S., Bourque, G., Wishart, D.S., Xia, J., 2018. MetaboAnalyst 4.0: towards more transparent and integrative metabolomics analysis. Nucleic Acids Res **46**, W486-W494.

Chong, J., Wishart, D.S., Xia, J., 2019. Using MetaboAnalyst 4.0 for Comprehensive and Integrative Metabolomics Data Analysis. Curr Protoc Bioinformatics **68**, e86.

Cohen, S.S., 1951. Gluconokinase and the oxidative path of glucose-6-phosphate utilization. J Biol Chem **189**, 617-628.

Demehri, F.R., Frykman, P.K., Cheng, Z., Ruan, C., Wester, T., Nordenskjold, A., Kawaguchi, A., Hui, T.T., Granstrom, A.L., Funari, V., Teitelbaum, D.H., Group, H.C.R., 2016. Altered fecal short chain fatty acid composition in children with a history of Hirschsprung-associated enterocolitis. J Pediatr Surg **51**, 81-86.

den Besten, G., Havinga, R., Bleeker, A., Rao, S., Gerding, A., van Eunen, K., Groen, A.K., Reijngoud, D.J., Bakker, B.M., 2014. The short-chain fatty acid uptake fluxes by mice on a guar gum supplemented diet associate with amelioration of major biomarkers of the metabolic syndrome. PLoS One **9**, e107392.

den Besten, G., van Eunen, K., Groen, A.K., Venema, K., Reijngoud, D.J., Bakker, B.M., 2013. The role of short-chain fatty acids in the interplay between diet, gut microbiota, and host energy metabolism. J Lipid Res **54**, 2325-2340.

Dickinson, H., Davies-Tuck, M., Ellery, S.J., Grieger, J.A., Wallace, E.M., Snow, R.J., Walker, D.W., Clifton, V.L., 2016. Maternal creatine in pregnancy: a retrospective cohort study. BJOG **123**, 1830-1838.

Dickinson, H., Ellery, S., Ireland, Z., LaRosa, D., Snow, R., Walker, D.W., 2014. Creatine supplementation during pregnancy: summary of experimental studies suggesting a treatment to improve fetal and neonatal morbidity and reduce mortality in high-risk human pregnancy. BMC Pregnancy Childbirth **14**, 150.

Elkin, E.R., Bridges, D., Harris, S.M., Loch-Caruso, R.K., 2020. Exposure to Trichloroethylene Metabolite S-(1,2-Dichlorovinyl)-L-cysteine Causes Compensatory Changes to Macronutrient Utilization and Energy Metabolism in Placental HTR-8/SVneo Cells. Chem Res Toxicol.

Elkin, E.R., Harris, S.M., Loch-Caruso, R., 2018. Trichloroethylene metabolite S-(1,2-dichlorovinyl)-l-cysteine induces lipid peroxidation-associated apoptosis via the intrinsic and extrinsic apoptosis pathways in a first-trimester placental cell line. Toxicol Appl Pharmacol **338**, 30-42.

Ellery, S.J., Della Gatta, P.A., Bruce, C.R., Kowalski, G.M., Davies-Tuck, M., Mockler, J.C., Murthi, P., Walker, D.W., Snow, R.J., Dickinson, H., 2017. Creatine biosynthesis and transport by the term human placenta. Placenta **52**, 86-93.

Fisher, J.W., Whittaker, T.A., Taylor, D.H., Clewell, H.J., 3rd, Andersen, M.E., 1989. Physiologically based pharmacokinetic modeling of the pregnant rat: a multiroute exposure model for trichloroethylene and its metabolite, trichloroacetic acid. Toxicol Appl Pharmacol **99**, 395-414.

Forand, S.P., Lewis-Michl, E.L., Gomez, M.I., 2012. Adverse birth outcomes and maternal exposure to trichloroethylene and tetrachloroethylene through soil vapor intrusion in New York State. Environ Health Perspect **120**, 616-621.

Forkert, P.G., Lash, L.H., Nadeau, V., Tardif, R., Simmonds, A., 2002. Metabolism and toxicity of trichloroethylene in epididymis and testis. Toxicol Appl Pharmacol **182**, 244-254.

Garcia-Flores, V., Romero, R., Miller, D., Xu, Y., Done, B., Veerapaneni, C., Leng, Y., Arenas-Hernandez, M., Khan, N., Panaitescu, B., Hassan, S.S., Alvarez-Salas, L.M., Gomez-Lopez, N., 2018. Inflammation-Induced Adverse Pregnancy and Neonatal Outcomes Can Be Improved by the Immunomodulatory Peptide Exendin-4. Front Immunol **9**, 1291.

Gil, A.M., Duarte, D., 2018. Biofluid Metabolomics in Preterm Birth Research. Reprod Sci **25**, 967-977.

Goeman, J.J., van de Geer, S.A., de Kort, F., van Houwelingen, H.C., 2004. A global test for groups of genes: testing association with a clinical outcome. Bioinformatics **20**, 93-99.

Graca, G., Moreira, A.S., Correia, A.J., Goodfellow, B.J., Barros, A.S., Duarte, I.F., Carreira, I.M., Galhano, E., Pita, C., Almeida Mdo, C., Gil, A.M., 2013. Mid-infrared (MIR) metabolic fingerprinting of amniotic fluid: a possible avenue for early diagnosis of prenatal disorders? Anal Chim Acta **764**, 24-31.

Gray, L.E., O'Hely, M., Ranganathan, S., Sly, P.D., Vuillermin, P., 2017. The Maternal Diet, Gut Bacteria, and Bacterial Metabolites during Pregnancy Influence Offspring Asthma. Front Immunol **8**, 365.

Hashemi, Z., Fouhse, J., Im, H.S., Chan, C.B., Willing, B.P., 2017. Dietary Pea Fiber Supplementation Improves Glycemia and Induces Changes in the Composition of Gut Microbiota, Serum Short Chain Fatty Acid Profile and Expression of Mucins in Glucose Intolerant Rats. Nutrients **9**.

Hassan, I., Kumar, A.M., Park, H.R., Lash, L.H., Loch-Caruso, R., 2016. Reactive Oxygen Stimulation of Interleukin-6 Release in the Human Trophoblast Cell Line HTR-8/SVneo by the Trichlorethylene Metabolite S-(1,2-Dichloro)-l-Cysteine. Biol Reprod **95**, 66.

Henschler, D., Romen, W., Elsasser, H.M., Reichert, D., Eder, E., Radwan, Z., 1980. Carcinogenicity study of trichloroethylene by longterm inhalation in three animal species. Arch Toxicol **43**, 237-248.

Higgins, M., Mc Auliffe, F., 2010. A review of maternal and fetal growth factors in diabetic pregnancy. Curr Diabetes Rev **6**, 116-125.

Huang, J., Mo, J., Zhao, G., Lin, Q., Wei, G., Deng, W., Chen, D., Yu, B., 2017. Application of the amniotic fluid metabolome to the study of fetal malformations, using Down syndrome as a specific model. Mol Med Rep **16**, 7405-7415.

Kumar, P., Prasad, A.K., Mani, U., Maji, B.K., Dutta, K.K., 2001. Trichloroethylene induced testicular toxicity in rats exposed by inhalation. Hum Exp Toxicol **20**, 585-589.

Laanpere, M., Altmae, S., Stavreus-Evers, A., Nilsson, T.K., Yngve, A., Salumets, A., 2010. Folate-mediated one-carbon metabolism and its effect on female fertility and pregnancy viability. Nutr Rev **68**, 99-113.

Lash, L.H., Anders, M.W., 1986. Cytotoxicity of S-(1,2-dichlorovinyl)glutathione and S-(1,2-dichlorovinyl)-L-cysteine in isolated rat kidney cells. J Biol Chem **261**, 13076-13081.

Lash, L.H., Anders, M.W., 1987. Mechanism of S-(1,2-dichlorovinyl)-L-cysteine- and S-(1,2-dichlorovinyl)-L-homocysteine-induced renal mitochondrial toxicity. Mol Pharmacol **32**, 549-556.

Lindsay, K.L., Hellmuth, C., Uhl, O., Buss, C., Wadhwa, P.D., Koletzko, B., Entringer, S., 2015. Longitudinal Metabolomic Profiling of Amino Acids and Lipids across Healthy Pregnancy. PLoS One **10**, e0145794.

Liu, J., Huang, H., Xing, X., Xi, R., Zhuang, Z., Yuan, J., Yang, F., Zhao, J., 2007. Comparative proteomic analysis on human L-02 liver cells treated with varying concentrations of trichloroethylene. Toxicol Ind Health **23**, 91-101.

Loch-Caruso, R., Hassan, I., Harris, S.M., Kumar, A., Bjork, F., Lash, L.H., 2019. Trichloroethylene exposure in mid-pregnancy decreased fetal weight and increased placental markers of oxidative stress in rats. Reprod Toxicol **83**, 38-45.

Lope, V., Perez-Gomez, B., Aragones, N., Lopez-Abente, G., Gustavsson, P., Plato, N., Silva-Mato, A., Pollan, M., 2009. Occupational exposure to chemicals and risk of thyroid cancer in Sweden. Int Arch Occup Environ Health **82**, 267-274.

Lorenz, M.A., Burant, C.F., Kennedy, R.T., 2011. Reducing time and increasing sensitivity in sample preparation for adherent mammalian cell metabolomics. Anal Chem **83**, 3406-3414.

Ly, A., Ishiguro, L., Kim, D., Im, D., Kim, S.E., Sohn, K.J., Croxford, R., Kim, Y.I., 2016. Maternal folic acid supplementation modulates DNA methylation and gene expression in the rat offspring in a gestation period-dependent and organ-specific manner. J Nutr Biochem **33**, 103-110.

Lynge, E., Anttila, A., Hemminki, K., 1997. Organic solvents and cancer. Cancer Causes Control **8**, 406-419.

McCullough, L.E., Miller, E.E., Calderwood, L.E., Shivappa, N., Steck, S.E., Forman, M.R., M, A.M., Maguire, R., Fuemmeler, B.F., Kollins, S.H., S, D.B., Huang, Z., Murtha, A.P., Murphy, S.K., Hebert, J.R., Hoyo, C., 2017. Maternal inflammatory diet and adverse

pregnancy outcomes: Circulating cytokines and genomic imprinting as potential regulators? Epigenetics **12**, 688-697.

Melody, S.M., Vincent, R., Mori, T.A., Mas, E., Barden, A.E., Waddell, B.J., Keelan, J.A., 2015. Effects of omega-3 and omega-6 fatty acids on human placental cytokine production. Placenta **36**, 34-40.

Menon, R., Jones, J., Gunst, P.R., Kacerovsky, M., Fortunato, S.J., Saade, G.R., Basraon, S., 2014. Amniotic fluid metabolomic analysis in spontaneous preterm birth. Reprod Sci **21**, 791-803.

Meyer, R.A., Sweeney, H.L., Kushmerick, M.J., 1984. A simple analysis of the "phosphocreatine shuttle". Am J Physiol **246**, C365-377.

Olsiewski, P.J., Kaczorowski, G.J., Walsh, C., 1980. Purification and properties of D-amino acid dehydrogenase, an inducible membrane-bound iron-sulfur flavoenzyme from Escherichia coli B. J Biol Chem **255**, 4487-4494.

Orczyk-Pawilowicz, M., Jawien, E., Deja, S., Hirnle, L., Zabek, A., Mlynarz, P., 2016. Metabolomics of Human Amniotic Fluid and Maternal Plasma during Normal Pregnancy. PLoS One **11**, e0152740.

Priyadarshini, M., Thomas, A., Reisetter, A.C., Scholtens, D.M., Wolever, T.M., Josefson, J.L., Layden, B.T., 2014. Maternal short-chain fatty acids are associated with metabolic parameters in mothers and newborns. Transl Res **164**, 153-157.

Rodenbeck, S.E., Sanderson, L.M., Rene, A., 2000. Maternal exposure to trichloroethylene in drinking water and birth-weight outcomes. Arch Environ Health **55**, 188-194.

Romero, R., Mazaki-Tovi, S., Vaisbuch, E., Kusanovic, J.P., Chaiworapongsa, T., Gomez, R., Nien, J.K., Yoon, B.H., Mazor, M., Luo, J., Banks, D., Ryals, J., Beecher, C., 2010. Metabolomics in premature labor: a novel approach to identify patients at risk for preterm delivery. J Matern Fetal Neonatal Med **23**, 1344-1359.

Ruckart, P.Z., Bove, F.J., Maslia, M., 2014. Evaluation of contaminated drinking water and preterm birth, small for gestational age, and birth weight at Marine Corps Base Camp Lejeune, North Carolina: a cross-sectional study. Environ Health **13**, 99.

Scheuermann-Freestone, M., Madsen, P.L., Manners, D., Blamire, A.M., Buckingham, R.E., Styles, P., Radda, G.K., Neubauer, S., Clarke, K., 2003. Abnormal cardiac and skeletal muscle energy metabolism in patients with type 2 diabetes. Circulation **107**, 3040-3046.

Schonfeld, P., Wojtczak, L., 2016. Short- and medium-chain fatty acids in energy metabolism: the cellular perspective. J Lipid Res **57**, 943-954.

Seegal, R.F., Brosch, K.O., Okoniewski, R.J., 1997. Effects of in utero and lactational exposure of the laboratory rat to 2,4,2',4'- and 3,4,3',4'-tetrachlorobiphenyl on dopamine function. Toxicol Appl Pharmacol **146**, 95-103.

Sharp, A.N., Heazell, A.E., Crocker, I.P., Mor, G., 2010. Placental apoptosis in health and disease. Am J Reprod Immunol **64**, 159-169.

Shimazu, T., Hirschey, M.D., Huang, J.Y., Ho, L.T., Verdin, E., 2010. Acetate metabolism and aging: An emerging connection. Mech Ageing Dev **131**, 511-516.

Shirasuna, K., Takano, H., Seno, K., Ohtsu, A., Karasawa, T., Takahashi, M., Ohkuchi, A., Suzuki, H., Matsubara, S., Iwata, H., Kuwayama, T., 2016. Palmitic acid induces interleukin-1beta secretion via NLRP3 inflammasomes and inflammatory responses through ROS production in human placental cells. J Reprod Immunol **116**, 104-112.

Shivu, G.N., Abozguia, K., Phan, T.T., Ahmed, I., Henning, A., Frenneaux, M., 2010. (31)P magnetic resonance spectroscopy to measure in vivo cardiac energetics in normal

myocardium and hypertrophic cardiomyopathy: Experiences at 3T. Eur J Radiol **73**, 255-259.

Spaans, F., de Vos, P., Bakker, W.W., van Goor, H., Faas, M.M., 2014a. Danger signals from ATP and adenosine in pregnancy and preeclampsia. Hypertension **63**, 1154-1160.

Spaans, F., Melgert, B.N., Chiang, C., Borghuis, T., Klok, P.A., de Vos, P., van Goor, H., Bakker, W.W., Faas, M.M., 2014b. Extracellular ATP decreases trophoblast invasion, spiral artery remodeling and immune cells in the mesometrial triangle in pregnant rats. Placenta **35**, 587-595.

Thorburn, A.N., McKenzie, C.I., Shen, S., Stanley, D., Macia, L., Mason, L.J., Roberts, L.K., Wong, C.H., Shim, R., Robert, R., Chevalier, N., Tan, J.K., Marino, E., Moore, R.J., Wong, L., McConville, M.J., Tull, D.L., Wood, L.G., Murphy, V.E., Mattes, J., Gibson, P.G., Mackay, C.R., 2015. Evidence that asthma is a developmental origin disease influenced by maternal diet and bacterial metabolites. Nat Commun **6**, 7320.

Virgiliou, C., Gika, H.G., Witting, M., Bletsou, A.A., Athanasiadis, A., Zafrakas, M., Thomaidis, N.S., Raikos, N., Makrydimas, G., Theodoridis, G.A., 2017. Amniotic Fluid and Maternal Serum Metabolic Signatures in the Second Trimester Associated with Preterm Delivery. J Proteome Res **16**, 898-910.

Wallimann, T., Wyss, M., Brdiczka, D., Nicolay, K., Eppenberger, H.M., 1992. Intracellular compartmentation, structure and function of creatine kinase isoenzymes in tissues with high and fluctuating energy demands: the 'phosphocreatine circuit' for cellular energy homeostasis. Biochem J **281 (Pt 1)**, 21-40.

Wartenberg, D., Reyner, D., Scott, C.S., 2000. Trichloroethylene and cancer: epidemiologic evidence. Environ Health Perspect **108 Suppl 2**, 161-176.

Weaver, G.A., Krause, J.A., Miller, T.L., Wolin, M.J., 1988. Short chain fatty acid distributions of enema samples from a sigmoidoscopy population: an association of high acetate and low butyrate ratios with adenomatous polyps and colon cancer. Gut **29**, 1539-1543.

Wellner, D., Meister, A., 1960a. Crystalline L-amino acid oxidase of Crotalus adamanteus. J Biol Chem **235**, 2013-2018.

Wellner, D., Meister, A., 1960b. Evidence for an intermediate in the oxidation of reduced L-amino acid oxidase by molecular oxygen. J Biol Chem **235**, PC12-13.

Wen, S.W., Guo, Y., Rodger, M., White, R.R., Yang, Q., Smith, G.N., Perkins, S.L., Walker, M.C., 2016. Folic Acid Supplementation in Pregnancy and the Risk of Pre-Eclampsia-A Cohort Study. PLoS One **11**, e0149818.

Wingren, G.B., Axelson, O., 1997. Occupational and Environmental Determinants for Benign Thyroid Disease and Follicular Thyroid Cancer. Int J Occup Environ Health **3**, 89-94.

Wu, K.L., Berger, T., 2007. Trichloroethylene metabolism in the rat ovary reduces oocyte fertilizability. Chem Biol Interact **170**, 20-30.

Wu, K.L., Berger, T., 2008. Ovarian gene expression is stable after exposure to trichloroethylene. Toxicol Lett **177**, 59-65.

Chapter IV. Apoptotic Responses Stimulated by the Trichloroethylene Metabolite *S*-(1,2-dichlorovinyl)-L-cysteine in BeWo Human Trophoblast Cells Depend on Cell Differentiation State

Abstract

During pregnancy, the placental villous cytotrophoblasts differentiate in a process involving cell fusion and multinucleation to create syncytiotrophoblasts, a cell type at the maternal-fetal interface that regulates gas, waste, and nutrient exchange between the mother and fetus. The human trophoblast BeWo cell line has been used as an *in vitro* model for this differentiation process, also known as syncytialization, including use as a model to study the impacts of toxicant exposure on placental cells. Apoptosis of syncytiotrophoblasts is associated with adverse pregnancy outcomes. In the current study, we exposed unsyncytialized BeWo cells, BeWo cells undergoing syncytialization, and syncytialized BeWo cells to *S*-(1,2-dichlorovinyl)-L-cysteine (DCVC), a metabolite of trichloroethylene (TCE), an industrial chemical and environmental contaminant. DCVC decreased cell viability, increased cell cytotoxicity, increased caspase 3/7 activity, and increased nuclear condensation or fragmentation with 48 hours of exposure to 50 µM DCVC in BeWo cells regardless of their differentiation status. Investigating mechanisms of apoptosis, DCVC increased hydrogen peroxide (H_2O_2) abundance and decreased *PRDX2* mRNA in all three models of BeWo cells. DCVC decreased tumor necrosis factor-receptor 1 (TNF-R1) concentration in media and decreased *NFKB1* mRNA expression in syncytialized BeWo cells but not in unsyncytialized BeWo cells nor in BeWo cells undergoing syncytialization. DCVC decreased *BCL2* mRNA expression in BeWo cells undergoing syncytialization and syncytialized BeWo cells, but not in unsyncytialized BeWo cells. Decreased

162

LGALS3 mRNA was seen in unsyncytialized BeWo cells. These data indicate that the oxidative stress or pro-inflammatory mechanisms underlying apoptosis in BeWo cells depend on differentiation state. Future directions should elaborate on defining the different pathways involved in DCVC-stimulated apoptosis for different placental cell types and attempt to modulate the adverse outcomes based on known molecular mechanisms.

Introduction

Many adverse pregnancy outcomes are attributable to abnormalities in placenta development (Ilekis *et al.*, 2016). Important classes of placental cells that have been studied with regard to adverse pregnancy outcomes include villous cytotrophoblasts and syncytiotrophoblasts. Villous cytotrophoblasts are the placental cells that differentiate *in vivo* into syncytiotrophoblast in a process involving cell fusion and multinucleation, known as syncytialization (Wang *et al.*, 2014). The syncytiotrophoblast serves as the maternal fetal interface that regulates gas, waste, and nutrient exchange between the mother and the fetus (Potgens *et al.*, 2002; Wang *et al.*, 2014). As such, disruption of the process of syncytialization or the resulting syncytiotrophoblasts could lead to adverse pregnancy outcomes.

Apoptosis of villous cytotrophoblasts, syncytiotrophoblasts, and other cytotrophoblasts is important as a mechanism for disruption of placental development and function. A specific example is that apoptosis of syncytiotrophoblasts is associated with intrauterine growth retardation and preeclampsia (Ishihara *et al.*, 2002), with further examples provided in a review by Sharp et al. (Sharp *et al.*, 2010). Loss of villous cytotrophoblasts and disrupted syncytia formation are proposed as stimuli for syncytiotrophoblast degeneration (Fox, 1970; Panigel and Myers, 1972; Castellucci *et al.*, 1990). Furthermore, apoptosis of invasive cytotrophoblasts is associated with preeclampsia (DiFederico *et al.*, 1999; Genbacev *et al.*, 1999).

Multiple biological processes can contribute to placental cell apoptosis. In BeWo and JEG-3 cells, placental cell lines representative of villous and extravillous cytotrophoblastic cells, respectively (Pattillo and Gey, 1968; Kohler and Bridson, 1971; Kohler *et al.*, 1971), overexpression of antioxidant response with selenium decreases apoptosis (Khera *et al.*, 2017). Additionally, a pro-inflammatory mechanism can contribute to apoptosis in placental cells. In WISH cells, IL-1β and NF-κB1 activation stimulate apoptosis (Saquib *et al.*, 2013), and IFN-γ promotes apoptosis in cultured human cytotrophoblast cells and rat placenta and uterus (Sun *et al.*, 2007). Finally, TNF-α increases apoptosis in both BeWo and JEG-3 cells (Al-Nasiry *et al.*, 2006) as well as in syncytiotrophoblasts isolated from placentae of uncomplicated pregnancies (Garcia-Lloret *et al.*, 2000).

TCE is commonly used as a metal degreaser and in the synthesis of various chemicals, including refrigerants (Agency for Toxic Substances and Disease Registry, 2007). *S*-(1,2-Dichlorovinyl)-L-cysteine (DCVC) is a TCE metabolite generated in the TCE glutathione (GSH) conjugation metabolic pathway (Lash *et al.*, 2014a) that is important for TCE toxicity. DCVC is toxic because it is further metabolized into unstable and reactive compounds, including 1,2-dichlorovinylthiol (DCVT), chlorothioketene (CTK), and chlorothionoacetyl chloride (CTAC) (Lash *et al.*, 2014a). Notably, DCVC stimulates apoptosis, necrosis, and mitochondrial dysfunction in kidney cells (Lash and Anders, 1986; Lash *et al.*, 1986; Lash *et al.*, 1994; Xu *et al.*, 2008; Lash *et al.*, 2014b). DCVC also stimulates ROS generation, pro-inflammatory response, and apoptosis in the HTR-8/SVneo extravillous cytotrophoblast cell line (Hassan *et al.*, 2016; Elkin *et al.*, 2018). The relevance of DCVC to toxicity is further supported by lack of toxicity of CYP-dervied TCE metabolites, such as dichloroacetate (DCA) and trichloroacetate

(TCA) (Lash *et al.*, 2014a), in HTR-8/SVneo cells (unpublished data). However, the impact of DCVC on the BeWo cell line has not been studied to our knowledge.

BeWo cells are a cell line that is representative of first-trimester villous cytotrophoblasts *in vitro* (Pattillo and Gey, 1968; Wice *et al.*, 1990). Cytotrophoblastic BeWo cells have been used to study the impact of toxicant exposure on placental cells (Zhang *et al.*, 1995; Zhang and Shiverick, 1997; Le Vee *et al.*, 2014; Wang *et al.*, 2015). The cytotrophoblastic BeWo cells can be induced to fuse and multinucleate, adopting important characteristics consistent with syncytiotrophoblasts (Wice *et al.*, 1990). Visual quantification of fusion and multinucleation is a method of assessing syncytialization (Matsuura *et al.*, 2011; Li *et al.*, 2015; Zheng *et al.*, 2016). Another common assessment of syncytialization involves investigating syncytin-1 and syncytin-2 as biomarkers (Vargas *et al.*, 2009). Forskolin, an adenylate cyclase activator (Daly, 1984), is commonly used to stimulate BeWo cell syncytialization (Wice *et al.*, 1990; Al-Nasiry *et al.*, 2006; Inadera *et al.*, 2010).

For the present study, we used the BeWo cell line to test the hypothesis that DCVC stimulates apoptosis in a manner that is dependent on the state of syncytialization such that the mechanism underlying apoptosis and magnitude of apoptosis differ as a consequence of the BeWo cell differentiation state.

<div align="center">

Materials and Methods

</div>

BeWo cell line

The BeWo human placental villous cytotrophoblast cell line (Patillo and Gey, 1968) was obtained from American Type Culture Collection (ATCC CCL-98), and its identity from its short tandem repeat (STR) profile was verified with fragment analysis (ABI 3730XL DNA Analyzer, Applied Biosystems, Waltham, MA) at the University of Michigan DNA Sequencing Core. The

cells were grown in F12-K Nutrient Mixture Kaighn's Modification with (+) L Glutamine (Gibco, Grand Island, NY). DMEM/F12 Nutrient Mixture (Gibco, Grand Island, NY) without phenol red was used whenever BeWo cells were treated with an exposure. Treatments for the cells were diluted in DMEM/F12 Nutrient Mixture. All media were supplemented with 10% (v/v) heat-inactivated fetal bovine serum (HI-FBS) and 1% (v/v) penicillin/streptomycin (P/S) (Gibco, Grand Island, NY). Cell cultures were washed three times with phosphate buffered saline (PBS) (Invitrogen Life Technologies, Carlsbad, CA) prior to detaching the cells with 0.25% trypsin-EDTA (Invitrogen Life Technologies, Carlsbad, CA) for subculture. For regular subculture, BeWo cells were plated at a 100,000 cells/mL in 25 mL in 175 cm^2 flasks (Corning Inc., Corning, NY) and subcultured at 70-80% confluence. Cell cultures were maintained in a 5% CO_2, 37°C controlled and humidified incubator. This work with human cell cultures was approved by the University of Michigan Institutional Biosafety Committee (IBCA00000100).

Exposures

DCVC was synthesized by the University of Michigan Medicinal Chemistry Core via a previously published method (McKinney *et al.*, 1959), and chemical identity of DCVC was verified periodically through proton nuclear magnetic resonance (NMR) spectroscopy and determined to be 98.7% pure by high-performance liquid chromatography (HPLC). DCVC was dissolved in PBS as a 1 mM stock solution and stored in 1 mL aliquots at -20°C.

The BeWo cells were plated at 100,000 cells/mL density in either 6 well or 96 well plates depending on the experiment and allowed 24 hours to adhere and acclimate prior to initiating treatment. The unsyncytialized BeWo cells were exposed to DCVC concentrations spanning from 1 µM to 100 µM. The effect of DCVC on forskolin-induced syncytialization of BeWo cells was evaluated using co-exposure to DCVC and forskolin. The cytotrophoblastic BeWo cells

166

were syncytialized by culturing the cells with 100 µM forskolin for 48 hours (Wice *et al.*, 1990; Al-Nasiry *et al.*, 2006; Inadera *et al.*, 2010). Forskolin was dissolved in dimethyl sulfoxide (DMSO) (Tocris Bioscience, Bristol, UK) to create a 100 mM forskolin stock solution, which was diluted 1:1000 in medium to create the 100 µM forskolin treatment. Hence, the vehicle control used in these experiments was 0.1% (v/v) DMSO. DCVC concentrations in these experiments ranged from 1-50 µM.

We also tested the effects of DCVC exposure on BeWo cells after the 48-hour forskolin-stimulated syncytialization, hereafter referred to as syncytialized BeWo cells receiving DCVC exposure. The concentration range of DCVC in these experiments was also 1-50 µM. DCVC concentrations were chosen based on past reports of effects of DCVC at similar concentrations (Xu *et al.*, 2008; Lash *et al.*, 2014b; Hassan *et al.*, 2016; Elkin *et al.*, 2018). In addition, the DCVC concentration range includes the average concentration of the DCVC precursor DCVG (13.4 µM) found in the blood of women exposed by inhalation to the US Occupational Safety and Health Administration permissible exposure level (Lash *et al.*, 1999; Agency for Toxic Substances and Disease Registry, 2007). Camptothecin (CPT) was purchased from Cayman Chemical (Ann Arbor, MI) and was used as a positive control in several experiments. CPT was dissolved in DMSO at 5.74 mM prior to administration to cell media.

Phalloidin-FITC and 4',6-diamidino-2-phenylindole, dihydrochloride (DAPI) staining

Cells were plated at a density of 200,000 cells/well in 2 mL/well in Corning Costar tissue culture-treated 6-well plates (Corning, NY; product number 3516) and allowed to adhere for 24 hours before treatment. After the 48-hour treatment, the medium was removed, and the cells were washed three times with PBS. Then, 3.7% formaldehyde was added to the wells for 5 minutes to fix the cells, and the cells were washed three times with PBS again. Next, phalloidin-

167

FITC (Sigma-Aldrich, St. Louis, MO) was applied at a concentration of 3.99 µM (from a stock solution of 0.399 mM in DMSO diluted 1:100 in PBS) for 40 minutes at room temperature. Cells were washed three times with PBS, and then incubated for 5 minutes at room temperature in 300 nM 4',6-diamidino-2-phenylindole, dihydrochloride (DAPI) (Thermo Fisher Scientific, Waltham, MA) (prepared from a 2.86 mM DAPI stock solution in dH_2O diluted in PBS). Cells were washed three times in PBS again prior to imaging using an EVOS microscope with fluorescence capabilities (Thermo Fisher Scientific, Waltham, MA). To obtain an accurate representation of the well, three images at 200X magnification were captured and analyzed per well: one near the top, one near the middle, and one near the bottom from a top-down direction.

Manual scoring of the images was performed to quantify cell multi-nucleation and fusion. The fusion index was calculated as follows: fusion index = [(N-S)/T]*100%, as previously described (Matsuura *et al.*, 2011; Li *et al.*, 2015; Zheng *et al.*, 2016). In the fusion index, N is the number of nuclei in syncytia, S is the total number of syncytia, and T is the total number of nuclei. As such, this index is interpreted as the number of fusion events per total nuclei. The range of this index is 0 to nearly 100 but not exactly 100. In the case of a fusion index of 0, no fusion has occurred, and in the case of nearly 100, all nuclei are within one syncytium (i.e., [(99-1)/99]*100% = 99%). Complementing the fusion index, the percentage of nuclei in syncytia, or (N/T)*100%, was calculated. Unlike the fusion index, the percentage of nuclei in syncytia does not decrease based on the number of syncytia (S) present, so the percentage of nuclei in syncytia is a value that increases relative to fusion index as the number of syncytia (S) increases or nuclei per syncytia (N) decreases. This general property is illustrated in **Table S4.1**. The numerical quantities used in the current study were manually assessed and verified by a research assistant given images without knowledge of treatment group.

Measurement of cell viability and cytotoxicity

BeWo cells were plated at a density of 10,000 cells/well in 100 µL/well in Corning Costar tissue cultured-treated 96-well plates (Corning, NY), and allowed to adhere for 24 hours before treatment. Cell viability and cytotoxicity were detected sequentially using the Multitox-Glo Multiplex Cytotoxicity Assay assessed on the Glomax Multi Plus Detection System (Promega, Madison, WI), as instructed by the manufacturers. For cell viability assessment, 50 µL of cell viability assay reagent was added to detect viability via fluorescence, and then plates were wrapped in aluminum foil and incubated at 37°C for 45 minutes prior to reading. The viability assay works by the principle of cell uptake of a fluorogenic peptide substrate (GF-AFC) that is cleaved by live cell protease activity to produce a fluorescence signal proportional to number of live cells. After the viability reading, 50 µL of cell cytotoxicity assay reagent was added to detect cell cytotoxicity via luminescence, and then plates were wrapped in aluminum foil and incubated at room temperature for 15 minutes prior to reading. This cytotoxicity assay works by the principle of using a luminogenic peptide substrate (AAF-aminoluciferin) that is cleaved by dead cell (i.e., cells with compromised membranes) protease activity to release the aminoluciferin product that produces a luminescent signal proportional to the number of dead cells. Cytotoxicity data were normalized to protein mass, which was determined from a separate set of cells in 96-well plates. Protein was collected in Pierce RIPA Lysis and Extraction Buffer (Thermo Fischer Scientific, Waltham, MA) and quantified using the bicinchoninic acid assay (Thermo Fisher Scientific, Waltham, MA). The average of nine different protein readings from three independent experiments for each experimental group was used for normalization.

Measurement of caspase 3/7 activity

Cells were plated in Corning Costar tissue culture-treated 96-well white, clear-bottom plates (Corning, NY) at a density of 10,000 cells/well in 100 µL/well and allowed to adhere for 24 hours before treatment. After treatment, caspase 3/7 activity was measured using a luminescence-based Caspase-Glo 3/7 Assay detected with the Glomax Multi Plus Detection System (Promega, Madison, WI) according to the manufacturer's instructions. The assay consisted of adding 100 µL of Caspase-Glo substrate in Caspase-Glo buffer followed by incubation at 37°C for one hour wrapped in aluminum foil to protect from light. The substrate is engineered to be specific in amino acid sequence to caspase 3/7: DEVD. Activity was luminogenically detected because the cleavage of the substrate, indicative of caspase activity, generates aminoluciferin, which reacts with luciferase to produce light (Niles et al., 2008). Caspase 3/7 activity was normalized to protein mass, which was determined from a separate set of cells in 96-well plates in Pierce RIPA Lysis and Extraction Buffer (Thermo Fischer Scientific, Waltham, MA). Protein was quantified using the bicinchoninic acid assay (Thermo Fisher Scientific, Waltham, MA). The average of nine different mass readings from three independent experiments for each experimental group was used for normalization.

Hoechst staining to detect nuclear condensation or fragmentation

Cells were plated in Corning Costar tissue culture-treated 6-well plates at a density of 200,000 cells/well in 2 mL/well and allowed to adhere for 24 hours before treatment. After the treatment, the medium was removed, and the cells were washed three times with PBS. The cells were fixed with 3.7% formaldehyde for 5 minutes, and then washed three times with PBS again. Next, Hoechst 33342 trihydrochloride, trihydrate (Invitrogen Life Technologies, Carlsbad, CA) at 0.5 µg/mL (from a 10 mg/mL stock solution diluted 1:20,000 in PBS) was added individually to each well to cover the cells. Cells were incubated in the Hoechst solution for 15 minutes, then

washed three times with PBS before imaging using an EVOS microscope with fluorescence capabilities (Thermo Fisher Scientific, Waltham, MA). Three images were taken per well at 400X magnification. To provide an accurate representation of the well, images were captured near the top, middle, and bottom of each well, going in a top-down direction.

Quantification consisted of using ImageJ (NIH, Bethesda, MD) set to a brightness threshold that highlighted nuclei sufficiently to visualize nuclear condensation. The settings were as follows: hue (0, 255), saturation (0, 255), brightness (165, 255). Under these settings, at least 10% of the nucleus had to be highlighted in order for the nucleus to be considered condensed. Criteria used to assess nuclear fragmentation include consideration of fragmentation into multiple pieces, jaggedness of the nuclei, and unequal size of nuclei subsequent to fragmentation.

Detection of hydrogen peroxide (H_2O_2) abundance

Cells were plated at a density of 10,000 cells/well in 100 µL/well in Corrning Costar tissue culture-treated 96-well white, clear-bottom plates (Corning, NY) and allowed to adhere for 24 hours before treatment. Hydrogen peroxide (H_2O_2) was detected using the ROS-Glo™ H_2O_2 assay (Promega, Madison, WI), performed according to the manufacturer's instructions. Six hours before the end of treatment, 20 µL of the H_2O_2 substrate solution containing a derivatized luciferin substrate was added to each well to bring the volume to 100 µL (specific to this protocol, treatments had been added at 80 µL volumes each). After 6 hours, 100 µL of the detection solution was added to each well. The assay works by the principle of addition of a derivatized luciferin substrate, which produces a luciferin precursor when reacting with H_2O_2. After 6 hours, addition of the detection solution generates a luciferin product that gives off a light signal proportional to the amount of H_2O_2 present extracellularly and intracellularly. The H_2O_2 abundance was normalized to protein mass, which was determined from a separate set of

171

cells in 96-well plates in Pierce RIPA Lysis and Extraction Buffer (Thermo Fischer Scientific, Waltham, MA). Protein was quantified using bicinchoninic acid assay (Thermo Fisher Scientific, Waltham, MA). The average of nine different protein readings from three independent experiments for each experimental group was used for normalization. Menadione (MD) was purchased from Sigma-Aldrich (St. Louis, MO) and used as a positive control. MD was directly dissolved in a stock solution of cell medium at a 1 mM concentration.

Detection of pro-inflammatory factors (IL-6, IFN-γ, CRP, and TNF-R1) in media

Cells were plated at 200,000 cells/well in 2 mL/well in Corning Costar tissue culture-treated 6-well plates (Corning, NY) and allowed to adhere for 24 hours before treatment. After treatment, the medium was collected and stored at -80°C until further processing. Cells were scraped and collected in a lysis buffer containing 0.5% (v/v) IGEPAL CA-630 (Sigma-Aldrich, St. Louis, MO), 250 mM NaCl (Sigma-Aldrich, St. Louis, MO), and 5% (v/v) of 1 mM Tris-HCl (pH 7.4) (Sigma-Aldrich, St. Louis, MO). Protein concentration from the cell lysate was measured using the bicinchoninic acid (BCA) assay (Thermo Fischer Scientific, Waltham, MA) according to the manufacturer's protocol. Cytokine concentrations in the medium were normalized to the mass of protein present. Media samples were thawed and pipetted into round-bottom 96-well plates to immediately prior to delivering the samples to the University of Michigan Immunologic Monitoring Core. The core performed ELISA assays using Duosets (R&D Systems, Minneapolis, MN) according to the manufacturer's recommended protocol.

RNA extraction

Cells were plated in Corning Costar tissue culture-treated 6-well plates at a density of 200,000 cells/well in 2 mL/well and allowed to adhere for 24 hours before treatment. After treatment, the medium was removed and RNA was extracted from the cells using a RNeasy

PLUS Mini Kit (Qiagen, Hilden, Germany) according to the manufacturer's instructions. Briefly, 1 mL of the RLT Buffer Plus reagent (Qiagen, Hilden, Germany) containing 1% (v/v) 2-mercaptoethanol (Sigma-Aldrich, St. Louis, MO) was placed in each well to generate cell lysate. Cell lysates were homogenized using QIA Shredders (Qiagen, Hilden, Germany) prior to continuation of the manufacturer protocol with gDNA elimination as the next step. Concentration and purity of RNA were determined using a Nanodrop 2000 UV-Vis Spectrophotometer (Thermo Fisher Scientific, Waltham, MA), and RNA was stored at -80°C until analyzed.

Quantitative real-time polymerase chain reaction (qRT-PCR)

To synthesize cDNA from the RNA samples, an iScript^{TM} cDNA synthesis kit (Bio-Rad Laboratories, Hercules, CA) was used according to the manufacturer's protocol. A Bio-Rad CFX Connect^{TM} Real-Time System (Bio-Rad Laboratories, Hercules, CA) was used to carry out the cDNA synthesis reaction. The protocol on the Bio-Rad CFX Connect^{TM} Real-Time System for the cDNA synthesis reaction was as follows: (1) 25°C for 5 minutes, (2) 42°C for 30 minutes, (3) 85°C for 5 minutes, and then (4) a cool down to 4°C. The cDNA was stored at -20°C until further use.

The qRT-PCR was performed using 25-µL reaction mixtures consisting of the following: 52.5% (v/v) SsoAdvanced^{TM} Universal SYBR® Green Supermix (Bio-Rad Laboratories, Hercules, CA), 0.28 µM of each (forward and reverse) primer, and 32 ng of cDNA template. Primer sequences are described in **Table S4.2** and were custom-made by Integrated DNA Technologies (Coralville, IA). A Bio-Rad CFX Connect^{TM} Real-Time System (Bio-Rad Laboratories, Hercules, CA) was used to perform qRT-PCR according to the manufacturer's

protocol. Analysis was performed using the ΔΔCt method (Yuan et al., 2006), and all samples were analyzed in duplicate. *B2M* served as the reference gene.

CyQUANT™ NF cell proliferation assay to measure DNA quantity (Used for supplemental data)

To assess cellular DNA content, the CyQUANT NF Cell Proliferation Assay kit (Thermo Fisher Scientific, Waltham, MA) was utilized. Cells were plated in Corning Costar tissue culture-treated 96-well white, clear-bottom plates (Corning, NY) at a density of 10,000 cells/well in 100 µL/well and allowed to adhere for 24 hours before treatment. After treatment, the medium was removed from the cells, and 100 µL of dye-binding solution (ratio of 1 µL of CyQUANT® NF dye reagent to 0.5 mL of 1x HBSS Buffer, as directed by the manufacturer) was added per well. After addition of the dye binding solution, cells were incubated in the dark at 37°C for 45 minutes prior to obtaining a fluorescence reading (excitation = 485 nm, emission = 530 nm) using the SpectraMax M2e Multi-Mode Microplate Reader (Molecular Devices, San Jose, CA). The fluorescence signal was proportional to DNA content.

ApoLive-Glo assay to measure cell viability and caspase 3/7 activity

BeWo cells were plated in Corning Costar tissue culture-treated 96-well white, clear-bottom plates at a density of 10,000 cells/well in 100 µL/well. Cells were allowed to adhere for 24 hours before treatment. Cell viability and caspase 3/7 were detected sequentially using the ApoLive-Glo assay from Promega (Madison, WI), performed as instructed by the manufacturer. To detect viability via fluorescence, 20 µL of cell viability reagent was added and plates were wrapped in aluminum foil and incubated at 37°C for 45 minutes. After the viability reading, 100 µL of Caspase-Glo substrate in Caspase-Glo buffer was added to detect caspase 3/7 activity via luminescence. Plates were wrapped again in aluminum foil and incubated at 37°C for one hour

prior to the caspase 3/7 activity reading. The scientific principles behind how the viability and caspase 3/7 activity measurements work on a molecular level have been described in previous sections in the current chapter. Luminescence was detected using the Glomax Multi Plus Detection System.

Statistical analysis

Statistical analyses included one-way ANOVA and mixed model ANOVA with treatment as fixed variable and experiment day as random variable. One-way ANOVA was performed using GraphPad Prism 7 (GraphPad Software, San Diego, CA). Mixed model ANOVA was performed using SPSS Software (IBM Corporation, Chicago, IL). Percentage data were transformed to fractions and arcsine transformed prior to statistical analysis. All ANOVAs were followed with Tukey's post-hoc comparison of means. All graphs were generated using GraphPad Prism 7 (GraphPad Software, San Diego, CA). A $p < 0.05$ was considered statistically significant.

Results

Effects of forskolin and DCVC co-treatment with forskolin on syncytialization

To verify our model of forskolin-stimulated syncytialization of BeWo cells, we exposed cytotrophoblastic BeWo cells to 0, 10, 20 50 or 100 µM of forskolin for 48 hours. These cells were co-stained with phalloidin-FITC and DAPI to identify the nuclei and plasma membranes, respectively, and thereby visualize cellular fusion and multinucleation (**Figure 4.1A**). As seen in **Figures 4.1B1 and 4.1B2**, forskolin increased the fusion index and percentage of nuclei in syncytia in a concentration-dependent manner, respectively. Treatment with 100 µM forskolin increased the fusion index and percentage of nuclei in syncytia by 671.8% and 531.8%, respectively, relative to control (0.1% DMSO) (p<0.0001). Because the indices of

175

syncytialization were substantially increased by 100 µM forskolin compared with lower forskolin concentrations, and because forskolin treatment for 48 hours is established as effective by others (Wice *et al.*, 1990; Al-Nasiry *et al.*, 2006; Inadera *et al.*, 2010), we used 100 µM forskolin exposures for 48 hours to stimulate syncytialization in BeWo cells in the remainder of our experiments.

To investigate DCVC effects on the process of syncytialization, 5 µM to 50 µM DCVC was added as a co-exposure with 100 µM forskolin. As expected, forskolin treatment alone increased indices of syncytialization relative to vehicle control, including: (1) increased fusion index by 625.6% (p<0.0001), (2) increased percentage of nuclei in syncytia by 510.8% (p<0.0001), (3) increased *ERVW-1* (syncytin-1) mRNA expression by 159.6% (p=0.0276), and (4) increased *ERVFRD-1* (syncytin-2) mRNA expression by 2241.2% (p=0.0130) (**Figures 4.1C1, 4.1C2, 4.1C3, 4.1C4**, respectively). However, treatment with DCVC did not significantly alter responses compared with forskolin-only treatment (**Figures 4.1C1-4.1C4**). The apparent reduction of forskolin-stimulated *ERVFRD-1* mRNA expression by co-treatment with 50 µM DCVC was not statistically significant (p=0.1714) (**Figure 4.1C4**).

Responses relevant to syncytialization were also measured in unsyncytialized BeWo cells exposed to 5-50 µM DCVC for 48 hours in the absence of forskolin. DCVC treatment at 5, 10, 20, or 50 µM for 48 hours did not stimulate an increase in the fusion index or an increase in the percentage of nuclei in syncytia relative to control (0 µM DCVC) (**Figures 4.1D1 and 4.1D2**, respectively). Furthermore, those DCVC treatments did not stimulate an increase in *ERVW-1* or *ERVFRD-1* mRNA expression relative to control (0 µM DCVC) (**Figures 4.1D3 and 4.1D4**, respectively).

Effects of DCVC on cell viability and cytotoxicity

Treatment for 48 hours with 50 μM but not lower concentrations of DCVC decreased cell

viability by 28.4% in unsyncytialized cytotrophoblastic BeWo cells relative to control (0 μM

DCVC exposure) (p<0.0001) (**Figure 4.2A1**). Cytotoxicity, which was used as a proxy for dead

cells, increased in unsyncytialized cytotrophoblastic BeWo cells exposed for 48 and 72 hours to

50 μM DCVC but not lower concentrations of DCVC, relative to control (0 μM DCVC) (84.8%

and 191.6% increase, respectively; p<0.0001 for both) (**Figures 4.2A2 and 4.2B2**, respectively).

After exposure for 72 hours on unsyncytialized BeWo cells, 10, 20 and 50 μM DCVC treatment

significantly reduced cell viability relative to control (0 μM DCVC) by 12.2% (p=0.023), 27.8%

(p<0.0001) and 57.4% (p<0.0001), respectively (**Figure 4.2B1**).

In BeWo cells undergoing forskolin-stimulated syncytialization, 50 μM DCVC decreased

cell viability relative to forskolin-only treatment by 42.6% (p<0.0001), whereas 1, 5, 10, and 20

μM DCVC did not (**Figure 4.2C1**). Although treatment with 20 μM DCVC modestly decreased

viability of cells undergoing forskolin-stimulated syncytialization compared with vehicle control

(without DCVC or forskolin) and lower concentrations of DCVC, this decrease was not

statistically different compared with the forskolin-only treatment (**Figure 4.2C1**). In this

experiment, the exposure duration was 48 hours to match the exposure duration used for

forskolin stimulation of syncytialization. Treatment with forskolin alone did not alter cell

viability relative to vehicle control. In BeWo cells undergoing forskolin-stimulated

syncytialization, exposure to both 20 and 50 μM DCVC increased cytotoxicity by 35.5% and

153.4%, respectively, relative to forskolin-only treatment (p=0.001 and <0.0001, respectively),

whereas lower concentrations of DCVC had no significant effects on cytotoxicity (**Figure

4.2C2**). Interestingly, forskolin only treatment increased cytotoxicity by 76.3% relative to

vehicle control (0.1% DMSO) (p<0.0001) (**Figure 4.2C2**).

A similar pattern was observed in BeWo cells exposed to DCVC after a 48-hour syncytialization with forskolin. Exposure for 48 hours to 50 µM DCVC decreased cell viability by 45.2% (p<0.0001) relative to control (0 µM DCVC), but 1, 2, 5, 10, or 20 µM DCVC had no significant effects (**Figure 4.2D1**). In syncytialized BeWo cells, 50 µM but not 1, 2, 5, 10, or 20 µM DCVC treatment for 48 hours increased cytotoxicity relative to control (0 µM DCVC) (151.5%; p<0.0001) (**Figure 4.2D2**).

Effects of DCVC on caspase 3/7 activity

Treatment of unsyncytialized cytotrophoblastic BeWo cells with 50 µM DCVC for 48 and 72 hours increased caspase 3/7 activity by 57.8% and 230.6%, respectively, relative to control (0 µM DCVC) (p<0.0001) (**Figures 4.3A and 4.3B**, respectively). Exposure to 100 µM DCVC for 72 hours increased caspase 3/7 activity by 145.2% relative to control (p<0.0001), reduced from the peak activation observed with 50 µM DCVC (**Figure 4.3B**). Exposure to 1, 2, 5, 10, or 20 µM DCVC did not increase caspase 3/7 activity at either 48 or 72 hours.

When DCVC exposure was concurrent with forskolin-stimulated cell syncytialization, 50 µM DCVC, but not 1, 5, 10, or 20 µM DCVC, increased caspase 3/7 activity relative to forskolin-only treatment (85.4%; p<0.0001) (**Figure 4.3C**). In BeWo cells that had been syncytialized, 48-hour exposure to 50 µM DCVC but not lower DCVC concentrations also increased caspase 3/7 activity relative to control (0 µM DCVC) (102.0% increase, p<0.0001) (**Figure 4.3D**). Forskolin treatment by itself did not change caspase 3/7 activity relative to vehicle control (0.1% DMSO) under any of the experimental conditions tested.

Effects of DCVC on nuclear condensation or fragmentation

Unsyncytialized cells exposed for 48 hours to 50 µM DCVC but not 5, 10 or 20 µM DCVC exhibited significantly increased percent of nuclei that were condensed or fragmented

compared to control (0 µM DCVC) (291.7% increase, p=0.0475) (**Figure 4.4B1**). Similarly, in BeWo cells undergoing forskolin-stimulated syncytialization, 50 µM DCVC significantly increased the percent of condensed or fragmented nuclei compared with forskolin alone (208.0% increase, p=0.0065) (**Figure 4.4B2**). Forskolin by itself did not increase nuclear condensation or fragmentation relative to control. Furthermore, 24- and 48-hour DCVC exposures of syncytialized BeWo cells significantly increased nuclear condensation or fragmentation at 50 µM DCVC but not lower DCVC concentrations (101.5% and 273.8% increase, respectively; p=0.0214 and 0.0256, respectively) (**Figures 4.4B3 and 4.4B4**, respectively). We performed the CyQuant assay for DNA quantity to evaluate the contribution of cell division to nuclear condensation. We observed no change in CyQuant detection of DNA quantity under any of the experimental conditions for assessment of nuclear condensation and fragmentation (**Figures S4.1A, S4.1C, and S4.1D**). At the 72-hour time point of exposure in unsyncytialized BeWo cells, however, 50 and 100 µM DCVC exposure decreased DNA quantity relative to control (0 µM DCVC) by 49.8% and 66.1%, respectively (p<0.0001) (**Figure S4.1B**).

Effects of DCVC on biomarkers of oxidative stress

In unsyncytialized BeWo cells, DCVC exposure increased generation of hydrogen peroxide (H_2O_2) after 48 hours of exposure to 20 and 50 µM DCVC by 47.1% and 259.3%, respectively, relative to control (0 µM DCVC) (p= 0.046 and <0.0001, respectively) (**Figure 4.5A1**). The hydrogen peroxide stimulation in unsyncytialized cells was accompanied by decreased *PRDX2* mRNA expression at 10, 20 and 50 µM DCVC relative to control (0 µM DCVC) by 20.5%, 23.9%, and 44.6%, respectively (p= 0.0202, 0.0057, and <0.0001, respectively) (**Figure 4.5A2**). However, *PRDX1* mRNA expression was unchanged by DCVC in unsyncytialized cells (**Figure 4.5A3**).

In BeWo cells undergoing forskolin-stimulated syncytialization, 50 µM DCVC increased generation of H_2O_2 by 148.3% relative to forskolin-only treatment (p<0.0001) (**Figure 4.5B1**). Interestingly, syncytialization by itself decreased H_2O_2 generation by 51.5% relative to vehicle control (p<0.0001) (**Figure 4.5B1**). Similar to unsyncytialized cells, 50 µM DCVC decreased *PRDX2* mRNA expression in BeWo cells undergoing syncytialization (62.9% decrease relative to forskolin-only treatment, p=0.0091) (**Figure 4.5B2**). No differences in *PRDX1* mRNA expression were found for DCVC effects on BeWo cells undergoing syncytialization (**Figure 4.5B3**).

After 24 hours of DCVC exposure, syncytialized BeWo cells exhibited decreased mRNA expression of *PRDX1* and *PRDX2* relative to control (0 µM DCVC). The *PRDX1* mRNA expression was significantly decreased by 10, 20, and 50 µM DCVC (50.6%, 39.6%, and 44.1% decrease, respectively; p=0.0067, 0.0427, and 0.0202, respectively), and the *PRDX2* mRNA expression was decreased by 20 and 50 µM DCVC (33.0% and 38.6% decrease, respectively; p=0.0223 and 0.0064, respectively) (**Figures 4.5C1 and 4.5C2**, respectively). In syncytialized BeWo cells, 50 µM DCVC increased H_2O_2 by 174.3% relative to control (0 µM DCVC) after a 48-hour exposure (p<0.0001) (**Figure 4.5D1**), with no significant changes observed at lower DCVC concentrations. After 48 hours, DCVC exposure had no significant effect on *PRDX1* and *PRDX2* mRNA in syncytialized BeWo cells (**Figures 4.5D2 and 4.5D3**, respectively).

Effects of DCVC on pro-inflammatory responses

To assess pro-inflammatory responses, interleukin-6 (IL-6), C-reactive protein (CRP), interferon-γ (IFN- γ), and tumor necrosis factor-receptor 1 (TNF-R1) were measured in cell culture media. In addition, changes in *NFKB1* mRNA expression were assessed. In unsyncytialized BeWo cells, DCVC exposures ranging from 5-50 µM had no significant effects

on *NFKB1* mRNA expression or on TNF-R1 and IL-6 media concentrations relative to control (0 µM DCVC) (**Figures 4.6A1, 4.6A2, and 4.6A3**, respectively). Equivalent DCVC exposures on unsyncytialized BeWo cells also had no significant effects on IFN-γ and CRP media concentrations relative to control (0 µM DCVC) (**Figures S4.2A1 and 4.2A2**, respectively). Similarly, DCVC had no significant effects on *NFKB1* mRNA, TNF-R1, or IL-6 responses in BeWo cells undergoing forskolin-stimulated syncytialization compared to forskolin-only treatment (**Figures 4.6B1, 4.6B2, and 4.6B3**, respectively). Negative results were also observed for CRP or IFN-γ media concentrations (**Figures S4.2B1 and S4.2B2**, respectively). Interestingly, syncytialization stimulated IL-6 release into media (91.0% increase comparing forskolin-only treatment to vehicle control; p=0.0028) (**Figure 4.6B3**).

In syncytialized cells, decreased *NFKB1* mRNA expression was significantly depressed after 24 hours of exposure to 5, 20, and 50 µM DCVC relative to control (44.8%, 45.1%, and 49.5% decrease, respectively; p= 0.0367, 0.0351, and 0.0181, respectively) (**Figure 4.6C1**). After 48 hours of exposure, *NFKB1* mRNA expression was significantly decreased only with the 10 µM DCVC exposure relative to control (47.8% decrease, p=0.0247) (**Figure 4.6C2**). In syncytialized cells, 48-hour treatment with 50 µM DCVC decreased TNF-R1 in cell media by 48.4% after 48 hours of exposure, compared with controls (p=0.0140) (**Figure 4.6C3**), but had no significant effect on IL-6 concentrations in cell media (**Figure 4.6C4**). In addition, DCVC had no significant effects on CRP or IFN-γ concentrations in media (**Figure S4.2C1 and S4.2C2**, respectively). Cell media concentrations of TNF-R1, IL-6, CRP, or IFN-γ were not measured for syncytialized BeWo cells at the 24-hour time point of DCVC exposure.

Effects of DCVC on expression of apoptotic pathway genes

We evaluated changes in mRNA expression of apoptotic pathway genes including *BCL2* (codes for B-cell lymphoma 2, apoptosis regulator), *BAK1* (codes for BCL2 antagonist/killer 1), and *LGALS3* (codes for Galectin-3). In unsyncytialized cells, DCVC had no statistically significant effects on *BCL2* and *BAK1* mRNA expression compared with controls (**Figures 4.7A1 and 4.7A2**, respectively), but *LGALS3* mRNA expression was significantly decreased relative to control at 20 µM DCVC (38.3% decrease, p=0.0066) (**Figure 4.7A3**). In cells undergoing syncytialization, forskolin treatment alone increased *BCL2* mRNA expression relative to its control (0.1% DMSO) (441.2% increase, p=0.0030) (**Figure 4.7B1**). Exposure to 20 µM and 50 µM DCVC depressed the forskolin-stimulated *BCL2* mRNA increase by 60.0% and 74.1%, respectively (p=0.0364 and 0.0073, respectively) (**Figure 4.7B1**). *BAK1* and *LGALS3* and mRNA expression were unchanged by syncytialization or DCVC co-treatment during syncytialization (**Figures 4.7B2 and 4.7B3**, respectively).

Similarly, syncytialized BeWo cells exhibited decreased *BCL2* mRNA expression following exposure to 20 and 50 µM DCVC for 24 hours relative to control (50.7% and 60.8% decrease, respectively; p= 0.0156 and 0.0037, respectively) (**Figure 4.7C1**). *BCL2* mRNA expression also decreased with 5, 10, and 20 µM DCVC treatments for 48 hours relative to control (0 µM DCVC) (65.5%, 74.7%, and 66.7% decrease, respectively; p=0.0004, 0.0002, and 0.0004, respectively) (**Figure 4.7D1**). *LGALS3* mRNA expression was unchanged by DCVC treatment in syncytialized BeWo after 24 and 48 hours of exposure (**Figures 4.7C2 and 4.7D2**, respectively). In experiments involving 48-hour DCVC exposure of syncytialized BeWo cells, the RNA yield for the 50 µM DCVC concentration was insufficient (**Figures 4.7D1 and 4.7D2**); therefore, no mRNA expression data could be obtained with the 50 µM DCVC concentration group.

Discussion

This study compares mechanisms by which unsyncytialized BeWo cells, BeWo cells undergoing syncytialization, and syncytialized BeWo cells undergo apoptosis in response to the trichloroethylene metabolite DCVC. DCVC was more effective at stimulating cell death observed in syncytialized BeWo cells compared to the two other BeWo models. The data suggest that DCVC-stimulated mechanisms of cell death had numerous similarities in unsyncytialzed BeWo cells and BeWo cells undergoing syncytialization but differed compared with the syncytialized BeWo cells. A prominent distinction is that decreased TNF-R1 media concentration and *NFKB1* mRNA expression were observed in the syncytialized BeWo cells but not in BeWo cells undergoing syncytialization or in unsyncytialized BeWo cells.

We observed that DCVC-induced cell death in the BeWo cells was consistent with apoptosis, regardless of whether the cells were unsyncytialized, undergoing syncytialization, or syncytialized at the time of DCVC exposure. Many of the responses occurred at similar concentrations in the three different BeWo models. For all three types of BeWo cells at 48 hours of DCVC exposure, increased cytotoxicity, increased caspase 3/7 activity, increased nuclear condensation or fragmentation was observed at 50 µM DCVC concentration relative to the respective controls. The corresponding decreased viability in all three cell types regardless of differentiation state adds validity to our results. The measurements of viability, which is a proxy for quantity of viable cells, and cytotoxicity, which was a proxy for number of dead cells, tested if the amount of viable cell decrease was coupled with an increase in dead cells normalized to total protein content. The normalization to protein accounts for the fact that lower protein quantity by itself hampers production of the aminoluciferase dead cell signal and is already reflected in a viability reading. Therefore, our results are consistent with DCVC stimulation of

deleterious downstream outcomes (cytotoxicity, caspase 3/7, percentage of nuclei condensed or fragmented) and suppression of viability. Additionally, our results revealed that 50 µM DCVC was almost always the lowest DCVC concentration necessary to elicit downstream effects in BeWo cells regardless of differentiation status.

Explanations exist for the similar effects of DCVC on caspase 3/7 activity and nuclear condensation or fragmentation regardless of BeWo differentiation status. Because caspase-3 is an executioner caspase downstream in apoptosis pathways at a point in which the intrinsic and extrinsic pathways of apoptosis converge (Parrish *et al.*, 2013), it is plausible that DCVC stimulates apoptosis. In addition, nuclear condensation and fragmentation are hallmarks of apoptosis (Matassov *et al.*, 2004; Errami *et al.*, 2013; Crowley *et al.*, 2016). Neither condensation nor fragmentation alone is sufficient for apoptosis, and apoptosis can happen in the presence of only one but not the other (Zhang *et al.*, 2001). Percentage of condensed or fragmented nuclei was chosen as an index that would capture most apoptotic nucleic while minimizing the chance of overlooking some apoptotic nuclei. Therefore, the increased percentage of nuclear condensation or fragmentation validates our observation that DCVC increased caspase 3/7 activity and increased percentage of nuclear condensation or fragmentation. Although it is possibile that some nuclei counted as positive were undergoing cell division, we suggest that the changes in percentage of nuclei condensed or fragmented most likely reflect apoptosis because we only observed DCVC-stimulated changes to DNA quantity after 72 hours but not at earlier time points in unsyncytialized BeWo cells (**Figure S4.1**).

DCVC stimulated larger changes in viability, cytotoxicity, and caspase 3/7 activity for syncytialized BeWo cells and BeWo cells undergoing syncytialization compared to unsyncytialized BeWo cells. A particularly important note is the larger DCVC-stimulated

184

increases in cytotoxicity and caspase 3/7 activity for syncytialized BeWo cells and BeWo cells undergoing syncytialization compared to unsyncytialized BeWo cells at the 48-hour time point. Because the DCVC-stimulated caspase 3/7 findings are similar in magnitude for a given BeWo model to the respective DCVC-stimulated cytotoxicity result, with the magnitudes associated with unsyncytialized BeWo cells as smallest, we suggest that increased cytotoxicity is at least partly driven by caspase 3/7. Together, the findings suggest that syncytialized BeWo cells and BeWo cells undergoing syncytialization may be most sensitive to DCVC-stimulated toxicity.

In contrast to the responses downstream in apoptotic signaling pathways and cellular responses, responses upstream in the apoptotic pathway were stimulated at lower concentrations of DCVC exposure for all three models of BeWo cells. These include transcriptional changes, such as DCVC-stimulated decreases in mRNA expression of *PRDX2* and *BCL2*, with *BCL2*-decreases most notable in BeWo cells undergoing syncytialization and syncytialized BeWo cells. In the unsyncytialized BeWo cells, a lower concentration, 10 µM DCVC, decreased *PRDX2* mRNA expression after 48 hours of exposure, but decreased viability was not observed until the 72-hour time point. Similarly, in syncytialized BeWo cells, 20 and 50 µM DCVC decreased *PRDX2* mRNA expression at 24 hours of exposure whereas decreased viability, increased cytotoxicity, and increased caspase 3/7 activity from 50 µM DCVC exposure were not observed until the 48-hour time point. Together, these findings suggest that transcriptional changes led to the more downstream changes of viability, cytotoxicity, caspase 3/7 activity, and nuclear condensation/fragmentation. Possible future work to confirm a sequence of events include knock-out or pharmacological inhibition experiments that are beyond the scope of the current study.

The DCVC-stimulated decreases in *PRDX1* and *PRDX2* observed in the current study could be relevant to placental health. Both peroxidredoxin proteins are reduced if syncytialization is inhibited in BeWo cells through hypoxia compared to normal syncytialization (Hu *et al.*, 2007). Moreover, BeWo cells with *PRDX2* knocked down are unable to syncytialize (Wu *et al.*, 2017). Both peroxiredoxin genes are highly expressed in the placenta (Fagerberg *et al.*, 2014). However, *PRDX1* is expressed at roughly twice the level of *PRDX2* (Fagerberg *et al.*, 2014). A possible explanation for our finding that DCVC decreased *PRDX2* to a greater extent than *PRDX1* is that *PRDX1* may be more essential to cytotrophoblasts and syncytiotrophoblasts than *PRDX2*. Both peroxiredoxin 1 and 2 scavenge hydrogen peroxide (H_2O_2), reduce other enzymes such as thioredoxins, and are anti-apoptotic through similar mechanisms (Ishii *et al.*, 2012). Whereas the anti-apoptotic mechanism for peroxiredoxin 1 involves ASK1 and JNK suppression, that for peroxiredoxin 2 involves ASK1 suppression (Ishii *et al.*, 2012). Both peroxiredoxins could also prevent apoptosis in a Bcl-2-dependent manner (Jin *et al.*, 2017; Lu *et al.*, 2019; Lu *et al.*, 2020; Yang *et al.*, 2020). Peroxiredoxin 1 could also activate inflammation and apoptosis via toll-like receptor-4 in the context of ischemia-reperfusion injury (Liu and Zhang, 2019). Therefore, whereas we found *PRDX1* and *PRDX2* responses to be relevant to H_2O_2 and *BCL2* responses, the impact of DCVC on ASK1 and JNK remain worthy considerations in investigating DCVC-stimulated cell death. Additionally, the role of peroxiredoxin 1 and 2 in relation to ROS and apoptotic outcomes, especially in relation to placenta, are worthy of future work.

BCL2 and *LGALS3* are critical in apoptosis and were modified by DCVC dependent on BeWo cell differentiation state. *BCL2* and *LGALS3* code for Bcl-2 and Galectin-3, respectively, proteins important with anti-apoptotic functions and capable of heterodimerization to inhibit

apoptosis (Yang *et al.*, 1996; Yang *et al.*, 2008; Newlaczyl and Yu, 2011). Interestingly, both Galectin-3 and Bcl-2 family proteins have a NWGR (Asp-Trp-Gly-Arg) motif in their carbohydrate recognition domains that is thought to contribute to their anti-apoptotic activity (Yang *et al.*, 1996; Akahani *et al.*, 1997; Colnot *et al.*, 1998). In unsyncytialized BeWo cells, DCVC decreased *LGALS3* mRNA expression at 20 µM DCVC whereas DCVC at various concentrations decreased *BCL2* mRNA expression in BeWo cells undergoing syncytialization and in syncytialized BeWo cells. In syncytialized BeWo cells or BeWo cells undergoing syncytialization, the decrease of either *BCL2* or *LGALS3* mRNA expression could be sufficient to allow apoptosis to occur because the protein products are structurally and functionally similar (Yang *et al.*, 1996; Akahani *et al.*, 1997; Colnot *et al.*, 1998; Yang *et al.*, 2008; Newlaczyl and Yu, 2011). Similarly, in unsyncytialized BeWo cells, a balance between *BCL2* and *LGALS3* may regulate apoptosis.

Interactions between NF-κB and ROS provide insight into the mechanism of action of DCVC towards apoptosis. Firstly, NF-κB reduces ROS by interacting with ferritin heavy chain or manganese superoxide dismutase (Papa *et al.*, 2005; Bubici *et al.*, 2006). Alternatively, in response to ROS, TNF-R1 becomes activated (Papa *et al.*, 2005), which increases NF-κB and its transcription (Bubici *et al.*, 2006; Wajant and Scheurich, 2011; Annibaldi and Meier, 2018). The ability of NF-κB to reduce ROS in the first mechanism may also be a way by which NF-κB compensates for the increased ROS in the second mechanism. In the case of DCVC exposure of syncytialized BeWo cells, the mechanism of NF-κB seems to favor a mechanism in which NF-κB reduces ROS (Papa *et al.*, 2005; Bubici *et al.*, 2006) with DCVC-stimulated suppression of *NFKB1*. Indeed, DCVC decreased *NFKB1* mRNA expression, increased H_2O_2 generation, and increased apoptosis, suggesting that *NFKB1* may activate a mechanism to reduce ROS in the

syncytialized BeWo cells (Papa *et al.*, 2005; Bubici *et al.*, 2006) as part of an anti-apoptotic response. Because TNF-R1 is a positive regulator of *NFKB* transcription (Bubici *et al.*, 2006; Wajant and Scheurich, 2011; Annibaldi and Meier, 2018), our data of decreased TNF-R1 and decreased *NFKB1* mRNA expression suggest that *NFKB1* may be regulated by TNF-R1 in syncytialized BeWo cells, as well. However, the extent to which TNF-R1 may respond to ROS in the context of DCVC exposure is currently unknown. The interaction among DCVC and ferritin heavy chain and manganese superoxide dismutase also remain unknown. These remain directions worthy of future investigation in order to understand mechanisms of DCVC-stimulated ROS more completely.

BeWo cell models have limitations as well as strengths. Forskolin stimulates unsyncytialized BeWo cells to adopt characteristics that are consistent with *in vivo* syncytialization and syncytiotrophoblasts, including increased cell fusion and multinucleation (Wice *et al.*, 1990; Wang *et al.*, 2014). Forskolin is more effective than other agents for stimulating cell fusion and other characteristics in BeWo cells that are consistent with normal syncytialization, including increased synthesis and secretion of human chorionic gonadotrophin (hCG) (Wice *et al.*, 1990). However, syncytiotrophoblasts in primary cell culture exhibit some different characterististics from BeWo b30 cells (a specific clone of BeWo cells) that have been syncytialized (Wice *et al.*, 1990). These include differing levels of expression of placental alkaline phosphatase, human placental lactogen, and Schwangerschafts protein 1 (Wice *et al.*, 1990). It has been proposed that syncytriotrophoblasts obtained from differentiating BeWo cells are biochemically representative of an early placenta stage near 10 weeks gestation age (Wice *et al.*, 1990).

We report here some novel findings in regard to syncytialization that contribute to our understanding of the relevance of *in vitro* syncytialization to *in vivo* syncytialization. We found that syncytialization decreased hydrogen peroxide generation, which has not been previously reported. This is consistent with literature indicating the importance in syncytialization of peroxiredoxin 1 and peroxiredoxin 2, which scavenge H_2O_2 (Hu *et al.*, 2007; Wu *et al.*, 2017). We also found that syncytialization increased interleukin-6 (IL-6) release, which has not been previously reported nor suggested to have a role in syncytialization, suggesting a noteworthy future direction. Our finding of increased *BCL2* mRNA expression with syncytialization is consistent with a prior report that syncytialization increases *BCL2* mRNA expression in BeWo cells and human primary cytotrophoblasts (Zheng *et al.*, 2016). Bcl-2 is anti-apoptotic, is thought to control excessive apoptosis during syncytialization (Huppertz *et al.*, 1998), and may account for why we did not observe syncytialization to increase caspase-3. In contrast, our finding of increased cytotoxicity with forskolin stimulation, which activates adenylate cyclase and increases cAMP (Daly, 1984), is consistent with a previous report showing that elevated levels of cAMP stimulate apoptosis for proper lymphocyte development and homeostasis (McConkey *et al.*, 1990). Follow-up of these findings would provide important information concerning the relevance of the BeWo *in vitro* syncytialization cell model for studies of human placental cell responses.

The DCVC concentrations used in the current study are relevant with respect to human occupational exposures and prior studies of DCVC toxicity. Firstly, women exposed by inhalation to 100 ppm TCE, which is the United States Occupational Safety and Health Administration permissible exposure level (Agency for Toxic Substances and Disease Registry, 2007), had an average of 13.4 µM of DCVG in their blood serum (Lash *et al.*, 1999). Because

DCVG is the TCE metabolic precursor to DCVC in a 1:1 stoichiometric ratio (Lash *et al.*, 2014a), the concentration range of 1-50 µM used in the present study encompasses blood concentrations relevant for occupational exposures to TCE. In comparison of DCVC to other TCE metabolites, we have observed that the TCE metabolites dichloroacetic acid (DCA) and trichloroacetic acid (TCA) (Lash *et al.*, 2014a) elicit very modest effects in unsyncytialized BeWo cells (**Figure S4.3**).

Secondly, the DCVC concentrations used in the present study have relevance to prior studies using DCVC. DCVC induces significant effects on cell apoptosis, mitochondrial dysfunction, and energy metabolism in HTR-8/SVneo placental cells, a cell line representative of extravillous cytotrophoblasts, with DCVC concentrations ranging from 5-100 µM, (Elkin *et al.*, 2018; Elkin *et al.*, 2019; Elkin *et al.*, 2020). These findings in HTR-8/SVneo cells are consistent with our findings of apoptosis in BeWo cells, although the impact of DCVC in BeWo cells on mitochondrial dysfunction and energy metabolism remain to be investigated. Because a prior study reported significant stimulation of apoptosis in HTR-8/SVneo cells following 24-hour exposure to 20 µM DCVC (Elkin *et al.*, 2018), whereas 48-hour exposure to 50 µM DCVC was required for significant stimulation of apoptosis in the BeWo cells, the HTR-8/SVneo cells may be more sensitive to DCVC compared to BeWo cells. Moreover, incubation with 10 µM DCVC for 4 hours or 5 µM DCVC for 24 hours blocked lipoteichoic acid (LTA)-stimulated release of tumor necrosis factor-α (TNF-α) from extraplacental membranes in culture (Boldenow *et al.*, 2015), highlighting the effectiveness of acute and low-concentration DCVC exposure in a related model. In kidney cells, DCVC stimulates significant apoptosis from concentrations ranging from 10-200 µM DCVC with 4- and 24-hour exposure durations. Decreased cellular respiration was

observed in human proximal tubular (hPT) kidney cells exposed to DCVC concentrations ranging from 10-500 µM DCVC at the 1, 4, 24, and 48 hour time points (Xu *et al.*, 2008).

Our findings of DCVC toxicity as dependent on particular cell type is consistent with a prior report. Looking at differences in DCVC-stimulated responses across passage generation in hPT kidney cells, Lash *et al.* found that cells at passage 4 exhibit greater DCVC-stimulated apoptosis compared to earlier passage cells especially at the 25 and 50 µM DCVC concentrations (Lash *et al.*, 2014b). This finding highlights that DCVC toxicity depends on the status of a cell type, whether it is differentiation state or passage number. Because of these differences in response to DCVC and because TCE is toxic to various organs, including kidney (Green *et al.*, 1997a; Xu *et al.*, 2008; Lash *et al.*, 2014b), liver (Bull, 2000), and lungs (Forkert *et al.*, 1985; Green *et al.*, 1997b), future studies should aim to characterize levels of DCVC toxicity in other cell types from other organs to further inform sensitive cell populations to DCVC exposure.

Particularly for the unsyncytialized BeWo cells, exposures were performed at 48 hours in duration or longer. Whereas this is consistent with time points for BeWo cells to achieve syncytialization, studies at earlier time points are informative. Similar to effects at 48 hours, DCVC increased the percentage of condensed or fragmented nuclei at the 24-hour time point of exposure in unsyncytialized BeWo cells (**Figure S4.4**). As such, unsyncytialized BeWo cells may serve as a good model for short-term exposures, as well. The relationship and mechanisms between short-term exposures and long-term exposures are currently unknown and worthy of future study. This is particularly true for transcriptional mechanisms that may initiate additional mechanisms.

In summary, the current study provides new information comparing DCVC-stimulated apoptotic responses in BeWo cells in three different states of differentiation: unsyncytialized

BeWo cells, BeWo cells undergoing syncytialization, and syncytialized BeWo cells. These responses were observed primarily at the 50 µM DCVC concentration for 48 hours of exposure, although decreased cell viability occurred with DCVC concentrations as low as 10 µM when exposure time was extended to 72 hours. Some responses, including increased H_2O_2 abundance, decreased *PRDX2* mRNA expression, and decreased *BCL2* mRNA expression, occurred at lower concentrations of DCVC and equivalent or shorter exposure durations, supporting potential roles for stimulating apoptosis. These findings can inform future studies of possible interventions for reducing TCE- and DCVC-stimulated toxicity in placental cells, as well as expand upon the sequence of events leading to apoptosis in BeWo cells. Importantly, the current study suggests that syncytiotrophoblasts may be more sensitive to DCVC than villous cytotrophoblasts, evidenced by differences in responses of syncytialized BeWo cells compared to unsyncytialized BeWo cells. Notably, the mechanisms proposed by which DCVC-stimulated apoptosis may occur differ by differentiation state of the BeWo cells (**Figures 4.8, 4.9, and 4.10**). Whereas the proposed mechanism involves *PRDX2* and H_2O_2 alterations in unsyncytialized BeWo cells (**Figure 4.8**) and BeWo cells undergoing syncytialization (**Figure 4.9**), the mechanism proposed in syncytialized BeWo cells (**Figure 4.10**) involves TNF-R1 and *NFKB1*, in addition to *PRDX2* and H_2O_2. As a whole, this study informs differing mechanisms of toxicity based on placental cell type, which can be used to understand differences in susceptibility to DCVC toxicity. Future studies can use these findings as a guideline for duration and concentrations of DCVC exposure likely to yield effects for additional cell types representing different organs to understand additional susceptible tissues.

(A) Visualization of forskolin-stimulated syncytialization		
Vehicle (0.1% DMSO)	10 µM Forskolin	20 µM Forskolin
50 µM Forskolin	100 µM Forskolin	
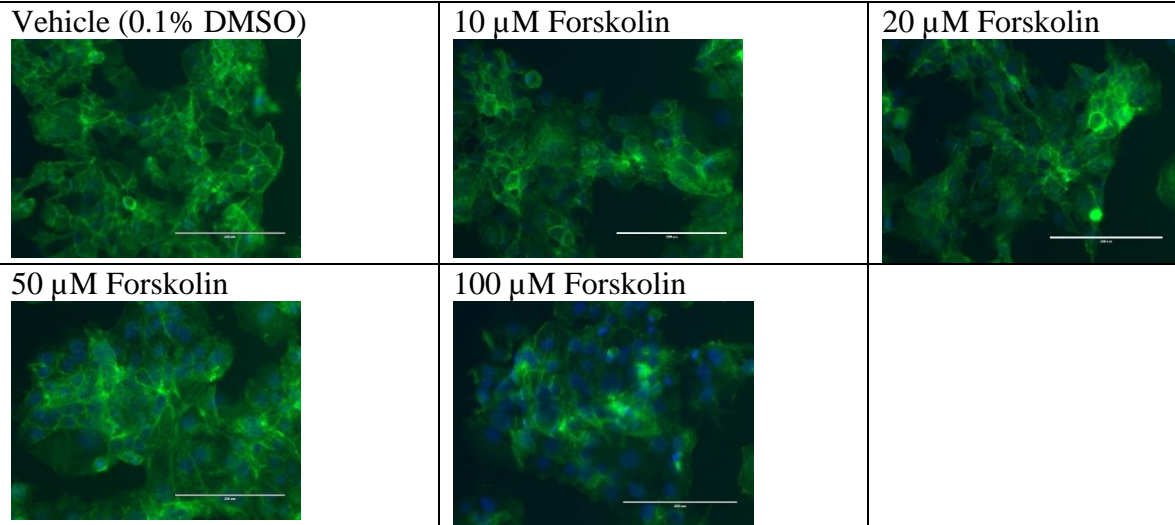
(B) Quantification of concentration-dependent response of forskolin-stimulated syncytialization

(B1)

(B2)
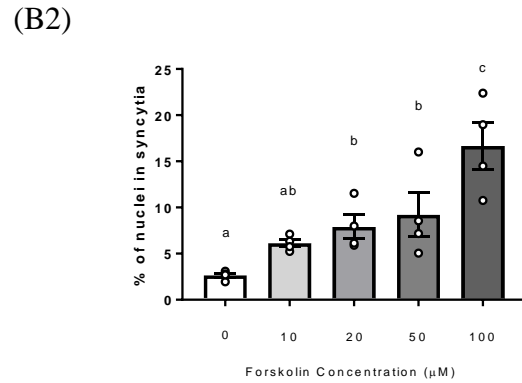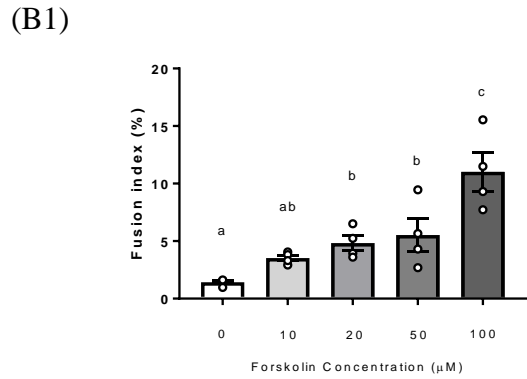
(C) DCVC effect on syncytialization

(C1)

(C2)

(C3)

(C4)

(D) DCVC exposure on unsyncytialized BeWo cells do not lead to any evidence of syncytialization
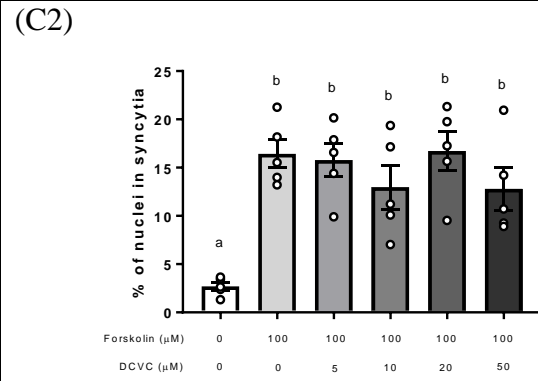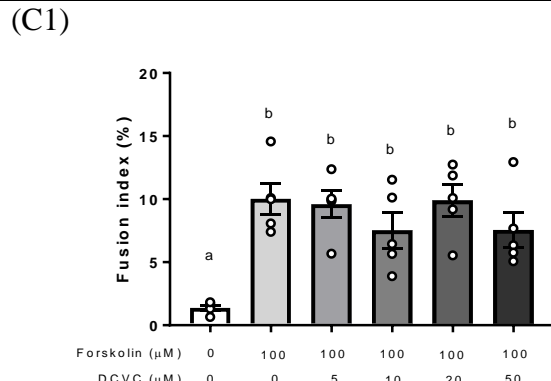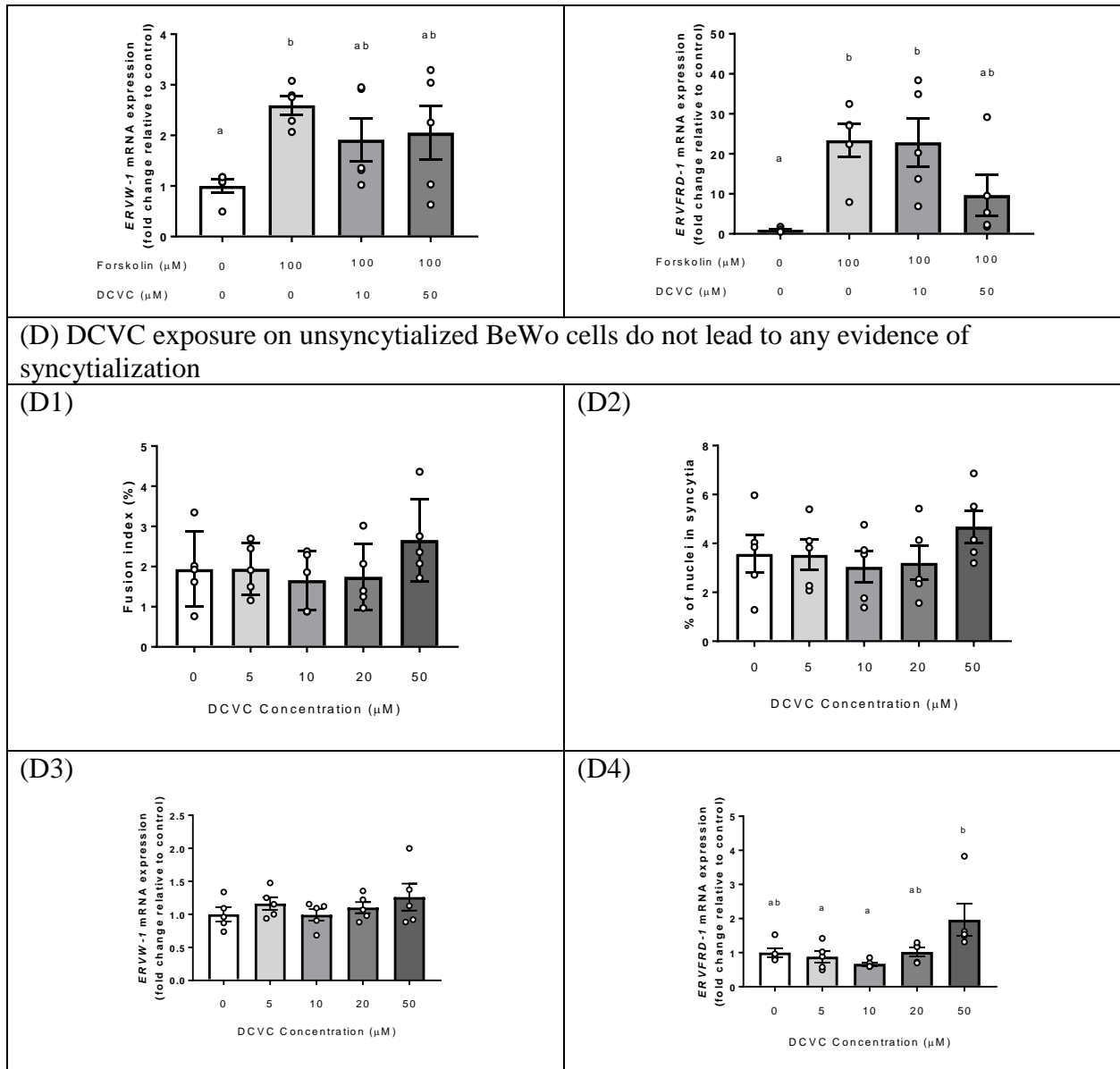
Figure 4.1. Concentration-dependent effects of forskolin on syncytialization with and without DCVC co-exposure. (A) Visualization of BeWo cell syncytialization. The green stain is a phalloidin-FITC membrane stain, and the blue stain corresponds to a 4',6-diamidino-2-phenylindole, dihydrochloride (DAPI) nuclear stain. (B) Quantification of staining assessment of syncytialization using the fusion index and percentage of nuclei in syncytia. N=4 independent experiments. (C) DCVC effects on forskolin-stimulated syncytialization. N=5 independent experiments. (D) DCVC effects on syncytialization metrics in the absence of forskolin. N=5 independent experiments. Statistical analysis was performed using one-way ANOVA followed by Tukey's post-hoc multiple comparisons of means. Statistical significance is indicated by non-overlapping letters. Error bars represent mean ± SEM.

	Cell viability	Cell cytotoxicity
(A) Unsyncytialized BeWo cells (48-hour exposure)	(A1)	(A2)
(B) Unsyncytialized BeWo cells (72-hour exposure)	(B1)	(B2)
(C) Exposure during syncytialization (48-hour exposure)	(C1)	(C2)
(D) BeWo cells after syncytialization (48-hour exposure)	(D1)	(D2)

Figure 4.2. Concentration-dependent effects of DCVC on cell viability and cytotoxicity. (A) Unsyncytialized BeWo cells exposed to DCVC for 48 hours. (B) Unsyncytialized BeWo cells exposed to DCVC for 72 hours. (C) BeWo cells co-exposed to DCVC while undergoing forskolin-stimulated syncytialization for 48 hours. (D) Syncytialized BeWo cells exposed to DCVC for 48 hours. Statistical analysis was performed using mixed models ANOVA followed by Tukey's post-hoc comparison of means. Statistical significance is denoted by non-overlapping letters. N=3 independent experiments with triplicate wells for each experiment. Cell viability was measured as relative fluorescence units (RFU) and cytotoxicity was measured as relative luminescence units (RLU)/mg protein. Camptothecin (CPT) was included as a positive control.
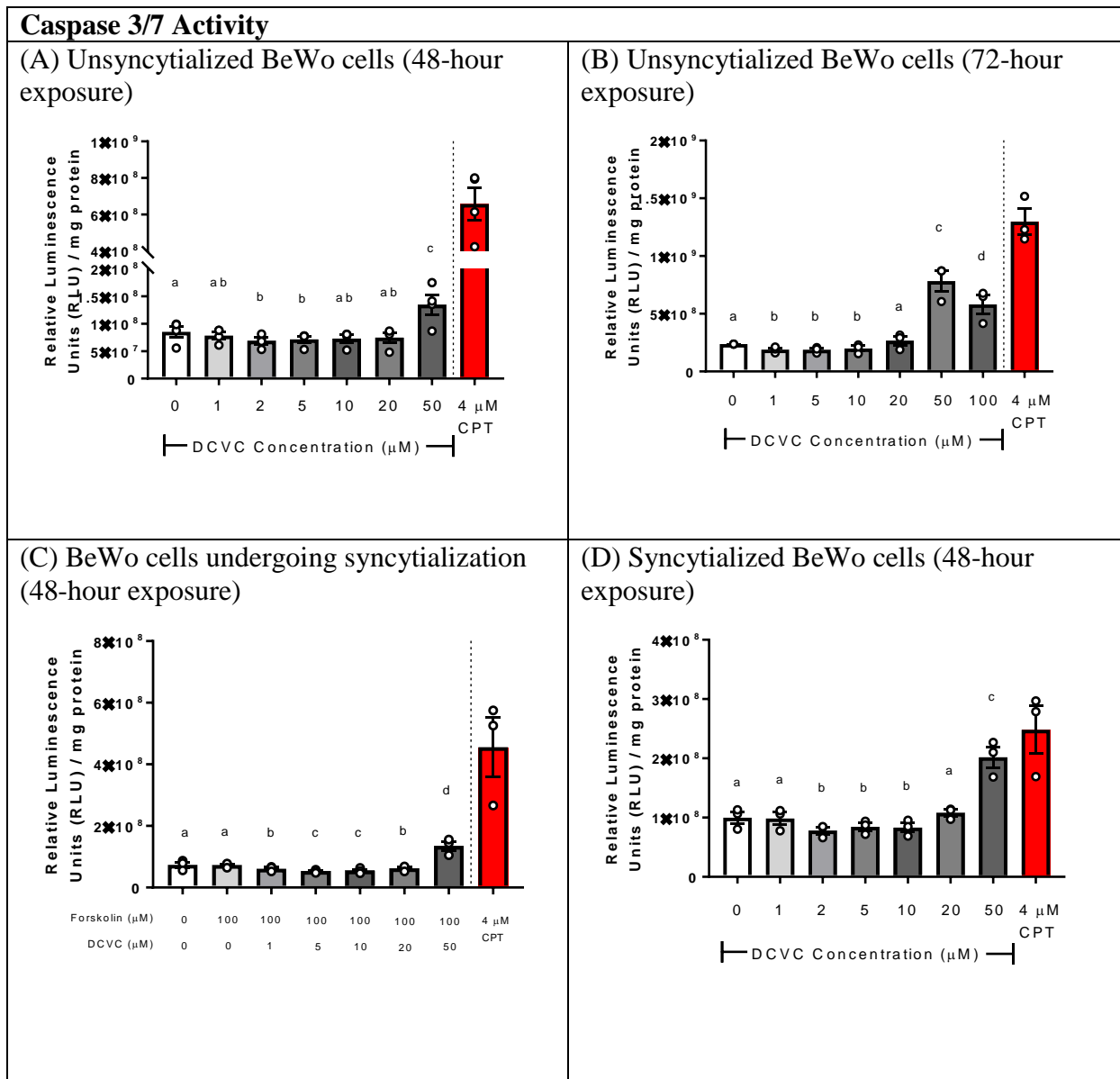
Figure 4.3. Effects of DCVC on caspase 3/7 activity. (A) Unsyncytialized BeWo cells exposed to DCVC for 48 hours. (B) Unsyncytialized BeWo cells exposed to DCVC for 72 hours. (C) BeWo cells co-exposed to DCVC while undergoing forskolin-stimulated syncytialization for 48 hours. (D) Syncytialized BeWo cells exposed to DCVC for 48 hours. Statistical analysis was performed using mixed models ANOVA followed by Tukey's post-hoc comparison of means. Statistical significance is denoted by non-overlapping letters. N=4 independent experiments for (A) and N=3 independent experiments for (B-D), performed in triplicate for each experiment. Camptothecin (CPT) was included as a positive control.

(A) Representative images of Hoechst staining to detect nuclear condensation or fragmentation (48-h exposures on unsyncytialized BeWo cells)

0 µM DCVC

5 µM DCVC

10 µM DCVC

20 µM DCVC

50 µM DCVC
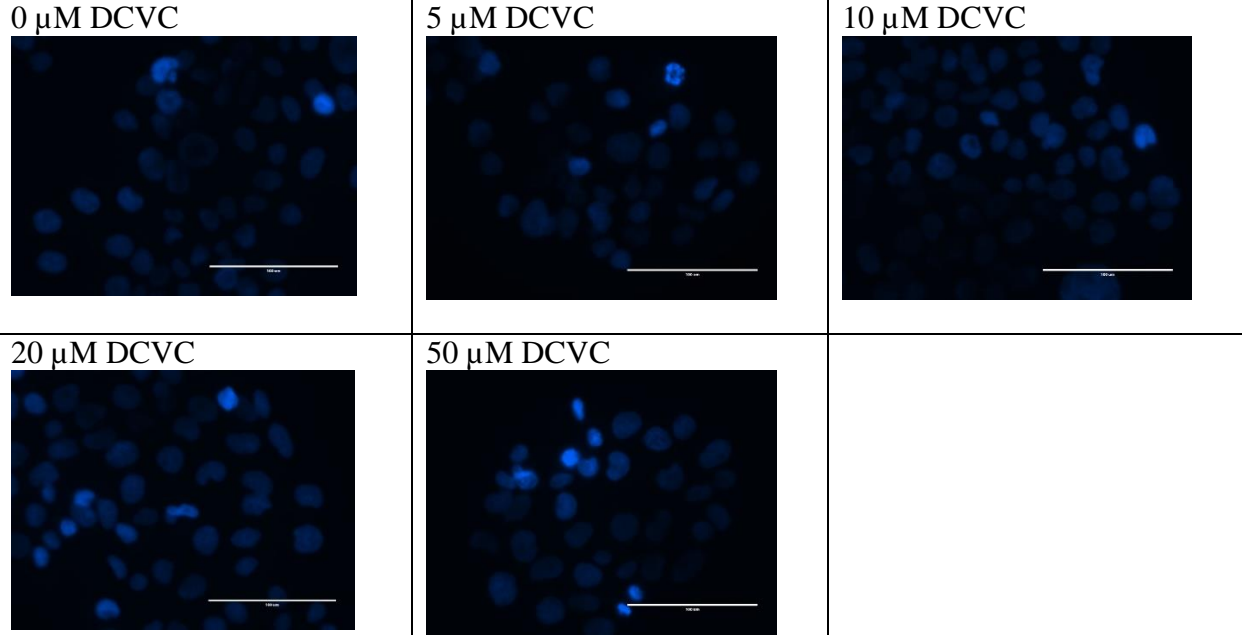
(B) Quantification results of Hoechst staining

(B1) Unsyncytialized BeWo cells (48-h exposure)

(B2) Process of syncytialization (48-h exposure)

(B3) Syncytialized BeWo cells (24-h exposure)

(B4) Syncytialized BeWo cells (48-h exposure)

198
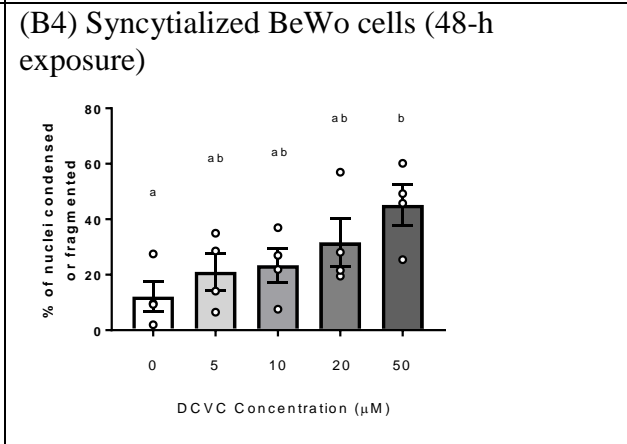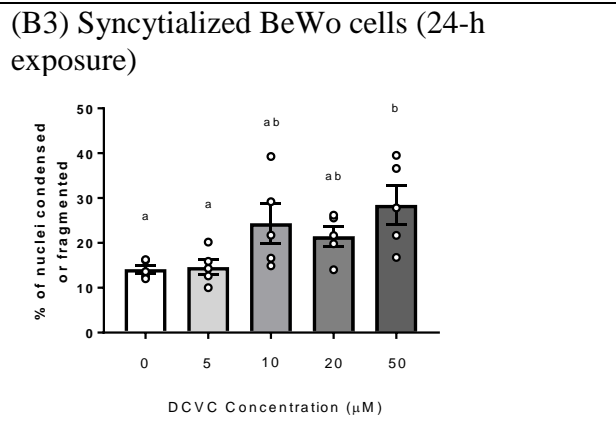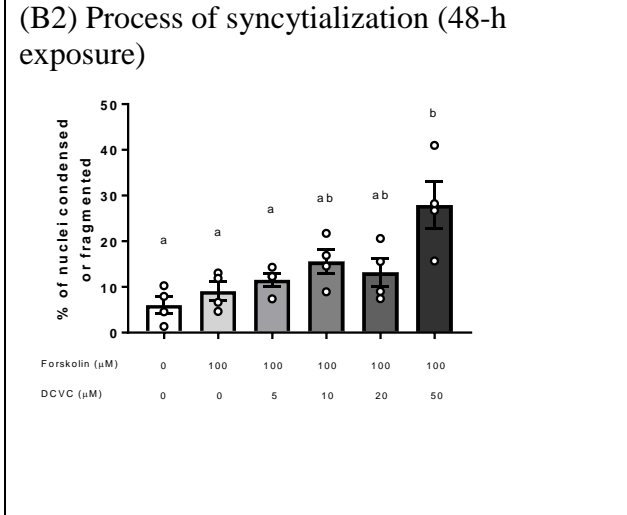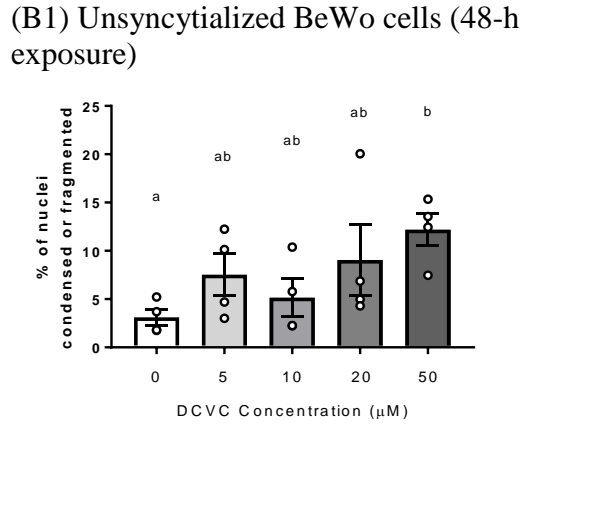
Figure 4.4. Effects of DCVC on nuclear condensation or fragmentation in BeWo cells. (A) Representative images of Hoechst 33342 staining to visualize nuclear condensation or fragmentation in unsyncytialized BeWo cells following 48-hour exposure to DCVC. (B) Quantification of DCVC effects on nuclear condensation or fragmentation in (B1) unsyncytialized BeWo cells exposed to DCVC for 48 hours, (B2) BeWo cells undergoing syncytialization for 48 hours, (B3) syncytialized BeWo cells exposed to DCVC for 24 hours, and (B4) syncytialized BeWo cells exposed to DCVC for 48 hours. Statistical analysis was performed using one-way ANOVA. Statistically significant differences are indicated by non-overlapping letters. Error bars represent mean ± SEM. N=4-5 independent experiments.

(A) Unsyncytialized BeWo cells (48-hour exposure)
(A1) (A2) (A3)
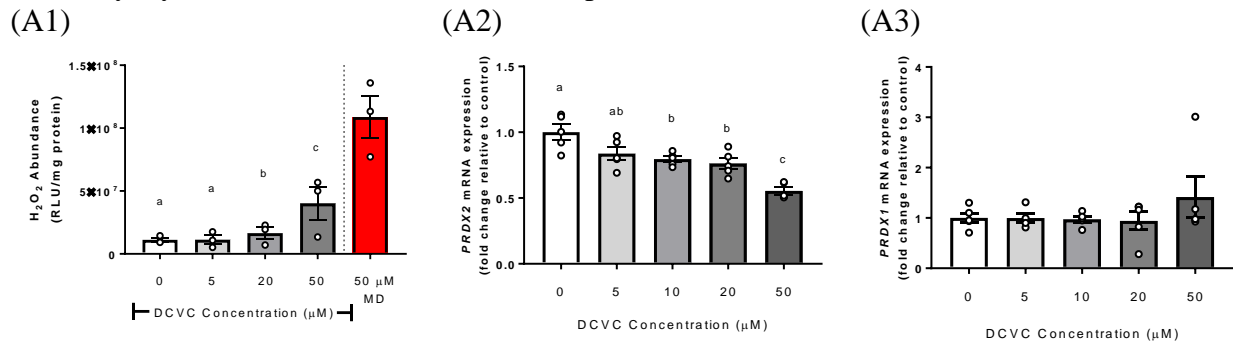
(B) Process of syncytialization (48-hour exposure)
(B1) (B2) (B3)
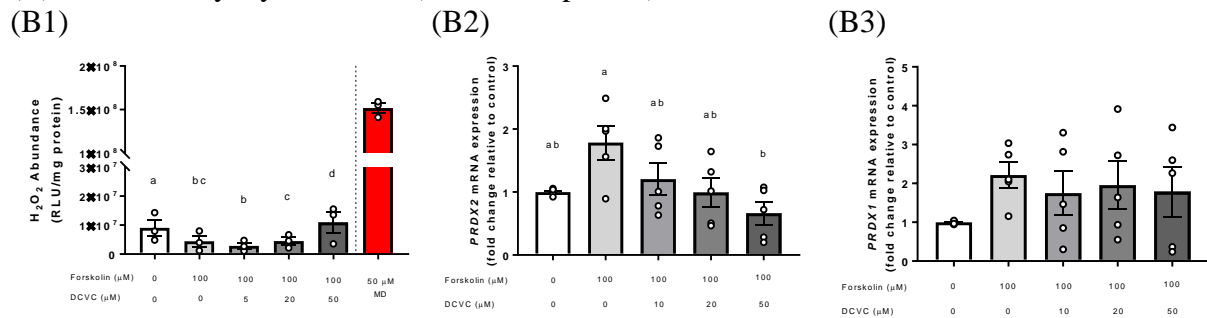
(C) Syncytialized BeWo cells (24-hour exposure)
(C1) (C2)
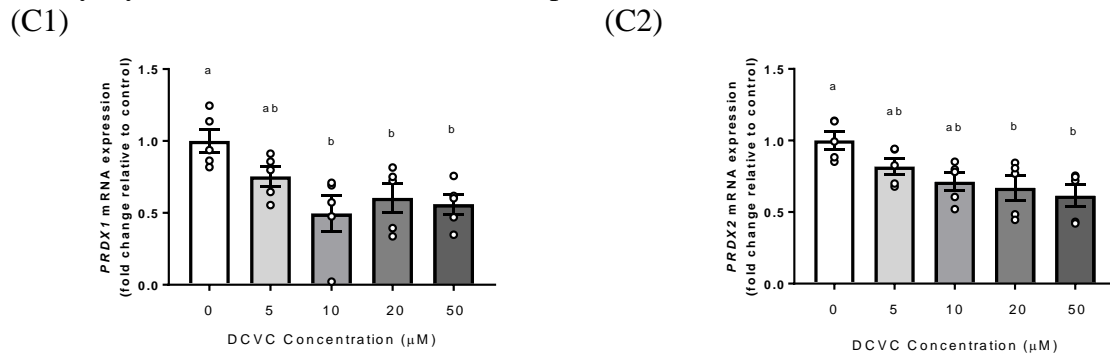
(D) Syncytialized BeWo cells (48-hour exposure)
(D1) (D2) (D3)
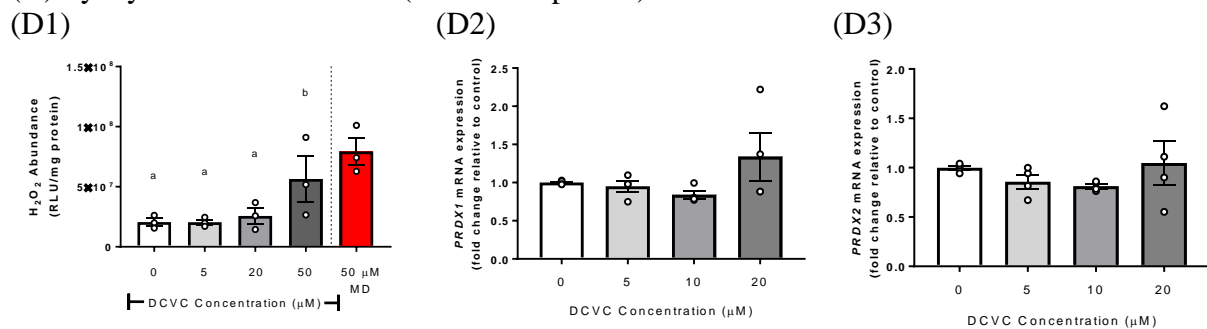
Figure 4.5. DCVC effects on H_2O_2 abundance, *PRDX1* mRNA expression, and *PRDX2* mRNA expression as biomarkers of oxidative stress. (A) Unsyncytialized BeWo cells exposed to DCVC for 48 hours. **(B)** BeWo cells co-treated with DCVC while undergoing forskolin-

200

stimulated syncytialization. (C) Syncytialized BeWo cells exposed to DCVC for 24 hours. (D) Syncytialized BeWo cells exposed to DCVC for 48 hours. For the mRNA expression data, statistical analysis was performed using one-way ANOVA followed by Tukey's post-hoc comparison of means, with N=4-5 independent experiments. For the H_2O_2 abundance data, statistical analysis was performed using mixed models ANOVA followed by Tukey's post-hoc comparison of means, with N=3 independent experiments performed in triplicate. Statistically significant differences are indicated by non-overlapping letters. Error bars for all graphs represent mean ± SEM. Menadione (MD) was included as a positive control for the experiments involving measurement of H_2O_2.

(A) Unsyncytialized BeWo cells (48-hour exposure)
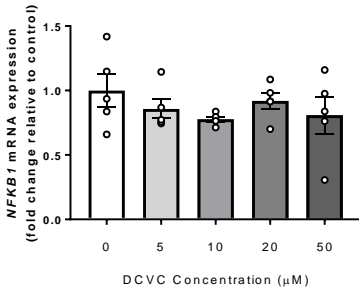
(A1)   (A2)   (A3)

(B) BeWo cells undergoing syncytialization (48-hour exposure)

(B1)   (B2)   (B3)
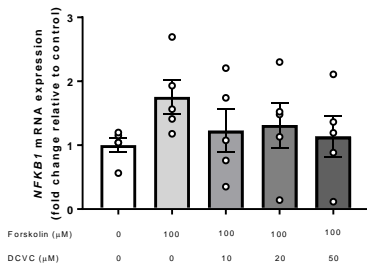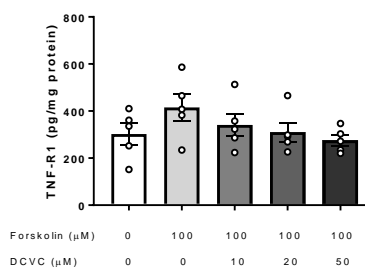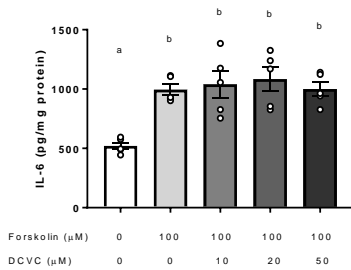
(C) Syncytialized BeWo cells

(C1) *NFBK1* mRNA expression (24-h exposure)
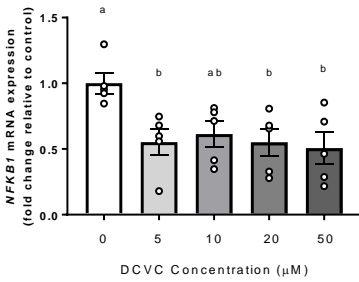
(C2) *NFKB1* mRNA expression (48-h exposure)
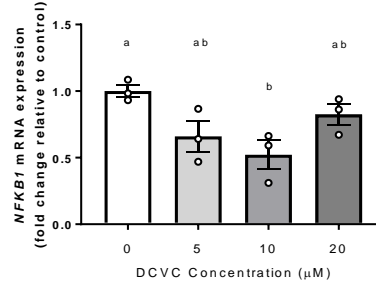
(C3) TNF-R1 (48-h exposure)
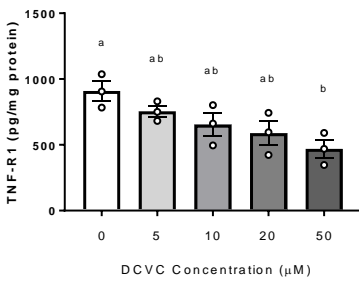
(C4) IL-6 (48-h exposure)
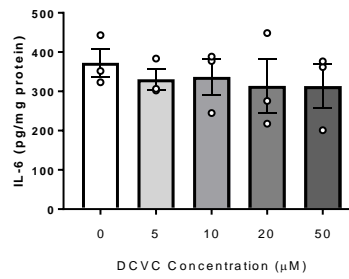
Figure 4.6. DCVC effects on *NFKB1* mRNA expression and cell media concentrations of TNF-R1 and IL-6 as biomarkers of pro-inflammatory response. (A) Unsyncytialized BeWo cells exposed to DCVC for 48 hours. (B) BeWo cells co-treated with DCVC while undergoing forskolin-stimulated syncytialization for 48 hours. (C1) Syncytialized BeWo cells exposed to DCVC for 24 hours. (C2-C4) Syncytialized BeWo cells exposed to DCVC for 48 hours. Data were analyzed using one-way ANOVA followed by Tukey's post-hoc comparison of means. Statistically significant differences are indicated by non-overlapping letters. For the TNF-R1 and IL-6 data, N=3, 5, and 3 independent experiments for unsyncytialized BeWo cells, BeWo cells undergoing syncytialization, and syncytialized BeWo cells, respectively. For the *NFKB1* mRNA expression data, N=5 independent experiments for all except N=4 for exposures on syncytialized cells for 48-hour duration. Error bars represent mean ± SEM.

(A) Unsyncytialized BeWo cells (48-hour exposure)
(A1) (A2) (A3)
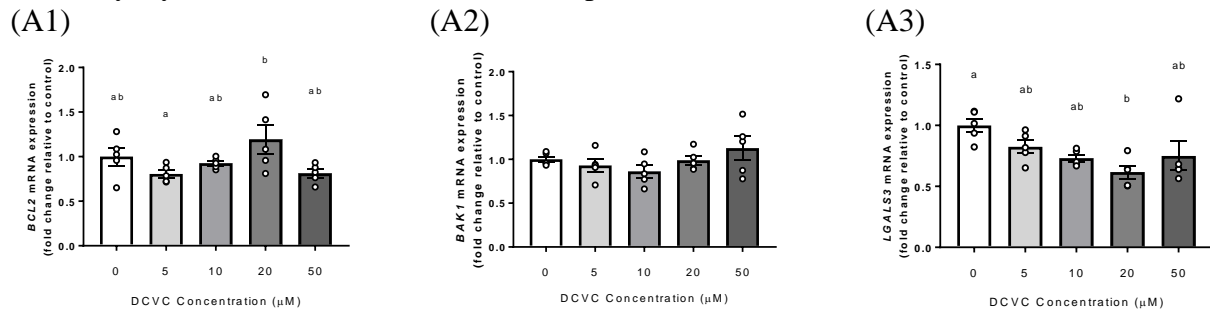
(B) BeWo cells undergoing syncytialization (48-hour exposure)
(B1) (B2) (B3)
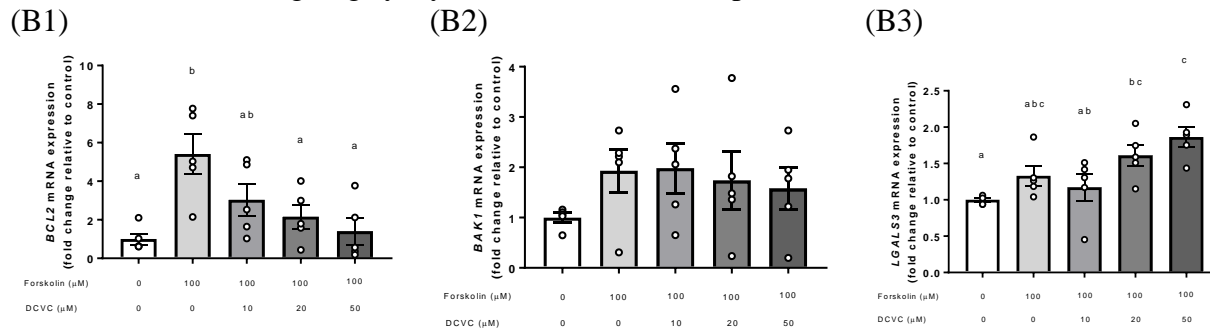
(C) Syncytialized BeWo cells (24-hour exposure)
(C1) (C2)
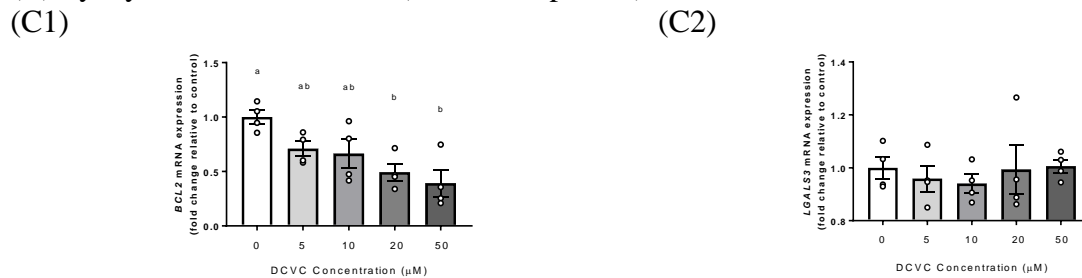
(D) Syncytialized BeWo cells (48-hour exposure)
(D1) (D2)
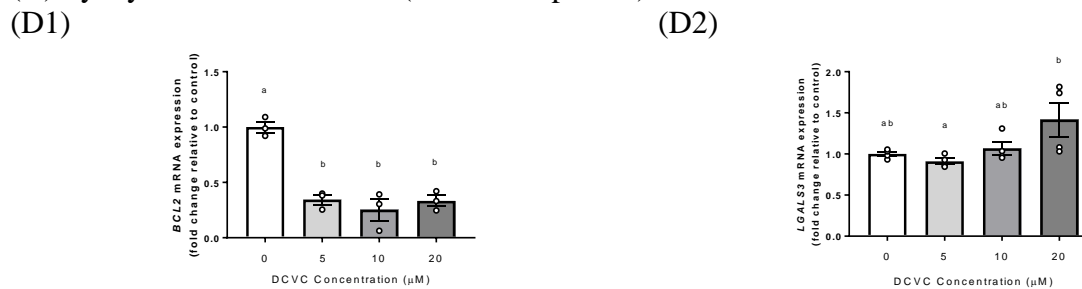
Figure 4.7. Effects of DCVC on apoptotic pathway genes *BCL2*, *BAK1*, and *LGALS3*. (A) Unsyncytialized BeWo cells exposed to DCVC for 48 hours. (B) BeWo cells co-treated with DCVC while undergoing forskolin-stimulated syncytialization for 48 hours. (C) Syncytialized BeWo cells exposed to DCVC for 24 hours. (D) Syncytialized BeWo cells exposed to DCVC for 48 hours. Data were analyzed using one-way ANOVA followed by Tukey's post-hoc comparison of means. Statistical significance is indicated by non-overlapping letters. Error bars represent mean ± SEM. N=5 independent experiments for the experiments in (A) and (B). N=4

independent experiments for the experiments in (C). N=3 and N=4 independent experiments for the *BCL2* and *LGALS3* outcomes, respectively, in Panel (D).
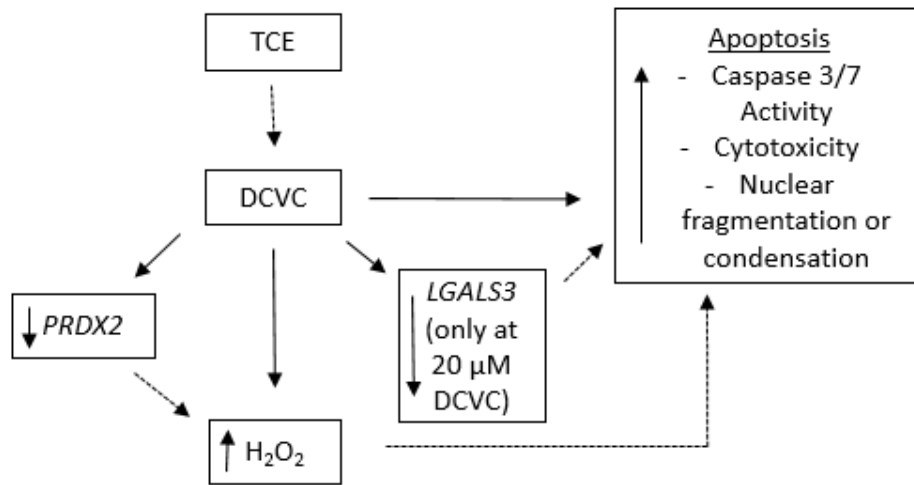
Figure 4.8. Simplified mechanism of apoptosis stimulated by DCVC in unsyncytialized BeWo cells. Solid arrows represent relationships observed and dashed arrows represent inferred relationships based on prior reports (not necessarily in placental cells). All endpoints were measured after 48 hours of exposure, with the exception of cytotoxicity and caspase 3/7 activity, which were measured at both the 48-hour and 72-hour time points.
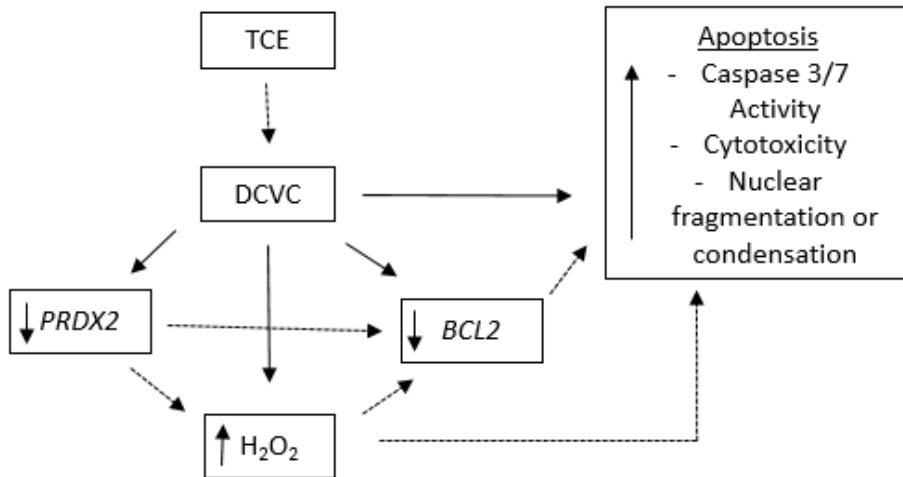
Figure 4.9. Simplified mechanism of apoptosis stimulated by DCVC in BeWo cells undergoing syncytialization. Solid arrows represent relationships observed and dashed arrows represent inferred relationships based on prior reports (not necessarily in placental cells). All endpoints were measured after 48 hours of exposure.
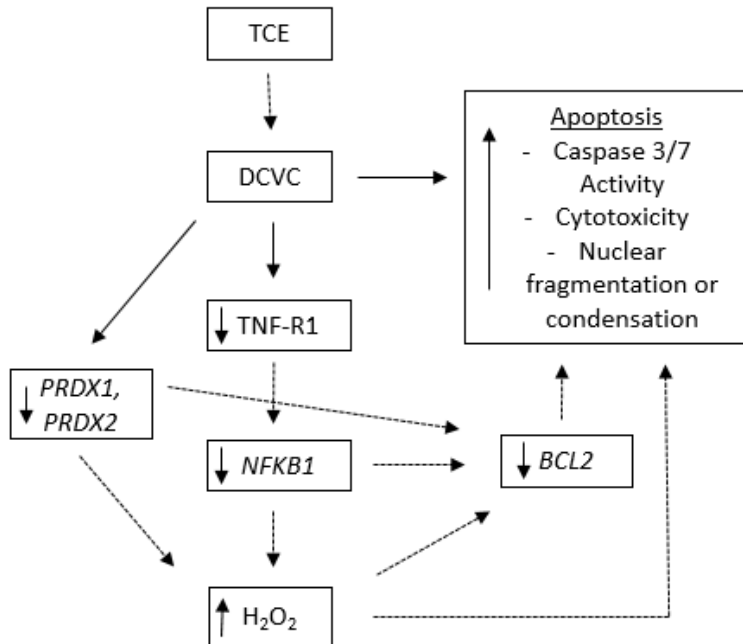
Figure 4.10. Simplified mechanism of apoptosis stimulated by DCVC in syncytialized BeWo cells. Solid arrows represent relationships observed and dashed arrows represent inferred relationships based on prior reports (not necessarily in placental cells). DCVC-stimulated alterations in the directions as depicted in the above endpoints occurred with the following exposures: *PRDX1*, 24 hours; *PRDX2*, 24 hours; TNF-R1, 48 hours; *NFKB1*, 24 and 48 hours; H_2O_2, 48 hours; *BCL2*, 24 and 48 hours; caspase 3/7 activity, 48 hours; cytotoxicity, 48 hours; nuclear fragmentation or condensation, 24 and 48 hours.

Table S4.1. Relationship between fusion index and percentage of nuclei in syncytia to characteristic of syncytialization.

	Low fusion index	**High fusion index**
Low percentage of nuclei in syncytia	Low syncytialization	Syncytialization favoring many nuclei per syncytia
High percentage of nuclei in syncytia	Syncytialization favoring low (e.g., two) nuclei per syncytia	High overall syncytialization

As depicted, high fusion index and percentage of nuclei in syncytia is indicative of high degree of syncytialization. Low fusion index and percentage of nuclei in syncytia is indicative of low degree of syncytialization. In the case of high fusion index but low percent of nuclei in syncytia, syncytialization is occurring in a manner favoring many nuclei per syncytia. In the case of low fusion index but high percentage of nuclei in syncytia, syncytialization is occurring in a manner favoring not many nuclei per syncytia.

Table S4.2. Primer sequences used for the current study. In the case of using the NCBI database, primers were selected to have as close to 60 degrees Celsius melting point for each primer as possible, have an amplicon size preferably between 75 and 150 base pairs, and be as close to 50% GC pairs in sequence as possible. Also, the criteria of the primer spanning an exon-exon junction was selected as a must.

B2M (Beta-2-microglobulin)	
Forward	5'-TGCCGTGTGAACCATGTG-3'
Reverse	5'-GCGGCATCTTCAAACCTC-3'
Source	Vreeburg, R.A.M, Bastiaan-Net, S., and Mes, J.J. (2011). Normalization genes for quantitative RT-PCR in differentiated Caco-2 cells used for food exposure studies. *Food Funct.* **2,** 124-129.
PRDX1 (Peroxiredoxin 1)	
Forward	5'-AACCTGGTTGAACCCCAAGC-3'
Reverse	5'-TATTTTCCTTTGTAGTCAGACAGGC-3'
Source	NCBI Nucleotide Database
PRDX2 (Peroxiredoxin 2)	
Forward	5'-AGACGAGCATGGGGAAGTTTG-3'
Reverse	5'-TGTCATCCACGTTGGGCTTA-3'
Source	NCBI Nucleotide Database
ERVFRD-1 (Syncytin-2)	
Forward	5'-GCTGTCCCTGGTGTTTCAGT-3'
Reverse	5'-CCTTCACTAGCAGCCTACCG-3'
Source	Vargas, A., Moreau, J., Landry, S, et al. (2009). Syncytin-2 plays an important role in the fusion of human trophoblast cells. *J. Mol. Biol.* **392,** 301-318.
ERVW-1 (Syncytin-1)	
Forward	5'-GATATTTGGCTAAGGAGGTGATGTC-3'
Reverse	5'-GAAGGCCCTTCATACCAATGA-3'
Source	Vargas, A., Moreau, J., Landry, S, et al. (2009). Syncytin-2 plays an important role in the fusion of human trophoblast cells. *J. Mol. Biol.* **392,** 301-318.
LGALS3 (Galectin-3)	
Forward	5'-GTGAAGCCCAATGCAAACAGA-3'
Reverse	5'-AGCGTGGGTTAAAGTGGAAGG-3'
Source	PrimerBank: (https://pga.mgh.harvard.edu/primerbank/) PrimerBank ID: 294345474c2
NFKB1 (Nuclear factor kappa B subunit 1)	
Forward	5'-AACAGAGAGGATTTCGTTTCCG-3'

Reverse	5'-TTTGACCTGAGGGTAAGACTTCT-3'
Source	PrimerBank: (https://pga.mgh.harvard.edu/primerbank/) PrimerBank ID: 259155300c1
BCL2 (**BCL2, B-cell lymphoma 2, apoptosis regulator**)	
Forward	5'-CATGCTGGGGCCGTACAG-3'
Reverse	5'-GAACCGGCACCTGCACAC-3'
Source	Wyrębska, A., Szymański, J., Gach, K., et al. (2013). Apoptosis-mediated cytotoxic effects of parthenolide and the new synthetic analog MZ-6 on two breast cancer cell lines. *Mol. Biol. Rep.* **40,** 1655-1663.
BAK1 (**BCL2 antagonist/killer 1**)	
Forward	5'-ATGGTCACCTTACCTCTGCAA-3'
Reverse	5'-TCATAGCGTCGGTTGATGTCG-3'
Source	PrimerBank: (https://pga.mgh.harvard.edu/primerbank/) PrimerBank ID: 109698605c2
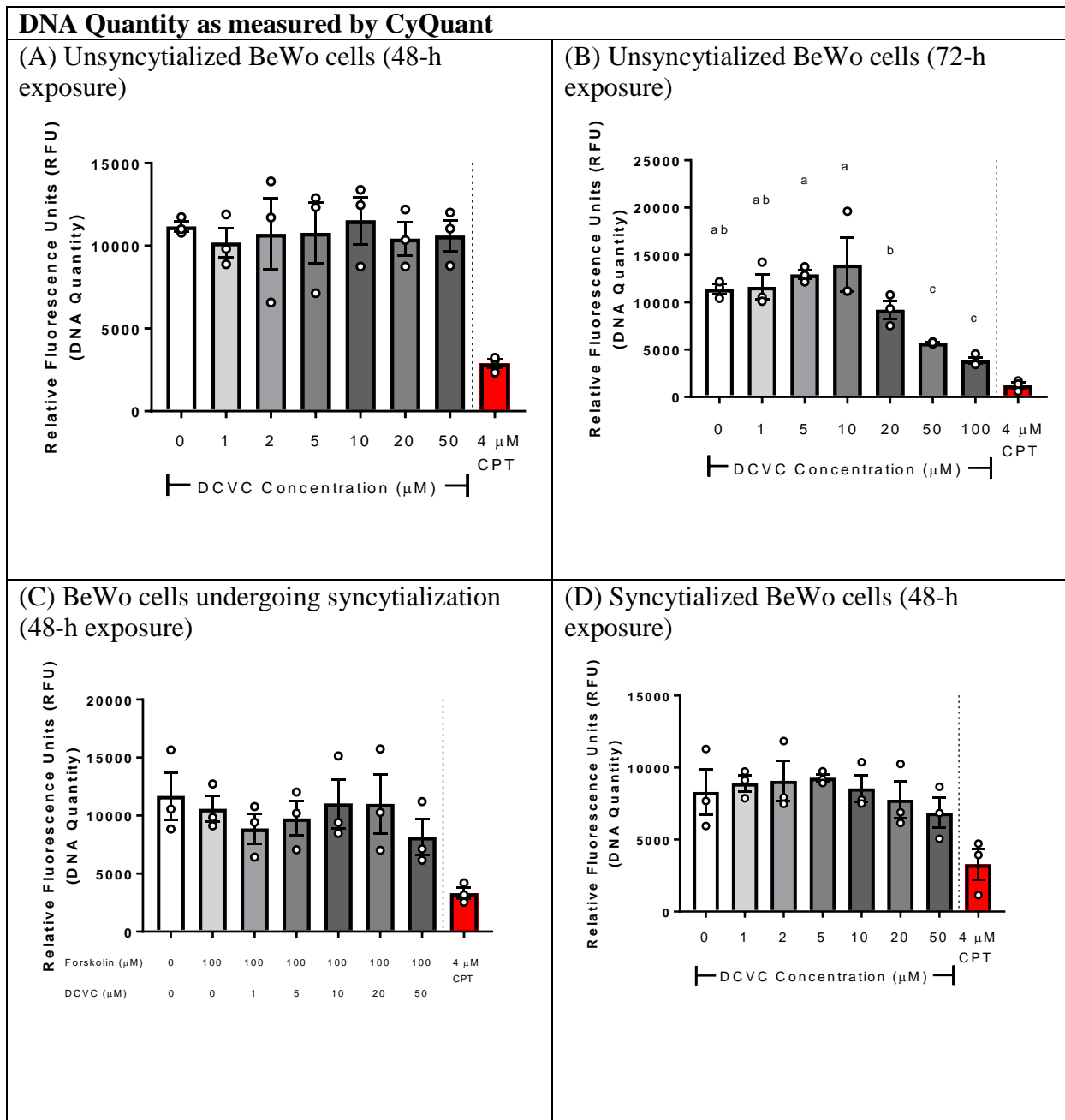
Figure S4.1. Effects of DCVC on DNA quantity. (A) Unsyncytialized BeWo cells exposed to DCVC for 48 hours. (B) Unsyncytialized BeWo cells exposed to DCVC for 72 hours. (C) BeWo cells co-treated with DCVC while undergoing forskolin-stimulated syn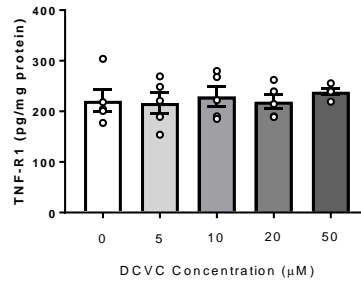cytialization for 48 hours. (D) Syncytialized BeWo cells exposed to DCVC for 48 hours. DCVC only decreases DNA quantity in unsyncytialized BeWo cells for the 72-hour time point. Statistical analysis was performed using mixed models ANOVA followed by Tukey's post-hoc comparison of means. Statistical significance is denoted by non-overlapping letters. N=3 independent experiments with triplicate wells for each experiment. Camptothecin (CPT) was included as a positive control.

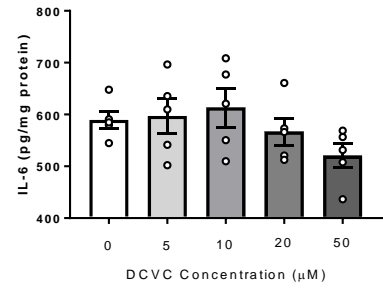|	IFN-γ (pg/mg protein)	CRP (pg/mg protein)
(A) Unsyncytialized BeWo cells (48-h exposure)	(A1)	(A2)
(B) BeWo cells undergoing syncytialization (48-h exposure)	(B1)	(B2)
(C) Syncytialized BeWo cells (48-h exposure)	(C1)	(C2)
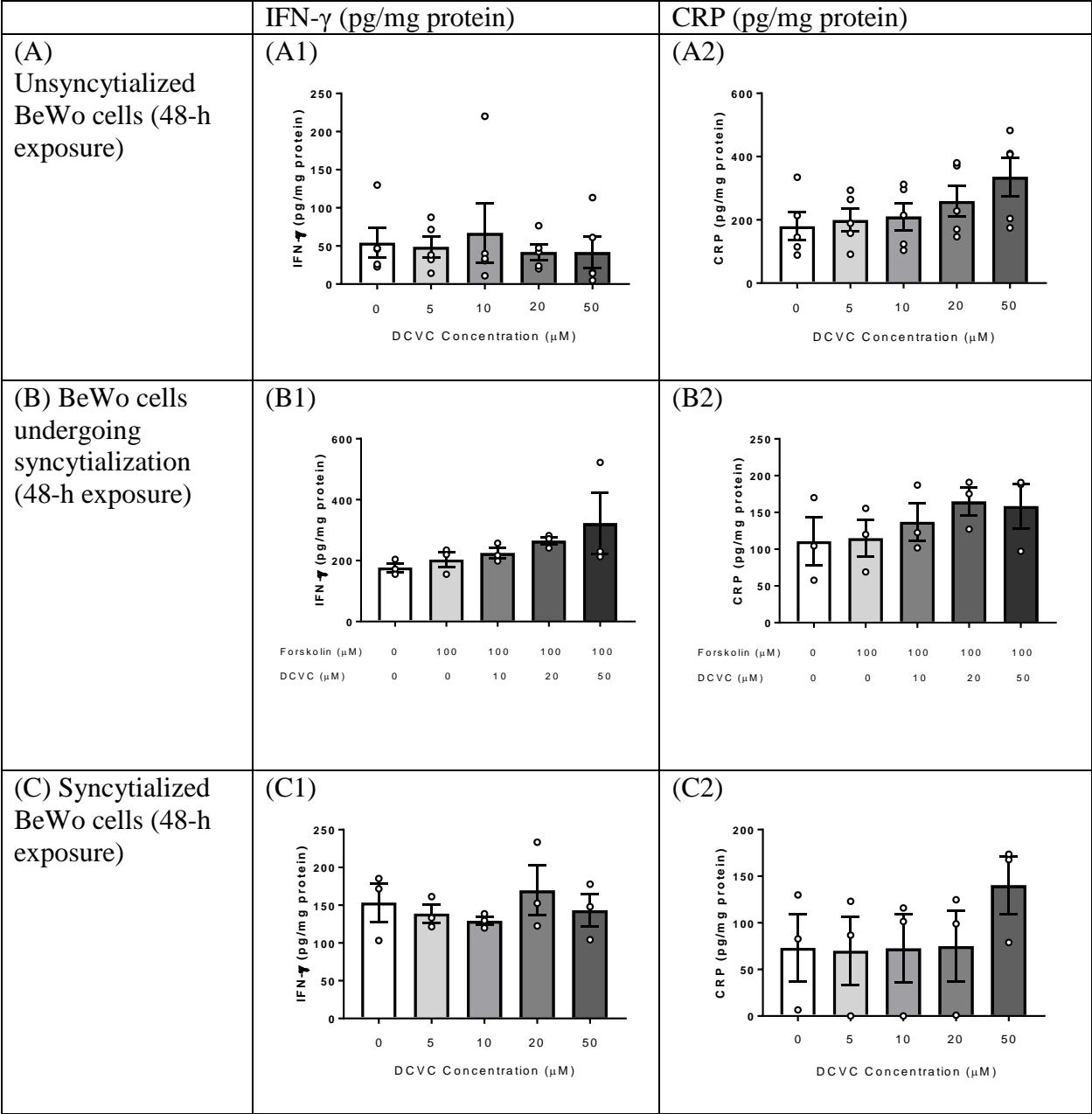
Figure S4.2. DCVC effects on pro-inflammatory endpoints in cell media IFN-γ and CRP unchanged in unsyncytialized BeWo cells, BeWo cells undergoing syncytialization, and syncytialized BeWo cells. (A) Unsyncytialized BeWo cells exposed to DCVC for 48 hours. (B) BeWo cells co-exposed to DCVC while undergoing forskolin-stimulated syncytialization for 48 hours. (C) Syncytialized BeWo cells exposed to DCVC for 48 hours. Data were analyzed using one-way ANOVA followed by Tukey's post-hoc comparison of means. Error bars represent mean ± SEM. N=3, 5, and 3 independent experiments for unsyncytialized BeWo cells, BeWo cells undergoing syncytialization, and syncytialized BeWo cells, respectively. As a few values for CRP on syncytialized BeWo cells were at or very close to zero, we are only including the graph for completion purposes and do not think the data is particularly reliable.
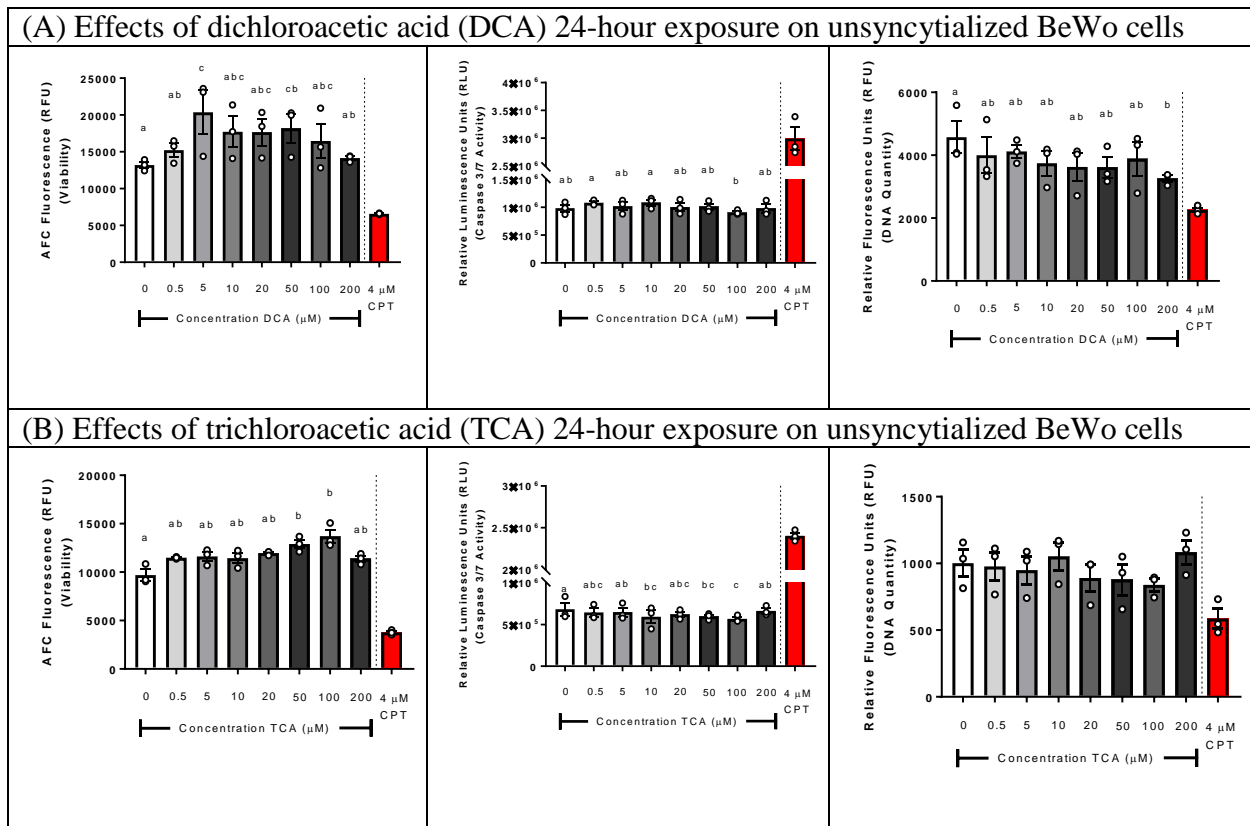
Figure S4.3. Effects of (A) dichloroacetic acid (DCA) and (B) trichloroacetic acid (TCA) on unsyncytialized BeWo cells at the 24-hour time point. Time was chosen to be consistent with that of previous studies looking at DCA and TCA exposure on other placental cells (unpublished data). Statistical analysis was performed using mixed models ANOVA followed by Tukey's post-hoc comparison of means with treatment as the fixed variable and experiment as the random variable. Statistical significance is denoted by non-overlapping letters. Error bars represent mean ± SEM. N=3 independent experiments performed in triplicate. RFU and RLU stand for relative fluorescence units and relative luminescence units, respectively. Camptothecin (CPT) was included as a positive control.

Nuclear Condensation or Fragmentation:
24-hour exposures on unsyncytialized BeWo cells
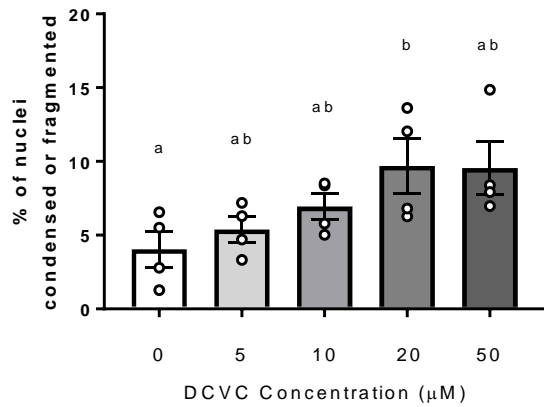
Figure S4.4. Effects on DCVC exposure on nuclear condensation or fragmentation at the 24-hour time point for unsyncytialized BeWo cells. The percentage data were converted to fractions and arcsine transformed prior to statistical analysis. One-way ANOVA followed by Tukey's post-hoc comparison of means was used to statistically analyze the data. Statistically significant differences are indicated by non-overlapping letters. Error bars represent mean ± SEM. N=4 independent experiments.

References

Agency for Toxic Substances and Disease Registry, 2007. Trichloroethylene Toxicity: What are the U.S. Standards for Trichloroethylene Exposure? In Agency for Toxic Substances and Disease Registry (ATSDR), E.H.a.M.E., (Ed.), Atlanta, GA, pp.

Akahani, S., Nangia-Makker, P., Inohara, H., Kim, H.R., Raz, A., 1997. Galectin-3: a novel antiapoptotic molecule with a functional BH1 (NWGR) domain of Bcl-2 family. Cancer Res **57**, 5272-5276.

Al-Nasiry, S., Spitz, B., Hanssens, M., Luyten, C., Pijnenborg, R., 2006. Differential effects of inducers of syncytialization and apoptosis on BeWo and JEG-3 choriocarcinoma cells. Hum Reprod **21**, 193-201.

Annibaldi, A., Meier, P., 2018. Checkpoints in TNF-Induced Cell Death: Implications in Inflammation and Cancer. Trends Mol Med **24**, 49-65.

Boldenow, E., Hassan, I., Chames, M.C., Xi, C., Loch-Caruso, R., 2015. The trichloroethylene metabolite S-(1,2-dichlorovinyl)-l-cysteine but not trichloroacetate inhibits pathogen-stimulated TNF-alpha in human extraplacental membranes in vitro. Reprod Toxicol **52**, 1-6.

Bubici, C., Papa, S., Pham, C.G., Zazzeroni, F., Franzoso, G., 2006. The NF-kappaB-mediated control of ROS and JNK signaling. Histol Histopathol **21**, 69-80.

Bull, R.J., 2000. Mode of action of liver tumor induction by trichloroethylene and its metabolites, trichloroacetate and dichloroacetate. Environ Health Perspect **108 Suppl 2**, 241-259.

Castellucci, M., Kaufmann, P., Bischof, P., 1990. Extracellular matrix influences hormone and protein production by human chorionic villi. Cell Tissue Res **262**, 135-142.

Colnot, C., Fowlis, D., Ripoche, M.A., Bouchaert, I., Poirier, F., 1998. Embryonic implantation in galectin 1/galectin 3 double mutant mice. Dev Dyn **211**, 306-313.

Crowley, L.C., Marfell, B.J., Waterhouse, N.J., 2016. Analyzing Cell Death by Nuclear Staining with Hoechst 33342. Cold Spring Harb Protoc **2016**.

Daly, J.W., 1984. Forskolin, adenylate cyclase, and cell physiology: an overview. Adv Cyclic Nucleotide Protein Phosphorylation Res **17**, 81-89.

DiFederico, E., Genbacev, O., Fisher, S.J., 1999. Preeclampsia is associated with widespread apoptosis of placental cytotrophoblasts within the uterine wall. Am J Pathol **155**, 293-301.

Elkin, E.R., Bridges, D., Harris, S.M., Loch-Caruso, R.K., 2020. Exposure to Trichloroethylene Metabolite S-(1,2-Dichlorovinyl)-L-cysteine Causes Compensatory Changes to Macronutrient Utilization and Energy Metabolism in Placental HTR-8/SVneo Cells. Chem Res Toxicol.

Elkin, E.R., Bridges, D., Loch-Caruso, R., 2019. The trichloroethylene metabolite S-(1,2-dichlorovinyl)-L-cysteine induces progressive mitochondrial dysfunction in HTR-8/SVneo trophoblasts. Toxicology **427**, 152283.

Elkin, E.R., Harris, S.M., Loch-Caruso, R., 2018. Trichloroethylene metabolite S-(1,2-dichlorovinyl)-l-cysteine induces lipid peroxidation-associated apoptosis via the intrinsic and extrinsic apoptosis pathways in a first-trimester placental cell line. Toxicol Appl Pharmacol **338**, 30-42.

Errami, Y., Naura, A.S., Kim, H., Ju, J., Suzuki, Y., El-Bahrawy, A.H., Ghonim, M.A., Hemeida, R.A., Mansy, M.S., Zhang, J., Xu, M., Smulson, M.E., Brim, H., Boulares,

216

A.H., 2013. Apoptotic DNA fragmentation may be a cooperative activity between caspase-activated deoxyribonuclease and the poly(ADP-ribose) polymerase-regulated DNAS1L3, an endoplasmic reticulum-localized endonuclease that translocates to the nucleus during apoptosis. J Biol Chem **288**, 3460-3468.

Fagerberg, L., Hallstrom, B.M., Oksvold, P., Kampf, C., Djureinovic, D., Odeberg, J., Habuka, M., Tahmasebpoor, S., Danielsson, A., Edlund, K., Asplund, A., Sjostedt, E., Lundberg, E., Szigyarto, C.A., Skogs, M., Takanen, J.O., Berling, H., Tegel, H., Mulder, J., Nilsson, P., Schwenk, J.M., Lindskog, C., Danielsson, F., Mardinoglu, A., Sivertsson, A., von Feilitzen, K., Forsberg, M., Zwahlen, M., Olsson, I., Navani, S., Huss, M., Nielsen, J., Ponten, F., Uhlen, M., 2014. Analysis of the human tissue-specific expression by genome-wide integration of transcriptomics and antibody-based proteomics. Mol Cell Proteomics **13**, 397-406.

Fisher, J.W., Whittaker, T.A., Taylor, D.H., Clewell, H.J., 3rd, Andersen, M.E., 1989. Physiologically based pharmacokinetic modeling of the pregnant rat: a multiroute exposure model for trichloroethylene and its metabolite, trichloroacetic acid. Toxicol Appl Pharmacol **99**, 395-414.

Forkert, P.G., Sylvestre, P.L., Poland, J.S., 1985. Lung injury induced by trichloroethylene. Toxicology **35**, 143-160.

Fox, H., 1970. Effect of hypoxia on trophoblast in organ culture. A morphologic and autoradiographic study. Am J Obstet Gynecol **107**, 1058-1064.

Garcia-Lloret, M.I., Winkler-Lowen, B., Guilbert, L.J., 2000. Monocytes adhering by LFA-1 to placental syncytiotrophoblasts induce local apoptosis via release of TNF-alpha. A model for hematogenous initiation of placental inflammations. J Leukoc Biol **68**, 903-908.

Genbacev, O., DiFederico, E., McMaster, M., Fisher, S.J., 1999. Invasive cytotrophoblast apoptosis in pre-eclampsia. Hum Reprod **14 Suppl 2**, 59-66.

Green, T., Dow, J., Ellis, M.K., Foster, J.R., Odum, J., 1997a. The role of glutathione conjugation in the development of kidney tumours in rats exposed to trichloroethylene. Chem Biol Interact **105**, 99-117.

Green, T., Mainwaring, G.W., Foster, J.R., 1997b. Trichloroethylene-induced mouse lung tumors: studies of the mode of action and comparisons between species. Fundam Appl Toxicol **37**, 125-130.

Hassan, I., Kumar, A.M., Park, H.R., Lash, L.H., Loch-Caruso, R., 2016. Reactive Oxygen Stimulation of Interleukin-6 Release in the Human Trophoblast Cell Line HTR-8/SVneo by the Trichlorethylene Metabolite S-(1,2-Dichloro)-l-Cysteine. Biol Reprod **95**, 66.

Hu, R., Jin, H., Zhou, S., Yang, P., Li, X., 2007. Proteomic analysis of hypoxia-induced responses in the syncytialization of human placental cell line BeWo. Placenta **28**, 399-407.

Huppertz, B., Frank, H.G., Kingdom, J.C., Reister, F., Kaufmann, P., 1998. Villous cytotrophoblast regulation of the syncytial apoptotic cascade in the human placenta. Histochem Cell Biol **110**, 495-508.

Ilekis, J.V., Tsilou, E., Fisher, S., Abrahams, V.M., Soares, M.J., Cross, J.C., Zamudio, S., Illsley, N.P., Myatt, L., Colvis, C., Costantine, M.M., Haas, D.M., Sadovsky, Y., Weiner, C., Rytting, E., Bidwell, G., 2016. Placental origins of adverse pregnancy outcomes: potential molecular targets: an Executive Workshop Summary of the Eunice Kennedy Shriver National Institute of Child Health and Human Development. Am J Obstet Gynecol **215**, S1-S46.

Inadera, H., Tachibana, S., Takasaki, I., Tatematsu, M., Shimomura, A., 2010. Hyperglycemia perturbs biochemical networks in human trophoblast BeWo cells. Endocr J **57**, 567-577.

Ishihara, N., Matsuo, H., Murakoshi, H., Laoag-Fernandez, J.B., Samoto, T., Maruo, T., 2002. Increased apoptosis in the syncytiotrophoblast in human term placentas complicated by either preeclampsia or intrauterine growth retardation. Am J Obstet Gynecol **186**, 158-166.

Ishii, T., Warabi, E., Yanagawa, T., 2012. Novel roles of peroxiredoxins in inflammation, cancer and innate immunity. J Clin Biochem Nutr **50**, 91-105.

Jin, X., Chen, C., Li, D., Su, Q., Hang, Y., Zhang, P., Hu, W., 2017. PRDX2 in Myocyte Hypertrophy and Survival is Mediated by TLR4 in Acute Infarcted Myocardium. Sci Rep **7**, 6970.

Khera, A., Vanderlelie, J.J., Holland, O., Perkins, A.V., 2017. Overexpression of Endogenous Anti-Oxidants with Selenium Supplementation Protects Trophoblast Cells from Reactive Oxygen Species-Induced Apoptosis in a Bcl-2-Dependent Manner. Biol Trace Elem Res **177**, 394-403.

Kohler, P.O., Bridson, W.E., 1971. Isolation of hormone-producing clonal lines of human choriocarcinoma. J Clin Endocrinol Metab **32**, 683-687.

Kohler, P.O., Bridson, W.E., Hammond, J.M., Weintraub, B., Kirschner, M.A., Van Thiel, D.H., 1971. Clonal lines of human choriocarcinoma cells in culture. Acta Endocrinol Suppl (Copenh) **153**, 137-153.

Lash, L.H., Anders, M.W., 1986. Cytotoxicity of S-(1,2-dichlorovinyl)glutathione and S-(1,2-dichlorovinyl)-L-cysteine in isolated rat kidney cells. J Biol Chem **261**, 13076-13081.

Lash, L.H., Chiu, W.A., Guyton, K.Z., Rusyn, I., 2014a. Trichloroethylene biotransformation and its role in mutagenicity, carcinogenicity and target organ toxicity. Mutat Res Rev Mutat Res **762**, 22-36.

Lash, L.H., Elfarra, A.A., Anders, M.W., 1986. Renal cysteine conjugate beta-lyase. Bioactivation of nephrotoxic cysteine S-conjugates in mitochondrial outer membrane. J Biol Chem **261**, 5930-5935.

Lash, L.H., Putt, D.A., Benipal, B., 2014b. Multigenerational study of chemically induced cytotoxicity and proliferation in cultures of human proximal tubular cells. Int J Mol Sci **15**, 21348-21365.

Lash, L.H., Putt, D.A., Brashear, W.T., Abbas, R., Parker, J.C., Fisher, J.W., 1999. Identification of S-(1,2-dichlorovinyl)glutathione in the blood of human volunteers exposed to trichloroethylene. J Toxicol Environ Health A **56**, 1-21.

Lash, L.H., Sausen, P.J., Duescher, R.J., Cooley, A.J., Elfarra, A.A., 1994. Roles of cysteine conjugate beta-lyase and S-oxidase in nephrotoxicity: studies with S-(1,2-dichlorovinyl)-L-cysteine and S-(1,2-dichlorovinyl)-L-cysteine sulfoxide. J Pharmacol Exp Ther **269**, 374-383.

Le Vee, M., Kolasa, E., Jouan, E., Collet, N., Fardel, O., 2014. Differentiation of human placental BeWo cells by the environmental contaminant benzo(a)pyrene. Chem Biol Interact **210**, 1-11.

Li, Y., Zheng, R., Wang, R., Lu, X., Zhu, C., Lin, H.Y., Wang, H., Yu, X., Fu, J., 2015. Involvement of nephrin in human placental trophoblast syncytialization. Reproduction **149**, 339-346.

Liu, Q., Zhang, Y., 2019. PRDX1 enhances cerebral ischemia-reperfusion injury through activation of TLR4-regulated inflammation and apoptosis. Biochem Biophys Res Commun **519**, 453-461.

Lu, E., Hu, X., Pan, C., Chen, J., Xu, Y., Zhu, X., 2020. Up-regulation of peroxiredoxin-1 promotes cell proliferation and metastasis and inhibits apoptosis in cervical cancer. J Cancer **11**, 1170-1181.

Lu, Y., Zhang, X.S., Zhou, X.M., Gao, Y.Y., Chen, C.L., Liu, J.P., Ye, Z.N., Zhang, Z.H., Wu, L.Y., Li, W., Hang, C.H., 2019. Peroxiredoxin 1/2 protects brain against H2O2-induced apoptosis after subarachnoid hemorrhage. FASEB J **33**, 3051-3062.

Matassov, D., Kagan, T., Leblanc, J., Sikorska, M., Zakeri, Z., 2004. Measurement of apoptosis by DNA fragmentation. Methods Mol Biol **282**, 1-17.

Matsuura, K., Jigami, T., Taniue, K., Morishita, Y., Adachi, S., Senda, T., Nonaka, A., Aburatani, H., Nakamura, T., Akiyama, T., 2011. Identification of a link between Wnt/beta-catenin signalling and the cell fusion pathway. Nat Commun **2**, 548.

McConkey, D.J., Orrenius, S., Jondal, M., 1990. Agents that elevate cAMP stimulate DNA fragmentation in thymocytes. J Immunol **145**, 1227-1230.

McKinney, L.L., Picken Jr., J.C., Weakley, F.B., Eldridge, A.C., Campbell, R.E., Cowan, J.C., Biester, H.E., 1959. Possible Toxic Factor of Trichloroethylene-extracted Soybean Oil Meal. Journal of the American Chemical Society **81**, 909-915.

Newlaczyl, A.U., Yu, L.G., 2011. Galectin-3--a jack-of-all-trades in cancer. Cancer Lett **313**, 123-128.

Panigel, M., Myers, R.E., 1972. Histological and ultrastructural changes in rhesus monkey placenta following interruption of fetal placental circulation by fetectomy or interplacental umbilical vessel ligation. Acta Anat (Basel) **81**, 481-506.

Papa, S., Bubici, C., Pham, C.G., Zazzeroni, F., Franzoso, G., 2005. NF-kappaB meets ROS: an 'iron-ic' encounter. Cell Death Differ **12**, 1259-1262.

Parrish, A.B., Freel, C.D., Kornbluth, S., 2013. Cellular mechanisms controlling caspase activation and function. Cold Spring Harb Perspect Biol **5**.

Pattillo, R.A., Gey, G.O., 1968. The establishment of a cell line of human hormone-synthesizing trophoblastic cells in vitro. Cancer Res **28**, 1231-1236.

Potgens, A.J., Schmitz, U., Bose, P., Versmold, A., Kaufmann, P., Frank, H.G., 2002. Mechanisms of syncytial fusion: a review. Placenta **23 Suppl A**, S107-113.

Saquib, Q., Al-Khedhairy, A.A., Ahmad, J., Siddiqui, M.A., Dwivedi, S., Khan, S.T., Musarrat, J., 2013. Zinc ferrite nanoparticles activate IL-1b, NFKB1, CCL21 and NOS2 signaling to induce mitochondrial dependent intrinsic apoptotic pathway in WISH cells. Toxicol Appl Pharmacol **273**, 289-297.

Sharp, A.N., Heazell, A.E., Crocker, I.P., Mor, G., 2010. Placental apoptosis in health and disease. Am J Reprod Immunol **64**, 159-169.

Sun, Q.H., Peng, J.P., Xia, H.F., Yang, Y., 2007. IFN-gamma promotes apoptosis of the uterus and placenta in pregnant rat and human cytotrophoblast cells. J Interferon Cytokine Res **27**, 567-578.

Vargas, A., Moreau, J., Landry, S., LeBellego, F., Toufaily, C., Rassart, E., Lafond, J., Barbeau, B., 2009. Syncytin-2 plays an important role in the fusion of human trophoblast cells. J Mol Biol **392**, 301-318.

Wajant, H., Scheurich, P., 2011. TNFR1-induced activation of the classical NF-kappaB pathway. FEBS J **278**, 862-876.

Wang, R., Dang, Y.L., Zheng, R., Li, Y., Li, W., Lu, X., Wang, L.J., Zhu, C., Lin, H.Y., Wang, H., 2014. Live cell imaging of in vitro human trophoblast syncytialization. Biol Reprod **90**, 117.

Wang, Z.Y., Lu, J., Zhang, Y.Z., Zhang, M., Liu, T., Qu, X.L., 2015. Effect of Bisphenol A on invasion ability of human trophoblastic cell line BeWo. Int J Clin Exp Pathol **8**, 14355-14364.

Wice, B., Menton, D., Geuze, H., Schwartz, A.L., 1990. Modulators of cyclic AMP metabolism induce syncytiotrophoblast formation in vitro. Exp Cell Res **186**, 306-316.

Wu, F., Tian, F., Zeng, W., Liu, X., Fan, J., Lin, Y., Zhang, Y., 2017. Role of peroxiredoxin2 downregulation in recurrent miscarriage through regulation of trophoblast proliferation and apoptosis. Cell Death Dis **8**, e2908.

Xu, F., Papanayotou, I., Putt, D.A., Wang, J., Lash, L.H., 2008. Role of mitochondrial dysfunction in cellular responses to S-(1,2-dichlorovinyl)-L-cysteine in primary cultures of human proximal tubular cells. Biochem Pharmacol **76**, 552-567.

Yang, G.Q., Huang, J.C., Yuan, J.J., Zhang, Q., Gong, C.X., Chen, Q., Xie, Q., Xie, L.X., Chen, R., Qiu, Z.M., Zhou, K., Xu, R., Jiang, G.H., Xiong, X.Y., Yang, Q.W., 2020. Prdx1 Reduces Intracerebral Hemorrhage-Induced Brain Injury via Targeting Inflammation- and Apoptosis-Related mRNA Stability. Front Neurosci **14**, 181.

Yang, R.Y., Hsu, D.K., Liu, F.T., 1996. Expression of galectin-3 modulates T-cell growth and apoptosis. Proc Natl Acad Sci U S A **93**, 6737-6742.

Yang, R.Y., Rabinovich, G.A., Liu, F.T., 2008. Galectins: structure, function and therapeutic potential. Expert Rev Mol Med **10**, e17.

Zhang, L., Connor, E.E., Chegini, N., Shiverick, K.T., 1995. Modulation by benzo[a]pyrene of epidermal growth factor receptors, cell proliferation, and secretion of human chorionic gonadotropin in human placental cell lines. Biochem Pharmacol **50**, 1171-1180.

Zhang, L., Shiverick, K.T., 1997. Benzo(a)pyrene, but not 2,3,7,8-tetrachlorodibenzo-p-dioxin, alters cell proliferation and c-myc and growth factor expression in human placental choriocarcinoma JEG-3 cells. Biochem Biophys Res Commun **231**, 117-120.

Zhang, M., Li, Y., Zhang, H., Xue, S., 2001. BAPTA blocks DNA fragmentation and chromatin condensation downstream of caspase-3 and DFF activation in HT-induced apoptosis in HL-60 cells. Apoptosis **6**, 291-297.

Zheng, R., Li, Y., Sun, H., Lu, X., Sun, B.F., Wang, R., Cui, L., Zhu, C., Lin, H.Y., Wang, H., 2016. Deep RNA sequencing analysis of syncytialization-related genes during BeWo cell fusion. Reproduction.

Chapter V. Toxicity of the Trichloroethylene Metabolite *S*-(1,2-dichlorovinyl)-L-cysteine in Human Placental Villous Trophoblast BeWo cells is Differentially Modulated by N-acetyl-L-cysteine and Aminooxyacetic Acid

Abstract

Trichloroethylene (TCE) is a known human carcinogen with toxicity primarily attributed to its metabolism to reactive metabolites. TCE metabolism by the glutathione (GSH) conjugation metabolic pathway is important for its toxicity. *S*-(1,2-Dichlorovinyl)-L-cysteine (DCVC) is a metabolite of TCE formed from the GSH conjugation pathway and is upstream of several toxic TCE metabolites. Despite knowledge that exposure to DCVC is toxic to placental cells via reactive oxygen species generation (ROS), pro-inflammatory response, and apoptosis, the contribution of DCVC metabolism modulation has not been reported previously as a means to modify DCVC toxicity in placental cells. The current study used N-acetyl-L-cysteine (NAC) and aminooxyacetic acid (AOAA) as pharmacological modifiers of DCVC metabolism to investigate DCVC toxicity in the human placental trophoblast BeWo cell model. DCVC-stimulated responses of unsyncytialized BeWo cells, BeWo cells undergoing syncytialization, and syncytialized BeWo cells were compared in order to ascertain BeWo syncytialization impacts on DCVC toxicity. NAC pre/co-treatment with DCVC either failed to inhibit or exacerbated DCVC-stimulated hydrogen peroxide (H_2O_2) abundance, *PRDX2* mRNA expression, and *BCL2* mRNA expression. Because the findings that NAC exacerbated or failed to modify DCVC outcomes might be due to increased expression of *CYP3A4* mRNA, which could favor the formation of the toxic *N*-acetyl-DCVC sulfoxide (NAcDCVCS), we used ketoconazole (KTZ) to inhibit CYP3A4 activity. However, KTZ inhibition of CYP3A4 failed to prevent DCVC or

DCVC/NAC-stimulated toxicity. The KTZ data suggest that interventions additional to CYP3A4

inhibition would be required to prevent DCVC or DCVC/NAC-stimulated toxicity. Moreover,

AOAA was ineffective as an inhibitor of cysteine conjugate β-lyase (CCBL) and did not affect

the percentage of nuclei condensed or fragmented, a measure of apoptosis, in unsyncytialized

BeWo cells, BeWo cells undergoing syncytialization, and syncytialized BeWo cells. Because

CCBL converts DCVC to 1,2-dichlorovinylthiol (DCVT), a toxic metabolite, the lack of ability

of AOAA to impact CCBL would hamper its ability to prevent DCVC-stimulated toxicity. We

found that syncytialized BeWo cells exhibit higher CCBL activity than unsyncytialized BeWo

cells, indicating that syncytialized BeWo cells may be more sensitive to DCVC toxicity.

Together, our data show that neither NAC nor AOAA mitigated DCVC toxicity. In addition, we

noted differences across BeWo differentiation state in CCBL activity and in response to NAC

pre/co-treatment. Future directions could investigate developing alternate methods of enzyme

inhibition to reduce DCVC toxicity, improvement in availability of methodologies to detect

reactive metabolites of TCE, and further definition of sensitive cell populations to DCVC

toxicity to increase understanding of DCVC toxicity modulation.

Introduction

Trichloroethylene (TCE) is a common volatile organic solvent found in over half of

Superfund Hazardous Waste Sites designated by the United States Environmental Protection

Agency (U.S. EPA) (United States Environmental Protection Agency, 2011a). Uses of TCE

include metal degreasing, synthesis of various chemicals, and the manufacture of adhesives

(Agency for Toxic Substances and Disease Registry, 2019). Significantly, TCE is classified as a

Group 1 known human carcinogen by the International Agency for Research on Cancer (IARC)

and concluded to be a human carcinogen by the U.S. EPA (United States Environmental

Protection Agency, 2011b; Guha *et al.*, 2012; International Agency for Research on Cancer, 2014). TCE has been found to act in part via an oxidative stress mechanism in rat kidneys (Siddiqi *et al.*, 2015) and increases oxidative stress markers in rat placenta (Loch-Caruso *et al.*, 2019). In epidemiological studies, TCE exposure has been associated with adverse pregnancy outcomes. These include associations with small for gestational age (SGA) via contaminated drinking water exposure (Ruckart *et al.*, 2014), low birth weight, SGA, and low term birth weight via inhalation (Forand *et al.*, 2012), and very low birth weight via contaminated drinking water exposure (Rodenbeck *et al.*, 2000). The TCE metabolite *S*-(1,2-dichlorovinyl)-L-cysteine (DCVC) is formed through the TCE glutathione (GSH) conjugation metabolic pathway (Lash *et al.*, 2014a). Further metabolism of DCVC produces transient reactive species such as 1,2-dichlorovinylthiol (DCVT), chlorothioketene (CTK), and chlorothionoacetyl chloride (CTAC) (Lash *et al.*, 2014a).

The toxicity of DCVC has been investigated in limited placental cell types. DCVC stimulates reactive oxygen species (ROS) generation and pro-inflammatory response in HTR-8/SVneo cells (Hassan *et al.*, 2016), a first-trimester human extravillous cytotrophoblastic cell line (Graham *et al.*, 1993). DCVC stimulates apoptotic responses that are associated with lipid peroxidation in the HTR-8/SVneo cell line, as well (Elkin *et al.*, 2018). DCVC also stimulates apoptosis and ROS generation in BeWo cells (Chapter 4), a cell line representing human villous cytotrophoblasts (Pattillo and Gey, 1968). In contrast, metabolites from the cytochrome P450-dependent oxidative pathway of TCE metabolism, dichloroacetic acid (DCA) and trichloroacetic acid (TCA), do not produce toxicity in HTR-8/SVneo cells (unpublished data) and exhibit markedly less toxicity in BeWo cells compared to DCVC (Chapter 4). Furthermore, DCVC

223

decreases lipoteichoic acid-stimulated increase of tumor necrosis factor-α (TNF-α) in media and mRNA expression in extraplacental membranes (Boldenow *et al.*, 2015).

Apoptosis is a mechanism critical to placental health regarding villous trophoblastic BeWo cells. BeWo cells can be cultured as cytotrophoblasts and can also be stimulated by forskolin to differentiate *in vitro* to form syncytiotrophoblastic cells (Wice *et al.*, 1990; Al-Nasiry *et al.*, 2006; Inadera *et al.*, 2010; Wang *et al.*, 2014). This differentiation process, known as syncytialization, requires the fusion and mutinucleation of cytotrophoblasts (Potgens *et al.*, 2002; Wang *et al.*, 2014). The process of syncytialization is characterized by some signs of apoptosis (Hu *et al.*, 2007) (Chapter 4). In human studies, apoptosis of syncytiotrophoblasts is associated with intrauterine growth retardation (IUGR) and preeclampsia (Ishihara *et al.*, 2002). Moreover, apoptosis developed more rapidly in a rat model of preeclampsia versus control rats (Mei *et al.*, 2020). Additional studies linking placental cell apoptosis and disease are summarized in a review by Sharp et al. (Sharp *et al.*, 2010). Together, these prior reports suggest that apoptosis of syncytiotrophoblasts has critical implications to placental health.

Molecular mechanisms underlying apoptosis in placental cells include ROS generation and pro-inflammatory response. In syncytiotrophoblasts, release of TNF-α was shown to contribute to apoptosis (Garcia-Lloret *et al.*, 2000; Chan and Guilbert, 2006). Similarly, the role of TNF-α and IFN-γ in promoting programmed cell death in syncytiotrophoblasts was demonstrated in another study (Garcia-Lloret *et al.*, 1996). ROS generation is a contributor to apoptosis in syncytiotrophoblasts, as well. Hydrogen peroxide exposure increased apoptosis in syncytiotrophoblasts (Moll *et al.*, 2007). Similarly, a ROS-dependent mechanism was proposed to explain hypoxia and reoxygenation-induced apoptosis in syncytiotrophoblasts (Belkacemi *et al.*, 2007). Adverse pregnancy outcomes are attributable to a ROS-dependent mechanism, as

well. For example, silencing of the peroxiredoxin 2 (Prdx2) gene, which codes for a ROS scavenger, prevents syncytialization from occurring and another publication shows that peroxiredoxin 1 (Prdx1) and Prdx2 are decreased in abnormal syncytialization occurring during hypoxia versus normal syncytialization (Hu *et al.*, 2007; Wu *et al.*, 2017). Additionally, hydrogen peroxide was increased in placenta or serum of preeclamptic patients compared with normal patients (Aris *et al.*, 2009; Li *et al.*, 2019).

N-acetyl-L-cysteine (NAC) is a chemical most notable for its antioxidant and ROS-scavenging properties, commonly attributable to its property as a precursor of reduced glutathione (GSH) (Aldini *et al.*, 2018). Because of ROS roles in DCVC toxicity and syncytialization, NAC pre/co-treatment may potentially modify DCVC toxicity or syncytialization. Additionally, NAC likely modulates metabolism downstream of DCVC in the GSH conjugation metabolic pathway of TCE. Specifically, NAC is cleaved by aminoacylase I into cysteine and an acetyl group (Uttamsingh and Anders, 1999; Uttamsingh *et al.*, 2000; Aldini *et al.*, 2018). The acetyl group contributes to metabolism of DCVC into N-acetyl-*S*-(1,2-dichlorovinyl)-L-cysteine (NAcDCVC) (Lash *et al.*, 2014a). However, NAC is not expected to impact the conversion of NAcDCVC back into DCVC because the enzyme responsible for cleaving NAC (aminoacylase I) is different from the enzyme responsible for cleaving NAcDCVC into DCVC (aminoacylase III) (Uttamsingh and Anders, 1999; Uttamsingh *et al.*, 2000; Lash *et al.*, 2014a). NAcDCVC is further converted by CYP3As into NAcDCVC sulfoxide (NAcDCVCS), which is toxic (Werner *et al.*, 1996; Lash *et al.*, 2014a). Thus, CYP3As are of particular interest in toxicity because these enzymes directly convert a non-toxic TCE metabolite (NAcDCVC) into the toxic metabolite NAcDCVCS (Werner *et al.*, 1996; Lash *et al.*, 2014a). Upstream, NAC serves as a precursor to GSH (Aldini *et al.*, 2018), which is used by glutathione

S-transferases (GSTs) (Allocati *et al.*, 2018) to initiate TCE metabolism by the GSH conjugation

pathway (Lash *et al.*, 2014a).

Another modulator of DCVC toxicity is aminooxyacetic acid (AOAA). AOAA is an

inhibitor of cysteine conjugate β-lyase (CCBL) in kidney (Elfarra and Anders, 1984; Lash *et al.*,

1986; Lash *et al.*, 1994), the enzyme responsible for converting DCVC into DCVT, a highly

reactive and toxic species (Lash *et al.*, 2014a). There are many isoforms of enzymes capable of

performing the CCBL reaction (Cooper and Pinto, 2006; Lash, 2010), and it is not currently

known which enzymes are most susceptible to AOAA inhibition. It is also currently not known

which CCBL-related enzymes are most relevant in placenta.

In the present study, we hypothesize that NAC and AOAA will modulate DCVC

metabolism and toxicity. We hypothesize that NAC contribution to DCVC acetylation will

outweigh the role of NAC as a ROS scavenger. We also hypothesize that AOAA will reduce

DCVC-stimulated toxicity if AOAA is an effective CCBL inhibitor in BeWo cells. The results

from this current study provide new knowledge on limitations of NAC and AOAA pre/co-

treatment for differential modulation of DCVC-stimulated toxicity.

Materials and Methods

Materials and reagents

N-acetyl-L-cysteine (NAC) and aminooxyacetic acid (as *O*-

(carboxymethyl)hydroxylamine hemihydrochloride) (AOAA), potassium phosphate dibasic

(K_2HPO_4), potassium phosphate monobasic (KH_2PO_4, anhydrous), sucrose, potassium hydroxide

(KOH), boric acid, and trichloroacetic acid were purchased from Sigma-Aldrich (St. Louis, MO).

S-(2-Benzothiazolyl)-L-cysteine (BTC) was purchased from Toronto Research Chemicals

(Toronto, ON). Ketoconazole (KTZ), an inhibitor of CYP3A4 (Gibbs et al., 2000; Lopez-

Barcons et al., 2017; Yang et al., 2017), was purchased from Sigma-Aldrich (St. Louis, MO).

Dimethyl sulfoxide (DMSO) was purchased from Tocris Bioscience (Tocris Bioscience, Bristol, UK). DCVC was synthesized by the University of Michigan Medicinal Chemistry Core using a previously published method (McKinney *et al.*, 1959). The identity of DCVC was verified using proton nuclear magnetic resonance (NMR) spectroscopy and the purity of DCVC stock solution was verified periodically by high-performance liquid chromatograph (HPLC) to be at least 98.7% pure. DCVC was dissolved in phosphate buffered saline (PBS) as a 1 mM stock solution and stored in 1 mL aliquots at -20°C. Camptothecin (CPT) was purchased from Cayman Chemical (Ann Arbor, MI) and was used as a positive control in several experiments. CPT was dissolved in DMSO at 5.74 mM prior to addition to cell media. Menadione (MD) was purchased from Sigma-Aldrich (St. Louis, MO) and included as a positive control for the experiments involving H_2O_2 detection. MD was directly dissolved in a stock solution of cell medium at a 1 mM concentration.

The BeWo cell line

The present study used the human villous trophoblast BeWo cell line, a cell line of male sex and representative of a first-trimester villous trophoblastic cell (Pattillo and Gey, 1968). BeWo cells were obtained from American Type Culture Collection (ATCC CCL-98). Identity of the BeWo cells was periodically verified through its short tandem repeat (STR) profile that was confirmed via fragment analysis on the ABI 3730XL DNA Analyzer from Applied Biosystems (Waltham, MA) at the University of Michigan DNA Sequencing Core. BeWo cells were grown, passaged, and plated with 1X F12-K Nutrient Mixture Kaighn's Modification with (+) L Glutamine (Gibco, Grand Island, NY). Chemical treatments were first diluted in 1X DMEM/F12 Nutrient Mixture (Gibco, Grand Island, NY), referred to as the treatment media, used for its

227

absence of phenol red. All media were supplemented with 10% (v/v) heat-inactivated fetal

bovine serum (HI-FBS) and 1% (v/v) penicillin/streptomycin (P/S) (Gibco, Grand Island, NY).

Three washes of phosphate buffered saline (PBS) (Invitrogen Life Technologies, Carlsbad, CA)

were performed prior to detaching the cells with 0.25% trypsin-EDTA (1X) (Invitrogen Life

Technologies, Carlsbad, CA) for subculture. For regular subculture, cells were plated at 100,000

cells/mL in 25 mL in 175 cm^2 flasks (Corning Inc., Corning, NY) and allowed to grow to 70-

80% confluence. Cell cultures were maintained in a 5% CO_2, 37°C controlled and humidified

incubator. This work with human cell cultures was approved by the University of Michigan

Institutional Biosafety Committee (IBCA00000100).

Exposures

Experimental exposures began after allowing 24 hours for the BeWo cells to adhere and

acclimate to the plate(s) used for experiments. To the unsyncytialized BeWo cells, the TCE

metabolite *S*-(1,2-dichlorovinyl)-L-cysteine (DCVC) was applied at concentrations ranging from

5 µM to 50 µM. These concentrations were chosen based on past reports that similar DCVC

concentrations elicited effects in placental and kidney cells (Xu *et al.*, 2008; Lash *et al.*, 2014b;

Hassan *et al.*, 2016; Elkin *et al.*, 2018). Additionally, this concentration range includes an

average concentration of DCVG (13.4 µM) found in the blood of women exposed by inhalation

to the permissible exposure limit of the U.S. Occupational Health and Safety Administration

(Lash *et al.*, 1999; Agency for Toxic Substances and Disease Registry, 2007). Although DCVC

was not measured in the aforementioned study, DCVG is the precursor to DCVC in a 1:1

stoichiometric ratio (Lash *et al.*, 2014a).

BeWo cells were syncytialized using 100 µM forskolin treatment for 48 hours based on

previous reports (Wice *et al.*, 1990; Al-Nasiry *et al.*, 2006; Inadera *et al.*, 2010) and verified as

228

maximally effective in our prior studies (Chapter 4). To test DCVC impacts on syncytialization, DCVC was applied from 10–50 µM concentrations as a co-treatment with forskolin. Because forskolin was dissolved in DMSO, cells in the vehicle control group were treated with 0.1% (v/v) DMSO, the final DMSO concentration in the DCVC exposure media.

Additional experiments tested the effect of DCVC on BeWo cells after they have been syncytialized using DCVC concentrations ranging from 5-50 µM. Because we observed in pilot experiments that the syncytialized BeWo cells approach reduced viability by 48 hours, 48 hours was the longest time of exposure of DCVC on these cells.

Cell cultures were exposed to NAC, AOAA or KTZ as pre/co-treatments to DCVC, with pre-treatments lasting 30 minutes. The NAC pre/co-treatment was applied at 5 mM concentration, a concentration shown previously to produce an ROS-dependent effect in BeWo cells (Inadera *et al.*, 2010) and other cells (Chen *et al.*, 2008; Sato *et al.*, 2009). The AOAA concentration of 1 mM was used because it reduces CCBL activity and DCVC-stimulated toxicity in kidney cells (Lash *et al.*, 1994). Likewise, KTZ was only applied at 1 µM concentration, a concentration previously reported to be nontoxic in various cell types (Lopez-Barcons *et al.*, 2017) and exceeds previously reported IC$_{50}$s of KTZ to CYP3A4 (Gibbs *et al.*, 2000; Yang *et al.*, 2018).

Hoechst staining to detect nuclear condensation or fragmentation

Cells were plated in Corning Costar tissue culture-treated 6-well plates (Corning, NY) at a density of 200,000 cells/well in 2 mL/well and allowed to adhere for 24 hours before treatment. After treatment, medium was removed, and the cells were washed three times with PBS. Formaldehyde (3.7%, v/v) was applied for 5 minutes to fix the cells, and the cells were washed three times with PBS again. Following this, 0.5 µg/mL Hoechst 33342 trihydrochloride,

trihydrate, prepared from a 10 mg/mL stock solution (Invitrogen Life Technologies, Carlsbad, CA) and diluted 1:20,000 in PBS, was added to each well. Plates were incubated with the Hoechst solution for 15 minutes, then washed three times with PBS before imaging using an EVOS microscope with fluorescence capabilities (Thermo Fisher Scientific, Waltham, MA). Going in a top-down direction, three images (one near the top, one near the middle, and one near the bottom) were captured per well at 400X magnification, to provide an accurate representation of the well, and analyzed.

Quantification consisted of using ImageJ (NIH, Bethesda, MD) set to a brightness threshold that would highlight nuclei that the authors considered sufficiently bright to be considered condensed. The settings were as follows: hue (0, 255), saturation (0, 255), brightness (165, 255). Under these settings, at least 10% of the nucleus had to be highlighted in order for the nucleus to be considered condensed. Criteria used to assess nuclear fragmentation included fragmentation into multiple pieces, jaggedness of the nucleic acid, and unequal size of nuclei subsequent to fragmentation.

Detection of hydrogen peroxide (H_2O_2) abundance

Cells were plated at a density of 10,000 cells/well in 80 µL/well on Corrning Costar tissue culture-treated 96-well white, clear-bottom plates (Corning, NY; product number 3610) and allowed to adhere for 24 hours before treatment. Treatment volumes were 80 µL. Hydrogen peroxide (H_2O_2) was detected using the ROS-Glo™ H_2O_2 assay system (Promega, Madison, WI) according to the manufacturer's instructions. Six hours before the end of treatment, 20 µL of the H_2O_2 substrate solution containing a derivatized luciferin substrate was added to each well to bring the volume of each well to 100 µL. After a 6-hour incubation with the luciferin substrate, 100 µL of the detection solution was added to each well to achieve 200 µL total per well. The

assay works by principle of a luciferin precursor that reacts with H_2O_2. Addition of the detection

solution 6 hours later generates a luciferin product that gives off a light signal that is proportional

to the amount of H_2O_2 present extracellularly and intracellularly in the well. H_2O_2 abundance

was normalized to protein mass, which was determined from a separate set of cells in 96-well

plates. Protein was isolated in Pierce RIPA Lysis and Extraction Buffer (Thermo Fischer

Scientific, Waltham, MA), and then quantified using bicinchoninic acid assay (Thermo Fisher

Scientific, Waltham, MA). The average of nine different protein readings from three independent

experiments for each experimental group was used for normalization.

RNA extraction

Cells were plated in Corning Costar tissue culture-treated 6-well plates at a density of

200,000 cells/well in 2 mL/well and allowed to adhere for 24 hours before treatment. After

treatment, the medium was removed and RNA was extracted from the cells using a RNeasy

PLUS Mini Kit (Qiagen, Hilden, Germany) according to the manufacturer's instructions. Cells

were first homogenized as previously described (Chapter 4). Briefly, 1 mL of the RLT Buffer

Plus reagent (Qiagen, Hilden, Germany) containing 1% (v/v) 2-mercaptoethanol (Sigma-Aldrich,

St. Louis, MO) was added to each well with medium removed. The cell lysates were

homogenized using QIA Shredders (Qiagen, Hilden, Germany) prior to continuation with the

manufacturer protocol, with subsequent gDNA elimination. Concentration and purity of RNA

were determined using a Nanodrop 2000 UV-Vis Spectrophotometer (Thermo Fisher Scientific,

Waltham, MA), and the RNA samples were stored at -80°C until further assayed.

Quantitative real-time polymerase chain reaction (qRT-PCR)

To synthesize cDNA from the RNA samples, an iScript™ cDNA synthesis kit (Bio-Rad

Laboratories, Hercules, CA) was used according to the manufacturer's protocol. A Bio-Rad CFX

Connect™ Real-Time System (Bio-Rad Laboratories, Hercules, CA) was used to carry out the cDNA synthesis reaction. The protocol on the Bio-Rad CFX Connect™ Real-Time System for the cDNA synthesis reaction was as follows: (1) 25°C for 5 minutes, (2) 42°C for 30 minutes, (3) 85°C for 5 minutes, and then (4) a cool down to 4°C. The cDNA was stored at -20°C until further use.

qRT-PCR was performed using 25-µL reaction mixtures consisting of the following: 52.5% (v/v) SsoAdvanced™ Universal SYBR® Green Supermix (Bio-Rad Laboratories, Hercules, CA), 0.28 µM of each primer (forward and reverse), and 32 ng of cDNA template. Primer sequences are described in **Table S5.1** and were custom made by Integrated DNA Technologies (Coralville, IA). A Bio-Rad CFX Connect™ Real-Time System was used to perform qRT-PCR according to the manufacturer's protocol. Analysis was performed using the ΔΔCt method (Yuan et al., 2006), and all samples were analyzed in duplicate. *B2M* served as the reference gene.

Measurement of cell viability and cytotoxicity

BeWo cells were plated in Corning Costar tissue culture-treated 96-well plates (Corning, NY) at a density of 10,000 cells/well in 100 µL/well and allowed to adhere for 24 hours before treatment. Cell viability and cytotoxicity were detected using the Multitox-Glo Multiplex Cytotoxicity Assay (Promega, Madison, WI), performed as instructed by the manufacturers. This assay works by the principle of using a fluorogenic peptide substrate (GF-AFC) that enters intact cells and is cleaved by live cell proteases to release a fluorescent molecule (AFC) and produce a fluorescence signal that is proportional to number of live cells. After treatment, 50 µL of cell viability assay reagent was added and plates were wrapped in aluminum foil and incubated at 37°C. Cell viability was detected via fluorescence reading 45 minutes after reagent application.

After the viability reading, cytotoxicity was assayed via a luminescence assay. The cytotoxicity assay works by the principle of using a luminogenic peptide substrate (AAF-aminoluciferin) that is cleaved by proteases that have leaked out of dead cells (i.e., cells without intact membrane) to release the aminoluciferin product that produces a luminescence signal proportional to number of dead cells. For the asaay, 50 µL cytotoxicity assay reagent was added to each well, then plates were wrapped in aluminum foil and incubated at room temperature for 15 minutes before luminescence was detected using the Glomax Multi Plus Detection System (Promega, Madison, WI). Cytotoxicity readings were normalized to protein mass, which was determined from a separate set of cells in 96-well plates. Protein was isolated in Pierce RIPA Lysis and Extraction Buffer (Thermo Fischer Scientific, Waltham, MA), and then quantified using bicinchoninic acid assay (Thermo Fisher Scientific, Waltham, MA). The average of nine different mass readings from three independent experiments for each experimental group was used for normalization.

Measurement of cysteine conjugate β-lyase (CCBL) activity

BeWo cells were plated in Corning Costar tissue culture-treated 6-well plates at a density of 200,000 cells/well in 2 mL/well and allowed to adhere for 24 hours before treatment. After treatment, cells were incubated in 200 µL of 0.1 M potassium phosphate buffer (pH 7.4) containing 0.25 M sucrose for 5 minutes before cells were scraped off the plate using a cell scraper (Fisher Scientific, Hampton, NH). The cell samples became the enzyme source and were frozen at -80°C until assayed. Potassium phosphate buffer (0.1 M, pH 7.4) consisted of potassium phosphate dibasic (K_2HPO_4) at 69.6 mM and potassium phosphate monobasic (KH_2PO_4, anhydrous) at 30.4 mM prior to addition of sucrose.

To perform the assay, cell samples were thawed, and then sonicated at 3.5 Hz twice for five seconds using a sonicator (MiSonix Sonicator 3000, Misonix Inc., Farmingdale, NY). The

assay followed the method of Dohn and Anders (1982) using BTC as substrate and a protocol previously described (Dohn and Anders, 1982) (Chapter 2). The substrate solution was made by suspending 10.15 mg of BTC in 4 mL ddH$_2$O. The mass of BTC added corresponds to a final BTC concentration in substrate solution of 4 mM. Potassium hydroxide (KOH) (1 M in ddH$_2$O) was added at 0.25 mL to dissolve BTC. After the BTC dissolved, 5 mL of boric acid (0.2 M in ddH$_2$O) was added. The solution pH was adjusted to 8.6 using 1 M KOH, and ddH$_2$O was then added to achieve 10 mL desired total volume. In aliquots, this substrate solution was added to 0.1 M potassium borate buffer (made from KOH and boric acid) in a 1.5:1.3 (v/v) ratio and incubated for 4 minutes at 37°C. Enzyme sample was added to this reaction mixture in a 1:14 (v/v) ratio. Incubation time with the enzyme sample was 30 minutes at 37°C.

After incubation, trichloroacetic acid at a 10% (w/v) concentration in ddH$_2$O was added to the reaction mixture in a 1:5 (v/v) ratio to terminate the reaction and precipitate protein. A negative control for each sample was made by adding 10% (w/v) trichloroacetic acid into the reaction mix before addition of the enzyme source (i.e., the cells). All samples were centrifuged at 11,000 x g for 1.25 minutes to remove precipitated protein. Absorbance of supernatant was measured at 321 nm wavelength with a molar extinction coefficient (ε) of 21,600 M^{-1} cm^{-1} for 321 nm using a SpectraMax M2e microplate reader (Molecular Devices, San Jose, CA). The absorbance corresponding to the negative control was subtracted from the absorbance corresponding to the appropriate reaction to generate a net absorbance used to convert absorbance into nmol of product produced/min/mL, which were converted into nmol/min/mg protein. Protein was assayed with bicinchoninic acid (BCA) using a kit from Thermo Fisher Scientific.

Statistical analysis

Statistical analyses included unpaired two-tailed t-tests, one-way ANOVA, and two-way ANOVA performed using GraphPad Prism 7 (GraphPad Software, San Diego, CA). Mixed models ANOVA was performed with treatment as fixed variable and experimental day as random variable using SPSS Software (IBM Corporation, Chicago, IL). In the case of percentage data, percentages were transformed to fractions and arcsine transformed prior to statistical analysis. All ANOVAs were followed with Tukey's post-hoc comparison of means. All graphs were generated using GraphPad Prism 7 (GraphPad Software, San Diego, CA). For all tests, a $p < 0.05$ was considered as statistically significant.

Results

Effects of DCVC with and without NAC pre/co-treatment on nuclear condensation or fragmentation

Representative images of DCVC-induced nuclear condensation or fragmentation in unsyncytialized BeWo cells are shown in **Figure 5.1A**. In unsyncytialized BeWo cells at the 48-hour time point, 20 µM DCVC increased the percentage of condensed or fragmented nuclei by 438.3% relative to nontreated control (absence of NAC or DCVC) (p= 0.0355), and NAC pre/co-treatment did not significantly modify this DCVC-induced response (**Figure 5.1B**). For BeWo cells undergoing forskolin-stimulated syncytialization, NAC treatment with forskolin only and NAC treatment with forskolin + DCVC elevated nuclear condensation or fragmentation by 624.5% and 601.3%, respectively, relative to vehicle control (0.1% DMSO only) (p=0.0026 and 0.0038, respectively) (**Figure 5.1C**). In syncytialized BeWo cells, NAC with 10 µM DCVC or 20 µM DCVC increased nuclear condensation or fragmentation by 75.9% and 97.8%, respectively, relative to nontreated control (absence of NAC or DCVC) (p=0.0293 and 0.0036,

respectively), but not in comparison to NAC treatment alone (**Figure 5.1D**). Thus, with exception of a few treatments done in combination, NAC did not modify DCVC-stimulated nuclear condensation or fragmentation.

Effects of DCVC with and without NAC pre/co-treatment on biomarkers of oxidative stress

Because NAC is a ROS scavenger either by itself or through its property as a GSH precursor (Aldini *et al.*, 2018), we measured abundance of hydrogen peroxide (H_2O_2). In unsyncytialized BeWo cells at 48 hours of exposure, 50 µM DCVC increased H_2O_2 abundance relative to control (absence of DCVC or NAC) by 83.9% (p<0.0001), and NAC plus 50 µM DCVC elicited even greater H_2O_2 abundance, increased by 80.5% compared to treatment with 50 µM DCVC without NAC (p<0.0001) (**Figure 5.2A1**). NAC alone did not significantly change H_2O_2 abundance.

A similar pattern was observed in BeWo cells undergoing syncytialization. In cells treated with forskolin to induce syncytialization, 50 µM DCVC increased H_2O_2 abundance by 61.4% relative to controls exposed to forskolin alone (p=0.037) (**Figure 5.2B1**). Cells exposed to NAC plus 50 µM DCVC (as well as forskolin) exhibited further increased H_2O_2 abundance relative to cells undergoing syncytialization in the presence of 50 µM DCVC alone (increased by 92.7%, p<0.0001) (**Figure 5.2B1**). NAC by itself or as pre/co-treatment to forskolin did not alter H_2O_2 abundance relative to respective controls (cells receiving only 0.1% DMSO or only forskolin, respectively) (**Figure 5.2B1**).

In cells already syncytialized, 48-hour exposures to NAC by itself decreased H_2O_2 abundance relative to control (absence of DCVC or NAC) by 31.4% (p=0.014). Treatment at 50 µM DCVC increased H_2O_2 abundance relative to control (absence of DCVC or NAC) by 55.6% (p<0.0001), similar to unsyncytialized cells and cells undergoing syncytialization. However, the

combination treatment of NAC with 50 µM DCVC did not alter H_2O_2 abundance relative to 50 µM DCVC treatment alone (**Figure 5.2C1**), in contrast to unsyncytialized cells and cells undergoing syncytialization. There were no significant changes with NAC treatment on *PRDX2* mRNA expression in unsyncytialized BeWo cells, BeWo cells undergoing syncytialization, or syncytialized BeWo cells (**Figures 5.2A2, 5.2B2, and 5.2C2**, respectively).

Effects of DCVC with and without NAC pre/co-treatment on apoptotic pathway genes

NAC alone had no significant effect on DCVC-stimulated decrease of *BCL2* mRNA expression in unsyncytialized BeWo cells (48-hour exposure), in BeWo cells undergoing syncytialization (48-hour exposure), and in syncytialized BeWo cells (24-hour exposure) (**Figures 5.3A1, 5.3B1, 5.3C1**, respectively). In contrast to findings with nuclear condensation/fragmentation and H_2O_2 abundance, the combination treatment of NAC and DCVC did not significantly alter the *BCL2* response compared with exposure to DCVC without NAC in all three differentiate states of BeWo cells (**Figures 5.3A1, 5.3B1, and 5.3C1**). *LGALS3* is another gene linked to cellular anti-apoptotic response (Yang *et al.*, 1996; Newlaczyl and Yu, 2011). Whereas the 50 µM DCVC effect was significant for *LGALS3* mRNA expression in two-way ANOVA in unsyncytialized BeWo cells (p=0.0188, in the direction of decrease), the effect of NAC was not significant (**Figure 5.3A2**). Neither NAC nor DCVC had an effect on *LGALS3* mRNA expression in BeWo cells undergoing syncytialization (48-hour exposures) or in syncytialized BeWo cells (24-hour exposures) (**Figures 5.3B2 and 5.3C2**, respectively). No significant effects were observed for *NFKB1* mRNA expression for the same experimental treatments on BeWo cells undergoing syncytialization or syncytialized BeWo cells (**Figure S5.1**).

237

Effects of DCVC with and without NAC pre/co-treatment on CYP3A4 mRNA expression

Because NAC failed to prevent or reverse a DCVC-stimulated response, even in the case of ROS-relevant outcomes such as hydrogen peroxide (H_2O_2), we measured *CYP3A4* mRNA expression because of its potential role in the formation of a toxic metabolite NAcDCVCS due to potential increased acetylation of DCVC in the presence of NAC. In unsyncytialized BeWo cells exposed for 48 hours and syncytialized BeWo cells exposed for 24 hours, the NAC effect from two-way ANOVA for *CYP3A4* mRNA was significant in the direction of increased *CYP3A4* mRNA expression (p=0.0275 and p=0.0344, respectively) (**Figures 5.4A and 5.4C**, respectively). In BeWo cells undergoing syncytialization, syncytialization by itself increased *CYP3A4* mRNA expression by 1150% (p=0.0265), but no changes in *CYP3A4* mRNA expression were elicited by treatment with DCVC or NAC (**Figure 5.4B**).

Effects of NAC and KTZ on DCVC-stimulated cell viability and cytotoxicity

We used ketoconazole (KTZ) as a CYP3A4 inhibitor to further investigate the potential role of CYP3A4 in DCVC and NAC toxicity. We performed these experiments with unsyncytialized cells and syncytialized cells, but not with cells undergoing syncytialization, because *CYP3A4* mRNA expression increased with syncytialization in the absence of other treatments (**Figure 5.4B**). In unsyncytialized BeWo cells receiving 48-hour treatments, neither KTZ, NAC, nor the combination of KTZ and NAC as pre/co-treatments to 50 µM DCVC prevented the 50 µM DCVC-stimulated decrease in cell viability and increase in cytotoxicity (**Figures 5.5A1 and 5.5A2**, respectively). Similarly, in syncytialized BeWo cells receiving 48-hour treatments, neither the KTZ, NAC, nor the combination of KTZ and NAC as pre/co-treatments to 50 µM DCVC prevented the 50 µM DCVC-stimulated decrease in cell viability (**Figure 5.5B1**). Cytotoxicity in syncytialized BeWo cells was reduced by KTZ and NAC alone

or in combination relative to control (absence of KTZ, NAC, or DCVC) by 52.9%, 33.9%, and 49.0%, respectively (p<0.0001) (**Figure 5.5B2**). Combined exposure to 50 µM DCVC with KTZ and NAC treatment, alone or in combination, also reduced cytotoxicity relative to treatment with 50 µM DCVC without KTZ or NAC by 47.8%, 49.7%, and 51.6%, respectively (p<0.0001) (**Figure 5.5B2**).

Effects of DCVC with and without AOAA pre/co-treatment on nuclear condensation or fragmentation

Exposure to 20 µM DCVC by itself did not statistically increase nuclear condensation or fragmentation in unsyncytialized BeWo cells, BeWo cells undergoing syncytialization, or syncytialized BeWo cells, although the direction for each was towards an increase (**Figures 5.6A, 5.6B, and 5.6C**, respectively). Moreover, AOAA did not significantly alter DCVC-induced nuclear condensation or fragmentation, regardless of BeWo cell differentiation state (**Figures 5.6A, 5.6B, and 5.6C**). Relative to vehicle control (0.1% DMSO), AOAA pre/co-treatment with forskolin increased nuclear condensation or fragmentation by 402.4% (p=0.0041) (**Figure 5.6B**). Treatment with 20 µM DCVC and forskolin in the absence of AOAA increased nuclear condensation or fragmentation by 280.4% relative to vehicle control (0.1% DMSO) (p=0.0355) (**Figure 5.6B**).

Effects of DCVC with and without AOAA pre/co-treatment on CCBL activity

BeWo cells exhibited CCBL activity regardless of differentiation state at 48-hour exposure time points. However, the CCBL activity in all three cases was unaltered by AOAA, DCVC, or AOAA pre/co-treatment with DCVC (**Figures 5.7A, 5.7B, and 5.7C**). Additionally, when comparing the control group (absence of DCVC or AOAA) for unsyncytialized BeWo cells to the control group (absence of DCVC or AOAA) for syncytialized BeWo cells,

syncytialized BeWo cells were found to have more CCBL activity than unsyncytialized BeWo cells by 54.8% (p=0.0319) (**Figure 5.7D**).

Effects of DCVC on KYAT1 mRNA expression

We investigated how CCBL activity results compare to mRNA expression of *KYAT1*, which codes for a specific CCBL, CCBL1. Similar to the finding that syncytialized BeWo cells have greater CCBL activity compared to unsyncytialized BeWo cells (**Figure 5.7D**), *KYAT1* mRNA expression was increased by forskolin-stimulated syncytialization by 123.8% (p=0.0034). Relative to forskolin treatment alone, DCVC co-treatments at 20 µM and 50 µM reduced *KYAT1* mRNA expression by 38.5% and 64.1%, respectively (p=0.0338 and 0.0011, respectively) (**Figure 5.8B**). *KYAT1* mRNA expression was not changed by DCVC exposure in unsyncytialized BeWo cells for 48 hours or syncytialized BeWo cells for 24 hours (**Figures 5.8A and 5.8C**, respectively).

Effects of DCVC on FMO3 and CYP2E1 mRNA expression

We investigated the relevance of the BeWo cells in genes for other pathways of DCVC metabolism and TCE metabolism. In unsyncytialized BeWo cells with treatment lasting for 48 hours, *FMO3* mRNA expression was decreased by 53.6% (p=0.0121) with 50 µM DCVC exposure relative to control (0 µM DCVC) (**Figure 5.9A1**). DCVC exposure during syncytialization for 48 hours or on syncytialized BeWo cells for 24 hours had no significant effect on *FMO3* mRNA expression (**Figures 5.9A2 and 5.9A3**, respectively). DCVC exposure on unsyncytialized BeWo cells for 48 hours or during syncytialization for 48 hours did not change *CYP2E1* mRNA expression (**Figures 5.9B1 and 5.9B2**, respectively). However, 50 µM DCVC exposure for 24 hours decreased *CYP2E1* mRNA expression by 56.6% relative to control (0 µM DCVC) in syncytialized BeWo cells (p=0.0124) (**Figure 5.9B3**).

Discussion

The current study is the first to our knowledge to use NAC and AOAA to modulate metabolism of the TCE metabolite, DCVC, and affect toxicity in BeWo cells. The TCE metabolite, DCVC, stimulated toxic responses in unsyncytialized BeWo cells, BeWo cells undergoing syncytialization, and syncytialized BeWo cells (Chapter 4). DCVC toxicity is attributable to its metabolism, which is supported by work utilizing the CCBL inhibitor, AOAA, to decrease DCVC-stimulated toxicity in kidney cells (Elfarra and Anders, 1984; Lash *et al.*, 1986; Lash *et al.*, 1994) and suppress DCVC-stimulated increase of interleukin-6 (IL-6) in HTR-8/SVneo cells (Hassan *et al.*, 2016). Mechanisms by which DCVC is toxic to BeWo cells and another placental cell line, the HTR-8/SVneo cells, involve ROS generation, pro-inflammatory response, and apoptosis (Hassan *et al.*, 2016; Elkin *et al.*, 2018) (Chapter 4). With respect to BeWo cells, DCVC increased nuclear condensation or fragmentation, a metric that quantifies apoptosis (Matassov *et al.*, 2004; Errami *et al.*, 2013; Crowley *et al.*, 2016). A pathway of DCVC metabolism is acetylation (Lash *et al.*, 2014a), and NAC is a provider of an acetyl group (Aldini *et al.*, 2018). As such, we investigated the ability of NAC and AOAA to modify numerous DCVC-stimulated responses.

Nuclear condensation or fragmentation results from this study indicate that neither NAC nor AOAA were effective at preventing a DCVC-stimulated response. This was true for any differentiation state of the BeWo cells. Although DCVC concentrations in the present study did not always increase nuclear condensation or fragmentation, the data nonetheless suggest that neither NAC nor AOAA would likely prevent a DCVC effect even if DCVC concentrations or sample sizes were increased. If anything, the trend suggested that NAC pre/co-treatment would exacerbate the DCVC response in syncytialized BeWo cells. Regardless, our prior finding

241

(Chapter 4) that DCVC did not alter DNA quantity under exposure conditions similar to those that produced changes in nuclear condensation or fragmentation increases the likelihood that nuclear condensation or fragmentation reflected apoptosis and not cell proliferation.

The nuclear condensation or fragmentation data also indicate that NAC or AOAA exposure could be detrimental during syncytialization. Exposure to NAC or AOAA with forskolin-stimulated syncytialization increased nuclear condensation or fragmentation relative to control. Because our primary interest was DCVC toxicity, we did not further investigate the mechanisms involved in responses to NAC or AOAA during forskolin-stimulated syncytialization. However, numerous mechanisms exist that could possibly explain an effect resulting from the combination of NAC and forskolin or the combination of AOAA and forskolin. Forskolin is a known adenylate cyclase activator (Daly, 1984) that increases intracellular cyclic adenosine monophosphate (cAMP) (Cooper, 2003) that is necessary for syncytialization (Gupta *et al.*, 2016). In rat retinal pigmented epithelial (RPE-J) cells cultured in the presence of L-cysteine, AOAA decreases cAMP relative to the absence of AOAA (Njie-Mbye *et al.*, 2012). Similarly, NAC at 0.5 mM decreases Aβ(25–35)-stimulated adenylate cyclase activity in the ventral hippocampus and frontal cortex in rats (Soomets *et al.*, 1999). Therefore, NAC or AOAA could have interfered with the forskolin-stimulated cAMP response necessary for normal syncytialization and thereby produced a toxic effect. Syncytialization is also likely associated with altered antioxidant activity because cAMP decrease has been associated with lower antioxidant activity (Saha *et al.*, 2008; Boyadjieva and Sarkar, 2013). However, NAC and AOAA differ in regard to antioxidant properties. NAC is commonly thought of as an antioxidant (Aldini *et al.*, 2018; Ezerina *et al.*, 2018). In contrast, AOAA has been reported to further increase palmitate-stimulated ROS augmentation in HepG2 cells (Sarna *et al.*,

2016) and exacerbate oxaliplatin-stimulated ROS production and apoptosis in HCT116 and HT29 cells (Yue *et al.*, 2020). Therefore, these differences are not as likely to explain a common mechanism of action for interaction with forskolin. Further investigation of these mechanisms requires additional experiments beyond the scope of the present thesis to explain why exposure of NAC or AOAA during syncytialization could be deleterious.

Our data on measures of ROS indicated that NAC exacerbated a DCVC-stimulated response. This is particularly notable for the hydrogen peroxide (H_2O_2) abundance data in unsyncytialized BeWo cells and BeWo cells undergoing syncytialization, in which DCVC-stimulated increase in H_2O_2 was augmented by NAC pre/co-treatment. Although NAC is a scavenger of ROS (Aldini *et al.*, 2018), the possibility exists that NAC and DCVC metabolism could interact to increase production of deleterious DCVC metabolites. NAC is metabolized to an acetyl group (Aldini *et al.*, 2018), which could be used to biotransform DCVC into NAcDCVC via N-acetyl-transferases (Lash *et al.*, 2014a). NAcDCVC itself is not toxic, but is metabolized to its sulfoxide, NAcDCVCS, which is toxic (Werner *et al.*, 1996; Lash *et al.*, 2014a). Our findings of increased toxicity stimulated by NAC pre/co-treatment with DCVC are consistent with the notion that NAC administration shifted DCVC metabolism towards increased production of toxic metabolites. The findings of no alterations provided by NAC pre/co-treatment relative to DCVC treatment alone likewise are consistent with the notion that NAC-stimulated changes to DCVC metabolism could counter anti-oxidant protective effects of NAC (Aldini *et al.*, 2018) as pre/co-treatment with DCVC. The effect of NAC on *CYP3A4* mRNA expression would favor formation of NAcDCVCS. Worthy future directions include studies that directly measure formation of NAcDCVCS or measurement of CYP3A4 activity to bolster the

conclusion that increased formation of NAcDCVCS is a mechanism of NAC exacerbation of DCVC-stimulated toxicity.

Notably, nearly all NAC-stimulated effects differed by the differentiation stage of the BeWo cells and by endpoint. For syncytialized but not unsyncytialized BeWo cells, NAC by itself exerted effects even in the absence of DCVC, as evidenced by changes in H_2O_2 abundance, cytotoxicity, and *BCL2* mRNA expression. This highlights that syncytialized BeWo cells are more susceptible than unsyncytialized BeWo cells to NAC. Additionally, the results from this study indicate that H_2O_2 abundance is an endpoint modifiable by DCVC and NAC pre/co-treatment more than *PRDX2* mRNA expression. Similarly, we saw that DCVC treatment or NAC pre/co-treatment had a greater effect on *BCL2* mRNA expression than on *LGALS3* mRNA expression. These findings show that DCVC and NAC acted on specific components within the oxidative stress response and apoptosis pathways, and that exact mechanisms depended on the differentiation state of the BeWo cells. As such, it is difficult to claim NAC as strictly an antioxidant or prooxidant in the BeWo cells, particularly the syncytialized cells.

We investigated the potential role of CYP3A4 on DCVC-stimulated toxicity using pharmacological inhibitors. These experiments were only performed on unsyncytialized and syncytialized BeWo cells because we found that *CYP3A4* mRNA was increased by syncytialization. We used KTZ as a CYP3A4 inhibitor at 1.0 µM concentration, which is consistent with other reports (Gibbs *et al.*, 2000; Lopez-Barcons *et al.*, 2017; Yang *et al.*, 2018) and higher than previously reported IC_{50} values to CYP3A4 of 0.3 or 0.4 µM in Caco-2 cells (Gibbs *et al.*, 2000) and 0.618 µM in human liver microsomes (Yang *et al.*, 2018). Neither KTZ, NAC, nor the combination of KTZ and NAC were toxic to the BeWo cells. We found that KTZ did not prevent DCVC or DCVC + NAC-stimulated toxicity in unsyncytialized BeWo cells. For

syncytialized BeWo cells, KTZ, NAC, and KTZ + NAC treatments with DCVC decreased cytotoxicity relative to DCVC-only treatment. However, this latter finding could be explained by the finding that KTZ, NAC, KTZ + NAC treatments in the absence of DCVC also lowered cytotoxicity relative to control (absence of DCVC, KTZ, or NAC). The inability of NAC to prevent DCVC-stimulated toxicity in syncytialized BeWo cells hampers a conclusion that KTZ, NAC, or KTZ + NAC pre/co-treatment prevents DCVC-stimulated cytotoxicity. It remains unclear how KTZ, NAC, or KTZ + NAC treatments could reduce cytotoxicity relative to control in syncytialized BeWo cells. Although we saw no indication that CYP3A4 inhibition prevented DCVC- or DCVC/NAC-stimulated toxicity, the possibility that NAC pre/co-treatment exacerbation of DCVC toxicity could depend on CYP3A4 is still valid in light of our *CYP3A4* mRNA data displaying a significant NAC effect of increased *CYP3A4*.

Although CYP3A4 may have a role in DCVC toxicity, inhibition with KTZ was insufficient to prevent toxicity. It is plausible that CYP3A4 inhibition alone failed to prevent DCVC toxicity because the cells had no mechanism to prevent the regeneration of DCVC from NAcDCVC. Indeed, whereas CYP3A4 inhibition by KTZ can result in less NAcDCVCS formation from NAcDCVC, the cells could still use aminoacylase III to convert NAcDCVC back into DCVC (Uttamsingh and Anders, 1999; Uttamsingh *et al.*, 2000; Lash *et al.*, 2014a), which could form reactive metabolites such as DCVT, CTK, and CTAC (Lash *et al.*, 2014a). Therefore, an alternative approach to reduce DCVC-stimulated toxicity would be to inhibit both CYP3A4 and aminoacylase III, which would theoretically "trap" the innocuous NAcDCVC metabolite. Ebselen seems to be a particularly good candidate for aminoacylase III inhibition (Tsirulnikov *et al.*, 2012; Hanavan *et al.*, 2015; Tan *et al.*, 2015). The proposed mechanism of inhibiting CYP3A4 and aminoaceylase III to reduce DCVC-stimulated toxicity is illustrated in **Figure**

245

5.10. Although reports suggest that CYP3A4 is a relevant CYP in BeWo cells (Pavek *et al.*, 2007; Suksawat *et al.*, 2019), the possibility exists that inhibition of other CYP3As may be more effective interventions for DCVC-stimulated toxicity. Finally, another possibility is that KTZ may not be an effective CYP3A4 inhibitor in BeWo cells. Validation of the role of metabolic inhibition of CYP3A on DCVC toxicity requires additional investigation that is beyond the scope of the current study.

AOAA was ineffective as a CCBL inhibitor in BeWo cells regardless of differentiation status. This is consistent with our finding that AOAA is ineffective as a CCBL inhibitor in rat placenta (Chapter 2), but differs from prior reports that AOAA inhibits CCBL in kidney (Elfarra and Anders, 1984; Lash *et al.*, 1986; Lash *et al.*, 1994). Nonetheless, the differences in response to AOAA are supported by previous findings that CCBL composition differs by organ (Cooper and Pinto, 2006; Lash, 2010). It is possible that BeWo cells and placenta contain CCBLs that are different than those of kidney, which confers the BeWo and placental cell resistance to AOAA as a CCBL inhibitor. Identifying the exact CCBLs in placenta remains important future work.

Although DCVC did not change CCBL activity (regardless of differentiation status), CCBL activity was higher in syncytialized BeWo cells compared with unsyncytialized BeWo cells. Our finding that the process of syncytialization increased mRNA expression of *KYAT1*, which codes for CCBL1, supports the notion that syncytialized cells have more CCBL activity than unsyncytialized cells. Because CCBL activity generates the toxic DCVT metabolite from DCVC, these findings help explain our prior finding that syncytialized BeWo cells were more susceptible than unsyncytialized BeWo cells to DCVC toxicity (Chapter 4). It remains unknown, however, how changes in CCBL activity correspond with multinucleation and cell fusion processes in other systems, such as slime molds and striated muscle cells (Potgens *et al.*, 2002).

Future experiments looking at such phenomena may inform basic biology questions of cell fusion and multinucleation, and define sensitive cell populations.

To our knowledge, we provide the first evidence that DCVC exposure altered mRNA expression of enzymes relevant to TCE metabolism in BeWo cells. A notable finding was that DCVC decreased *FMO3* mRNA expression in unsyncytialized BeWo cells while not affecting *KYAT1* mRNA expression. If these findings translate to the level of protein activity, this raises the possibility that unsyncytialized BeWo cells exposed to DCVC have less induction of FMO3 activity relative to CCBL activity. This could mean that the DCVC to 1,2-dichlorovinylthiol (DCVT) conversion via CCBL would be more relevant to these cells than the DCVC to DCVC sulfoxide (DCVCS) conversion via FMO3 (Lash *et al.*, 2014a). In syncytialized BeWo cells, DCVC exposure decreased *CYP2E1* but not *KYAT1* mRNA expression. Because CYP2E1 is a major CYP that metabolizes TCE in its initial step in the CYP-dependent oxidative pathway (Lash *et al.*, 2014a), this finding raises the possibility that DCVC exposure in syncytialized BeWo cells decreased the relevance of the CYP-dependent oxidative pathway in these cells. Additionally, based on observation of Cq values, it seems that BeWo cells have higher levels of *KYAT1* mRNA compared to *FMO3* or *CYP2E1* mRNA regardless of differentiation state (data not shown). Interestingly, we observed *KYAT1* but not *FMO3* or *CYP2E1* mRNA expression changed by syncytialization. Future experiments can measure activities of multiple enzymes involved in TCE metabolism across different cell types or tissues. Together, these experiments can inform which metabolites could be in highest abundance following TCE or DCVC exposure.

In summary, NAC and AOAA differentially modulated DCVC-stimulated toxicity. **Figure 5.11** summarizes the knowledge of NAC and AOAA on DCVC metabolism modulation highlighting contributions of the current study. We have shown for the first time that NAC

increased DCVC toxicity relative to DCVC treatment alone. The mechanism of NAC exacerbation of DCVC cytotoxicity could be attributable to increased metabolism towards the toxic NAcDCVCS metabolite. Consistent with *in vivo* data showing the ineffectiveness of AOAA for CCBL activity inhibition in rat placenta (Chapter 2), AOAA was an ineffective CCBL inhibitor in BeWo cells regardless of differentiation status. This could mean that AOAA was unable to block the CCBL-catalyzed conversion of DCVC into the toxic DCVT. A key finding from the CCBL experiments was the discovery that syncytialized BeWo cells had higher CCBL activity compared to unsyncytialized BeWo cells. This discovery offers an explanation for our prior finding that syncytialized BeWo cells were more susceptible to DCVC toxicity (Chapter 4). Future directions could measure concentrations of TCE metabolites, such as DCVT and NAcDCVCS, to verify that changes in enzyme activity or mRNA expression correlate with changes in metabolite abundance. Additional noteworthy considerations include the need to define mechanisms explaining the different sensitives among placental and other cell populations to DCVC exposure, investigate mechanisms of co-exposure toxicity or reduction in toxicity, and use of tissue-specific enzyme activity to inform alternate methods of enzyme inhibition.

(A) Hoechst staining in unsyncytialized BeWo cells			
0 µM DCVC, 0 mM NAC	0 µM DCVC, 5 mM NAC	20 µM DCVC, 0 mM NAC	20 µM DCVC, 5 mM NAC

(B) Quantification in unsyncytialized BeWo cells (48-hour exposure)

(C) Quantification in BeWo cells undergoing syncytialization (48-hour exposure)

(D) Quantification in syncytialized BeWo cells (48-hour exposure)
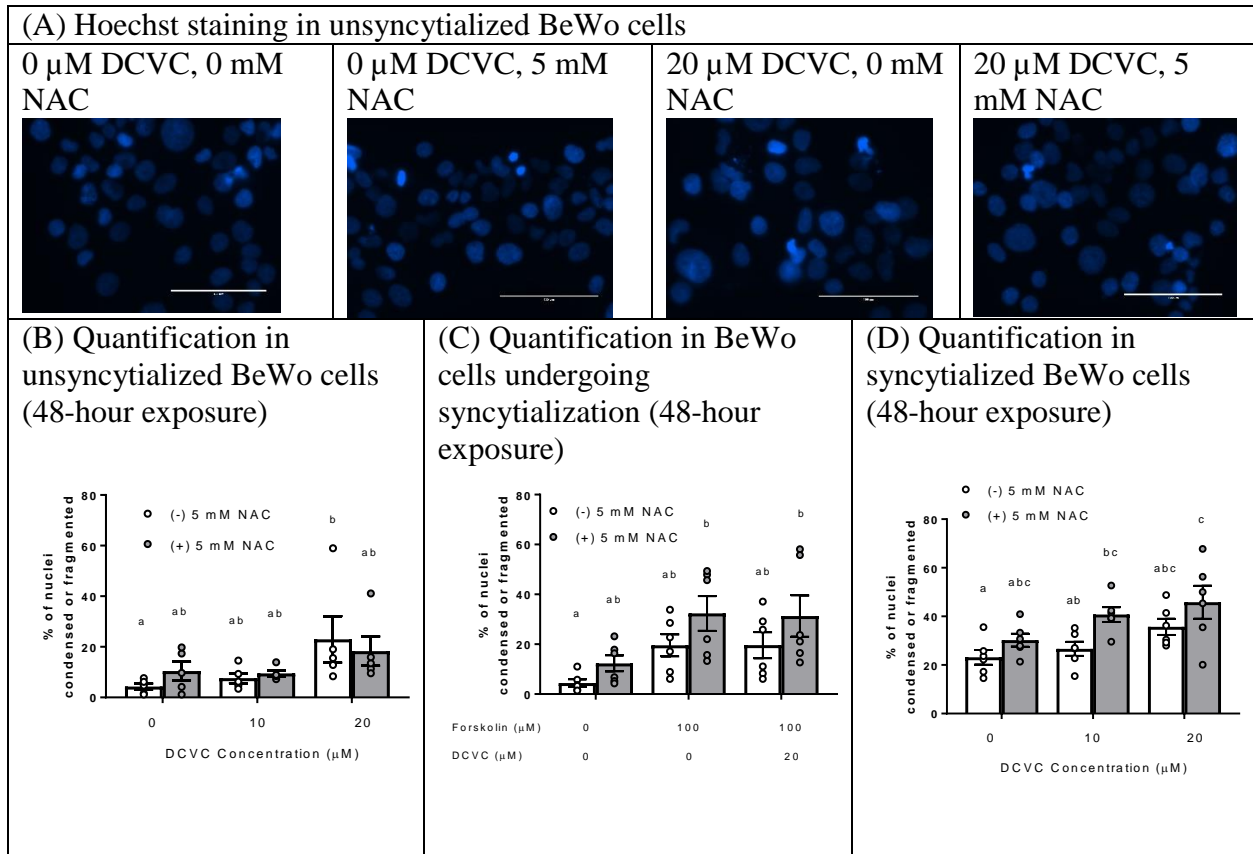
Figure 5.1. Effects of DCVC with and without NAC pre/co-treatment on nuclear condensation or fragmentation. (A) Representative images of Hoechst staining to detect nuclear condensation or fragmentation. (B) Unsyncytialized BeWo cells received treatment(s) for 48 hours. (C) BeWo cells received treatment(s) for 48 hours while undergoing forskolin-stimulated syncytialization. (D) Syncytialized BeWo cells received treatment(s) for 48 hours. Statistical analysis was performed using two-way ANOVA followed by Tukey's post-hoc comparison of means. Statistical significance is indicated by non-overlapping letters. Error bars represent mean ± SEM. N=6 independent experiments.

(A) Unsyncytialized BeWo cells (48-hour exposure)
(A1)   (A2)

(B) BeWo cells undergoing syncytialization (48-hour exposure)
(B1)   (B2)
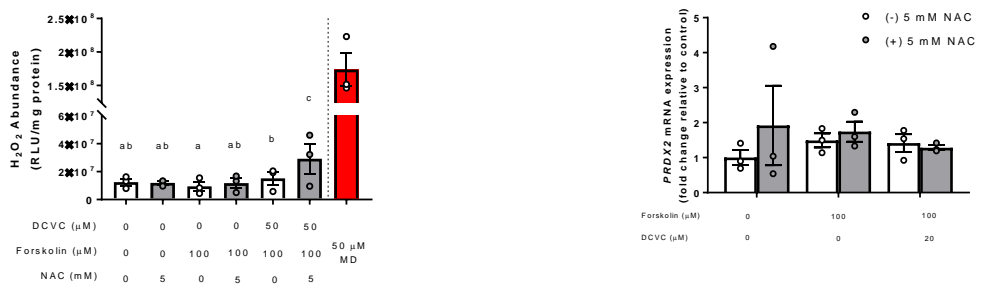
(C) Syncytialized BeWo cells
(C1) (48-hour exposure)   (C2) (24-hour exposure)
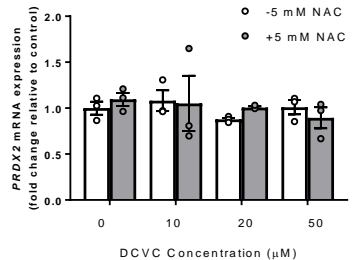
Figure 5.2. Effects of DCVC with and without NAC pre/co-treatment on H_2O_2 abundance and *PRDX2* mRNA expression as biomarkers of oxidative stress. (A) Unsyncytialized BeWo cells received treatment(s) for 48 hours. (B) BeWo cells received treatment(s) while undergoing forskolin-stimulated syncytialization for 48 hours. (C) Syncytialized BeWo cells received treatment(s) for (C1) 48 hours and (C2) 24 hours. For the *PRDX2* mRNA expression data, data were analyzed by two-way ANOVA followed by Tukey's post-hoc comparison of means, with N=3 independent experiments. For the H_2O_2 abundance data, statistical analysis was performed using mixed models ANOVA followed by Tukey's post-hoc comparison of means, with N=3 independent experiments performed in triplicate. Non-overlapping letters signify statistically significant differences. Error bars represent mean ± SEM. Menadione (MD) was included as a positive control for the H_2O_2 experiments.
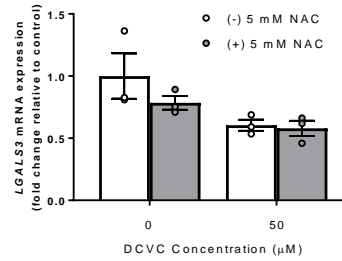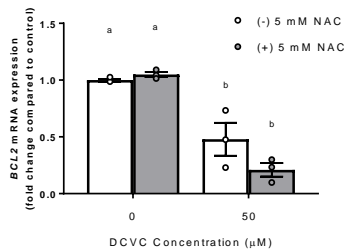
250

(A) Unsyncytialized BeWo cells (48-hour exposure)
(A1)   (A2)

(B) BeWo cells undergoing syncytialization (48-hour exposure)
(B1)   (B2)
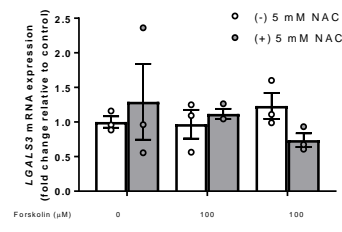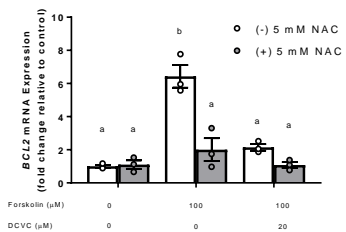
(C) Syncytialized BeWo cells (24-hour exposure)
(C1)   (C2)
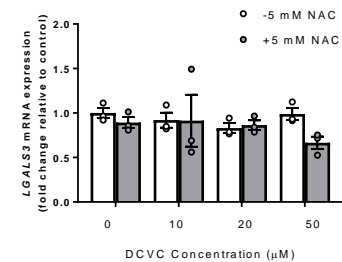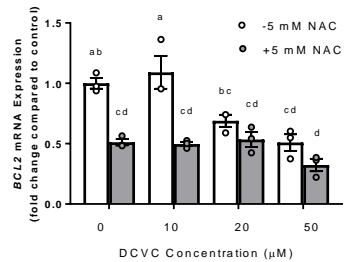
Figure 5.3. Effects of DCVC with and without NAC pre/co-treatment on apoptotic pathway genes *BCL2* and *LGALS3*. (A) Unsyncytialized BeWo cells received treatment(s) for 48 hours. (B) BeWo cells received treatment(s) while undergoing forskolin-stimulated syncytialization for 48 hours. (C) Syncytialized BeWo cells received treatment(s) for 24 hours. For the *LGALS3* data in unsyncytialized BeWo cells, *LGALS3* is unchanged by NAC for BeWo cells, however, p=0.0188 for the DCVC effect. Data were analyzed by two-way ANOVA followed by Tukey's post-hoc comparison of means. Non-overlapping letters signify statistically significant differences. Error bars represent mean ± SEM. N=3 independent experiments.

(A) Unsyncytialized BeWo cells (48-hour exposure)
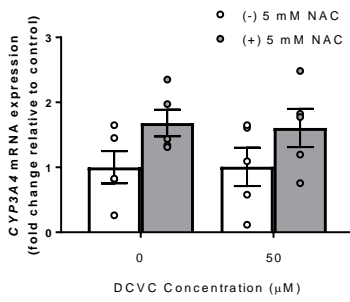
(B) BeWo cells undergoing syncytialization (48-hour exposure)
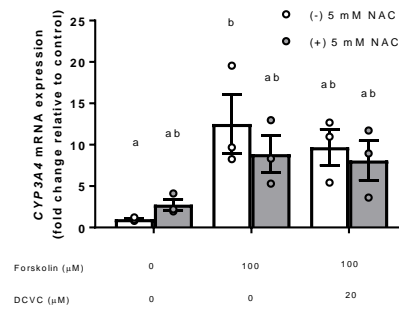
(C) Syncytialized BeWo cells (24-hour exposure)
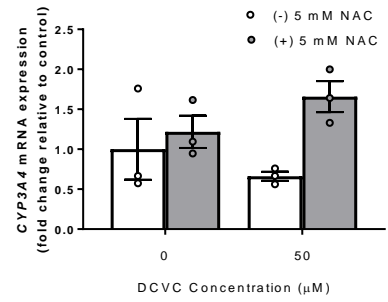
Figure 5.4. Effects of DCVC with and without NAC pre/co-treatment on *CYP3A4* mRNA expression. (A) Unsyncytialized BeWo cells received treatment(s) for 48 hours. (B) BeWo cells received treatment(s) while undergoing forskolin-stimulated syncytialization for 48 hours. (C) Syncytialized BeWo cells received treatment(s) for 24 hours. Data were analyzed by two-way ANOVA followed by Tukey's post-hoc comparison of means. Error bars represent mean ± SEM. Non-overlapping letters signify statistically significant differences. Independent experiments with unsyncytialized BeWo cells, BeWo cells undergoing syncytialization, and syncytialized BeWo cells were repeated five, three, and three times, respectively.

(A) Unsyncytialized BeWo cells (48-hour exposure)

(A1)

(A2)
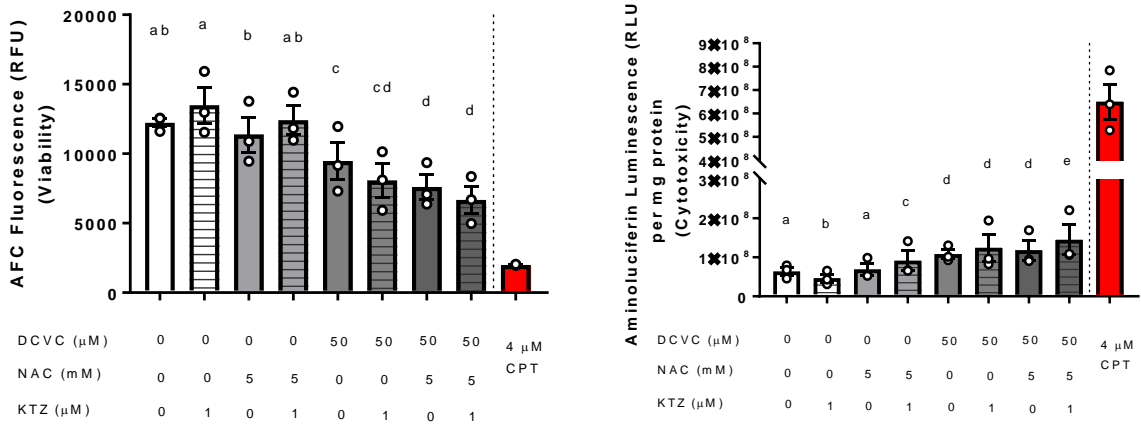
(B) Syncytialized BeWo cells (48-hour exposure)

(B1)

(B2)
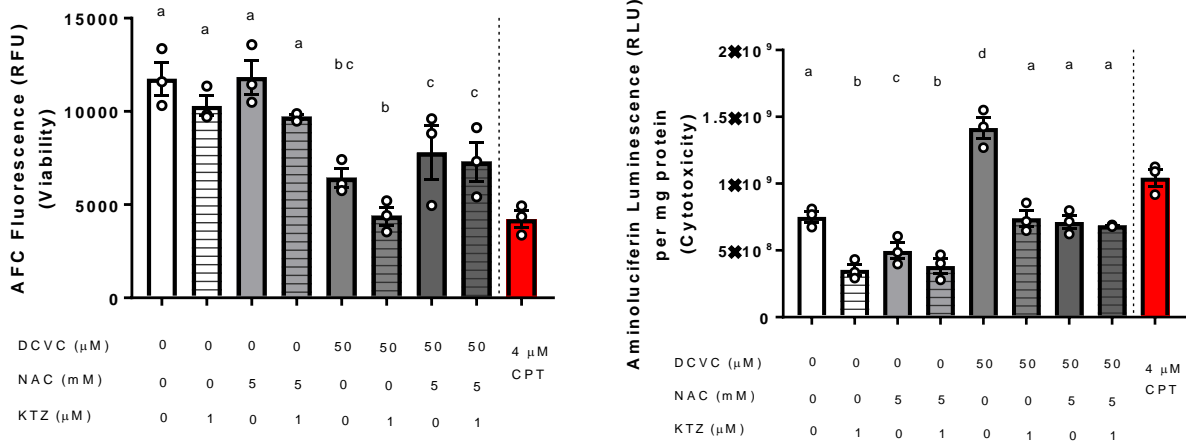
Figure 5.5. Effects of NAC and KTZ on DCVC-stimulated cell viability and cytotoxicity.
Effects are shown for (A) unsyncytialized BeWo cells receiving treatment(s) for 48 hours and
(B) syncytialized BeWo cells receiving treatment(s) for 48 hours. Statistical analysis was
performed using mixed models ANOVA followed by Tukey's post-hoc comparison of means.
Statistically significant differences are indicated by non-overlapping letters. Error bars represent
mean ± SEM. N=3 independent experiments with each experiment performed in triplicate. Cell
viability was measured as relative fluorescence units (RFU) and cytotoxicity was measured as
relative luminescence units (RLU)/mg protein. Camptothecin (CPT) was included as a positive
control.

(A) Unsyncytialized BeWo cells (48-hour exposure)
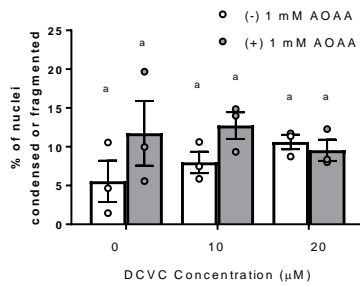
(B) BeWo cells undergoing syncytialization (48-hour exposure)
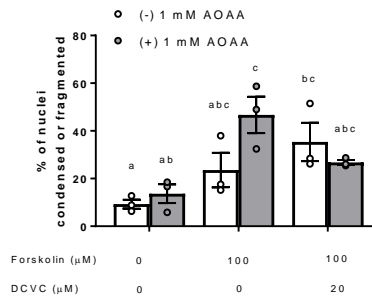
(C) Syncytialized BeWo cells (48-hour exposure)
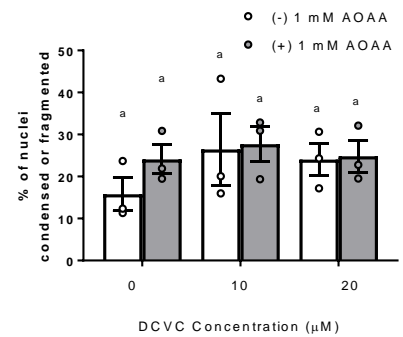
Figure 5.6. Effects of DCVC with and without AOAA pre/co-treatment on nuclear condensation or fragmentation. **(A)** Unsyncytialized BeWo cells received treatment(s) for 48 hours. **(B)** BeWo cells received treatment(s) while undergoing forskolin-stimulated syncytialization for 48 hours. **(C)** Syncytialized BeWo cells received treatment(s) for 48 hours. Statistical analysis was performed using two-way ANOVA followed by Tukey's post-hoc comparison of means. Statistical significance is indicated by non-overlapping letters. N=3 independent experiments.
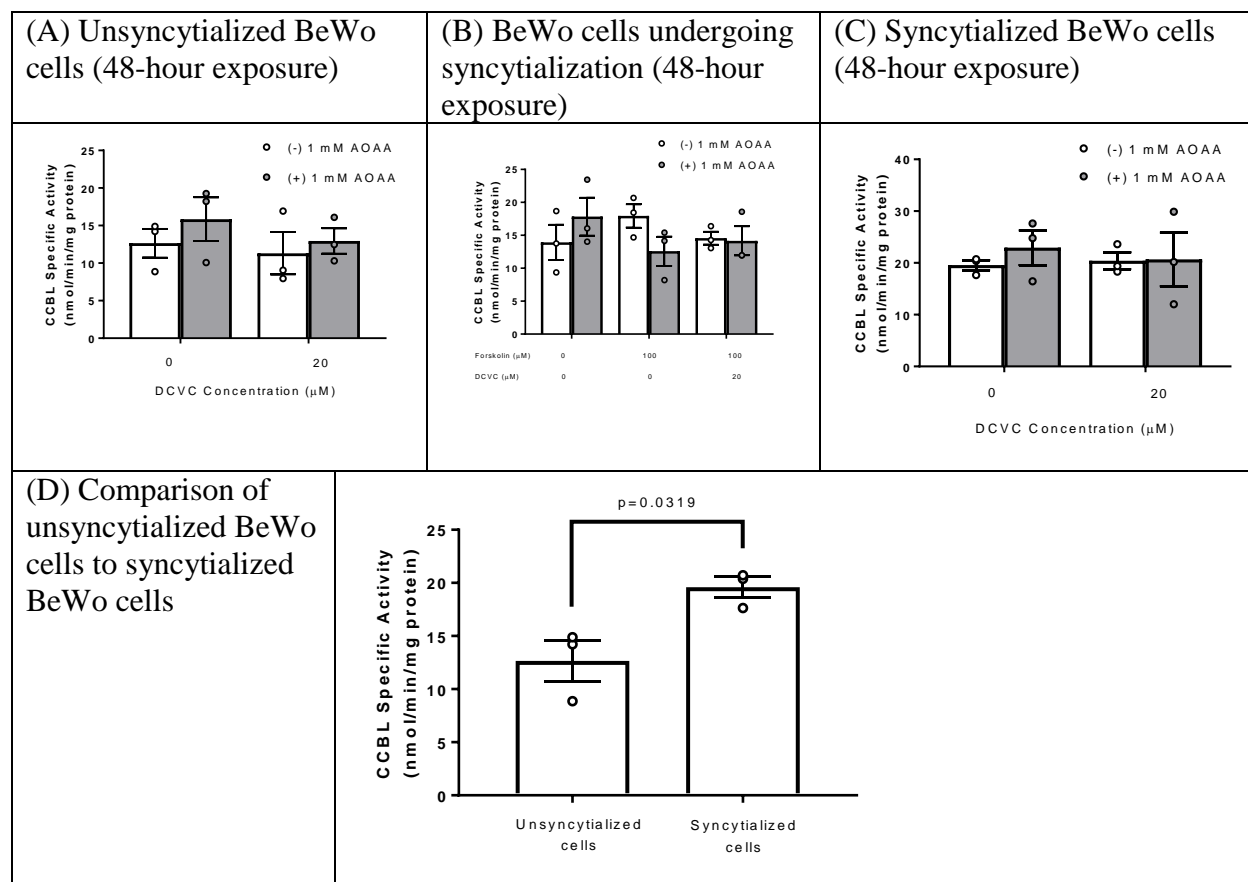
Figure 5.7. Effects of DCVC with and without AOAA pre/co-treatment on CCBL activity.
(A) Unsyncytialized BeWo cells received treatment(s) for 48 hours. (B) BeWo cells received
treatment(s) while undergoing forskolin-stimulated syncytialization for 48 hours. (C)
Syncytialized BeWo cells received treatment(s) for 48 hours. (D) Comparison of CCBL activity
in unsyncytialized BeWo cells versus syncytialized BeWo cells. Groups in (D) were taken from
the respective groups in (A) and (C). For the comparisons within unsyncytialized BeWo cells,
within BeWo cells undergoing syncytialization, and within syncytialized BeWo cells (A, B, and
C), statistical analysis was performed using two-way ANOVA followed by Tukey's post-hoc
comparison of means. For the comparison between the control unsyncytialized BeWo cells and
the control syncytialized BeWo cells (D), statistical analysis was performed using a two-tailed
unpaired t-test. Error bars represent mean ± SEM. N=3 independent experiments.

(A) Unsyncytialized BeWo cells (48-hour exposure)
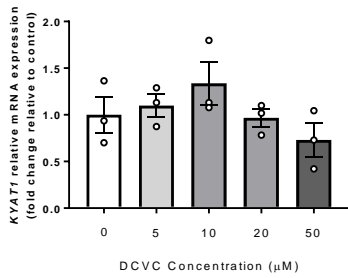
(B) BeWo cells undergoing syncytialization (48-hour exposure)
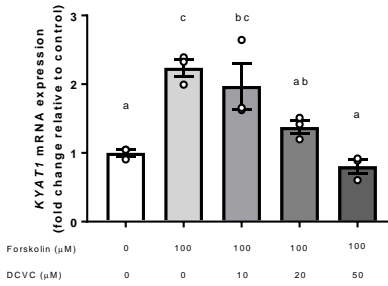
(C) Syncytialized BeWo cells (24-hour exposure)
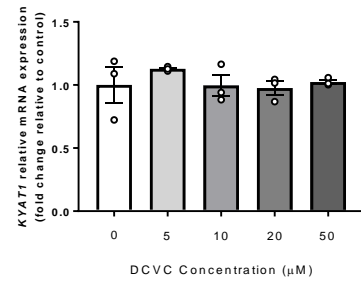
Figure 5.8. Effects of DCVC on *KYAT1* mRNA expression. (A) Unsyncytialized BeWo cells exposed to DCVC for 48 hours. (B) BeWo cells exposed to DCVC while undergoing forskolin-stimulated syncytialization for 48 hours. (C) Syncytialized BeWo cells exposed to DCVC for 24 hours. Statistical analysis was performed using one-way ANOVA followed by Tukey's post-hoc comparison of means. Non-overlapping letters indicate statistical significance. Error bars represent mean ± SEM. N=3 independent experiments.

(A) Unsyncytialized BeWo cells (48-hour exposure)
(A1)   (A2)
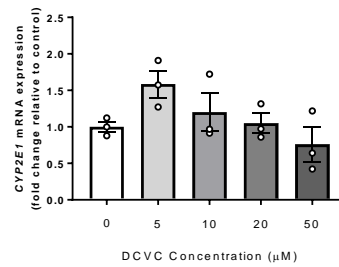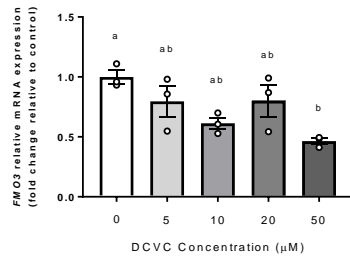
(B) BeWo cells undergoing syncytialization (48-hour exposure)
(B1)   (B2)
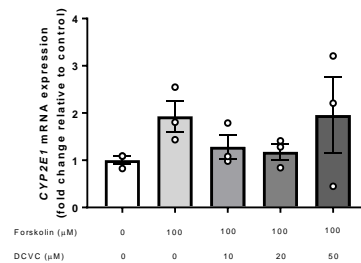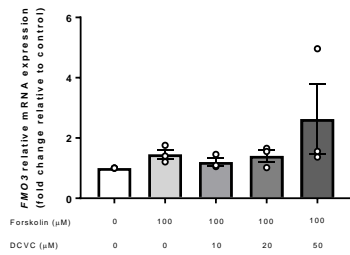
(C) Syncytialized BeWo cells (24-hour exposure)
(C1)   (C2)
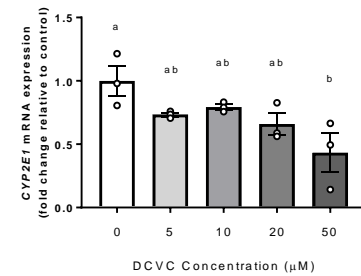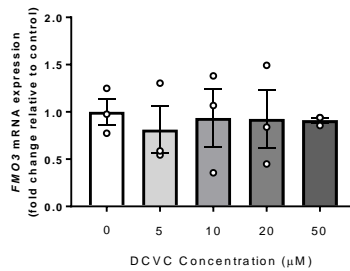
Figure 5.9. Effects of DCVC on *FMO3* and *CYP2E1* mRNA expression. (A) Unsyncytialized BeWo cells exposed to DCVC for 48 hours. (B) BeWo cells exposed to DCVC while undergoing forskolin-stimulated syncytialization for 48 hours. (C) Syncytialized BeWo cells exposed to DCVC for 24 hours. Statistical analysis was performed using one-way ANOVA followed by Tukey's post-hoc comparison of means. Statistical significance is indicated by non-overlapping letters. Error bars represent mean ± SEM. N=3 independent experiments.
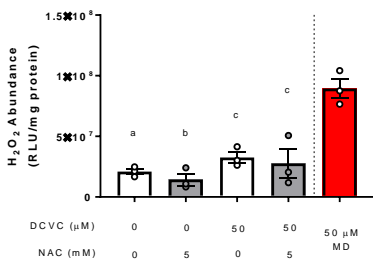
257
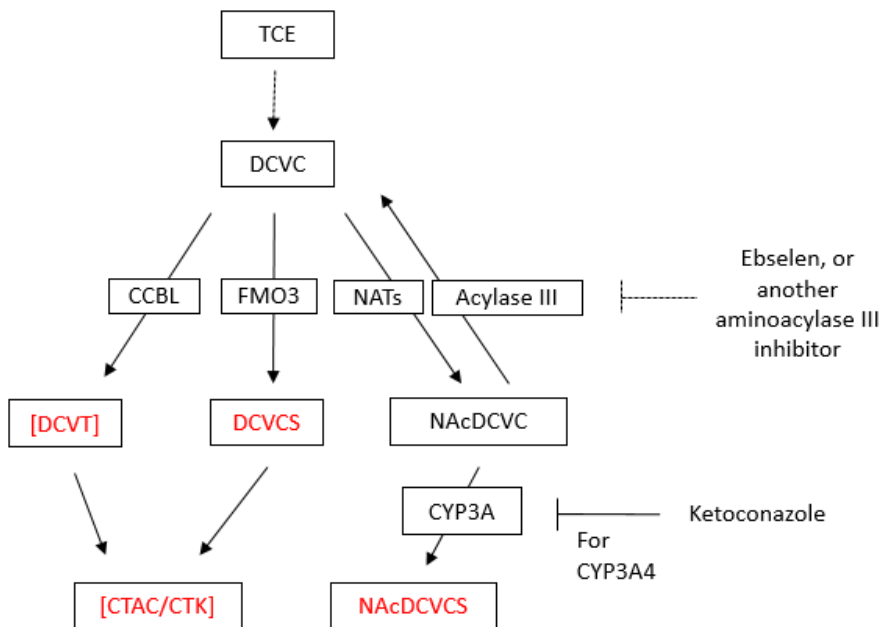
Figure 5.10. Proposed model for targeting _S_-(1,2-dichlorovinyl)-L-cysteine (DCVC) metabolism to reduce toxicity. The current study suggests that CYP3A4 inhibition alone is not sufficient to reduce DCVC-stimulated toxicity, even in the presence of N-acetyl-L-cysteine (NAC). A strategy to reduce DCVC toxicity proposed is the administration of CYP3A inhibition and aminoacylase III inhibition to prevent N-acetyl-DCVC (NAcDCVC) from being metabolized to either DCVC or NAcDCVC sulfoxide (NAcDCVCS), as shown above. NAcDCVCS itself is toxic, and DCVC can be metabolized to toxic metabolites via cysteine conjugate β-lyase (CCBL) or flavin-containing monooxygenase 3 (FMO3). Whereas unstable metabolites appear in brackets, metabolites known to be toxic appear in red. Enzymes are depicted by placement within arrows between metabolites. The dashed symbol with ebselen indicates a method uninvestigated in the current study but suggested for future studies. Other abbreviations: DCVT, 1,2-dichlorovinylthiol; DCVCS, DCVC sulfoxide; CTAC, chlorothionoacetyl chloride; CTK, chlorothioketene; NAT, _N_-acetyltransferase; CYP, cytochrome P450. This figure was modified from a figure by Lash et al. 2014 (Lash _et al._, 2014).
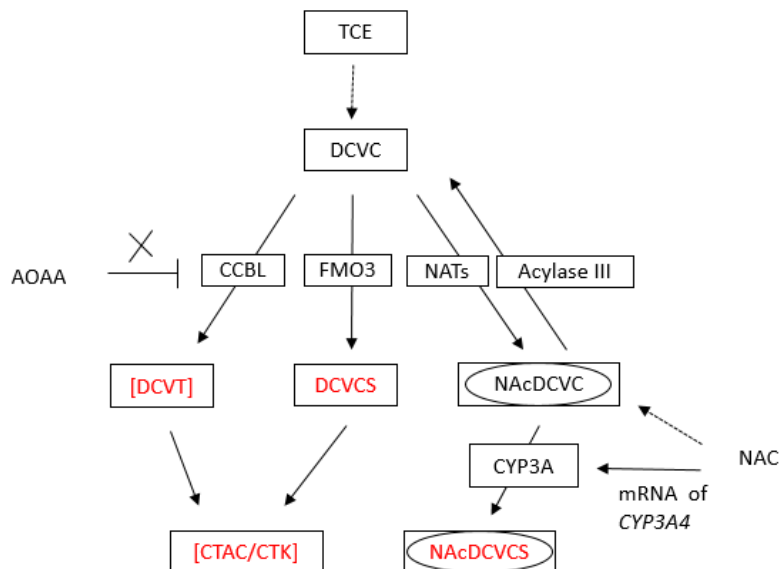
Figure 5.11. Proposed mechanism of action of aminooxyacetic acid (AOAA) and N-acetyl-L-cysteine (NAC) on *S*-(1,2-dichlorovinyl)-L-cysteine (DCVC) metabolism in BeWo cells. In the placental BeWo cells, AOAA was ineffective as a cysteine conjugate β-lyase (CCBL) inhibitor. It is proposed that NAC can increase N-acetyl-*S*-(1,2-dichlorovinyl)-L-cysteine sulfoxide (NAcDCVCS) production. Supporting evidence from the current study is that NAC has a significant effect on *CYP3A4* mRNA expression in the direction of increase. Ultimately, because of the toxicity of NAcDCVCS and the ability of AOAA to inhibit CCBL in BeWo cells, NAC and AOAA were unable to prevent DCVC-stimulated toxicity. Unstable metabolites appear in brackets, metabolites known to be toxic appear in red, and metabolites recoverable in urine are circled. Enzymes are depicted by placement within arrows between metabolites. Other Abbreviations: DCVT, 1,2-dichlorovinylthiol; DCVCS, DCVC sulfoxide; NAcDCVC, N-acetyl-*S*-(1,2-dichlorovinyl)-L-cysteine; CTAC, chlorothionoacetyl chloride; CTK, chlorothioketene; FMO, flavin-containing monooxygenase; NAT, *N*-acetyltransferase; CYP, cytochrome P450. This figure was based in part from Lash et al. 2014 (Lash *et al.*, 2014).

Table S5.1. Primer sequences used for the current study. In the case of using the NCBI database, primers were selected to have as close to 60 degrees Celsius melting point for each primer as possible, have an amplicon size preferably between 75 and 150 base pairs, and be as close to 50% GC pairs in sequence as possible. An absolute criterion of the primer was inclusion of an exon-exon junction.

B2M (Beta-2-microglobulin)	
Forward	5'-TGCCGTGTGAACCATGTG-3'
Reverse	5'-GCGGCATCTTCAAACCTC-3'
Source	Vreeburg, R.A.M, Bastiaan-Net, S., and Mes, J.J. (2011). Normalization genes for quantitative RT-PCR in differentiated Caco-2 cells used for food exposure studies. *Food Funct.* **2,** 124-129.
PRDX2 (Peroxiredoxin 2)	
Forward	5'-AGACGAGCATGGGGAAGTTTG-3'
Reverse	5'-TGTCATCCACGTTGGGCTTA-3'
Source	NCBI Nucleotide Database
BCL2 (BCL2, B-cell lymphoma 2, apoptosis regulator)	
Forward	5'-CATGCTGGGGCCGTACAG-3'
Reverse	5'-GAACCGGCACCTGCACAC-3'
Source	Wyrębska, A., Szymański, J., Gach, K., et al. (2013). Apoptosis-mediated cytotoxic effects of parthenolide and the new synthetic analog MZ-6 on two breast cancer cell lines. *Mol. Biol. Rep.* **40,** 1655-1663.
LGALS3 (Galectin-3)	
Forward	5'-GTGAAGCCCAATGCAAACAGA-3'
Reverse	5'-AGCGTGGGGTTAAAGTGGAAGG-3'
Source	PrimerBank: (https://pga.mgh.harvard.edu/primerbank/) PrimerBank ID: 294345474c2
NFKB1 (Nuclear factor kappa B subunit 1)	
Forward	5'-AACAGAGAGGATTTCGTTTCCG-3'
Reverse	5'-TTTGACCTGAGGGTAAGACTTCT-3'
Source	PrimerBank: (https://pga.mgh.harvard.edu/primerbank/) PrimerBank ID: 259155300c1
FMO3 (Flavin-containing monooxygenase 3)	
Forward	5'-AAGAACGGGTTACCATGGGG-3'
Reverse	5'-TGTAAATGCTAGCCCTGCCC-3'
Source	NCBI Nucleotide Database
KYAT1 (Kynurenine aminotransferase 1)	
Forward	5'-CCAGTGGATGGTCTACGACG-3'
Reverse	5'-CTCCCGTTCAAAGCTCTCG-3'

Source	PrimerBank: (https://pga.mgh.harvard.edu/primerbank/) PrimerBank ID: 95147550c1
***CYP2E1* (Cytochrome P450, family 2, subfamily E, polypeptide 1)**	
Forward	5'-GGGAAACAGGGCAATGAGAG-3'
Reverse	5'-GGAAGGTGGGGTCGAAAGG-3'
Source	PrimerBank: (https://pga.mgh.harvard.edu/primerbank/) PrimerBank ID: 75709190c3
***CYP3A4* (Cytochrome P450, family 3, subfamily A, polypeptide 4)**	
Forward	5'-TGCACATAGCCCAGCAAAGA-3'
Reverse	5'-TGGGTTCCATATAGATAGAGGAGCA-3'
Source	NCBI Nucleotide Database

(A) BeWo cells undergoing syncytialization (48-hour exposure)
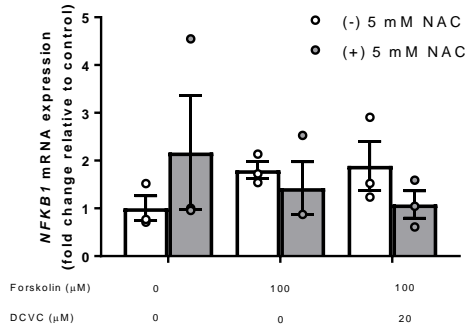
(B) Syncytialized BeWo cells (48-hour exposure)
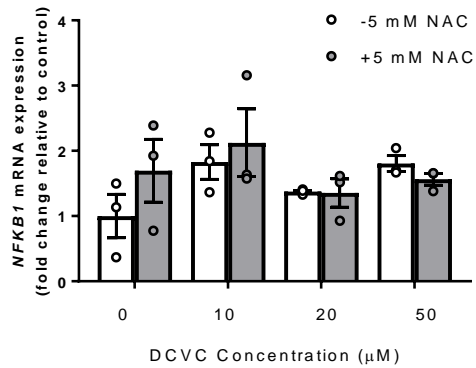
Figure S5.1. Effects of DCVC with and without NAC pre/co-treatment on *NFKB1* mRNA expression. Effects are shown for (A) BeWo cells undergoing syncytialization and (B) syncytialized BeWo cells. Data were analyzed by two-way ANOVA followed by Tukey's post-hoc comparison of means. N=3 independent experiments. Analysis was not performed on unsyncytialized BeWo cells for *NFKB1* mRNA expression because DCVC by itself did not change *NFKB1* mRNA expression in those cells (**Figure 4.6**).

References

Agency for Toxic Substances and Disease Registry, 2007. Trichloroethylene Toxicity: What are the U.S. Standards for Trichloroethylene Exposure? In Agency for Toxic Substances and Disease Registry (ATSDR), E.H.a.M.E., (Ed.), Atlanta, GA, pp.

Agency for Toxic Substances and Disease Registry, 2019. Toxicological Profile for Trichloroethylene. In U.S. Department of Health and Human Services, A.f.T.S.a.D.R.A., (Ed.), Atlanta, GA, pp.

Al-Nasiry, S., Spitz, B., Hanssens, M., Luyten, C., Pijnenborg, R., 2006. Differential effects of inducers of syncytialization and apoptosis on BeWo and JEG-3 choriocarcinoma cells. Hum Reprod **21**, 193-201.

Aldini, G., Altomare, A., Baron, G., Vistoli, G., Carini, M., Borsani, L., Sergio, F., 2018. N-Acetylcysteine as an antioxidant and disulphide breaking agent: the reasons why. Free Radic Res **52**, 751-762.

Allocati, N., Masulli, M., Di Ilio, C., Federici, L., 2018. Glutathione transferases: substrates, inihibitors and pro-drugs in cancer and neurodegenerative diseases. Oncogenesis **7**, 8.

Aris, A., Benali, S., Ouellet, A., Moutquin, J.M., Leblanc, S., 2009. Potential biomarkers of preeclampsia: inverse correlation between hydrogen peroxide and nitric oxide early in maternal circulation and at term in placenta of women with preeclampsia. Placenta **30**, 342-347.

Belkacemi, L., Bainbridge, S.A., Dickinson, M.A., Smith, G.N., Graham, C.H., 2007. Glyceryl trinitrate inhibits hypoxia/reoxygenation-induced apoptosis in the syncytiotrophoblast of the human placenta: therapeutic implications for preeclampsia. Am J Pathol **170**, 909-920.

Boldenow, E., Hassan, I., Chames, M.C., Xi, C., Loch-Caruso, R., 2015. The trichloroethylene metabolite S-(1,2-dichlorovinyl)-l-cysteine but not trichloroacetate inhibits pathogen-stimulated TNF-alpha in human extraplacental membranes in vitro. Reprod Toxicol **52**, 1-6.

Boyadjieva, N.I., Sarkar, D.K., 2013. Cyclic adenosine monophosphate and brain-derived neurotrophic factor decreased oxidative stress and apoptosis in developing hypothalamic neuronal cells: role of microglia. Alcohol Clin Exp Res **37**, 1370-1379.

Chan, G., Guilbert, L.J., 2006. Ultraviolet-inactivated human cytomegalovirus induces placental syncytiotrophoblast apoptosis in a Toll-like receptor-2 and tumour necrosis factor-alpha dependent manner. J Pathol **210**, 111-120.

Chen, L., Liu, L., Huang, S., 2008. Cadmium activates the mitogen-activated protein kinase (MAPK) pathway via induction of reactive oxygen species and inhibition of protein phosphatases 2A and 5. Free Radic Biol Med **45**, 1035-1044.

Cooper, A.J., Pinto, J.T., 2006. Cysteine S-conjugate beta-lyases. Amino Acids **30**, 1-15.

Cooper, D.M., 2003. Regulation and organization of adenylyl cyclases and cAMP. Biochem J **375**, 517-529.

Crowley, L.C., Marfell, B.J., Waterhouse, N.J., 2016. Analyzing Cell Death by Nuclear Staining with Hoechst 33342. Cold Spring Harb Protoc **2016**.

Daly, J.W., 1984. Forskolin, adenylate cyclase, and cell physiology: an overview. Adv Cyclic Nucleotide Protein Phosphorylation Res **17**, 81-89.

Dohn, D.R., Anders, M.W., 1982. Assay of cysteine conjugate beta-lyase activity with S-(2-benzothiazolyl)cysteine as the substrate. Anal Biochem **120**, 379-386.

Elfarra, A.A., Anders, M.W., 1984. Renal processing of glutathione conjugates. Role in nephrotoxicity. Biochem Pharmacol **33**, 3729-3732.

Elkin, E.R., Harris, S.M., Loch-Caruso, R., 2018. Trichloroethylene metabolite S-(1,2-dichlorovinyl)-l-cysteine induces lipid peroxidation-associated apoptosis via the intrinsic and extrinsic apoptosis pathways in a first-trimester placental cell line. Toxicol Appl Pharmacol **338**, 30-42.

Errami, Y., Naura, A.S., Kim, H., Ju, J., Suzuki, Y., El-Bahrawy, A.H., Ghonim, M.A., Hemeida, R.A., Mansy, M.S., Zhang, J., Xu, M., Smulson, M.E., Brim, H., Boulares, A.H., 2013. Apoptotic DNA fragmentation may be a cooperative activity between caspase-activated deoxyribonuclease and the poly(ADP-ribose) polymerase-regulated DNAS1L3, an endoplasmic reticulum-localized endonuclease that translocates to the nucleus during apoptosis. J Biol Chem **288**, 3460-3468.

Ezerina, D., Takano, Y., Hanaoka, K., Urano, Y., Dick, T.P., 2018. N-Acetyl Cysteine Functions as a Fast-Acting Antioxidant by Triggering Intracellular H2S and Sulfane Sulfur Production. Cell Chem Biol **25**, 447-459 e444.

Forand, S.P., Lewis-Michl, E.L., Gomez, M.I., 2012. Adverse birth outcomes and maternal exposure to trichloroethylene and tetrachloroethylene through soil vapor intrusion in New York State. Environ Health Perspect **120**, 616-621.

Garcia-Lloret, M.I., Winkler-Lowen, B., Guilbert, L.J., 2000. Monocytes adhering by LFA-1 to placental syncytiotrophoblasts induce local apoptosis via release of TNF-alpha. A model for hematogenous initiation of placental inflammations. J Leukoc Biol **68**, 903-908.

Garcia-Lloret, M.I., Yui, J., Winkler-Lowen, B., Guilbert, L.J., 1996. Epidermal growth factor inhibits cytokine-induced apoptosis of primary human trophoblasts. J Cell Physiol **167**, 324-332.

Gibbs, M.A., Baillie, M.T., Shen, D.D., Kunze, K.L., Thummel, K.E., 2000. Persistent inhibition of CYP3A4 by ketoconazole in modified Caco-2 cells. Pharm Res **17**, 299-305.

Graham, C.H., Hawley, T.S., Hawley, R.G., MacDougall, J.R., Kerbel, R.S., Khoo, N., Lala, P.K., 1993. Establishment and characterization of first trimester human trophoblast cells with extended lifespan. Exp Cell Res **206**, 204-211.

Guha, N., Loomis, D., Grosse, Y., Lauby-Secretan, B., El Ghissassi, F., Bouvard, V., Benbrahim-Tallaa, L., Baan, R., Mattock, H., Straif, K., International Agency for Research on Cancer Monograph Working, G., 2012. Carcinogenicity of trichloroethylene, tetrachloroethylene, some other chlorinated solvents, and their metabolites. Lancet Oncol **13**, 1192-1193.

Hanavan, P.D., Borges, C.R., Katchman, B.A., Faigel, D.O., Ho, T.H., Ma, C.T., Sergienko, E.A., Meurice, N., Petit, J.L., Lake, D.F., 2015. Ebselen inhibits QSOX1 enzymatic activity and suppresses invasion of pancreatic and renal cancer cell lines. Oncotarget **6**, 18418-18428.

Hassan, I., Kumar, A.M., Park, H.R., Lash, L.H., Loch-Caruso, R., 2016. Reactive Oxygen Stimulation of Interleukin-6 Release in the Human Trophoblast Cell Line HTR-8/SVneo by the Trichlorethylene Metabolite S-(1,2-Dichloro)-l-Cysteine. Biol Reprod **95**, 66.

Hu, R., Jin, H., Zhou, S., Yang, P., Li, X., 2007. Proteomic analysis of hypoxia-induced responses in the syncytialization of human placental cell line BeWo. Placenta **28**, 399-407.

Inadera, H., Tachibana, S., Takasaki, I., Tatematsu, M., Shimomura, A., 2010. Hyperglycemia perturbs biochemical networks in human trophoblast BeWo cells. Endocr J **57**, 567-577.

International Agency for Research on Cancer, 2014. Trichloroethylene, Tetrachloroethylene, and Some Other Chlorinated Agents. (IARC Monographs on the Evaluation of Carcinogenic Risks to Humans). IARC Working Group on the Evaluation of Carcinogenic Risk to Humans, Lyon, France, pp.

Ishihara, N., Matsuo, H., Murakoshi, H., Laoag-Fernandez, J.B., Samoto, T., Maruo, T., 2002. Increased apoptosis in the syncytiotrophoblast in human term placentas complicated by either preeclampsia or intrauterine growth retardation. Am J Obstet Gynecol **186**, 158-166.

Lash, L.H., 2010. Role of Bioactivation Reactions in Chemically Induced Nephrotoxicity. In Gad, S.C., (Ed.), Pharmaceutical Sciences Encyclopedia: Drug Discovery, Development, and Manufacturing. John Wiley & Sons, Inc., Hoboken, NJ, pp. 1-21.

Lash, L.H., Chiu, W.A., Guyton, K.Z., Rusyn, I., 2014a. Trichloroethylene biotransformation and its role in mutagenicity, carcinogenicity and target organ toxicity. Mutat Res Rev Mutat Res **762**, 22-36.

Lash, L.H., Elfarra, A.A., Anders, M.W., 1986. Renal cysteine conjugate beta-lyase. Bioactivation of nephrotoxic cysteine S-conjugates in mitochondrial outer membrane. J Biol Chem **261**, 5930-5935.

Lash, L.H., Putt, D.A., Benipal, B., 2014b. Multigenerational study of chemically induced cytotoxicity and proliferation in cultures of human proximal tubular cells. Int J Mol Sci **15**, 21348-21365.

Lash, L.H., Putt, D.A., Brashear, W.T., Abbas, R., Parker, J.C., Fisher, J.W., 1999. Identification of S-(1,2-dichlorovinyl)glutathione in the blood of human volunteers exposed to trichloroethylene. J Toxicol Environ Health A **56**, 1-21.

Lash, L.H., Sausen, P.J., Duescher, R.J., Cooley, A.J., Elfarra, A.A., 1994. Roles of cysteine conjugate beta-lyase and S-oxidase in nephrotoxicity: studies with S-(1,2-dichlorovinyl)-L-cysteine and S-(1,2-dichlorovinyl)-L-cysteine sulfoxide. J Pharmacol Exp Ther **269**, 374-383.

Li, J., Tong, C., Xu, P., Wang, L., Han, T.L., Wen, L., Luo, X., Tan, B., Zhu, F., Gui, S., Gao, R., Qi, H., Baker, P.N., 2019. QSOX1 regulates trophoblastic apoptosis in preeclampsia through hydrogen peroxide production. J Matern Fetal Neonatal Med **32**, 3708-3715.

Loch-Caruso, R., Hassan, I., Harris, S.M., Kumar, A., Bjork, F., Lash, L.H., 2019. Trichloroethylene exposure in mid-pregnancy decreased fetal weight and increased placental markers of oxidative stress in rats. Reprod Toxicol **83**, 38-45.

Lopez-Barcons, L., Maurer, B.J., Kang, M.H., Reynolds, C.P., 2017. P450 inhibitor ketoconazole increased the intratumor drug levels and antitumor activity of fenretinide in human neuroblastoma xenograft models. Int J Cancer **141**, 405-413.

Matassov, D., Kagan, T., Leblanc, J., Sikorska, M., Zakeri, Z., 2004. Measurement of apoptosis by DNA fragmentation. Methods Mol Biol **282**, 1-17.

McKinney, L.L., Picken Jr., J.C., Weakley, F.B., Eldridge, A.C., Campbell, R.E., Cowan, J.C., Biester, H.E., 1959. Possible Toxic Factor of Trichloroethylene-extracted Soybean Oil Meal. Journal of the American Chemical Society **81**, 909-915.

Mei, Z., Huang, B., Qian, X., Zhang, Y., Teng, B., 2020. Gastrodin improves preeclampsia-induced cell apoptosis by regulation of TLR4/NF-kappaB in rats. Food Sci Nutr **8**, 820-829.

Moll, S.J., Jones, C.J., Crocker, I.P., Baker, P.N., Heazell, A.E., 2007. Epidermal growth factor rescues trophoblast apoptosis induced by reactive oxygen species. Apoptosis **12**, 1611-1622.

Newlaczyl, A.U., Yu, L.G., 2011. Galectin-3--a jack-of-all-trades in cancer. Cancer Lett **313**, 123-128.

Njie-Mbye, Y.F., Kulkarni, M., Opere, C.A., Ohia, S.E., 2012. Mechanism of action of hydrogen sulfide on cyclic AMP formation in rat retinal pigment epithelial cells. Exp Eye Res **98**, 16-22.

Pattillo, R.A., Gey, G.O., 1968. The establishment of a cell line of human hormone-synthesizing trophoblastic cells in vitro. Cancer Res **28**, 1231-1236.

Pavek, P., Cerveny, L., Svecova, L., Brysch, M., Libra, A., Vrzal, R., Nachtigal, P., Staud, F., Ulrichova, J., Fendrich, Z., Dvorak, Z., 2007. Examination of Glucocorticoid receptor alpha-mediated transcriptional regulation of P-glycoprotein, CYP3A4, and CYP2C9 genes in placental trophoblast cell lines. Placenta **28**, 1004-1011.

Potgens, A.J., Schmitz, U., Bose, P., Versmold, A., Kaufmann, P., Frank, H.G., 2002. Mechanisms of syncytial fusion: a review. Placenta **23 Suppl A**, S107-113.

Rodenbeck, S.E., Sanderson, L.M., Rene, A., 2000. Maternal exposure to trichloroethylene in drinking water and birth-weight outcomes. Arch Environ Health **55**, 188-194.

Ruckart, P.Z., Bove, F.J., Maslia, M., 2014. Evaluation of contaminated drinking water and preterm birth, small for gestational age, and birth weight at Marine Corps Base Camp Lejeune, North Carolina: a cross-sectional study. Environ Health **13**, 99.

Saha, S., Li, Y., Anand-Srivastava, M.B., 2008. Reduced levels of cyclic AMP contribute to the enhanced oxidative stress in vascular smooth muscle cells from spontaneously hypertensive rats. Can J Physiol Pharmacol **86**, 190-198.

Sarna, L.K., Sid, V., Wang, P., Siow, Y.L., House, J.D., O, K., 2016. Tyrosol Attenuates High Fat Diet-Induced Hepatic Oxidative Stress: Potential Involvement of Cystathionine beta-Synthase and Cystathionine gamma-Lyase. Lipids **51**, 583-590.

Sato, N., Ueno, T., Kubo, K., Suzuki, T., Tsukimura, N., Att, W., Yamada, M., Hori, N., Maeda, H., Ogawa, T., 2009. N-Acetyl cysteine (NAC) inhibits proliferation, collagen gene transcription, and redox stress in rat palatal mucosal cells. Dent Mater **25**, 1532-1540.

Sharp, A.N., Heazell, A.E., Crocker, I.P., Mor, G., 2010. Placental apoptosis in health and disease. Am J Reprod Immunol **64**, 159-169.

Siddiqi, A., Nafees, S., Rashid, S., Sultana, S., Saidullah, B., 2015. Hesperidin ameliorates trichloroethylene-induced nephrotoxicity by abrogation of oxidative stress and apoptosis in wistar rats. Mol Cell Biochem **406**, 9-20.

Soomets, U., Mahlapuu, R., Tehranian, R., Jarvet, J., Karelson, E., Zilmer, M., Iverfeldt, K., Zorko, M., Graslund, A., Langel, U., 1999. Regulation of GTPase and adenylate cyclase activity by amyloid beta-peptide and its fragments in rat brain tissue. Brain Res **850**, 179-188.

Suksawat, T., Jarukamjorn, K., Chatuphonprasert, W., 2019. Effects of rifampicin on the expressions of drug transporter OATP1B1, drug metabolizing enzymes CYP3A4 and CYP3A5, and nuclear receptors PXR and AhR in human HepG2 and BeWo cells. Isan Journal of Pharmaceutical Sciences **15**, 118-128.

Tan, S.M., Deliyanti, D., Figgett, W.A., Talia, D.M., de Haan, J.B., Wilkinson-Berka, J.L., 2015. Ebselen by modulating oxidative stress improves hypoxia-induced macroglial Muller cell and vascular injury in the retina. Exp Eye Res **136**, 1-8.

Tsirulnikov, K., Abuladze, N., Bragin, A., Faull, K., Cascio, D., Damoiseaux, R., Schibler, M.J., Pushkin, A., 2012. Inhibition of aminoacylase 3 protects rat brain cortex neuronal cells from the toxicity of 4-hydroxy-2-nonenal mercapturate and 4-hydroxy-2-nonenal. Toxicol Appl Pharmacol **263**, 303-314.

United States Environmental Protection Agency, 2011a. EPA Releases Final Health Assessment for TCE. In Newsroom, U.S.E.P.A., (Ed.), Washington, D.C., pp.

United States Environmental Protection Agency, 2011b. Trichloroethylene: CASRN 79-01-6 (IRIS Assessment). In Integrated Risk Information System (IRIS), U.S.E.P.A.U.S.E., (Ed.), Washington, D.C., pp.

Uttamsingh, V., Anders, M.W., 1999. Acylase-catalyzed deacetylation of haloalkene-derived mercapturates. Chem Res Toxicol **12**, 937-942.

Uttamsingh, V., Baggs, R.B., Krenitsky, D.M., Anders, M.W., 2000. Immunohistochemical localization of the acylases that catalyze the deacetylation of N-acetyl-L-cysteine and haloalkene-derived mercapturates. Drug Metab Dispos **28**, 625-632.

Wang, R., Dang, Y.L., Zheng, R., Li, Y., Li, W., Lu, X., Wang, L.J., Zhu, C., Lin, H.Y., Wang, H., 2014. Live cell imaging of in vitro human trophoblast syncytialization. Biol Reprod **90**, 117.

Werner, M., Birner, G., Dekant, W., 1996. Sulfoxidation of mercapturic acids derived from tri- and tetrachloroethene by cytochromes P450 3A: a bioactivation reaction in addition to deacetylation and cysteine conjugate beta-lyase mediated cleavage. Chem Res Toxicol **9**, 41-49.

Wice, B., Menton, D., Geuze, H., Schwartz, A.L., 1990. Modulators of cyclic AMP metabolism induce syncytiotrophoblast formation in vitro. Exp Cell Res **186**, 306-316.

Wu, F., Tian, F., Zeng, W., Liu, X., Fan, J., Lin, Y., Zhang, Y., 2017. Role of peroxiredoxin2 downregulation in recurrent miscarriage through regulation of trophoblast proliferation and apoptosis. Cell Death Dis **8**, e2908.

Xu, F., Papanayotou, I., Putt, D.A., Wang, J., Lash, L.H., 2008. Role of mitochondrial dysfunction in cellular responses to S-(1,2-dichlorovinyl)-L-cysteine in primary cultures of human proximal tubular cells. Biochem Pharmacol **76**, 552-567.

Yang, L., Yan, C., Zhang, F., Jiang, B., Gao, S., Liang, Y., Huang, L., Chen, W., 2018. Effects of ketoconazole on cyclophosphamide metabolism: evaluation of CYP3A4 inhibition effect using the in vitro and in vivo models. Exp Anim **67**, 71-82.

Yang, R.Y., Hsu, D.K., Liu, F.T., 1996. Expression of galectin-3 modulates T-cell growth and apoptosis. Proc Natl Acad Sci U S A **93**, 6737-6742.

Yue, T., Zuo, S., Bu, D., Zhu, J., Chen, S., Ma, Y., Ma, J., Guo, S., Wen, L., Zhang, X., Hu, J., Wang, Y., Yao, Z., Chen, G., Wang, X., Pan, Y., Wang, P., Liu, Y., 2020. Aminooxyacetic acid (AOAA) sensitizes colon cancer cells to oxaliplatin via exaggerating apoptosis induced by ROS. J Cancer **11**, 1828-1838.

Chapter VI. Alterations in Energy Metabolism Stimulated by the Trichloroethylene Metabolite *S*-(1,2-dichlorovinyl)-L-cysteine in the BeWo Human Placental Trophoblast Model During Syncytialization

Abstract

Syncytialization is a crucial event of placentation that forms the syncytiotrophoblasts comprising the maternal-fetal interface. The process is characterized by changes in amino acid and energy metabolism. Exposure to the trichloroethylene (TCE) metabolite *S*-(1,2-dichlorovinyl)-L-cysteine (DCVC) stimulates changes in energy metabolism in HTR-8/SVneo placental cells. In the current study, we exposed human villous trophoblastic BeWo cells to forskolin at 100 µM for 48 hours to stimulate syncytialization and investigated how DCVC treatment at 10 and 20 µM during syncytialization altered metabolites involved in energy metabolism using a metabolomics platform. Notable changes stimulated by syncytialization in the absence of DCVC included increased adenosine monophosphate (AMP) and guanosine monophosphate (GMP) and decreased aspartate and glutamate. In contrast, DCVC treatment during syncytialization decreased oleic acid, aspartate, proline, uridine diphosphate (UDP), UDP-D-glucose, uridine monophosphate (UMP), and cytidine monophosphate (CMP) relative to forskolin treatment alone, but did not increase any measured metabolites. Pathway analysis revealed multiple pathways in amino acid metabolism and sugar metabolism that were altered with forskolin-stimulated syncytialization alone and DCVC treatment during syncytialization (p<0.05). Analysis of ratios of metabolites within the pathways revealed that DCVC during syncytialization changed metabolite ratios in the same or different direction of syncytialization alone, indicating the complex nature of the relationship between syncytialization and DCVC

treatment. Together, the metabolic changes stimulated by DCVC treatment during syncytialization suggest energy metabolism and amino acid abundance as potential mechanisms by which DCVC could impact syncytialization and pregnancy. Future work could explore the relevance of the findings to TCE reproductive toxicity, including the detection of additional metabolites or assessment of the enzymes in the metabolic pathways that may be targets of TCE or DCVC.

Introduction

In the placenta, the differentiation of cytotrophoblasts into syncytiotrophoblasts is a process known as syncytialization and is crucial for a healthy pregnancy (Wice *et al.*, 1990; Potgens *et al.*, 2002; Wang *et al.*, 2014). Multinucleation and cell fusion occur as cytotrophoblasts differentiate into syncytiotrophoblasts (Wang *et al.*, 2014), which become the outermost layer of the villous tree of the fetal side of the placenta and hence the maternal-fetal interface (Cantle *et al.*, 1987; Robbins *et al.*, 2010; Wang *et al.*, 2014). These syncytiotrophoblasts are the cells responsible for the transport of nutrients, gas, and waste between mother and fetus (Potgens *et al.*, 2002; Wang *et al.*, 2014). As such, abnormalities of syncytialization or syncytiotrophoblast function could impair fetal growth and development.

Apoptosis of villous cytotrophoblasts, syncytiotrophoblasts, and other trophoblasts is associated with adverse pregnancy outcomes such as preeclampsia and intrauterine growth restriction, as reviewed by Sharp *et al.* (Sharp *et al.*, 2010). A pattern of apoptosis of syncytiotrophoblasts, in particular, has been described in which apoptosis initiates locally and then expands to encompass the entire syncytium (Longtine *et al.*, 2012). Mechanisms by which syncytiotrophoblast apoptosis are executed include decreased Bcl-2, which is associated with both preeclampsia and intrauterine growth retardation (Ishihara *et al.*, 2002). Caspase-3

activation is downstream in the mechanism by which apoptosis in villous cytotrophoblasts is carried out, and is associated with intrauterine growth restriction (Endo *et al.*, 2005; Huppertz *et al.*, 2006). Thus, there is a clear link between syncytiotrophoblast apoptosis and adverse pregnancy outcomes.

The BeWo human placental trophoblast cell line is a popular *in vitro* model for studying syncytialization (Pattillo and Gey, 1968). BeWo cells are villous trophoblasts that can be stimulated to syncytialize by forskolin (Daly, 1984; Wice *et al.*, 1990), producing a cell phenotype that is similar to syncytialization as it occurs *in vivo* (Wice *et al.*, 1990). An appropriate condition used to syncytialize the cytotrophoblastic BeWo cells is administration of 100 µM forskolin for 48 hours (Wice *et al.*, 1990; Al-Nasiry *et al.*, 2006; Inadera *et al.*, 2010) (Chapter 4).

Studies characterizing the molecular effects of forskolin-stimulated syncytialization of BeWo cells indicate a role for cellular redox regulation. These include findings that hypoxia inhibits syncytialization and alters the proteome of BeWo cells stimulated with forskolin (Hu *et al.*, 2007). Additional findings from the prior study include alterations in proteins with relevance to oxidative stress (peroxiredoxin 1, peroxiredoxin 2), among others (Hu *et al.*, 2007). Another study reported that peroxiredoxin 2 knockdown prevents BeWo cell syncytialization in response to forskolin (Wu *et al.*, 2017), which suggests that syncytialization involves reactive oxygen species (ROS) regulation. Furthermore, syncytin-1, a biomarker of syncytialization (Vargas *et al.*, 2009), is regulated by redox-sensitive proteins such as p38 and protein kinase A (Gupta *et al.*, 2016). Moreover, forskolin reduces cell viability and proliferation in BeWo cells (Al-Nasiry *et al.*, 2006) and reduced cell viability is associated with increased ROS in BeWo cells (Chapter 4).

Environmental exposures have the potential to disrupt syncytialization, especially because numerous toxicants disrupt cellular ROS regulation (Jones and Sies, 2015). For this study, we focused on a common environmental contaminant, trichloroethylene (TCE), a chemical used as a metal degreaser and in the synthesis of various chemicals (Agency for Toxic Substances and Disease Registry, 2019). In epidemiological studies, TCE exposure has been associated with adverse pregnancy outcomes, including low birth weight and small for gestational age (Rodenbeck *et al.*, 2000; Forand *et al.*, 2012; Ruckart *et al.*, 2014). In addition, TCE modifies oxidative stress markers in a pregnant Wistar rat model of fetal growth restriction (Loch-Caruso *et al.*, 2019). *S*-(1,2-Dichlorovinyl)-L-cystine (DCVC) is a metabolite of TCE through its glutathione conjugation pathway (Lash *et al.*, 2014). *In vitro* studies using DCVC exposure to HTR-8/SVneo extravillous placental cells (Graham *et al.*, 1993) demonstrated that DCVC stimulates apoptosis, ROS generation, and pro-inflammatory response (Hassan *et al.*, 2016; Elkin *et al.*, 2018). Thus, there is overlap between the mechanism of DCVC toxicity and the mechanism of syncytialization in regard to ROS, suggesting that DCVC may disrupt syncytialization. Importantly, TCE metabolites from its cytochrome P450-dependent oxidative pathway, trichloroacetic acid and dichloroacetic acid (Lash *et al.*, 2014), are non-toxic to HTR-8/SVneo cells (unpublished data).

Another possibile mechanism through which DCVC could disrupt syncytialization is through alteration of energy metabolism metabolites. Energy metabolites, particularly amino acids, are altered by DCVC treatment of HTR-8/SVneo placental cells (Elkin *et al.*, 2020). DCVC also targets intracellular signaling relevant to the mitochondria (Elkin *et al.*, 2019), where generation of energy metabolites such as adenosine triphosphate (ATP), crucial for pregnancy, takes place (Spaans *et al.*, 2014; Sferruzzi-Perri *et al.*, 2019). With respect to syncytialization, a

recent study discovered that syncytialization alters amino acid phosphorylation and collagen metabolic process in BeWo cells (Zheng *et al.*, 2016). In addition, slime mold multinucleation involves energy utilization and amino acid turnover (Wright and Anderson, 1959; Liddel and Wright, 1961). Thus, we hypothesize that syncytialization and DCVC exposure during syncytialization will alter energy utilization and amino acid turnover in manners consistent with important pregnancy outcomes. The present study investigates modifications to energy metabolism stimulated by exposure to the TCE metabolite DCVC during syncytialization using a targeted metabolomics approach.

Materials and Methods

The BeWo cell line

The BeWo human placental villous cytotrophoblast cell line (Pattillo and Gey, 1968) was used for the present study. BeWo cells were obtained through the American Type Culture Collection (ATCC CCL-98) and their identity was verified by short tandem repeat profile with fragment analysis on the ABI 3730XL DNA Analyzer from Applied Biosystems (Waltham, MA) at the University of Michigan DNA Sequencing Core. The cells were maintained in F12-K Nutrient Mixture Kaighn's Modification medium with (+) L Glutamine (Gibco, Grand Island, NY). For cell treatments, DMEM/F12 Nutrient Mixture medium (Gibco, Grand Island, NY) was used so that the exposure media were without phenol red. All media were supplemented with 10% (v/v) heat-inactivated fetal bovine serum (HI-FBS) and 1% (v/v) penicillin/streptomycin (P/S) (Gibco, Grand Island, NY). Three washes of phosphate buffered saline (PBS) (Invitrogen Life Technologies, Carlsbad, CA) were performed prior to detaching the cells with 0.25% trypsin-EDTA (Invitrogen Life Technologies, Carlsbad, CA) during subculture. All cells were kept in a 5% CO_2, 37°C controlled and humidified incubator. For regular subculture, cells were

272

plated at a 100,000 cells/mL concentration in 25 mL in 175 cm^2 flasks (Corning Inc., Corning, NY) and passaged at about 70-80% confluence. This work with human cell cultures was approved by the University of Michigan Institutional Biosafety Committee (IBCA00000100).

Exposures

We applied 100 µM forskolin exposure for 48 hours to promote BeWo cell syncytialization, consistent with prior reports (Wice *et al.*, 1990; Al-Nasiry *et al.*, 2006; Inadera *et al.*, 2010) and verified by us (Chapter 4). The vehicle control for any experiments using forskolin was 0.1% dimethyl sulfoxide (DMSO) (Tocris Bioscience, Bristol, UK). The TCE metabolite *S*-(1,2-dichlorovinyl)-L-cysteine (DCVC) was synthesized by the University of Michigan Medicinal Chemistry Core via published methods (McKinney *et al.*, 1959). The chemical identity of DCVC was verified through proton nuclear magnetic resonance (NMR) spectroscopy and determined to be 98.7% pure by high-performance liquid chromatography (HPLC). DCVC was added to cultures at 10 and 20 µM concentrations. These DCVC concentrations were chosen based on prior findings of efficacy for elicitation of metabolic changes (Elkin *et al.*, 2020). Moreover, the DCVC concentration range is similar to the average concentration of DCVG (13.4 µM), a precursor of DCVC (Lash *et al.*, 2014), found in the blood of women exposed to occupationally relevant doses TCE (Lash *et al.*, 1999; Agency for Toxic Substances and Disease Registry, 2007). DCVC was applied as a co-treatment with forskolin to investigate the effect of DCVC on syncytialization. To prepare for the experiment, cells were plated in 10-cm tissue culture dishes (Corning Inc., product 430167) at a density of 800,000 cells per dish in 8 mL volume. After 24 hours, the cells were treated according to the experimental groups in **Figure 6.1**.

Sample preparation for metabolomics analysis

After the 48-hour treatment duration, medium was removed from the cells, and a gentle, quick wash with 150 mM ammonium acetate was performed. Following the ammonium acetate wash, liquid nitrogen was poured over the cells and allowed to evaporate from the dishes. Cell dishes were then stored at -80°C until delivery to the University of Michigan Metabolomics Core on dry ice for analysis. The targeted platform used at the University of Michigan Metabolomics Core for these plates was the Tricarboxylic acid (TCA) Plus Platform. Metabolites detected through the TCA plus platform include metabolites in energy utilization (e.g., metabolites in glycolysis, TCA cycle, pentose phosphate pathway) and amino acids. At the Core, cell culture dishes were removed from -80°C storage and maintained on wet ice throughout processing. To each 10-cm dish, a 1.5-mL mixture of methanol, chloroform and water (8:1:1) containing isotope-labeled internal standards was added. Dishes were gently agitated to release cells and then scraped to homogenize the cells. The resulting cell mixtures were transferred to microtubes. Microtubes were mixed on a vortex mixer and allowed to incubate at 4°C for 10 minutes to complete metabolite extraction. Samples were mixed a second time, and then centrifuged at 14,000 RPM for 10 minutes at 4°C. From each sample, an aliquot of 100 µL of the extraction solvent was transferred to an autosampler vial for liquid chromatography-mass spectrometry (LC-MS) analysis. A volume of 10 µL of each sample was removed and pooled in a separate autosampler vial for a separate run for quality control purposes.

Liquid chromatography-mass spectrometry (LC-MS) analysis

Glycolysis, tricarboxylic acid, pentose phosphate pathway, and additional analyses were performed on an Agilent system consisting of a 1290 UPLC coupled with a 6520 Quadrupole-Time-of-flight (QTOF) mass spectrometer (Agilent Technologies, Santa Clara, CA). Metabolites

were separated on a 150 x 1 mm Luna NH$_2$ Hilic column (Phenomenex, Torrance, CA) using 10 mM ammonium acetate in water, adjusted to pH 9.9 with ammonium hydroxide, as mobile phase A. Acetonitrile was used as mobile phase B. The flow rate was 0.075 mL/minute and the gradient was linear from 20% to 100% mobile phase A over 15 minutes, followed by isocratic elution at 100% mobile phase A for 5 minutes. The system was returned to starting conditions (20% mobile phase A) and held there for 10 minutes to allow for column re-equilibration before injecting another sample. The mass spectrometer was operated in ESI negative mode according to previously published conditions (Lorenz *et al.*, 2011).

Data processing

Data were processed using MassHunter Quantitative analysis version B.07.00. Metabolites in the glycolysis, tricarboxylic acid, and pentose phosphate pathways were normalized to the nearest isotope-labeled internal standard and quantitated using two replicated injections of five standards to create a linear calibration curve with high accuracy for each standard. The locally estimated scatterplot smoothing (LOESS) method (Dunn *et al.*, 2011; Thonusin *et al.*, 2017) was used as a signal and drift correction method using Metabodrift (Thonusin *et al.*, 2017). Because of the presence of internal standards, quantities arising from this method are reported in absolute concentrations. These absolute concentrations were normalized to protein mass to arrive at a reporting unit of pmol metabolite per µg protein and used in data analyses. Other compounds in the analysis were normalized to the nearest internal standard, and the peak areas were used for differential analysis between groups. The LOESS method using Metabodrift (Dunn *et al.*, 2011; Thonusin *et al.*, 2017) was also utilized as a signal and drift correction method for these data. Data from this method of processing were reported in the unit of relative responses (RR) and were used in data analyses.

Some metabolites were detected more than once. Guanosine monophosphate (GMP) and phosphoenolpyruvate (PEP) were detected as both absolute concentrations and relative responses: in both cases, the values from the absolute concentrations were used because of decreased total variance (for each metabolite, defined as the aggregate of the variance from each experimental group). Also, 3-phosphoserine was detected twice using the method with relative response with similar values within each treatment group: the second set of values, which had lower variance within each treatment group, was used in the current study.

Pathway analysis

Pathway analysis was performed using Metaboanalyst 4.0 (Chong *et al.*, 2018; Chong *et al.*, 2019) and selecting *Homo sapiens* (KEGG) within the pathway library. Because pathway analysis could only be performed for comparison of two groups, four sets of comparisons were made: (1) Vehicle control (0.1% DMSO) versus forskolin, (2) forskolin versus forskolin + 10 µM DCVC, (3) forskolin versus forskolin + 20 µM DCVC, and (4) forskolin + 10 µM DCVC versus forskolin + 20 µM DCVC. Because of the non-Gaussian distribution of the processed data, data were generalized log-transformed prior to analysis. Other choices made within the program include: Pathway enrichment analysis (global test as opposed to global ANCOVA); and pathway topology analysis (relative between-ness centrality as opposed to out-degree centrality).

Detection of MMP-1, MMP-2, MMP-3, and MMP-9 in media

BeWo cells were plated at a 200,000 cells/well density in 2 mL/well of 6-well tissue culture plates (Corning, Corning, NY) and allowed to adhere for 24 hours before treatment. Upon completion of treatment, medium was collected and stored at -80°C until further processing. Protein was collected in a lysis buffer featuring 0.5% (v/v) IGEPAL CA-630 (Sigma-Aldrich, St. Louis, MO), 250 mM NaCl (Sigma-Aldrich, St. Louis, MO), and 5% (v/v) of Tris-

HCl (1 M, pH 7.4). Protein concentration was measured using the Pierce bicinchoninic acid (BCA) protein assay kit (Thermo Fischer Scientific, Waltham, MA) according to the manufacturer's protocol, to allow for analyte concentration normalization to mass of protein. Directly prior to delivery, the media samples were thawed and pipetted into round-bottom 96-well plates, and then submitted to the University of Michigan Immunologic Monitoring Core. The Immunologic Monitoring Core performed enzyme-linked immunosorbent assays to detect the analytes of interest using Duosets (R&D Systems, Minneapolis, MN) according to the manufacturer's recommended protocol.

Enrichment analyses

Enrichment analyses for location and drug pathway were performed using Metaboanalyst 4.0 (Chong *et al.*, 2018; Chong *et al.*, 2019). The library for the location enrichment analysis contained 73 metabolite sets pertaining to organ, tissue, or subcellular localization. The library for the drug pathway enrichment analysis contained 461 metabolite sets pertaining to drug pathways. All enrichment analyses were done using the same types of comparisons as in pathway analysis and performed on the processed data that subsequently underwent generalized log-transformation.

Statistical analysis

The sample size from all experiments in the current study is five independent replicates. To analyze up- or down-regulated individual metabolites, statistical analysis was conducted using unpaired two-tailed t-tests in the case of the forskolin treatment to vehicle (0.1% v/v DMSO) comparison to investigate the impact of syncytialization. In the case of the comparison of the forskolin alone, forskolin + 10 µM DCVC, and forskolin + 20 µM DCVC treatment groups, statistical analysis was conducted using one-way analysis of variance (ANOVA)

followed by Tukey's post-hoc comparison of means. The data from the same forskolin group

was used in all analyses. All processed metabolomics data were generalized log-transformed

prior to statistical analysis because of non-Gaussian distribution, with the exception of ratio data,

which used the processed but not generalized log-transformed data in order to obtain accurate

ratios. Pathway and enrichment analyses were conducted using Metaboanalyst 4.0 (Chong *et al.*,

2018; Chong *et al.*, 2019) with the settings described in the respective previous sections, and also

consisted of generalized log-transformation of the processed data for comparison of two

treatment groups at a time. Statistical analyses were performed using GraphPad Prism 7

(GraphPad Software Inc.; San Diego, CA, USA), with the exception of the analyses from

Metaboanalyst 4.0, which automatically computed p-values. P-values computed by

Metaboanalyst 4.0 were adjusted for multiple comparisons (Chong *et al.*, 2019) and were similar

in magnitude to those computed by GraphPad Prism 7.0, whether from t-tests for one-way

ANOVA.

Results

Quantity of metabolites measured

A total of 54 metabolites were measured from the BeWo cells using the TCA plus

metabolomics platform, and concentrations or relative responses are listed in **Table S6.1**. Each

of the following sets of metabolites was detected as an aggregate (i.e., within the set, it was not

possible to distinguish one from the other): (1) citrate and isocitrate, (2) fructose 6-phosphate and

glucose 6-phosphate, (3) ribose 5-phosphate and xylulose 5-phosphate, (4) leucine and

isoleucine, and (5) hexose (glucose etc.). Each of these sets was considered as one metabolite in

the counting of total. Additionally, the aforementioned sets were excluded from pathway and

enrichment analyses because those analyses could not assign an aggregate of metabolites to a

specific compound. Three metabolites were counted more than once, as further discussed in the methods section along with what set of values were used; these metabolites were not double-counted in the total number (54) of detected metabolites.

Metabolites altered by forskolin-stimulated syncytialization

The effect of forskolin-stimulated syncytialization on metabolites was assessed by comparing forskolin-only treatment to vehicle control (**Figure 6.2A**). Forskolin treatment altered nine of the 54 detected metabolites (**Figure 6.3; Table S6.2**). Five out of the nine alterations were decreases, and four of the nine alterations were increases. Interestingly, two of the increases were monophosphate products: adenosine monophosphate and guanine monophosphate. Analysis of fold-change versus p-value in response to forskolin treatment revealed that 32 metabolites had a fold-change less than one but that eight metabolites had a fold-change greater than 2.

Metabolites altered by DCVC treatment during forskolin-stimulated syncytialization

To investigate if DCVC exposure could alter metabolites during forskolin-stimulated syncytialization, treatment with 10 or 20 µM DCVC was compared with forskolin-only treatment. Exposure to 10 µM DCVC during forskolin-stimulated syncytialization decreased two metabolites. Analysis of fold-change versus p-value indicates that 37 of the 54 metabolites had a fold-change less than one in the same comparison (**Figure 6.2B; Table S6.2**). Exposure to 20 µM DCVC during forskolin-stimulated syncytialization decreased seven metabolites. In this comparison, 37 of the 54 metabolites had a fold-change less than one (**Figure 6.2C; Table S6.2**). Concentration-dependent changes in metabolites were observed for DCVC exposure during forskolin-stimulated syncytialization: comparison of the 20 µM DCVC group to the 10 µM DCVC group revealed that 20 µM DCVC decreased two metabolites. In this comparison, 20 out

279

of 54 metabolites had a fold-change less than one (**Figure 6.2D; Table S6.2**). Whereas both metabolites changed by 10 µM DCVC were also within the seven metabolites changed by 20 µM DCVC relative to forskolin-only treatment, one of the metabolites changed in the 20 µM DCVC versus 10 µM DCVC comparison was not included in the seven metabolites changed in the 20 µM DCVC to forskolin-only treatment comparison (**Table S6.2**).

Associations of metabolites changed by syncytialization versus metabolites changed by DCVC treatment during syncytialization

Among the metabolites significantly altered by syncytialization (comparing forskolin-only and vehicle control groups), three metabolites (oleic acid, aspartate, and uridine diphosphate D-glucose) were also significantly altered by DCVC treatment during syncytialization (**Figure 6.3**). Oleic acid decreased by 40.5% with 20 µM DCVC (p=0.0344), whereas a 69.2% increase was seen with syncytialization (forskolin-only treatment) (p=0.0152). In the case of aspartate and uridine diphosphate D-glucose, 20 µM DCVC further decreased (by 40.2% and 44.2%, respectively; p=0.0310 and 0.0255, respectively) concentrations seen with syncytialization (forskolin-only treatment) (by 38.5% and 57.3%, respectively; p=0.0068 and 0.0060, respectively). We next visualized associations between metabolite fold-changes across different comparisons to assess changes associated with syncytialization versus changes associated with DCVC treatment during syncytialization. Comparison of fold change of 10 µM DCVC co-treatment versus 20 µM DCVC co-treatment led to statistically significant association (p<0.0001 for Spearman correlation), indicating that changes stimulated by 10 µM DCVC co-treatment are similar to changes stimulated by 20 µM DCVC co-treatment (**Figure 6.4A**). Neither comparison of 10 or 20 µM DCVC treatment to syncytialization by itself were statistically significant (p=0.1182 and 0.9893 for Spearman correlation, respectively) (**Figures 6.4B and 6.4C**).

KEGG pathway analysis

Our data input identified 47 pathways that were able to be analyzed by Metaboanalyst 4.0 (**Figure 6.5A**). Of these, 13 pathways were statistically altered in response to forskolin treatment to induce syncytialization (p<0.05). Four of these 13 pathways had a corresponding pathway impact above 0.1, indicating that measured metabolites had relevance to those pathways. Impacted pathways included histidine metabolism (p=0.0038; pathway impact=0.2213), ascorbate and aldarate metabolism (p=0.0120; pathway impact=0.5), pentose and glucuronate interconversions (p=0.0120; pathway impact=0.2031), and amino sugar and nucleotide sugar metabolism (p=0.0120; pathway impact=0.1031). Six of the 13 statistically altered pathways had a corresponding pathway impact of 0, which indicates that very few, if any, of the important metabolites in the pathway were detected.

Because Metaboanalyst limited pathway analysis to comparison of two groups, three comparisons were undertaken to assess alterations by DCVC treatment during syncytialization. Exposure to 10 µM DCVC significantly increased one pathway, arginine and proline metabolism, relative to forskolin-only treatment (p=0.0262, pathway impact=0.2744). Three additional pathways (starch and sucrose metabolism, galactose metabolism, and pyrimidine metabolism) had p-values between 0.05 and 0.06 (**Figure 6.5B**).

Following treatment with 20 µM DCVC during syncytialization, 16 pathways were statistically significantly altered in comparison with forskolin-only treatment. Eight out of the 16 pathways had a pathway impact above 0.1: (1) pyrimidine metabolism (p=0.000015; pathway impact=0.1305), (2) arginine and proline metabolism (p=0.0006; pathway impact=0.2744), (3) ascorbate and aldarate metabolism (p=0.0029; pathway impact=0.5), (4) pentose and glucuronate interconversions (p=0.0029; pathway impact=0.2031), (5) amino sugar and nucleotide sugar

metabolism (p=0.0029; pathway impact=0.1031), (6) alanine, aspartate and glutamate metabolism (p=0.0055; pathway impact=0.5345), (7) arginine biosynthesis (p=0.0184; pathway impact=0.1777), and (8) histidine metabolism (p=0.0202; pathway impact=0.2213). Five of the 16 identified pathways had a pathway impact of 0 (metabolites analyzed in the pathway were few and/or unimportant). For the third comparison of 10 µM DCVC versus 20 µM DCVC during syncytialization, none of the 54 pathways achieved statistical significance. The lowest p-value for that comparison was 0.05904 in the case of fatty acid biosynthesis (pathway impact=0), and the next lowest was for pyrimidine metabolism (p=0.0650; pathway impact=0.1305).

Analysis of metabolite ratios within pathways

To distinguish specific points within metabolic pathways, ratios between known consecutive metabolites of a pathway were analyzed. Additionally, ratios of biological importance, such as ratios of metabolites near the beginning and end of a pathway, were assessed. The totality of metabolite ratios analyzed are listed in **Tables S6.3 through S6.7** along with their treatment-dependent fold changes and p-values. Details within specific pathways are presented in subsequent sections. In totality of analysis, forskolin-stimulated syncytialization (forskolin-only treatment) significantly changed 16 of 48 ratios analyzed (p<0.05). Treatment with 20 µM DCVC during syncytialization significantly changed 18 of the 48 ratios (p<0.05). Both 10 and 20 µM µM DCVC changed 5 of the 18 ratios relative to forskolin-only treatment. Comparison of 20 µM DCVC treatment versus 10 µM DCVC treatment during syncytialization identified 8 of the 18 ratios significantly altered with one additional change that was not observed in the 20 µM DCVC treatment comparison to forskolin-only treatment. Of the ratios changed by forskolin or any comparison within DCVC co-treatment, nine (adenosine triphosphate (ATP) to adenosine diphosphate (ADP), ADP to adenosine monophosphate (AMP),

citrate and isocitrate to succinate, phosphoenolpyruvate to succinate, ornithine to proline, histidine to aspartate, phenylalanine to succinate, oleic acid to palmitic acid, and uridine diphosphate (UDP)-D-glucose to uridine monophosphate (UMP)) were in common to each other. In the case of citrate and isocitrate to succinate, phosphoenolpyruvate to succinate, histidine to aspartate, phenylalanine to succinate, and ornithine to proline, DCVC treatment during syncytialization served to further a change in the same direction as that produced by syncytialization. However, in the case of ATP to ADP, ADP to AMP, UDP-D-glucose to UMP, and oleic acid to palmitic acid, DCVC treatment during syncytialization made changes in the opposite direction as the change with syncytialization.

Analysis of metabolite ratios within the purine and pyrimidine metabolism pathway

Metabolite ratios altered within the purine and pyrimidine metabolism pathways are shown in **Figures 6.6 and 6.7,** and in **Table S6.3**. Forskolin-stimulated syncytialization (forskolin-only treatment) altered the following ratios: ATP to ADP (56.6% decrease, p=0.0410), ADP to AMP (50.8% decrease, p=0.0051), GDP to GMP (57.0% decrease, p=0.0096), and UDP to CMP (42.1% decrease, p=0.0218) (**Figures 6.6B, 6.6C, 6.6E, and 6.7C**, respectively). Treatment with 20 µM DCVC during syncytialization altered the following ratios relative to forskolin-only treatment: ATP to ADP (51.4% increase, p=0.0142), ADP to AMP (72.8% increase, p=0.0049), ATP to AMP (166.7% increase, p=0.0086), UMP to cytidine monophosphate (CMP) (42.6% decrease, p<0.0001), and glutamine to UMP (243.1% increase, p<0.0001) (**Figures 6.6B, 6.6C, 6.6D, 6.7B, and 6.7D**, respectively). Metabolite ratio analysis comparing 20 µM DCVC versus 10 µM DCVC treatment during syncytialization revealed the following differences: ADP to AMP (65.8% increase, p=0.0074), ATP to AMP (117.4% increase, p=0.0209), UMP to CMP (31.3% decrease, p<0.0001), glutamine to UMP (136.6%

increase; p=0.0001), and inosine to hypoxanthine (55.6% decrease, p=0.0484) (**Figures 6.6C, 6.6D, 6.7B, 6.7D, and 6.6F**, respectively). DCVC treatment at 10 µM during syncytialization altered the UMP to CMP ratio relative to forskolin only treatment (16.5% decrease, p=0.0010) (**Figure 6.7B**).

Analysis of metabolite ratios within the glycolysis, tricarboxylic acid (TCA) cycle, and pentose phosphate pathways

Ratios analyzed within glycolysis, the TCA cycle, and pentose phosphate pathway are in **Figures 6.8, 6.9, 6.10, and Table S6.4**. Metabolite ratios specific to glycolysis that were changed only included a decrease in the fructose 1,6-bisphosphate to phosphoenolpyruvate ratio in the case of forskolin-stimulated syncytialization (forskolin-only treatment) relative to its control (0.1% DMSO) (48.7% decrease, p=0.0024) (**Figure 6.8B**). Although a change in response to forskolin treatment occurred within a specific portion of the glycolysis pathway, to understand if glycolysis as a whole was impacted, the ratio of glucose 6-phosphate and fructose 6-phosphate (early in glycolysis) to phosphoenolpyruvate (late in glycolysis) for each sample was analyzed. This ratio was not changed in response to forskolin exposure (p=0.4974) (**Table S6.4**). Relative to forskolin-only treatment, no DCVC treatment during syncytialization changed this ratio (lowest p-value was 0.8680 in the case of the 10 µM DCVC versus 20 µM DCVC treatment during syncytialization comparison) (**Table S6.4**).

Within the TCA cycle, the citrate and isocitrate to succinate ratio was decreased in response to forskolin treatment (54.1% decrease, p=0.0061) and when 10 µM DCVC treatment during syncytialization and 20 µM DCVC treatment during syncytialization were each compared to syncytialization alone (49.3% and 47.1% decrease, respectively; p=0.0011 and p=0.0015, respectively) (**Figure 6.9B**). The phosphoenolpyruvate to succinate ratio was decreased by

forskolin treatment (50.2% decrease, p=0.0007) and 20 µM DCVC treatment during syncytialization compared to forskolin-only treatment (55.8% decrease, p=0.0103) (**Figure 6.9C**). Forskolin treatment did not change any of the ratios we calculated for the pentose phosphate pathway. However, two of the ratios for the pentose phosphate pathway, ribose 5-phosphate and xylulose 5-phosphate to 6-phosphogluconate and ribose 5-phosphate and xylulose 5-phosphate to sedoheptulose 7-phosphate, were decreased for the 20 µM DCVC treatment during syncytialization to forskolin-only treatment comparison (75.1% and 68.7% decrease, respectively; p=0.0455 and 0.0090, respectively) (**Figures 6.10B and 6.10C**, respectively).

Analysis of metabolite ratios within amino acid metabolism pathways

Analysis of amino acid metabolism pathways are included in **Figures 6.11, 6.12, 6.13, 6.14, and Table S6.5**. Forskolin-stimulated syncytialization (forskolin-only treatment) changed the following three metabolite ratios: Glutamate to succinate (73.6% decrease, p=0.0029), histidine to aspartate (63.1% increase, p=0.0046), ornithine to proline (42.6% increase, p=0.0030), phenylalanine to succinate (68.8% decrease, p=0.0053), and taurine to alanine (34.4% decrease, p=0.0138) (**Figures 6.11C, 6.12C, 6.13B, 6.14B, and Table S6.5**, respectively). The asparagine to aspartate ratio was increased in the 20 µM DCVC treatment during syncytialization group compared to the forskolin-only treatment and the 10 µM DCVC treatment during syncytialization groups (61.7% and 63.5% increase, respectively; p=0.0366 and 0.0335, respectively) (**Figure 6.11B**). The ornithine to proline ratio was increased in the 10 µM DCVC and 20 µM DCVC treatments during syncytialization groups relative to the forskolin-only treatment group (65.1% and 109.6% increase, respectively; p=0.0091 and 0.0001, respectively) (**Figure 6.13B**). The histidine to aspartate ratio was increased in the 20 µM DCVC treatment during syncytialization group comparison to the forskolin-only treatment and the 10

μM DCVC treatment during syncytialization groups (61.4% and 51.1% increase, respectively; p=0.0195 and 0.0369, respectively) (**Figure 6.12C**). The phenylalanine to succinate ratio was decreased in the 10 μM DCVC and 20 μM DCVC treatments during syncytialization groups relative to the forskolin-only treatment group (54.3% and 63.7% decrease, respectively; p=0.0152 and 0.0054, respectively) (**Figure 6.14B**).

Analysis of metabolite ratios within glutathione metabolism

Analysis of glutathione metabolism is included in **Figure 6.15 and Table S6.6**. Only one calculated ratio for glutathione (GSH) metabolism was altered: Glutathione disulfide to nicotinamide adenine dinucleotide phosphate. This ratio was decreased with forskolin-stimulated syncytialization (forskolin-only treatment) (57.9% decrease, p=0.0487), and none of the comparisons with DCVC treatment during syncytialization altered this ratio (**Figure 6.15B**).

Analysis of other metabolite ratios of interest

Additional analysis of metabolites ratios as they relate to pathways is included in **Figure 6.16 and Table S6.7**. Other metabolite ratios altered by forskolin-stimulated syncytialization (forskolin-only treatment) included the following: Oleic acid to palmitic acid (99.8% increase, p=0.0104), UDP-D-glucose to UDP-D-glucuronate (31.7% decrease, p=0.0272), and UDP-D-glucose to UMP (58.1% decrease, p=0.0266) (**Table S6.7**). A few other metabolite ratios were altered in comparisons involving DCVC treatment during syncytialization. DCVC treatment at 20 μM during syncytialization altered the following ratios relative to forskolin-only treatment: Phosphocreatine to ATP (82.4% decrease, p=0.0074) (**Figure 6.16B**), phosphocreatine to ADP (72.0% decrease, p=0.00126) (**Figure 6.16C**), stearic acid to oleic acid (116.9% increase, p=0.0072) (**Table S6.7**), oleic acid to palmitic acid (53.5% decrease, p=0.0148) (**Table S6.7**), and UDP-D-glucose to UMP (100.6% increase, p=0.0091) (**Table S6.7**). DCVC treatment at 10

µM during syncytialization decreased the phosphocreatine to ATP ratio relative to forksolin only treatment (59.7% decrease, p=0.0465) (**Figure 6.16B**). DCVC treatment at 20 µM during syncytialization altered the following ratios relative to DCVC treatment at 10 µM during syncytialization: Stearic acid to oleic acid (72.0% increase, p=0.0324) and UDP-D-glucose to UMP (84.1% increase, p=0.0163) (**Table S6.7**). It is noteworthy that both of the ratios consisting of phosphocreatine were only altered when performing the comparisons involving DCVC treatment compared to forskolin-only treatment and not when investigating forskolin-only treatment compared to vehicle (0.1% DMSO).

Effects of syncytialization and DCVC during syncytialization on concentrations of matrix metalloproteinases (MMP)-1, MMP-2, MMP-3, and MMP-9 in media

Changes in media concentrations of the matrix metalloproteinases MMP-1, MMP-2, MMP-3, and MMP-9 due to syncytialization and DCVC treatment are shown in **Figure 6.17**. Forskolin-stimulated syncytialization (forskolin-only treatment) increased MMP-2 379.6% (p=0.0001), an effect that was reduced by DCVC treatment at 20 and 50 µM during syncytialization relative to forskolin-only treatment (44.2% and 68.6% decrease, respectively; p=0.0351 and 0.0007, respectively) (**Figure 6.17B**). Treatment with 50 µM DCVC during syncytialization increased MMP-1 relative to control (forskolin-only treatment) by 340.5% (p=0.0299) (**Figure 6.17A**). Neither syncytialization nor DCVC treatment during syncytialization significantly changed MMP-3 or MMP-9 (**Figures 6.17C and 6.17D**, respectively).

Enrichment analysis identifying organs, tissues, or subcellular structures altered by syncytialization

Our input data of metabolites led to the corresponding analysis of 28 organs, tissues, or subcellular structures that could be associated with the effects of forskolin-stimulated syncytialization on detected metabolites (**Table S6.8**). Out of these 28, eight were statistically significant (p<0.05) in the comparison of forskolin-only treatment to vehicle control (0.1% DMSO). The top five were liver (p=0.0062), endoplasmic reticulum (p=0.0069), peroxisome (p=0.0078), Golgi apparatus (p=0.0120), and heart (p=0.0233).

Enrichment analysis identifying organs, tissues, or subcellular structures altered by DCVC during syncytialization

The same comparison groups used in the corresponding pathway analysis section were used here to assess impacts of DCVC exposure during syncytialization (**Tables S6.9, S6.10, and S6.11**). Comparison of the 10 µM DCVC treatment during forskolin-stimulated syncytialization with the forskolin-only treatment comparison revealed only one out of 28 organs, tissues, or subcellular structures that was significantly altered (thyroid gland; p=0.0161) (**Table S6.9**). For the 20 µM DCVC treatment during syncytialization versus forskolin-only treatment comparison, 13 out of the 28 structures were significantly altered – the top five were placenta (p=0.000065), skin (p=0.00093), Golgi apparatus (p=0.0029), thyroid gland (p=0.0031), and mitochondria (p=0.0040) (**Table S6.10**). For the 20 µM DCVC treatment versus 10 µM DCVC treatment during syncytialization comparison, two out of the 28 were significantly altered. The top two were kidney (p=0.0290) and erythrocyte (p= 0.0474) (**Table S6.11**). The p-values corresponding to placenta for the first and third-mentioned comparisons were 0.2248 and 0.1391, respectively.

Enrichment analysis identifying drug pathways altered by syncytialization

There were 357 drug pathways analyzed for association with forskolin-stimulated syncytialization from our input data of metabolites. Of these 357 drug pathways, 13 appeared as significantly altered by forskolin treatment. The lowest p-value from this set was 0.0277, and eleven pathways shared this p-value. The names of these pathways are reported in **Table S6.12**.

Enrichment analysis identifying drug pathways altered by DCVC during syncytialization

The set of three comparisons mentioned previously in this results section is relevant here, as well, for analysis of drug pathways as associated with DCVC treatment during syncytialization (**Tables S6.13, S6.14, and S6.15**). For the 10 µM DCVC treatment during syncytialization versus forskolin-only treatment comparison, four out of the 357 drug pathways were significantly altered: these included morphine metabolism pathway (p=0.0274), sorafenib metabolism pathway (p=0.0274), celecoxib metabolism pathway (p=0.0356), and ibuprofen metabolism pathway (p=0.0356) (**Table S6.13**). For the 20 µM DCVC treatment during syncytialization versus forskolin-only treatment comparison, 52 out of the 357 drug pathways were significantly altered (**Table S6.14**): the lowest p-value from this set was 0.00038, which 30 pathways shared. For the 20 µM DCVC treatment versus 10 µM DCVC treatment during syncytialization comparison, none of the 357 drug pathways were significantly altered. The lowest p-value from this set was 0.1526, which four pathways shared (**Table S6.15**).

Discussion

This study provides novel information regarding metabolic changes during placental cell syncytialization and the impact of DCVC, a metabolite of TCE, on energy metabolism during syncytialization. The major changes in energy metabolism observed in the present study are summarized in **Figure 6.18**, which provides a proposed model of how DCVC treatment during

syncytialization impacts energy metabolism. **Figure 6.18** also highlights multiple KEGG

pathway regions that could be deserving of further investigation, such as arginine biosynthesis.

DCVC treatment during syncytialization affected multiple endpoints that were affected by

syncytialization by itself, especially with regard to the pathway and metabolite ratio analyses.

Metabolites altered

Our findings of altered metabolites with forskolin-stimulated syncytialization (forskolin-

only treatment) and DCVC treatment during syncytialization provides insight into specific

metabolites and classes of metabolites in energy metabolism changed by syncytialization and

DCVC. Thematically, forskolin-stimulated syncytialization decreased abundance of cellular

acidic amino acids (e.g., glutamate and aspartate) and increased abundance of purine

monophosphates (adenosine monophosphate (AMP) and guanosine monophosphate (GMP)). On

the other hand, DCVC treatment during syncytialization decreased pyrimidine phosphates

(uridine diphosphate (UDP), uridine monophosphate (UMP), and cytidine monophosphate

(CMP)) and altered the abundance of other metabolites not part of a specific energy metabolite

group. Similar to our findings, forskolin does not affect amino acid system transporter A (SysA),

which mediates the transport of neutral amino acids (Novak *et al.*, 2006). Changes in energy

metabolites in BeWo cells undergoing syncytialization is consistent with energy utilization and

protein turnover previously observed in slime molds multinucleation (Wright and Anderson,

1959; Liddel and Wright, 1961). Likewise, our results support findings that DCVC modifies

energy metabolism outcomes in HTR-8/SVneo placental cells (Elkin *et al.*, 2020). However, the

impact of forskolin on transport of acidic and basic amino acids has not been investigated

previously, and our data suggest that acidic amino acids could be a target for forskolin-

stimulation. Investigations of transport and mechanisms surrounding this could be a worthy future direction.

From prior studies, it is known that forskolin activates adenylate cyclase to increase intracellular cyclic AMP (cAMP) (Daly, 1984). Although we did not measure cAMP directly, it is plausible that our data on increased AMP is a consequence of the increased cAMP breakdown by cyclic nucleotide phosphodiesterase (Nair, 1966; Fischer and Amrhein, 1974) into AMP. Whether phosphodiesterase activity increases more than other enzymes stimulated by cAMP is not presently clear, however. Our data showing increased GMP following syncytialization could be a consequence of increased phosphodiesterase activity, perhaps by cAMP stimulation, in converting cyclic GMP (cGMP) to GMP. However, the role of forskolin on GMP or cGMP has not been previously studied in BeWo cells.

The impact of DCVC treatment on energy metabolites during forskolin-stimulated syncytialization is generally consistent with prior reports of DCVC effects on placental cells, while contributing new information about possible mechanisms of action. The finding that DCVC altered pyrimidine phosphates (UDP, UMP and CMP) has not been previously reported. Because oleic acid is protective against apoptosis in syncytiotrophoblasts (Colvin *et al.*, 2017), the oleic acid decrease we observed might have a role in the DCVC-stimulated apoptosis in HTR-8/SVneo placental cells (Elkin *et al.*, 2018) and BeWo cells (Chapter 4). Additionally, proline and aspartate, both decreased by DCVC treatment during syncytialization, have important roles in pregnancy. Proline is crucial for polyamine synthesis during pregnancy and has been suggested to ameliorate intrauterine growth restriction (Wu *et al.*, 2005; Wu *et al.*, 2008). Aspartate is also decreased in cases of early-onset preeclampsia (Kawasaki *et al.*, 2019)

and, in addition to glutamate, preferentially locates in placenta as opposed to maternal or fetal circulation (Hoeltzli *et al.*, 1990).

Of three metabolites altered by both forskolin treatment and DCVC treatment during syncytialization, the change produced by DCVC treatment further decreased the response to forskolin treatment for two metabolites (aspartate and UDP-D-glucose) and suppressed an increased response to forskolin treatment for one metabolite (oleic acid). These findings highlight that DCVC exposure during syncytialization failed to elicit many changes in metabolites altered by syncytialization, and that the direction of change could either be exacerbation or reversal of the syncytialization effect. Furthermore, changes stimulated by syncytialization did not correlate well with changes stimulated by DCVC treatment during syncytialization. The conclusion is also consistent with our finding that of 14 metabolites altered by forskolin-stimulated syncytialization or any comparison involving DCVC treatment during syncytialization, eight metabolites were altered by DCVC treatment, nine metabolites were altered by forskolin treatment, and three metabolites were altered in both cases. In contrast, changes stimulated by different concentrations of DCVC correlated well with each other.

Purine and pyrimidine metabolism

Ratio analysis within the purine metabolism pathway revealed that forskolin-stimulated syncytialization increased the formation of ATP relative to ADP, which was increased relative to AMP. DCVC treatment during syncytialization reversed all those forskolin-stimulated changes. Although the increased AMP relative to ADP stimulated by syncytialization was not unexpected given the role of forskolin as increasing cAMP (Daly, 1984; Wice *et al.*, 1990), the finding that DCVC treatment during syncytialization reversed this hallmark of forksolin-stimulated syncytialization is novel. Because extracellular ATP is known to be vasoconstrictive and pro-

inflammatory during pregnancy (Spaans *et al.*, 2014) and causes albuminuria with pro-inflammatory response in rats (Faas *et al.*, 2010), it is plausible that the DCVC-stimulated effect would be detrimental for pregnancy. Future directions can serve to further characterize pregnancy-related outcomes resulting from DCVC exposure during pregnancy, understand how extracellular ATP is manifest in intracellular ATP, and investigate the relationship between DCVC and enzymes involved in conversion between the adenosine phosphates, such as CD39, CD73, and alkaline phosphatase (Spaans *et al.*, 2014). Interestingly, syncytialization also increased GMP relative to GDP, showing that guanosine phosphates may also be as relevant to syncytialization. The mechanism linking changes in adenosine phosphates with changes in guanosine phosphates remain unknown in the context of syncytialization.

Ratios analyzed within the pyrimidine metabolism pathway revealed that forskolin-stimulated syncytialization favored the formation of CMP relative to UDP whereas DCVC treatment during syncytialization favored the formation of CMP and glutamine relative to UMP. We suggest these changes in pyrimidine metabolism stimulated by DCVC during syncytialization, especially regarding glutamine, could be an adaptive response to improve pregnancy outcome. In support of this, glutamine has been proposed to improve pregnancy outcomes in mice and other mammals (Ren *et al.*, 2013; Wu *et al.*, 2015), reduces alcohol-stimulated maternal hypercapnia during pregnancy (Sawant *et al.*, 2014), and appropriate levels prevent hypoglycemia during pregnancy (Metzger *et al.*, 1971). However, the roles of UMP, UDP, or CMP in pregnancy remain outstanding questions and their understanding would be needed to further place these findings in context.

Glycolysis, tricarboxylic acid (TCA) cycle, and pentose phosphate pathways

Despite the inability of forskolin-stimulated syncytialization or DCVC treatment during syncytialization to affect glycolysis or gluconeogenesis in pathway analysis by Metaboanalyst (p>0.05), forskolin treatment altered a portion of glycolysis. Specifically, the ratio of fructose 1,6-bisphosphate to phosphoenolpyruvate was decreased by forskolin treatment. Although these are not consecutive metabolites in glycolysis, the possibility exists that syncytialization preferentially shifted glycolysis overall to favor the late portion of glycolysis (e.g., phosphoenolpyruvate) as opposed to the earlier portion of glycolysis (e.g., fructose 1,6-bisphosphate). Investigation of additional metabolites in glycolysis would address that possibility. Additionally, the change in metabolite ratio could be attributable to a substrate that feeds into phosphoenolpyruvate but not fructose 1,6-bisphosphate, such as oxaloacetate and 2-phospho-D-glycerate (Holt and Wold, 1961; Chang and Lane, 1966; Bar-Even *et al.*, 2012), which were not measured in the current study.

For the TCA cycle, ratio analysis indicated that both forskolin-stimulated syncytialization and DCVC treatment during syncytialization favored the production of succinate relative to phosphoenolpyruvate and citrate and isocitrate. Whereas succinate is a direct precursor of succinyl coenzyme A (Hager, 1962), isocitrate can be converted to 2-oxoglutarate (Plaut and Sung, 1954), which can be converted to succinyl coenzyme A (Kerscher and Oesterhelt, 1981a; Kerscher and Oesterhelt, 1981b). Succinyl coenzyme A was not measured in the current study, and its measurement would be needed to further conclusions about the impact of DCVC on the TCA cycle. The pentose phosphate pathway was a pathway in which DCVC treatment during syncytialization favored production of 6-phosphogluconate and sedoheptulose 7-phosphate relative to ribose 5-phosphate and xylulose 5-phosphate. Future analysis can consider the role of

6-phosphogluconate dehydrogenase, which converts 6-phosphogluconate into 6-ribulose 5-phosphate (Dickens and Glock, 1951; Yoon *et al.*, 1989), which can be converted to D-xylulose 5-phosphate by an epimerase (Dickens and Williamson, 1956). Identification of the relationship between DCVC and these enzymes can help inform the mechanism of action of DCVC.

Amino acid and glutathione metabolism

Forskolin-stimulated syncytialization favored the abundance of (1) histidine relative to aspartate, (2) succinate relative to glutamate, (3) nicotinamide adenine dinucleotide phosphate (NADP) relative to glutathione disulfide (GSSG), (4) succinate relative to phenylalanine, and (5) ornithine relative to proline. In contrast, DCVC treatment during syncytialization favored abundance of (1) asparagine relative to aspartate, (2) histidine relative to aspartate, (3) succinate relative to phenylalanine, and (4) ornithine relative to proline. With regard to the ornithine to proline ratio that is within the arginine metabolism pathway, the direction of change by both syncytialization and DCVC treatment during syncytialization was towards the direction of increased arginine and nitric acid as opposed to proline. Because arginine has been suggested to promote embryonic survival (Zeng *et al.*, 2008) and is a treatment for preeclampsia because of its role as a precursor of the vasodilator nitric oxide (Aouache *et al.*, 2018), the current study would have benefitted from actual detection of arginine or other metabolites that are located closer to nitric oxide in the arginine metabolism pathway. These detections could further knowledge about the relationship of syncytialization or DCVC treatment to vasodilation or vasoconstriction during pregnancy.

The finding that DCVC treatment during syncytialization increased aspartate relative to asparagine may be relevant to pregnancy. Asparagine has been implicated to be important in rat fetal growth (Newburg and Fillios, 1979), so it may be possible that the increase in the

asparagine to aspartate ratio stimulated by DCVC treatment during syncytialization could be a compensatory change in amino acid supply. Additional metabolite ratios in amino acid metabolism altered in the current study have implications for adverse pregnancy outcomes. These include decreased succinate as associated with preeclampsia (Bahado-Singh *et al.*, 2012; Bahado-Singh *et al.*, 2015) and decreased phenylalanine as also associated with preeclampsia (Bahado-Singh *et al.*, 2012; Bahado-Singh *et al.*, 2015). Additionally, the finding that DCVC treatment during syncytialization altered three ratios (histidine to aspartate, succinate to phenylalanine, and ornithine to proline) in the same direction as syncytialization and no ratios the other way around was notable. This suggests that on the level of amino acid metabolism, DCVC treatment during syncytialization could more likely be further promoting syncytialization as opposed to opposing syncytialization.

The finding that forskolin-stimulated syncytialization increased the NADP to GSSG ratio but did not alter the glutathione (GSH) to GSSG ratio is contrary to findings in slime mold, in which multinucleation is accompanied by decreased GSH (Allen *et al.*, 1985). Possible explanations for the different findings include the different methods used to stimulate multinucleation (i.e., a specific differentiation media, not forskolin, was used to stimulate multinucleation of the slime molds (Allen *et al.*, 1985)) and differences in methodology used to detect GSH. Nevertheless, the finding of the increased NADP to GSSG ratio by syncytialization raises considerations. The first is whether NADP may have a greater impact than GSH in regulating glutathione reductase, which generates GSSG from GSH and NADP (Worthington and Rosemeyer, 1976; Bohme *et al.*, 2000). The second is whether syncytialization is accompanied by glutathione reductase inhibition.

Oleic acid and matrix metalloproteinases

Because oleic acid was increased by forskolin-stimulated syncytialization and decreased by DCVC treatment during syncytialization in our current study, we investigated manifestations of the effects on oleic acid with a focus on matrix metalloproteinases (MMPs). Consistent with prior reports that oleic acid positively correlates with multiple matrix metalloproteinases (MMPs) (Yamaguchi *et al.*, 2002; Soto-Guzman *et al.*, 2010), we found that DCVC treatment during syncytialization decreased MMP-2 and oleic acid. MMP-2 and oleic acid were increased by syncytialization. Increased extracellular MMP-2 is suggested to have relevance to adverse pregnancy outcomes (Palei *et al.*, 2012; Nissi *et al.*, 2013) as well as hold importance to syncytialization (Sawicki *et al.*, 2000; Xu *et al.*, 2002). Interestingly, although MMP-1 increased with DCVC treatment during syncytialization, MMP-3 and MMP-9 were unchanged by syncytialization or DCVC treatment during syncytialization. **Figure 6.17E** shows a model by which syncytialization and DCVC treatment during syncytialization could impact MMPs and oleic acid. Although MMP-1 and MMP-2 are classified as a collagenase and a gelatinase, respectively, and cleave different substrates (Li *et al.*, 2020), the meaning of these differences, as well as other differences among MMPs, remain unclear in the context of syncytialization. However, our data still suggest that selective regulation of MMPs, possibly attributable to oleic acid, would be plausible mechanisms for regulation of syncytialization or execution of the effects of DCVC treatment during syncytialization. Additional future directions could consider the extent by which alternative mechanisms, including AMP-activated protein kinase that enchances MMP-1 and MMP-2 production (Um *et al.*, 2017), could be responsible for a MMP effect.

Enrichment analyses and other considerations

Enrichment analysis identified syncytialization-associated changes that did not necessarily translate to placenta effects. As one plausible explanation, cell fusion and multinucleation are events that are not limited to placental cells, but also occur in muscle cells, slime molds, and osteoclasts (Potgens *et al.*, 2002). It is also unknown if the enrichment analysis specifically considers syncytialization events and if so, the contribution of syncytialization as a placenta-specific pathway. Because we observed placenta as the most associated organ with 20 µM DCVC treatment during syncytialization relative to forskolin only treatment, we suggest that BeWo cells are capable of responding in a manner that is specific to placenta. Further, this finding may indicate that BeWo cells have the ability to respond to DCVC in a placenta-specific manner that is not reflective of responses in other organs. Drug pathway enrichment analysis revealed that none of the top 13 drug pathways associated with syncytialization were in the top 30 pathways associated with the 20 µM DCVC treatment during syncytialization versus syncytialization alone comparison. This suggests there is a difference between syncytialization and DCVC treatment during syncytialization. Nevertheless, these results can be used to generate hypotheses about alterations in drug metabolism with DCVC exposure and pregnancy.

An overall limitation in the current study lies with the limited number of metabolites able to be quantified and the different methods for quantification (e.g., relative versus absolute processed and reported values) in the metabolomics analysis. Overcoming these limitations would allow for more specific inferences to pathways and adverse pregnancy outcomes. Additionally, the cells used in the study have limitations. Although forskolin-stimuation of BeWo cells produces features consistent with normal syncytialization (Wice *et al.*, 1990), results may differ for placental cells *in vivo*. Nevertheless, forskolin presents benefits compared to other

agents that have been proposed to stimulate syncytialization. The other candidates that could stimulate syncytialization included theophylline, cholera toxin, 8-Br-cAMP, and dibutyryl-cAMP, of which the last two require up to 1 mM to induce cell fusion (Wice *et al.*, 1990).

Conclusion

In summary, both forskolin-stimulated syncytialization and DCVC treatment during forskolin-stimulated syncytialization elicited effects on metabolites involved in energy metabolism. Notable and novel findings indicate that syncytialization and DCVC treatment during syncytialization provide opposing effects on metabolite ratios involving ATP, ADP, and AMP, suggesting that DCVC effects on adenosine phosphates may contribute a mechanism to oppose syncytialization. In contrast, histidine to aspartate, succinate to phenylalanine, and ornithine to proline ratios are examples of same direction of change promoted by syncytialization and DCVC treatment during syncytialization. Additionally, acidic amino acids, glutamate and aspartate, and nucleotide monophosphates may be likely targets of DCVC because these classes of metabolites were altered by DCVC. Furthermore, DCVC failed to increase the abundance of any measured metabolite. Finally, our work identified a potential role for MMPs in the mechanism of syncytialization that is modifiable by DCVC treatment during syncytialization. The notion of DCVC treatment as not simply a positive or negative regulator of syncytialization is consistent with the idea that syncytialization is a complex process (Gupta *et al.*, 2016). Important future directions include understanding how changes in specific portions of the pathways have relation to other pathway portions and use of the discoveries in the current study to inform approaches at DCVC toxicity modulation possibly through targeting specific enzymes.

Chemical	Treatment group			
	1	2	3	4
Forskolin (μM)	0	100	100	100
DCVC (μM)	0	0	10	20

Syncytialization

DCVC effect during
syncytialization

Figure 6.1. Summary and purposes of treatment groups used in the metabolomics study design. Comparison of the first two treatment groups, groups 1 and 2, test the effect of syncytialization on metabolomics outcomes. Comparison of groups 2, 3, and 4, investigate the effect of DCVC treatment on forskolin-stimulated syncytialization. Group 1 is the vehicle control group exposed to 0.1% (v/v) dimethyl sulfoxide (DMSO).
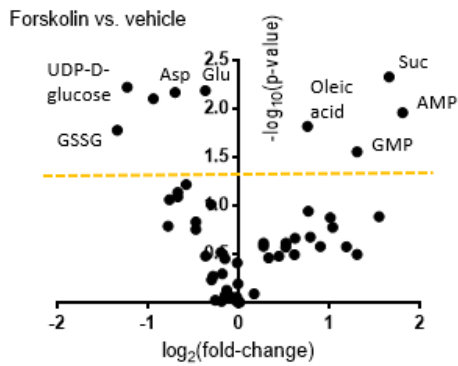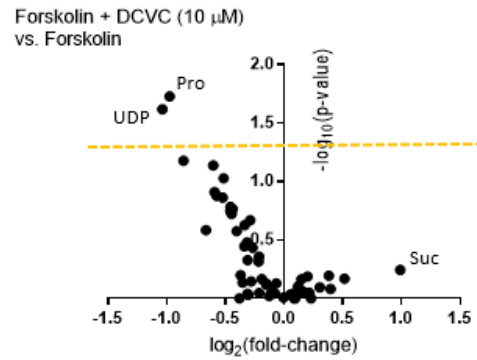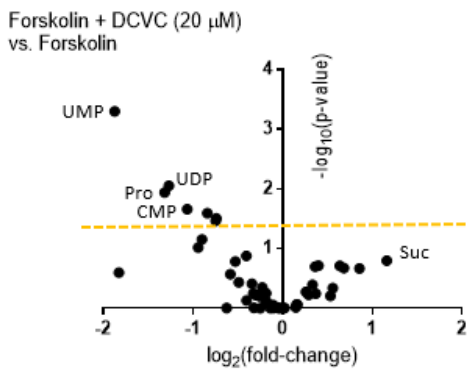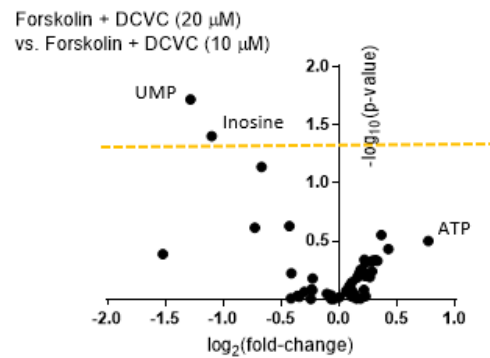
Figure 6.2. Volcano plots displaying the negative[log$_{10}$(p-value)] as a function of the log$_2$(fold-change) for each individual metabolite comparison. Graphs show four different comparisons, corresponding to the effect of: (A) syncytialization, comparing forskolin-only treatment to vehicle control; (B) 10 µM DCVC during syncytialization, comparing 10 µM DCVC treatment during syncytialization to forkskolin-only treatment; (C) 20 µM DCVC during syncytialization, comparing 20 µM DCVC treatment during syncytialization to forskolin-only treatment, and (D) DCVC concentration response, comparing 20 µM DCVC during syncytialization versus 10 µM DCVC during syncytialization. Individual points correspond to individual metabolites detected. The dashed gold lines correspond to the threshold of p=0.05 (approximately where y=1.3 on each graph). Axes ranges differ among the graphs to clearly show metabolites.

Figure 6.3. Summary of specific metabolites altered by syncytialization or DCVC treatment during syncytialization. Metabolites highlighted in blue or red indicate metabolites increased or decreased, respectively, in response to forskolin-stimulated syncytialization and/or DCVC co-treatment. The metabolites in smallest, moderate, and largest text sizes were significantly different at $p<0.05$, $p<0.01$, and $p<0.001$, respectively. In the case of DCVC effect during syncytialization, a metabolite was listed if it changed with at least 20 µM DCVC treatment, with the exception of inosine (marked with an asterisk), which was decreased in the 20 µM DCVC group compared to the 10 µM DCVC group.

(A)

log₂(fold-change):
10 μM DCVC vs. 20 μM DCVC exposure during syncytialization

(B)

log₂(fold-change):
Syncytialization vs. 10 μM DCVC exposure during syncytialization

(C)

log₂(fold-change):
Syncytialization vs. 20 μM DCVC exposure during syncytialization
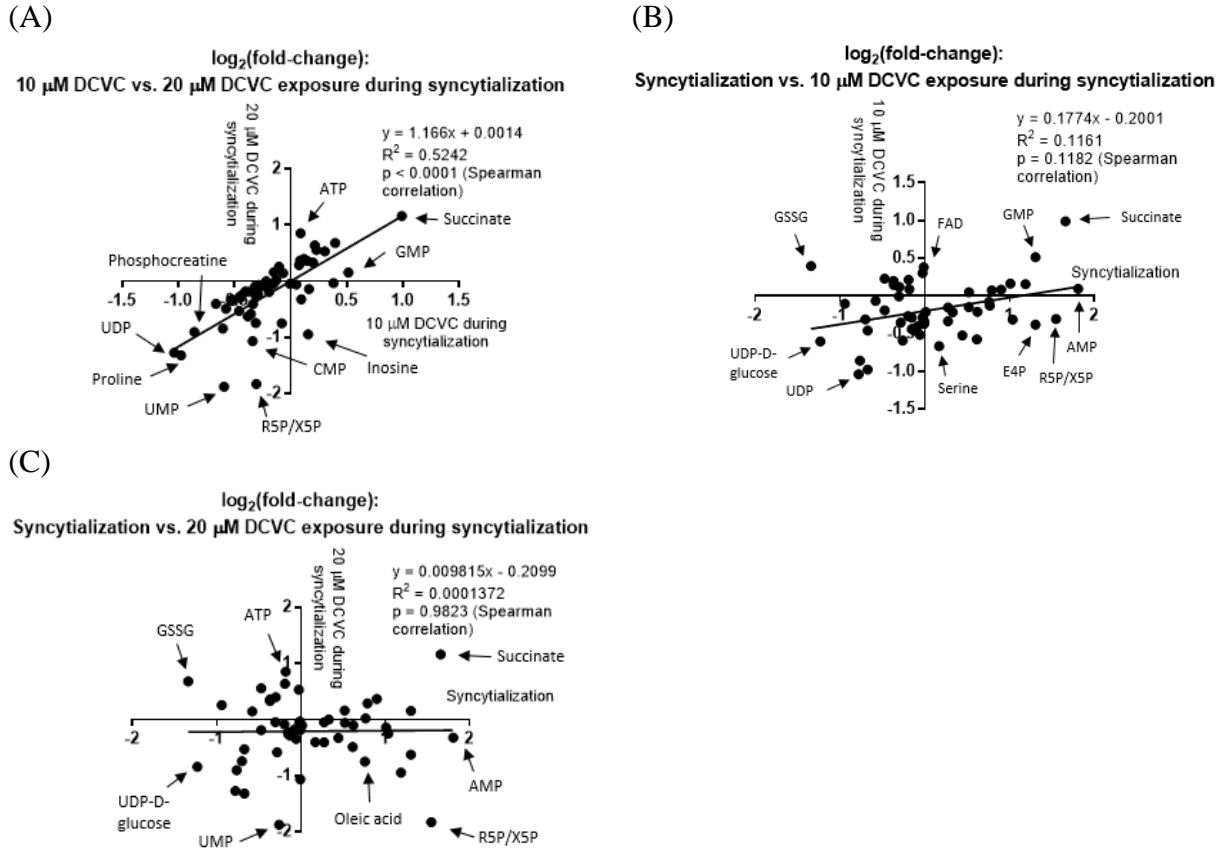
Figure 6.4. Scatterplots showing associations between metabolite fold-changes across different comparisons to visualize changes associated with syncytialization versus changes associated with DCVC treatment during syncytialization. Comparisons displayed correspond to (A) the 20 µM DCVC treatment during syncytialization versus 10 µM DCVC treatment during syncytialization comparison, (B) the 10 µM DCVC treatment during syncytialization versus syncytialization alone comparison, and (C) the 20 µM DCVC treatment during syncytialization versus syncytialization alone comparison. X and Y axes are in units of log₂(fold-change), and individual data points represent individual metabolites detected in the cells.

(A) Process of syncytialization:
Vehicle (0.1% DMSO) versus forskolin
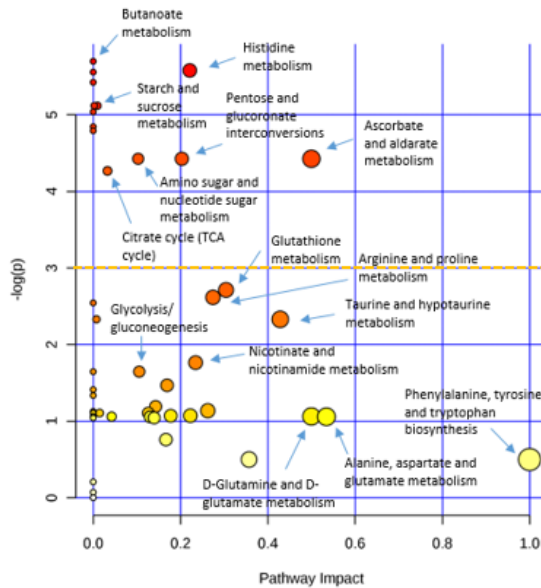
(B) DCVC effect during syncytialization:
Forskolin versus forskolin + DCVC (10 µM)
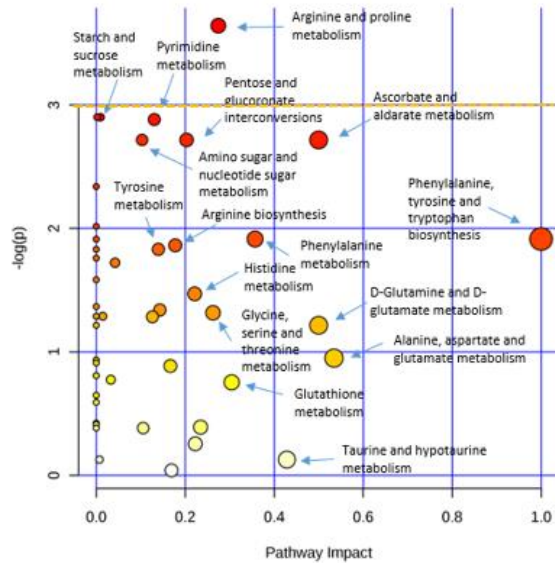
(C) DCVC effect during syncytialization:
Forskolin versus forskolin + DCVC (20 µM)
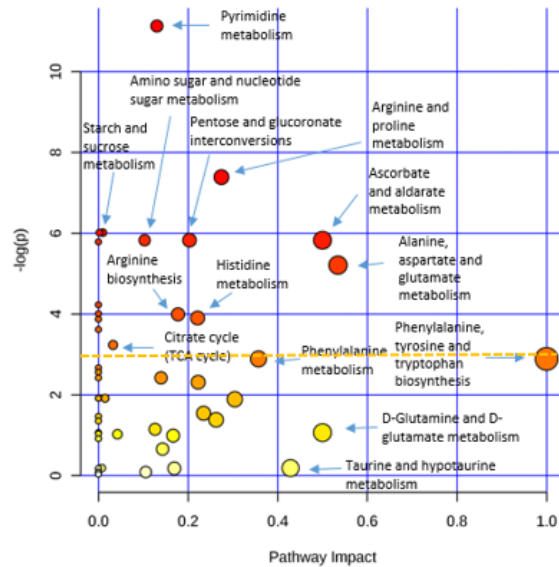
(D) DCVC concentration effect during syncytialization:
Forskolin + DCVC (20 µM) versus forskolin + DCVC (10 µM)
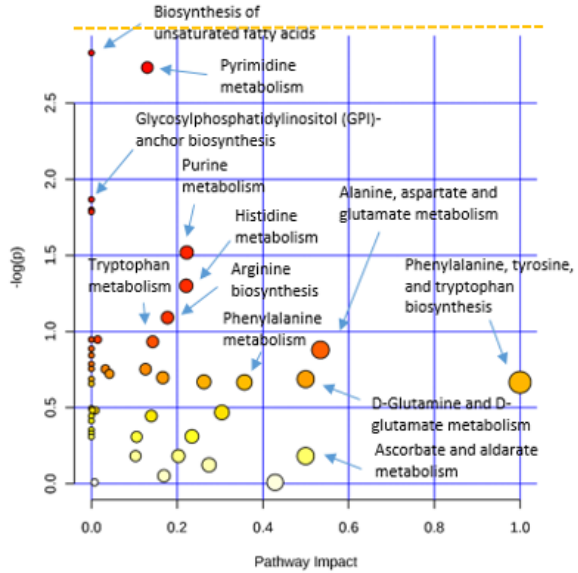
Figure 6.5. KEGG pathways altered by forskolin-stimulated syncytialization or DCVC treatment during syncytialization. Individual figures represent the effect of (A) syncytialization, comparing forskolin-only treatment to vehicle control; (B) 10 µM DCVC during syncytialization, comparing 10 µM DCVC treatment during syncytialization to forkskolin-only treatment; (C) 20 µM DCVC during syncytialization, comparing 20 µM DCVC treatment during syncytialization to forskolin-only treatment, and (D) DCVC concentration response, comparing 20 µM DCVC during syncytialization versus 10 µM DCVC during syncytialization. Pathway analysis (specific for *Homo sapiens*) was performed by Metaboanalyst 4.0 on the data (generalized log-transformed). The circle color corresponds to significance of the

pathway (white to red in order of increasing significance) whereas circle size corresponds to pathway impact, which is calculated as the matched metabolites as a cumulative percentage contributing to total pathway importance. A horizontal yellow dashed line indicates negative(log(p))=3, which corresponds to a p=0.05 under the $\log_e$ (or ln) scale used in this analysis. Axes ranges differ among the graphs to clearly label pathways.

(A)
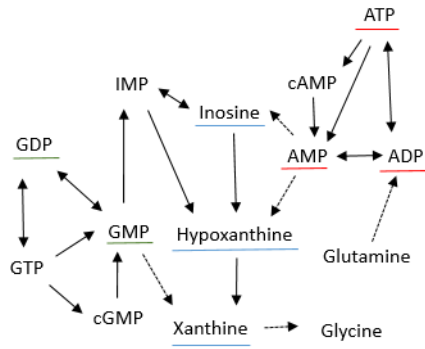
(B)
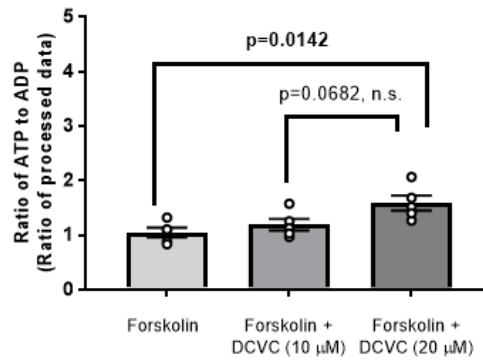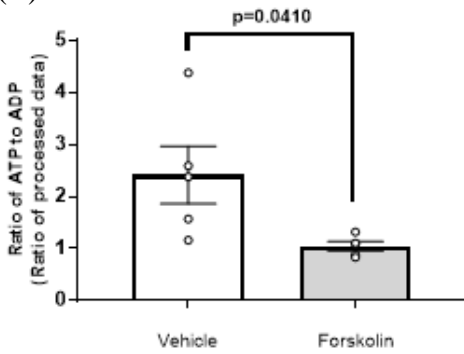
(C)
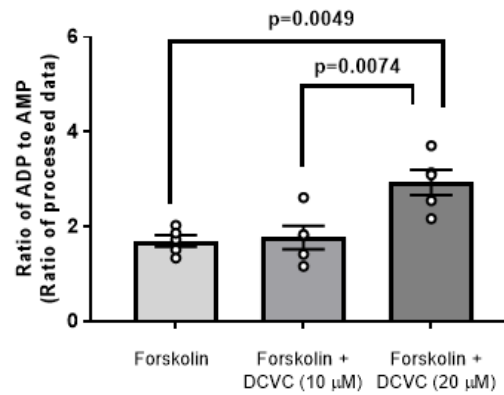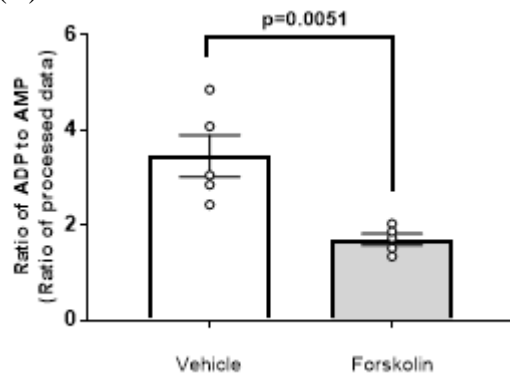
(D)
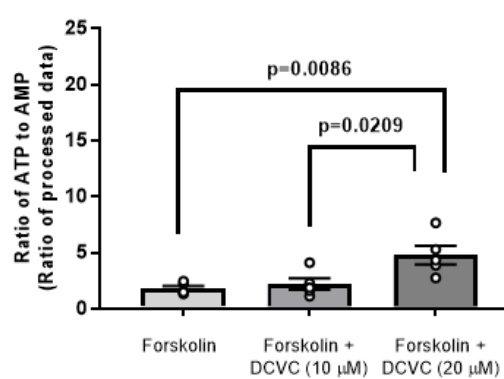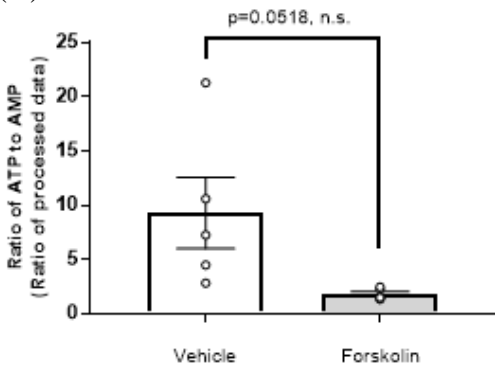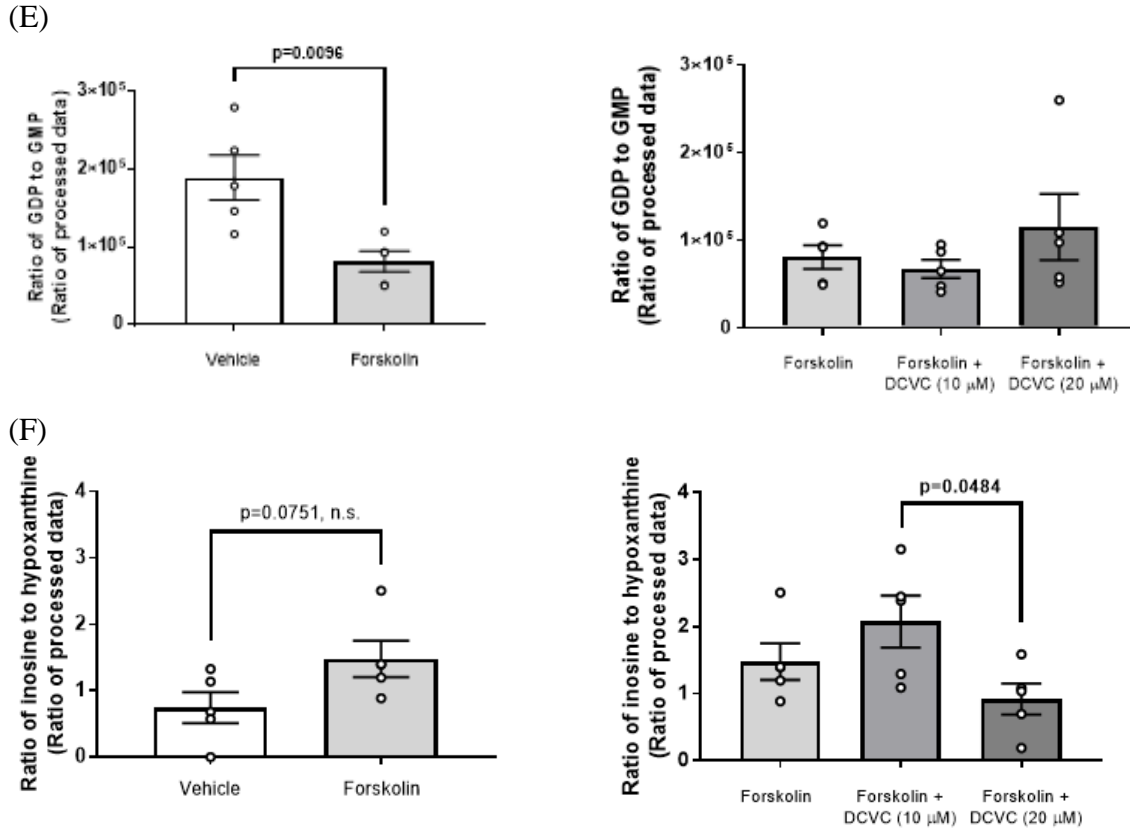
Figure 6.6. Purine metabolism as modified by syncytialization and DCVC treatment during syncytialization. (A) Simplified depiction of the purine metabolism KEGG pathway in *Homo sapiens*. Metabolites underlined in red correspond to metabolites that are part of a ratio altered by both syncytialization and DCVC treatment, compared to forskolin-only treatment. Metabolites underlined in green correspond to metabolites that are part of a ratio altered by syncytialization only. Metabolites underlined in blue correspond to metabolites that were analyzed in ratio analysis but not altered by syncytialization nor DCVC treatment, compared to forskolin-only treatment. Specific metabolite ratios changed by syncytialization or DCVC treatment during syncytialization are shown for: (B) the ATP to ADP ratio; (C) the ADP to AMP ratio; (D) the ATP to AMP ratio; (E) the GDP to GMP ratio; and (F) the inosine to hypoxanthine ratio. The inosine to hypoxanthine ratio was indicated as nonsignifiant in (A) because of lack of statistical significance compared to control (forskolin-only treatment). In the graphs, error bars represent mean ± SEM. N= 5 independent experiments. Abbreviations: ATP, adenosine triphosphate; ADP, adenosine diphosphate; AMP, adenosine monophosphate; cAMP, cyclic AMP; GTP, guanosine triphosphate; GDP, guanosine diphosphate; GMP, guanosine monophosphate; cGMP, cyclic GMP; IMP, inosine monophosphate.

(A)
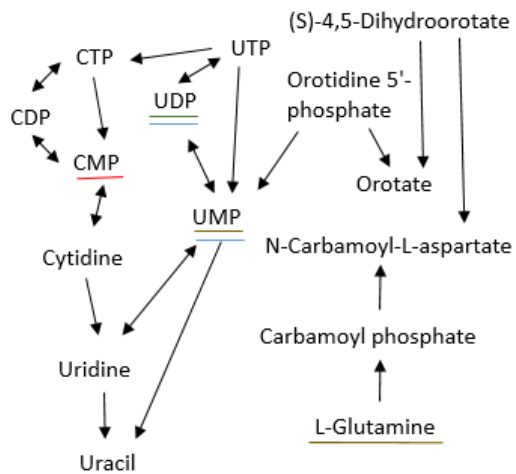
(B)
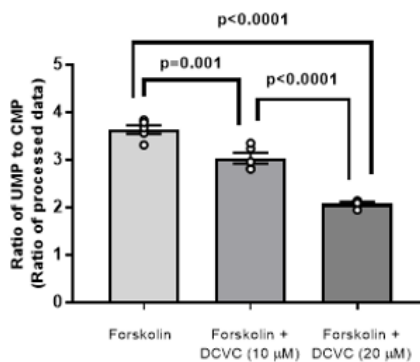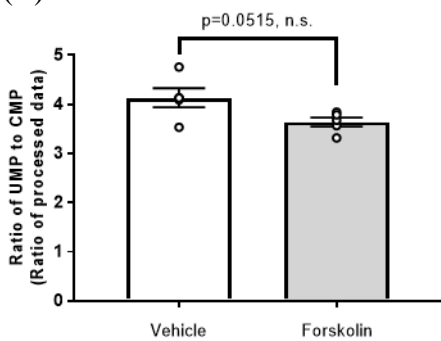
(C)
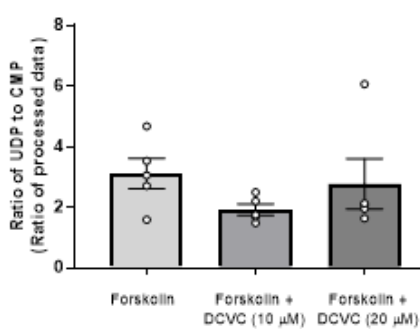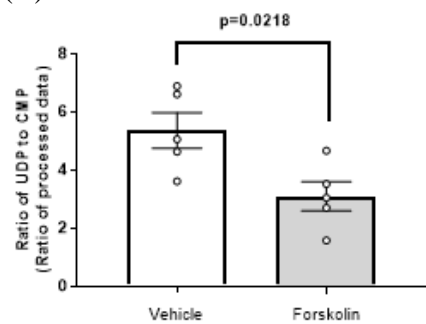
(D)
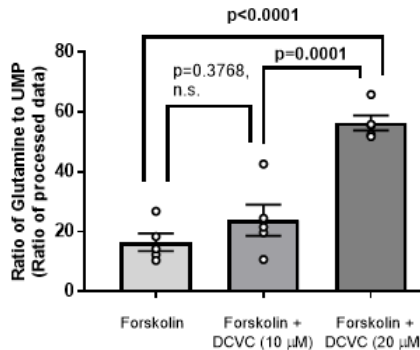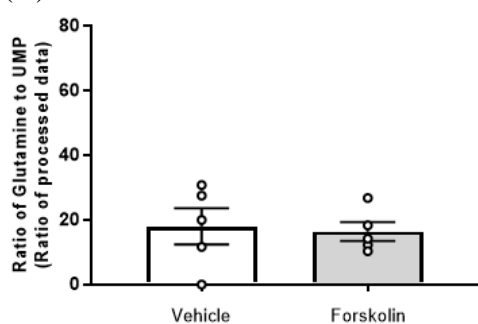
Figure 6.7. Pyrimidine metabolism as modified by syncytialization and DCVC treatment during syncytialization. (A) Simplified depiction of the pyrimidine metabolism KEGG pathway in *Homo sapiens*. Metabolites underlined in red correspond to metabolites that are part of a ratio altered by both syncytialization and DCVC treatment, compared to forskolin-only treatment. Metabolites underlined in green correspond to metabolites that are part of a ratio altered by syncytialization only. Metabolites underlined in dark gold correspond to metabolites that are part of a ratio altered by DCVC treatment only. Metabolites underlined in blue correspond to metabolites that were analyzed in ratio analysis but not altered by syncytialization nor DCVC treatment, compared to forskolin-only treatment. Specific metabolite ratios changed by syncytialization or DCVC treatment during syncytialization are shown for: (B) the UMP to CMP ratio; (C) the UDP to CMP ratio; and (D) the glutamine to UMP ratio. In the graphs, error bars represent mean $\pm$ SEM. N= 5 independent experiments. Abbreviations: CTP, cytidine triphosphate; CDP, cytidine diphosphate; CMP, cytidine monophosphate; UTP, uracil triphosphate; UDP, uracil diphosphate; UMP, uracil monophosphate.

(A)
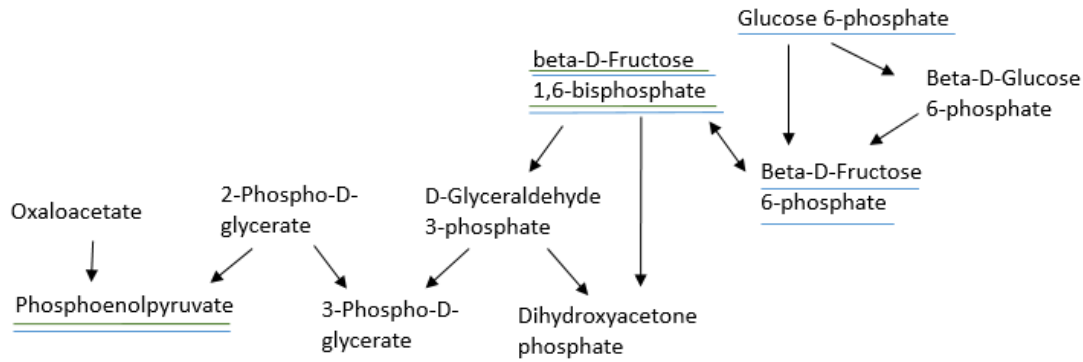
(B)
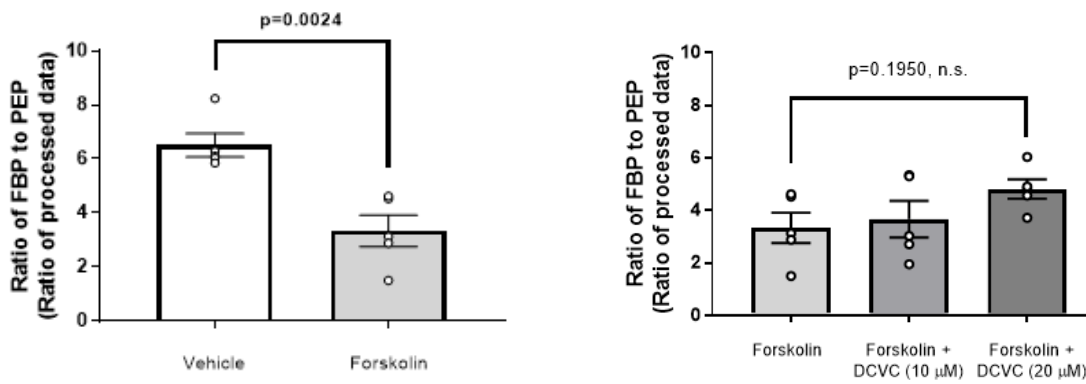
Figure 6.8. Glycolysis or gluconeogenesis as modified by syncytialization and DCVC treatment during syncytialization. (A) Simplified depiction of the glycolysis or gluconeogenesis KEGG pathway in *Homo sapiens*. Metabolites underlined in green correspond to metabolites that are part of a ratio altered by syncytialization only. Metabolites underlined in blue correspond to metabolites that were analyzed in ratio analysis but not altered by syncytialization nor DCVC treatment, compared to forskolin-only treatment. Specific metabolite ratios changed by syncytialization or DCVC treatment during syncytialization are shown for: (B) the FBP to PEP ratio. In the graphs, error bars represent mean ± SEM. N= 5 independent experiments. Abbreviations: FBP, fructose 1,6-bisphosphate; PEP, phosphoenolpyruvate.
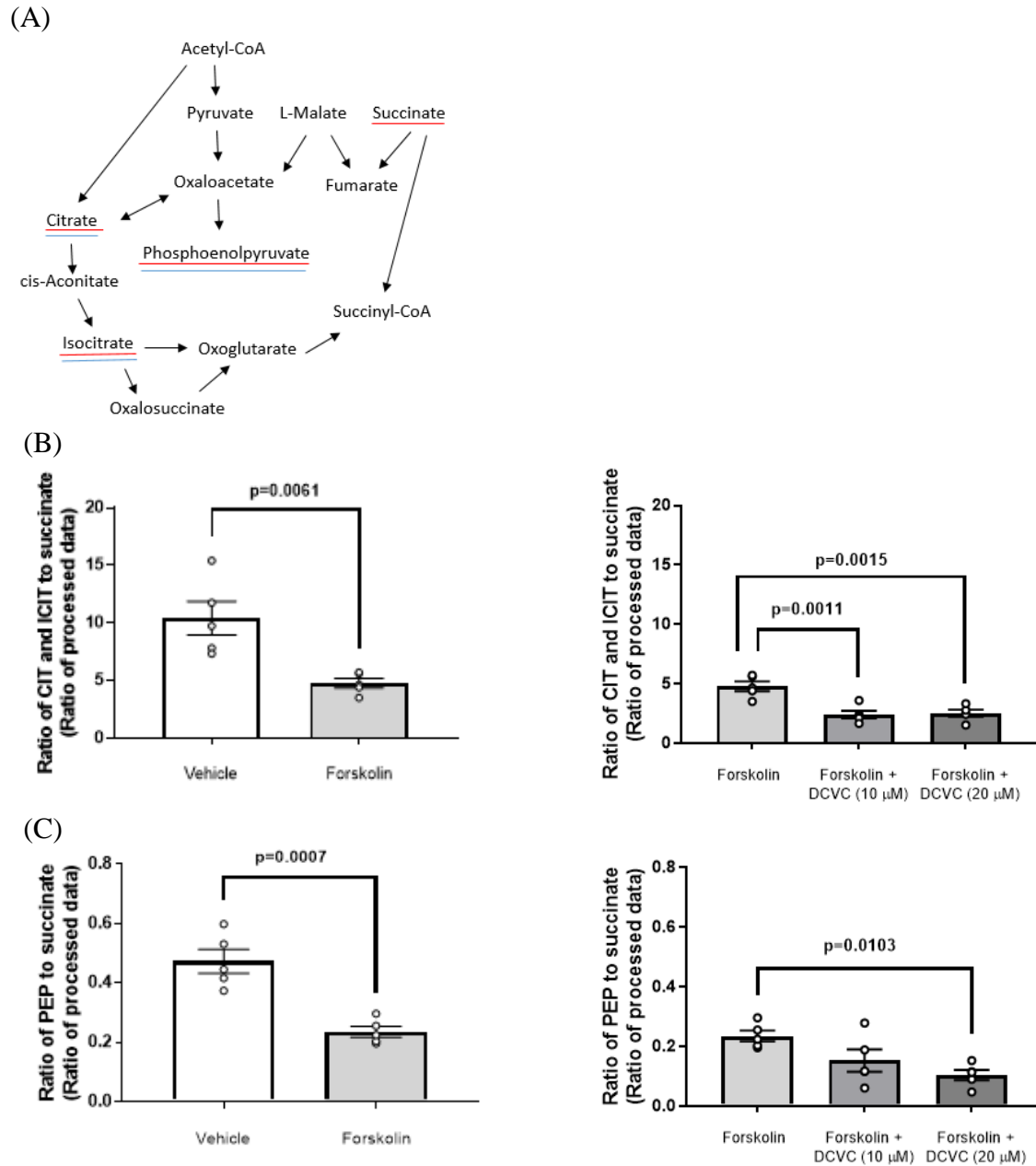
Figure 6.9. Tricarboxylic acid (TCA) cycle as modified by syncytialization and DCVC treatment during syncytialization. (A) Simplified depiction of the TCA cycle KEGG pathway in *Homo sapiens*. Metabolites underlined in red correspond to metabolites that are part of a ratio altered by both syncytialization and DCVC treatment, compared to forskolin-only treatment. Metabolites underlined in blue correspond to metabolites that were analyzed in ratio analysis but not altered by syncytialization nor DCVC treatment, compared to forskolin-only treatment. Specific metabolite ratios changed by syncytialization or DCVC treatment during syncytialization are shown for: (B) the CIT and ICIT to succinate ratio; and (C) the PEP to succinate ratio. In the graphs, error bars represent mean ± SEM. N= 5 independent experiments. Abbreviations: CIT, citrate; ICIT, isocitrate; PEP, phosphoenolpyruvate.

311
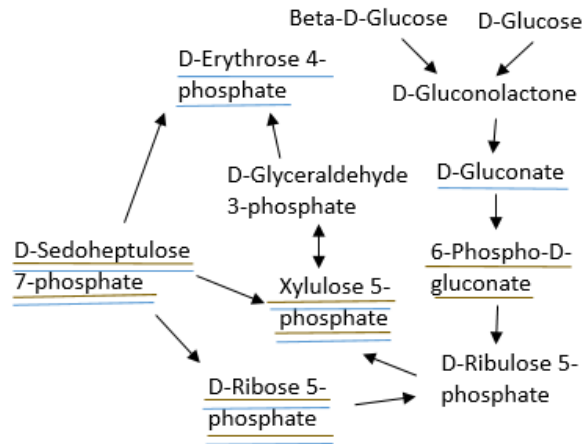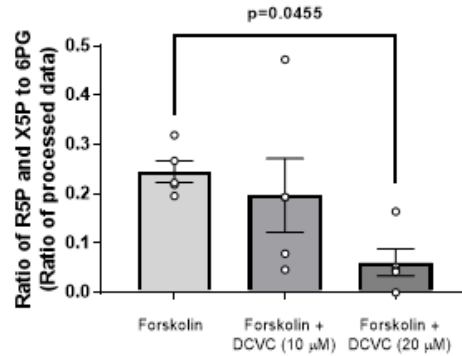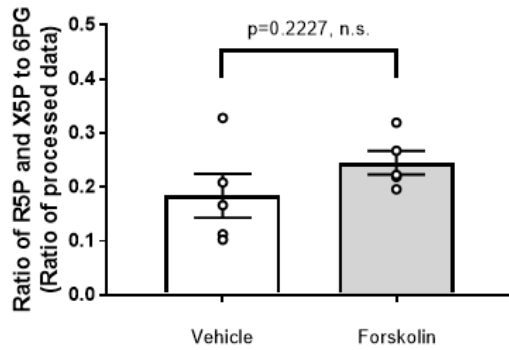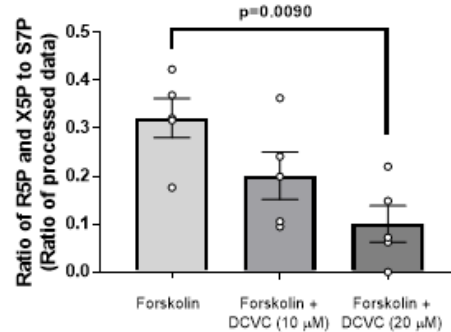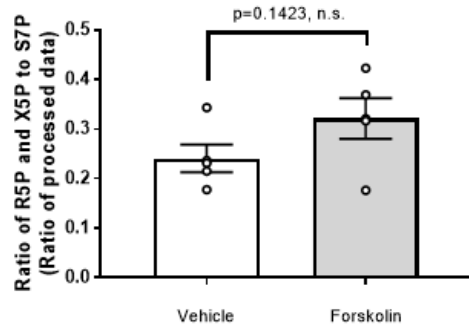
Figure 6.10. Pentose phosphate pathway as modified by syncytialization and DCVC treatment during syncytialization. (A) Simplified depiction of the pentose phosphate KEGG pathway in *Homo sapiens*. Metabolites underlined in dark gold correspond to metabolites that are part of a ratio altered by DCVC treatment only. Metabolites underlined in blue correspond to metabolites that were analyzed in ratio analysis but not altered by syncytialization nor DCVC treatment, compared to forskolin-only treatment. Specific metabolite ratios changed by syncytialization or DCVC treatment during syncytialization are shown for: (B) the R5P and X5P to 6PG ratio; and (C) the R5P and X5P to S7P ratio. In the graphs, error bars represent mean ± SEM. N= 5 independent experiments. Abbreviations: R5P, ribose 5-phosphate; X5P, xylulose 5-phosphate; 6PG, 6-phosphogluconate; S7P, sedoheptulose 7-phosphate.

312
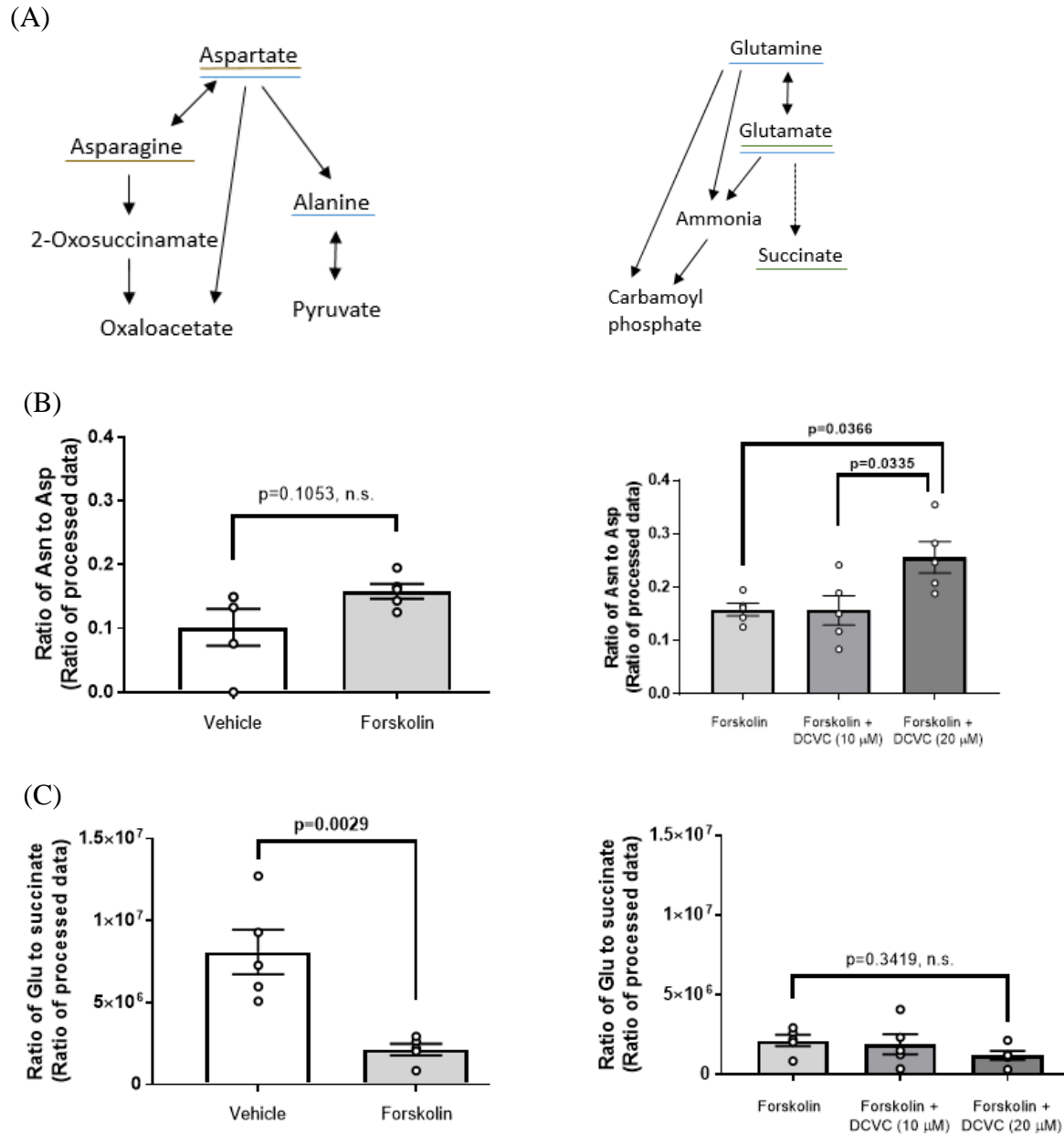
Figure 6.11. Alanine, aspartate, and glutamate metabolism as modified by syncytialization and DCVC treatment during syncytialization. (A) Simplified depiction of two portions of alanine, aspartate, and glutamate metabolism KEGG pathway in *Homo sapiens*. Metabolites underlined in green correspond to metabolites that are part of a ratio altered by syncytialization only. Metabolites underlined in dark gold correspond to metabolites that are part of a ratio altered by DCVC treatment only. Metabolites underlined in blue correspond to metabolites that were analyzed in ratio analysis but not altered by syncytialization nor DCVC treatment, compared to forskolin-only treatment. Specific metabolite ratios changed by syncytialization or DCVC treatment during syncytialization are shown for: (B) the Asn to Asp ratio; and (C) the Glu to succinate ratio. In the graphs, error bars represent mean ± SEM. N= 5 independent experiments. Abbreviations: Asn, Asparagine; Asp, Aspartate; Glu, Glutamate.

313
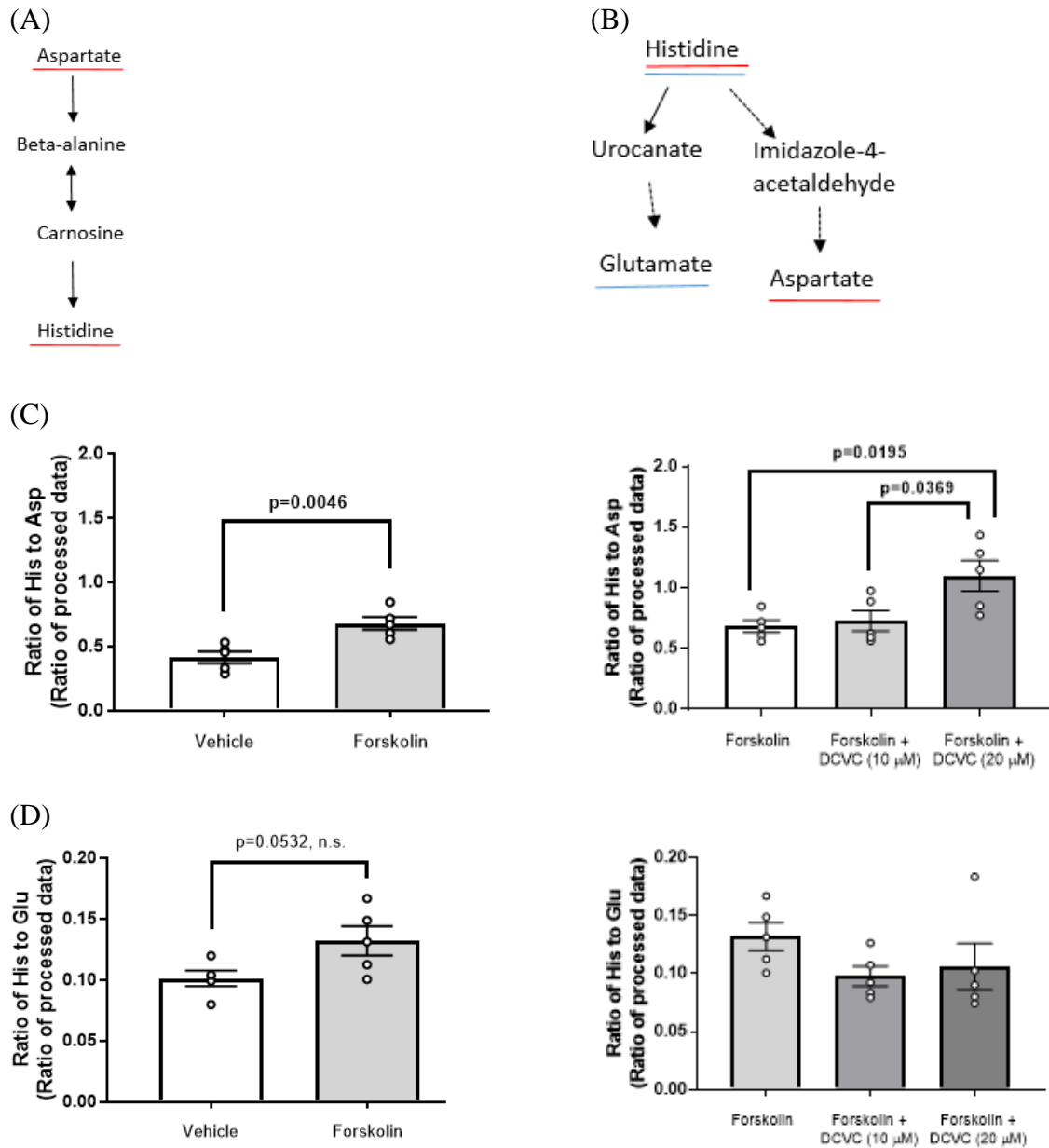
Figure 6.12. Beta-alanine metabolism and histidine metabolism as modified by syncytialization and DCVC treatment during syncytialization. Simplified depiction of the (A) the beta-alanine metabolism and (B) histidine metabolism KEGG pathways in *Homo sapiens*. Metabolites underlined in red correspond to metabolites that are part of a ratio altered by both syncytialization and DCVC treatment, compared to forskolin-only treatment. Metabolites underlined in blue correspond to metabolites that were analyzed in ratio analysis but not altered by syncytialization nor DCVC treatment, compared to forskolin-only treatment. Specific metabolite ratios changed by syncytialization or DCVC treatment during syncytialization are shown for: (B) the His to Asp ratio; and (C) the His to Glu ratio. In the graphs, error bars represent mean ± SEM. N= 5 independent experiments. Abbreviations: His, Histidine; Asp, Aspartate; Glu, Glutamate.

314
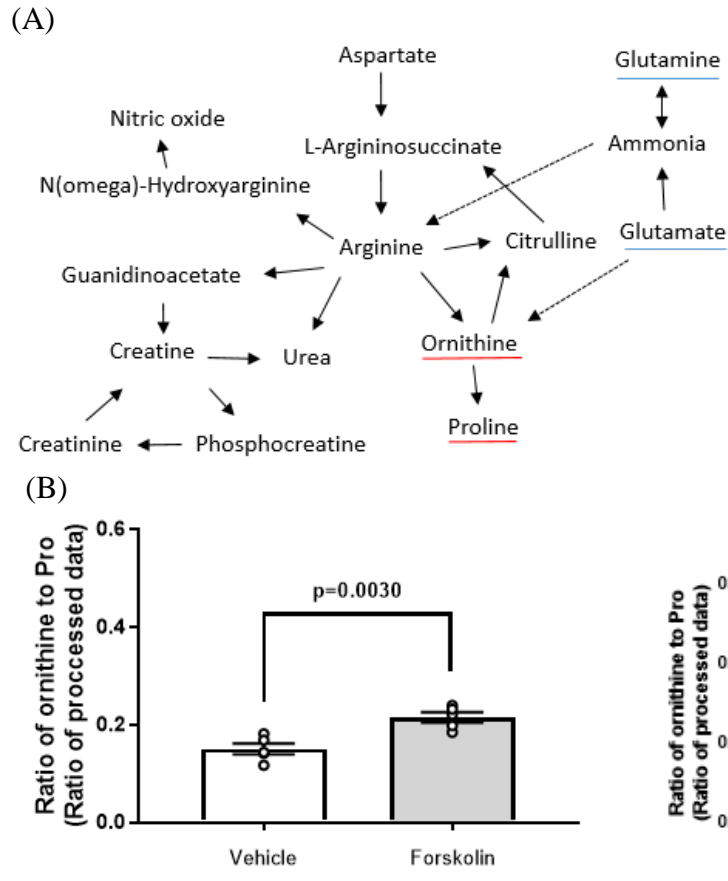
Figure 6.13. Arginine and proline metabolism as modified by syncytialization and DCVC treatment during syncytialization. (A) Simplified depiction of the arginine and proline metabolism KEGG pathway in *Homo sapiens*. Metabolites underlined in red correspond to metabolites that are part of a ratio altered by both syncytialization and DCVC treatment, compared to forskolin-only treatment. Metabolites underlined in blue correspond to metabolites that were analyzed in ratio analysis but not altered by syncytialization nor DCVC treatment, compared to forskolin-only treatment. Specific metabolite ratios changed by syncytialization or DCVC treatment during syncytialization are shown for: (B) the ornithine to Pro ratio. In the graphs, error bars represent mean ± SEM. N= 5 independent experiments. Abbreviation: Pro, proline.

(A)

(B)
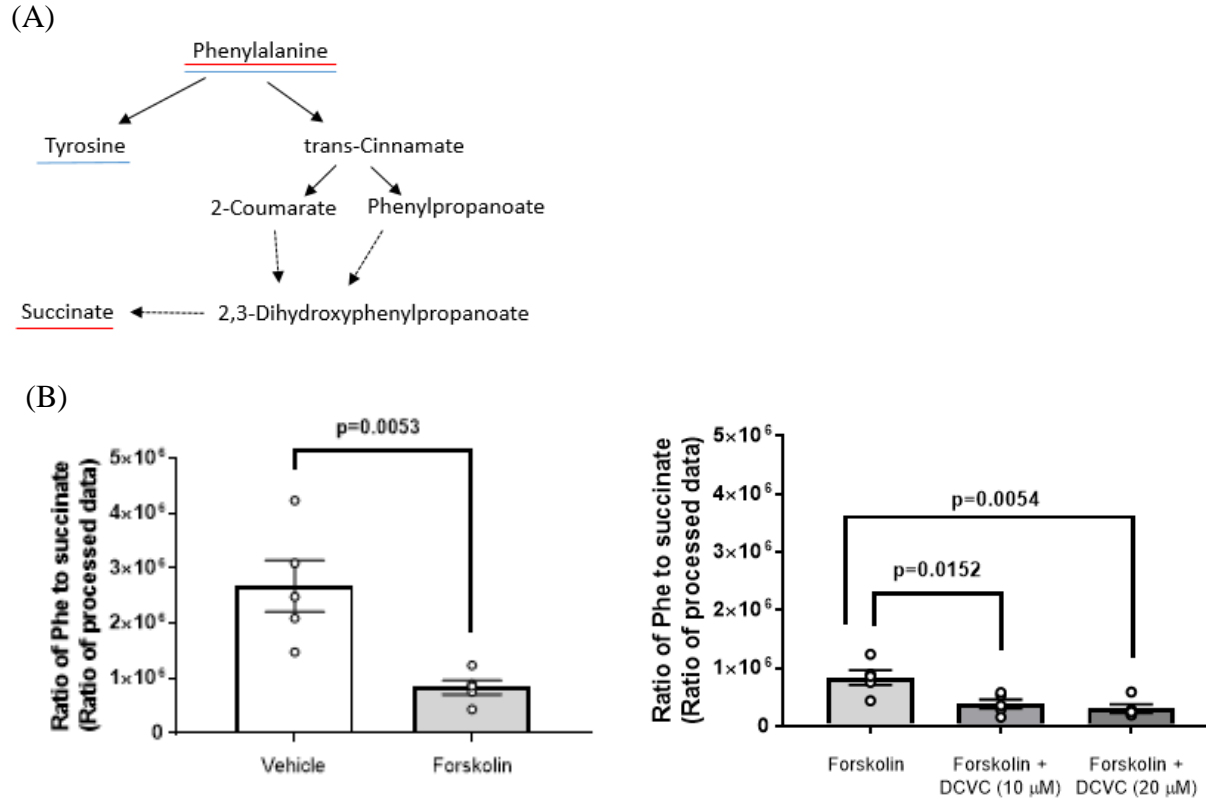
Figure 6.14. Phenylalanine metabolism as modified by syncytialization and DCVC treatment during syncytialization. (A) Simplified depiction of the phenylalanine metabolism KEGG pathway in *Homo sapiens*. Metabolites underlined in red correspond to metabolites that are part of a ratio altered by both syncytialization and DCVC treatment, compared to forskolin-only treatment. Metabolites underlined in blue correspond to metabolites that were analyzed in ratio analysis but not altered by syncytialization nor DCVC treatment, compared to forskolin-only treatment. Specific metabolite ratios changed by syncytialization or DCVC treatment during syncytialization are shown for: (B) the Phe to succinate ratio. In the graphs, error bars represent mean ± SEM. N= 5 independent experiments. Abbreviation: Phe, phenylalanine.
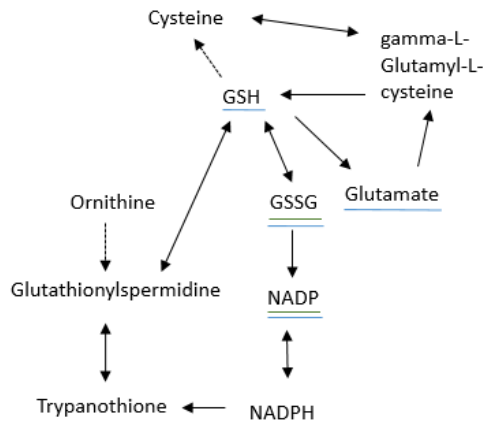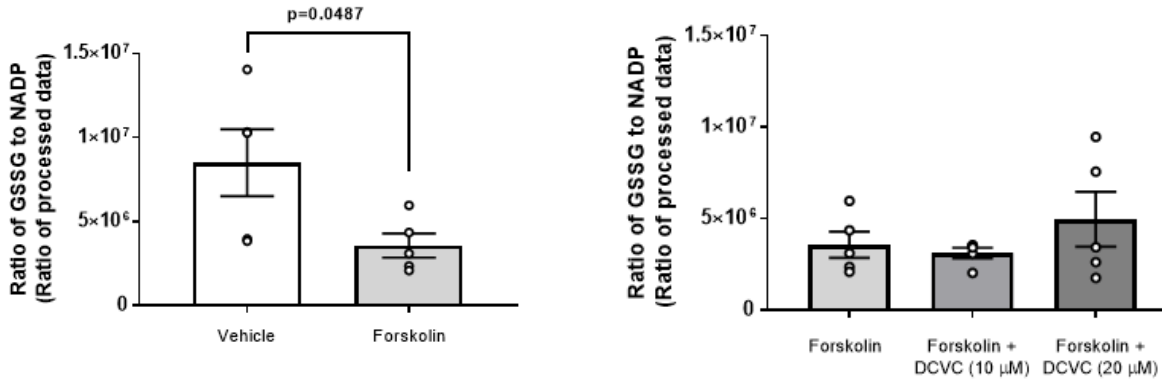
Figure 6.15. Glutathione (GSH) metabolism as modified by syncytialization or DCVC treatment during syncytialization. (A) Simplified depiction of the glutathione metabolism KEGG pathway in *Homo sapiens*. Metabolites underlined in green correspond to metabolites that are part of a ratio altered by syncytialization only. Metabolites underlined in blue correspond to metabolites that were analyzed in ratio analysis but not altered by syncytialization nor DCVC treatment, compared to forskolin-only treatment. Specific metabolite ratios changed by syncytialization or DCVC treatment during syncytialization are shown for: (B) the GSSG to NADP ratio. In the graphs, error bars represent mean ± SEM. N= 5 independent experiments. Other abbreviations: GSSG, glutathione disulfide; NADP, nicotinamide adenine dinucleotide phosphate; NADPH, nicotinamide adenine dinucleotide phosphate hydrogen.
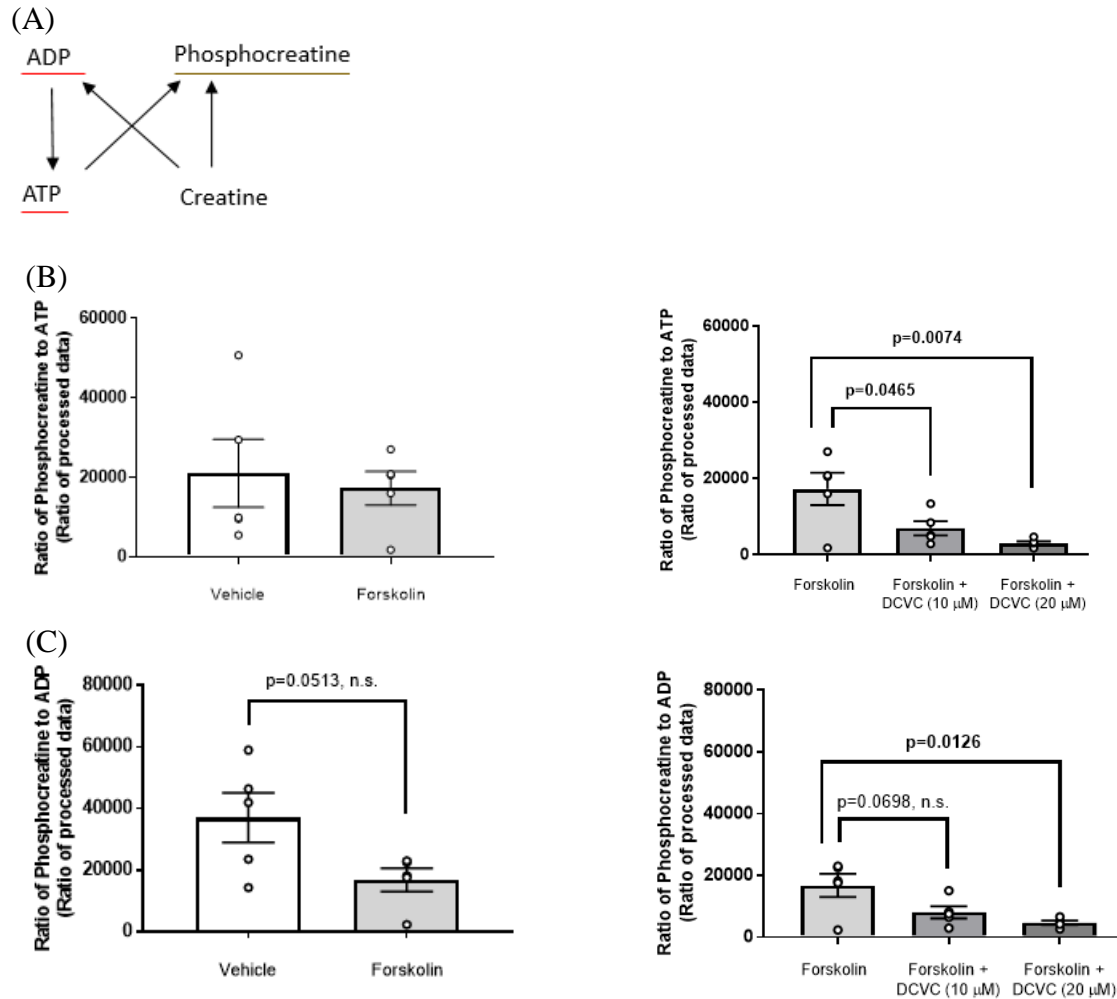
Figure 6.16. Phosphocreatine shuttling as modified by syncytialization and DCVC treatment during syncytialization. (A) Depiction of phosphocreatine shuttling. Metabolites underlined in red correspond to metabolites that are part of a ratio altered by both syncytialization and DCVC treatment, compared to forskolin-only treatment. Metabolites underlined in dark gold correspond to metabolites that are part of a ratio altered by DCVC treatment only. Specific metabolite ratios changed by syncytialization or DCVC treatment during syncytialization are shown for: (B) the phosphocreatine to ATP ratio and (C) the phosphocreatine to ADP ratio. A graph corresponding to the ATP to ADP ratio had already been shown in **Figure 6.6B**. In the graphs, error bars represent mean ± SEM. N= 5 independent experiments. Abbreviations: ATP, adenosine triphosphate; ADP, adenosine diphosphate.
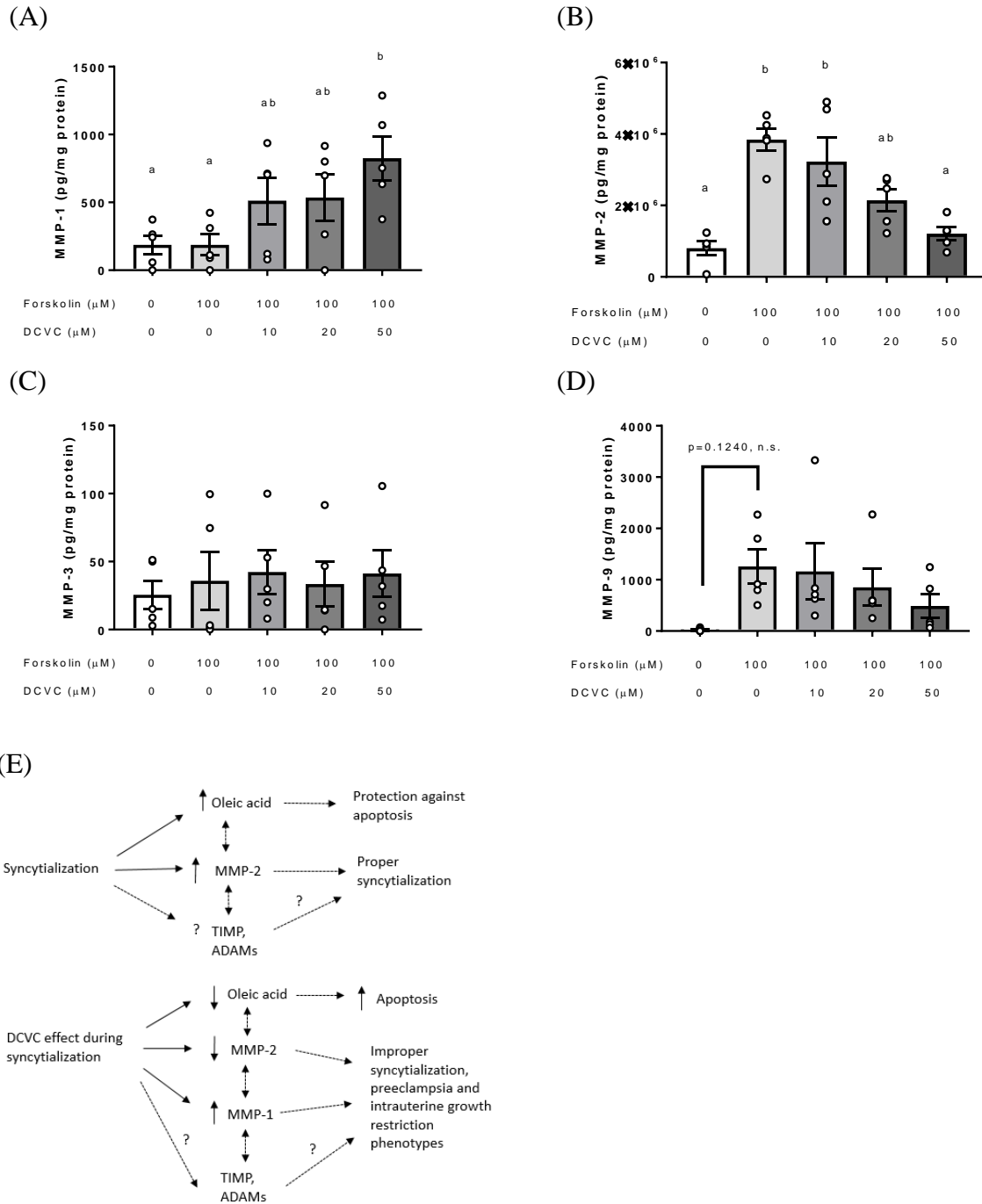
Figure 6.17. Effect of syncytialization and DCVC treatment during syncytialization on matrix metalloproteinase (MMP) concentrations in BeWo cell media. Effect on (A) MMP-1, (B) MMP-2, (C) MMP-3, and (D) MMP-9. Statistical significance is denoted by non-overlapping letters. Error bars represent mean ± SEM. N=5 independent experiments. (E) Proposed mechanism by which DCVC co-treatment may act to stimulate adverse pregnancy outcomes involving oleic acid and MMPs. Solid lines indicate relationships confirmed by current study to date. Dotted lines indicate relationships inferred by previous literature. Dotted lines with a

question mark above indicate relationships untested previously. High likelihood exists that the relationships are also mediated by tissue inhibitors of metalloproteinases (TIMPs) and a disintegrin and metalloproteinases (ADAMs).
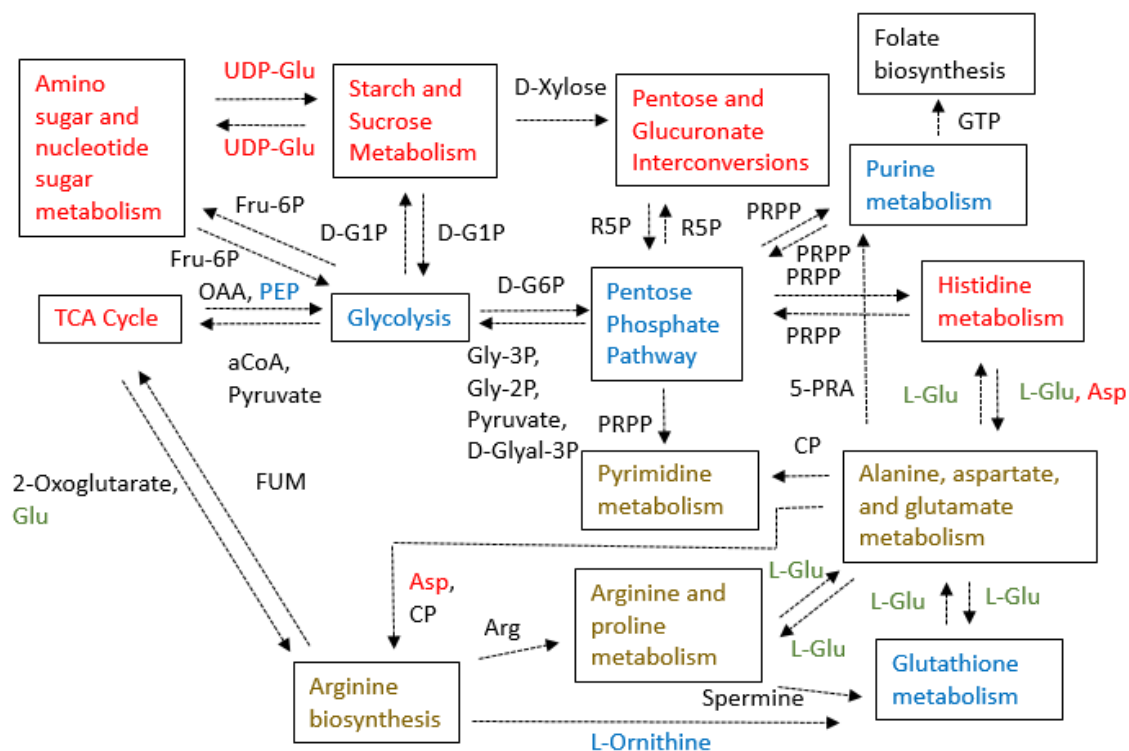
Figure 6.18. The effect of syncytialization or DCVC treatment during syncytialization on a simplified depiction portraying relationships among KEGG metabolism pathways. Boxed names are individual KEGG pathways, and unboxed names are critical metabolites that connect the pathways. Red names indicate metabolites or pathways altered in both syncytialization and DCVC treatment during syncytialization. Green names indicate metabolites or pathways altered in syncytialization only. Dark gold names indicate metabolites or pathways altered by DCVC treatment during syncytialization only. Blue names indicate metabolites or pathways unaltered by neither syncytialization nor DCVC treatment during syncytialization, compared to forskolin-only treatment. Black names indicate metabolites or pathways not detected in the current study. Metabolite concentrations or relative responses and Metaboanalyst 4.0 pathway analysis results were used in determining metabolite and pathway significance, respectively. Dashed arrows indicate multi-step processes. Abbreviations: aCoA, acetyl coenzyme A; OAA, oxaloacetate; D-G1P, alpha-D-glucose 1-phosphate; UDP-Glu, uridine diphosphate-glucose; R5P, D-ribulose 5-phosphate; PRPP, phosphoribosyl pyrophosphate; FUM, fumarate; CP, carbamoyl phosphate, Gly-3P, glycerate 3-phosphate; Gly-2P, glycerate 2-phosphate; D-Glyal-3P, D-glyceraldehyde 3-phosphate; D-G6P, alpha-D-glucose 6-phosphate; 5-PRA, 5-phosphoribosylamine; Fru-6P, fructose 6-phosphate; GTP, guanosine triphosphate.

Table S6.1. Concentrations or relative responses of detected metabolites.

I. Metabolites measured as relative concentrations (Units: Relative response (RR))			

Stearic Acid (Relative response)

	Vehicle (0.1% DMSO)	Forskolin	Forskolin + DCVC (10 μM)	Forskolin + DCVC (20 μM)
	8983063.51130517	3577837.32705119	5431447.91171993	5596887.95485907
	5309191.82737296	4970376.93938718	4555250.233188	3689164.71627745
	2316491.86649554	3955183.14662995	4221499.02388262	6932041.9166587
	5952094.30303425	5883524.81876735	5779520.33984377	8184450.2131122
	5903087.30347712	4743309.14831395	5142683.13674597	6085090.48027335
Average	5692785.76233701	4626046.27602992	5026080.12907606	6097527.05623615

Oleic Acid (Relative response)

	Vehicle (0.1% DMSO)	Forskolin	Forskolin + DCVC (10 μM)	Forskolin + DCVC (20 μM)
	1080628.7038924	2469380.74722079	2597896.95143052	1100786.69353322
	1634979.19089547	1850275.3172575	3021027.28454472	1366968.94107996
	1151241.59875212	2076607.73829589	3055181.68577114	1486500.1225454
	1300022.32983317	2928630.99824654	1314864.35304729	2184215.7507185
	2325587.1253798	3348756.51462918	2006869.7928271	1403874.40248789
Average	1498491.78975059	2534730.26312998	2399168.01352415	1508469.18207299

Palmitic Acid (Relative response)

	Vehicle (0.1% DMSO)	Forskolin	Forskolin + DCVC (10 μM)	Forskolin + DCVC (20 μM)
	6808559.7598119	2643544.24796784	4221843.74678367	3782355.21897362
	4226931.12878125	3621361.50290839	3572248.14937695	2965763.03767177
	2205836.73832168	3502112.10792534	3336952.18620769	5000208.09952605
	4436110.22027933	4070100.36120745	4482519.35830523	6190033.73623017
	4673870.68947895	3506856.88492195	3596481.19482056	4354955.74273263
Average	4470261.70733462	3468795.02098619	3842008.92709882	4458663.16702685

Hexose (glucose, etc.) (Relative response)

	Vehicle (0.1% DMSO)	Forskolin	Forskolin + DCVC (10 μM)	Forskolin + DCVC (20 μM)
	5103597.09754602	3236554.83207516	2624231.87819794	3068304.84111315
	3562483.66006332	3271849.91222307	2413077.00625465	2256955.40781663
	2696991.31249283	3941753.28921425	1326403.17785934	3537069.76059081
	3077305.92642198	5006211.2079981	2995553.93221561	2635258.95097011
	5310893.73056186	3539723.23792435	3926256.25510115	3467773.37614554
Average	3950254.34541720	3799218.49588699	2657104.44992574	2993072.46732725

Hypoxanthine (Relative response)

	Vehicle (0.1% DMSO)	Forskolin	Forskolin + DCVC (10 μM)	Forskolin + DCVC (20 μM)
	701843.204092439	412361.312438637	445150.040148062	736871.929020986
	316348.270692475	276694.687377403	362304.453406435	280665.348952527
	373662.72878256	389438.649146639	208190.872017565	390254.729447692
	423512.514897494	754888.292820714	426661.683034317	368544.364462013
	453634.391719787	403352.761139326	398850.450338736	360260.500438105
Average	453800.222036951	447347.140584544	368231.499789023	427319.374464264

Gluconate (Relative response)

	Vehicle (0.1% DMSO)	Forskolin	Forskolin + DCVC (10 μM)	Forskolin + DCVC (20 μM)
	1174019.21649567	1750110.34386574	2505808.61216436	4686597.69396932
	989449.199527297	2264130.59324959	2361972.44666252	1491445.40192058
	668630.841360544	1243439.68713348	553218.637550705	1260908.34596076
	1454140.92606625	3471006.37472047	1776220.85938873	1412845.59411985
	1410192.97895479	972137.022021575	1680767.73738885	995264.705119501
Average	1139286.63248091	1940164.80419817	1775597.65863103	1969412.34821800

Glutamate (Relative response)

	Vehicle (0.1% DMSO)	Forskolin	Forskolin + DCVC (10 μM)	Forskolin + DCVC (20 μM)
	10196860.6384147	6657977.13275369	10476261.2873121	5349117.87845842
	11066260.5969455	7826781.92650512	9878505.93224222	11084413.2448821
	9803838.60082761	8669008.41356904	6800052.84766124	12266120.0710548
	9031997.83100949	7763643.07617403	10107909.2765198	11477316.7015036
	11591719.1258661	9160111.38198923	8748392.2489722	10253004.7676401
Average	10338135.3586127	8015504.38619822	9202224.31854151	10085994.5327078

Aspartate (Relative response)

	Vehicle (0.1% DMSO)	Forskolin	Forskolin + DCVC (10 μM)	Forskolin + DCVC (20 μM)
	2298719.23327588	1171271.67868016	1408887.06810831	683939.718936933
	2404797.0408211	1299069.37398625	1031865.5261527	641757.272000444
	2134695.24981922	1582802.43195329	963776.054962218	1276084.04734685
	3253270.97557796	2326734.8402766	1841762.09408527	1219084.63716756
	2783007.1919358	1537316.45847726	1134262.43855932	916358.344019551
Average	2574897.93828599	1583438.95667471	1276110.63637356	947444.803894268

Glutathione (GSH) (Relative response)

	Vehicle (0.1% DMSO)	Forskolin	Forskolin + DCVC (10 μM)	Forskolin + DCVC (20 μM)
	2574666.109163	1285849.40637094	1254483.51606688	1478818.67530848
	2927994.16493215	1602271.82557549	1276637.17257534	1069787.35073975
	1910890.29904556	1014690.19270616	1553677.20230736	904679.966742162
	2071224.15968098	3313869.00354071	1496296.93124825	1437571.34604358
	775544.877295789	1219651.34066514	1021975.90568927	740217.653758553
Average	2052063.92202350	1687266.35377169	1320614.14557742	1126214.99851850

Phosphocreatine (Relative response)

	Vehicle (0.1% DMSO)	Forskolin	Forskolin + DCVC (10 μM)	Forskolin + DCVC (20 μM)
	454551.85697831	204145.607313613	170327.276045687	166500.194239367
	331298.315353717	229572.247003832	118184.314470439	79845.1898154739
	327141.221602214	392386.471035413	56773.3791944169	162681.548258016
	225983.170758931	142106.168398271	170606.813829002	136937.291475438
	735899.770019573	254872.974355581	159090.696530966	108539.658896785
Average	414974.866942549	244616.693621342	134996.496014102	130900.776537016

Uridine diphosphate (UDP) (Relative response)

	Vehicle (0.1% DMSO)	Forskolin	Forskolin + DCVC (10 μM)	Forskolin + DCVC (20 μM)

	645917.427355274	685432.235277347	436125.045207122	418813.65094107
	708233.487450085	415523.832544218	240783.787879113	149322.836801892
	687704.267413249	738559.7411582	126486.345980097	228260.125587615
	622884.198806184	637076.097748023	226058.655670003	198968.80097381
	2243486.70168367	385204.353116313	364186.855151468	190509.666703531
Average	981645.216541692	572359.251968820	278728.137977561	237175.016201584

UDP-N-acetyl-D-glucosamine (Relative response)

	Vehicle (0.1% DMSO)	Forskolin	Forskolin + DCVC (10 μM)	Forskolin + DCVC (20 μM)
	1782091.14925734	623398.03069108	1053190.40632734	980826.99666882
	1389152.1717686	840427.278962086	1006461.05855669	925033.71417051
	1385336.5941752	1108560.53518808	459082.750381614	1334937.78073005
	1406524.11354646	824793.293644988	813160.978492501	903923.213684079
	2841716.48009302	1191122.61079255	936267.416660438	1345672.19231531
Average	1760964.10176812	917660.34985576	853632.52208372	1098078.77951375

UDP-D-glucose (Relative response)

	Vehicle (0.1% DMSO)	Forskolin	Forskolin + DCVC (10 μM)	Forskolin + DCVC (20 μM)
	1610529.88578895	562057.932063174	716843.058101649	423761.325061167
	1153370.52970799	603653.583800584	411361.31671166	257849.105844303
	1323388.77217408	877137.445441189	216649.958037673	460385.335574967
	965530.681537843	620664.959285628	505202.612512754	435340.78231225
	2982747.36867778	764352.265866518	406015.18419757	335618.145122503
Average	1607113.44757733	685573.23729142	451214.42591226	382590.93878304

N-Acetyl-glucosamine-1-phosphate (Relative response)

	Vehicle (0.1% DMSO)	Forskolin	Forskolin + DCVC (10 μM)	Forskolin + DCVC (20 μM)
	43060.1555538728	28792.6430909685	44353.3760728178	28383.926971332
	40381.6049585973	25506.0935043795	33120.413095387	21967.6488991945
	32464.622344282	28573.6052892275	16864.0613345608	32436.429164985
	39668.0370959446	51546.8241798381	32571.277467623	34611.8056822476
	78406.5822631106	34306.757902136	20952.1543814387	30724.9733272983
Average	46796.2004431615	33745.1847933099	29572.2564703655	29624.9568090115

Uridine monophosphate (UMP) (Relative response)

	Vehicle (0.1% DMSO)	Forskolin	Forskolin + DCVC (10 μM)	Forskolin + DCVC (20 μM)
	387164.713937517	746068.767065474	954965.645731668	147057.19856209
	624199.533063653	508739.353949539	404353.744112558	178483.972039197
	783958.841280369	862223.558524544	242437.757393647	234030.291084895
	332907.394128567	500941.662747765	254134.091538829	217688.176473857
	2105823.44642235	919099.419671158	490000.716821029	187427.58654357
Average	846810.785766491	707414.552391696	469178.391119546	192937.444940722

Glutathione disulfide (GSSG) (Relative response)

	Vehicle (0.1% DMSO)	Forskolin	Forskolin + DCVC (10 μM)	Forskolin + DCVC (20 μM)
	5157060.43478775	2452228.71313292	5313680.17179217	3878517.90734591
	3868058.76340793	1415574.1478066	3564541.30930056	3633697.98898544
	4574057.8957487	3268557.94742999	865149.438860533	4758626.4367129
	4171230.95663982	2490552.45481477	3471727.4877796	3813336.61022054

	13992628.2236502	2931170.8827408	3310475.47992373	4080398.0202422
Average	6352607.25484688	2511616.82918502	3305114.77753132	4032915.39270140

Cytidine monophosphate (CMP) (Relative response)

	Vehicle (0.1% DMSO)	Forskolin	Forskolin + DCVC (10 μM)	Forskolin + DCVC (20 μM)
	93645.9812971805	194089.470130283	294246.610610406	68998.9077829792
	152481.987441027	153345.031417315	143133.82641875	91401.6516727605
	189727.163031354	241678.549275991	72217.4414239354	110767.095373784
	94116.9844755483	136250.797325772	90480.1163943396	101522.091896064
	442310.976824141	242427.506718835	165384.849112367	89424.0586510191
Average	194456.618613850	193558.270973639	153092.568791960	92422.7610753214

UDP-D-glucuronate (Relative response)

	Vehicle (0.1% DMSO)	Forskolin	Forskolin + DCVC (10 μM)	Forskolin + DCVC (20 μM)
	152791.862043021	121821.670320996	115555.027263174	122394.180426833
	153263.124950914	103049.920759709	98464.1991803553	64913.9129158291
	164183.400601146	153548.657752835	43037.407327095	92689.6512297803
	169462.156677757	158869.940931369	92412.7096221748	75730.4630910972
	396535.481284785	112905.051441851	123696.35645341	95170.5916234926
Average	207247.205111525	130039.048241352	94633.1399692418	90179.7598574064

Guanosine diphosphate (GDP) (Relative response)

	Vehicle (0.1% DMSO)	Forskolin	Forskolin + DCVC (10 μM)	Forskolin + DCVC (20 μM)
	138855.665416501	180817.019995708	239851.50791973	457088.139898694
	160097.828763909	144789.276503541	249079.154962596	193156.756887486
	109043.985677624	185935.782753223	88134.427533928	297822.845243087
	180183.403948	278208.138602849	221139.568898053	231263.003427751
	479676.477920829	146679.770442953	287446.560007494	276865.218885692
Average	213571.472345373	187285.997659655	217130.243864360	291239.192868542

Leucine & isoleucine (Relative response)

	Vehicle (0.1% DMSO)	Forskolin	Forskolin + DCVC (10 μM)	Forskolin + DCVC (20 μM)
	11343654.5307601	9912566.24124498	6715326.94664157	9168638.37367567
	8834100.50444693	10406711.9940073	6464509.41503418	6008179.73080259
	6647467.13467104	9345839.59034407	2769562.35416773	8837845.86698693
	7632107.83816127	10797693.8615505	7467129.59109134	6874405.70560619
	18096763.2415142	7599536.25529325	11576347.9934083	8521944.86953362
Average	10510818.6499107	9612469.58848802	6998575.26006862	7882202.90932100

Valine (Relative response)

	Vehicle (0.1% DMSO)	Forskolin	Forskolin + DCVC (10 μM)	Forskolin + DCVC (20 μM)
	41863997.0013018	59415334.1512695	44711418.6221319	58227676.2257195
	40947500.1817221	72867101.330966	36796509.1816118	37151100.417638
	41302326.797836	53635102.1823053	52018076.0333312	50271208.2448146
	48083692.0590495	73936154.6525552	44321870.8356226	45032381.5195939
	77549463.0793953	42177430.2994955	61587925.6476063	37445448.0374934
Average	49949395.8238609	60406224.5233183	47887160.0640608	45625562.8890519

Alanine (Relative response)

	Vehicle (0.1% DMSO)	Forskolin	Forskolin + DCVC (10 μM)	Forskolin + DCVC (20 μM)
	1251761.77259576	1156696.88229286	1640231.91714714	1061674.71952721
	1199734.83264185	1003110.99653245	1260390.19749639	1041966.79796466
	1044063.47284301	1590270.49164745	525921.754890769	1675263.60767559
	662383.09602826	984716.455139082	1026112.96163433	969155.672613549
	1097776.87606626	1622019.5604579	1261055.5765126	1400777.76733933
Average	1051144.01003503	1271362.87721395	1142742.48153625	1229767.71302407

Phenylalanine (Relative response)

	Vehicle (0.1% DMSO)	Forskolin	Forskolin + DCVC (10 μM)	Forskolin + DCVC (20 μM)
	4242006.26355555	3147478.1964243	2403584.9887673	3175526.17366259
	3219119.14634314	3164968.73743551	2299841.20428549	1998914.92635796
	2387673.93396912	3204109.27716673	881279.736587924	2868154.59127969
	2602605.48387078	4001978.15664152	2514593.65235578	2353168.08829021
	5287830.31731118	2672339.65484187	3775387.07067325	2810842.62246749
Average	3547847.02900995	3238174.80450199	2374937.33053395	2641321.28041159

Proline (Relative response)

	Vehicle (0.1% DMSO)	Forskolin	Forskolin + DCVC (10 μM)	Forskolin + DCVC (20 μM)
	4410509.14315248	3212930.91963301	1509874.37547466	1630644.43907842
	4383537.44288163	3984053.9780354	1216813.66058772	908547.193515211
	4023562.95024057	2799667.31269328	580835.943408454	1519074.29202187
	3227231.97099285	3279498.85463706	1142787.40283567	1051955.99256528
	9450002.84262297	2731683.65740384	3692704.79519709	1315197.72733954
Average	5098968.86997810	3201566.94448052	1628603.23550072	1285083.92890406

Tyrosine (Relative response)

	Vehicle (0.1% DMSO)	Forskolin	Forskolin + DCVC (10 μM)	Forskolin + DCVC (20 μM)
	2408423.93067313	1658435.64947996	1669482.34893131	1427875.31954282
	2258255.00289601	1682948.63917859	1558202.79137452	1545613.54309392
	1728680.32768422	1969713.10178216	916205.174969534	1938657.30475188
	1705017.07104411	2340243.17295009	1681970.0762979	1583296.34815492
	2467920.48007969	1855176.56981293	1950341.75944492	1618402.95096117
Average	2113659.36247543	1901303.42664075	1555240.43020364	1622769.09330094

Inosine (Relative response)

	Vehicle (0.1% DMSO)	Forskolin	Forskolin + DCVC (10 μM)	Forskolin + DCVC (20 μM)
	0	575868.640851873	1063134.59321198	140366.597238706
	419830.468932748	387624.726164021	886815.244877786	304905.560332782
	254146.296299846	346438.13593634	656595.524612478	272311.383914118
	482408.070402302	905047.384387647	552377.193066114	585622.820080736
	260596.492745321	1011862.633655	435906.987860136	374280.836612713
Average	283396.265676043	645368.304198976	718965.908725699	335497.439635811

Taurine (Relative response)

	Vehicle (0.1% DMSO)	Forskolin	Forskolin + DCVC (10 μM)	Forskolin + DCVC (20 μM)
	34832116.7998706	22087965.9626573	36718502.277578	22568531.8347089
	37175004.244683	20423154.2509749	24250668.8701759	23197132.1593347

	33959463.3280719	30696726.7625361	15479791.9381939	31278122.9072844
	28325168.2069816	24156553.1910148	24500870.9051007	24855195.7896179
	25101322.9693925	31859201.1741884	27757953.2438995	23240257.1151208
Average	31878615.1097999	25844720.2682743	25741557.4469896	25027847.9612133

Threonine (Relative response)

	Vehicle (0.1% DMSO)	Forskolin	Forskolin + DCVC (10 μM)	Forskolin + DCVC (20 μM)
	1164192.6125416	1118774.44172737	703292.191779367	1151171.71986693
	1216930.32449122	1344506.14018676	716758.251996643	667721.77963068
	871606.507158474	1117090.64442412	405109.392504064	1050846.38976126
	922920.811346582	1906531.83579642	725747.459244199	770551.640353699
	0	902359.916186898	1735056.19408761	909668.447427323
Average	835130.051107575	1277852.59566431	857192.697922377	909991.995407978

Ornithine (Relative response)

	Vehicle (0.1% DMSO)	Forskolin	Forskolin + DCVC (10 μM)	Forskolin + DCVC (20 μM)
	804030.731589232	711888.477623132	486108.936173583	681677.792198983
	623789.299996837	737260.128653208	476929.423049256	430887.119421208
	474636.187931985	672819.584103773	211225.678164372	634166.237526866
	546844.64217889	764019.639681086	556043.319400091	504811.559963168
	1362557.22626383	542315.657116506	799644.431607857	618591.440049595
Average	762371.617592155	685660.697435541	505990.357679032	574026.829831964

Glutamine (Relative response)

	Vehicle (0.1% DMSO)	Forskolin	Forskolin + DCVC (10 μM)	Forskolin + DCVC (20 μM)
	11945289.8254137	9164974.33853216	10199986.2175945	9689465.67942537
	12500063.1523097	9340994.43741836	9906358.61657095	9374614.04771588
	9149185.65110307	12259097.8300695	4770369.69419618	13003653.0748484
	9177487.68623987	13452335.4094325	10838604.0826682	11276585.9144576
	0	9551327.32152035	10551850.5325479	10478556.7482073
Average	8554405.26301327	10753745.8673946	9253433.82871555	10764575.0929309

Methionine (Relative response)

	Vehicle (0.1% DMSO)	Forskolin	Forskolin + DCVC (10 μM)	Forskolin + DCVC (20 μM)
	592505.248066773	444152.393732023	331688.121731243	436233.022518756
	445223.95873605	474945.791698838	308923.914637661	284287.681428199
	328083.189185964	425541.776217965	128986.105409223	420456.768371393
	390539.490487559	652239.056046085	356234.734328076	353377.738612674
	0	392273.467466704	534796.959338014	407941.937534404
Average	351270.377295269	477830.497032323	332125.967088843	380459.429693085

Asparagine (Relative response)

	Vehicle (0.1% DMSO)	Forskolin	Forskolin + DCVC (10 μM)	Forskolin + DCVC (20 μM)
	306056.6941342	228639.496465658	212044.475228957	242705.024835956
	359386.823685761	186611.913832089	195594.16750488	181320.447802217
	318863.709890896	262044.821493868	80833.8104264451	265266.819919936
	247776.730653648	292094.761533788	216117.399992834	229229.888016946
	0	248159.245229985	274135.692067005	226041.032888935
Average	246416.791672901	243510.047711078	195745.109044024	228912.642692798

Serine (Relative response)

	Vehicle (0.1% DMSO)	Forskolin	Forskolin + DCVC (10 μM)	Forskolin + DCVC (20 μM)
	246259.44751448	324428.726300696	170511.016591597	423002.177011066
	245650.830649712	255943.296805446	147604.040966249	132050.745107001
	219143.616103128	215763.528855643	50365.0829176607	233445.770317545
	274516.871459558	577445.576718414	175765.873216621	195787.535363497
	400440.106802223	185499.539191126	437980.505213508	195357.79921253
Average	277202.174505820	311816.133574265	196445.303781127	235928.805402328

Tryptophan (Relative response)

	Vehicle (0.1% DMSO)	Forskolin	Forskolin + DCVC (10 μM)	Forskolin + DCVC (20 μM)
	1372489.99556618	788253.357168473	807663.450518481	707500.337736937
	1122413.58558275	744813.10258015	796412.159224484	732620.047209912
	811610.599075742	987077.993122173	331562.185094567	970198.786332832
	886507.715688728	1014820.75406683	899130.718260305	843168.405478302
	894436.610484804	902871.864936989	848175.018914986	931141.99393615
Average	1017491.70127964	887567.414374923	736588.706402565	836925.914138827

Xanthine (Relative response)

	Vehicle (0.1% DMSO)	Forskolin	Forskolin + DCVC (10 μM)	Forskolin + DCVC (20 μM)
	590302.025695044	467280.828151001	346876.017340094	585424.330320352
	429574.316314556	378796.636209808	340223.360533151	274446.065267453
	326287.69464977	460049.938823525	166785.67639351	396812.068176301
	378514.029267081	623034.958457026	354938.3140946	335840.492600153
	731990.70120991	393795.523118429	546182.976562623	454210.344558645
Average	491333.753427272	464591.576951958	351001.268984796	409346.660184581

Histidine (Relative response)

	Vehicle (0.1% DMSO)	Forskolin	Forskolin + DCVC (10 μM)	Forskolin + DCVC (20 μM)
	1222968.71443757	991340.787979862	877146.502956747	982289.915234937
	1140411.22547602	787305.208083144	913436.455259294	822834.123185479
	972879.63173437	1139109.7616317	539851.830364185	985104.37370831
	941914.087402447	1296302.68374535	1086350.35380326	1036712.12575555
	926139.168189361	1031204.23800577	1105872.45669494	1051859.80743311
Average	1040862.56544795	1049052.53588917	904531.519815685	975760.069063477

3-Phosphoserine (Relative response)

	Vehicle (0.1% DMSO)	Forskolin	Forskolin + DCVC (10 μM)	Forskolin + DCVC (20 μM)
	1231661.63905574	634376.645931474	1182163.28667798	570145.549100882
	1241235.29558227	655299.28593687	992071.998687401	848327.533902546
	999435.318337713	997897.056163873	78881.2516908852	1131279.32765401
	787271.6560686	597550.772362055	926644.983570854	966135.731032963
	1732476.1656398	1123991.05779469	647889.107274331	918188.265246278
Average	1198416.01493682	801822.963637793	765530.125580290	886815.281387336

Lysine (Relative response)

	Vehicle (0.1% DMSO)	Forskolin	Forskolin + DCVC (10 μM)	Forskolin + DCVC (20 μM)

	1256660.88109214	869652.757308284	513744.969548776	792030.761590202
	866169.423880891	987418.493356993	520138.043973971	396896.167617712
	601703.364818574	986460.986097304	112876.465891973	693665.024904138
	818777.215685111	0	587092.413430996	474528.919345792
	0	683212.88399536	993865.980145295	742747.518808663
Average	708662.177095343	705349.024151588	545543.574598202	619973.678453301

II. Metabolites measured as absolute concentration and normalized to protein (Units: pmol/µg protein)

Nicotinamide adenine dinucleotide (NAD) (pmol/µg protein)

	Vehicle (0.1% DMSO)	Forskolin	Forskolin + DCVC (10 µM)	Forskolin + DCVC (20 µM)
	2.512408041	2.106652992	3.148497671	3.625955015
	2.385852219	2.174842643	2.542743101	2.984764575
	1.053241991	2.428894436	0.638498238	2.589431237
	1.495720425	5.85646457	1.908604939	3.083416378
	3.240356039	2.76192841	7.625911006	2.450495068
Average	2.137515743	3.06575661	3.172850991	2.946812455

Succinate (SUC) (pmol/µg protein)

	Vehicle (0.1% DMSO)	Forskolin	Forskolin + DCVC (10 µM)	Forskolin + DCVC (20 µM)
	1.703093977	2.543016556	8.330499233	16.10042428
	2.170219945	3.518507554	6.491699533	9.996673157
	0.770305684	4.241699003	1.660184916	10.01823461
	1.240298284	9.107839054	4.316164187	9.458343242
	1.246777346	3.110622096	23.89671458	4.767429293
Average	1.426139047	4.504336853	8.93905249	10.06822092

Ribose 5-phosphate & xylulose 5-phosphate (R5P & X5P) (pmol/µg protein)

Units: pmol/µg protein	Vehicle (0.1% DMSO)	Forskolin	Forskolin + DCVC (10 µM)	Forskolin + DCVC (20 µM)
	0.227773237	0.387335443	1.408464282	0.169374061
	0.325449587	0.345835944	0.547649001	0.174126778
	0.232593052	0.439961997	0.084493685	0.477933432
	0.192264922	2.014695697	0.166168137	0.203293387
	0.266245396	0.447900557	0.733925725	0
Average	0.248865239	0.727145928	0.588140166	0.204945532

Flavin adenine dinucleotide (FAD) (pmol/µg protein)

Units: pmol/µg protein	Vehicle (0.1% DMSO)	Forskolin	Forskolin + DCVC (10 µM)	Forskolin + DCVC (20 µM)
	0.151034716	0.052364344	0.240234386	0.080859811
	0.166830931	0.087093666	0.16795638	0.106806589
	0.075879083	0.12080502	0.055173856	0.164451934
	0.063842232	0.144817552	0.093240837	0.167232668
	0.138567877	0.18579586	0.212334377	0.058236056
Average	0.119230968	0.118175288	0.153787967	0.115517412

Erythrose 4-Phosphate (E4P) (pmol/µg protein)

	Vehicle (0.1% DMSO)	Forskolin	Forskolin + DCVC (10 µM)	Forskolin + DCVC (20 µM)
	8.157250779	2.272840201	16.17954389	6.010695038
	4.262950786	8.053224475	7.728650957	5.409879586

	1.277958761	3.112437343	1.438108088	9.898652169
	3.649866932	30.83773592	5.065637725	7.999987735
	2.226808455	4.14130445	6.752652229	2.048201957
Average	3.914967143	9.683508478	7.432918578	6.273483297

Fructose 6-phosphate & glucose 6-phosphate (F6P & G6P) (pmol/µg protein)

	Vehicle (0.1% DMSO)	Forskolin	Forskolin + DCVC (10 µM)	Forskolin + DCVC (20 µM)
	2.583601509	3.230561626	5.718755308	5.267814328
	3.423073182	2.634837937	4.268601975	4.302948439
	1.324955227	3.462942036	0.895104763	4.31558929
	3.159625941	14.20994424	3.603083419	5.518673139
	2.617617752	3.356595921	7.163270019	3.214738886
Average	2.621774722	5.378976352	4.329763097	4.523952816

Sedoheptulose 7-phosphate (S7P) (pmol/µg protein)

	Vehicle (0.1% DMSO)	Forskolin	Forskolin + DCVC (10 µM)	Forskolin + DCVC (20 µM)
	1.282433373	1.206156524	3.879572892	1.140541295
	1.377359714	0.93584822	2.745851084	2.802180569
	0.677253421	1.389225017	0.890338996	2.170419633
	0.894199895	4.75938268	1.574069718	2.809401472
	1.149949479	2.54091571	3.039774417	0.928822
Average	1.076239176	2.16630563	2.425921421	1.970272994

Adenosine monophosphate (AMP) (pmol/µg protein)

	Vehicle (0.1% DMSO)	Forskolin	Forskolin + DCVC (10 µM)	Forskolin + DCVC (20 µM)
	2.22928311	7.371546416	17.73390332	9.653842529
	4.603465593	6.408469763	10.02720341	11.54446467
	2.473878321	10.03555051	2.638267844	9.877139135
	3.844682004	31.95891773	8.594408619	14.89845906
	5.132023061	8.23585817	29.36664694	5.278488174
Average	3.656666418	12.80206852	13.67208603	10.25047871

Guanosine monophosphate (GMP) (pmol/µg protein)

	Vehicle (0.1% DMSO)	Forskolin	Forskolin + DCVC (10 µM)	Forskolin + DCVC (20 µM)
	0.949893578	1.511727141	5.020870595	1.758213781
	1.374913923	1.550151515	3.826359918	3.704769784
	0.610545073	2.014445056	0.924762436	3.043790399
	0.803849684	5.446565642	2.535953908	3.956753765
	1.714677648	2.954046664	6.943680508	2.541494849
Average	1.090775981	2.695387204	3.850325473	3.001004516

Citrate & isocitrate (CIT & ICIT) (pmol/µg protein)

	Vehicle (0.1% DMSO)	Forskolin	Forskolin + DCVC (10 µM)	Forskolin + DCVC (20 µM)
	20.04101895	14.30240541	20.10824349	24.9039243
	17.01766637	12.38034457	14.90018721	25.26417531
	7.517133919	19.76033261	3.558957003	24.51030888
	9.117503625	40.26148274	15.55888752	26.39417839
	19.22439186	17.82976091	40.14712529	15.96465496
Average	14.58354294	20.90686525	18.8546801	23.40744837

6-Phosphogluconate (6PG) (pmol/µg protein)

	Vehicle (0.1% DMSO)	Forskolin	Forskolin + DCVC (10 µM)	Forskolin + DCVC (20 µM)
	2.020133516	1.448090138	2.979943897	3.243144935
	1.9545711	1.762767551	2.834339765	3.784738496
	0.709157845	2.008384684	1.067303955	2.909222086
	1.869742905	6.307301655	3.576043789	4.788333532
	1.275495911	2.010306158	3.786650067	1.824198111
Average	1.565820255	2.707370037	2.848856295	3.309927432

Nicotinamide adenine dinucleotide phosphate (NADP) (pmol/µg protein)

	Vehicle (0.1% DMSO)	Forskolin	Forskolin + DCVC (10 µM)	Forskolin + DCVC (20 µM)
	1.297819561	0.411018751	1.499869221	0.4098734
	1.007640977	0.456413968	1.155227254	1.386243727
	0.44201914	0.749275374	0.425134206	1.388148311
	0.405539277	1.057745671	0.987346851	2.173351976
	0.995808022	1.403090958	0.966933153	0.539382955
Average	0.829765395	0.815508944	1.006902137	1.179400074

Phosphoenolpyruvate (PEP) (pmol/µg protein)

	Vehicle (0.1% DMSO)	Forskolin	Forskolin + DCVC (10 µM)	Forskolin + DCVC (20 µM)
	1.019389633	0.649581738	0.968538835	0.767341594
	0.810402955	0.690770367	0.762620802	1.156927533
	0.320494431	0.864017084	0.462691584	0.905175333
	0.55310764	2.045845707	0.816773572	1.447928874
	0.661787143	0.922327987	1.455742652	0.542422661
Average	0.67303636	1.034508577	0.893273489	0.963959199

Adenosine diphosphate (ADP) (pmol/µg protein)

	Vehicle (0.1% DMSO)	Forskolin	Forskolin + DCVC (10 µM)	Forskolin + DCVC (20 µM)
	10.82866734	11.1895863	20.73431637	35.84161726
	14.04707046	13.03137309	18.13796142	29.43924233
	7.054577274	17.36894386	3.755229213	31.03713965
	15.69843466	59.66881479	22.47673919	32.33186504
	12.47546768	11.06170632	53.92549153	16.35991426
Average	12.02084348	22.46408487	23.80594754	29.00195571

Fructose 1,6-bisphosphate (FBP) (pmol/µg protein)

	Vehicle (0.1% DMSO)	Forskolin	Forskolin + DCVC (10 µM)	Forskolin + DCVC (20 µM)
	6.411887221	2.035235111	2.62573712	3.719698462
	4.948563162	1.995760456	2.31012425	5.285969706
	2.64081915	3.914514461	0.905751308	5.467536175
	3.340991079	3.079679175	4.364336339	5.381722253
	3.873956722	4.261802064	7.718745803	2.662456246
Average	4.243243467	3.057398253	3.584938964	4.503476568

Adenosine triphosphate (ATP) (pmol/µg protein)

	Vehicle (0.1% DMSO)	Forskolin	Forskolin + DCVC (10 µM)	Forskolin + DCVC (20 µM)

	47.44641598	9.915070784	20.0525312	74.16448978
	33.4240421	14.3123025	22.79260526	44.74719708
	11.09888575	14.49837465	4.232818336	52.29192421
	40.74059774	78.94727219	35.40194012	41.06983018
	14.51043606	12.25325486	55.57974082	22.93466603
Average	29.44407553	25.985255	27.61192715	47.04162146

Below are duplicate measurements that were not used

3-phosphoserine (duplicate – not used)

	Vehicle (0.1% DMSO)	Forskolin	Forskolin + DCVC (10 μM)	Forskolin + DCVC (20 μM)
	1223296.39988493	627148.784327659	1176312.35607987	559025.790770423
	1231713.04090067	627093.870703473	987111.344850652	839817.753864484
	993249.806328151	992505.285573434	70000.0502570201	1118503.27091267
	782968.607180161	586031.409551877	916121.460926119	957469.131058504
	4593396.11423264	1115261.7167805	643939.977080099	906985.015732987
Average	1764924.79370531	789608.213387389	758697.037838752	876360.192467814

GMP (duplicate – not used)

	Vehicle (0.1% DMSO)	Forskolin	Forskolin + DCVC (10 μM)	Forskolin + DCVC (20 μM)
	69384.7592724389	213436.04574124	454617.558156657	170032.612251211
	134224.542787707	157768.149707528	390376.801374495	207002.805322597
	12560.9952014022	222141.732494345	156672.582708375	229168.665241053
	118408.618062833	323295.13708953	230421.949411317	231436.207627368
	462817.288684281	312985.566448983	325150.657251106	267859.293315077
Average	159479.240801732	245925.326296325	311447.909780390	221099.916751461

Phosphoenolpyruvate (duplicate – not used)

	Vehicle (0.1% DMSO)	Forskolin	Forskolin + DCVC (10 μM)	Forskolin + DCVC (20 μM)
	22801.1838297166	18168.6794515709	8533.18931296423	
	13409.5244461231	10293.8671749891	9538.90343508598	6088.89611069714
	13573.3515877345	17223.0967455805	2694.80728955237	11720.8744565169
	25451.0619327432	29368.7773587766	17752.6958296976	12016.3356277916
	52158.967571701	10634.7104696581	4843.0216406369	11094.9077533408
Average	25478.8178736037	17137.8262401150	8672.52350158742	10230.2534870866

Table S6.2. Metabolites increased or decreased in response to forskolin-stimulated syncytialization and DCVC treatment during syncytialization. Metabolites altered by any scenario are listed first and followed by metabolites that are not altered in any scenario. The values placed in **boldface** correspond to values associated with a $p < 0.05$. In the case of DCVC-stimulated responses, the first values for p-value and fold-change correspond to the 10 µM DCVC to syncytialization comparison. The second and third values correspond to the 20 µM DCVC to syncytialization comparison and the 20 µM DCVC to 10 µM DCVC comparison, respectively.

Metabolite	Change in response to syncytialization (forskolin-only treatment)		Change in response to DCVC treatment during syncytialization (10 µM, 20 µM, 20 vs. 10 µM)	
	p-value	**Fold-change**	**p-value**	**Fold-change**
Succinate	**0.0047**	**3.1584**	0.5705, 0.1592, 0.6224	1.9845, 2.2352, 1.1263
Uridine diphosphate (UDP)-D-glucose	**0.0060**	**0.42659**	0.0729, **0.0255**, 0.8247	0.65816, **0.55806**, 0.84791
Glutamate	**0.0065**	**0.77533**	0.6483, 0.4017, 0.9016	1.1481, 1.2583, 1.0960
Aspartate	**0.0068**	**0.61495**	0.4704, **0.0310,** 0.2350	0.80591, **0.59835**, 0.74245
UDP-N-acetyl-D-glucosamine	**0.0079**	**0.52111**	0.8714, 0.5298, 0.2805	0.93023, 1.1966, 1.2864
Adenosine monophosphate (AMP)	**0.0110**	**3.5010**	>0.9999, 0.9839, 0.9862	1.0680, 0.80069, 0.74974
Oleic acid	**0.0152**	**1.6915**	0.9056, **0.0344**, 0.0726	0.94652, **0.59512**, 0.62875
Glutathione – oxidized (GSSG)	**0.0167**	**0.39537**	0.8314, 0.2113, 0.4667	1.3159, 1.6057, 1.2202
Guanine monophosphate (GMP)	**0.0278**	**2.4711**	0.6785, 0.8657, 0.9391	1.4285, 1.1134, 0.77942
Proline	0.0732	0.62789	**0.0187, 0.0114**, 0.9583	**0.50869, 0.40139**, 0.78907
Uridine diphosphate (UDP)	0.1629	0.58306	**0.0241**, **0.0088**, 0.8426	**0.48698**, **0.41438**, 0.85092
Inosine	0.2649	2.2773	0.8667, 0.0962, **0.0395**	1.1140, 0.51985, **0.46664**
Cytidine monophosphate (CMP)	0.6423	0.99538	0.3577, **0.0218**, 0.2435	0.79094, **0.47749**, 0.60371
Uridine monophosphate (UMP)	0.9445	0.83539	0.1232, **0.0005**, **0.0190**	0.66323, **0.27274**, **0.41122**

Stearic acid	0.5836	0.81262	0.7896, 0.1923, 0.4757	1.0865, 1.3181, 1.2132
Palmitic acid	0.3306	0.77597	0.6858, 0.2008, 0.5957	1.1076, 1.2854, 1.1605
Hexose (glucose etc.)	0.9214	0.96177	0.0938, 0.3873, 0.6290	0.69938, 0.78781, 1.1264
Hypoxanthine	0.8798	0.98578	0.7155, 0.9751, 0.8348	0.82314, 0.95523, 1.1605
Gluconate	0.1142	1.7030	0.9540, 0.9856, 0.9906	0.91518, 1.0151, 1.1092
3-Phosphoserine	0.0605	0.66907	0.7414, 0.9644, 0.5888	0.95474, 1.1060, 1.1584
Glutathione – reduced (GSH)	0.5356	0.82223	0.7323, 0.2687, 0.6657	0.78269, 0.66748, 0.85280
Phosphocreatine	0.0867	0.58947	0.0664, 0.0699, 0.9995	0.55187, 0.53513, 0.96966
N-Acetyl-glucosamine-1-phosphate	0.1470	0.72111	0.6822, 0.8292, 0.9637	0.87634, 0.87790, 1.0018
UDP-D-glucuronate	0.0813	0.62746	0.1790, 0.1640, 0.9983	0.72773, 0.69348, 0.95294
Guanine diphosphate (GDP)	0.9706	0.87692	0.8940, 0.1939, 0.3703	1.1594, 1.5551, 1.3413
Leucine/isoleucine	0.8756	0.91453	0.1651, 0.6001, 0.6062	0.72807, 0.82000, 1.1263
Valine	0.2435	1.2093	0.2359, 0.1325, 0.9280	0.79275, 0.75531, 0.95277
Alanine	0.2628	1.2095	0.7446, 0.9863, 0.8319	0.89883, 0.96728, 1.0762
Phenylalanine	0.7446	0.91272	0.1897, 0.6059, 0.6534	0.73342, 0.81568, 1.1122
Tyrosine	0.3523	0.89953	0.2146, 0.4497, 0.8524	0.81799, 0.85350, 1.0434
Taurine	0.0972	0.81072	0.9826, 0.9849, >0.9999	0.99601, 0.96839, 0.97227
Threonine	0.3199	1.5301	0.1326, 0.3660, 0.7773	0.67081, 0.71213, 1.0616
Ornithine	0.8484	0.89938	0.1724, 0.6295, 0.5931	0.73796, 0.83719, 1.1345
Glutamine	0.3464	1.2571	0.4826, 0.9988, 0.4574	0.86048, 1.0010, 1.1633
Methionine	0.3320	1.3603	0.1372, 0.5625, 0.5753	0.69507, 0.79622, 1.1455
Asparagine	0.3892	0.98820	0.3323, 0.9490, 0.4891	0.80385, 0.94005, 1.1694

Serine	0.8122	1.1249	0.2607, 0.7395, 0.6459	0.63000, 0.75663, 1.2010
Tryptophan	0.3037	0.87231	0.3679, 0.9342, 0.5582	0.82990, 0.94294, 1.1362
Xanthine	0.8768	0.94557	0.2655, 0.7593, 0.6328	0.75551, 0.88109, 1.1662
Histidine	0.9937	1.0079	0.4392, 0.8816, 0.7182	0.86224, 0.93013, 1.0787
Lysine	0.9971	0.99532	0.6325, 0.5586, 0.9915	0.77344, 0.87896, 1.1364
Nicotinamide adenine dinucleotide (NAD)	0.2436	1.4343	0.9317, 0.9965, 0.9001	1.0349, 0.96120, 0.92876
Ribose 5-phosphate / Xylulose 5-phosphate (R5P/X5P)	0.1297	2.9218	0.9317, 0.2515, 0.4100	0.80883, 0.28185, 0.34846
Flavin adenine dinucleotide (FAD)	0.9729	0.99115	0.6403, 0.9974, 0.5993	1.3014, 0.97751, 0.75115
Erythrose 4-phosphate (E4P)	0.3179	2.4735	0.9986, 0.9912, 0.9968	0.76759, 0.64785, 0.84401
Fructose 6-phosphate / glucose 6-phosphate (F6P/G6P)	0.1677	2.0517	0.9140, 0.9949, 0.8719	0.80494, 0.84104, 1.0449
D-sedoheptulose 7-phosphate (S7P)	0.1331	2.0128	0.8884, 0.9987, 0.8661	1.1198, 0.90951, 0.81218
Citrate / Isocitrate (CIT/ICIT)	0.2674	1.4336	0.7618, 0.8656, 0.4613	0.90184, 1.1196, 1.2415
6-phosphogluconate (6PG)	0.2111	1.7290	0.9088, 0.5949, 0.8359	1.0523, 1.2226, 1.1618
Adenosine diphosphate (ADP)	0.2645	1.8688	0.9999, 0.5678, 0.5773	1.0597, 1.2910, 1.2183
Nicotinamide adenine dinucleotide phosphate (NADP)	0.9447	0.98282	0.8065, 0.6204, 0.9454	1.2347, 1.4462, 1.1713
Phosphoenolpyruvate (PEP)	0.2174	1.5371	0.9001, 0.9881, 0.9545	0.86348, 0.93180, 1.0791
Fructose 1,6-bisphosphate (FBP)	0.1759	0.72053	0.9998, 0.4592, 0.4684	1.1725, 1.4730, 1.2562
Adenosine triphosphate (ATP)	0.5045	0.88253	0.9616, 0.2145, 0.3155	1.0626, 1.8103, 1.7037

Table S6.3. Metabolite ratios with relevance to purine and pyrimidine metabolism analyzed and degree of change. Abbreviations: ATP, adenosine triphosphate; ADP, adenosine diphosphate; AMP, adenosine monophosphate; GDP, guanosine diphosphate, GMP, guanosine monophosphate; UDP, uridine diphosphate; UMP, uridine monophosphate; CMP, cytidine monophosphate. In the case of DCVC-stimulated responses, the first values for p-value and fold-change correspond to the 10 µM DCVC to syncytialization comparison. The second and third values correspond to the 20 µM DCVC to syncytialization comparison and the 20 µM DCVC to 10 µM DCVC comparison, respectively.

Metabolite Ratio	Change in response to syncytialization (forskolin-only treatment)		Change in response to DCVC treatment during syncytialization (10 µM, 20 µM, 20 vs. 10 µM)	
	p-value	**Fold-change**	**p-value**	**Fold-change**
ATP to ADP	**0.0410**	**0.43414**	0.6599, **0.0142**, 0.0682	1.1346, **1.5136**, 1.3340
ADP to AMP	**0.0051**	**0.49161**	0.9709, **0.0049, 0.0074**	1.0425, **1.7280, 1.6576**
ATP to AMP	0.0518	0.19333	0.8737, **0.0086, 0.0209**	1.2270, **2.6672, 2.1737**
GDP to GMP	**0.0096**	**0.42963**	0.9125, 0.5837, 0.3614	0.82939, 1.4219, 1.7144
UDP to UMP	0.0805	0.64730	0.8035, 0.3894, 0.1546	0.74871, 1.5388, 2.0552
UMP to CMP	0.0515	0.88087	**0.0010, <0.0001, <0.0001**	**0.83525, 0.57356, 0.68669**
UDP to CMP	**0.0218**	**0.57943**	0.3373, 0.9068, 0.5611	0.61794, 0.89029, 1.4407
Glutamine to UMP	0.8060	0.91114	0.3768, **<0.0001, 0.0001**	1.4498, **3.4306, 2.3663**
Inosine to hypoxanthine	0.0751	1.9874	0.3776, 0.4223, **0.0484**	1.4034, 0.62243, **0.44352**
Xanthine to hypoxanthine	0.9198	0.98308	0.5036, 0.7171, 0.9308	0.86063, 0.90447, 1.0509
Inosine to xanthine	0.0956	2.0760	0.2211, 0.6683, 0.0526	1.7014, 0.65494, 0.38493

Table S6.4. Metabolite ratios with relevance to glycolysis, tricarboxylic acid-cycle and pentose phosphate pathway analyzed and degree of change. The values placed in **boldface** correspond to values associated with a $p<0.05$. Abbreviations: G6P, glucose 6-phosphate; F6P, fructose 6-phosphate; FBP, fructose 1,6-bisphosphate; PEP, phosphoenolpyruvate; CIT, citrate; ICIT, isocitrate; 6PG, 6-phosphogluconate; R5P, ribose 5-phosphate; X5P, xylulose 5-phosphate; S7P, sedoheptulose 7-phosphate; E4P, erythrose 4-phosphate. In the case of DCVC-stimulated responses, the first values for p-value and fold-change correspond to the 10 µM DCVC to syncytialization comparison. The second and third values correspond to the 20 µM DCVC to syncytialization comparison and the 20 µM DCVC to 10 µM DCVC comparison, respectively.

Glycolysis (aka glycolysis or gluconeogenesis)				
Ratio	Change in response to syncytialization (forskolin-only treatment)		Change in response to DCVC treatment during syncytialization (10 µM, 20 µM, 20 vs. 10 µM)	
	p-value	Fold-change	p-value	Fold-change
G6P/F6P to FBP	0.1331	2.8572	0.7265, 0.4459, 0.8810	0.73610, 0.57130, 0.77611
FBP to PEP	**0.0024**	**0.51272**	0.9096, 0.1950, 0.3546	1.0998, 1.4439, 1.3128
G6P/F6P to PEP	0.4974	1.1372	0.9901, 0.9257, 0.8680	0.97382, 1.0731, 1.1020
Tricarboxylic acid cycle				
Ratio	Change in response to syncytialization (forskolin-only treatment)		Change in response to DCVC treatment during syncytialization (10 µM, 20 µM, 20 vs. 10 µM)	
	p-value	Fold-change	p-value	Fold-change
PEP to CIT/ICIT	0.6561	1.0477	0.5989, 0.8068, 0.2766	1.2854, 0.81772, 0.63616
CIT/ICIT to succinate	**0.0061**	**0.45943**	**0.0011**, **0.0015**, 0.9750	**0.50671**, **0.52851**, 1.0430
PEP to succinate	**0.0007**	**0.49755**	0.1044, **0.0103**, 0.4169	0.64814, **0.44247**, 0.68268
Pentose Phosphate Pathway				
Ratio	Change in response to syncytialization (forskolin-only treatment)		Change in response to DCVC treatment during syncytialization (10 µM, 20 µM, 20 vs. 10 µM)	
	p-value	Fold-change	p-value	Fold-change
6PG to gluconate	0.9256	1.0229	0.7979, 0.2845, 0.6204	1.2080, 1.5140, 1.2533
R5P/X5P to 6PG	0.2227	1.3332	0.7630, **0.0455**, 0.1516	0.80437, **0.24897**, 0.30952
R5P/X5P to S7P	0.1423	1.3348	0.1594, **0.0090**, 0.2645	0.62503, **0.31314**, 0.50100
S7P to E4P	0.8894	1.0505	0.9771, 0.9705, 0.9002	1.0612, 0.93043, 0.87676

Gluconate to E4P	0.8582	0.93114	0.8672, 0.9974, 0.8331	0.80353, 1.0263, 1.2773
R5P/X5P to gluconate	0.2283	1.4843	0.8584, 0.1590, 0.3467	0.83484, 0.38202, 0.45760
Gluconate to S7P	0.8405	1.0737	0.7997, 0.9561, 0.6333	0.64806, 1.1564, 1.7845

Table S6.5. Metabolite ratios with relevance to amino acid metabolism analyzed and degree of change. The values placed in **boldface** correspond to values associated with a p<0.05. In the case of DCVC-stimulated responses, the first values for p-value and fold-change correspond to the 10 µM DCVC to syncytialization comparison. The second and third values correspond to the 20 µM DCVC to syncytialization comparison and the 20 µM DCVC to 10 µM DCVC comparison, respectively.

Ratio	Change in response to syncytialization (forskolin-only treatment)		Change in response to DCVC treatment during syncytialization (10 µM, 20 µM, 20 vs. 10 µM)	
	p-value	**Fold-change**	**p-value**	**Fold-change**
Phenylalanine to tyrosine	0.7075	1.0387	0.4324, 0.9370, 0.6296	0.85421, 0.96073, 1.1247
Glutamine to glutamate	0.0755	1.5904	0.1582, 0.5076, 0.6847	0.73324, 0.84647, 1.1544
Asparagine to aspartate	0.1053	1.5575	0.9987, **0.0366**, **0.0335**	0.98936, **1.6174**, **1.6348**
Glutamate to succinate	**0.0029**	**0.26449**	0.9365, 0.3419, 0.5221	0.89701, 0.56437, 0.62917
Aspartate to alanine	0.0663	0.49607	0.9616, 0.2276, 0.3330	0.93815, 0.59482, 0.63404
Ornithine to proline	**0.0030**	**1.4261**	**0.0091**, **0.0001**, 0.0704	**1.6512**, **2.0956**, 1.2692
Taurine to alanine	**0.0138**	**0.65575**	0.3854, 0.9883, 0.4616	1.1362, 1.0145, 0.89293
Serine to tryptophan	0.4513	1.2263	0.6033, 0.8348, 0.9153	0.72084, 0.83554, 1.1591
Serine to 3-phosphoserine	0.1869	1.8794	0.8686, 0.6976, 0.9479	0.79890, 0.67539, 0.84540
Histidine to glutamate	0.0532	1.3042	0.2492, 0.4337, 0.9117	0.74113, 0.80417, 1.0851
Histidine to aspartate	**0.0046**	**1.6313**	0.9328, **0.0195**, **0.0369**	1.0685, **1.6143**, **1.5109**
Phenylalanine to succinate	**0.0053**	**0.31246**	**0.0152**, **0.0054**, 0.8358	**0.45674**, **0.36312**, 0.79503

Table S6.6. Metabolite ratios with relevance to glutathione metabolism analyzed and degree of change. The values placed in **boldface** correspond to values associated with a p<0.05. Abbreviations: GSH, glutathione; GSSG, glutathione disulfide; NADP, nicotinamide adenine dinucleotide phosphate. In the case of DCVC-stimulated responses, the first values for p-value and fold-change correspond to the 10 µM DCVC to syncytialization comparison. The second and third values correspond to the 20 µM DCVC to syncytialization comparison and the 20 µM DCVC to 10 µM DCVC comparison, respectively.

Ratio	Change in response to syncytialization (forskolin-only treatment)		Change in response to DCVC treatment during syncytialization (10 µM, 20 µM, 20 vs. 10 µM)	
	p-value	**Fold-change**	**p-value**	**Fold-change**
GSH to GSSG	0.2391	1.6682	0.9178, 0.3024, 0.4994	0.84285, 0.38353, 0.45505
GSSG to NADP	**0.0487**	**0.42058**	0.9422, 0.5852, 0.4019	0.87297, 1.3893, 1.5914
GSH to NADP	0.5302	0.79446	0.5888, 0.4257, 0.9551	0.68096, 0.58899, 0.86494
GSH to glutamate	0.8451	1.0661	0.5005, 0.3270, 0.9383	0.69059, 0.59930, 0.86780

Table S6.7. Other important metabolite ratios analyzed and degree of change. The values placed in **boldface** correspond to values associated with a p<0.05. Abbreviations: ATP, adenosine triphosphate; ADP, adenosine diphosphate; UDP, uracil diphosphate; UMP, uracil monophosphate; NAD, nicotinamide adenine dinucleotide; NADP, nicotinamide adenine dinucleotide phosphate. In the case of DCVC-stimulated responses, the first values for p-value and fold-change correspond to the 10 µM DCVC to syncytialization comparison. The second and third values correspond to the 20 µM DCVC to syncytialization comparison and the 20 µM DCVC to 10 µM DCVC comparison, respectively.

Ratio	Change in response to syncytialization (forskolin-only treatment)		Change in response to DCVC treatment during syncytialization (10 µM, 20 µM, 20 vs. 10 µM)		Significance
	p-value	Fold-change	p-value	Fold-change	
Phosphocreatine to ATP	0.7008	0.82006	**0.0465**, **0.0074**, 0.5736	**0.40296**, **0.17623**, 0.43732	Phosphocreatine shuttling
Phosphocreatine to ADP	0.0513	0.45260	0.0698, **0.0126**, 0.6124	0.48155, **0.27981**, 0.58106	Phosphocreatine shuttling
Stearic acid to oleic acid	0.0873	0.45750	0.6871, **0.0072**, **0.0324**	1.2613, **2.1688**, **1.7195**	Fatty acid biosynthesis
Stearic acid to palmitic acid	0.2863	1.0679	0.9311, 0.8271, 0.6189	0.98386, 1.0265, 1.0433	Fatty acid biosynthesis
Oleic acid to palmitic acid	**0.0104**	**1.9980**	0.7006, **0.0148**, 0.0634	0.86949, **0.46450**, 0.53423	Fatty acid biosynthesis
UDP-D-glucose to UDP-D-glucuronate	**0.0272**	**0.68268**	0.7184, 0.3205, 0.7537	0.89962, 0.80699, 0.89704	Multiple pathways
NAD to NADP	0.0943	1.5143	0.8058, 0.9718, 0.9147	0.75697, 0.91227, 1.2052	Source of co-factor
UDP-D-glucose to UMP	**0.0266**	**0.41856**	0.9446, **0.0091**, **0.0163**	1.0896, **2.0056**, **1.8408**	Peripheral to pyrimidine metabolism

Table S6.8. Enrichment analysis of organ, tissue, and subcellular structures predicted to be altered by forksolin-stimulated syncytialization (comparison of vehicle control versus forskolin-only treatment) based on the metabolite alterations.

	Total Compounds	Hits	Statistic Q[a]	Expected Q[a]	Raw p	Holm p	FDR[b]
Liver	234	6	32.1	11.111	0.006218	0.1741	0.073087
Endoplasmic Reticulum	53	6	38.092	11.111	0.006938	0.18732	0.073087
Peroxisome	37	4	43.102	11.111	0.007831	0.2036	0.073087
Golgi Apparatus	14	2	53.164	11.111	0.011962	0.29905	0.083733
Heart	8	1	49.452	11.111	0.023283	0.5588	0.093133
Neuron	69	1	49.452	11.111	0.023283	0.5588	0.093133
Smooth Muscle	9	1	49.452	11.111	0.023283	0.5588	0.093133
Skin	125	4	26.934	11.111	0.027756	0.58287	0.097145
Nervous Tissue	12	1	30.59	11.111	0.097248	1	0.30255
Bladder	87	4	22.083	11.111	0.1123	1	0.31443
Thyroid Gland	12	1	22.79	11.111	0.16293	1	0.36422
Adrenal Gland	30	1	17.116	11.111	0.23464	1	0.36422
Platelet	108	4	14.983	11.111	0.26751	1	0.36422
Nerve Cells	35	3	14.977	11.111	0.26826	1	0.36422
Testes	72	3	14.548	11.111	0.27639	1	0.36422
Brain	122	2	14.502	11.111	0.27713	1	0.36422
Kidney	164	3	14.441	11.111	0.27844	1	0.36422
Erythrocyte	34	2	14.386	11.111	0.2793	1	0.36422
Skeletal Muscle	123	12	12.375	11.111	0.31758	1	0.36422
Epidermis	216	14	12.187	11.111	0.32181	1	0.36422
Muscle	160	11	11.831	11.111	0.33004	1	0.36422
Mitochondria	98	7	11.822	11.111	0.33026	1	0.36422
Placenta	183	10	13.253	11.111	0.33512	1	0.36422
Pancreas	118	9	12.755	11.111	0.33533	1	0.36422
Fibroblasts	183	9	13.181	11.111	0.34035	1	0.36422
Spleen	170	6	12.554	11.111	0.34221	1	0.36422
Intestine	251	10	12.764	11.111	0.35121	1	0.36422
Prostate	267	29	9.0146	11.111	0.45264	1	0.45264

[a]The equation for the Q statistics can be found in Goeman *et al.* 2004 (Goeman *et al.*, 2004). Q can be considered as a squared covariance aggregate between metabolite concentrations and treatment. [b]FDR refers to false discovery rate.

Table S6.9. Enrichment analysis results of organ, tissue, and subcellular structures predicted to be altered when comparing DCVC treatment at 10 µM during syncytialization to forskolin-stimulated syncytialization alone based on the metabolite alterations.

	Total Compounds	Hits	Statistic Q^a	Expected Q^a	Raw p	Holm p	FDR[b]
Thyroid Gland	12	1	53.59	11.111	0.016078	0.4502	0.4502
Golgi Apparatus	14	2	33.777	11.111	0.066095	1	0.62222
Skin	125	4	28.271	11.111	0.066666	1	0.62222
Mitochondria	98	7	15.672	11.111	0.22163	1	0.78474
Placenta	183	10	15.057	11.111	0.22477	1	0.78474
Liver	234	6	12.903	11.111	0.30323	1	0.78474
Spleen	170	6	11.661	11.111	0.35455	1	0.78474
Endoplasmic Reticulum	53	6	11.361	11.111	0.35655	1	0.78474
Kidney	164	3	12.541	11.111	0.35672	1	0.78474
Skeletal Muscle	123	12	10.766	11.111	0.37972	1	0.78474
Muscle	160	11	10.423	11.111	0.39358	1	0.78474
Prostate	267	29	9.0028	11.111	0.41274	1	0.78474
Peroxisome	37	4	9.0204	11.111	0.4254	1	0.78474
Fibroblasts	183	9	8.3702	11.111	0.49732	1	0.78474
Heart	8	1	5.3025	11.111	0.52215	1	0.78474
Neuron	69	1	5.3025	11.111	0.52215	1	0.78474
Smooth Muscle	9	1	5.3025	11.111	0.52215	1	0.78474
Testes	72	3	7.139	11.111	0.54698	1	0.78474
Nerve Cells	35	3	6.3932	11.111	0.60335	1	0.78474
Bladder	87	4	4.6333	11.111	0.60681	1	0.78474
Pancreas	118	9	6.3886	11.111	0.62376	1	0.78474
Epidermis	216	14	5.5766	11.111	0.6784	1	0.78474
Adrenal Gland	30	1	1.9487	11.111	0.70052	1	0.78474
Erythrocyte	34	2	4.2407	11.111	0.70788	1	0.78474
Intestine	251	10	4.8927	11.111	0.71356	1	0.78474
Platelet	108	4	3.8162	11.111	0.72868	1	0.78474
Brain	122	2	2.4227	11.111	0.82338	1	0.85388
Nervous Tissue	12	1	0.30018	11.111	0.88051	1	0.88051

[a]The equation for the Q statistics can be found in Goeman *et al.* 2004 (Goeman *et al.*, 2004). Q can be considered as a squared covariance aggregate between metabolite concentrations and treatment. [b]FDR refers to false discovery rate.

Table S6.10. Enrichment analysis results of organ, tissue, and subcellular structures predicted to be altered when comparing DCVC treatment at 20 µM during syncytialization to forskolin-stimulated syncytialization alone based on the metabolite alterations.

	Total Compounds	Hits	Statistic Q^a	Expected Q^a	Raw p	Holm p	FDR[b]
Placenta	183	10	44.6	11.111	6.46E-05	0.00181	0.00181
Skin	125	4	46.463	11.111	0.000931	0.025139	0.013035
Golgi Apparatus	14	2	62.119	11.111	0.002943	0.076512	0.022037
Thyroid Gland	12	1	68.427	11.111	0.003148	0.078704	0.022037
Mitochondria	98	7	33.69	11.111	0.004033	0.096802	0.022587
Liver	234	6	33.003	11.111	0.00655	0.15065	0.030566
Pancreas	118	9	40.332	11.111	0.010097	0.22213	0.040387
Spleen	170	6	34.986	11.111	0.013221	0.27763	0.041591
Skeletal Muscle	123	12	37.715	11.111	0.013368	0.27763	0.041591
Endoplasmic Reticulum	53	6	32.592	11.111	0.015221	0.28921	0.04262
Muscle	160	11	33.751	11.111	0.020403	0.36725	0.051934
Intestine	251	10	28.138	11.111	0.026445	0.44957	0.061706
Peroxisome	37	4	30.177	11.111	0.03915	0.62639	0.084322
Kidney	164	3	30.644	11.111	0.056144	0.84217	0.11229
Testes	72	3	27.652	11.111	0.075069	1	0.13352
Epidermis	216	14	19.683	11.111	0.083604	1	0.13352
Brain	122	2	28.166	11.111	0.084332	1	0.13352
Bladder	87	4	27.032	11.111	0.085832	1	0.13352
Nerve Cells	35	3	24.348	11.111	0.10749	1	0.15841
Platelet	108	4	21.689	11.111	0.11541	1	0.16157
Erythrocyte	34	2	22.464	11.111	0.12858	1	0.17144
Fibroblasts	183	9	16.865	11.111	0.18428	1	0.23454
Prostate	267	29	11.889	11.111	0.32783	1	0.39909
Heart	8	1	5.5794	11.111	0.51117	1	0.55049
Neuron	69	1	5.5794	11.111	0.51117	1	0.55049
Smooth Muscle	9	1	5.5794	11.111	0.51117	1	0.55049
Nervous Tissue	12	1	0.61959	11.111	0.82888	1	0.85958
Adrenal Gland	30	1	0.32677	11.111	0.87536	1	0.87536

[a]The equation for the Q statistics can be found in Goeman *et al.* 2004 (Goeman *et al.*, 2004). Q can be considered as a squared covariance aggregate between metabolite concentrations and treatment. [b]FDR refers to false discovery rate.

Table S6.11. Enrichment analysis results of organ, tissue, and subcellular structures predicted to be altered when comparing DCVC treatment at 20 µM during syncytialization to DCVC treatment at 10 µM during syncytialization based on the metabolite alterations.

	Total Compounds	Hits	Statistic Q[a]	Expected Q[a]	Raw p	Holm p	FDR[b]
Kidney	164	3	37.021	11.111	0.02904	0.81313	0.4497
Erythrocyte	34	2	31.171	11.111	0.047391	1	0.4497
Brain	122	2	26.426	11.111	0.076237	1	0.4497
Nerve Cells	35	3	25.121	11.111	0.079957	1	0.4497
Intestine	251	10	22.033	11.111	0.10562	1	0.4497
Testes	72	3	21.826	11.111	0.12601	1	0.4497
Pancreas	118	9	21.744	11.111	0.12836	1	0.4497
Placenta	183	10	19.016	11.111	0.13907	1	0.4497
Spleen	170	6	19.927	11.111	0.14454	1	0.4497
Platelet	108	4	18.297	11.111	0.18956	1	0.53077
Skin	125	4	15.767	11.111	0.23142	1	0.54163
Fibroblasts	183	9	15.163	11.111	0.24749	1	0.54163
Bladder	87	4	15.039	11.111	0.25147	1	0.54163
Muscle	160	11	13.72	11.111	0.27588	1	0.55177
Skeletal Muscle	123	12	12.419	11.111	0.31066	1	0.57991
Prostate	267	29	10.92	11.111	0.3647	1	0.63822
Epidermis	216	14	8.1654	11.111	0.49547	1	0.7592
Liver	234	6	8.4086	11.111	0.5117	1	0.7592
Peroxisome	37	4	7.1375	11.111	0.53123	1	0.7592
Mitochondria	98	7	7.301	11.111	0.54598	1	0.7592
Endoplasmic Reticulum	53	6	6.5705	11.111	0.59479	1	0.7592
Adrenal Gland	30	1	3.1958	11.111	0.62121	1	0.7592
Thyroid Gland	12	1	3.1523	11.111	0.62363	1	0.7592
Heart	8	1	0.7057	11.111	0.81753	1	0.86405
Neuron	69	1	0.7057	11.111	0.81753	1	0.86405
Smooth Muscle	9	1	0.7057	11.111	0.81753	1	0.86405
Golgi Apparatus	14	2	1.7081	11.111	0.83319	1	0.86405
Nervous Tissue	12	1	0.001744	11.111	0.99087	1	0.99087

[a]The equation for the Q statistics can be found in Goeman *et al.* 2004 (Goeman *et al.*, 2004). Q can be considered as a squared covariance aggregate between metabolite concentrations and treatment. [b]FDR refers to false discovery rate.

Table S6.12. Enrichment analysis results of top 13 drug pathways altered by forskolin-stimulated syncytialization (comparison of vehicle control versus forskolin-only treatment). All other drug pathways had a raw p-value of greater than 0.05.

	Total Compounds	Hits	Statistic Q^a	Expected Q^a	Raw p	Holm p	FDR[b]
Abacavir Action Pathway	5	2	33.127	11.111	0.02765	1	0.36464
Delavirdine Action Pathway	4	2	33.127	11.111	0.02765	1	0.36464
Didanosine Action Pathway	6	2	33.127	11.111	0.02765	1	0.36464
Efavirenz Action Pathway	4	2	33.127	11.111	0.02765	1	0.36464
Emtricitabine Action Pathway	4	2	33.127	11.111	0.02765	1	0.36464
Lamivudine Action Pathway	5	2	33.127	11.111	0.02765	1	0.36464
Nevirapine Action Pathway	4	2	33.127	11.111	0.02765	1	0.36464
Rilpivirine Action Pathway	4	2	33.127	11.111	0.02765	1	0.36464
Stavudine Action Pathway	4	2	33.127	11.111	0.02765	1	0.36464
Zalcitabine Action Pathway	5	2	33.127	11.111	0.02765	1	0.36464
Zidovudine Action Pathway	4	2	33.127	11.111	0.02765	1	0.36464
Disulfiram Action Pathway	79	8	25.719	11.111	0.042536	1	0.36464
Valproic Acid Metabolism Pathway	37	7	23.614	11.111	0.043143	1	0.36464

[a]The equation for the Q statistics can be found in Goeman *et al.* 2004 (Goeman *et al.*, 2004). Q can be considered as a squared covariance aggregate between metabolite concentrations and treatment. [b]FDR refers to false discovery rate.

Table S6.13. Enrichment analysis results of the top 6 drug pathways altered when comparing DCVC treatment at 10 µM during syncytialization compared to forskolin-stimulated syncytialization alone. All other drug pathways had a raw p-value of greater than 0.1.

	Total Compounds	Hits	Statistic Q^a	Expected Q^a	Raw p	Holm p	FDR[b]
Morphine Metabolism Pathway	6	2	45.833	11.111	0.027439	1	0.93648
Sorafenib Metabolism Pathway	9	2	45.833	11.111	0.027439	1	0.93648
Celecoxib Metabolism Pathway	13	3	32.099	11.111	0.035559	1	0.93648
Ibuprofen Metabolism Pathway	15	3	32.099	11.111	0.035559	1	0.93648
Tamoxifen Action Pathway	27	4	23.884	11.111	0.097934	1	0.93648
Tamoxifen Metabolism Pathway	27	4	23.884	11.111	0.097934	1	0.93648

[a]The equation for the Q statistics can be found in Goeman *et al.* 2004 (Goeman *et al.*, 2004). Q can be considered as a squared covariance aggregate between metabolite concentrations and treatment. [b]FDR refers to false discovery rate.

Table S6.14. Enrichment analysis results of the top 30 drug pathways altered when comparing DCVC treatment at 20 µM during syncytialization compared to forskolin-stimulated syncytialization alone. The next highest raw p-value was 0.00428 (for morphine metabolism pathway and sorafenib metabolism pathway).

	Total Compounds	Hits	Statistic Q[a]	Expected Q[a]	Raw p	Holm p	FDR[b]
Amikacin Action Pathway	20	12	49.233	11.111	0.000382	0.1363	0.004543
Arbekacin Action Pathway	20	12	49.233	11.111	0.000382	0.1363	0.004543
Azithromycin Action Pathway	20	12	49.233	11.111	0.000382	0.1363	0.004543
Chloramphenicol Action Pathway	20	12	49.233	11.111	0.000382	0.1363	0.004543
Clarithromycin Action Pathway	20	12	49.233	11.111	0.000382	0.1363	0.004543
Clindamycin Action Pathway	20	12	49.233	11.111	0.000382	0.1363	0.004543
Clomocycline Action Pathway	20	12	49.233	11.111	0.000382	0.1363	0.004543
Demeclocycline Action Pathway	20	12	49.233	11.111	0.000382	0.1363	0.004543
Doxycycline Action Pathway	20	12	49.233	11.111	0.000382	0.1363	0.004543
Erythromycin Action Pathway	20	12	49.233	11.111	0.000382	0.1363	0.004543
Gentamicin Action Pathway	20	12	49.233	11.111	0.000382	0.1363	0.004543
Josamycin Action Pathway	20	12	49.233	11.111	0.000382	0.1363	0.004543
Kanamycin Action Pathway	20	12	49.233	11.111	0.000382	0.1363	0.004543
Lincomycin Action Pathway	20	12	49.233	11.111	0.000382	0.1363	0.004543
Lymecycline Action Pathway	20	12	49.233	11.111	0.000382	0.1363	0.004543
Methacycline Action Pathway	20	12	49.233	11.111	0.000382	0.1363	0.004543
Minocycline Action Pathway	20	12	49.233	11.111	0.000382	0.1363	0.004543
Neomycin Action Pathway	20	12	49.233	11.111	0.000382	0.1363	0.004543

Netilmicin Action Pathway	20	12	49.233	11.111	0.000382	0.1363	0.004543
Oxytetracycline Action Pathway	20	12	49.233	11.111	0.000382	0.1363	0.004543
Paromomycin Action Pathway	20	12	49.233	11.111	0.000382	0.1363	0.004543
Rolitetracycline Action Pathway	20	12	49.233	11.111	0.000382	0.1363	0.004543
Roxithromycin Action Pathway	20	12	49.233	11.111	0.000382	0.1363	0.004543
Spectinomycin Action Pathway	20	12	49.233	11.111	0.000382	0.1363	0.004543
Streptomycin Action Pathway	20	12	49.233	11.111	0.000382	0.1363	0.004543
Telithromycin Action Pathway	20	12	49.233	11.111	0.000382	0.1363	0.004543
Tetracycline Action Pathway	20	12	49.233	11.111	0.000382	0.1363	0.004543
Tigecycline Action Pathway	20	12	49.233	11.111	0.000382	0.1363	0.004543
Tobramycin Action Pathway	20	12	49.233	11.111	0.000382	0.1363	0.004543
Troleandomycin Action Pathway	20	12	49.233	11.111	0.000382	0.1363	0.004543

[a]The equation for the Q statistics can be found in Goeman *et al.* 2004 (Goeman *et al.*, 2004). Q can be considered as a squared covariance aggregate between metabolite concentrations and treatment. [b]FDR refers to false discovery rate.

Table S6.15. Enrichment analysis results of the top 4 drug pathways altered when comparing DCVC treatment at 20 µM during syncytialization compared to DCVC treatment at 10 µM during syncytialization. The next highest raw p-value was 0.21366, shared by 118 different drug pathways.

	Total Compounds	Hits	Statistic Q[a]	Expected Q[a]	Raw p	Holm p	FDR[b]
Glibenclamide Action Pathway	5	1	23.804	11.111	0.15256	1	0.3789
Gliclazide Action Pathway	6	1	23.804	11.111	0.15256	1	0.3789
Nateglinide Action Pathway	5	1	23.804	11.111	0.15256	1	0.3789
Repaglinide Action Pathway	5	1	23.804	11.111	0.15256	1	0.3789

[a]The equation for the Q statistics can be found in Goeman *et al.* 2004 (Goeman *et al.*, 2004). Q can be considered as a squared covariance aggregate between metabolite concentrations and treatment. [b]FDR refers to false discovery rate.

References

Agency for Toxic Substances and Disease Registry, 2007. Trichloroethylene Toxicity: What are the U.S. Standards for Trichloroethylene Exposure? In Agency for Toxic Substances and Disease Registry (ATSDR), E.H.a.M.E., (Ed.), Atlanta, GA, pp.

Agency for Toxic Substances and Disease Registry, 2019. Toxicological Profile for Trichloroethylene. In U.S. Department of Health and Human Services, A.f.T.S.a.D.R.A., (Ed.), Atlanta, GA, pp.

Al-Nasiry, S., Spitz, B., Hanssens, M., Luyten, C., Pijnenborg, R., 2006. Differential effects of inducers of syncytialization and apoptosis on BeWo and JEG-3 choriocarcinoma cells. Hum Reprod **21**, 193-201.

Allen, R.G., Newton, R.K., Sohal, R.S., Shipley, G.L., Nations, C., 1985. Alterations in superoxide dismutase, glutathione, and peroxides in the plasmodial slime mold Physarum polycephalum during differentiation. J Cell Physiol **125**, 413-419.

Aouache, R., Biquard, L., Vaiman, D., Miralles, F., 2018. Oxidative Stress in Preeclampsia and Placental Diseases. Int J Mol Sci **19**.

Bahado-Singh, R.O., Akolekar, R., Mandal, R., Dong, E., Xia, J., Kruger, M., Wishart, D.S., Nicolaides, K., 2012. Metabolomics and first-trimester prediction of early-onset preeclampsia. J Matern Fetal Neonatal Med **25**, 1840-1847.

Bahado-Singh, R.O., Syngelaki, A., Akolekar, R., Mandal, R., Bjondahl, T.C., Han, B., Dong, E., Bauer, S., Alpay-Savasan, Z., Graham, S., Turkoglu, O., Wishart, D.S., Nicolaides, K.H., 2015. Validation of metabolomic models for prediction of early-onset preeclampsia. Am J Obstet Gynecol **213**, 530 e531-530 e510.

Bar-Even, A., Flamholz, A., Noor, E., Milo, R., 2012. Rethinking glycolysis: on the biochemical logic of metabolic pathways. Nat Chem Biol **8**, 509-517.

Bohme, C.C., Arscott, L.D., Becker, K., Schirmer, R.H., Williams, C.H., Jr., 2000. Kinetic characterization of glutathione reductase from the malarial parasite Plasmodium falciparum. Comparison with the human enzyme. J Biol Chem **275**, 37317-37323.

Cantle, S.J., Kaufmann, P., Luckhardt, M., Schweikhart, G., 1987. Interpretation of syncytial sprouts and bridges in the human placenta. Placenta **8**, 221-234.

Chang, H.C., Lane, M.D., 1966. The enzymatic carboxylation of phosphoenolpyruvate. II. Purification and properties of liver mitochondrial phosphoenolpyruvate carboxykinase. J Biol Chem **241**, 2413-2420.

Chong, J., Soufan, O., Li, C., Caraus, I., Li, S., Bourque, G., Wishart, D.S., Xia, J., 2018. MetaboAnalyst 4.0: towards more transparent and integrative metabolomics analysis. Nucleic Acids Res **46**, W486-W494.

Chong, J., Wishart, D.S., Xia, J., 2019. Using MetaboAnalyst 4.0 for Comprehensive and Integrative Metabolomics Data Analysis. Curr Protoc Bioinformatics **68**, e86.

Colvin, B.N., Longtine, M.S., Chen, B., Costa, M.L., Nelson, D.M., 2017. Oleate attenuates palmitate-induced endoplasmic reticulum stress and apoptosis in placental trophoblasts. Reproduction **153**, 369-380.

Daly, J.W., 1984. Forskolin, adenylate cyclase, and cell physiology: an overview. Adv Cyclic Nucleotide Protein Phosphorylation Res **17**, 81-89.

Dickens, F., Glock, G.E., 1951. Direct oxidation of glucose-6-phosphate, 6-phosphogluconate and pentose-5-phosphates by enzymes of animal origin. Biochem J **50**, 81-95.

Dickens, F., Williamson, D.H., 1956. Pentose phosphate isomerase and epimerase from animal tissues. Biochem J **64**, 567-578.

Dunn, W.B., Broadhurst, D., Begley, P., Zelena, E., Francis-McIntyre, S., Anderson, N., Brown, M., Knowles, J.D., Halsall, A., Haselden, J.N., Nicholls, A.W., Wilson, I.D., Kell, D.B., Goodacre, R., Human Serum Metabolome, C., 2011. Procedures for large-scale metabolic profiling of serum and plasma using gas chromatography and liquid chromatography coupled to mass spectrometry. Nat Protoc **6**, 1060-1083.

Elkin, E.R., Bridges, D., Harris, S.M., Loch-Caruso, R.K., 2020. Exposure to Trichloroethylene Metabolite S-(1,2-Dichlorovinyl)-L-cysteine Causes Compensatory Changes to Macronutrient Utilization and Energy Metabolism in Placental HTR-8/SVneo Cells. Chem Res Toxicol.

Elkin, E.R., Bridges, D., Loch-Caruso, R., 2019. The trichloroethylene metabolite S-(1,2-dichlorovinyl)-L-cysteine induces progressive mitochondrial dysfunction in HTR-8/SVneo trophoblasts. Toxicology **427**, 152283.

Elkin, E.R., Harris, S.M., Loch-Caruso, R., 2018. Trichloroethylene metabolite S-(1,2-dichlorovinyl)-l-cysteine induces lipid peroxidation-associated apoptosis via the intrinsic and extrinsic apoptosis pathways in a first-trimester placental cell line. Toxicol Appl Pharmacol **338**, 30-42.

Endo, H., Okamoto, A., Yamada, K., Nikaido, T., Tanaka, T., 2005. Frequent apoptosis in placental villi from pregnancies complicated with intrauterine growth restriction and without maternal symptoms. Int J Mol Med **16**, 79-84.

Faas, M.M., van der Schaaf, G., Borghuis, T., Jongman, R.M., van Pampus, M.G., de Vos, P., van Goor, H., Bakker, W.W., 2010. Extracellular ATP induces albuminuria in pregnant rats. Nephrol Dial Transplant **25**, 2468-2478.

Fischer, U., Amrhein, N., 1974. Cyclic nucleotide phosphodiesterase of Chlamydomonas reinhardtii. Biochim Biophys Acta **341**, 412-420.

Forand, S.P., Lewis-Michl, E.L., Gomez, M.I., 2012. Adverse birth outcomes and maternal exposure to trichloroethylene and tetrachloroethylene through soil vapor intrusion in New York State. Environ Health Perspect **120**, 616-621.

Goeman, J.J., van de Geer, S.A., de Kort, F., van Houwelingen, H.C., 2004. A global test for groups of genes: testing association with a clinical outcome. Bioinformatics **20**, 93-99.

Graham, C.H., Hawley, T.S., Hawley, R.G., MacDougall, J.R., Kerbel, R.S., Khoo, N., Lala, P.K., 1993. Establishment and characterization of first trimester human trophoblast cells with extended lifespan. Exp Cell Res **206**, 204-211.

Gupta, S.K., Malhotra, S.S., Malik, A., Verma, S., Chaudhary, P., 2016. Cell Signaling Pathways Involved During Invasion and Syncytialization of Trophoblast Cells. Am J Reprod Immunol **75**, 361-371.

Hager, L.P., 1962. Succinyl CoA synthetase. In Boyer, P.D., Lardy, H., Myrback, K., (Eds.), The Enzymes. Academic Press, New York, pp. 387-399.

Hassan, I., Kumar, A.M., Park, H.R., Lash, L.H., Loch-Caruso, R., 2016. Reactive Oxygen Stimulation of Interleukin-6 Release in the Human Trophoblast Cell Line HTR-8/SVneo by the Trichlorethylene Metabolite S-(1,2-Dichloro)-l-Cysteine. Biol Reprod **95**, 66.

Hoeltzli, S.D., Kelley, L.K., Moe, A.J., Smith, C.H., 1990. Anionic amino acid transport systems in isolated basal plasma membrane of human placenta. Am J Physiol **259**, C47-55.

Holt, A., Wold, F., 1961. The isolation and characterization of rabbit muscle enolase. J Biol Chem **236**, 3227-3231.

Hu, R., Jin, H., Zhou, S., Yang, P., Li, X., 2007. Proteomic analysis of hypoxia-induced responses in the syncytialization of human placental cell line BeWo. Placenta **28**, 399-407.

Huppertz, B., Kadyrov, M., Kingdom, J.C., 2006. Apoptosis and its role in the trophoblast. Am J Obstet Gynecol **195**, 29-39.

Inadera, H., Tachibana, S., Takasaki, I., Tatematsu, M., Shimomura, A., 2010. Hyperglycemia perturbs biochemical networks in human trophoblast BeWo cells. Endocr J **57**, 567-577.

Ishihara, N., Matsuo, H., Murakoshi, H., Laoag-Fernandez, J.B., Samoto, T., Maruo, T., 2002. Increased apoptosis in the syncytiotrophoblast in human term placentas complicated by either preeclampsia or intrauterine growth retardation. Am J Obstet Gynecol **186**, 158-166.

Jones, D.P., Sies, H., 2015. The Redox Code. Antioxid Redox Signal **23**, 734-746.

Kawasaki, K., Kondoh, E., Chigusa, Y., Kawamura, Y., Mogami, H., Takeda, S., Horie, A., Baba, T., Matsumura, N., Mandai, M., Konishi, I., 2019. Metabolomic Profiles of Placenta in Preeclampsia. Hypertension **73**, 671-679.

Kerscher, L., Oesterhelt, D., 1981a. The catalytic mechanism of 2-oxoacid:ferredoxin oxidoreductases from Halobacterium halobium. One-electron transfer at two distinct steps of the catalytic cycle. Eur J Biochem **116**, 595-600.

Kerscher, L., Oesterhelt, D., 1981b. Purification and properties of two 2-oxoacid:ferredoxin oxidoreductases from Halobacterium halobium. Eur J Biochem **116**, 587-594.

Lash, L.H., Chiu, W.A., Guyton, K.Z., Rusyn, I., 2014. Trichloroethylene biotransformation and its role in mutagenicity, carcinogenicity and target organ toxicity. Mutat Res Rev Mutat Res **762**, 22-36.

Lash, L.H., Putt, D.A., Brashear, W.T., Abbas, R., Parker, J.C., Fisher, J.W., 1999. Identification of S-(1,2-dichlorovinyl)glutathione in the blood of human volunteers exposed to trichloroethylene. J Toxicol Environ Health A **56**, 1-21.

Li, K., Tay, F.R., Yiu, C.K.Y., 2020. The past, present and future perspectives of matrix metalloproteinase inhibitors. Pharmacol Ther **207**, 107465.

Liddel, G.U., Wright, B.E., 1961. The effect of glucose on respiration of the differentiating slime mold. Dev Biol **3**, 265-276.

Loch-Caruso, R., Hassan, I., Harris, S.M., Kumar, A., Bjork, F., Lash, L.H., 2019. Trichloroethylene exposure in mid-pregnancy decreased fetal weight and increased placental markers of oxidative stress in rats. Reprod Toxicol **83**, 38-45.

Longtine, M.S., Barton, A., Chen, B., Nelson, D.M., 2012. Live-cell imaging shows apoptosis initiates locally and propagates as a wave throughout syncytiotrophoblasts in primary cultures of human placental villous trophoblasts. Placenta **33**, 971-976.

Lorenz, M.A., Burant, C.F., Kennedy, R.T., 2011. Reducing time and increasing sensitivity in sample preparation for adherent mammalian cell metabolomics. Anal Chem **83**, 3406-3414.

McKinney, L.L., Picken Jr., J.C., Weakley, F.B., Eldridge, A.C., Campbell, R.E., Cowan, J.C., Biester, H.E., 1959. Possible Toxic Factor of Trichloroethylene-extracted Soybean Oil Meal. Journal of the American Chemical Society **81**, 909-915.

Metzger, B.E., Hare, J.W., Freinkel, N., 1971. Carbohydrate metabolism in pregnancy. IX. Plasma levels of gluconeogenic fuels during fasting in the rat. J Clin Endocrinol Metab **33**, 869-872.

Nair, K.G., 1966. Purification and properties of 3',5'-cyclic nucleotide phosphodiesterase from dog heart. Biochemistry **5**, 150-157.

Newburg, D.S., Fillios, L.C., 1979. A requirement for dietary asparagine in pregnant rats. J Nutr **109**, 2190-2197.

Nissi, R., Talvensaari-Mattila, A., Kotila, V., Niinimaki, M., Jarvela, I., Turpeenniemi-Hujanen, T., 2013. Circulating matrix metalloproteinase MMP-9 and MMP-2/TIMP-2 complex are associated with spontaneous early pregnancy failure. Reprod Biol Endocrinol **11**, 2.

Novak, D., Quiggle, F., Haafiz, A., 2006. Impact of forskolin and amino acid depletion upon System A activity and SNAT expression in BeWo cells. Biochimie **88**, 39-44.

Palei, A.C., Sandrim, V.C., Amaral, L.M., Machado, J.S., Cavalli, R.C., Duarte, G., Tanus-Santos, J.E., 2012. Association between matrix metalloproteinase (MMP)-2 polymorphisms and MMP-2 levels in hypertensive disorders of pregnancy. Exp Mol Pathol **92**, 217-221.

Pattillo, R.A., Gey, G.O., 1968. The establishment of a cell line of human hormone-synthesizing trophoblastic cells in vitro. Cancer Res **28**, 1231-1236.

Plaut, G.W., Sung, S.C., 1954. Diphosphopyridine nucleotide isocitric dehydrogenase from animal tissues. J Biol Chem **207**, 305-314.

Potgens, A.J., Schmitz, U., Bose, P., Versmold, A., Kaufmann, P., Frank, H.G., 2002. Mechanisms of syncytial fusion: a review. Placenta **23 Suppl A**, S107-113.

Ren, W., Luo, W., Wu, M., Liu, G., Yu, X., Fang, J., Li, T., Yin, Y., Wu, G., 2013. Dietary L-glutamine supplementation improves pregnancy outcome in mice infected with type-2 porcine circovirus. Amino Acids **45**, 479-488.

Robbins, J.R., Skrzypczynska, K.M., Zeldovich, V.B., Kapidzic, M., Bakardjiev, A.I., 2010. Placental syncytiotrophoblast constitutes a major barrier to vertical transmission of Listeria monocytogenes. PLoS Pathog **6**, e1000732.

Rodenbeck, S.E., Sanderson, L.M., Rene, A., 2000. Maternal exposure to trichloroethylene in drinking water and birth-weight outcomes. Arch Environ Health **55**, 188-194.

Ruckart, P.Z., Bove, F.J., Maslia, M., 2014. Evaluation of contaminated drinking water and preterm birth, small for gestational age, and birth weight at Marine Corps Base Camp Lejeune, North Carolina: a cross-sectional study. Environ Health **13**, 99.

Sawant, O.B., Ramadoss, J., Hankins, G.D., Wu, G., Washburn, S.E., 2014. Effects of L-glutamine supplementation on maternal and fetal hemodynamics in gestating ewes exposed to alcohol. Amino Acids **46**, 1981-1996.

Sawicki, G., Radomski, M.W., Winkler-Lowen, B., Krzymien, A., Guilbert, L.J., 2000. Polarized release of matrix metalloproteinase-2 and -9 from cultured human placental syncytiotrophoblasts. Biol Reprod **63**, 1390-1395.

Sferruzzi-Perri, A.N., Higgins, J.S., Vaughan, O.R., Murray, A.J., Fowden, A.L., 2019. Placental mitochondria adapt developmentally and in response to hypoxia to support fetal growth. Proc Natl Acad Sci U S A **116**, 1621-1626.

Sharp, A.N., Heazell, A.E., Crocker, I.P., Mor, G., 2010. Placental apoptosis in health and disease. Am J Reprod Immunol **64**, 159-169.

Soto-Guzman, A., Navarro-Tito, N., Castro-Sanchez, L., Martinez-Orozco, R., Salazar, E.P., 2010. Oleic acid promotes MMP-9 secretion and invasion in breast cancer cells. Clin Exp Metastasis **27**, 505-515.

Spaans, F., de Vos, P., Bakker, W.W., van Goor, H., Faas, M.M., 2014. Danger signals from ATP and adenosine in pregnancy and preeclampsia. Hypertension **63**, 1154-1160.

Thonusin, C., IglayReger, H.B., Soni, T., Rothberg, A.E., Burant, C.F., Evans, C.R., 2017. Evaluation of intensity drift correction strategies using MetaboDrift, a normalization tool for multi-batch metabolomics data. J Chromatogr A **1523**, 265-274.

Um, J.Y., Lee, S.A., Park, J.H., Shin, J.M., Park, I.H., Lee, H.M., 2017. Role of adenosine monophosphate-activated protein kinase on cell migration, matrix contraction, and matrix metalloproteinase-1 and matrix metalloproteinase-2 production in nasal polyp-derived fibroblasts. Am J Rhinol Allergy **31**, 357-363.

Vargas, A., Moreau, J., Landry, S., LeBellego, F., Toufaily, C., Rassart, E., Lafond, J., Barbeau, B., 2009. Syncytin-2 plays an important role in the fusion of human trophoblast cells. J Mol Biol **392**, 301-318.

Wang, R., Dang, Y.L., Zheng, R., Li, Y., Li, W., Lu, X., Wang, L.J., Zhu, C., Lin, H.Y., Wang, H., 2014. Live cell imaging of in vitro human trophoblast syncytialization. Biol Reprod **90**, 117.

Wice, B., Menton, D., Geuze, H., Schwartz, A.L., 1990. Modulators of cyclic AMP metabolism induce syncytiotrophoblast formation in vitro. Exp Cell Res **186**, 306-316.

Worthington, D.J., Rosemeyer, M.A., 1976. Glutathione reductase from human erythrocytes. Catalytic properties and aggregation. Eur J Biochem **67**, 231-238.

Wright, B.E., Anderson, M.L., 1959. Biochemical differentiation in the slime mold. Biochim Biophys Acta **31**, 310-322.

Wu, F., Tian, F., Zeng, W., Liu, X., Fan, J., Lin, Y., Zhang, Y., 2017. Role of peroxiredoxin2 downregulation in recurrent miscarriage through regulation of trophoblast proliferation and apoptosis. Cell Death Dis **8**, e2908.

Wu, G., Bazer, F.W., Datta, S., Johnson, G.A., Li, P., Satterfield, M.C., Spencer, T.E., 2008. Proline metabolism in the conceptus: implications for fetal growth and development. Amino Acids **35**, 691-702.

Wu, G., Bazer, F.W., Hu, J., Johnson, G.A., Spencer, T.E., 2005. Polyamine synthesis from proline in the developing porcine placenta. Biol Reprod **72**, 842-850.

Wu, X., Xie, C., Zhang, Y., Fan, Z., Yin, Y., Blachier, F., 2015. Glutamate-glutamine cycle and exchange in the placenta-fetus unit during late pregnancy. Amino Acids **47**, 45-53.

Xu, P., Alfaidy, N., Challis, J.R., 2002. Expression of matrix metalloproteinase (MMP)-2 and MMP-9 in human placenta and fetal membranes in relation to preterm and term labor. J Clin Endocrinol Metab **87**, 1353-1361.

Yamaguchi, T., Nakamura, H., Kihara, Y., Taguchi, M., Yoshikawa, H., Otsuki, M., 2002. Long-term overexpression of membrane type-1 matrix metalloproteinase and matrix metalloproteinase-2 in oleic acid-induced pancreatitis in rats. Pancreas **24**, 348-356.

Yoon, H., Anderson, C.D., Anderson, B.M., 1989. Kinetic studies of Haemophilus influenzae 6-phosphogluconate dehydrogenase. Biochim Biophys Acta **994**, 75-80.

Zeng, X., Wang, F., Fan, X., Yang, W., Zhou, B., Li, P., Yin, Y., Wu, G., Wang, J., 2008. Dietary arginine supplementation during early pregnancy enhances embryonic survival in rats. J Nutr **138**, 1421-1425.

Zheng, R., Li, Y., Sun, H., Lu, X., Sun, B.F., Wang, R., Cui, L., Zhu, C., Lin, H.Y., Wang, H., 2016. Deep RNA sequencing analysis of syncytialization-related genes during BeWo cell fusion. Reproduction.

Chapter VII. Conclusions

The objective of this dissertation is to investigate mechanisms of trichloroethylene (TCE)-stimulated toxicity and potential modulation of TCE reproductive and developmental toxicity by targeting TCE metabolism in timed-pregnant Wistar rats and human placental trophoblast BeWo cells (Pattillo and Gey, 1968). Whereas the timed-pregnant Wistar rat has been used in the context of TCE previously (Loch-Caruso *et al.*, 2019), BeWo cells (Pattillo and Gey, 1968), which represent a villous placental cell type capable of syncytialization *in vitro* (Potgens *et al.*, 2002; Wang *et al.*, 2014), have not been previously used to study TCE toxicity. TCE, an organic solvent with multiple industrial purposes (Agency for Toxic Substances and Disease Registry, 2019), is known to target the reproductive (Healy *et al.*, 1982; Manson *et al.*, 1984; Lamb and Hentz, 2006; Loch-Caruso *et al.*, 2019) and developmental systems (Saillenfait *et al.*, 1995). The findings of this dissertation provide mechanistic evidence to support epidemiological associations between TCE exposure and adverse pregnancy outcomes (Rodenbeck *et al.*, 2000; Forand *et al.*, 2012; Ruckart *et al.*, 2014).

Using the TCE metabolite *S*-(1,2-dichlorovinyl)-L-cysteine (DCVC), prior reports suggest that TCE toxicity is at least partially attributable to CCBL activity from the glutathione (GSH) conjugation metabolic pathway of TCE metabolism because aminooxyacetic acid (AOAA) inhibits cysteine conjugate β-lyase (CCBL) activity in kidney cells and reduces DCVC-stimulated toxicity (Elfarra and Anders, 1984; Lash *et al.*, 1986; Lash *et al.*, 1994). N-acetyl-L-cysteine metabolism releases an acetyl group (Aldini *et al.*, 2018), which may augment DCVC metabolism to *N*-acetyl DCVC (NAcDCVC) (Lash *et al.*, 2014a). Prior studies have shown

mitochondrial dysfunction and apoptosis as mechanisms associated with DCVC-stimulated toxicity in kidney cells (Xu *et al.*, 2008; Lash *et al.*, 2014b). Importantly, reactive oxygen species (ROS) generation, pro-inflammatory response, apoptosis, mitochondrial dysfunction, and energy metabolism alteration are mechanisms of DCVC-stimulated toxicity in HTR-8/SVneo extravillous placental cells (Hassan *et al.*, 2016; Elkin *et al.*, 2018; Elkin *et al.*, 2019; Elkin *et al.*, 2020). In contrast, metabolites from the cytochrome P450-dependent oxidative pathway of TCE metabolism, trichloroacetic acid (TCA) and dichloroacetic acid (DCA) (Lash *et al.*, 2014a), do not produce toxicity in HTR-8/SVneo cells (unpublished data). *In vivo*, TCE exposure reduces fetal weight and increases markers of oxidative stress in timed-pregnant Wistar rats (Loch-Caruso *et al.*, 2019).

Because the toxicity of TCE is dependent on its metabolism, we hypothesized that NAC and AOAA would modify TCE- or DCVC-stimulated toxicity in Wistar rats and BeWo cells, respectively. This dissertation is the first to show that AOAA pre/co-treatment to TCE prevents TCE-stimulated decreased fetal weight (Chapter 2). This finding suggests that TCE-induced reduction of fetal weight is dependent on CCBL activity that converts DCVC to the toxic metabolite 1,2-dichlorovinylthiol (DCVT), consistent with prior studies with kidney cells (Elfarra and Anders, 1984; Lash *et al.*, 1986; Lash *et al.*, 1994). Significantly, AOAA reduced CCBL activity in maternal kidney but not maternal liver or placenta in the present study, suggesting that kidney may have a role in the AOAA-stimulated prevention of fetal weight decrease (Chapter 2). NAC pre/co-treatment to TCE altered placental dimensions consistent with a delayed developmental progression (Furukawa *et al.*, 2011), indicating that NAC pre/co-treatment to TCE could have an adverse effect on placenta. In support of this, NAC pre/co-treatment exacerbated DCVC-stimulated hydrogen peroxide abundance (Chapter 5).

Immunohistochemistry staining of placenta revealed that expression of enzymes known to bioactivate TCE differed as a function of placenta zone, indicating that placental capability to bioactivate TCE depends on placental zone. By itself, TCE did not stimulate many changes to rat placenta. This is contrary to previous studies of TCE or DCVC-stimulated toxicity in placenta (Hassan *et al.*, 2016; Elkin *et al.*, 2018; Elkin *et al.*, 2019; Loch-Caruso *et al.*, 2019; Elkin *et al.*, 2020) and findings in this dissertation that DCVC stimulated effects in human placental BeWo cells (Chapters 4, 5, and 6).

A significant portion of the dissertation investigated responses in energy metabolism in response to TCE exposure of timed-pregnant Wistar rats and DCVC exposure of BeWo cells undergoing forskolin-stimulated syncytialization (Chapters 3 and 6, respectively). Syncytialization is the multinucleation and fusion process of the placenta (Potgens *et al.*, 2002; Wang *et al.*, 2014). Because metabolomics analyses have been widely used to identify energy metabolism metabolites that are associated with adverse pregnancy outcomes (Romero *et al.*, 2010; Menon *et al.*, 2014; Huang *et al.*, 2017; Virgiliou *et al.*, 2017; Gil and Duarte, 2018), we hypothesized that TCE would modify energy metabolites of rat amniotic fluid that have relevance to pregnancy. Similarly, because multinucleation in slime molds involve changes in energy metabolism (Allen *et al.*, 1985; Allen *et al.*, 1988) and DCVC targets energy metabolism in HTR-8/SVneo placental cells (Elkin *et al.*, 2020), we hypothesized that DCVC would alter energy metabolites in BeWo cells undergoing syncytialization. Significantly, we found that TCE-stimulated decreases in metabolites responsible for direct energy supply, including adenosine triphosphate (ATP), adenosine diphosphate (ADP), and guanosine diphosphate (GDP) in amniotic fluid for both male and female fetal sex. KEGG pathways altered by TCE in amniotic fluid of both sexes as discovered from Metaboanalyst 4.0 analysis included folate

biosynthesis and pentose phosphate pathway. A sex-specific difference was noted for TCE-stimulated increased arginine in females but not males, which relates to arginine and proline metabolism. This suggests that the decreased susceptibility of females to TCE toxicity (Chapter 2) may be related, at least in part, to increased ability to vasodilate as a consequence of increased arginine (Aouache *et al.*, 2018). A similar metabolomics approach could yield important results for other environmental toxicants or interventions.

Novel insights inform how DCVC exposure during forskolin-stimulated syncytialization of BeWo cells could exacerbate or reverse the energy metabolism responses observed with syncytialization. Whereas DCVC treatment further decreased the syncytialization-stimulated decrease in aspartate and uridine diphosphate (UDP)-D-glucose, DCVC treatment during syncytialization decreased the syncytialization-stimulated increase in oleic acid. Together, these show the complex relationship between syncytialization and DCVC treatment during syncytialization. Some similar KEGG pathways were altered by both syncytialization and DCVC treatment during syncytialization, including starch and sucrose metabolism and histidine metabolism. Purine metabolism was a KEGG pathway in which metabolite ratios altered by syncytialization were reversed by DCVC treatment during syncytialization. For example, whereas syncytialization increased adenosine monophosphate at the expense of adenosine diphoshphate (ADP), DCVC treatment during syncytialization increased ADP at the expense of AMP. Following up on the oleic acid finding by investigating matrix metalloproteinases (MMPs), some of which are positively associated with oleic acid and are important in syncytialization (Sawicki *et al.*, 2000; Xu *et al.*, 2002; Yamaguchi *et al.*, 2002; Soto-Guzman *et al.*, 2010), we found that MMP-2 increased with syncytialization but decreased with DCVC treatment during sycytialization. Because MMP-2 has a critical role in polarization of

syncytiotrophoblasts (Sawicki *et al.*, 2000), we suggest DCVC hinders proper syncytialization. We also found that DCVC treatment during syncytialization increased MMP-1 relative to syncytialization only. Importantly and with regard to metabolomics-specific findings, we also found many more changes in response to DCVC exposure in cells compared to those for TCE exposure in rats.

This dissertation showed that DCVC stimulated apoptosis in unsyncytialized BeWo cells, BeWo cells undergoing syncytialization, and syncytialized BeWo cells. Importantly, we showed that DCVC was more toxic to syncytialized BeWo cells and to BeWo cells undergoing syncytialization compared to unsyncytialized BeWo cells. Increased caspase 3/7 activity, increased nuclear condensation or fragmentation, increased cytotoxicity, and decreased cell viability were stimulated by DCVC in BeWo cells regardless of differentiation state. Importantly, the apoptosis in unsyncytialized BeWo cells, BeWo cells undergoing syncytialization, and syncytialized BeWo cells was characterized by increased hydrogen peroxide generation and decreased *PRDX2* mRNA expression, consistent with increased cellular ROS generation. However, the decreased nuclear factor kappa B subunit 1 *NFKB1* mRNA expression and decreased tumor necrosis factor receptor 1 (TNF-R1) was observed only in syncytialized BeWo cells, suggesting that a pro-inflammatory response may be more relevant to DCVC toxicity on syncytialized BeWo cells compared to unsyncytialized BeWo cells or BeWo cells undergoing syncytialization. We also found some novel responses regarding syncytialization, including increased interleukin-6 in media and decreased hydrogen peroxide abundance, suggesting a need to further characterize the process.

This dissertation also investigated how NAC and AOAA pre/co-treatment modulated DCVC-stimulated toxicity in BeWo cells. NAC was found to either exacerbate or not affect

360

DCVC-stimulated toxicity. In particular, the exacerbation of hydrogen peroxide abundance in unsyncytialized BeWo cells and BeWo cells undergoing sycytialization by NAC showed that NAC was not functioning strictly as an antioxidant, a property of NAC (Aldini *et al.*, 2018). Of novelty, we showed that the effect of NAC but not DCVC was statistically significant for *CYP3A4* mRNA expression in unsyncytialized BeWo cells and syncytialized BeWo cells. This is important because increased *CYP3A4* mRNA favors increased production of N-acetyl DCVC sulfoxide (NAcDCVCS), a toxic DCVC metabolite (Werner *et al.*, 1996; Lash *et al.*, 2014a), and NAC could provide an acetyl group (Aldini *et al.*, 2018) to promote the production of NAcDCVCS. Because CYP3A4 inhibition with ketaconazole pre/co-treatment was not sufficient to reduce toxicity in unsyncytialized BeWo cells and BeWo cells, it is possibile that aminoacylase III contributed to metabolism to the reactive DCVT (Lash *et al.*, 2014a) and would also need to be inhibited to prevent regeneration of DCVC in order to reduce toxicity. Similar to the finding that AOAA exerted no effect on CCBL activity in rat placenta, AOAA exerted no effect on CCBL activity in unsyncytialized BeWo cells, BeWo cells undergoing syncytialization, and syncytialized BeWo cells. However, a significant observation from the CCBL activity assays in BeWo cells was that syncytialized BeWo cells have higher CCBL activity than unsyncytialized BeWo cells. This may explain why syncytialized BeWo cells were more susceptible to DCVC-stimulated toxicity than unsyncytialized BeWo cells and suggests that differences in DCVC toxicity as a function of cell differentiation state can be considerable.

Strengths arose from the use of the Wistar rat model that could not have been achieved through use of BeWo cells alone. Firstly, the Wistar rat model allowed investigation into organs other than the placenta. Our results of cysteine conjugate β-lyase (CCBL) activity suggest that the kidney, as opposed to liver or placenta, may have a more significant role for the AOAA-

stimulated prevention of TCE-stimulated decreased fetal weight. Within the placenta, the histology and immunohistochemistry (IHC) findings revealed regions of the placenta most capable of TCE biotransformation or responsible for toxic outcomes. Finally, including sex of the placenta in our analysis allowed us to identify sex-specific changes in response to TCE treatment. Future studies investigating TCE reproductive toxicity are likely to encounter similar important nuances in effects and should expand upon them.

The *in vitro* BeWo human placental trophoblast cell model complemented the rat model in this thesis. Firstly, AOAA as an ineffective modulator of CCBL was confirmed in both the rat model and the BeWo cells. This novel finding contrasts from findings in kidney cells (Elfarra and Anders, 1984; Lash *et al.*, 1986; Lash *et al.*, 1994) and suggests that the composition of CCBL enzymes in rat placenta is more similar to human placenta compared to rat kidney. Additionally, the use of the BeWo cell line allowed us to observe a placenta process, syncytialization, *in vitro*, which would be more difficult to accomplish in an *in vivo* rat model. Given that notable differences between rats and humans may exist in enzymes responsible for TCE biotransformation (Lash *et al.*, 2000; Lash *et al.*, 2014a; Rusyn *et al.*, 2014), the importance of work that translates the relevance of findings from laboratory animals to humans cannot be overstated as a crucial future direction.

In general, we observed that treatment with the TCE metabolite, *S*-(1,2-dichlorovinyl)-L-cysteine (DCVC), stimulated more responses in BeWo cells than treatment with TCE to timed-pregnant Wistar rats. This was seen with the metabolomics studies (Chapters 3 and 6), particularly with the pathway and ratio analysis. Additionally, we observed that DCVC stimulates apoptosis in BeWo cells but that TCE failed to stimulate several apoptotic responses in rat placenta (Chapters 2, 4, and 5). The difference in concentrations at the target cells is one

possible explanation for the differences in response. Although concentrations of DCVC and dosage of TCE were chosen as relevant to occupational exposures (Lash *et al.*, 1999; Agency for Toxic Substances and Disease Registry, 2007), it remains unknown how relevant a dosage of 480 mg TCE/kg/day is to an *in vitro* concentration of 20 µM DCVC. Another consideration is the difference in species between the *in vivo* model (rat) and the BeWo model (human) because there are notable differences in TCE biotransformation between humans and rats. An example is the higher activity of CCBL in rat kidney compared to human kidney (Stevens *et al.*, 1986; Elfarra *et al.*, 1987; Lash *et al.*, 1990). Although our CCBL values in BeWo cells versus rat placenta did not suggest that rats have higher CCBL activity than humans, understanding CCBL activity variation by organ and species is crucial to comprehending differences in susceptibility to DCVC toxicity. Finally, the role that other organs can exert on TCE toxicity *in vivo* but not *in vitro* can be considerable. For example, because the liver is a major site of CYP-dependent metabolism of TCE (Lash *et al.*, 2014a), the rats could be exposed to higher concentrations of TCE metabolites through the CYP-dependent metabolic pathway of TCE (Lash *et al.*, 2014a) compared to the BeWo cells.

Despite aforementioned differences between BeWo cell responses to DCVC and rat responses to TCE, notable similarities exist between results from the two models. In both models, NAC was found to either exacerbate or not affect TCE or DCVC responses but failed to minimize a TCE or DCVC response. We suggest that NAC could push metabolism towards increased production of the toxic N-acetyl DCVC sulfoxide (NAcDCVCS), but actual detection of metabolites would strengthen this speculation. As a whole, the NAC studies challenge the notion of NAC administration as a protective measure for TCE toxicity, and suggest instead that the provision of NAC could be detrimental if administred with TCE or DCVC. Accordingly, the

argument for NAC toxicity is more specific to the context of TCE or DCVC metabolism than by itself.

AOAA failed to inhibit CCBL activity in rat placenta as well as in BeWo cells, regardless of BeWo differentiation status. Furthermore, the finding that syncytialized BeWo cells exhibited greater CCBL activity than unsyncytialized BeWo cells supports the notion that placenta cell differentiation states have differing levels of CCBL, consistent with findings of differential distribution of CCBL in placental zones of rats. These findings suggest that different placental cell types have different abilities for bioactivating DCVC and potentially other toxicants. Discovering the exact composition of CCBLs in placenta and the relationship to other organs remains important future work.

Although this dissertation did not observe many effects in rat placenta, the rat study contributes significantly to the current understanding of TCE toxicity to the placenta. Firstly, this dissertation is the first to show that modification of CCBL activity by AOAA prevented TCE-induced decreased fetal weight, implying that the GSH conjugation pathway of TCE metabolism downstream of DCVC is important for fetal growth. In the absence of TCE exposure, AOAA decreased fetal weight, showing that the impact of AOAA depended on the presence of TCE. These findings highlight that DCVC metabolism was critical to TCE toxicity in pregnancy. This dissertation shows that CCBL activity was profoundly different across tissues, which supports and expands upon previous literature (Lash, 2010). Nonetheless, our finding of placental CCBL activity was the first to indicate that placenta has CCBL activity but also acknowledges that there is a need to further characterize exact placental enzymes capable of CCBL activity and develop or identify inhibitors of CCBL for tissues besides the kidney. This dissertation would also be bolstered by the detection of 1,2-dichlorovinylthiol (DCVT) and other metabolites downstream

364

of DCVC via CCBL activity. In light of findings that DCVC has been found at low concentrations in mouse serum (Kim *et al.*, 2009a; Kim *et al.*, 2009b; Luo *et al.*, 2018), important future directions also include the need to consider if rats are more capable of generating DCVC than mice or if low concentrations of DCVC *in vivo* are sufficient to produce the observed fetal weight effects. Secondly, our work suggests a need to understand further the enzymes involved in TCE metabolism in placenta.

In summary, this dissertation contributes to our understanding of TCE and DCVC toxicity during pregnancy. In the Wistar rat, because few changes were observed in placenta in response to TCE exposure, we were unable to infer a sequence of events that could contribute to an adverse outcome, such as decreased fetal weight. However, the AOAA effect on CCBL activity in maternal kidney suggests that AOAA-stimulated prevention of TCE-stimulated deceased fetal weight may be attributable to maternal kidney. Additionally, the effect of NAC pre/co-treatment to TCE, suggestive to favor delayed placenta development, supports the possibility that NAC in combination with TCE or DCVC could be harmful. The BeWo cells provided insight into DCVC-stimulated mechanisms underlying apoptosis, allowing separate analysis of effects on unsyncytialized BeWo cells, BeWo cells undergoing syncytialization, and syncytialized BeWo cells. Significantly, we found that the syncytialized BeWo cells responded differently to DCVC compared to unsyncytialized BeWo cells and BeWo cells undergoing syncytialization. The syncytialized BeWo cell response involved more interaction with factors regulating pro-inflammatory response, notably tumor necrosis factor receptor 1 (TNF-R1) and mRNA of *NFKB1*. Regardless of the differentiation state of the BeWo cells, reactive oxygen species generation was suggested to play a major role in apoptosis. Also significant was the finding that syncytialized BeWo cells have greater CCBL activity than unsyncytialized BeWo

cells, which may explain why syncytialized BeWo cells are more susceptible to DCVC toxicity than unsyncytialized BeWo cells. Metabolomics analysis suggest that DCVC in BeWo cells or TCE in Wistar rats affect direct energy supply involving purine metabolism. A simplified depiction of a model of TCE and DCVC toxicity from this dissertation is shown in **Figure 7.1**.

Overall, we suggest that TCE exposure is toxic during pregnancy and this toxicity likely is attributable to metabolism downstream of DCVC. Importantly, we suggest that modulation of enzymes capable of bioactivation of TCE or DCVC is a potentially promising method for reducing TCE stimulated toxicity, as demonstrated by the AOAA prevention of TCE-stimulated decreased fetal weight. Targeting additional mechanisms by which TCE or DCVC could stimulate apoptosis, such as the generation of reactive oxygen species, is also promising. Major considerations for future work include improved analytical methods to detect TCE metabolites, especially reactive metabolites thought to contribute to TCE toxicity. An important future consideration is the *in vivo* exposure correlation and relation to an *in vitro* exposure. Finally, agents thought to be protective, such as NAC, should be individually evaluated for possibility of toxicant bioactivation or other mechanisms that could actually be of harm to health.
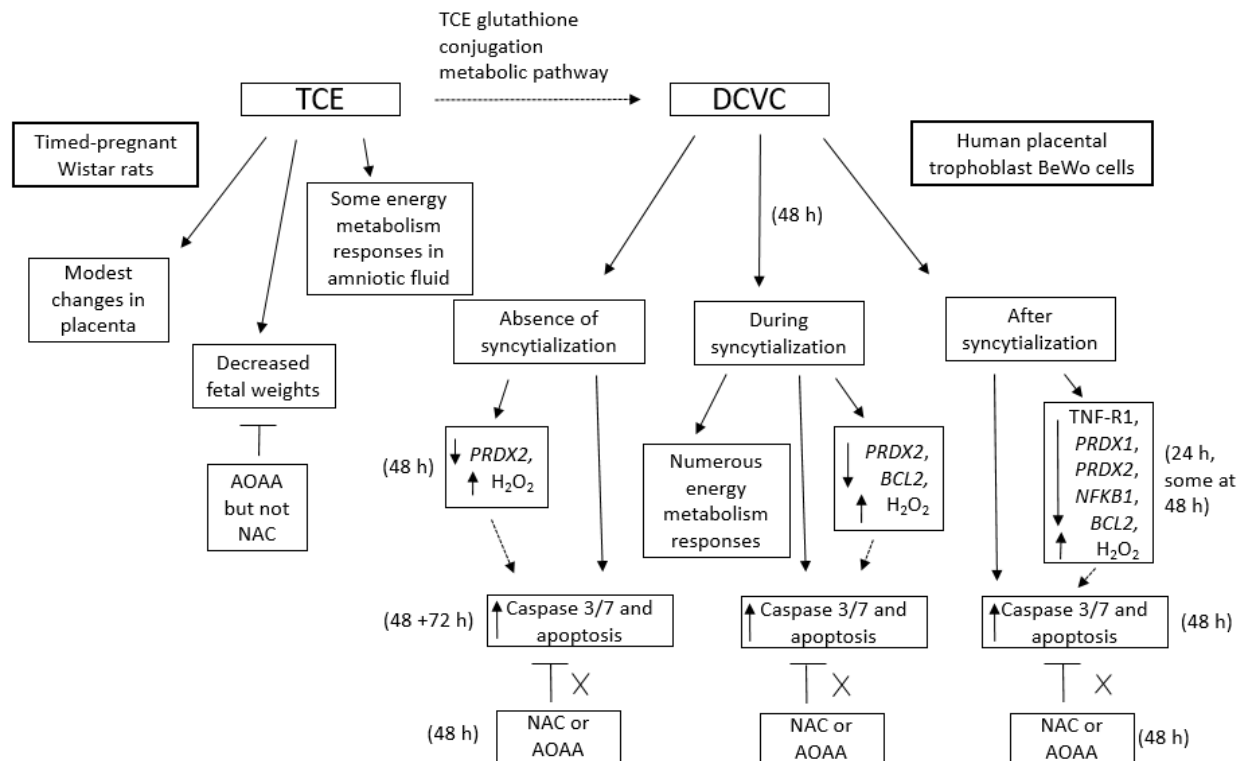
Figure 7.1. Simplified model of TCE or DCVC toxicity from this dissertation. We found that TCE decreased fetal weight in timed-pregnant Wistar rats, an effect prevented by AOAA but not NAC pre/co-treatment (Chapter 2). TCE stimulated modest changes in rat placenta (Chapter 2). This dissertation found and discussed some metabolites in energy metabolism in amniotic fluid that were altered by TCE treatment (Chapter 3). We saw that DCVC could stimulate some distinct mechanisms towards apoptosis dependent on the differentiation state of the BeWo cells, or whether the BeWo cells were unsyncytialized, undergoing syncytialization, or syncytialized (Chapter 4). This dissertation found that NAC or AOAA pre/co-treatment did not prevent DCVC-stimulated toxicity in unsyncytialized BeWo cells, BeWo cells undergoing syncytialization, and syncytialized BeWo cells and that NAC could exacerbate some DCVC-stimulated responses (Chapter 5). Significantly, syncytialized BeWo cells have more CCBL activity than unsyncytialized BeWo cells, which can explain why syncytialized BeWo cells are more susceptible to DCVC toxicity than unsyncytialized BeWo cells (Chapters 4 and 5). Finally, this dissertation showed how DCVC-treatment during BeWo cell syncytialization could stimulate changes in metabolites in energy metabolism, some changes that furthered a change stimulated by syncytialization and some changes that reversed a change stimulated by syncytialization (Chapter 6).

367

References

Agency for Toxic Substances and Disease Registry, 2007. Trichloroethylene Toxicity: What are the U.S. Standards for Trichloroethylene Exposure? In Agency for Toxic Substances and Disease Registry (ATSDR), E.H.a.M.E., (Ed.), Atlanta, GA, pp.

Agency for Toxic Substances and Disease Registry, 2019. Toxicological Profile for Trichloroethylene. In U.S. Department of Health and Human Services, A.f.T.S.a.D.R.A., (Ed.), Atlanta, GA, pp.

Aldini, G., Altomare, A., Baron, G., Vistoli, G., Carini, M., Borsani, L., Sergio, F., 2018. N-Acetylcysteine as an antioxidant and disulphide breaking agent: the reasons why. Free Radic Res **52**, 751-762.

Allen, R.G., Balin, A.K., Reimer, R.J., Sohal, R.S., Nations, C., 1988. Superoxide dismutase induces differentiation in microplasmodia of the slime mold Physarum polycephalum. Arch Biochem Biophys **261**, 205-211.

Allen, R.G., Newton, R.K., Sohal, R.S., Shipley, G.L., Nations, C., 1985. Alterations in superoxide dismutase, glutathione, and peroxides in the plasmodial slime mold Physarum polycephalum during differentiation. J Cell Physiol **125**, 413-419.

Aouache, R., Biquard, L., Vaiman, D., Miralles, F., 2018. Oxidative Stress in Preeclampsia and Placental Diseases. Int J Mol Sci **19**.

Elfarra, A.A., Anders, M.W., 1984. Renal processing of glutathione conjugates. Role in nephrotoxicity. Biochem Pharmacol **33**, 3729-3732.

Elfarra, A.A., Lash, L.H., Anders, M.W., 1987. Alpha-ketoacids stimulate rat renal cysteine conjugate beta-lyase activity and potentiate the cytotoxicity of S-(1,2-dichlorovinyl)-L-cysteine. Mol Pharmacol **31**, 208-212.

Elkin, E.R., Bridges, D., Harris, S.M., Loch-Caruso, R.K., 2020. Exposure to Trichloroethylene Metabolite S-(1,2-Dichlorovinyl)-L-cysteine Causes Compensatory Changes to Macronutrient Utilization and Energy Metabolism in Placental HTR-8/SVneo Cells. Chem Res Toxicol.

Elkin, E.R., Bridges, D., Loch-Caruso, R., 2019. The trichloroethylene metabolite S-(1,2-dichlorovinyl)-L-cysteine induces progressive mitochondrial dysfunction in HTR-8/SVneo trophoblasts. Toxicology **427**, 152283.

Elkin, E.R., Harris, S.M., Loch-Caruso, R., 2018. Trichloroethylene metabolite S-(1,2-dichlorovinyl)-l-cysteine induces lipid peroxidation-associated apoptosis via the intrinsic and extrinsic apoptosis pathways in a first-trimester placental cell line. Toxicol Appl Pharmacol **338**, 30-42.

Forand, S.P., Lewis-Michl, E.L., Gomez, M.I., 2012. Adverse birth outcomes and maternal exposure to trichloroethylene and tetrachloroethylene through soil vapor intrusion in New York State. Environ Health Perspect **120**, 616-621.

Furukawa, S., Hayashi, S., Usuda, K., Abe, M., Hagio, S., Ogawa, I., 2011. Toxicological pathology in the rat placenta. J Toxicol Pathol **24**, 95-111.

Gil, A.M., Duarte, D., 2018. Biofluid Metabolomics in Preterm Birth Research. Reprod Sci **25**, 967-977.

Healy, T.E., Poole, T.R., Hopper, A., 1982. Rat fetal development and maternal exposure to trichloroethylene 100 p.p.m. Br J Anaesth **54**, 337-341.

Hassan, I., Kumar, A.M., Park, H.R., Lash, L.H., Loch-Caruso, R., 2016. Reactive Oxygen Stimulation of Interleukin-6 Release in the Human Trophoblast Cell Line HTR-8/SVneo by the Trichlorethylene Metabolite S-(1,2-Dichloro)-l-Cysteine. Biol Reprod **95**, 66.

Huang, J., Mo, J., Zhao, G., Lin, Q., Wei, G., Deng, W., Chen, D., Yu, B., 2017. Application of the amniotic fluid metabolome to the study of fetal malformations, using Down syndrome as a specific model. Mol Med Rep **16**, 7405-7415.

Kim, S., Collins, L.B., Boysen, G., Swenberg, J.A., Gold, A., Ball, L.M., Bradford, B.U., Rusyn, I., 2009a. Liquid chromatography electrospray ionization tandem mass spectrometry analysis method for simultaneous detection of trichloroacetic acid, dichloroacetic acid, S-(1,2-dichlorovinyl)glutathione and S-(1,2-dichlorovinyl)-L-cysteine. Toxicology **262**, 230-238.

Kim, S., Kim, D., Pollack, G.M., Collins, L.B., Rusyn, I., 2009b. Pharmacokinetic analysis of trichloroethylene metabolism in male B6C3F1 mice: Formation and disposition of trichloroacetic acid, dichloroacetic acid, S-(1,2-dichlorovinyl)glutathione and S-(1,2-dichlorovinyl)-L-cysteine. Toxicol Appl Pharmacol **238**, 90-99.

Lamb, J.C., Hentz, K.L., 2006. Toxicological review of male reproductive effects and trichloroethylene exposure: assessing the relevance to human male reproductive health. Reprod Toxicol **22**, 557-563.

Lash, L.H., 2010. Role of Bioactivation Reactions in Chemically Induced Nephrotoxicity. In Gad, S.C., (Ed.), Pharmaceutical Sciences Encyclopedia: Drug Discovery, Development, and Manufacturing. John Wiley & Sons, Inc., Hoboken, NJ, pp. 1-21.

Lash, L.H., Chiu, W.A., Guyton, K.Z., Rusyn, I., 2014a. Trichloroethylene biotransformation and its role in mutagenicity, carcinogenicity and target organ toxicity. Mutat Res Rev Mutat Res **762**, 22-36.

Lash, L.H., Elfarra, A.A., Anders, M.W., 1986. Renal cysteine conjugate beta-lyase. Bioactivation of nephrotoxic cysteine S-conjugates in mitochondrial outer membrane. J Biol Chem **261**, 5930-5935.

Lash, L.H., Fisher, J.W., Lipscomb, J.C., Parker, J.C., 2000. Metabolism of trichloroethylene. Environ Health Perspect **108 Suppl 2**, 177-200.

Lash, L.H., Nelson, R.M., Van Dyke, R.A., Anders, M.W., 1990. Purification and characterization of human kidney cytosolic cysteine conjugate beta-lyase activity. Drug Metab Dispos **18**, 50-54.

Lash, L.H., Putt, D.A., Benipal, B., 2014b. Multigenerational study of chemically induced cytotoxicity and proliferation in cultures of human proximal tubular cells. Int J Mol Sci **15**, 21348-21365.

Lash, L.H., Putt, D.A., Brashear, W.T., Abbas, R., Parker, J.C., Fisher, J.W., 1999. Identification of S-(1,2-dichlorovinyl)glutathione in the blood of human volunteers exposed to trichloroethylene. J Toxicol Environ Health A **56**, 1-21.

Lash, L.H., Sausen, P.J., Duescher, R.J., Cooley, A.J., Elfarra, A.A., 1994. Roles of cysteine conjugate beta-lyase and S-oxidase in nephrotoxicity: studies with S-(1,2-dichlorovinyl)-L-cysteine and S-(1,2-dichlorovinyl)-L-cysteine sulfoxide. J Pharmacol Exp Ther **269**, 374-383.

Loch-Caruso, R., Hassan, I., Harris, S.M., Kumar, A., Bjork, F., Lash, L.H., 2019. Trichloroethylene exposure in mid-pregnancy decreased fetal weight and increased placental markers of oxidative stress in rats. Reprod Toxicol **83**, 38-45.

Luo, Y.S., Furuya, S., Chiu, W., Rusyn, I., 2018. Characterization of inter-tissue and inter-strain variability of TCE glutathione conjugation metabolites DCVG, DCVC, and NAcDCVC in the mouse. J Toxicol Environ Health A **81**, 37-52.

Manson, J.M., Murphy, M., Richdale, N., Smith, M.K., 1984. Effects of oral exposure to trichloroethylene on female reproductive function. Toxicology **32**, 229-242.

Menon, R., Jones, J., Gunst, P.R., Kacerovsky, M., Fortunato, S.J., Saade, G.R., Basraon, S., 2014. Amniotic fluid metabolomic analysis in spontaneous preterm birth. Reprod Sci **21**, 791-803.

Pattillo, R.A., Gey, G.O., 1968. The establishment of a cell line of human hormone-synthesizing trophoblastic cells in vitro. Cancer Res **28**, 1231-1236.

Potgens, A.J., Schmitz, U., Bose, P., Versmold, A., Kaufmann, P., Frank, H.G., 2002. Mechanisms of syncytial fusion: a review. Placenta **23 Suppl A**, S107-113.

Rodenbeck, S.E., Sanderson, L.M., Rene, A., 2000. Maternal exposure to trichloroethylene in drinking water and birth-weight outcomes. Arch Environ Health **55**, 188-194.

Romero, R., Mazaki-Tovi, S., Vaisbuch, E., Kusanovic, J.P., Chaiworapongsa, T., Gomez, R., Nien, J.K., Yoon, B.H., Mazor, M., Luo, J., Banks, D., Ryals, J., Beecher, C., 2010. Metabolomics in premature labor: a novel approach to identify patients at risk for preterm delivery. J Matern Fetal Neonatal Med **23**, 1344-1359.

Ruckart, P.Z., Bove, F.J., Maslia, M., 2014. Evaluation of contaminated drinking water and preterm birth, small for gestational age, and birth weight at Marine Corps Base Camp Lejeune, North Carolina: a cross-sectional study. Environ Health **13**, 99.

Rusyn, I., Chiu, W.A., Lash, L.H., Kromhout, H., Hansen, J., Guyton, K.Z., 2014. Trichloroethylene: Mechanistic, epidemiologic and other supporting evidence of carcinogenic hazard. Pharmacol Ther **141**, 55-68.

Saillenfait, A.M., Langonne, I., Sabate, J.P., 1995. Developmental toxicity of trichloroethylene, tetrachloroethylene and four of their metabolites in rat whole embryo culture. Arch Toxicol **70**, 71-82.

Sawicki, G., Radomski, M.W., Winkler-Lowen, B., Krzymien, A., Guilbert, L.J., 2000. Polarized release of matrix metalloproteinase-2 and -9 from cultured human placental syncytiotrophoblasts. Biol Reprod **63**, 1390-1395.

Soto-Guzman, A., Navarro-Tito, N., Castro-Sanchez, L., Martinez-Orozco, R., Salazar, E.P., 2010. Oleic acid promotes MMP-9 secretion and invasion in breast cancer cells. Clin Exp Metastasis **27**, 505-515.

Stevens, J.L., Robbins, J.D., Byrd, R.A., 1986. A purified cysteine conjugate beta-lyase from rat kidney cytosol. Requirement for an alpha-keto acid or an amino acid oxidase for activity and identity with soluble glutamine transaminase K. J Biol Chem **261**, 15529-15537.

Virgiliou, C., Gika, H.G., Witting, M., Bletsou, A.A., Athanasiadis, A., Zafrakas, M., Thomaidis, N.S., Raikos, N., Makrydimas, G., Theodoridis, G.A., 2017. Amniotic Fluid and Maternal Serum Metabolic Signatures in the Second Trimester Associated with Preterm Delivery. J Proteome Res **16**, 898-910.

Wang, R., Dang, Y.L., Zheng, R., Li, Y., Li, W., Lu, X., Wang, L.J., Zhu, C., Lin, H.Y., Wang, H., 2014. Live cell imaging of in vitro human trophoblast syncytialization. Biol Reprod **90**, 117.

Werner, M., Birner, G., Dekant, W., 1996. Sulfoxidation of mercapturic acids derived from tri- and tetrachloroethene by cytochromes P450 3A: a bioactivation reaction in addition to

deacetylation and cysteine conjugate beta-lyase mediated cleavage. Chem Res Toxicol **9**, 41-49.

Xu, F., Papanayotou, I., Putt, D.A., Wang, J., Lash, L.H., 2008. Role of mitochondrial dysfunction in cellular responses to S-(1,2-dichlorovinyl)-L-cysteine in primary cultures of human proximal tubular cells. Biochem Pharmacol **76**, 552-567.

Xu, P., Alfaidy, N., Challis, J.R., 2002. Expression of matrix metalloproteinase (MMP)-2 and MMP-9 in human placenta and fetal membranes in relation to preterm and term labor. J Clin Endocrinol Metab **87**, 1353-1361.

Yamaguchi, T., Nakamura, H., Kihara, Y., Taguchi, M., Yoshikawa, H., Otsuki, M., 2002. Long-term overexpression of membrane type-1 matrix metalloproteinase and matrix metalloproteinase-2 in oleic acid-induced pancreatitis in rats. Pancreas **24**, 348-356.